Bioclastic Accumulations along the Western Margin of the Early Triassic Montney Formation

by

Shelby Sanders

A thesis submitted in partial fulfillment of the requirements for the degree of

Master of Science

Department of Earth and Atmospheric Sciences
University of Alberta

© Shelby Sanders, 2016

Abstract

Two bioclastic intervals within the Early Triassic Montney Formation in British Columbia, Canada, were examined for sedimentological and paleontological evidence of their deposition. Twenty seven core were analyzed for sedimentological characteristics and then sampled for further paleontological and petrological analyses. The analyses allowed for the construction of three facies associations that describe the depositional characteristics of these two units.

These two bioclastic intervals represent some of the first calcified body fossils preserved within th Western Canada Sedimentary Basin after the P-Tr boundary. Preserved calcified body fossils are rare within the Montney Formation (Zonneveld, 2011). Their presence within these sections and absence within the rest of the basin allow insight to the unstable conditions within the Peace River Embayment in the Early Triassic.

The first of the two bioclastic horizons, the *Claraia* Zone”, has been mistakenly interpreted as an offshore turbidite fan. Analysis of core has revealed that this unit is a bioclastic interval that shows lithological characteristics inconsistent with this interpretation. The “*Claraia* Zone” has been delineated and mapped using core data sets and wire line log characteristics. Core were logged and facies identified based on lithological characteristics of the units.

Two facies associations were connected to this horizon. The first, the fan-derived bottom current modified deposits, consists of heterolithic very fine sandstone interbedded with fine bituminous siltston These beds contain lenticular to flaser bedding that has been found to be remarkably similar to bottom current deposits from the Pleistocene of the Gulf of Mexico. The second facies association consists of distal bottom current modified deposits wherein a biological signal was able to be preserved. The primary facies of this association is the laminated bioclastic siltstone which is also the primary facies connected to the “*Claraia* Zone”. The bioclasts within this zone showed evidence of transport and/or winnowing in the form of highly fragmented and disarticulated valves. Similar contacts and grading found between this facies and the heterolithic facies allowed them to be connected to the same depositional mechanism.

Finally, evidence of the possibility of bottom current modification was compared with the criteria for identifying bottom current deposits. The small scale sedimentary analysis showed evidence in the form of the heterolithic facies and the winnowing or bioclasts within the laminated bioclastic siltstone facies. The medium scale was based on the deposit shape which was extrapolated to be parallel to paleoshoreline from analysis of cross sections and isopach maps. Large scale evidence was linked to the location of the

basin at the western margin of Pangea in the Early Triassic which would have been subjected to strong westerly winds and storms. Therefore it was interpreted that the “*Claraia* Zone” was the result of wind derived bottom current deposition/modification

The second, the Altares Packstone Member, was identified as the earliest example of *in situ* biogenic carbonate development in northwestern North America after the P-Tr boundary. These packstone beds are late Smithian in age and occur just below the Smithian/Spathian boundary (SMSP) that is correlated across the Montney Formation. They are interpreted to be a series of biostromes that were exhumed and eroded several times throughout their development and make up the final facies association within this study.

The bioclastic packstone units appear in small packages, commonly no thicker than a few centimeters in core, but these packages are repeated through the horizon, and often have thin, calcified beds on either side that grade into the thicker packstone. Articulated brachiopod, bivalve, and ammonoid shells were observed within thin-sections through the packstone, along with several examples of vertebrate material. The abundance of articulated valve material (particularly of Pectinoids) in the center of the deposit indicates that these deposits likely occurred *in situ*.

Biostromes have been referred to being the result of Allogenic Taphonomic Feedback, but without the necessary evidence of hard ground preferring organisms that theory cannot be substantiated here. These biostrome beds are discrete features that are not correlatable across large distances. Therefore, although these beds contain low concentrations of bitumen and could act as a baffle to exploration, their discret nature indicates that they are not a complete obstruction.

Preface

The material within this thesis represents the combined work of the primary author, Shelby Sanders, as well as Dr. John-Paul Zonneveld, Dr. Thomas Moslow, and Beth Haverslew.

Acknowledgements

I would like to acknowledge Dr. John-Paul Zonneveld as my supervisor through my program for his guidance and aid. Dr. Murray Gingras and the rest of the Ichnology Research Group should be acknowledged for their support and aid in my work, specifically Reed Meyers and Carolyn Furlong for their help around the lab. Dr. Stacy Gibb should be recognized for introducing me to the methods of using fossil whitening to gain high quality photos for this thesis and subsequent publications. Dr. Tom Moslow and Beth Haverslew at Progress Energy Canada Ltd. should be recognized for the data they have provided me with as well as some insight into the bioclastic horizons of interest. Progress Energy Canada Ltd. provided funding through the Montney grant and the British Columbia core storage facility gave us access to the materials for this study. The Isolab at the University of Washington processed the isotope samples used for this body of work.

TABLE OF CONTENTS

TITLE PAGE I

ABSTRACT II

PREFACE IV

ACKNOWLEDGEMENTS V

TABLE OF CONTENTS VI

LIST OF TABLES X

LIST OF FIGURES XI

CHAPTER 1: INTRODUCTION 1

- 1.1 Introduction 1
- 1.2 Context 1
- 1.3 Argument 4
- 1.4 Roadmap 6
- 1.5 References 6
- Figure Captions 10

CHAPTER 2: SEDIMENTOLOGY AND TAPHONOMY OF THE "CLARAIA ZONE" IN BRITISH COLUMBIA, CANADA 11

- 2.1 Introduction 11
- 2.2 Background/Methods 11
  - *2.2.1 Montney & Bioclastic Units 11*
  - *2.2.2 Triassic 14*
  - *2.2.3 Methods 15*
- 2.3 Resul ts 15
  - *2.3.1 Facies 15*
    - 2.3.1a Laminated siltstone (SL1) 18
    - 2.3.1b Laminated bioclastic siltstone (LBS) 18
    - 2.3.1c Rippled to laminated heterolithic very fine sandstone to fine siltstone (SL 22

2.3.1d Calcisphere massive to laminated siltstone subfacies (CA) 26

2.3.1e Calcite cemented concretions subfacies (CO) 27

2.3.1f Massive siltstone (SL3) 30

2.3.1g Bioturbated/mottled siltstone (SL4) 30

2.3.1h Heterolithic convoluted laminated fine to coarse siltstone (SL5 31

2.3.1i *Planolites* bioturbated siltstone (BF1) 34

2.3.2 Identifiable axa 34

2.4 Discussion 35

2.4.1 Bioclasts 35

2.4.2 Facies Association and Paleoenvironmental Interpretation 38

2.4.2a Proximal bottom current modified deposit 40

2.4.2b Distal bottom current modified deposit 40

2.4.2c Bottom Current Deposition 44

2.4.3 Comparison with Similar Deposits 47

2.5 Conclusions 47

2.6 References 50

Figure Captions 56

List of Tables 58

CHAPTER 3: THE ALTARES PACKSTONE MEMBER OF THE EARLY TRIASSIC MONTNEY FORMATION, NE-BRITISH COLUMBIA 60

3.1 Introduction 60

3.2 Background 61

3.2.1 Triassic 61

3.2.2 Montney stratigraphy and fossil occurrence 62

3.3 Methods 65

3.4 Results 65

3.4.1 Bioclast Characterization 65

3.4.1a Ammonoids 71

3.4.1b Bivalves 73

3.4.1c Brachiopods 73

3.4.1d Vertebrates 73

3.4.2 Facies 75

3.4.2a Massive bioclastic packstone (MBP) 75

3.4.3 Facies Associations 75

3.4.3a FA3: Biostromes 80

3.5 Discussion 83

3.5.1 Biological and Sedimentological Analyses 83

3.5.2 Analogues 87

3.5.2a Middle Triassic Biostromes 87

3.5.2b Muschelkalk *Placunopsis* Biostromes 89

3.5.2c Sinbad Limestone and Virgin Limestone 90

3.6 Conclusion 90

3.7 References 91

Figure Captions 98

List of Tables 100

CHAPTER 4: SUMMARY AND CONCLUSIONS 101

4.1 ***“Claraia* Zone”** 101

4.2 Altares Packstone Member 101

4.3 Conclusions 106

4.4 References 109

Figure Captions 110

List of Tables 111

REFERENCES 112

APPENDIX A: OXYGENATION IN THE “CLARAIA ZONE” OF THE LOWER TRIASSIC MONTNEY FORMATION OF BRITISH COLUMBIA, CANADA 124

A.1 Introduction 124

A.2 Background 124

A.2.1 Triassic *124*

A.2.2 **The Montney Formation and the “*Claraia* Zone”** *125*

A.2.3 Previous Sulfur Isotope Studies *126*

A.3 Methods 126

A.4 Resul ts 129

A.5 Discussion 129

A.6 Conclusions 134

A.7 References 134

Figure Captions 137

List of Tables 138

APPENDIX B: FOSSIL IDENTIFICATION BY DEPTH WITHIN CORES 139

APPENDIX C: THIN SECTION DESCRIPTIONS BY WELL AND DEPTH (M) 146

APPENDIX D: WELL DATA 168

APPENDIX E: CORE LITHOLOGY LOGS 178

List of Tables

2.1: TABLE OF CORES ANALYZED AND PRESENCE OR ABSENCE OF THE PACKSTONE BED HORIZON OR THE "*CLARAIA* ZONE". 17

2.2: SUMMARY OF FACIES WITH DESCRIPTIONS OF MINEROLOGY, GRAIN SIZE, SEDIMENTARY STRUCTURES, TRACE FOSSILS, AND BODY FOSSILS FOUND IN EACH FACIES. 19

2.3: SUMMARY OF CONTACTS BETWEEN EACH FACIES IN AND AROUND THE *"CLARAIA* ZONE". G = GRADATIONAL, S = SHARP, C = SCOUR, OW = OCCUR WITHIN. 39

3.1: TABLE OF CORES ANALYZED AND PRESENCE OR ABSENCE OF THE PACKSTONE BED HORIZON OR THE "*CLARAIA* ZONE". 66

3.2: TABULAR SUMMARY OF FACIES, WHICH DETAILS EACH FACIES' MINEROLOGY, GRAIN SIZE, SEDIMENTARY STRUCTURES, TRACE FOSSILS, AND BODY FOSSILS THAT HAVE BEEN IDENTIFIED. 76

3.3: TABLE OF FACIES CONTACTS. G = GRADATIONAL, S = SHARP, C = SCOUR, OW = OCCURS WITHIN 78

3.4: SUMMARY AND DESCRIPTION OF THE THREE FACIES ASSOCIATIONS. 82

4.1: SUMMARY OF FACIES WITH DESCRIPTIONS OF MINEROLOGY, GRAIN SIZE, SEDIMENTARY STRUCTURES, TRACE FOSSILS, AND BODY FOSSILS FOUND IN EACH FACIES. 102

A.1: THE TABLE OF THE RAW SULFUR ISOTOPE DATA INCLUDING SULFUR CONTENT OF EACH SAMPLE AND THE ACCURACY AND PRECISION OF EACH DATA POINT. 130

List of Figures

1.1: MAP OF CORE DATASETS IN RELATION TO THE MONTNEY FORMATION AS A WHOLE DURING THE DIENERIAN-SMITHIAN BOUNDARY. THE TWO DELTAS ARE KNOWN TO BE PRESENT ON OPPOSITE SIDES OF THE BOUNDARY. THE RED BLOCK IN THE INSET MAP SHOWS THE LOCATION OF THE ABOVE MAP IN RELATION TO MODERN GEOGRAPHICAL BOUNDARIES OF CANADA. (THE MONTNEY MAP WAS COMPILED AND MODIFIED FROM BARCLAY ET AL, 1990; PANEK, 2000; ZONNEVELD ET AL, 2010A; ZONNEVELD ET AL, 2010B; ZONNEVELD AND MOSLOW, 2014; AND ZONNEVELD, PERS. COMM.; THE MAP OF THE PROVINCES AND COASTLINE OF CANADA WAS MODIFIED FROM GOVERNMENT OF CANADA, 2001)..2

1.2: THE STRATIGRAPHIC FRAMEWORK OF THE LOWER AND MIDDLE TRIASSIC IN THE WESTERN CANADA SEDIMENTARY BASIN, AND THE LOCATION AND CORRELATION OF THE MONTNEY FORMATION WITH ITS OUTCROP EQUIVALENTS. WITH FORMATION NAMES REPRESENTED FOR BOTH ABOVE AND BELOW THE PINE RIVER (MODIFIED FROM ZONNEVELD, 2011; COMPILED FROM TOZER, 1994; ORCHARD AND TOZER, 1997; ORCHARD AND ZONNEVELD, 2009). 4

1.3: NORTH AMERICAN PALEOMAP SHOWING THE LOCATION OF NORTH AMERICA IN RELATION TO THE PALEO-EQUATOR AND THE LOCATION OF THE PEACE RIVER EMBAYMENT WITHIN THE CONTINENT (MODIFIED FROM BLAKEY ET AL., 1993). 5

2.1: MAP OF CORE DATASETS IN RELATION TO THE MONTNEY FORMATION AS A WHOLE DURING THE GREISBACHIAN. THE RED DOTS EACH REPRESENT A SEPARATE CORE AND THEY ARE ALL LOCATED WELL WITHIN THE OFFSHORE PORTION OF THE FORMATION. THE PEDIGREE-RING DELTA IS KNOWN TO BE GREISBACHIAN IN AGE, BUT THE DIXONVILLE HAS ONLY BEEN CONFIRMED TO BE SMITHIAN, ALTHOUGH THERE ARE SAND BODIES OF GREISBACHIAN AGE THAT ARE LOCATED WESTWARD IN THE PEACE RIVER ARCH FROM THE DELTA LOCATION. THE MEOSIN HIGH IN THE SOUTHWEST IS BASED ON SUBAERIAL EXPOSURE IN THE OUTCROP BELT. THE RED BLOCK IN THE INSET MAP SHOWS THE LOCATION OF THE ABOVE MAP IN RELATION TO MODERN GEOGRAPHICAL BOUNDARIES OF CANADA. (THE MONTNEY MAP WAS COMPILED AND MODIFIED FROM BARCLAY ET AL, 1990; PANEK, 2000; ZONNEVELD ET AL, 2010A; ZONNEVELD ET AL, 2010B; ZONNEVELD AND MOSLOW, 2014; AND ZONNEVELD, PERS. COMM.). 12

2.2: THE STRATIGRAPHIC FRAMEWORK OF THE LOWER AND MIDDLE TRIASSIC IN THE

WESTERN CANADA SEDIMENTARY BASIN, AND THE LOCATION AND CORRELATION OF THE MONTNEY FORMATION WITH ITS OUTCROP EQUIVALENTS WITH THE HORIZON OF INTEREST TO THIS PAPER HIGHLIGHTED IN GREY ON THE RIGHT (MODIFIED FROM ZONNEVELD, 2011; COMPILED FROM TOZER, 1994; ORCHARD AND TOZER, 1997; ORCHARD AND ZONNEVELD, 2009). 13

2.3: THE LOCATION AND STUDY AREA OF ALL WELLS LOGGED FOR THIS STUDY. THESE WELLS WERE SELECTED AS THEY APPEARED TO HAVE CORE WITHIN THE "*CLARAIA* ZONE" BASED ON WIRELINE GAMMA LOG SIGNATURES 16

2.4: SL1: LAMINATED SILTSTONE FACIES. A) MACROSCOPIC EXAMPLE FROM 14-29-080-20W6. B) THIN SECTION EXAMPLE FROM 14-29-080-20W6. C) THIN SECTION EXAMPLE FROM 15-02-080-16W6. MACROSCOPICALLY AND MICROSCOPICALLY LAMINAE CAN BE FOLLOWED ACROSS THE FACE OF THE CORE OR SLIDE IN THE FINE GRAINED, GRAY, BITUMINOUS SILTSTONE. D) THIN SECTION PHOTOGRAPH SHOWING THE CONTINUOUS LAMINATED FROM SAMPLE IRG-SA-1412-066...21

2.5: LBS: LAMINATED BIOCLASTIC SILTSTONE FACIES. A) MACROSCOPIC EXAMPLE FROM 14-29-080-20W6. B) THIN SECTION EXAMPLE FROM A-10-J/094-B-9. C) THIN SECTION EXAMPLE FROM C-007-J/094-B-8. BOTH THIN SECTIONS B AND C ARE SCANNED IN PLAIN LIGHT AND ARE HALF STAINED FOR CALCIUM CARBONATE. A SHOWS THE GRADUAL INCREASE IN BIOCLASTS THAT OCCURS AT THE BASE OF THE FACIES. THE LAMINATED HAS OF BIOCLASTIC MATERIAL IS VISIBLE IN B AND C. D)THIN SECTION PHOTOGRAPH SHOWING CALCISPHERES ALONGSIDE THE BIOCLASTIC MATERIAL AS WELL AS AN ANKERITE ALTERED VALVE FROM 3-30-082-20W6. 22

2.6: THIN SECTIONS OF LBS: A) SEPARATE LAYERS OF CONCENTRATED *CLARAIA* MATERIAL (BC13). B) A LARGE CONCENTRATION OF *CLARAIA* MATERIAL AT THE BASE OF THE SECTION WITH A SUDDEN CUTOFF ABOUT A THIRD OF THE WAY FROM THE TOP OF THE SECTION (BC5). C) INCREASING UPWARD CONCENTRATION OF *CLARAIA* MATERIAL (14-29-080-20W6). D) HIGH CONCENTRATION OF *CLARAIA* MATERIAL INCREASING UPWARD IN THE SECTION (14-29-080-20W6). 23

2.7: THIN SECTION PHOTOGRAPHS IN PLANE POLARIZED LIGHT WITHIN LBS. A, B) LENSES OF BIOCLASTIC MATERIAL FROM 14-29-080-20W6. C, D, E) EXAMPLES OF THE SHELL STACKING PATTERN AND THE FRAGMENTED NATURE OF THE SHELLS WITHIN LBS FROM A-18-D/094-A-13. F) CALCISPHERES ALONGSIDE BIOCLASTS WITH PREFERENTIAL DOLOMITIZATION OF CALCISPHERES FROM A-18-D/094-A-13. 24

2.8: SL2: HETEROLITHIC FINE GRAINED SANDSTONE INTERBEDDED WITH FINE SILTSTONE A) EXAMPLE FROM 3-30-082-20W6. THIS EXAMPLE SHOWS RAPID INTERBEDDING BETWEEN THE TWO LITHOLOGIES AS WELL AS MULTIPLE SCOUR SURFACES. B) EXAMPLE FROM 08-30-082-20W6. THIS SAMPLE SHOWS MULTIPLE FINE GRAINED DRAPES OVER SANDSTONE RIPPLES THAT WOULD NOT BE IDENTIFIABLE SAVE FOR THE FINE GRAINED MATERIAL. THIS HORIZON IS MUCH MORE DISCRETE COMPARED TO A. (SC) SCOUR SURFACE, (D) FLASER/FINE GRAINED OFFSHOOTS, (L) LENTICULAR BEDDING. C) THIN SECTION VIEW OF THE HETEROLITHIC STRUCTURES PRESERVED IN THE TOP PART OF THE SECTION, BUT SOMEWHAT OBSCURED IN THE BASE OF THE SECTION (IRG-SA-1412-66). D) POSSIBLE HCS FEATURE FROM B-65-J/094-B-16. E) THIN SECTION PHOTOGRAPH OF THE SEPARATED COARSE AND FINE GRAINED SECTIONS WITH RIPPLES (IRG-SA-1412-066). F) THIN SECTION PHOTOGRAPH OF A COARSENING UPWARD SEQUENCE (IRG-SA-1412-066). 25

2.9: PRESERVED ORIGINAL SHELL MATERIAL (F) ON BEDDING PLANE FROM B-065-J/094-B-16. 27

2.10: CA: CALCISPHERE LAMINATED TO MASSIVE SILTSTONE. A) MACROSCOPIC EXAMPLE OF MASSIVE TO LAMINATED SILTSTONE WITH CALCISPHERES GRADING IN AND OUT FROM A-008-D/094-A-13. B) ANOTHER LAMINATED SILTSTONE WITH CALCISPHERES FROM A-005-C/094-G-10. C) THIN SECTION WITH CALCISPHERES WITHIN LAMINAE FROM C-074-G/094-B-09. D) THIN SECTION PHOTO OF A PARTIALLY DOLOMITIZED CALCISPHERES FROM A-18-D/094-A-13. E) THIN SECTION PHOTO OF CALCISPHERE HORIZON (BC20). F) CALCISPHERES ALONGSIDE BIOCLASTS WITH PREFERENTIAL DOLOMITIZATION OF CALCISPHERES FROM A-18-D/094-A-13...28

2.11: CO: CALCITE CONCRETIONS COMMON THROUGHOUT THE INTERVALS STUDIED. A, E) CONCRETIONS FROM 14-29-080-20W6 THAT DO NOT SHOW AN INTERNAL FABRIC. B) CONCRETION FROM C-074-G/094-B-9 THAT SHOWS PYRITE (RED ARROW) AROUND THE EDGE OF THE CONCRETION. C) CONCRETION FROM C-007-J/094-B-8 THAT SHOWS THE VARIATION IN CALCITE TO DOLOMITE THROUGH THE CONCRETION. BOTH THIN SECTIONS B AND C WERE HALF STAINED WITH A DOUBLE CALCITE STAIN. D) CONCRETION FROM 14-29-080-20W6 IN WHICH ONE CAN FOLLOW THE BEDS FROM OUTSIDE OF THE CONCRETION THROUGH IT. F) THIN SECTION PHOTO OF THE EDGE OF A CONCRETION (BC19). G) EUHEDRAL PYRITE AROUND THE RIM OF A CALCITE CEMENTED CONCRETION (BC19). 29

2.12: SL3: MASSIVE SILTSTONE FACIES. A) A-005-C/094-G-10 B, C) 14-29-080-20W6 MASSIVE

FINE GRAINED BITUMINOUS SILTSTONE THAT SHOWS NO EVIDENCE OF BIOTURBATION. THESE THIN SECTIONS EXHIBIT A BROWN COLORATION NOT SEEN IN OTHER SECTIONS. D) THIN SECTION PHOTO OF MASSIVE FINE GRAINED SILTSTONE (IRG-SA-1412-036).31

2.13: SL4: BIOTURBATED/MOTTLED SILTSTONE. A) A08-07-085-18W6 SHOWS BIOTURBATION INDUCED MOTTLING OF THE SEDIMENT. B) EXAMPLE FROM A-005-C/094-G-10 WHICH SHOWS UNIDENTIFIABLE BURROWS VISIBLE DUE TO LITHOLOGICAL VARIATION IN THE SILTSTONE. C) THIN SECTION PHOTOGRAPH OF THE COARSE GRAINED LENSES AND DISCONTINUOUS COARSE AND FINE GRAINED LAYERS (IRG-SA-1412-025). 32

2.14: SL5: SOFT SEDIMENT DEFORMED HETEROLITHIC COARSE GRAINED SILTSTONE AND FINE GRAINED SILTSTONE. A) AN ISOLATED FEATURE IN A08-07-085-18W6. B) THE STRATA IS MORE COMPLETELY CONVOLUTED FROM A-07-19-085-15W6. C) THIN SECTION SHOWING NEAR COMPLETE CONVOLUTION OF THE HETEROLITHIC BEDS (BC16). D) THE MIDDLE OF THIS THIN SECTION SHOWS CONVOLUTED TEXTURE WHILE THE OUTER BEDS STILL RETAIN THE BEDFORMS (IRG-SA-1412-066). 33

2.15: BF1: *PLANOLITES* BIOTURBATED SILTSTONE. A) A-005-C/094-G-10 B) A-005-C/094-G-10 LAYERS OF *PLANOLITES* BIOTURBATED SILTSTONE WITH VERY LITTLE LITHOLOGICAL VARIATION. C) B-065-J/094-B-16 *PLANOLITES* IN DISCRETE SAND LAYERS WITHIN FINE GRAINED SILTSTONE. (P) *PLANOLITES*. D) *PLANOLITES* BURROWS PRESERVED IN THE COARSE GRAINED HORIZON THAT HAVE BEEN SLIGHTLY FLATTENED (BC26). 35

2.16: BEDDING PLANE IMPRESSIONS OF PECTINOIDS. A, B) B-50-H/094-B-16 SHOWING LARGE VALVES THAT ARE SOMEWHAT FRAGMENTED AND DISARTICULATED. C) B-50-H/094-B-16 SHOWING SMALL VERY FRAGMENTED VALVES. 36

2.17: AMMONOIDS FROM VARIOUS CORES NEAR THE "*CLARAIA* ZONE": A) NEW AMMONOID FROM A-10-J/094-B-9 B) *WORDEIOCERAS WORDIEI* FROM A-10-J/094-B-9 C, E) *OPHIOCERAS* SP. FROM 08-30-082-20W6 D) *OPHIOCERAS*? FROM A-005-C/094-G-10 SURROUNDED BY PECTINOIDS. 37

2.18: THE BOTTOM CURRENT DEPOSITIONAL ENVIRONMENT WITH THE CURRENT SHOWN PRODUCING THE TWO DIFFERENT FACIES ASSOCIATIONS. A) REPRESENTS THE FAN DERIVED BOTTOM CURRENT MODIFIED DEPOSITS THAT ARE CLOSER TO THE SOURCE INPUT OF COARSE GRAINED SEDIMENT (ARROWS). WHEN THE CURRENT IS ACTIVE (BLUE) BIVALVE SHELLS AND RIPPLE STRUCTURES ARE CREATED, WITH SUSPENSION SEDIMENTATION BETWEEN CURRENT ACTIVITY. B) REPRESENTS THE DISTAL BOTTOM

CURRENT MODIFIED DEPOSITS WHERE WINNOWING OF FINE GRAINED SEDIMENT WITH THE DEPOSITION OF BIVALVE MATERIAL IN CONCENTRATED HORIZONS BY THE CURRENT ACTIVITY (BLUE). 41

2.19: CORE LITHOGRAPHIC DESCRIPTION OF WELL API: 03-30-082-20W6. THERE ARE TWO DISTINCT SECTIONS TO THIS CORE: THE LOWER SHOWING WHAT IS TYPICAL OF FACIES SL2 AND THE FIRST FACIES ASSOCIATION, AND THE UPPER SHOWING WHAT IS TYPICAL OF LBS AND THE SECOND FACIES ASSOCIATION. 42

2.20: STRIKE SECTION THROUGH THE "*CLARAIA* ZONE" ACROSS THE STUDY AREA. HORIZON B, A SUPPOSED FLOODING SURFACE IS USED AS THE DATUM. EXCEPT FOR ONE LONG, 02-07-085-23W6, THE "*CLARAIA* ZONE" APPEARS TO HAVE A CONSISTENT DISTANCE FROM THE CONTACT WITH THE BELLOY FORMATION...45

2.21: ISOPACH CONTOUR OF THE MEASURED DEPTH OF THE TOP OF THE "*CLARAIA* ZONE" ACROSS THE STUDY AREA. THERE WERE 155 WELLS USED TO CREATE THIS CONTOUR. 46

2.22: MAP OF THE MONTNEY FORMATION DURING THE GREISBACHIAN WITH POSSIBLE DIRECTION OF WIND DRIVEN BOTTOM CURRENTS THE CURRENTS COULD BE CONSTRAINED BY THE RIDGE AT THE SOUTHWEST, BUT THERE ARE NO DATA IN THAT AREA. SHELLS AND SAND COULD BE BROUGHT IN FROM THE EAST, OR THE SHELLS COULD BE FROM A MORE LOCAL SOURCE. (THE MONTNEY MAP WAS COMPILED AND MODIFIED FROM BARCLAY ET AL, 1990; PANEK, 2000; ZONNEVELD ET AL, 2010A; ZONNEVELD ET AL, 2010B; ZONNEVELD AND MOSLOW, 2014; AND ZONNEVELD, PERS. COMM.). 48

2.23: THE DEPOSITIONAL MODELS FOR THE FORMATION OF BOTH FACIES ASSOCIATIONS. A-D REPRESENTS THE FORMATION OF THE FAN DERIVED BOTTOM CURRENT MODIFIED DEPOSITS. A, E-G REPRESENT THE FORMATION OF THE DISTAL BOTTOM CURRENT MODIFIED DEPOSITS. A) REPRESENTS THE BACKGROUND CONDITIONS OF THE FORMATION WITH MOSTLY SUSPENSION DEPOSITION. B) A BOTTOM WATER CURRENT WINNOWS THE SEDIMENT ALREADY DEPOSITED AND LEAVES RIPPLE STRUCTURES. C) BACKGROUND CONDITIONS RETURN AND SUSPENSION DERIVED SEDIMENT IS DEPOSITED OVER THE RIPPLES. PROCESSES B AND C ARE REPEATED UNTIL A DEPOSIT SUCH AS D IS FORMED. E) REPRESENTS A DISTAL CURRENT PROCESS WHERE BIVALVE SHELLS ARE TRANSPORTED INTO THE SYSTEM AND CONCENTRATED IN THE WINNOWING OF THE FINE GRAINED SEDIMENT. F) BACKGROUND CONDITIONS RETURN AND

SUSPENSION DERIVED SEDIMENT IS DEPOSITED OVER THE BIVALVES. PROCESSES E AND F ARE REPEATED UNTIL A DEPOSIT SUCH AS G IS FORMED. 49

3.1: MAP OF CORE DATASETS IN RELATION TO THE MONTNEY FORMATION AS A WHOLE DURING THE DIENERIAN-SMITHIAN BOUNDARY. THE TWO DELTAS ARE KNOWN TO BE PRESENT ON OPPOSITE SIDES OF THE BOUNDARY. THE RED BLOCK IN THE INSET MAP SHOWS THE LOCATION OF THE ABOVE MAP IN RELATION TO MODERN GEOGRAPHICAL BOUNDARIES OF CANADA. (THE MONTNEY MAP WAS COMPILED AND MODIFIED FROM BARCLAY ET AL., 1990; PANEK, 2000; ZONNEVELD ET AL., 2010A; ZONNEVELD ET AL., 2010B; ZONNEVELD AND MOSLOW, 2014; AND ZONNEVELD, PERS. COMM.; THE MAP OF THE PROVINCES AND COASTLINE OF CANADA WAS MODIFIED FROM GOVERNMENT OF CANADA, 2001)..63

3.2: THE STRATIGRAPHIC FRAMEWORK OF THE LOWER AND MIDDLE TRIASSIC IN THE WESTERN CANADA SEDIMENTARY BASIN, AND THE LOCATION AND CORRELATION OF THE MONTNEY FORMATION WITH ITS OUTCROP EQUIVALENTS. WITH FORMATION NAMES REPRESENTED FOR BOTH ABOVE AND BELOW THE PINE RIVER (MODIFIED FROM ZONNEVELD, 2011; COMPILED FROM TOZER, 1994; ORCHARD AND TOZER, 1997; ORCHARD AND ZONNEVELD, 2009). 64

3.3: STRIKE SECTION THROUGH THE STUDY AREA, INSET MAP. HORIZON B IS USED AS THE DATUM, AS IT IS A FLOODING SURFACE. 67

3.4: ISOPACH MAP OF THE TOP OF HORIZON B THROUGH THE STUDY AREA. WELLS WERE CENTRALIZED ALONG THE NW-SE TREND. 68

3.5: DIAGRAMS OF THE THICK AND THIN PACKSTONE BED STRUCTURES. A) THE LARGER, MORE CEMENTED PACKSTONE BEDS. B) THE SMALLER PACKSTONE BED STRUCTURE.
69

3.6: FACIES MBP: THIN SECTION VIEWS OF THE BIOCLASTIC PACKSTONE. ALL OF THE SECTIONS ARE SCANNED IN PLANE LIGHT, HAVE DOUBLE CALCITE STAINING, AND THE LEFT SIDE OF E HAS STAINING FOR ARAGONITE. A) REPETITION OF THE FACIES WITHIN THE THIN SECTION SHOWING THE HIATUS OF CALCITE CEMENTATION OUTSIDE OF THE PACKSTONE (WELL API = A-64-A/094-B-08). B) ANOTHER REPRESENTATION OF THE PACKSTONE IN A THINNER HORIZON THAT PINCHES OUT TO THE RIGHT OF THE THIN SECTION. C) THIS SAMPLE SHOWS A BRACHIOPOD WITH PARTICULARLY INFLATED VALVES IN THE CENTER OF THE THIN SECTION. THE INTERNAL CAVITY ONLY IS CRYSTALIZED

AROUND THE RIM (SAMPLE IRG-SA-1412-061). D) GRADATION OUT OF PACKSTONE BACK INTO SILTSTONE FACIES (SAMPLE BC38). E) THE PACKSTONE IS MOSTLY MADE OF AMMONOIDS THAT HAS CAUSED THE BEDDING TO BE DISTORTED AROUND THE PACKSTONE (WELL API = A-64-A/094-B-8). THIS IS ONE OF THE FEW EXAMPLES WHICH HAS AN ABUNDANCE OF BIOCLASTS OTHER THAN BIVALVES AND BRACHIOPODS. F) DEFORMATION OF THE BEDS BELOW THE PACKSTONE AS WELL AS SHELLS THAT ARE NOT ORIENTED PERPENDICULAR TO BEDDING (SAMPLE BC39). 70

3.7: VARIOUS PICTURES OF THE BIOCLASTS WITHIN THE PACKSTONE BEDS. A) DISARTICULATED VALVES ALONGSIDE WHOLE AMMONOIDS. B) EXPOSED BEDDING PLANE MADE OF DISARTICULATED BIVALVES ON THE TOP OF A BIOCLASTIC PACKSTONE BED (WELL API = 8-30-082-20W6). C) SHELL STRUCTURE OF *CLARAIA* VALVES FROM THE “*CLARAIA* ZONE”. D) VALVES WITH SPARY CALCITE RIMS WITHIN A PACKSTONE BED (PHOTOGRAPHED IN CROSS-POLARIZED LIGHT). E) DISSOLVED AND DOLOMITIZED DISARTICULATED VALVES FROM AROUND A PACKSTONE BED. F) PACKSTONE BED THAT HAS MULTIPLE EROSION SURFACES ONTOP OF ONE ANOTHER WITHIN THE BED...72

3.8: FOSSILS FOUND IN AND CLOSE TO HORIZON B IN CORES. A) PYRITIZED AMMONOID THAT COULD POSSIBLY BE *OPHIOCERAS* SP. B) IMPRESSION OF *HYPOPHICERAS* SP. OR *TOMPOPHICERAS* SP. C) TEREBRATULIDE IMPRESSIONS. D) *CLARAIA CLARAE* IMPRESSIONS. E) VERTEBRATE RIBS AND BACKBONE. F) *CLARAIA STACHEI*. 74

3.9: FACIES MBP: BIOCLASTIC PACKSTONE FACIES A) PACKSTONE BEDS FROM 16-17-083-25W6. A SHOWS REPETITION OF THE FACIES WITH THE COMMON WAVY APPEARANCE OF THE FACIES. B) PACKSTONE FROM 14-29-080-20W6 SHOWS LARGE THICK BIVALVE SHELLS WITHIN IT ALONG WITH VERTEBRATE MATERIAL. C) PACKSTONE FROM 13-11-081-20W6 SHOWS ANOTHER VARIATION OF THE FACIES WITH THE SCOURED BASE AND THE GRADING UP. D) PACKSTONE BEDS FROM 16-17-083-25W6. SIMILAR TO A SHOWS THE REPETITION ALONG WITH SOFT SEDIMENT DEFORMATION..79

3.10: CORRELATION OF PACKSTONE BEDS BETWEEN FOUR WELLS. THE BEDS ARE NOT CORRELATABLE ACROSS SHORT DISTANCES IN WHICH EVEN EROSION SURFACES ARE CORRELATABLE. 81

3.11: DIAGRAM OF THE LOCATION OF FA3 WITHIN THE SAME ENVIRONMENT AS FA1 AND FA2. 83

3.12: BEDFORMS FOUND IN AND AROUND THE ALTARES PACKSTONE MEMBER. A) STARVED

MUD DRAPED RIPPLES FROM C-74-G/094-B-8. B) PACKSTONE PINCHING OUT ON THE BACK OF A CORE PIECE FROM 13-11-081-20W6. 86

3.13: SUCCESSION THROUGH PART OF THE ALTARES PACKSTONE MEMBER IN 16-17-083-25W6 SHOWING THE INCREASE AND DECREASE IN THICKNESS OF PACKSTONE BEDS ON A SMALL SCALE AND SEDIMENTARY STRUCTURES THAT ARE FOUND ALONGSIDE THE PACKSTONE BEDS. 88

3.14: FORMATION OF BIOSTROMES IN THE MIDDLE MONTNEY FORMATION BASED ON ZONNEVELD (2001). A) DEPOSITION OF SILTSTONE IN BACKGROUND CONDITIONS. B) STORM OR CURRENT BRINGS IN DISARTICULATED VALVES AND LIVE OPPORTUNIST LARVAE AND ADULTS WHO RECOLONIZE THE PATCH. C) SHELLS SERVE AS A HARD SUBSTRATE FOR OTHER COLONIZERS WHICH IN TURN PROVIDE PREY FOR NEKTOBENTHIC ORGANISMS AS WELL AS NEKTONIC FAUNA. D) EITHER LOW OXYGEN KILLS OFF FAUNA OR SUDDEN SEDIMENTATION BURIES THE ORGANISMS. THIS IS A RETURN TO BACKGROUND CONDITIONS, BUT BENEATH THE SEDIMENT-WATER INTERFACE THE PACKSTONE IS CEMENTED. E) A STORM OR CURRENT UNCOVERS AND ERODES INTO THE PACKSTONE ALLOWING IT TO BECOME A HARDGROUND AGAIN. 89

4.1: THE BOTTOM CURRENT DEPOSITIONAL ENVIRONMENT WITH THE CURRENT SHOWN PRODUCING THE TWO DIFFERENT FACIES ASSOCIATIONS. A) REPRESENTS THE FAN DERIVED BOTTOM CURRENT MODIFIED DEPOSITS THAT ARE CLOSER TO THE SOURCE INPUT OF COARSE GRAINED SEDIMENT (ARROWS). WHEN THE CURRENT IS ACTIVE (BLUE) BIVALVE SHELLS AND RIPPLE STRUCTURES ARE CREATED, WITH SUSPENSION SEDIMENTATION BETWEEN CURRENT ACTIVITY. B) REPRESENTS THE DISTAL BOTTOM CURRENT MODIFIED DEPOSITS WHERE WINNOWING OF FINE GRAINED SEDIMENT WITH THE DEPOSITION OF BIVALVE MATERIAL IN CONCENTRATED HORIZONS BY THE CURRENT ACTIVITY (BLUE). 104

4.2: CORE LITHOGRAPHIC DESCRIPTION OF WELL API: 03-30-082-20W6. THERE ARE TWO DISTINCT SECTIONS TO THIS CORE: THE LOWER SHOWING WHAT IS TYPICAL OF FACIES SL2 AND THE FIRST FACIES ASSOCIATION, AND THE UPPER SHOWING WHAT IS TYPICAL OF LBS AND THE SECOND FACIES ASSOCIATION. 105

4.3: FORMATION OF BIOSTROMES IN THE MIDDLE MONTNEY FORMATION BASED ON ZONNEVELD (2001). A) DEPOSITION OF SILTSTONE IN BACKGROUND CONDITIONS. B) STORM OR CURRENT BRINGS IN DISARTICULATED VALVES AND LIVE OPPORTUNIST LARVAE AND ADULTS WHO RECOLONIZE THE PATCH. C) SHELLS SERVE AS A

HARD SUBSTRATE FOR OTHER COLONIZERS WHICH IN TURN PROVIDE PREY FOR NEKTOBENTHIC ORGANISMS AS WELL AS NEKTONIC FAUNA. D) EITHER LOW OXYGEN KILLS OFF FAUNA OR SUDDEN SEDIMENTATION BURIES THE ORGANISMS. THIS IS A RETURN TO BACKGROUND CONDITIONS, BUT BENEATH THE SEDIMENT-WATER INTERFACE THE PACKSTONE IS CEMENTED. E) A STORM OR CURRENT UNCOVERS AND ERODES INTO THE PACKSTONE ALLOWING IT TO BECOME A HARDGROUND AGAIN. 106

4.4: DIAGRAMS OF THE THICK AND THIN PACKSTONE BED STRUCTURES. A) THE LARGER, MORE CEMENTED PACKSTONE BEDS. B) THE SMALLER PACKSTONE BED STRUCTURE. 107

4.5: MAP OF THE MONTNEY FORMATION DURING THE GREISBACHIAN WITH POSSIBLE DIRECTION OF WIND DRIVEN BOTTOM CURRENTS. THE CURRENTS COULD BE CONSTRAINED BY THE RIDGE AT THE SOUTHWEST, BUT THERE IS NO DATA IN THAT AREA. SHELLS AND SAND COULD BE BROUGHT IN FROM THE EAST, OR THE SHELLS COULD BE FROM A MORE LOCAL SOURCE. (THE MONTNEY MAP WAS COMPILED AND MODIFIED FROM BARCLAY ET AL, 1990; PANEK, 2000; ZONNEVELD ET AL, 2010A; ZONNEVELD ET AL, 2010B; ZONNEVELD AND MOSLOW, 2014; AND ZONNEVELD, PERS. COMM.). 108

A.1: MAP OF CORE DATASETS IN RELATION TO THE MONTNEY FORMATION AS A WHOLE DURING THE GREISBACHIAN. THE RED DOTS EACH REPRESENT A SEPARATE CORE AND THEY ARE ALL LOCATED WELL WITHIN THE OFFSHORE PORTION OF THE FORMATION. THE PEDIGREE-RING DELTA IS KNOWN TO BE GREISBACHIAN IN AGE, BUT THE DIXONVILLE HAS ONLY BEEN CONFIRMED TO BE SMITHIAN, ALTHOUGH THERE ARE SAND BODIES OF GREISBACHIAN AGE THAT ARE LOCATED WESTWARD IN THE PEACE RIVER ARCH FROM THE DELTA LOCATION. THE MEOSIN HIGH IN THE SOUTHWEST IS BASED ON SUBAERIAL EXPOSURE IN THE OUTCROP BELT. THE RED BLOCK IN THE INSET MAP SHOWS THE LOCATION OF THE ABOVE MAP IN RELATION TO MODERN GEOGRAPHICAL BOUNDARIES OF CANADA. (THE MONTNEY MAP WAS COMPILED AND MODIFIED FROM BARCLAY ET AL, 1990; PANEK, 2000; ZONNEVELD ET AL, 2010A; ZONNEVELD ET AL, 2010B; ZONNEVELD AND MOSLOW, 2014; AND ZONNEVELD, PERS. COMM.). 126

A.2: THE STRATIGRAPHIC FRAMEWORK OF THE LOWER AND MIDDLE TRIASSIC IN THE WESTERN CANADA SEDIMENTARY BASIN, AND THE LOCATION AND CORRELATION OF THE MONTNEY FORMATION WITH ITS OUTCROP EQUIVALENTS WITH THE HORIZON OF INTEREST TO THIS PAPER HIGHLIGHTED IN GREY ON THE RIGHT (MODIFIED FROM ZONNEVELD, 2011; COMPILED FROM TOZER, 1994; ORCHARD AND TOZER, 1997; AND

ZONNEVELD, 2009). 127

A.3: CORE LITHOLOGY LOG OF C-065-F/094-B-08 ALONGSIDE THE Δ^{34}S DATA POINTS FOR THE CORE. 132

A.4: CORE LITHOLOGY LOG OF C-006-L/094-B-08 ALONGSIDE THE Δ^{34}S DATA POINTS FOR THE CORE. 133

Chapter 1: Introduction

1.1 Introduction

The bioclastic units of the Lower Triassic Montney Formation in British Columbia and Alberta, Canada, are of particular interest because they represent the main biotic records of metazoan life in the immediate aftermath of the Permian-Triassic mass extinction within the Western Canada Sedimentary Basin. The underlying Permian Belloy Formation represents a shallow marine carbonate ramp succession deposited on the west Pangaean margin (Beauchamp and Desrochers, 1997; Moslow, 2000; Henderson et al., 2002). Mineralogically the Montney Formation and the Belloy Formation are similar, differing primarily in the abundance and nature of skeletal carbonate material. This loss is due to the loss of the Paleozoic Fauna (*sensu* Sepkoski, 1981) at the end-Permian extinction. Delayed biotic recovery and failure of the Paleozoic Fauna to resume their dominance accentuated the gap in carbonate-dominated successions in the Peace River Embayment, and resulted in microbial-dominated carbonate sections in other parts of the world (e.g., Hallam, 1991; Flugel, 1994; Lehrmann, 1999; Payne et al, 2004; Erwin, 2007; Meyer et al., 2011; Zonneveld, 2011; Greene et al., 2011).

The paucity of carbonate deposits in the Montney Formation has been attributed to a variety of reasons, ranging from oceanic acidification to anoxia (Rampino and Caldeira, 2005; oods, 2005; Zonneveld, 2011; Payne et al., 2014). An exception to this, the Coquinal Dolomite middle member (CDMM) of the Montney Formation (Mackenzie Dolomite Lentil / MDL in outcrop) is a notable exception to this (Gibson and Poulton, 1994; Paull et al., 1997; Davies et al., 1997) and occurs solely in Alberta. The CDMM/MDL occurs at the Dienerian-Smithian (=Induan-Olenekian boundary; Paull et al., 1997; Orchard and Zonneveld, 2009) and includes a low-diversity assemblage dominated by bivalves, gastropods and lingulide brachiopods (Markhasin, 1997; Kendall, 1999; Paull et al., 1997).

This thesis identifies two additional bioclastic intervals which contain calcified body fossils: th "*Claraia* Zone" (mid-Dienerian) and the Altares Packstone Member, which occurs in the late Smithian, just below the Smithian-Spathian boundary (Golding et al., 2015). Only the Altares Packstone Member of these two new bioclastic intervals contains a significant amount of carbonate deposition. Delineation and sedimentary analysis of the bioclastic units aid in understanding their deposition in an otherwise siliciclastic unit. Investigating the deposition of the bioclasts, as well as the fossils assemblage contained within the units, starts to unravel some of the questions regarding life in this unique and important time period in the history of the Peace River Embayment.

The goal of this body of work is to determine how the "*Claraia* Zone" and the Altares Packstone Member were deposited, describe the fauna that are present within the units and clarify their role in the expansion of marine biotic diversity in the Western Canada Sedimentary Basin.

1.2 Context

The Montney Formation is a westward thickening package of primarily heterogeneous bituminous siltstone and very fine grained sandstone (Edwards et al., 1994; Davies et al., 1997) (Fig. 1.1). It was identified in the subsurface and named by Armitage (1962), and subsequently has been determined to represent the entirety of the Lower Triassic in the Western Canada Sedimentary Basin (Orchard and Tozer, 1997; Orchard and Zonneveld, 2009). The Montney Formation also outcrops along the frontal

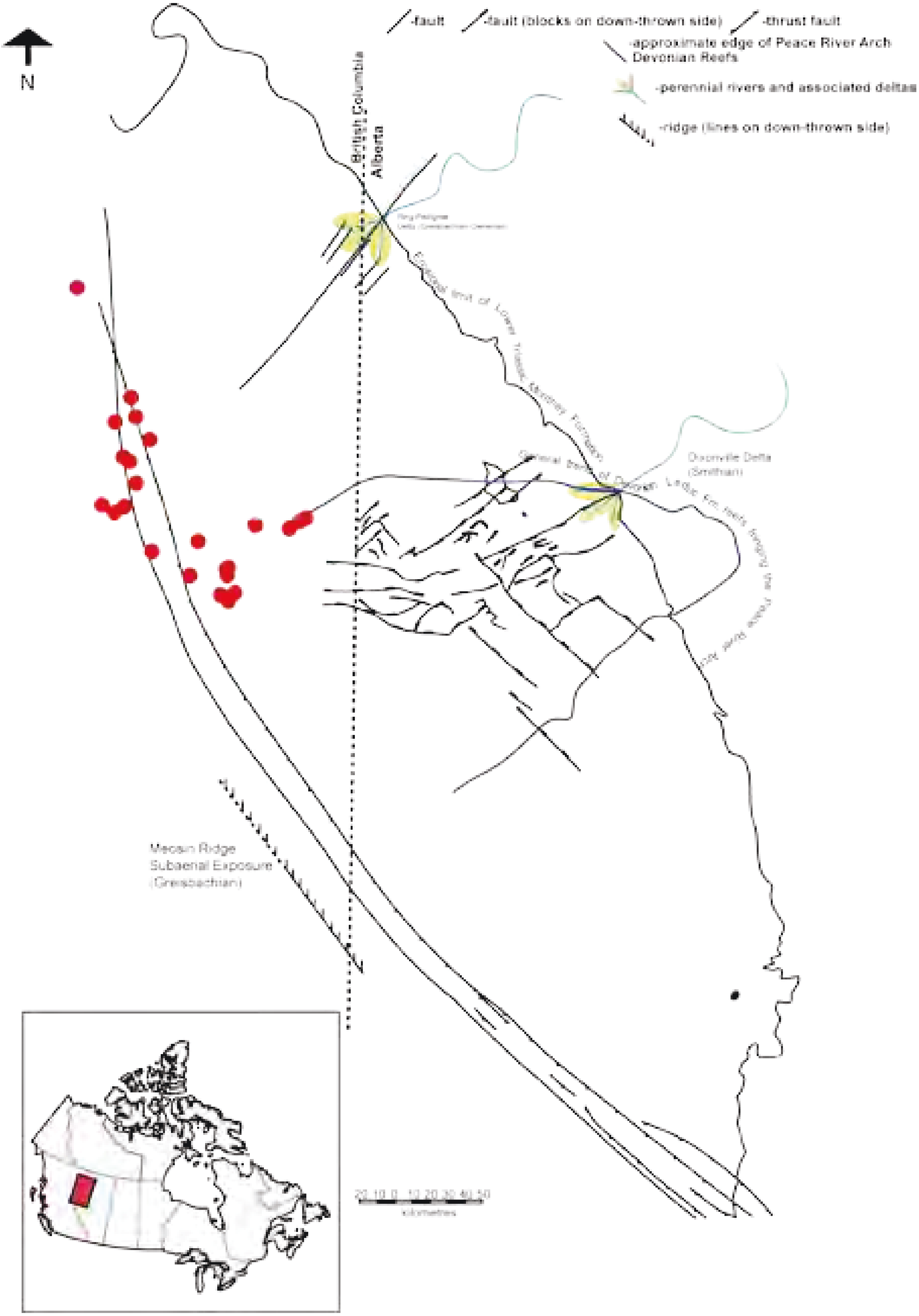
N
-fault
-fault (blocks on down-thrown side)
-thrust fault
-approximate edge of Peace River Arch Devonian Reefs
-perennial rivers and associated deltas
-ridge (lines on down-thrown side)
British Columbia
Alberta
Erosional limit of Lower Triassic Montney Formation
General trend of Devonian Leduc Fm. reefs fringing the Peace River Arch
Dixonville Delta
(Smithian)
Mecain Ridge
Subaerial Exposure
(Greisbachian)
20 10 0 10 20 30 40 50
kilometres

ranges of the Canadian Cordillera, where it is stratigraphically equivalent to the Toad and Grayling Formations south of the Pine River, and the Sulphur Mountain Formation north of the Pine River (Fig 1.2). Deposition occurred within the Peace River Embayment along the northwestern coast of Pangea on a clastic ramp that was located at approximately 30°N Latitude (Habicht, 1979; Tozer, 1982; Wilson et al., 1994) (Fig. 1.3). Immediately preceding the Permian-Triassic boundary the Belloy Formation was deposited in a carbonate ramp setting (Barclay et al., 1990; Beauchamp and Desrochers, 1997; Moslow, 2000; Henderson et al., 2002). The boundary is diachronous throughout most of the basin, and has been found to be conformable in some locations, such as at the Opal Creek outcrop (Schoepfer et al., 2012). Accommodation space within the basin is attributed to the collapse of the Devonian Reef Complex, which was a result of extensional tectonics beneath the Peace River Arch, and allowed for a large package of sediment, in some cases over 350m thick, to be deposited in 5 million years (Barclay et al., 1990; Edwards et al., 1994; Davies, 1997).

The Triassic in Western Canada has been previously described as being deposited along a passive margin (Gibson and Barclay, 1989; Edwards et al., 1994), however there has been some thought recently for an active tectonic regime west of the basin with some areas of subaerial exposure during the deposition of the Montney Formation (Ferri and Zonneveld 2008; Zonneveld et al., 2010a,b; 2015). These western highs may have been secondary sources of sediment for the Montney Formation and may have provided a western margin / restriction to a basin previously thought to have been open to the Panthalassan Ocean. Nonetheless, perennial and ephemeral deltas are currently thought to be the main sources of sediment in the formation (Zonneveld and Moslow, 2014). These deltas were identified both on the presence of unusually diverse trace fossils, as well as swelling clays which are not present anywhere else within the basin (Zonneveld et al., 2010a, b; Zonneveld and Moslow, 2013).

The succession identified as the Montney Formation in Alberta represents only what is considered the Lower Montney Formation in British Columbia (Wilson, 2009). The British Columbia “upper Montney” is referred to as the “basal Doig siltstone” by the Alberta government. These contrasting terminologies required the author to make the decision to conform to the British Columbia terminology for the entirety of this thesis to remain consistent with the location of the deposits. It should be noted that the British Columbia paradigm follows the established lithostratigraphic nomenclature and, from an academic / mapping perspective, is a more consistent choice than the Alberta pick.

As mentioned previously, carbonate units within the Montney Formation are rare, and several of the units within Alberta have been used to mark significant boundaries; e.g., Coquinal Dolomite Middle Member (Paull et al., 1997; Kendal et al., 1998; Kendal, 1999). A bathymetric rise / shallowing of the Aragonite and Carbonate Compensation Depths during the earliest Triassic has been invoked to explain, at least partially, the scarcity of calcium carbonate body fossils (Woods and Bottjer, 2000; Rampino and Caldeira, 2005; Zonneveld, 2011). Whatever the cause, the bioclastic units within the Montney Formation represent a large portion of what is known about shelly fauna after the Permian-Triassic boundary within

Figure 1.1 (Previous page)**:** Map of core datasets in relation to the Montney Formation as a whole during the Dienerian-Smithian boundary. The two deltas are known to be present on opposite sides of the boundary. The red block in the inset map shows the location of the above map in relation to modern geographical boundaries of Canada. (The Montney map was compiled and modified from Barclay et al, 1990; Panek, 2000; Zonneveld et al, 2010a; Zonneveld et al, 2010b; Zonneveld and Moslow, 2014; and Zonneveld, pers. comm.; the Map of the provinces and coastline of Canada was modified from Government of Canada, 2001).

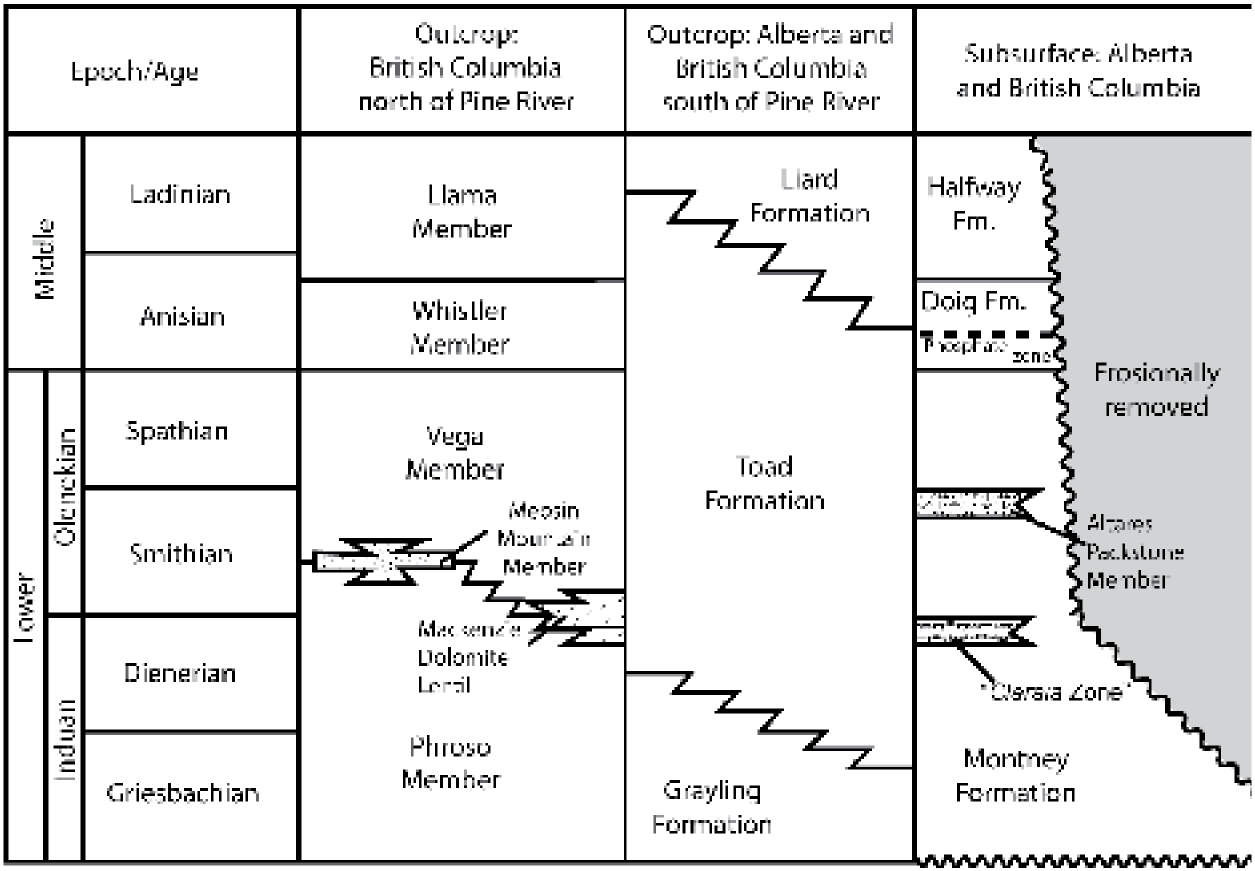
Epoch/Age
Outcrop: British Columbia north of Pine River
Outcrop: Alberta and British Columbia south of Pine River
Subsurface: Alberta and British Columbia
Middle
Lower
Olenekian
Induan
Ladinian
Anisian
Spathian
Smithian
Dienerian
Griesbachian
Llama Member
Whistler Member
Vega Member
Meosin Mountain Member
Mackenzie Dolomite Lentil
Phroso Member
Liard Formation
Toad Formation
Grayling Formation
Halfway Fm.
Doig Fm.
Phosphate zone
Erosionally removed
Altares Packstone Member
"Claraia Zone"
Montney Formation

Figure **1.2:** The stratigraphic framework of the Lower and Middle Triassic in the Western Canada Sedimentary Basin, and the location and correlation of the Montney Formation with its outcrop equivalents. With formation names represented for both above and below the Pine River (modified from Zonneveld, 2011; compiled from Tozer, 1994; Orchard and Tozer, 1997; Orchard and Zonneveld, 2009).

the basin. There are other fossils present, but they are composed of materials that are less susceptible to dissolution (i.e. phosphatic vertebrate fossils and linguilide brachiopods).

Trace fossils are also reduced in abundance, size, and distribution throughout the Montney (Zonneveld et al., 2010a,b). This absence, compounded with the lack of body fossils makes it even more difficult to determine the sedimentary processes that operated during deposition of the Montne Formation. Therefore, sedimentologists must make use of the evidence that has been preserved in the form of body fossils, sedimentary structures, and trace fossils wherever present. Each instance allows for another glimpse into the depositional history of this unique and important formation.

Beside the academic interest in the Montney Formation as a valuable record of the Lower Triassic, the Montney Formation is also as an unconventional, locally liquids-rich, tight gas reservoir (Bird et al., 1994; Davies et al., 1997; Wood, 2012). The two horizons discussed within this thesis are of interest to the industry as potential producing horizons (Moslow, pers. comm.).

1.3 Argument

Through detailed sedimentary analysis of cores, the author has interpreted that both of the bioclastic deposits have been influenced by storm and current modification The "*Claraia* Zone" was transported from shallower settings and deposited through bottom water ocean currents that were likely

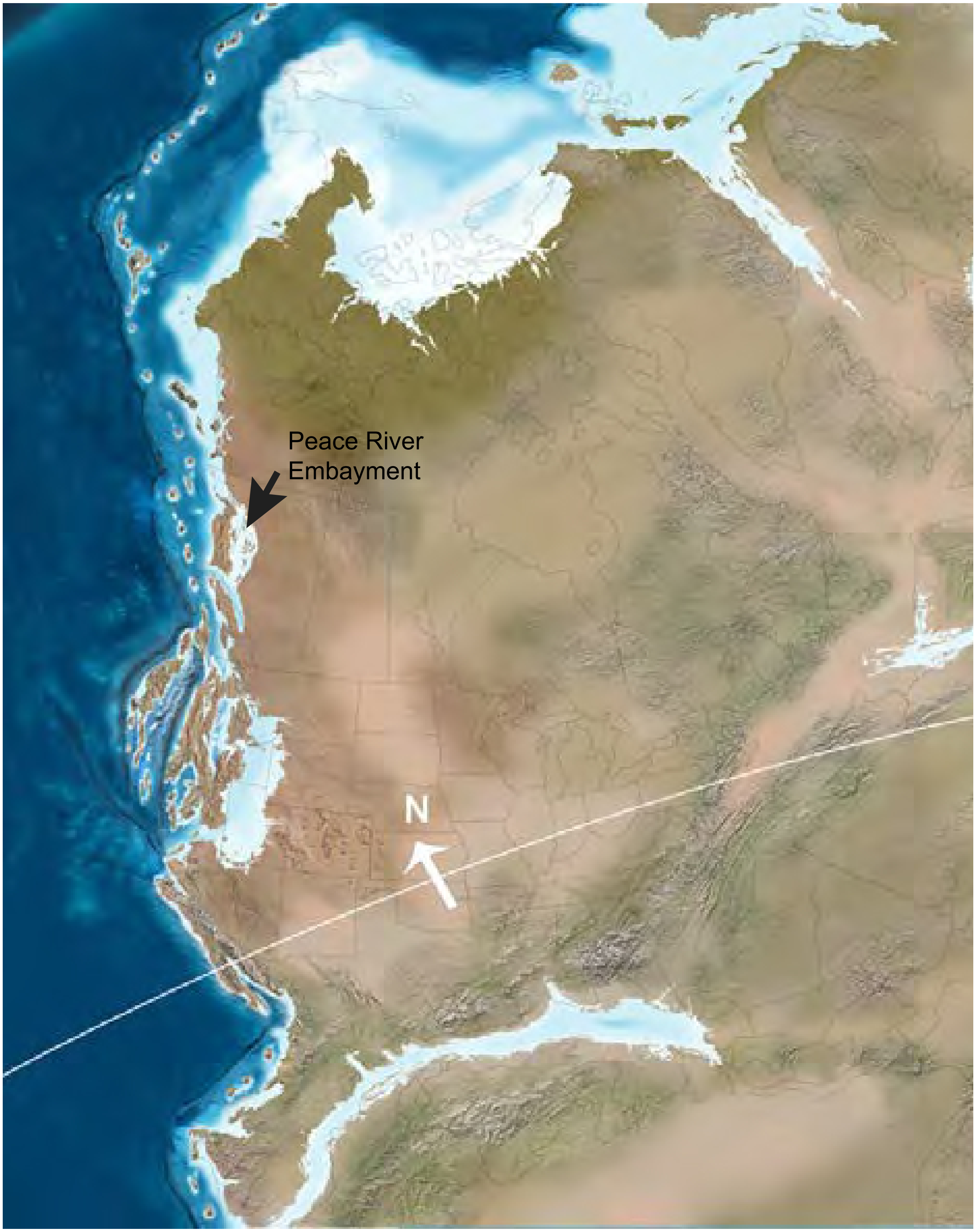
Peace River
Embayment
N

Figure 1.3: North American paleomap showing the location of North America in relation to the paleo-equator and the location of the Peace River Embayment within the continent (modified from Blakey et al., 1993).

driven by wind, similar to the Loop Current in the Gulf of Mexico. Analyzing the taphonomy of the shells and correlating the sedimentary facies across the study area lead to these conclusions. There is a possible oxygenation interval through the “*Claraia* Zone” as recorded by the sulfur isotopes from pyrite. This is only one stream of evidence, but it goes to substantiate the reasons for the occurrence of the shells through the interval.

The Montney Altares Packstone Member from the Late Smithian is the result of the formation of the first identified biostromes along the northwestern coast of Pangea after the Permian riassic mass extinction. These thin packstone beds were attempts at restarting the carbonate factory in the Peace River Embayment. Present evidence suggests that they were ultimately unsuccessful, however they are another indication of the adverse, and unstable, environmental conditions that organisms were subjected to following the extinction. The development, intermittent nature, and ultimate demise of these beds may reflect fluctuations in the Oxygen Minimum Zone along the northwestern Pangea coas

1.4 Roadmap

Through the course of this body of work the author will outline the evidence for the argument presented above in relation to both the “*Claraia* Zone” and the Altares Packstone Member. A small scale analysis of these two horizons allows for the understanding of the interactions between the biosphere and lithosphere in the basin at these two discrete times.

The second chapter of this thesis will be focused on the “*Claraia* Zone”, analyzing the relationship of facies that are found within this horizon, as well as the fossils that were found within it. This chapter primarily focuses on the relationship between the taphonomy and sedimentology of the deposits and how it changes across the study area. The same techniques of mapping, correlation, sedimentological and paleontological analyses were used to draw the conclusions in this and the subsequent chapter.

The third chapter focuses primarily on the bioclastic units, the Altares Packstone Member, which are located in the Late Smithian of the Montney Formation. Both this bioclastic zone and the previous one are located in the same study area, which allows inferences to be made about the changing environment in some of the deep basin sections of the Montney Formation.

This fine scale study of these horizons attempts to determine depositional models of these unique deposits in the Lower Triassic Montney Formation of British Columbia, Canada. Evidence from both the taphonomy of the preserved organisms and the sediments themselves has been amalgamated and examined to derive the conclusions and interpretations herein.

1.5 References

Armitage, J. H., 1962, Triassic Oil and Gas Occurrences in Northeastern British Columbia, Canada: Journal of the Alberta Society of Petroleum Geologists, v. 10, no. 2, p. 35–56.

Barclay, J., F. Krause, R. Campbell, and J. Utting, 1990, Dynamic casting and growth faulting: Dawson Creek graben complex, Carboniferous-Permian Peace River embayment, western Canada: Bulletin of Canadian Petroleum Geology, v. 38, no. 1, p. 115–145.

Beauchamp, B., and A. Desrochers, 1997, Permian warm- to very cold- water carbonates and cherts in northwest Pangea, in N. P. James, and J. A. D. Clarke, eds., Cool-Water Carbonates: SEPM

(Society for Sedimentary Geology).

Blakey, R.C., Basham, E.L., and Cook, M.J., 1993, Early and Middle Triassic paleogeography, Colorado Plateau and vicinity, in Morales, M., ed., Aspects of Mesozoic Geology and Paleontology of the Colorado Plateau: Museum of Northern Arizona Bulletin 59, p. 13-26.

Bird, T., J. Barclay, R. Campbell, and P. Lee, 1994, Triassic Gas Resources of Western Canada Sedimentary Basin, Interior Plains-Geological Play Analysis and Resource Assessment: Western Canadian and International Expertise [Program book with expanded abstracts], p. 352–353.

Davies, G. R., 1997, The Triassic of the Western Canada Sedimentary Basin: tectonic and stratigraphic framework, paleogeography, paleoclimate and biota: Bulletin of Canadian Petroleum Geology, v. 45, no. 4, p. 434–460.

Davies, G. R., T. F. Moslow, and M. D. Sherwin, 1997, The Lower Triassic Montney Formation, west-central Alberta: Bulletin of Canadian Petroleum Geology, v. 45, no. 4, p. 474–505.

Edwards, D. E., J. E. Barclay, D. W. Gibson, G. E. Kvill, and E. Halton, 1994, Triassic Strata of the Western Canada Sedimentary Basin, in G. D. Mossop, and I. Shetsen, eds., Geological Atlas of the Western Canada Sedimentary Basin: Canadian Society of Petroleum Geologists and Alberta Research Council.

Erwin, D., 2007, Disparity: Morphological pattern and developmental context: Palaeontology, v. 50, p. 57–73.

Ferri, F., and J. Zonneveld, 2008, Were Triassic rocks of the Western Canada Sedimentary Basin deposited in a foreland: Canadian Society of Petroleum Geologists Reservoir, v. 35, no. 10, p. 12–14.

Flügel, E., 1994, Pangean shelf carbonates: controls and paleoclimatic significance of Permian and Triassic reefs: Geological Society of America Special Papers, v. 288, p. 247–266.

Gibson, D., and J. Barclay, 1989, Middle Absaroka sequence the Triassic stable craton, in Ricketts, BD, ed., Western Canada Sedimentary Basin - A case history: Calgary, p. 219–231.

Gibson, D., and T. Poulton, 1994, Field Guide to the Triassic and Jurassic stratigraphy and depositional environments in the Rocky Mountain Foothills and Front Ranges in the Banff, Jasper and Cadomin areas, Alberta: Geological Survey of Canada, Open File Report No. 2780, 85 p.

Golding, M., M. Orchard, J.-P. Zonneveld, and N. Wilson, 2015, Determining the age and depositional model of the Doig Phosphate Zone in northeastern British Columbia using conodont biostratigraphy: Bulletin of Canadian Petroleum Geology, v. 63, no. 2, p. 143–170.

Government of Canada; Natural Resources Canada; Earth Sciences Sector; Canada Centre for Mapping and Earth, 2001, Coastline and Boundaries of Canada.

Greene, S. E., D. J. Bottjer, H. Hagdorn, and J.-P. Zonneveld, 2011, The Mesozoic return of Paleozoic faunal constituents: A decoupling of taxonomic and ecological dominance during the recovery from the end-Permian mass extinction: Palaeogeography, Palaeoclimatology, Palaeoecology, v.

308, no. 1-2, p. 224–232, doi:10.1016/j.palaeo.2010.08.019.

Habicht, J. K. A., 1979, Paleoclimate, paleomagnetism, and continental drift: American Association of Petroleum Geologists Studies in Geology 9.

Hallam, A., 1991, Relative importance of regional tectonics and eustasy for the Mesozoic of the Andes, in D. Macdonald, ed., Sedimentation, tectonics and eustasy, sea-level changes at active margins: International Association of Sedimentologists Special Publication 12, p. 189–200.

Henderson, C., S. Mei, and B. Wardlaw, 2002, New conodont definitions at the Guadalupian-Lopingian boundary, in L. Hills, C. Henderson, and E. Bamber, eds., Carboniferous and Permian of the World: Canadian Society of Petroleum Geologists Memoir 19, p. 725–735.

Kendall, D. R., 1999, Sedimentology and Stratigraphy of the Lower Triassic Montney Formation, Peace River Basin, subsurface of northwestern Alberta, Master of Science: Calgary, Alberta, The University of Calgary, 368 p.

Kendall, D. R., R. Panek, and C. M. Henderson, 1998, Coquina facies of the Lower Triassic Montney Formation, Peace River Embayment, northwestern Alberta.

Lehrmann, D. J., 1999, Early Triassic calcimicrobial mounds and biostromes of the Nanpanjiang basin, south China: Geology, v. 27, no. 4, p. 359–362.

Markhasin, B., 1997, Sedimentology and Stratigraphy of the Lower Triassic Montney Formation, Subsurface of Northwestern Alberta, Master of Science: Calgary, Alberta, University of Calgary, 154 p.

Meyer, K., M. Yu, A. Jost, B. Kelley, and J. L. Payne, 2011, d13C evidence that high primary productivity delayed recovery from end-Permian mass extinction: Earth and Planetary Science Letters, v. 302, p. 378–384.

Moslow, T. F., 2000, Reservoir architecture of a fine-grained turbidite system: Lower Triassic Montney Formation, Western Canada Sedimentary Basin, in Deep-water Reservoirs of the World, Conference Proceedings, Gulf Coast SEPM. P. Weimer, RM Slatt, J. Coleman, NC Rosen, H. Nelson, AH Bouma, MJ Styzen, and DT Lawrence (eds.): SEPM, p. 686–713.

Orchard, M. J., and E. T. Tozer, 1997, Triassic conodont biochronology, its calibration with the ammonoid standard, and a biostratigraphic summary for the Western Canada Sedimentary Basin: Bulletin of Canadian Petroleum Geology, v. 45, no. 4, p. 675–692.

Orchard, M. J., and J.-P. Zonneveld, 2009, The Lower Triassic Sulphur Mountain Formation in the Wapiti Lake area: lithostratigraphy, conodont biostratigraphy, and a new biozonation for the lower Olenekian (Smithian)Earth Science Sector (ESS) Contribution 20080714.: Canadian Journal of Earth Sciences, v. 46, no. 10, p. 757–790, doi:10.1139/E09-051.

Panek, R., 2000, The Sedimentology and Stratigraphy of the Lower Triassic Montney Formation in the Subsurface of the Peace River Area, Northwestern Alberta, Master of Science: Calgary, Alberta, University of Calgary.

Paull, R. K., R. A. Paull, and T. S. Laudon, 1997, Conodont biostratigraphy of the Lower Triassic Mackenzie Dolomite Lentil, Sulphur Mountain Formation in the Cadomin area, Alberta: Bulletin of Canadian Petroleum Geology, v. 45, no. 4, p. 708–714.

Payne, J. L., D. Altiner, D. J. DePaolo, J. L. Hinojosa, L. R. Kump, K. V. Lau, D. J. Lehrmann, K. Maher, A. Paytan, and S. Shen, 2014, The End-Permian Mass Extinction and its Aftermath: Insights from Non-Traditional Isotope System: Vancouver, BC.

Payne, J. L., D. J. Lehrmann, J. Wei, M. Orchard, D. Schrag, and A. Knoll, 2004, Large Perturbations of the Carbon Cycle During Recovery from the End-Permian Extinction: Science, v. 305, no. 5683, p. 506–509, doi:10.1126/science.1097023.

Rampino, M. R., and K. Caldeira, 2005, Major perturbation of ocean chemistry and a “Strangelove Ocean” after the end-Permian mass extinction: Terra Nova, v. 17, no. 6, p. 554–559, doi:10.1111/j.1365-3121.2005.00648.x.

Schoepfer, S. D., C. M. Henderson, G. H. Garrison, J. Foriel, P. D. Ward, D. Selby, J. C. Hower, T. J. Algeo, and Y. Shen, 2013, Termination of a continent-margin upwelling system at the Permian–Triassic boundary (Opal Creek, Alberta, Canada): Global and Planetary Change, v. 105, p. 21–35, doi:10.1016/j.gloplacha.2012.07.005.

Sepkoski Jr, J. J., 1981, A factor analytic description of the Phanerozoic marine fossil record: Paleobiology, p. 36–53.

Tozer, E., 1982, Marine Triassic faunas of North America: their significance for assessing plate and terrane movements: Geologische Rundschau, v. 71, no. 3, p. 1077–1104.

Tozer, E. T., 1994, Canadian Triassic ammonoid faunas: Geological Survey of Canada.

Wilson, N., 2009, Integrated regional model for the deposition and evolution of the Montney Formation, NE British Columbia.

Wilson, K. M., D. Pollard, W. W. Hay, S. L. Thompson, and C. N. Wold, 1994, General circulation model simulations of Triassic climates: preliminary results: Geological Society of America Special Papers, v. 288, p. 91–116.

Wood, J., 2012, Water Distribution in the Montney Tight Gas Play of the Western Canadian Sedimentary Basin: Significance for Resource Evaluation: Society of Petroleum Engineers, doi:10.2118/161824-MS.

Woods, A. D., 2005, Paleoceanographic and paleoclimatic context of Early Triassic time: Comptes Rendus Palevol, v. 4, no. 6-7, p. 463–472, doi:10.1016/j.crpv.2005.07.003.

Woods, A. D., and D. J. Bottjer, 2000, Distribution of ammonoids in the Lower Triassic Union Wash Formation (Eastern California): Evidence for paleoceanographic conditions during recovery from the end-Permian mass extinction: Palaios, v. 15, p. 535–545.

Zonneveld, J.-P., 2011, Suspending the Rules: Unraveling the ichnological signature of the Lower Triassic post-extinction recovery interval: Palaios, v. 26, no. 11, p. 677–681, doi:10.2110/palo.2011.S06.

Zonneveld, J.-P., C. Furlong, A. Gegolick, M. K. Gingras, M. Golding, T. F. Moslow, M. J. Orchard, T. Playter, D. Prenoslo, and S. C. Sanders, 2015, Stratigraphic architecture of the Montney Formation, Peace district, Alberta and British Columbia: Banff, Canada. Gussow Geoscience Conference: Banff, Canada.

Zonneveld, J.-P., M. K. Gingras, and T. W. Beatty, 2010a, Diverse ichnofossil assemblages following the P-T mass extinction, Lower Triassic, Alberta and British Columbia, Canada: Evidence for shallow marine refugia on the northwestern coast of Pangea: Palaios, v. 25, no. 6, p. 368–392, doi:10.2110/palo.2009.p09-135r.

Zonneveld, J.-P., R. B. MacNaughton, J. Utting, T. W. Beatty, S. G. Pemberton, and C. M. Henderson, 2010b, Sedimentology and ichnology of the Lower Triassic Montney Formation in the Pedigree-Ring/Border-Kahntah River area, northwestern Alberta and northeastern British Columbia: Bulletin of Canadian Petroleum Geology, v. 58, no. 2, p. 115–140.

Zonneveld, J.-P, and T. F. Moslow, 2013, Regional outcrop to subsurface correlation of the Montney Formation: An evolving understanding of Lower Mesozoic tectono-stratigraphic evolution in Western Canada: Pennsylvania.

Zonneveld, J.-P., and T. F. Moslow, 2014, Perennial River Deltas of the Montney Formation: Alberta and British Columbia Subcrop Edge.

Figure Captions

1.1: Map of core datasets in relation to the Montney Formation as a whole during the Dienerian-Smithian boundary. The two deltas are known to be present on opposite sides of the boundary. The red block in the inset map shows the location of the above map in relation to modern geographical boundaries of Canada. (The Montney map was compiled and modified from Barclay et al, 1990; Panek, 2000; Zonneveld et al, 2010a; Zonneveld et al, 2010b; Zonneveld and Moslow, 2014; and Zonneveld, pers. comm.; the Map of the provinces and coastline of Canada was modified from Government of Canada, 2001).

1.2: The stratigraphic framework of the Lower and Middle Triassic in the Western Canada Sedimentary Basin, and the location and correlation of the Montney Formation with its outcrop equivalents. With formation names represented for both above and below the Pine River (modified from Zonneveld, 2011; compiled from Tozer, 1994; Orchard and Tozer, 1997; Orchard and Zonneveld, 2009).

1.3: North American paleomap showing the location of North America in relation to the paleo-equator and the location of the Peace River Embayment within the continent (modified from Blakey et al., 1993)

Chapter 2: Sedimentology and Taphonomy of the “*Claraia* Zone” in British Columbia, Canada

2.1 Introduction

Bioclastic units may occur in both clastic and carbonate dominated successions. Bioclastic units have always posed a problem for sedimentological and paleontological analyses as taphonomic processes may obscure or alter patterns, and they are susceptible to a variety of early and late stage diagenetic processes (e.g., Stanley et al., 1967; Kidwell, 1991; Best et al., 2007; Best and Kidwell, 2000). The bioclasts within a system may have arrived through transport or *in situ* growth, but it is also possible that a combination of these mechanisms affected the biotic signal that is preserved within strata. Taphonomic features are important in identifying the history of a deposit and can completely change the interpretation when compared with a solely sedimentological interpretation. To aid in taphonomic interpretation, Kidwell and Holland (1991) have composed a list of macroscopic features of shells of bioclastic horizons, with emphasis on bivalve deposition, that summarize the basic taphonomic factors useful to sedimentologists.

In fine-grained successions, bed forms that clearly indicate depositional environment may be subtle or absent, thus rendering interpretation difficult. Bioclastic intervals are a small window that gives more information about the fine-grained succession that could not otherwise be obtained from the sediment itself. This study focuses on a Lower Triassic siltstone-dominated succession in the lower Montney Formation of northeastern British Columbia, Canada. This unit is devoid of bioturbation, which may reflect regional environmental constraints (e.g., dysoxia, marine acidity, etc…) or an absence of available bioturbators in sediments deposited shortly after the end-Permian extinction event (Wignall and Hallam, 1996; Twitchett and Wignall, 1996; Zonneveld et al., 2010a). Thus, the taxonomic composition and taphonomic characters of bioclastic intervals in this succession provide crucial information for sedimentological and palaeoecological analyses.

This study focuses on the lower part of the Montney Formation in the western subcrop belt, on an interval colloquially referred to by some practitioners both as the northern ‘turbidite zone’ and, more recently, as evidence has not supported this depositional interpretation, as the “*Claraia* Zone”. This manuscript focuses on describing the taxonomic composition, taphonomic character and sedimentological features of the “*Claraia* Zone” through sedimentary core analysis, thin section petrography and wire line log correlation, and provides a depositional model and palaeoecological interpretation for the genesis of this important unit.

2.2 Background/Methods

2.2.1 Montney & Bioclastic Units

The Montney Formation is a westward thickening package of bituminous siltstone and fine grained sandstone in western Alberta and northeastern British Columbia, Canada (Edwards et al, 1994; Davies et al., 1997) (Fig. 2.1). It was first identified by Armitage (1962) and has been targeted by petroleum exploration companies in Western Canada as both a conventional target (from the 1950s through the 1990s), and more recently as an unconventional, locally liquids-rich, tight gas reservoir. (Bird

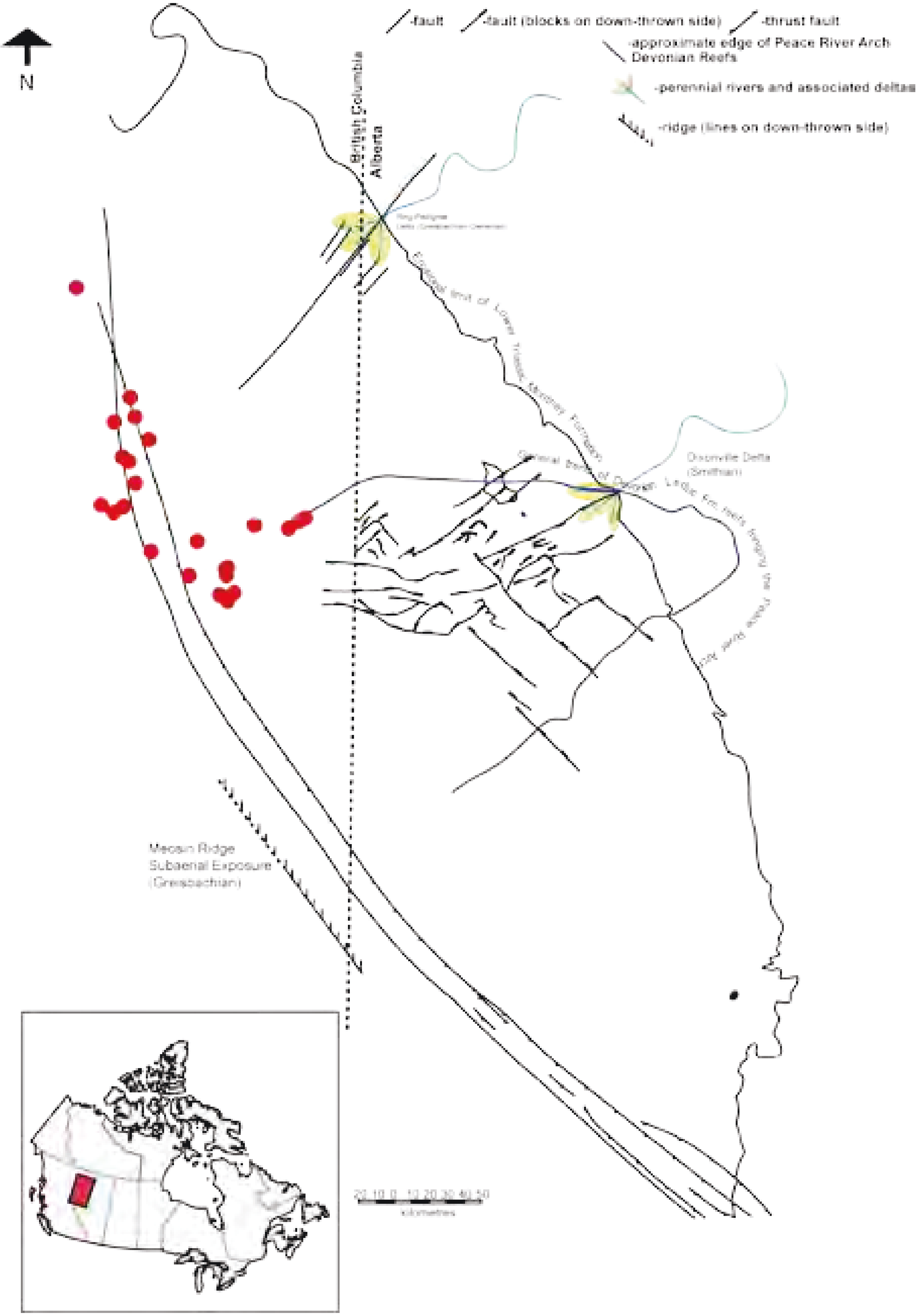

N
-fault
-fault (blocks on down-thrown side)
-thrust fault
-approximate edge of Peace River Arch Devonian Reefs
-perennial rivers and associated deltas
-ridge (lines on down-thrown side)
British Columbia
Alberta
Ring/Pedigree Delta (Greisbachian-Dienerian)
Erosional limit of Lower Triassic Montney Formation
General trend of Devonian Leduc Fm. reefs fringing the Peace River Arch
Dixonville Delta (Smithian)
Meosin Ridge Subaerial Exposure (Greisbachian)
20 10 0 10 20 30 40 50
kilometres

et al., 1994; Davies et al., 1997; Wood, 2012). The subsurface Montney, and its outcrop equivalents in the western deformation belt along the eastern thrust sheets of the Canadian Rocky Mountains (Toad, Grayling, and Sulphur Mountain Formations), were deposited in the Peace River Basin (Edwards et al, 1994; Davies et al., 1997) (Fig. 2.2). The Montney Formation has been interpreted as being deposited along a clastic ramp on the western margin of Pangea, with deeper sedimentary facies deposited in the west (Edwards et al., 1994; Davies et al, 1997). Although the deposits span both Alberta and British Columbia, the Alberta units generally represent more proximally deposited facies, with the shoreline truncated along the eastern erosional edge by a series of later Mesozoic unconformities including: the Late Triassic Coplin Unconformity, the sub-Jurassic unconformity, and several sub-Cretaceous unconformities. Units which span the entirety of the Montney Formation on the eastern (Alberta) side of

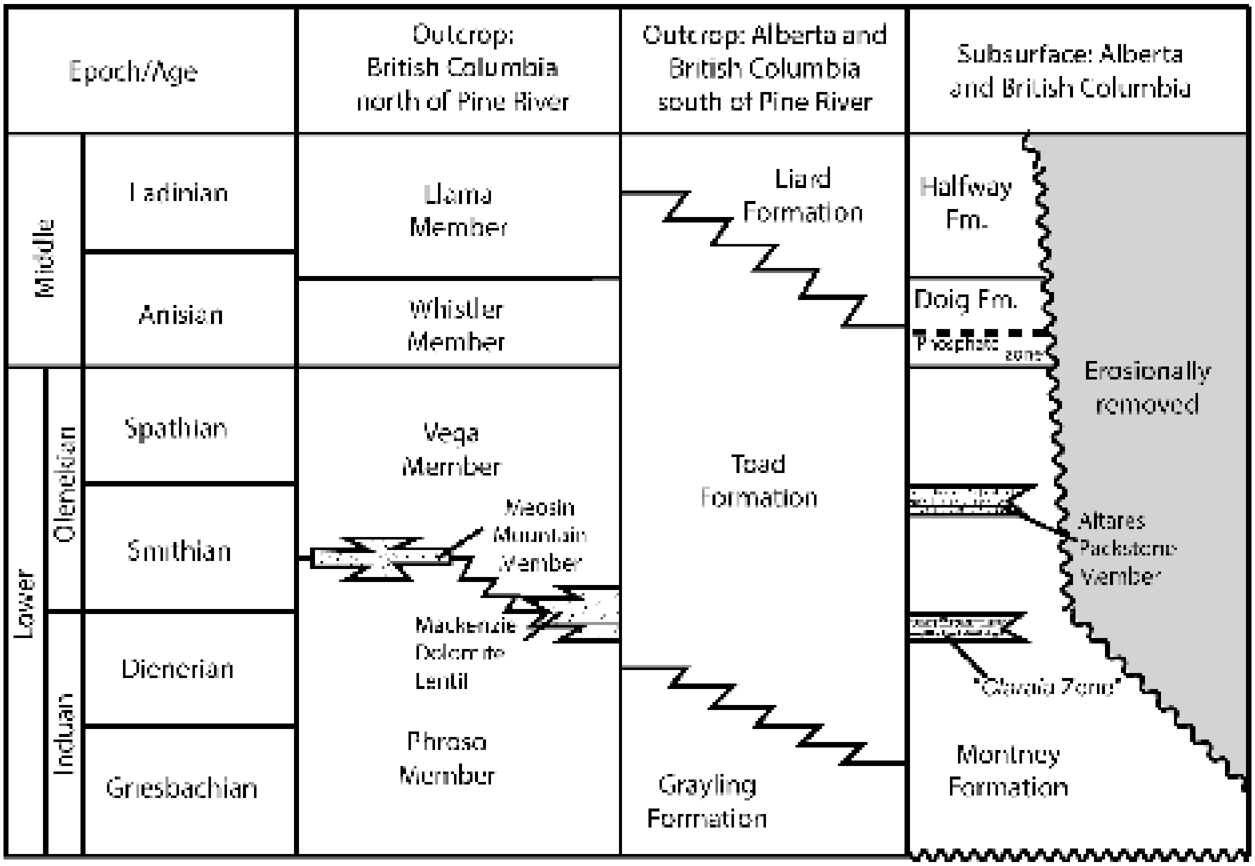
Epoch/Age
Outcrop: British Columbia north of Pine River
Outcrop: Alberta and British Columbia south of Pine River
Subsurface: Alberta and British Columbia
Middle
Ladinian
Anisian
Lower
Olenekian
Spathian
Smithian
Induan
Dienerian
Griesbachian
Llama Member
Whistler Member
Vega Member
Meosin Mountain Member
Mackenzie Dolomite Lentil
Phroso Member
Liard Formation
Toad Formation
Grayling Formation
Halfway Fm.
Doig Fm.
Phosphate zone
Erosionally removed
Altares Packstone Member
"Clavaia Zone"
Montney Formation

Figure 2.2: The stratigraphic framework of the Lower and Middle Triassic in the Western Canada Sedimentary Basin, and the location and correlation of the Montney Formation with its outcrop equivalents with the horizon of interest to this paper highlighted in grey on the right (modified from Zonneveld, 20 1; compiled from Tozer, 1994; Orchard and Tozer, 1997; Orchard and Zonneveld, 2009).

Figure 2.1 (Opposite Page): Map of core datasets in relation to the Montney Formation as a whole during the Greisbachian. The red dots each represent a separate core and they are all located well within the offshore portion of the formation. The Pedigree-Ring Delta is known to be Greisbachian in age, but the Dixonville has only been confirmed to be Smithian, although there are sand bodies of Greisbachian age that are located westward in the Peace River Arch from the delta location. The Meosin High in the southwest is based on subaerial exposure in the outcrop belt. The red block in the inset map shows the location of the above map in relation to modern geographical boundaries of Canada. (The Montney map was compiled and modified from Barclay et al, 1990; Panek, 2000; Zonneveld et al, 2010a; Zonneveld et al, 2010b; Zonneveld and Moslow, 2014; and Zonneveld, pers. comm.).

the basin are temporally equivalent to the Lower Montney Formation in the western (British Columbia) part of the basin, whereas the Upper Montney in British Columbia is an expansion of what is referred to as the Basal Doig Siltstone member in Alberta (Wilson, 2009). The Alberta terminology is based on an unpublished consultant report, and has not been formally established in the literature. Due to a lack of clear lithological distinctions between the two units, and because all of the data presented herein are located in British Columbia, this study will conform to the British Columbia stratigraphic paradigm.

Thick Montney fossil accumulations, which occur on the eastern side of the basin, are typically included in the Coquinal Dolomite Middle Member (informal subsurface terminology), or as the Mackenzie Dolomite Lentil of the Sulphur Mountain Formation (formal outcrop terminology) (Gibson, 1974; 1993; Mederos, 1995; Markhasin, 1997; Davies et al., 1997; Paull et al, 1997; Kendall et al, 1998; Zonneveld and Orchard, 2009). The fossils in these horizons consist dominantly of shells of lingulide brachiopods and molds of bivalve and gastropod shells in a dolomitic matrix (Gibson, 1974; 1993; Markhasin, 1997; Davies et al., 1997; Kendall, 1999).

The ‘Montney coquina play’, which has been identified as early Smithian in age (Mederos, 1995; Markhasin, 1997; Paull et al., 1997; Kendall, 1999), was previously exploited as a conventional reservoir play in the southeastern end of the basin, typically near the subcrop limit. Porosity and permeability, measured on both outcrop and hand samples are high, with porosity ranging from 5 to 25% and permeabilities in the upper millidarcy to darcy range (Mederos, 1995; Markhasin, 1997). To date, all other Montney plays, both conventional and unconventional alike, are hosted in predominantly clastic strata, either siltstone or very fine- to fine-grained sandstone

This study focuses on a bioclastic-rich horizon recently identified in the northwestern part of the basin, which are currently being investigated as unconventional plays by a number of exploration companies. This unit, referred to informally as the “*Claraia* Zone”, consists primarily of bivalve shells encased in laminated bituminous siltstone. The bioclastic horizons of the “*Claraia* Zone” represent nearly all of the preserved calcareous body fossils in the lower Montney Formation. In intervals above and below this horizon, Montney fossils are represented either by locally abundant impressions of shells, devoid of preserved shell material, or fossils composed of minerals not susceptible to dissolution (e.g., calcium phosphate / apatite). The preferential preservation of calcite body fossils within the “*Claraia* Zone” and the Altares Packstone Member indicates that this pattern of preservation (and non-preservation through the rest of the formation) is unlikely to be related to burial diagenesis and has been attributed to syndepositional changes in the Aragonite Compensation Depth (ACD) and/or Calcite Compensation Depth (CCD) (Rampino and Caldeira, 2005; Zonneveld, 2011).

2.2.2 Triassic

The Montney Formation represents the entirety of the Lower Triassic in the Western Canada Sedimentary Basin (Orchard and Tozer 1997, Orchard and Zonneveld, 2009). Thus, fossils within the Montney Formation record the recovery of northwestern Pangaean marine biotas after the Permian-Triassic Mass Extinction on the eastern margin of Panthalassa. The Peace River Basin at this time was located at approximately 30°N latitude, and was characterized by an arid climate on the east margin of the Panthalassa Ocean (Habicht, 1979; Tozer, 1982; Wilson et al., 1994; Kidder and Worsley, 2004). Diversity after the extinction event was low in the world’s oceans and cosmopolitan taxa (organisms with widespread / global distribution) dominated the world’s marine biotas (i.e., Sepkoski, 1981; Erwin, 2000; Bambach, 2006; Payne and Clapham, 2012). Recovery did not occur until the Middle Triassic at the earliest, and was possibly delayed by increased alkalinity and/or expansion of oxygen minimum zones (e.g., Sepkoski, 1981; Woods, 2005; Payne et al., 2014). In the Montney Formation, trace fossils are also of very low abundance and diversity, pointing towards a stressed environment during deposition (Zonneveld et al, 2010a; 2010b). High diversity occurs only in successions that have been interpreted as perennial deltaic (Zonneveld et al, 2010a; Zonneveld and Moslow, 2014).

2.2.3 Methods

The “*Claraia* Zone” was initially identified in subsurface cores by geologists from Progress Energy Canada Ltd. Two wells (C-006-L/094-B-08 and the C-065- F/094-B-08) are herein considered the informal ‘type wells’ for this unit, and were the first cores through the *Claraia* Zone” logged in this study. Lithological character and well log characteristics (particularly gamma ray and density log signatures) were noted for each zone, and subsequently used to identify the same interval in other cores. A total of twenty-seven cores through the “*Claraia* Zone” were logged in detail (Fig. 2.3)(Table 2.1). The “*Claraia* Zone”, and any other bioclastic zones identified within analyzed cores, were logged on a decimeter scale to aid in capturing any small scale variability within the zone. Bedding plane impressions were noted, and select specimens were taken for further photography and identification. Samples were taken at horizons of interest for petrographic and geochemical analyses. Thin sections were then analyzed and described for diagenetic and sedimentary characteristics.

The core gamma and down hole gamma log signatures, which were matched to the core, were used to identify the “*Claraia* Zone” in other (non-cored) wells within the study area . Well log cross sections were made and correlated with logged cores to determine the extent, distribution, and thickness of the interval. Isopach maps were also constructed to extrapolate the “*Claraia* Zone” between and beyond known core locations.

A sedimentary framework has subsequently been constructed based on facies characteristics that have been documented in multiple cores and taphonomic observations from bedding planes and thin section. Through the above methods, the distribution of the “*Claraia* Zone”, and comparison to modern and ancient analogues have allowed the depositional environment of the succession to be interpreted and have facilitated hypotheses regarding the chemistry and biologic composition of the interval at the time of deposition.

2.3 Results

2.3.1 Facies

A diverse range of lithofacies were identified in the 27 wells, which were analyzed for this stud . Grain size references allude to the Udden-Wentworth grain-size classification scheme (entworth, 1922). Carbonate facies classification refers to the Dunham classification (Dunham, 1962). Use of the ter

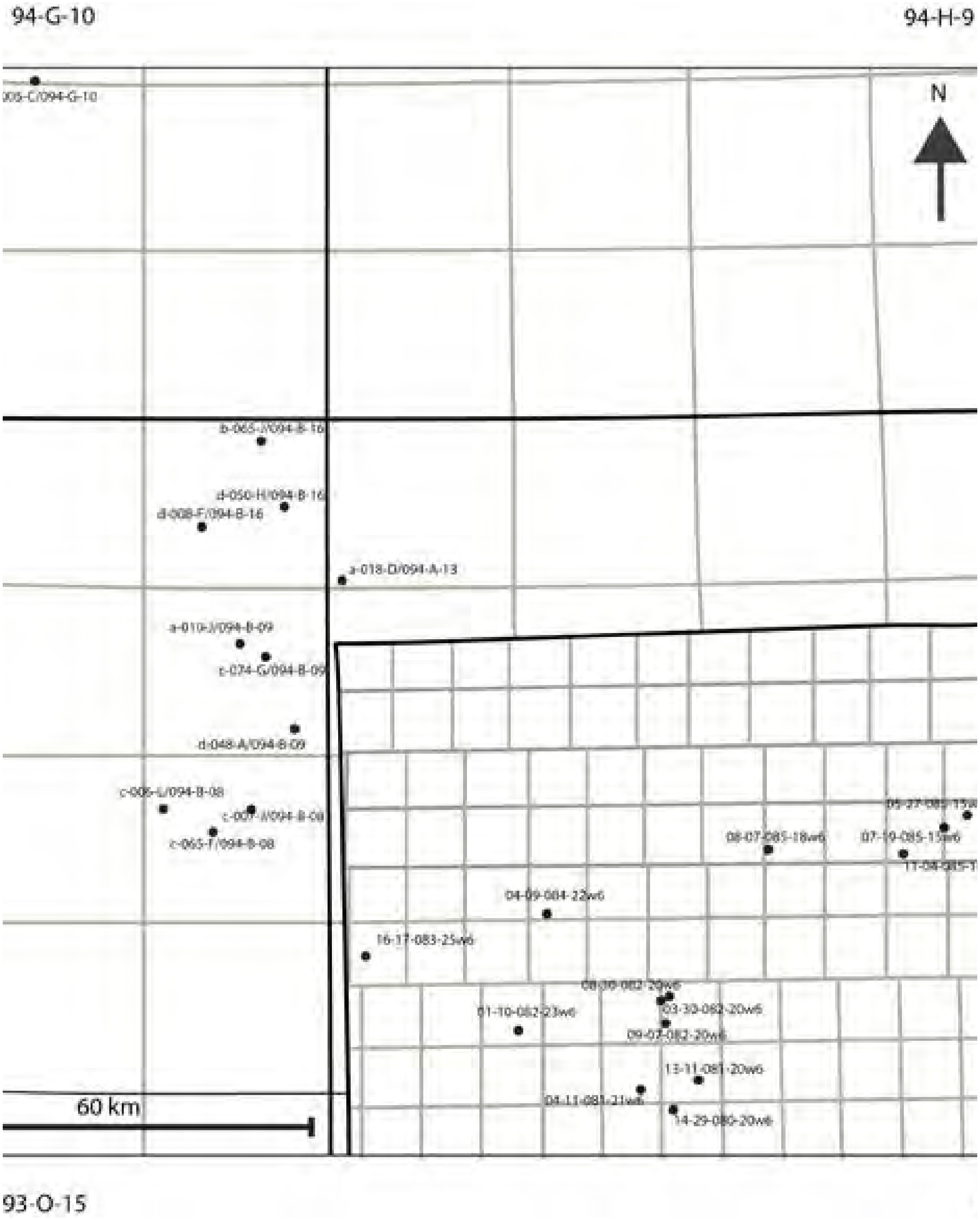
94-G-10
94-H-9
06-C/094-G-10
N
b-065-J/094-B-16
d-050-H/094-B-16
d-008-F/094-B-16
a-018-D/094-A-13
a-010-J/094-B-09
c-074-G/094-B-09
d-048-A/094-B-09
c-006-L/094-B-08
c-007-J/094-B-08
c-065-F/094-B-08
05-27-085-15w
08-07-085-18w6
07-19-085-15w6
11-08-085-1
04-09-084-22w6
16-17-083-25w6
08-30-082-20w6
01-10-082-23w6
03-30-082-20w6
09-07-082-20w6
13-11-081-20w6
04-11-081-21w6
14-29-080-20w6
60 km
93-O-15

Figure 2.3: The location and study area of all wells logged for this study. These wells were selected as they appeared to have core within the “Claraia Zone” based on wireline gamma log signatures.

Well I.D.	***Cored Interval***	***“Claraia Zone” MD (m)***	***Packstone Beds MD (m)***	***Presence of “Claraia Zone”***	***Presence of Packstone Beds***
200/a-005-C 094-G-10/00	1854-1872; 2025.5-2043.5	1995	1870.3	x	
200/b-065-J 094-B-16/00	2102-2126	2122.8	1975.6		
200/b-050-H 094-B-16/00	2049.83-2077.3	2142.5	2052.7		x
200/d-008-F 094-B-16/00	2268-2286	2296.5	2177.5		
200/a-010-J 094-B-09/00	2310-2328.27	2318.1	2158.8	x	
200/c-074-G 094-B-09/00	1855-1864; 1954-1945.9	2112.1	1947.2	x	x
200/a-008-D 094-A-13/00	2162-2180	2176.1	2068.4	x	
102/08-07-085-18W6/00	1814-1832		1693		
100/09-21-085-16W6/00	1620.4-1638.85	1750.7	1608.4		x
100/16-17-083-25W6/00	2230-2530	2425.1	2384.1	x	x
100/01-10-082-23W6/00	1995-2013.4	2055.6	2018.6		appears as LBS
100/03-30-082-20W6/00	1899-1926	1900.3		x	
100/09-07-082-20W6/00	2022-2040	2010.2	1956.6		
100/04-11-081-21W6/02	2175.9-2212.17; 2139.75-2175.9		2228.3	x?	
100/14-29-080-20W6/00	2485-2584.05	2570.7	2519.8	x	x
200/c-006-L 094-B-08/00	2610-2845	2781	2660	x	x
200/c-65-F 094-B-08/00	2180-2575	2504	2375	x	x
8-30-82-20w6	1897-1915.45				x
13-11-81-20w6	2306-2323.92				x

Table 2.1: Table of cores analyzed and presence or absence of the packstone bed horizon or the “Claraia Zone”.

calcispheres is based on Versteegh et al. (2009). The facies identified and described herein were found within and around the "*Claraia* Zone" in these wells. Facies identified and described include: Laminated siltstone (SL1), Rippled to laminated heterolithic very fine sandstone to fine siltstone (SL2), Calcispher massive to laminated siltstone subfacies (CA), Calcite cemented concretions subfacies (CO), Massive siltstone (SL3), Bioturbated/mottled siltstone (SL4), Heterolithic convoluted laminated fine to coarse siltstone (SL5), Planolites bioturbated siltstone (BF1) (Table 2.2).

2.3.1a Laminated siltstone (SL1)

This facies consists of fine to coarse siltstone deposited in distinct laminae (Fig. 2.4). Distinct beds of coarser grained material are common within finer grained intervals. These laminae are sometimes discontinuous, perhaps indicating that bioturbation has had an effect on preservation of primary physical sedimentary structures. There is little to no bioturbation otherwise visible in this facies. SL1 is present in all of the cores that were logged for this study, it is the most common facies, and is found in association with nearly every other facies. In thin section, SL1 is most often observed as medium to fine grained silt that sometimes alternates with beds of the coarser and finer material. This allows the bedding to be visible both macroscopically and microscopically. Without a change in lithology, the bedding can be indistinct microscopically. Bitumen is concentrated in the fine grained layers of this facies. The grains within this facies are typically angular to subangular, but are moderately well sorted. Coarser grains can often be limited to their own layer separate from the much finer grains (Fig. 2.4d). The cement is indistinct in many of the sections due to abundance of interstitial bitumen, likely silica, but there are examples where this facies is cemented with calcite. In those cases, more bioclastic material is commonly preserved within this facies. SL1 is typically made up mostly of quartz (roughly 50-60% of the grains) with small amounts (typically 1-5% each depending on the individual section) of plagioclase feldspar, clay minerals, and calcite or dolomite grains that are likely detrital in nature. The dolomite and calcite components can reach levels of up to 10% in some sections.

2.3.1b Laminated bioclastic siltstone (LBS)

This facies consist of laminated siltstone interspersed with moderate to very abundant bioclastic material in the form of bivalve shells (Fig. 2.5). This facies is typically taxonomically monogeneric. The shells are oriented concordant with bedding and are often flattened along those planes. The contacts on these horizons are often sharp, but when they are conformable they exhibit a rapid upwards increase in the proportion of bioclasts from the base of the facies and a rapid decrease from abundant bioclasts to laminated siltstone at the top of the facies (Fig. 2.5a; Fig. 2.6). Sharp surfaces are common within the facies as well, similar to SL2 below. LBS is most often identifiable in thin section as a hash of *Claraia* valve fragments that are oriented concordant with bedding (Fig. 2.7). The fine-grained siltstone material is rich with bitumen and there are occasional pyrite framboids present alongside the valve fragments. In some cases the only indication of bedding are the valve fragments. Valves were occasionally observed to be stacked on top of one another, and in some samples calcispheres were observed to be present within the same horizon (Fig. 2.7 c-f). Dolomitization is not common within this facies, and dolomite typically occurs solely as detrital grains. In the few examples in which dolomitization was observed to have occurred, it appears to have preferentially affected the calcispheres and the space between the valves prior to affecting the bioclasts. In the 3-30-082-20w6 core, the calcite of several *Claraia* valves was altered to ankerite. Lenses of haphazardly arranged shell material occur within this facies and may either

Facies	***Minerology***	***Thickness***	***Grain Size***	***Sed. Structures***	***Trace Fossils***	***Body Fossils***	***Taphonomy***
MBP	quartz, clay minerals, detrital dolomite or calcite, plagioclase, silica or sometimes calcite cement, and high concentration of bitumen	1-10cm	Fine to coarse silt with pebble or larger size bioclasts	soft sediment deformation, scour, crinkled lamination		ammonoids, brachiopods (terebratulids), bivalves	valves can be disarticulated or articulated, articulated valves often have cement in the cavity. Valves do not appear to be abbraided, and ammonoids are whole.
SL1	quartz, bioclastic hash, some clay minerals, silica cement, and high concentration of bitumen	2cm-10m	fine silt, angular-subangular, mod. well sorted	planar lamination		bivalve and ammonoid impressions	disarticulated bivalve impressions. Sometimes there is fracturing, most ammonoids appear complete
LBS	quartz, silica or calcite cement, clay minerals, pyrite, high bitumen concentration in fine grained fraction	10-20cm	fine silt, angular-subangular, poor-mod. well sorted	planar lamination		Claraia sp.	fractured, disarticulated, sorted and stacked valves concentrated in beds
SL2	Calcispheres (either dolomite or calcite), quartz, small clay fraction occasionally, silica or calcite cement	20cm-5m	fine and coarse silt to very fine sand, angular, well sorted	starved and climbing ripples, flaser and lenticular bedding, mud drapes, scour surfaces	occasional Planolities		
CA	calcite or dolomite cement, pyrite rim, quartz grains, and some clay fraction	20-30cm	fine silt, round calcispheres	massive to planar lamination		occassional Claraia sp.	disarticulated, unfractured valves

Table 2.2: Summary of facies with descriptions of minerology, grain size, sedimentary structures, trace fossils, and body fossils found in each facies.

Facies	***Minerology***	***Thickness***	***Grain Size***	***Sed. Structures***	***Trace Fossils***	***Body Fossils***	***Taphonomy***
CO	clay minerals, quartz, pyrite layers, silica cement	5-20cm	fine or coarse silt	lense shaped features with mostly planar lamination		bivalves	abbraided, fractured, and disarticulated valves
SL3	quartz, clay minerals, detrital dolomite, silica cement	20-50cm	fine silt, angular, well sorted	massive	none observed		
SL4	quartz, clay minerals, pyrite, silica cement	3-10m	fine to coarse silt, angular, mod. well sorted	mottled/bioturbated	observed, but not identified		
SL5	quartz, clay minerals, pyrite, silica cement	5-20cm	fine and coarse silt to very fine sand, angular, well sorted	soft sediment deformation, scour			
BF1	quartz, clay minerals, detrital dolomite or calcite, plagioclase, silica or sometimes calcite cement, and high concentration of bitumen	5-20cm	fine to coarse silt, angular, well sorted	planar lamination, scour	Planolities, Phycosiphon		

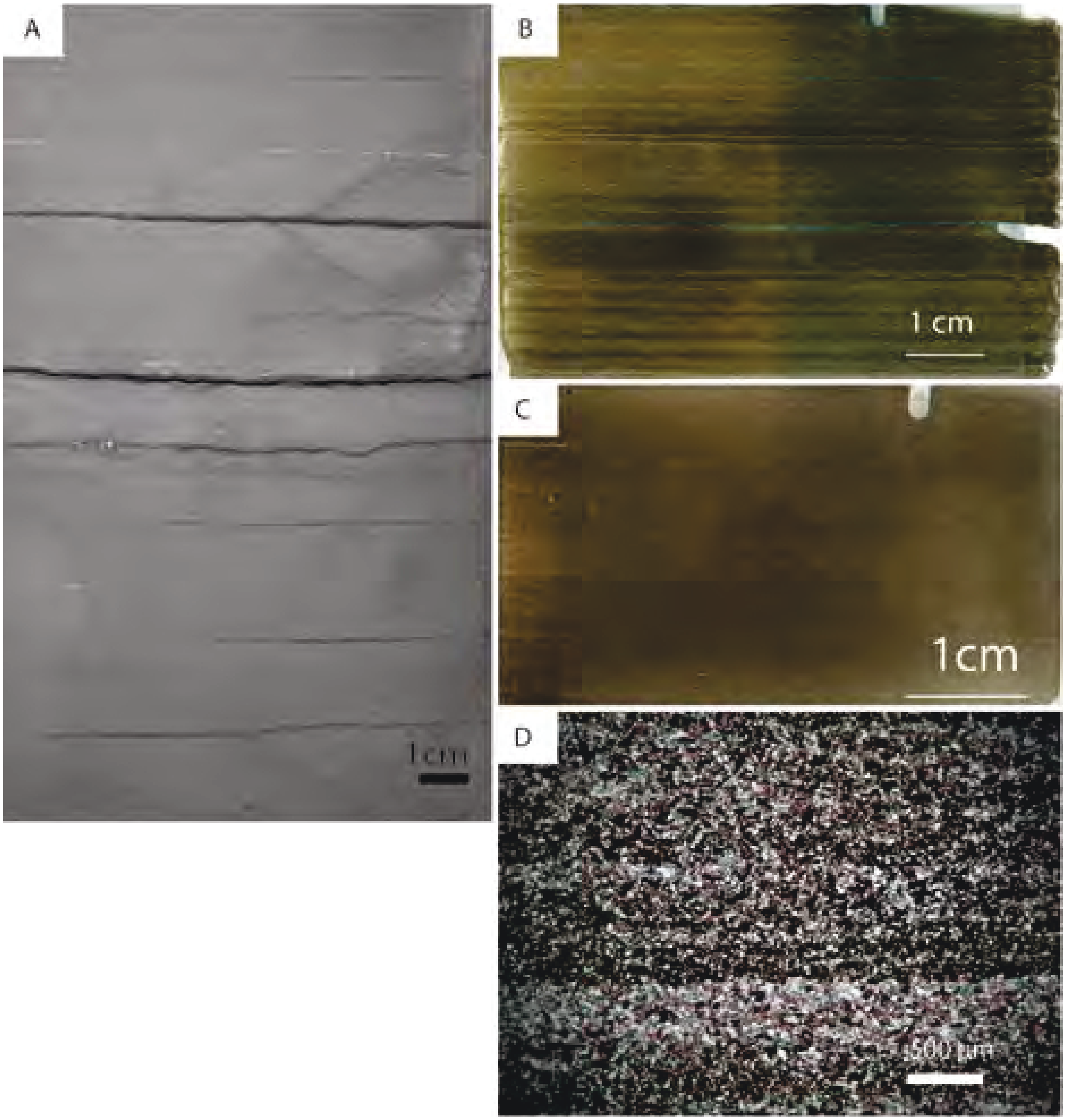

Figure 2.4: SL1: Laminated Siltstone facies. A) Macroscopic example from 14-29-080-20w6. B) Thin section example from 14-29-080-20w6. C) Thin section example from 15-02-080-16w6. Macroscopically and microscopically laminae can be followed across the face of the core or slide in the fine grained, gray, bituminous siltstone. D) Thin section photograph showing the continuous laminated from sample IRG-SA-1412-066.

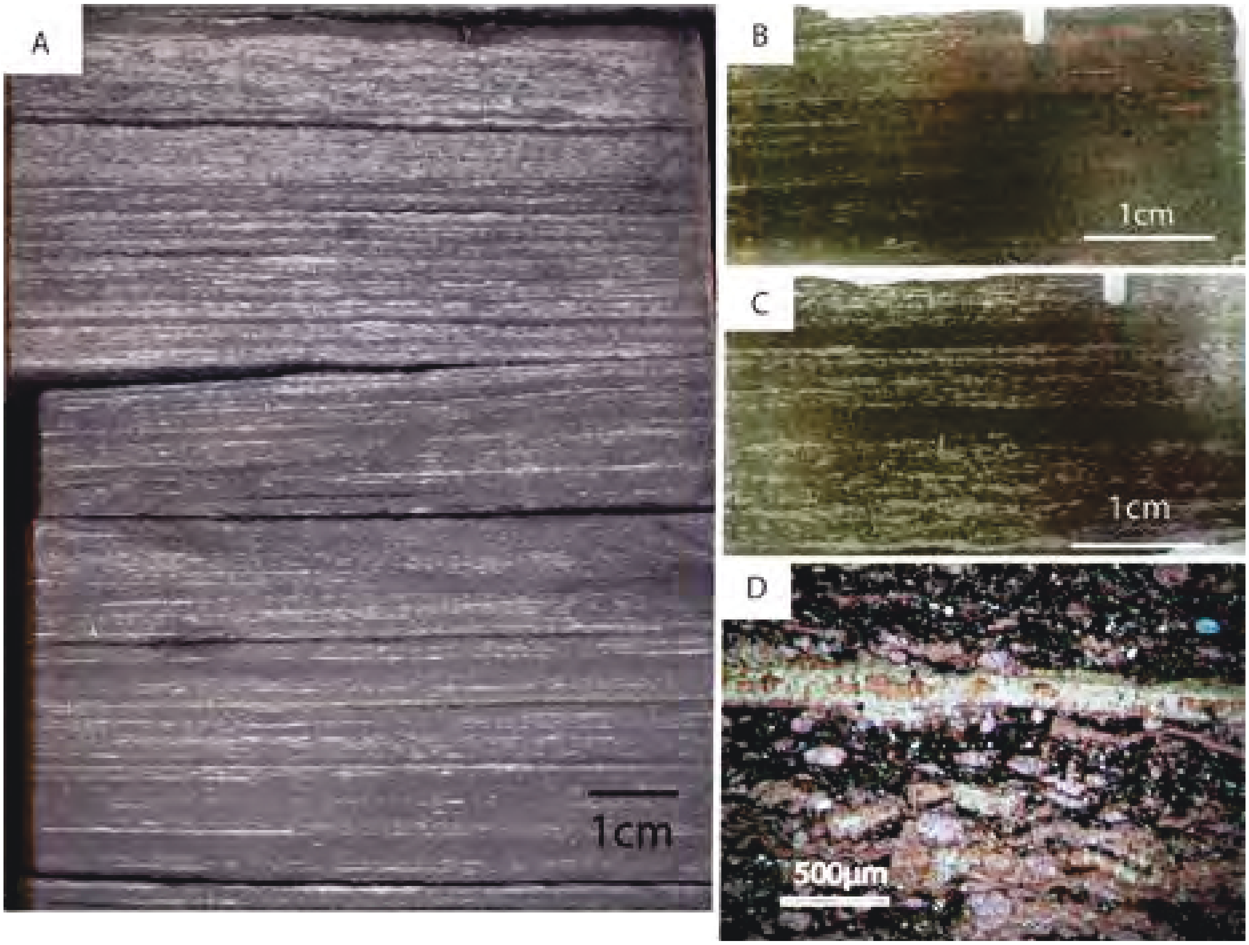

Figure 2.5: LBS: Laminated bioclastic siltstone facies. A) Macroscopic example from 14-29-080-20w6. B) Thin section example from A-10-J/094-B-9. C) Thin section example from C-007-J/094-B-8. Both thin sections B and C are scanned in plain light and are half stained for calcium carbonate. A shows the gradual increase in bioclasts that occurs at the base of the facies. The laminated has of bioclastic material is visible in B and C. D)Thin section photograph showing calcispheres alongside the bioclastic material as well as an ankerite altered valve from 3-30-082-20w6.

reflect the occurrence of agglutinated foraminifera or the fecal pellets of fish (Fig. 2.7 a-b) The grains within LBS are typically poorly to moderately well sorted, depending on the individual section, but the grains themselves are angular to subangular (fig 2.7c-e). The siltstone surrounding the bioclasts is similar in nature to SL1, primarily consisting of quartz with an unidentifiable cement (obscured by the prevalence of bitumen in the horizon, most likely silica). There are also small amounts (~5%) of detrital dolomite, phosphate, and pyrite within this facies, although pyrite can be found concentrated in some very discrete beds with concentrations up to 20-30%.

2.3.1c Rippled to laminated heterolithic very fine sandstone to fine siltstone (SL

This facies consists of dark grey, fine siltstone interbedded with white to light grey, coarse siltstone and very fine sandstone (Fig. 2.8). Ripples are often present in the coarser material, disappearing within the fine portions. Because of the color difference between the two grain sizes, bedforms and bioturbation, such as *Planolites*, can be identified. In several cases, the ripples were only identifiable by the drapes of dark fine siltstone over them. Very often the ripples can be identified as

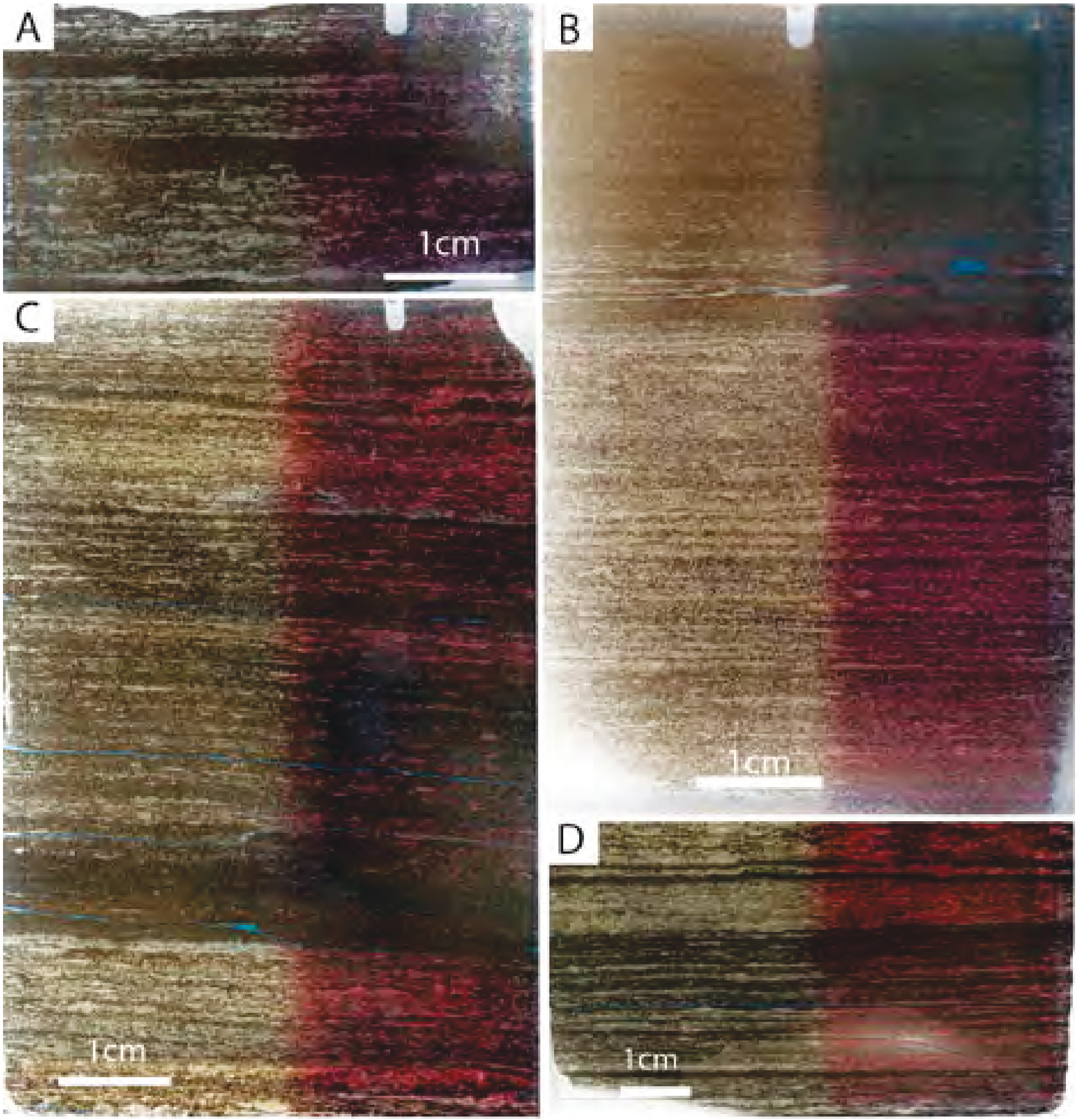

Figure 2.6: Thin sections of LBS: A) Separate layers of concentrated Claraia material (BC13). B) A large concentration of Claraia material at the base of the section with a sudden cutoff about a third of the way from the top of the section (BC5). C) Increasing upward concentration of Claraia material (14-29-080-20w6). D) High concentration of Claraia material increasing upward in the section (14-29-080-20w6).

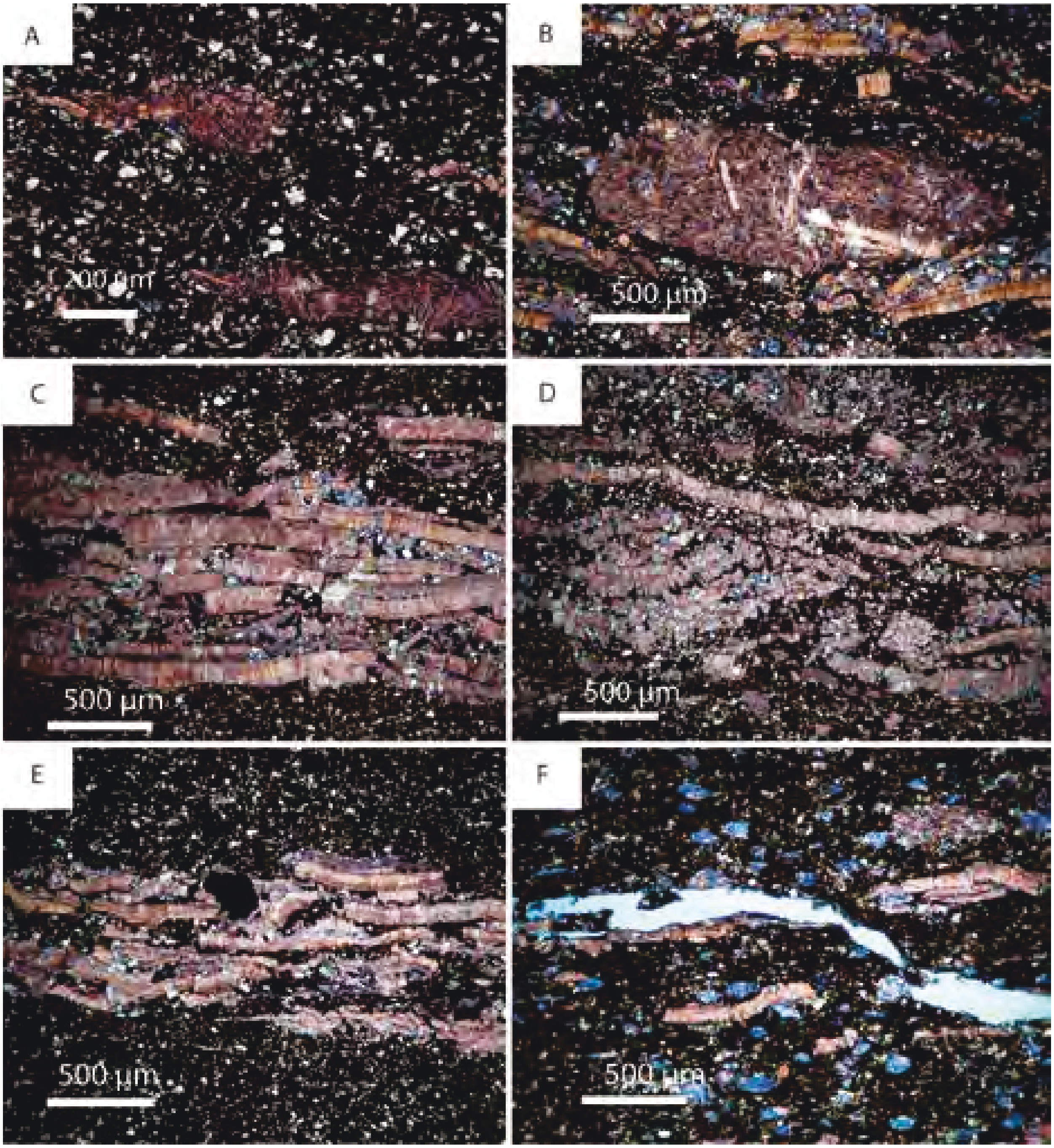
A
200 µm
B
500 µm
C
500 µm
D
500 µm
E
500 µm
F
500 µm

Figure 2.7: Thin section photographs in plane polarized light within LBS. A, B) lenses of bioclastic material from 14-29-080-20w6. C, D, E) Examples of the shell stacking pattern and the fragmented nature of the shells within LBS from A-18-D/094-A-13. F) Calcispheres alongside bioclasts with preferential dolomitization of calcispheres from A-18-D/094-A-13.

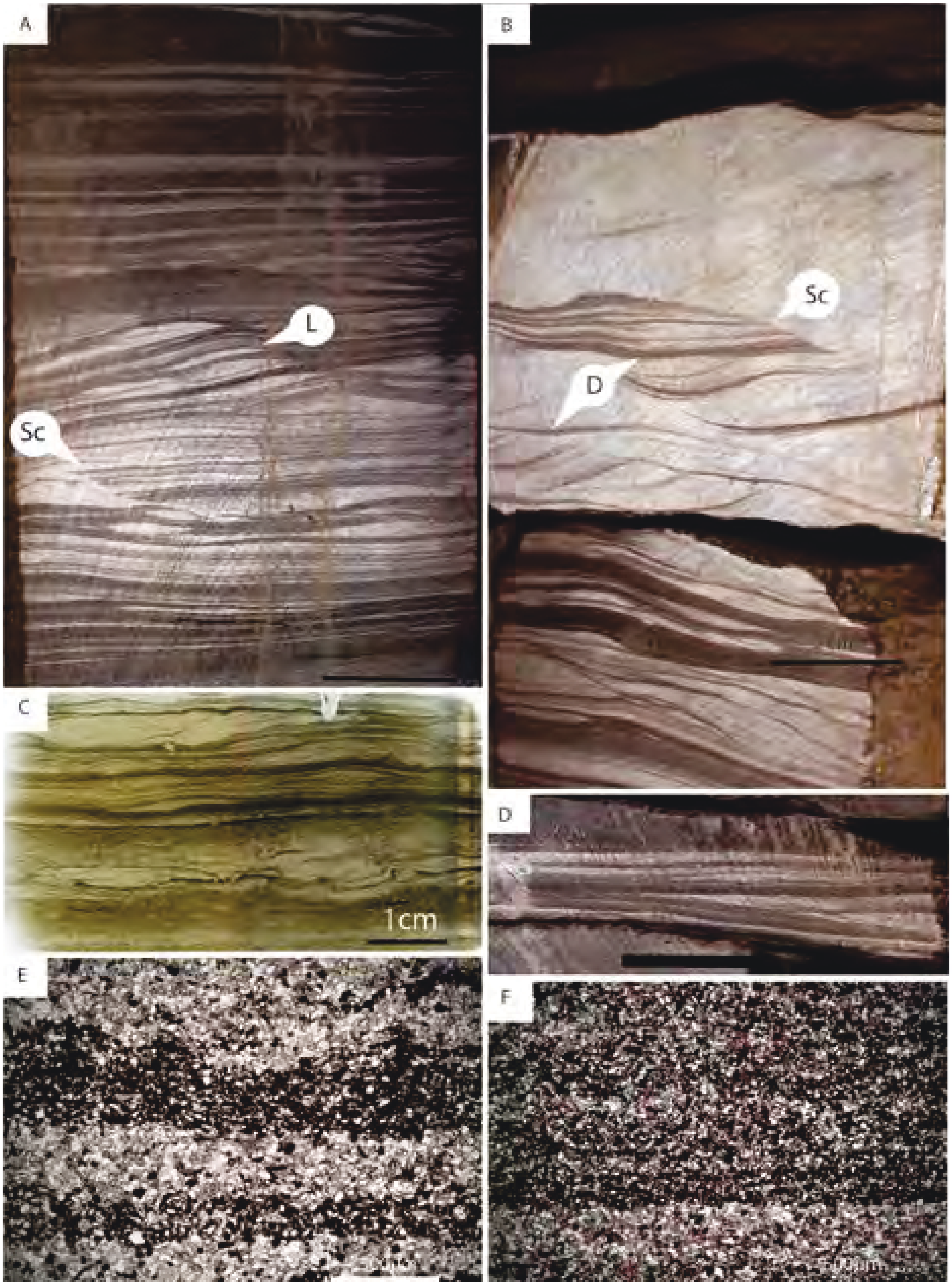
A
B
L
Sc
Sc
D
C
1cm
D
E
F

starved, but there are a few cases where climbing ripples can be identified (Fig. 2.8a, b). Scour surfaces and sharp bases are very common within the facies, with repetition of the coarse grained material overlying the fine-grained siltstone. The base of the horizon is most often a scour or a sharp contact with the facies below it. Usually the contacts at the top of this horizon are gradational and nearly always are with SL1, although this facies can be in contact with bioturbated facies as well as occur in conjunction with the heterolithic convoluted very fine sandstone to fine siltstone facies. In thin section, inverse gradin is visible occasionally within this facies, and bitumen is concentrated in the fine grained horizons. In the B-65-J/094-B-16 core, bioclasts were preserved within the coarse grained horizons of SL2 (Fig. 2.9). The coarse horizons of SL2 are often cemented by carbonate. Both the coarse and fine grained horizons are well sorted and made of angular grains (fig 2.8 e-f). The grains are primarily quartz (80%), with small portions of pyrite and clay minerals (3-5%), but the fine grained horizons typically have a higher proportion of clay that is concordant with the bedding in those horizons.

2.3.1d Calcisphere massive to laminated siltstone subfacies (CA)

This facies contains dark grey fine-grained siltstone that either appears planar laminated or massive with abundant matrix supported calcispheres (Fig. 2.10). CA horizons usually appear abruptly, but there is no evidence of erosion or scour at the base or the top of these horizons. The beds usually are no more than 20 cm in thickness-often less-, but can occur multiple times through a core. The facies usually surrounding CA are the laminated siltstone facies and the laminated bioclastic siltstone facies (Fig. 2.10). The siltstone grains can be fine to coarse and in some cases show an alternation of layers that appear as laminations. The fine grained siltstone in these layers are rich in bitumen. The minerology and nature of the grains within CA are primarily derived from the facies within which it is contained, e.g., SL1, LBS. The primary difference is the presence of calcite or dolomite nearly spherical grains (calcispheres) that are much larger than the surrounding grains (Fig 2.10d, e).

Calcispheres are observed in thin section as nearly circular calcite grains much larger than any surrounding grains by several orders of magnitude. They have been described as algal spores, radiolarians, and acritarchs, but are still generally agreed to be of unknown origin (Marszalek, 1975; Kazmierczak and Kremer 2005; Versteegh et al., 2009; Milliken et al., 2012). While describing them as radiolarians is convenient to explain the source of silica cement in the rocks they are contained within, it does not explain how they occur alongside other body fossils that have not suffered similar dissolution (Fig. 2.7f). It is more likely they were originally calcite tests.

The calcispheres can be the only calcite grains within a fine-grained siltstone or the calcisphere subfacies can be part of a bioclastic horizon. Infrequently, the calcispheres will be preferentially

---

Figure 2.8 (Previous page): SL2: Heterolithic fine grained sandstone interbedded with fine siltston A) example from 3-30-082-20w6. This example shows rapid interbedding between the two lithologies as well as multiple scour surfaces. B) Example from 08-30-082-20w6. This sample shows multiple fine grained drapes over sandstone ripples that would not be identifiable save for the fine grained material This horizon is much more discrete compared to A. (Sc) scour surface, (D) Flaser/fine grained offshoots (L) Lenticular bedding. C) Thin section view of the heterolithic structures preserved in the top part of the section, but somewhat obscured in the base of the section (IRG-SA-1412-66). D) Possible HCS feature from B-65-J/094-B-16. E) Thin section photograph of the separated coarse and fine grained sections with ripples (IRG-SA-1412-066). F) Thin section photograph of a coarsening upward sequence (IRG-SA-1412-066).

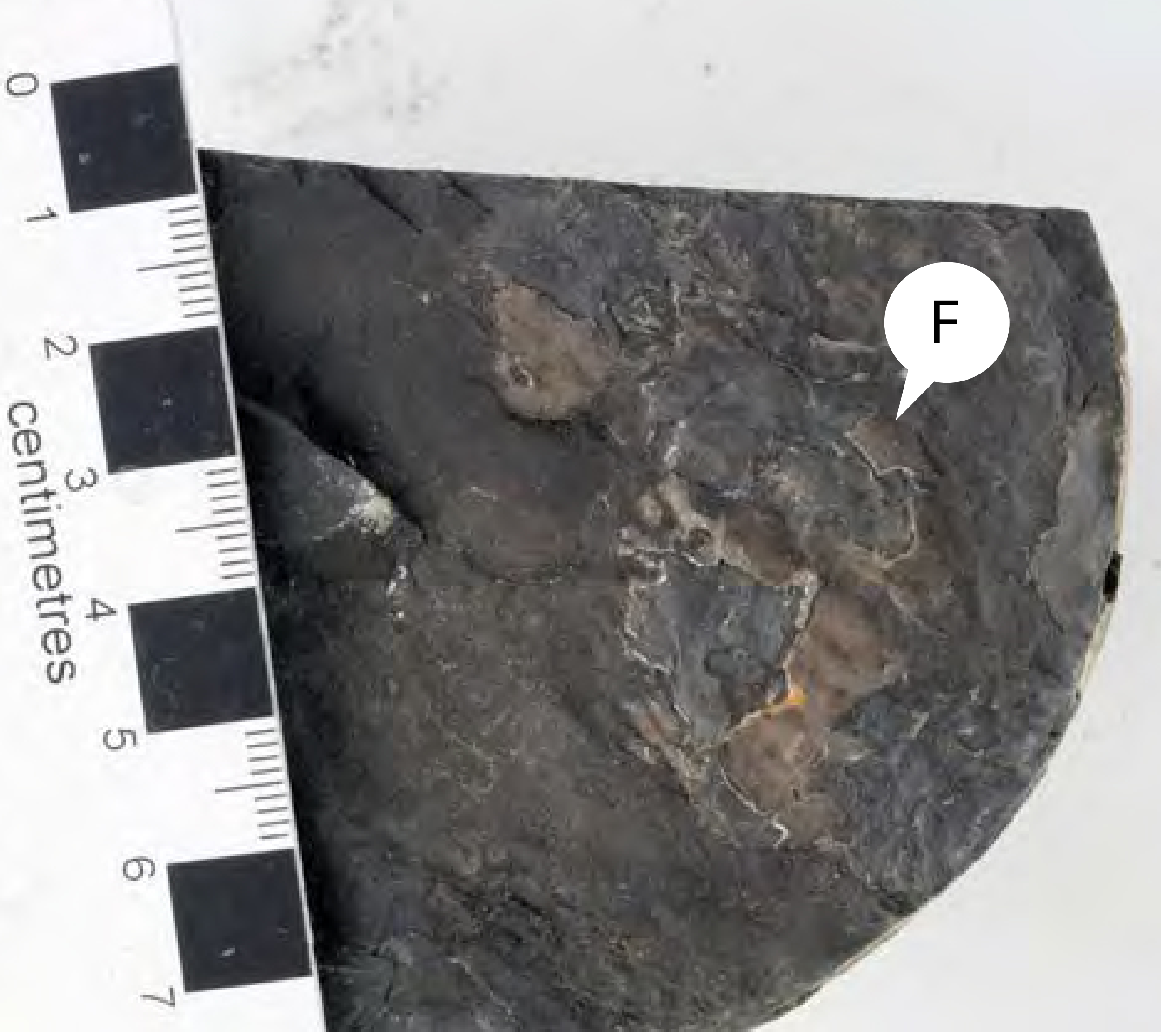

2.9: Preserved original shell material (F) on bedding plane from B-065-J/094-B-16.

dolomitized compared to the surrounding bioclastic material (Fig. 2.10d). The dolomitized calcispheres that are in the presence of unaltered calcite bivalve shells were likely dolomitized prior to deposition (Fig. 2.10d), however it is possible that in cases where both the bivalve shells and calcispheres have undergone dolomitization that it occurred after deposition as a part of diagenesis.

2.3.1e Calcite cemented concretions subfacies (CO)

These concretions often occur within SL1 and SL2. They retain the same grain size as the surrounding facies, but have been pervasively cemented with calcite (Fig. 2.11a). Bed forms are often preserved within these concretions that are not visible in the surrounding rock due to compaction (Fig. 2.11d). Individual beds can commonly be traced from the surrounding rock into the concretion, highlighting the degree of compaction in adjacent intervals. CO usually appears as ellipsoid, calcite-cemented bodies within the core and in thin section. In rare examples dolomite rims or pyrite around the margins, occur (Fig. 2.11 b, c, f, g). A few of the concretions contain a skeletal packstone which is

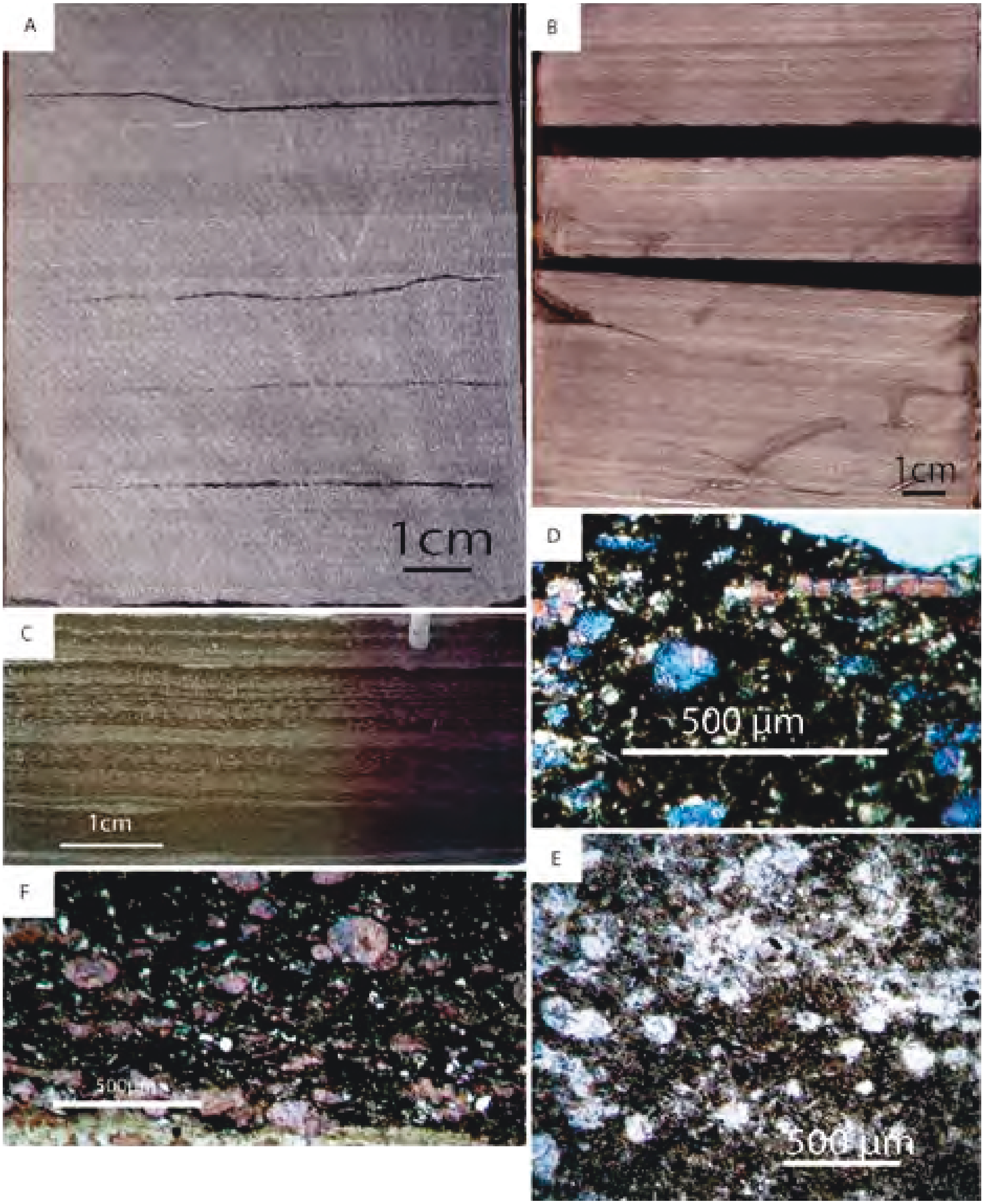

Figure 2.10: CA: Calcisphere laminated to massive siltstone. A) Macroscopic example of massive to laminated siltstone with calcispheres grading in and out from A-008-D/094-A-13. B) Another laminated siltstone with calcispheres from A-005-C/094-G-10. C) Thin section with calcispheres within laminae from C-074-G/094-B-09. D) Thin section photo of a partially dolomitized calcispheres from A-18-D/094-A-13. E) Thin section photo of calcisphere horizon (BC20). F) Calcispheres alongside bioclasts with preferential dolomitization of calcispheres from A-18-D/094-A-13.

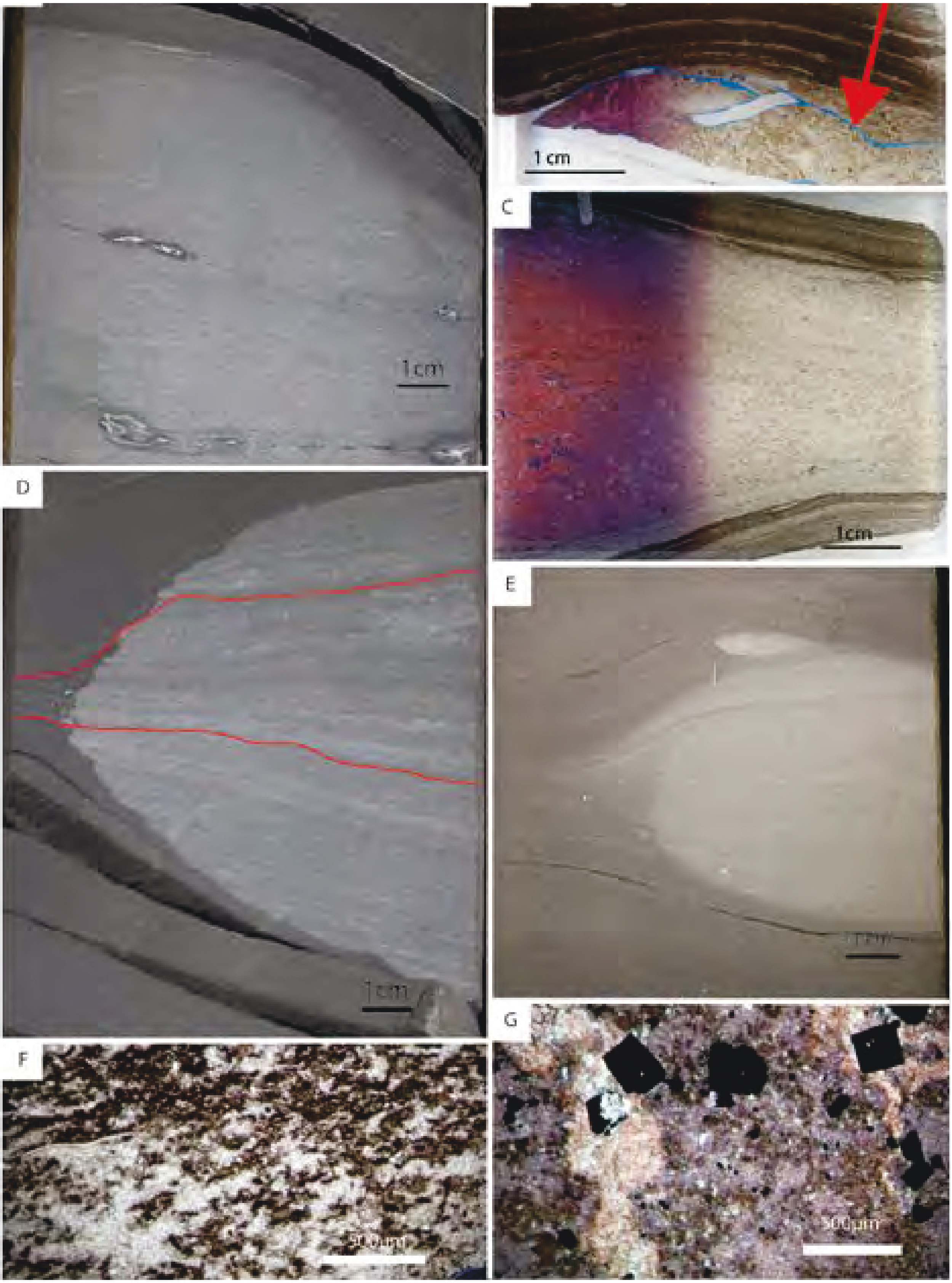
1 cm
C
1cm
1cm
D
E
1cm
1cm
F
500μm
G
500μm

very low in bitumen content and consist, at center, almost exclusively of bivalve material with randomly oriented bioclasts. The minerology of CO is typically the same of the surrounding facies, except for the calcite or dolomite cement, euhedral pyrite rim, and occasional occurrence of calcispheres, e.g., IRG-SA-1504-024 (fig 2. 1g).

2.3.1f Massive siltstone (SL3)

This facies consists of dark grey fine-grained siltstone. SL3 appears to be massive (Fig. 2.12). It is often in contact with SL1, LBS, CA, and the bioturbated/mottled siltstone. In thin section, SL3 shows no bed forms, and is primarily fine-grained silt with a high bitumen content. There is no evidence of bioturbation visible in thin section as there is no variation in lithology. There are gradational to indistinct contacts with the laminated siltstone and the mottled siltstone of SL4. It is often more identifiable in thin section than in core. The grains within the massive siltstone are much finer than those found in even the laminated siltstone of SL1. They are typically brown in color compared to the dark grey to black that seems to be found in nearly every other facies due to their high bitumen content (Fig. 2.12b, c). The grains within this facies are angular and very well sorted (Fig. 2.12d). There is no evidence of dolomite in this facies, but sometimes it has been found to surround broken *Claraia* valves. The concordance of the valves is the only aspect that hints at the bedding of the facies. The grains otherwise are primarily quartz (~70%) and a small portion of clay minerals (5-10%). There are occasional pyrite layers where the pyrite concentration can reach levels as high as 30-40% of the grains present.

2.3.1g Bioturbated/mottled siltstone (SL4)

This facies consists of dark grey, fine grained siltstone that has a mottled fabric or discontinuous laminae (Fig. 2.13). The type of bioturbation is not evident either due to lack of lithological variation, the size of the burrows, or thorough reworking of the sediment. In Figure 2.13, the burrows can be seen due to the lithological variation that surrounds the burrows in the sediment. The burrows are not identifiable in Figure 2.13 because the coarse sediment concentration is still much too small to outline the entire burrow. This facies can be found adjacent SL3 and SL1. Amount of bioturbation varies between 20-100% and is often hard to determine. In thin section this facies is distinct from the laminated siltstone and massive siltstone by the discontinuous laminations and lenses of coarse grains. It is only identifiable through that lithological variation. These small coarse grained lenses do not have much lithological difference between them and the surrounding grains other than the difference in grain size and lack of bitumen within them (Fig. 2.13c). Similar to SL1, this facies is primarily quartz (around 50-60%) with small fractions of plagioclase, clay minerals, and detrital calcite or dolomite (all around 3-5%). The grains are moderately well sorted and subangular to angular. The cement is the same between the coarse and fine grained beds, most likely silica, but often it is obscured by bitumen in the fine grained portions

---

Figure 2.11 (Previous page): CO: Calcite concretions common throughout the intervals studied. A, E) Concretions from 14-29-080-20w6 that do not show an internal fabric. B) Concretion from C-074-G/094-B-9 that shows pyrite (red arrow) around the edge of the concretion. C) Concretion from C-007-J/094-B-8 that shows the variation in calcite to dolomite through the concretion. Both thin sections B and C were half stained with a double calcite stain. D) Concretion from 14-29-080-20w6 in which one can follow the beds from outside of the concretion through it. F) Thin section photo of the edge of a concretion (BC19). G) Euhedral pyrite around the rim of a calcite cemented concretion (BC19).

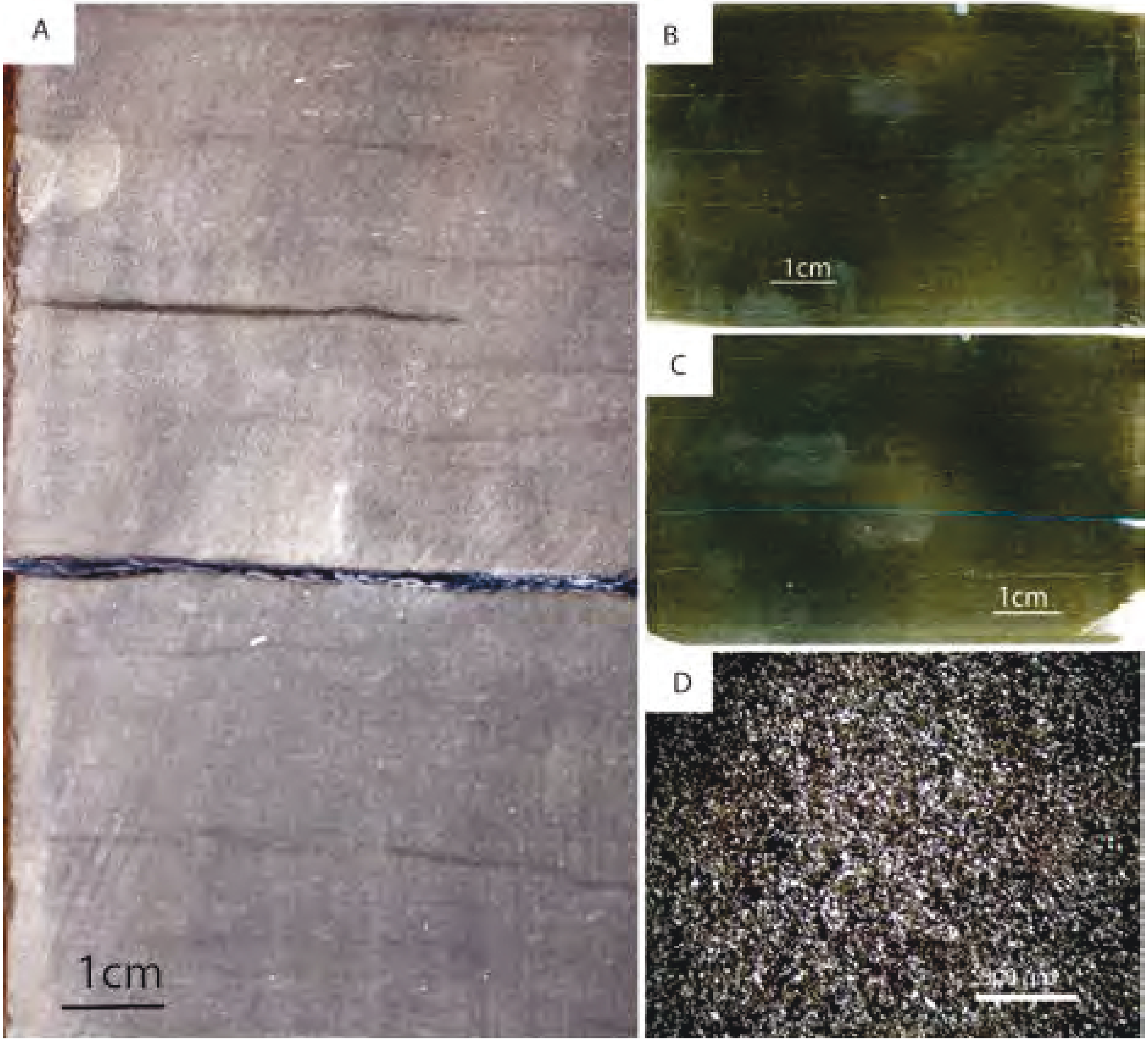

Figure 2.12: SL3: Massive siltstone facies. A) a-005-C/094-G-10 B, C) 14-29-080-20w6 Massive fine grained bituminous siltstone that shows no evidence of bioturbation. These thin sections exhibit a brown coloration not seen in other sections. D) Thin section photo of massive fine grained siltstone (IRG-SA-1412-036).

2.3.1h Heterolithic convoluted laminated fine to coarse siltstone (SL5

This facies consists of heterolithic, white to light grey, coarse grained siltstone and dark grey, fine grained siltstone (Fig. 2.14). The bed forms in SL5 have been effected by soft sediment deformation which in some cases has completely removed traces of the original structures, and in others only slightly contorted the beds. Figure 2.14a shows both an isolated convolution and figure 2.14b shows the overwhelming imprint of the convolution on the core. These beds usually occur in conjunction with SL2, as well as SL1, and often show evidence of scour surfaces throughout the facies and at the base of the beds. Similar to SL2, bitumen in this facies is concentrated in the fine grained layers. Figure 2.14c, d shows that the convolutions can occur on a microscopic scale as well as on the macroscopic scale. It is possible, as observed in thin section, for the horizon to be completely disturbed so that the bedding is lost, as well as for the bedding to be only slightly disturbed from its original orientation. Some

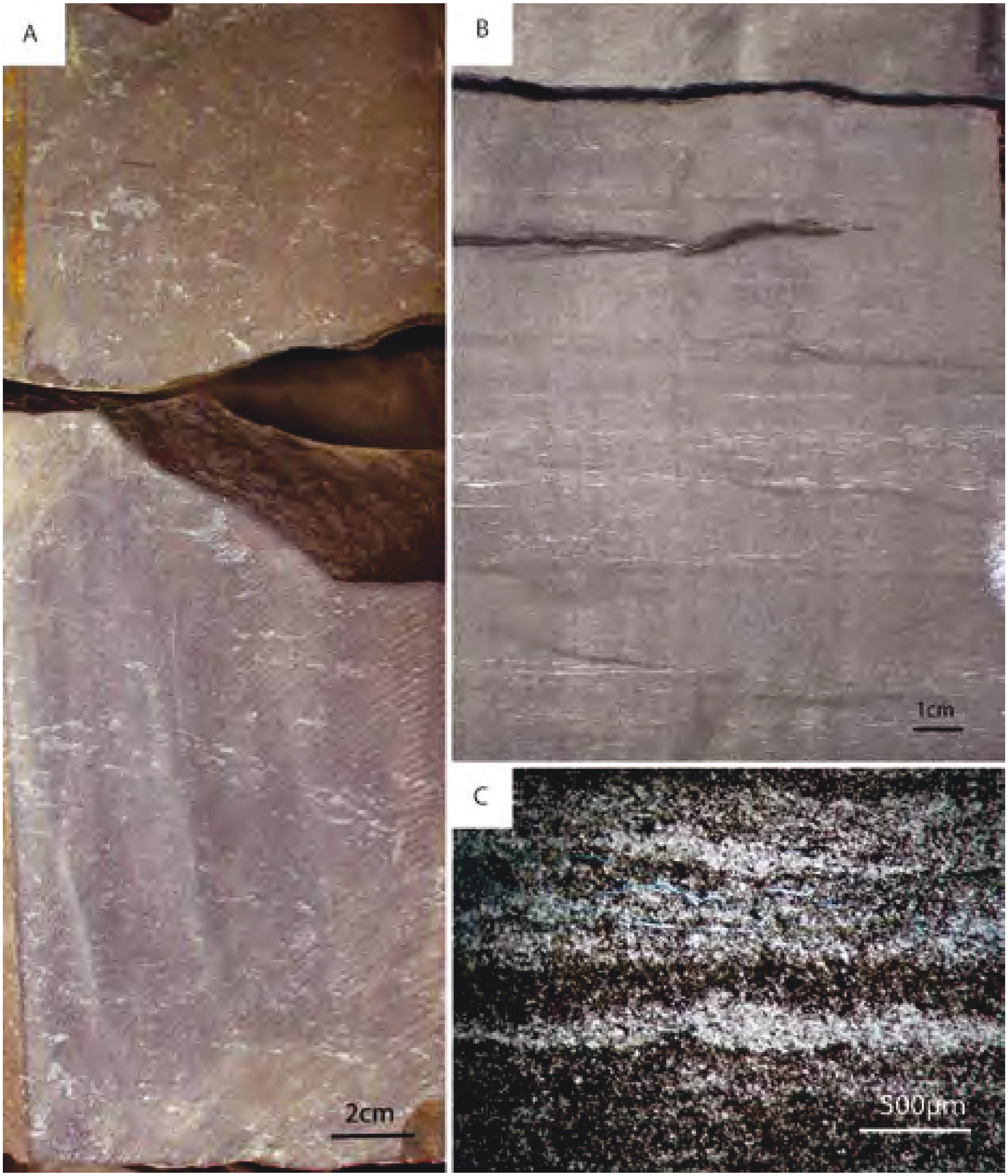

Figure 2.13: SL4: Bioturbated/Mottled siltstone. A) A08-07-085-18w6 shows bioturbation induced mottling of the sediment. B) Example from A-005-C/094-G-10 which shows unidentifiable burrows visible due to lithological variation in the siltstone. C) Thin section photograph of the coarse grained lenses and discontinuous coarse and fine grained layers (IRG-SA-1412-025)

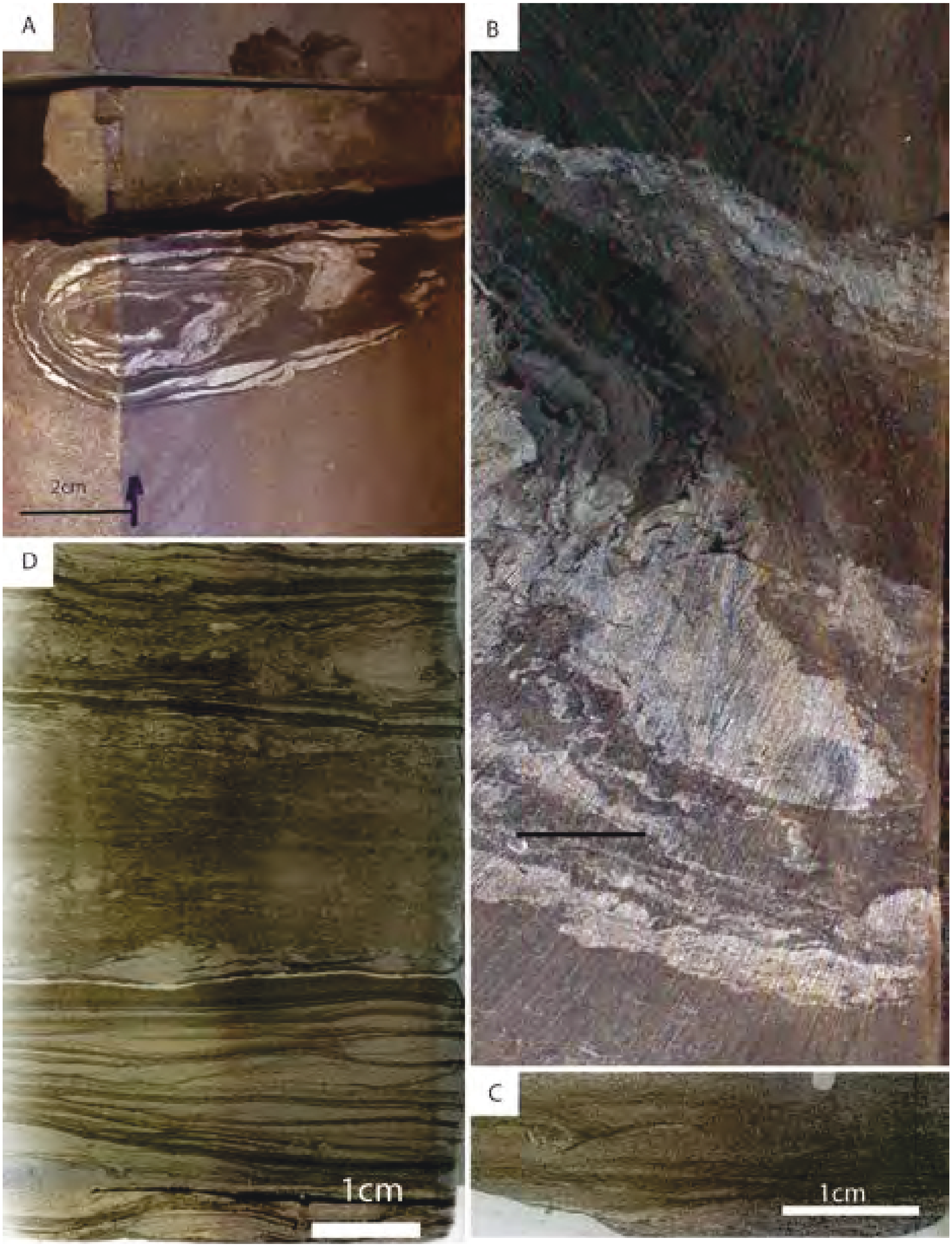
A
2cm
B
D
1cm
C
1cm

of the more complete disturbance could have been derived from bioturbation (Fig. 2.14d). This facies is mIneralogically similar to SL2, and could be classified as a subfacies of it. There is often calcite cement in the coarse horizons, and the grains are primarily composed of quartz grains that are angular and well sorted when the beds are still intact. The sorting is disturbed extensively when the beds have been erased. In those cases, the sorting becomes very poor, and the texture of the bed becomes homogenous.

2.3.1i *Planolites* bioturbated siltstone (BF1)

This facies mainly consists of heterolithic light grey coarse grained siltstone and dark grey fine grained siltstone (Fig. 2.15a-c). *Planolites,* and sometimes *Phycosiphon,* are visible due to the lithological difference and usually the burrows disturb approximately 30% of the sediment. The burrows disrupt the laminae, and the *Planolites* burrows are around 0.5cm in diameter or less (Fig. 2.15c). BF1 grades in and out of SL2, and is only present in a few cores, e.g., C-060-C/094-A-13. The burrows are found to be flattened in thin section (fig 2.15c), and are made up of the coarse grained portion of the sediment This facies is much more common outside of the ”*Claraia* Zone” than it is within the zone, particularly close to the boundary with the Upper Montney and to the east near the Turbidite intervals of the Middle Montney. The minerology of this facies is similar to the rippled to laminated heterolithic very fine sandstone to fin siltstone, but it does not show evidence of calcite cementation (Fig 2.15d). It is made primarily of quartz grains that are well sorted, but angular, with small portions of clay minerals that are more prevalent in the fine grained beds.

2.3.2 Identifiabl taxa

The primary identifiable taxa within the cores are pectinoid bivalves, ammonoids, and rare vertebrate material, particularly *Listricanthus* spines. Using the classification outlined by Newell and Boyd (1994), the most common bivalves found within the cores were *Claraia* cf. *clarae* and *C.* cf. *stachei.* Both occur below, within, and above the “*Claraia* Zone”. The bivalves were identified primarily on shape and the external ornamentation as all of the examples documented within and around the “*Claraia* Zone” were impressions. None of the samples included a complete hinge line or internal view to provide a clearer identification (Fig. 2.16). Similarl , few ammonoids were found which were not preserved as impressions and those that are calcified are only crudely preserved. Only two ammonoid impressions still preserved the suture pattern, one of which appeared to be a new taxon, and a second identified herein as *Wordeioceras wordiei* in A-18-D/094-A-13 (Fig. 2.17 a, b). Therefore, most of the identifications were based on shape and coiling pattern, and can only be so reliable. Nevertheless, cf. *Ophioceras* sp. were observed in many cores, supporting the interpretation of this horizon within the *Ophioceras* zone of the Late Griesbachian, based on ammonoid and bivalve biostratigraphy (Tozer, 1994; Balini et al, 2010; McRoberts, 2010). However, this age assignment does not hold up with conodont biostratigraphy conducted by Golding et al. (2014) on the 16-17-83-25w6 core and the location of the “*Claraia* Zone” within the core (Progress energy, unpublished report). According to biozonation of Golding et al. (2014), the “*Claraia* Zone” falls within the Late Deinerian *Neospathodus cristagalli* zone.

Figure 2.14 (Previous page): SL5: Soft sediment deformed heterolithic coarse grained siltstone and fine grained siltstone. A) An isolated feature in A08-07-085-18w6. B) The strata is more completely convoluted from A-07-19-085-15w6. C) Thin section showing near complete convolution of the heterolithic beds (BC16). D) The middle of this thin section shows convoluted texture while the outer beds still retain the bedforms (IRG-SA-1412-066).

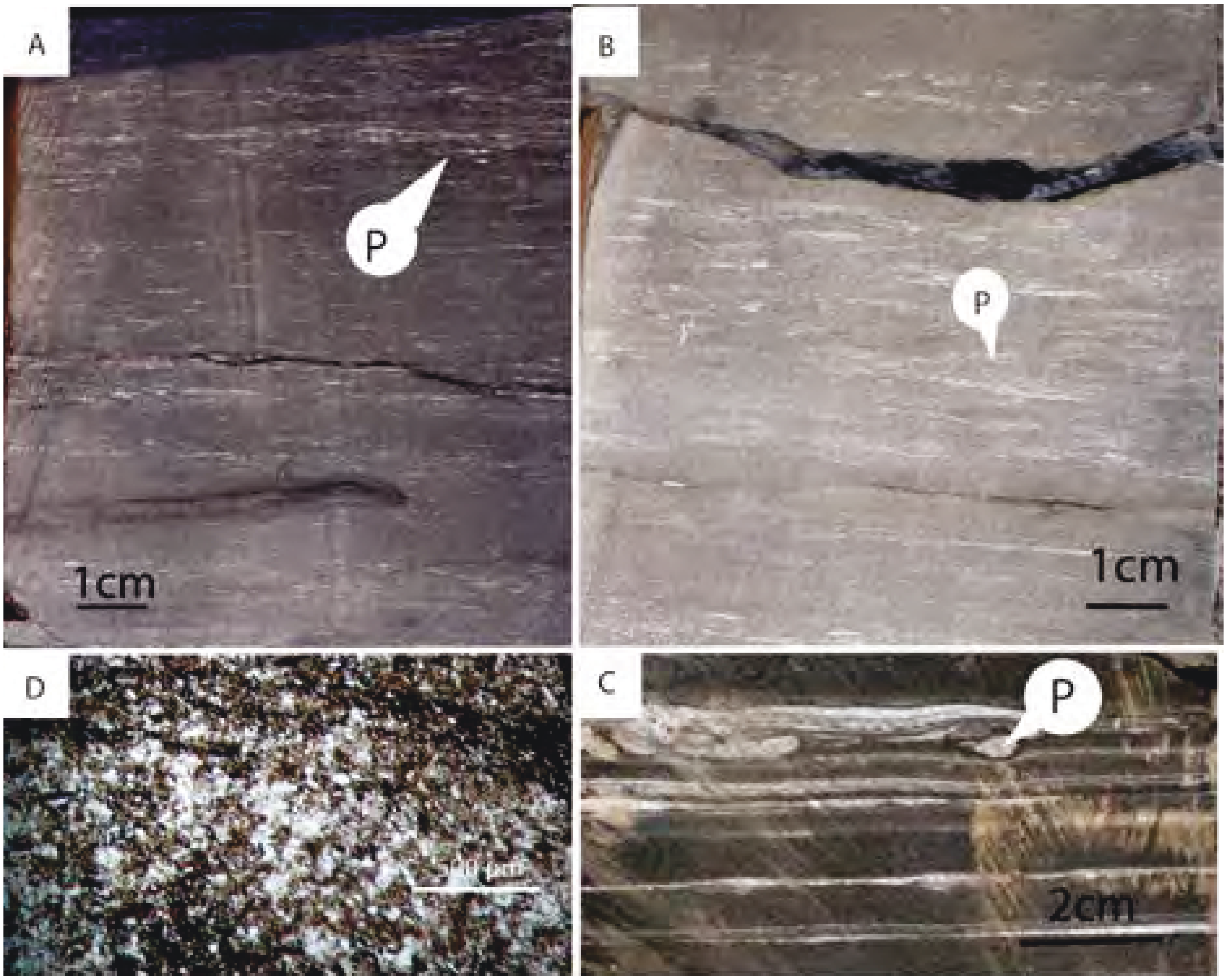

Figure 2.15: BF1: Planolites bioturbated siltstone. A) A-005-C/094-G-10 B) A-005-C/094-G-10 Layers of Planolites bioturbated siltstone with very little lithological variation. C) B-065-J/094-B-16 Planolites in discrete sand layers within fine grained siltstone. (P) Planolites. D) Planolites burrows preserved in the coarse grained horizon that have been slightly flattened (BC26)

2.4 Discussion

2.4.1 Bioclasts

The bioclastic beds in the "*Claraia* Zone" cannot be attributed to event beds, as has been done in some other bioclastic accumulations in shale and siltstone dominated successions, such as the Mississippian Barnett Shale of Texas or the Triassic *Claraia* beds of the Western United States (Utah, Idaho, and Wyoming) (Boyer et al, 2004; Milliken et al, 2012). Some of the beds are not sharp based, and there are several occurrences where the ratio of shell material to clastic sediment gradually increases upwards in the cores. This indicates that these beds are most likely not formed through event deposition (e.g., turbidites, tempestites). However, the shell material has been sorted by size and is very often disarticulated (Fig. 2.16). In thin section, LBS is often made up of highly fragmented material; although the shells in LBS are thick in comparison to other bioclastic horizons. The fragmentation and size sorting may indicate the shells in these units have been transported. The shells in this horizon are infrequently seen in a vertical stacking pattern (Fig. 2.7), but it is unlikely that storms alone would have caused this stacking

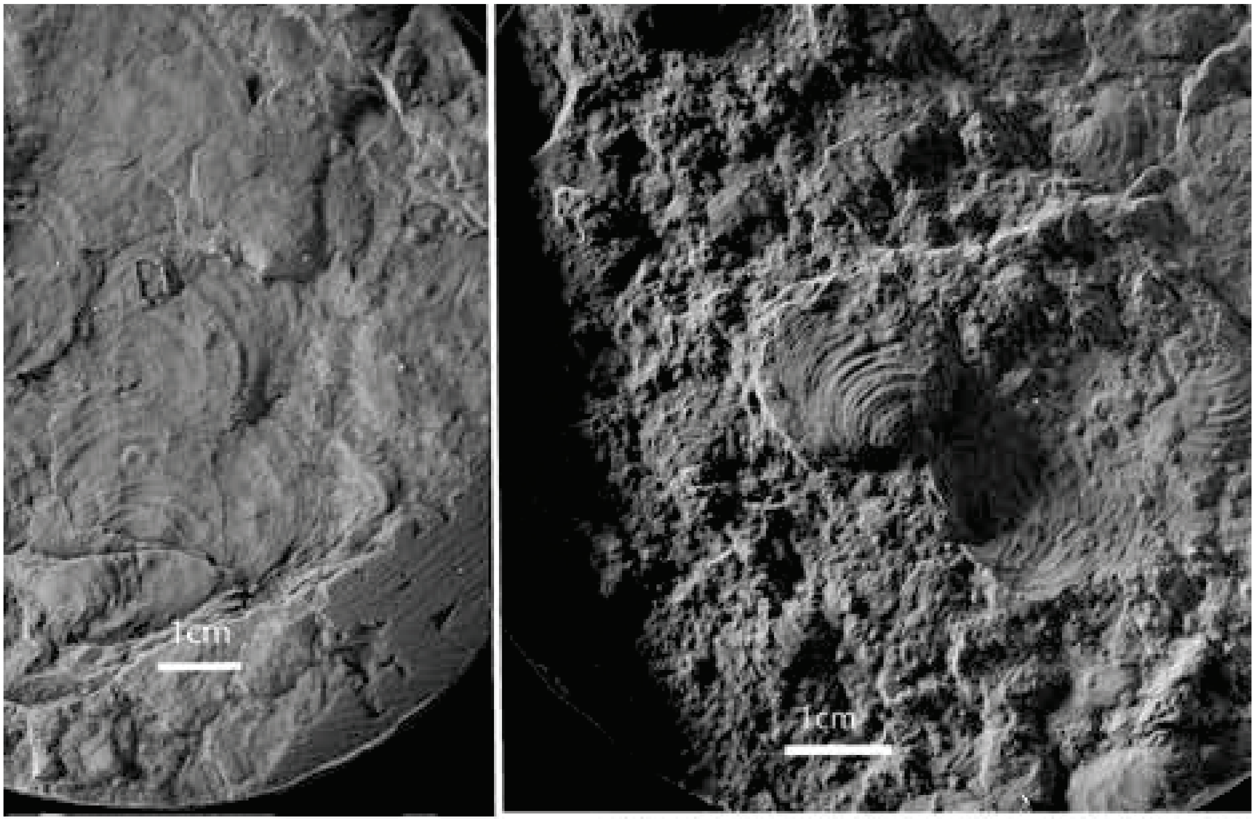

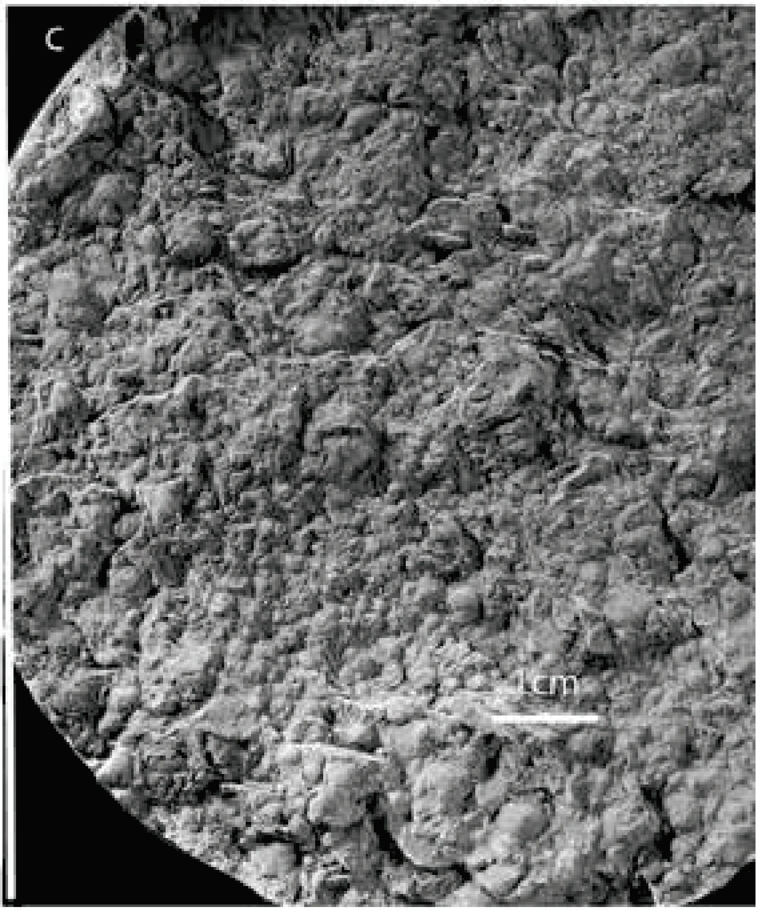

Figure 2.16: Bedding plane impressions of Pectinoids. A, B) B-50-H/094-B-16 showing large valves that are somewhat fragmented and disarticulated. C) B-50-H/094-B-16 showing small very fragmented valves.

Figure 2.17 (Opposing page): Ammonoids from various cores near the “Claraia Zone”: A) New ammonoid from A-10-J/094-B-9 B) Wordeioceras wordiei from A-10-J/094-B-9 C, E) Ophioceras sp. from 08-30-082-20w6 D) Ophioceras? From A-005-C/094-G-10 surrounded by Pectinoids.

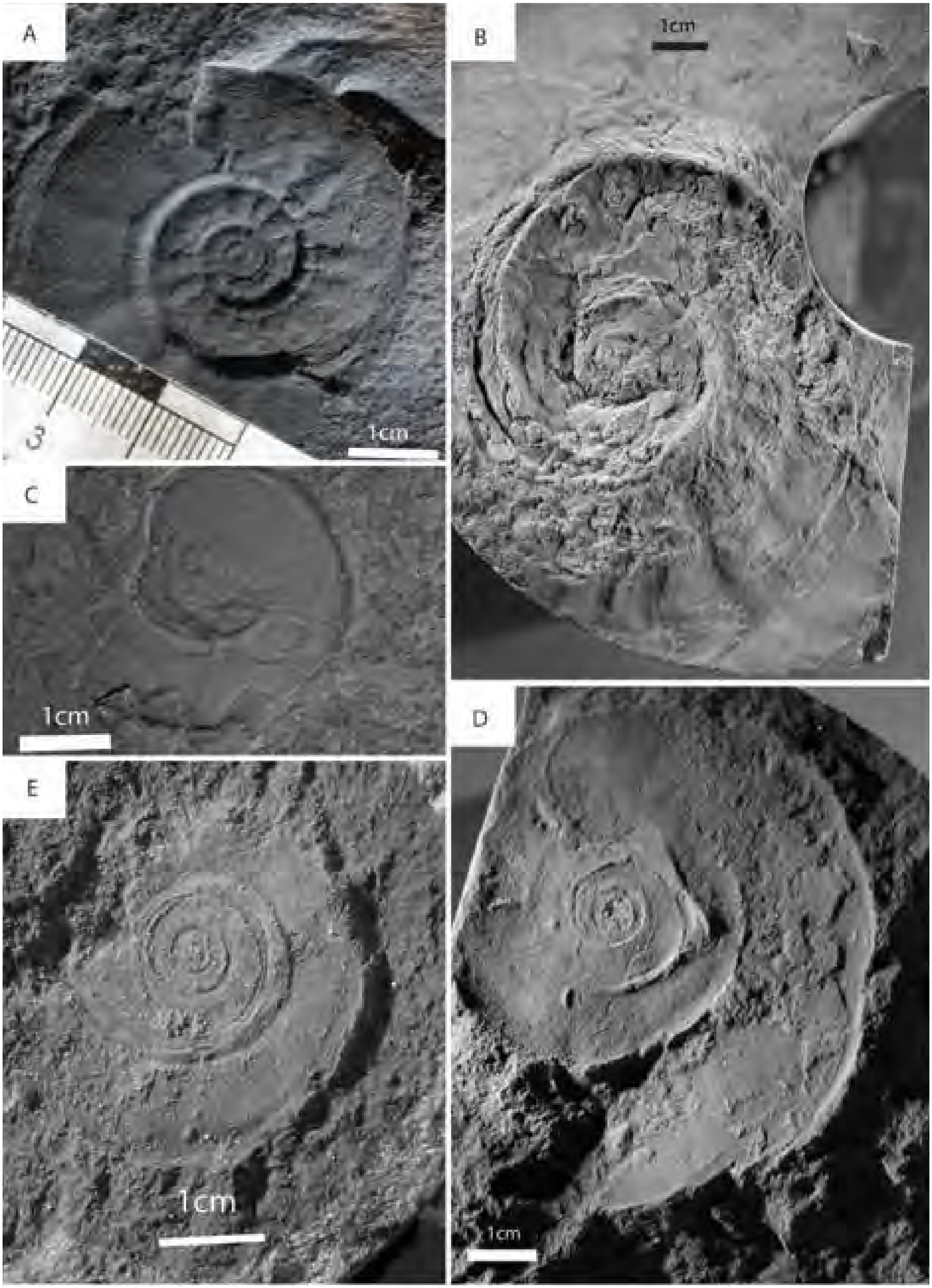
A
B
1cm
3
1cm
C
1cm
D
E
1cm
1cm

pattern as suggested by Kidwell and Boscense (1991). Winnowing would have reduced the fine grained sediment surrounding the bioclasts, and could just as easily have concentrated the bioclasts in the beds as a shell pavement (Kidwell and Jablonski, 1983). Storm influence, howeve , may be substantiated by the rare HCS horizon within SL2 (Fig. 2.8d).

Kidwell (1986) noted that differences in sediment accumulation and bioclast contribution are the main factors which influence grading in bioclastic units such as the *Claraia* Zone". As mentioned previously, the abundance of bioclasts in core frequently increases up section (Fig. 2.5; Fig. 2.6). It appears the percent abundance of bioclasts in the section can increase from around 10-20% up to 50-60% of the rock volume (Fig. 2.6). Therefore, there is an increase in bioclasts into the system and/or a decrease in clastic input to form these bioclastic zones.

An additional factor could be a chemical preservation bias due to increased CCD and ACD (Woods, 2005; Zonneveld 2011). This theory may explain the occurrence of shells with preserved carbonate within the "*Claraia* Zone", and the occurrence of bivalve impressions devoid of preserved carbonate in other Montney horizons. This clearly indicates a bias in fossil preservation, even without external evidence in the form of geochemical data, which have presently been difficult to find due to t lack of useful sources of isotope data. In fact, most of the bedding planes that were used to identify the fossils within the horizons were impressions that were either found outside of the horizons or between the cemented layers within the horizon.

Chemical changes alone are not likely the reason why the bioclasts appear concentrated in the "*Claraia* Zone". Winnowing of clastic material, non-deposition, could be attributed both to the fragmentary and disarticulated nature of the bioclasts, both observed within the laminated bioclastic facies (LBS) and on other bedding planes. The bioclast fragments are primarily in a random arrangement and with no indication that two adjacent fragments are from the same valve (Fig. 2.7). Rarely, the fragments are closely spaced and can be followed along what was once a complete valve which is evidence of compaction (Zuschin et al., 2003). Another mechanism for these accumulations to occur would be an increase of shell input due to sudden recolonization during oxygenation events, and/or subsequent die off of a single generation. Howeve , fragmentation, as is seen in thin section and core bedding planes, is unusual for an assemblage that would have remained in place, therefore it is more likely these bioclasts have been transported from their original habitat in an ongoing process.

It was originally hypothesized that the bioclasts appear through this specific interval due to an oxygenation event. However, current evidence from sulfur isotope data indicates that is likely that this was an oxic environment even before the "*Claraia* Zone" (see Appendix A). Therefore, it is likely that oxygen was not the limiting factor on the appearance of bioclasts.

2.4.2 Facies Association and Paleoenvironmental Interpretation

The contacts found between each facies can be found in Table 2.3. The calcisphere siltstone and the calcite cemented concretions are considered to be subfacies as they are found within other facies and do not occur separately. Therefore, they are marked as occurring within (ow) on the table.

		SL1	LBS	SL2	CA	CO	SL3	HB	SL4	SL5	BF1
Laminated Fine siltstone	**SL1**	■	g/s	s/c	s/g/ow	ow	g	s/g/c	g/c/s	s/g	g
Laminated bioclastic siltstone	**LBS**	g/s	■	s/g	s/g/ow	ow	g/s			s/g	
Heterolithic rippled to laminated siltstone to very fine sandstone	**SL2**	s/c	s/g	■	g/ow	ow		s		g	
Laminated to massive calcisphere siltstone	**CA**	s /g/ow	s/g/ow	g/ow	■						
Calcite cemented concretions	**CO**	ow	ow	ow		■		ow			
Massive siltstone	**SL3**	g	g/s				■	s/c	g		
Massive Bioclastic Packstone	**MBP**	s/g/c		s		ow	s/c	■			
Bioturbated mottled siltstone	**SL4**	g/c/s					g		■		
Heterolithic convoluted laminated siltstone and vf sandstone	**SL5**	s/g	s/g	g						■	
Planolites Bioturbated siltstone	**BF1**	g									■

Table 2.3: Summary of contacts between each facies in and around the “Claraia Zone”. G = gradational, S = sharp, C = scour, OW = occur within.

2.4.2a Proximal bottom current modified deposit

The sand associated with the heterolithic facies within the formation (e.g., SL2, SL5, and BF1) was likely sourced from turbidite fans or tempestites, the evidence of which is discussed later, similar to those found by Shanmugam et al. (1993a) (Fig. 2.18a). It was then reworked by discontinuous bottom currents to create the isolated rippled features that are found within several of the facies (Ito, 1996; Viana et al., 1998; Stow et al., 2002). The discontinuous nature of the bottom currents, likely caused by storms or variations in wind intensity, allowed for the background deposition of the laminated siltstone and massive siltstone (SL1, SL3, and SL4) to develop between the deposition of the sand layers (Hollister and McCave, 1984; Faugeres et al., 1993; Shanmugam et al., 1993a). This facies association is found in many cores, both within and outside of the "*Claraia* Zone", and likely was an ongoing mechanism in the deep basin parts of the Montney Formation (Fig. 2.19).

SL2 shows evidence of structures produced by traction deposition (e.g., starved ripples etc.) in the very fine sand horizons that are interbedded with fine-grained siltstone, which was deposited fro suspension. Shanmugam et al (1993a) identified similar traction structures in the Pleistocene of the Gulf of Mexico, and attributed these structures to the Loop Current, a wind driven current that runs through the gulf. The structures observed in SL2 are remarkably similar to Pleistocene examples, displaying isolated sand beds with mud drapes on the ripples, starved ripples, mud offshoots, flas , and lenticular bedding (Shanmugam et al 1993a, b). Similarly, these facies appear in what should be a more distal / offshore portion of the Montney formation (as can be seen in Fig. 2.1).

Deposits interpreted as turbidites were found in two cores that are located much further east from the "*Claraia* Zone" (5-27-85-15w6, 07-19-085-15w6) and turbidites have been identified in the heart of the Peace River embayment within a series of structurally controlled basins (Davies et al., 1997; Moslow, 2000). Coarse-grained sediment in SL2 could have been sourced from such turbidites, and cores such as B-65-J/094-B-16, which contain SL2, could be located more proximal to the turbidity current deposits similar to the bottom current reworked interchannel sequences identified by Shanmugam (1993) and Ito (1996) or from storm input. Bioturbation is a prevalent method used to identify bottom current deposits (Stow et al, 2002), but is not applicable in this case. Bioturbation is rare within the Montney Formation for various reasons mentioned previously. However, the presence of bioturbation in specific facies related to this facies association (e.g., SL4 and BF1) falls in line with the popular idea that bioturbation is a required feature of a contourite/bottom current deposit (Stow and Faugeres, 2008).

2.4.2b Distal bottom current modified deposit

The absence of the sand within the laminated bioclastic siltstone and the siltstone facies surrounding LBS evidences that this facies association was deposited distal to any source of coarse grained sediment (Fig. 2.18b). In this distal facies association, due to the absence of coarse grained sediment, bioclasts were winnowed and concentrated by the same bottom currents that likely produced the previous facies association (Kidwell and Bosence, 1991). The bioclasts similarly accumulate in discrete horizons (LBS) that are separated by the laminated siltstone, mottled siltstone, and massive siltstone. Even outside of the LBS horizons, impressions of bioclasts are present in the laminated siltstone horizons. These impressions show evidence of fragmentation and size sorting (Fig. 2.16). It is likely that the bioclasts preserved as impressions underwent the same depositional mechanisms as those in the

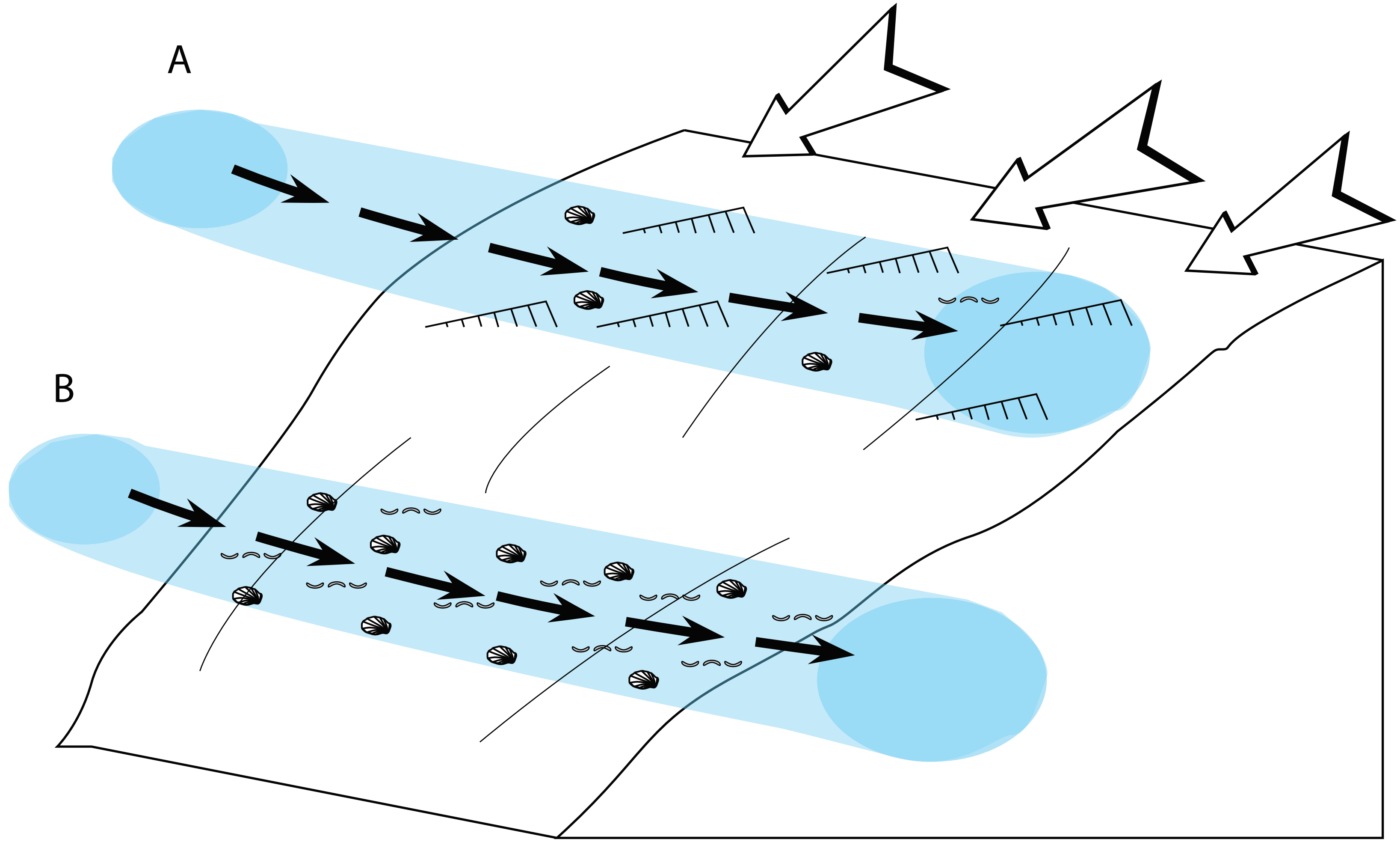

Figure 2.18 (Opposing page): The bottom current depositional environment with the current shown producing the two different facies associations. A) Represents the fan derived bottom current modified deposits that are closer to the source input of coarse grained sediment (arrows). When the current is active (blue) bivalve shells and ripple structures are created, with suspension sedimentation between current activity. B) Represents the distal bottom current modified deposits where winnowing of fine grained sediment with the deposition of bivalve material in concentrated horizon by the current activity (blue).

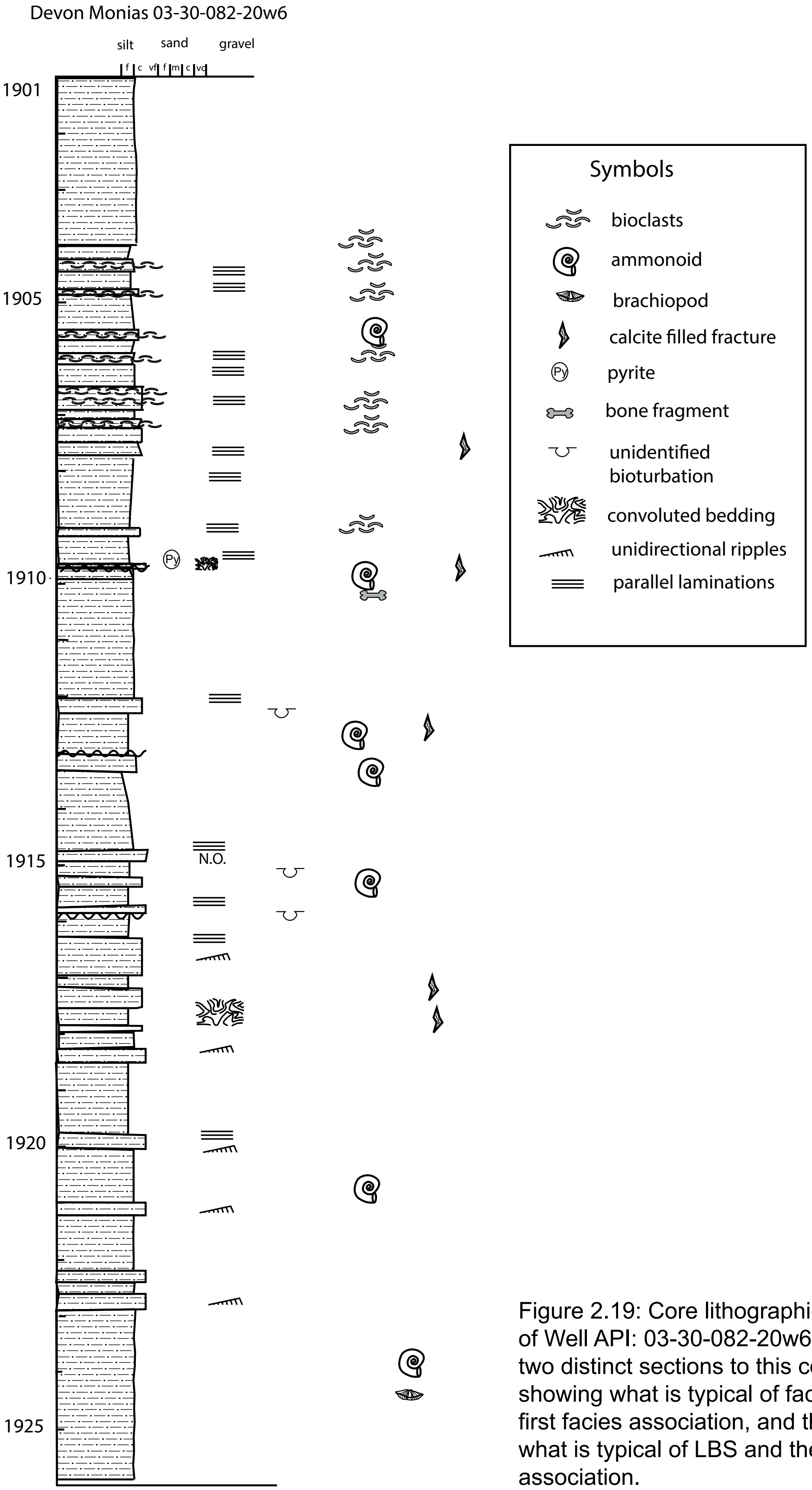
Devon Monias 03-30-082-20w6
silt
sand
gravel
f
c
vf
f
m
c
vc
1901
1905
1910
1915
1920
1925
Py
N.O.
Symbols
bioclasts
ammonoid
brachiopod
calcite filled fracture
pyrite
bone fragment
unidentified bioturbation
convoluted bedding
unidirectional ripples
parallel laminations

Figure 2.19: Core lithographic description of Well API: 03-30-082-20w6. There are two distinct sections to this core: the lower showing what is typical of facies SL2 and the first facies association, and the upper showing what is typical of LBS and the second facies association.

“*Claraia* Zone”, hinting at the prevalence of the process through at least this time interval. This also may help to explain mechanisms that influence younger bioclastic deposits in the formation, such as those discussed in the next chapter.

While no bivalve dominated contour current deposit has been identified within the literature, there are several instances where foraminifera, diatoms, radiolarians, and other bioclastic material has been a part of contour current beds or been the main constituent of the beds (e.g., Viana et al., 1998; Zhenzhong et al., 1995; Faugeres and Stow, 2008; Stow and Faugeres, 2008). The bioclastic material in these deposits is often highly abraded similar to what is see in the “*Claraia* Zone” (Faugeres and Stow, 2008; Stow and Faugeres, 2008). Additionally, one of the factors used in differentiating bottom current deposits from other depositional mechanisms is the presence of sharp contacts at the top of beds, a common feature in both FA1 and FA2 (Hollister, 1967).

All of the strata within the fine siltstone facies have been compacted and do not preserve any sedimentary structures beyond lamination, therefore it has been necessary to derive conclusions about the depositional environment from the surrounding facies. Similar to FA1, LBS will often have repetition of the bioclastic intervals, with sharp contacts sometimes occurring mid facies. The facies is repeated again above the contact, often with an increased bioclastic component. This repetition of facies and scour at the top of beds is one of the criteria Shanmugam et al (1993a; Shanmugam, 1997) used to isolate the current reworked deposits from the nearby turbidite deposits. The repetition within FA1 and FA2, as well as the common sharp tops and scour surfaces further supports the interpretation that both of these deposits are the result of the same depositional mechanism.

The “*Claraia* Zone” is typified by the laminated bioclastic facies (LBS) and A2, but LBS often grades in and out with the laminated siltstone facies (SL1), the massive siltstone facies (SL3), and the calcisphere siltstone subfacies (CA). The calcispheres, which are characteristic of CA, also occur intermixed with the LBS bioclasts as observed in the 03-30-082-20w6 core (Fig. 2.10d, f). The same horizon is expressed as a ripple to laminated heterolithic siltstone to fine grained sandstone with one occurrence of a possible HCS bed in the B-65-J/094-B-16 core (Fig. 2.8d). In 03-30-082-20w6, the core it grades out of the rippled to laminated heterolithic very fine sandstone to fine siltstone (SL2) and th convoluted heterolithic very fine sandstone to fine siltstone (SL4) into what is typically seen in the *Claraia* Zone” (e.g., LBS) (Fig. 2.17).

In B-65-J/094-B-16, bioclasts are preserved within the coarse grained horizons, and in one example original shell material was preserved on a bedding plane (Fig. 2.9). This preservation is not shown in other wells with similar heterolithic material outside of the “*Claraia* Zone”, and indicates FA1 in this well is actually another representation of the “*Claraia* Zone”. The actual appearance of the shell material should be attributed to something besides the depositional environment, as mentioned above. The coarse grained sediment in SL2 may represent deposition closer to the sediment source, or closer to the contour current itself, compared with LBS (Shanmugam et al., 1993a). It is also noted that there are current ripple structures within LBS in A-18-D/094-A-13, which further substantiates this explanation. Inverse grading within this lithofacies further supports the bottom current modification/deposition interpretation (Fig. 2.8f). LBS could be argued to exhibit this in the gradual increase in bioclastic component at the base and within some sections (Fig. 2.5a).

2.4.2c Bottom Current Deposition

Contourites are currently defined to be the deposits of bottom currents in a broad sense, although the original definition of the term was specific to deposits formed by contour currents, currents tha followed sea floor contour surfaces (Heezen and Holliste , 1964; Hollister, 1967; Stow et al., 2002). The broadening of the term came about due to the difficulty/impossibility of determining depths in ancien deposits, however the term is still rife with problems in defining the limits of what is a contourite (see Rebesco et al., 2008). Therefore the author chose to follow the example of Shanmugam et al. (1993) and refer to the "*Claraia* Zone" deposits as bottom current deposits, as that is the mechanism that formed them.

Stow et al. (1998) proposed three stages of criteria for recognizing contourites/bottom current deposits in modern and ancient systems at three different scales (small, medium, and large). The small scale, representing sedimentary analysis is addressed above. The large scale takes into context the basin as a whole. A thermohaline current did likely occur offshore of Pangea within this area (Kutzbach et al, 1990), but these deposits cannot be related directly to a thermohaline current as they are likely shallower than most thermohaline deposits. There are other forces such as wind, which can drive bottom currents. There have been many studies which show the likelihood of mega monsoons and westerlies that affected Pangea along its western margin (Loope et al, 2004; Barron, 1989; Kidder and Worsley, 2004). Therefore, the likelihood is higher that these are deposits of wind driven currents, which, in the Gulf of Mexico, can still create high velocities at depths as deep as 100m (Cooper et al, 1990). The medium scale can be related to the exploration scale of seismic interpretation. The "*Claraia* Zone" has been identified as trending parallel to the paleo-shoreline, and typically occurs shallower in the subsurface eastwards towards the shoreline (Fig. 2.20, 2.21). The "*Claraia* Zone" is fairly uniform in thickness, and is similar to the slope-plastered sheets described in Faugeres et al, (1999), Stow (2001), and Stow et al. (2002).

The taphonomic evidence, as discussed above, further supports this interpretation. Fragmentation, size sorting, and disarticulation provides evidence of transport of the bioclasts. An accumulation of bioclasts requires either a sudden increase in bioclasts being introduced to the system with a stable sedimentation rate, or a decrease in sedimentation with constant input of bioclasts. Winnowing would explain the accumulation of bioclasts. Winnowing, a primary mechanism in bottom current deposition, is one of the methods in which LBS could be deposited.

It was mentioned at the beginning of the paper that the "*Claraia* Zone" was initially referred to as the "Turbidite Zone" by industry workers based on its horizon of occurrence and log similarities to turbidite units described previously from the center of the Peace River embayment (e.g., Davies et al., 1997; Moslow, 2000). This is a misnomer as there is no conclusive evidence for the occurrences of turbidites specifically within this zone in the study area. The heterolithic facies are the only features that could possibly indicate turbidite influence. Howeve , the reverse grading, and the isolated starved ripples with mud drapes indicate otherwise (Fig. 2.8a, b, f). This is true in the laminated bioclastic unit as well. Bioclasts can be grouped with larger sedimentary grains, and are often deposited alongside them (Maiklem, 1968), therefore locations where the density of bioclasts increases up section would be contrary to what one would expect from a waning flow deposit (Fig. 2.6)

Secondly, while the *"Claraia* Zone" may be attributed to currents generated by storms or wind, it is unlikely that these are tempestites. There is minimal evidence of storm deposition in the study interval,

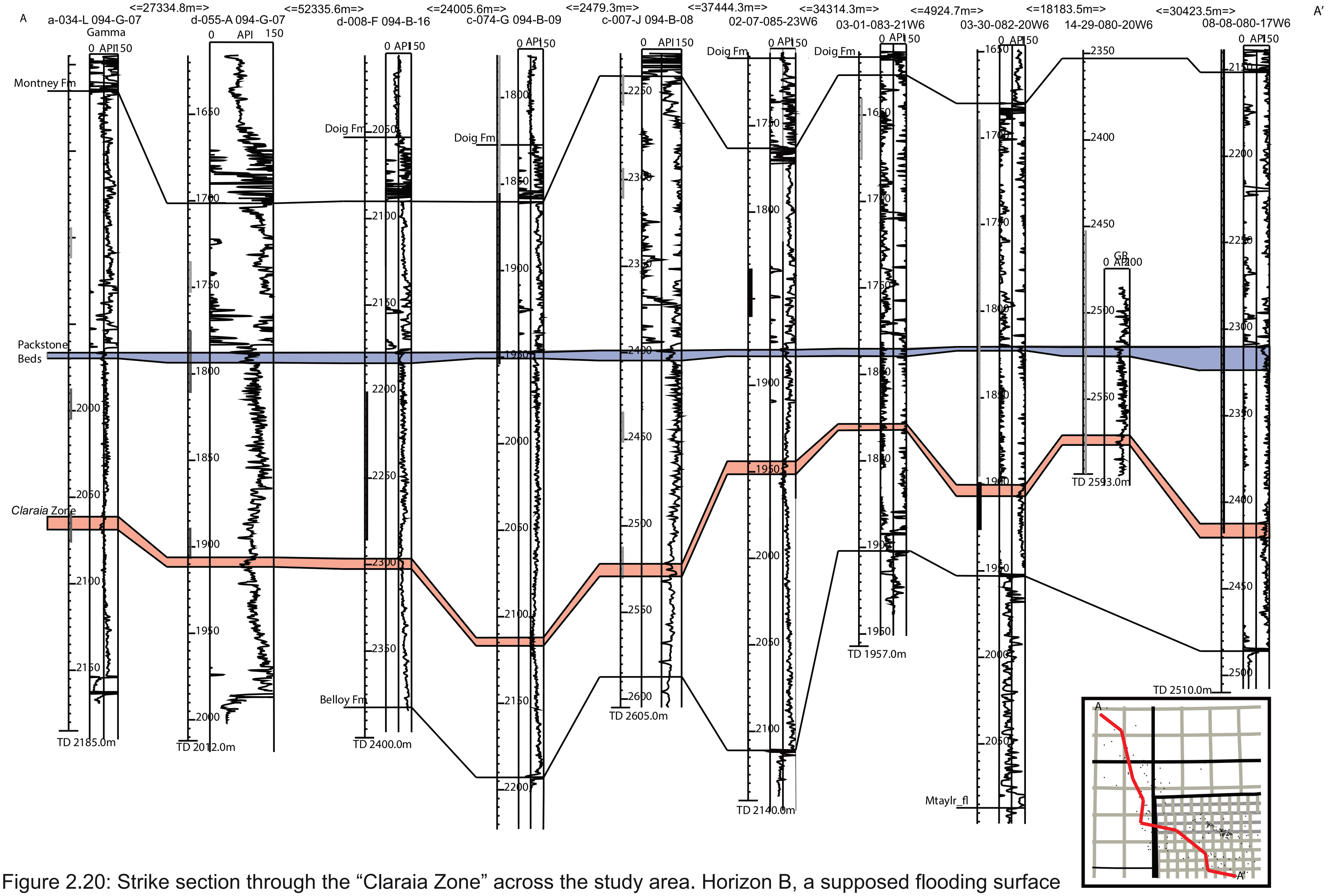

Figure 2.20: Strike section through the “Claraia Zone” across the study area. Horizon B, a supposed flooding surface is used as the datum. Except for one long, 02-07-085-23w6, the “Claraia Zone” appears to have a consistent distance from the contact with the Belloy Formation.

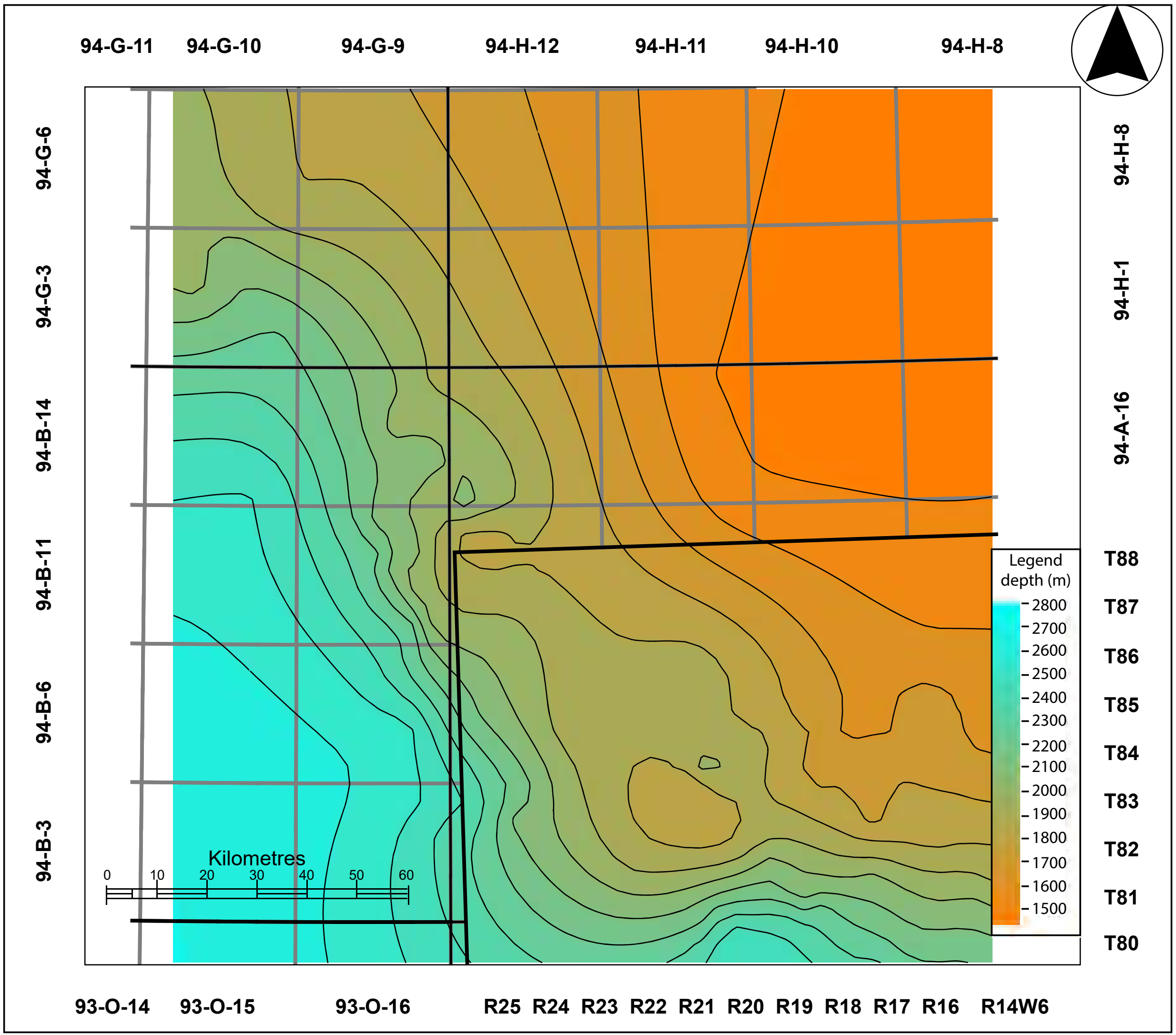

94-G-11
94-G-10
94-G-9
94-H-12
94-H-11
94-H-10
94-H-8
94-G-6
94-G-3
94-B-14
94-B-11
94-B-6
94-B-3
94-H-8
94-H-1
94-A-16
T88
T87
T86
T85
T84
T83
T82
T81
T80
Legend
depth (m)
2800
2700
2600
2500
2400
2300
2200
2100
2000
1900
1800
1700
1600
1500
Kilometres
0
10
20
30
40
50
60
93-O-14
93-O-15
93-O-16
R25
R24
R23
R22
R21
R20
R19
R18
R17
R16
R14W6

Figure 2.21: Isopach contour of the measured depth of the top of the "Claraia Zone" across the study area. There were 155 wells used to create this contour.

---

the sum of which was discussed above (Fig. 2.8d; 2.7 c-e). The prevalence of mud layers (Fig. 2.8a, b) interspersed with the sand layers in SL2 would have to be attributed to a great many storms with enough time for the suspension sediment to accumulate between each one. While the occasional storm could have affected the horizon, creating the few HCS features, there would be much more evidence for storm deposition preserved if that had been the primary mechanism. Storms could have been a likely mechanism in transporting in large amounts of sediment which could contribute to the formation of convoluted facies (SL5) with eventual dewatering.

Finally, the "*Claraia* Zone" could not be the product of *in situ* deposition of shells. It was discussed previously in section 2.4.1 that the state of the shells in the "*Claraia* Zone" is much degraded from what would be expected from an *in situ* deposit. The shells are broken, disarticulated, and sorted by size (Fig. 2.18, 2.7). While an *in situ* deposit could be monotaxic, it would not show this degree of degradation of the shells.

2.4.3 Comparison with Similar Deposits

Facies LBS is similar in sedimentological architecture to bioclastic deposits which occur in the Mississippian Barnett Shale (Milliken et al, 2012), although the *"Claraia* Zone" does not always have a sharp base. Both FA2 and the bioclastic beds within the Barnett Shale represent preserved calcareous body fossils in a laminated fine grained bituminous clastic matrix. At first glance the bioclastic horizons look similar, bioclasts oriented concordant to bedding. However the nature of the bioclasts, and the signal preserved by them is different. It is notable as well that LBS consists primarily of a single taxon, which likely reflects a monotypic living population (as could be likely with the prevalence of cosmopolitan taxa and opportunists in the Early Triassic or due to a deeper basin setting). This is in stark contrast with the Mississippian beds, which have several different taxonomic groups with varying sizes of taxa. The shells in both cases have been compacted and are oriented parallel to the bedding plane in a fine grained bituminous rock, which affords them their similarit , but it is the actual characteristics of the shells which highlight the differences in their deposition

The *Halobia* and *Monotis* beds of the Upper Triassic, particularly of Williston Lake, are laminated bioclastic siltstones, much like those found within the *"Claraia* Zone" (Zonneveld et al., 2004). However, the valves within these beds are found primarily as whole articulated or disarticulated valves and occur in much thicker, denser accumulations. They were interpreted to have been deposited in the distal portion of the Peace River Basin, similar to the "*Claraia* Zone", but Zonneveld et al. (2004) determined that due to their taphonomy and the life position of *Gryphaea* specimens, these beds were deposited *in situ*, with relatively little transport.

The Dinwoody Formation and the Virgin Limestone are part of the Early Triassic deposits in the Western United States, which formed around the same time period as the "*Claraia* Zone" and yet record a completely different ecological signature (Boyer et al., 2004; Mata and Bottje , 2011). Event beds that are made up of single taxa have been identified by Boyer et al (2004) in the Early Triassic of Western United States. These beds were likely deposited closely, both in time and space, to the beds in the "*Claraia* Zone", but they have both a broader range, and better preservation, of the taxa. It is notable that preservation in the Montney Formation is so drastically different from the sandstone and limestone deposits found in the Dinwoody Formation and Virgin Limestone. Here, as before in the Mississippian, the beds are identified as event deposits, and appear to be sharply separated from other beds in outcrop

2.5 Conclusions

The Montney Formation in North Eastern British Columbia, Canada provides a unique view of the western margin of Pangea during the Early Triassic. The "*Claraia* Zone", likewise, is one of the few zones where body fossil material of calcareous organisms is preserved, and the first above the contact with the Permian Belloy Formation.

Sedimentary and taphonomic analysis of core datasets associated with the wire line log signature of the "*Claraia* Zone" have led to the conclusion that the deposits of the "*Claraia* Zone", were formed by bottom current reworking and winnowing of sediment and the shells of opportunistic species. Because the "*Claraia* Zone" is one of the first records of calcified body fossils in the Peace River Basin after th Permian-Triassic boundary, this indicates that while the organisms did not live in this environment, they

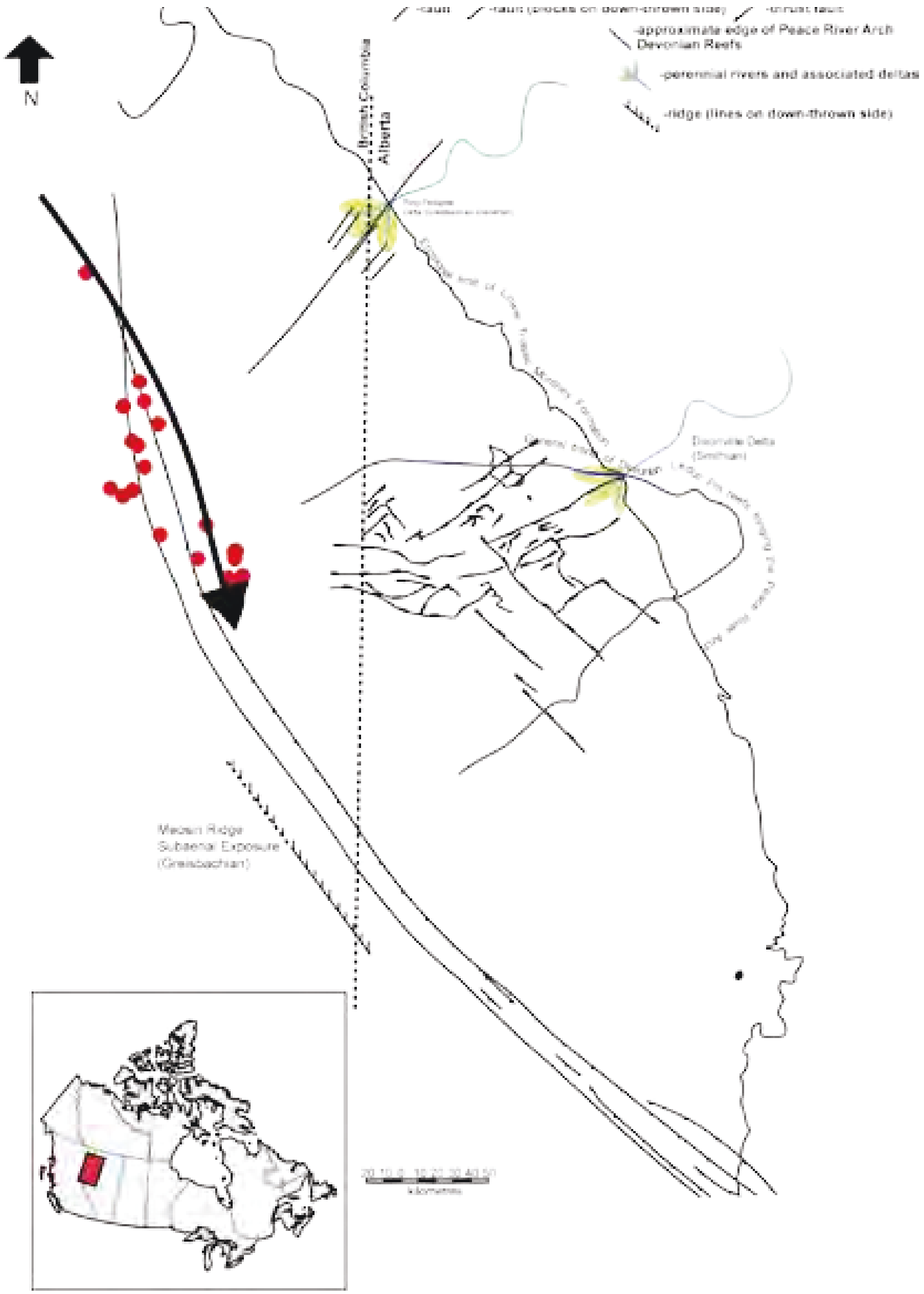

-fault
-fault (blocks on down-thrown side)
-thrust fault
-approximate edge of Peace River Arch Devonian Reefs
-perennial rivers and associated deltas
-ridge (lines on down-thrown side)
N
British Columbia
Alberta
Dixonville Delta
(Smithian)
Meosin Ridge
Subaerial Exposure
(Greisbachian)
20 10 0 10 20 30 40 50
kilometres

Figure 2.22: Map of the Montney Formation during the Greisbachian with possible direction of wind driven bottom currents The currents could be constrained by the ridge at the southwest, but there are no data in that area. Shells and sand could be brought in from the east, or the shells could be from a more local source. (The Montney map was compiled and modified from Barclay et al, 1990; Panek, 2000; Zonneveld et al, 2010a; Zonneveld et al, 2010b; Zonneveld and Moslow, 2014; and Zonneveld, pers. comm.).

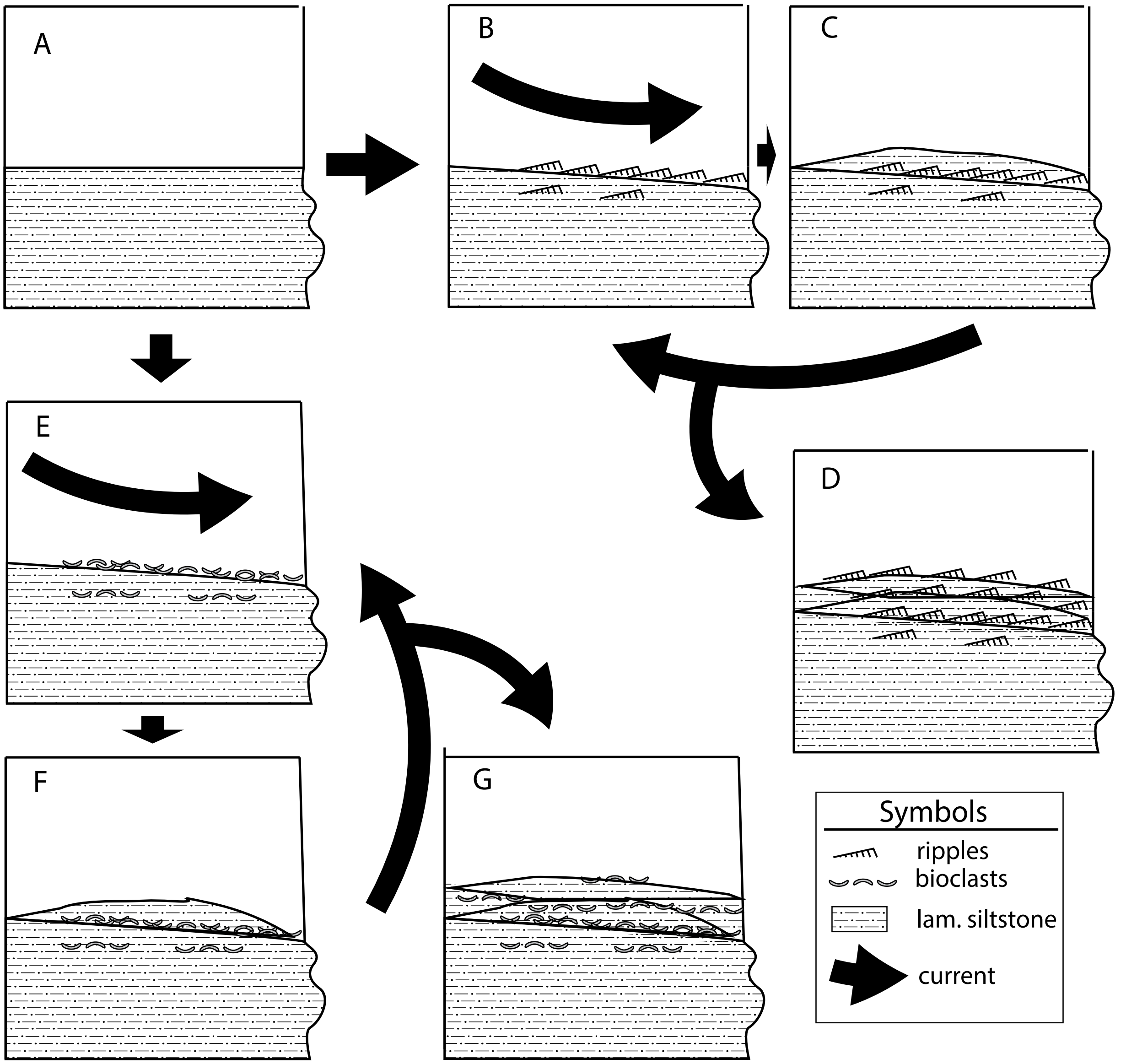

Figure 2.23: The depositional models for the formation of both facies associations. A-D represents the formation of the fan derived bottom current modified deposits. A, E-G represent the formation of the distal bottom current modified deposits. A) Represents the background conditions of the formation with mostly suspension deposition. B) A bottom water current winnows the sediment already deposited and leaves ripple structures. C) Background conditions return and suspension derived sediment is deposited over the ripples. Processes B and C are repeated until a deposit such as D is formed. E) Represents a distal current process where bivalve shells are transported into the system and concentrated in the winnowing of the fine grained sediment. F) Background conditions return and suspension derived sediment is deposited over the bivalves. Processes E and F are repeated until a deposit such as G is formed.

were present elsewhere in the basin (Fig. 2.22; 2.23).

The location and alignment of the deposit with the known paleo-shoreline within the Montney Formation substantiate this conclusion, and although a current has not been identified, there is the possibility that with oriented core datasets, a prevailing current direction could be gleaned from the ripple structures of the heterolithic rippled to laminated very fine sandstone to fine siltstone facies (SL2)

Identification of the current direction could also aid in further identifying the structures of SL2 as the result of bottom water currents rather than turbidites (Fig. 2.23).

The shells contained within these layers are uniquely preserved primarily with their original calcite, but examination of bedding planes outside of the "*Claraia* Zone" has indicated that it is not unique for shells to have accumulated in these areas, but preservation is the key difference between the "Claraia Zone" and other parts of the Lower Montney in British Columbia. The identification of this differenc provides evidence of a chemical imbalance in the Peace River Basin during deposition of the Lower Montney Formation.

Finally, the identification of this current modified deposit provides evidence to substantiate th known prevalence of storms and mega monsoons on the western coast of Pangea. If current directions from SL2 can be determined, this may be able to aid in finding the pathways of the currents, which would have been influenced by storms and monsoons. Additionally, it may aid in locating or even substantiating evidence of any areas of subaerial exposure within the basin at the time. More information about these deposits can only aid in our understanding of the Peace River Basin during the Triassic, and the flow of the ocean around the western coast of Pangea as a whole.

2.6 References

Armitage, J. H., 1962, Triassic Oil and Gas Occurrences in Northeastern British Columbia, Canada: Journal of the Alberta Society of Petroleum Geologists, v. 10, no. 2, p. 35–56.

Balini, M., S. G. Lucas, J. F. Jenks, and J. A. Spielmann, 2010, Triassic ammonoid biostratigraphy: an overview: Geological Society, London, Special Publications, v. 334, no. 1, p. 221–262, doi:10.1144/SP334.10.

Bambach, R. K., 2006, Phanerozoic biodiversity mass extinctions: Annual Review of Earth and Planetary Sciences, v. 34, p. 127–155.

Barclay, J., F. Krause, R. Campbell, and J. Utting, 1990, Dynamic casting and growth faulting: Dawson Creek graben complex, Carboniferous-Permian Peace River embayment, western Canada: Bulletin of Canadian Petroleum Geology, v. 38, no. 1, p. 115–145.

Barron, E. J., 1989, Climate variations and the Appalachians from the late paleozoic to the present: Results from model simulations: Geomorphology, v. 2, no. 1-3, p. 99–118, doi:10.1016/0169-555X(89)90008-1.

Best, M. M. R., and S. M. Kidwell, 2000, Bivalve taphonomy in tropical mixed siliciclastic-carbonate settings. I. Environmental variation in shell condition: Paleobiology, v. 26, no. 1, p. 80–102, doi:10.1666/0094-8373(2000)026<0080:BTITMS>2.0.CO;2.

Best, M. M., T. C. Ku, S. M. Kidwell, and L. M. Walter, 2007, Carbonate preservation in shallow marine environments: Unexpected role of tropical siliciclastics: The Journal of geology, v. 115, no. 4, p. 437–456.

Bird, T., J. Barclay, R. Campbell, and P. Lee, 1994, Triassic Gas Resources of Western Canada Sedimentary Basin, Interior Plains-Geological Play Analysis and Resource Assessment: Western

Canadian and International Expertise [Program book with expanded abstracts], p. 352–353.

Boyer, D. L., D. J. Bottjer, and M. L. Droser, 2004, Ecological Signature of Lower Triassic Shell Beds of the Western United States: Palaios, v. 19, no. 4, p. 372–380, doi:10.1669/0883-1351(2004)019<0372:ESOLTS>2.0.CO;2.

Cooper, C., G. Z. Forristall, and T. M. Joyce, 1990, Velocity and hydrographic structure of two Gulf of Mexico warm-core rings: Journal of Geophysical Research: Oceans (1978–2012), v. 95, no. C2, p. 1663–1679.

Davies, G. R., T. F. Moslow, and M. D. Sherwin, 1997, The Lower Triassic Montney Formation, west-central Alberta: Bulletin of Canadian Petroleum Geology, v. 45, no. 4, p. 474–505.

Dunham, R. J., 1962, Classification of carbonate rocks according to depositional textures, in Classification of Carbonate Rocks--A Symposium: AAPG, Memoir, p. 108–121.

Edwards, D. E., J. E. Barclay, D. W. Gibson, G. E. Kvill, and E. Halton, 1994, Triassic Strata of the Western Canada Sedimentary Basin, in G. D. Mossop, and I. Shetsen, eds., Geological Atlas of the Western Canada Sedimentary Basin: Canadian Society of Petroleum Geologists and Alberta Research Council.

Erwin, D. H., 2000, The Permo-Triassic extinction: Shaking the Tree: Readings from Nature in the History of Life, v. 189.

Faugères, J. C., M. L. Mézerais, and D. A. Stow, 1993, Contourite drift types and their distribution in the North and South Atlantic Ocean basins: Sedimentary Geology, v. 82, no. 1, p. 189–203.

Faugères, J.-C., and D. Stow, 2008, Contourite drifts: nature, evolution and controls: Developments in sedimentology, v. 60, p. 257–288.

Faugères, J.-C., D. A. Stow, P. Imbert, and A. Viana, 1999, Seismic features diagnostic of contourite drifts: Marine Geology, v. 162, no. 1, p. 1–38.

Gibson, D., 1993, Triassic: Sedimentary cover of the craton in Canada. DF Stott and JD Aitken (eds.). Geological Survey of Canada, Geology of Canada, v. 5, p. 294–320.

Gibson, D. W., 1974, Triassic rocks of the Southern Canadian Rocky Mountains: Ottawa, [s.n.], Bulletin / Geological survey of Canada;no. 230.

Golding, M., M. Orchard, J.-P. Zonneveld, C. Henderson, and L. Dunn, 2014, An exceptional record of the sedimentology and biostratigraphy of the Montney and Doig formations in British Columbia: Bulletin of Canadian Petroleum Geology, v. 62, no. 3, p. 157–176.

Government of Canada; Natural Resources Canada; Earth Sciences Sector; Canada Centre for Mapping and Earth, 2001, Coastline and Boundaries of Canada.

Habicht, J. K. A., 1979, Paleoclimate, paleomagnetism, and continental drift: American Association of Petroleum Geologists Studies in Geology 9.

Heezen, B. C., and C. Hollister, 1964, Deep-sea current evidence from abyssal sediments: Marine

Geology, v. 1, no. 2, p. 141–174.

Hollister, C. D., 1967, Sediment distribution and deep circulation in the western North Atlantic: Columbia University.

Hollister, C. D., and I. N. McCave, 1984, Sedimentation under deep-sea storms: Nature, v. 309, no. 5965, p. 220–225, doi:10.1038/309220a0.

Ito, M., 1996, Sandy contourites of the lower Kazusa Group in the Boso Peninsula, Japan: Kuroshio-Current-influenced deep-sea sedimentation in a Plio-Pleistocene forearc basin: Journal of Sedimentary Research, v. 66, no. 3.

Kaźmierczak, J., and B. Kremer, 2005, Early post-mortem calcified Devonian acritarchs as a source of calcispheric structures: Facies, v. 51, no. 1-4, p. 554–565.

Kendall, D. R., 1999, Sedimentology and Stratigraphy of the Lower Triassic Montney Formation, Peace River Basin, subsurface of northwestern Alberta, Master of Science: Calgary, Alberta, The University of Calgary, 368 p.

Kendall, D. R., R. Panek, and C. M. Henderson, 1998, Coquina facies of the Lower Triassic Montney Formation, Peace River Embayment, northwestern Alberta.

Kidder, D. L., and T. R. Worsley, 2004, Causes and consequences of extreme Permo-Triassic warming to globally equable climate and relation to the Permo-Triassic extinction and recovery: Palaeogeography, Palaeoclimatology, Palaeoecology, v. 203, no. 3-4, p. 207–237, doi:10.1016/S0031-0182(03)00667-9.

Kidwell, S. M., 1986, Models for fossil concentrations: paleobiologic implications: Paleobiology, p. 6–24.

Kidwell, S. M., 1991, Taphonomic feedback (live/dead interactions) in the genesis of bioclastic beds: keys to reconstructing sedimentary dynamics., in G. Einsele, W. Ricken, and A. Seilacher, eds., Cycles and Events in Stratigraphy: Berlin, Springer-Verlag, p. 268–282.

Kidwell, S. M., and D. W. Bosence, 1991, Taphonomy and time-averaging of marine shelly faunas: Taphonomy: releasing the data locked in the fossil record. Plenum, New York, p. 115–209.

Kidwell, S. M., and S. M. Holland, 1991, Field Description of Coarse Bioclastic Fabrics: PALAIOS, v. 6, no. 4, p. 426, doi:10.2307/3514967.

Kidwell, S. M., and D. Jablonski, 1983, Taphonomic feedback ecological consequences of shell accumulation, in Biotic interactions in recent and fossil benthic communities: Springer, p. 195–248.

Kutzbach, J. E., P. J. Guetter, and W. M. Washington, 1990, Simulated circulation of an idealized ocean for Pangaean time: Paleoceanography, v. 5, no. 3, p. 299–317, doi:10.1029/PA005i003p00299.

Loope, D. B., M. B. Steiner, C. M. Rowe, and N. Lancaster, 2004, Tropical westerlies over Pangaean sand seas: 100 million years of cross-equatorial flow: Sedimentolog , v. 51, no. 2, p. 315–322, doi:10.1046/j.1365-3091.2003.00623.x.

Maiklem, W., 1968, Some hydraulic properties of bioclastic carbonate grains: Sedimentology, v. 10, no. 2, p. 101–109.

Markhasin, B., 1997, Sedimentology and Stratigraphy of the Lower Triassic Montney Formation, Subsurface of Northwestern Alberta, Master of Science: Calgary, Alberta, University of Calgary, 154 p.

Marszalek, D., 1975, Calcisphere ultrastructure and skeletal aragonite from the alga Acetabularia antillana: Journal of Sedimentary Research, v. 45, no. 1.

Mata, S. A., and D. J. Bottjer, 2011, Origin of Lower Triassic microbialites in mixed carbonate-siliciclastic successions: ichnology, applied stratigraphy, and the end-Permian mass extinction: Palaeogeography, Palaeoclimatology, Palaeoecology, v. 300, no. 1, p. 158–178.

McRoberts, C. A., 2010, Biochronology of Triassic bivalves: Geological Society, London, Special Publications, v. 334, no. 1, p. 201–219, doi:10.1144/SP334.9.

Mederos, S., 1995, Sedimentology and sequence stratigraphy of the Montney Formation in the Sturgeon Lake A and B pool, MSc: Edmonton, University of Alberta, 229 p.

Milliken, K. L., W. L. Esch, R. M. Reed, and T. Zhang, 2012, Grain assemblages and strong diagenetic overprinting in siliceous mudrocks, Barnett Shale (Mississippian), Fort Worth Basin, Texas: Aapg Bulletin, v. 96, no. 8, p. 1553–1578.

Moslow, T. F., 2000, Reservoir architecture of a fine-grained turbidite system: Lower Triassic Montney Formation, Western Canada Sedimentary Basin, in Deep-water Reservoirs of the World, Conference Proceedings, Gulf Coast SEPM. P. Weimer, RM Slatt, J. Coleman, NC Rosen, H. Nelson, AH Bouma, MJ Styzen, and DT Lawrence (eds.): SEPM, p. 686–713.

Newell, N., and D. Boyd, 1995, Pectinoid bivalves of the Permian-Triassic crisis.: Bulletin of the American Museum of Natural History, no. 227, p. 5 – 95.

Orchard, M. J., and E. T. Tozer, 1997, Triassic conodont biochronology, its calibration with the ammonoid standard, and a biostratigraphic summary for the Western Canada Sedimentary Basin: Bulletin of Canadian Petroleum Geology, v. 45, no. 4, p. 675–692.

Orchard, M. J., and J.-P. Zonneveld, 2009, The Lower Triassic Sulphur Mountain Formation in the Wapiti Lake area: lithostratigraphy, conodont biostratigraphy, and a new biozonation for the lower Olenekian (Smithian)Earth Science Sector (ESS) Contribution 20080714.: Canadian Journal of Earth Sciences, v. 46, no. 10, p. 757–790, doi:10.1139/E09-051.

Panek, R., 2000, The Sedimentology and Stratigraphy of the Lower Triassic Montney Formation in the Subsurface of the Peace River Area, Northwestern Alberta, Master of Science: Calgary, Alberta, University of Calgary.

Paull, R. K., R. A. Paull, and T. S. Laudon, 1997, Conodont biostratigraphy of the Lower Triassic Mackenzie Dolomite Lentil, Sulphur Mountain Formation in the Cadomin area, Alberta: Bulletin of Canadian Petroleum Geology, v. 45, no. 4, p. 708–714.

Payne, J. L., D. Altiner, D. J. DePaolo, J. L. Hinojosa, L. R. Kump, K. V. Lau, D. J. Lehrmann, K. Maher, A. Paytan, and S. Shen, 2014, The End-Permian Mass Extinction and its Aftermath: Insights from Non-Traditional Isotope System: Vancouver,BC.

Payne, J. L., and M. E. Clapham, 2012, End-Permian mass extinction in the oceans: an ancient analog for the twenty-first century?: Annual Review of Earth and Planetary Sciences, v. 40, p. 89–111.

Rampino, M. R., and K. Caldeira, 2005, Major perturbation of ocean chemistry and a “Strangelove Ocean” after the end-Permian mass extinction: Terra Nova, v. 17, no. 6, p. 554–559, doi:10.1111/j.1365-3121.2005.00648.x.

Rebesco, M., A. Camerlenghi, and A. Van Loon, 2008, Contourite research: a field in full development: Contourites, Developments in Sedimentology, v. 60, p. 3–10.

Sepkoski Jr, J. J., 1981, A factor analytic description of the Phanerozoic marine fossil record: Paleobiology, p. 36–53.

Shanmugam, G., 1997, The Bouma sequence and the turbidite mind set: Earth-Science Reviews, v. 42, no. 4, p. 201–229.

Shanmugam, G., T. Spalding, and D. Rofheart, 1993, Process sedimentology and reservoir quality of deep-marine bottom-current reworked sands (sandy contourites): an example from the Gulf of Mexico: AAPG Bulletin, v. 77, no. 7, p. 1241–1259.

Shanmugam, G., T. D. Spalding, and D. H. Rofheart, 1993, Traction structures in deep-marine, bottom-current-reworked sands in the Pliocene and Pleistocene, Gulf of Mexico: Geology, v. 21, no. 10, p. 929, doi:10.1130/0091-7613(1993)021<0929:TSIDMB>2.3.CO;2.

Stanley, D. J., D. J. Swift, and H. G. Richards, 1967, Fossiliferous concretions on Georges Bank: Journal of Sedimentary Research, v. 37, no. 4.

Stow, D. A. V., 2001, Deep-Sea Sediment Drifts, in J. H. Steele, K. K. Turekian, and S. A. Thorpe, eds., Encyclopedia of Ocean Sciences: London, Academic Press.

Stow, D., and J.-C. Faugères, 2008, Contourite facies and the facies model: Developments in Sedimentology, v. 60, p. 223–256.

Stow, D. A., J.-C. Faugères, J. A. Howe, C. J. Pudsey, and A. R. Viana, 2002, Bottom currents, contourites and deep-sea sediment drifts: current state-of-the-art: Geological Society, London, Memoirs, v. 22, no. 1, p. 7–20.

Stow, D. A., J.-C. Faugères, A. Viana, and E. Gonthier, 1998, Fossil contourites: a critical review: Sedimentary Geology, v. 115, no. 1, p. 3–31.

Tozer, E., 1982, Marine Triassic faunas of North America: their significance for assessing plate and terrane movements: Geologische Rundschau, v. 71, no. 3, p. 1077–1104.

Tozer, E. T., 1994, Canadian Triassic ammonoid faunas: Geological Survey of Canada.

Twitchett, R. J., and P. B. Wignall, 1996, Trace fossils and the aftermath of the Permo-Triassic mass extinction: evidence from northern Italy: Palaeogeography, Palaeoclimatology, Palaeoecology, v. 124, no. 1, p. 137–151.

Versteegh, G. J., T. Servais, M. Streng, A. Munnecke, and D. Vachard, 2009, A discussion and proposal concerning the use of the term calcispheres: Palaeontology, v. 52, no. 2, p. 343–348.

Viana, A., J.-C. Faugères, and D. Stow, 1998, Bottom-current-controlled sand deposits—a review of modern shallow-to deep-water environments: Sedimentary Geology, v. 115, no. 1, p. 53–80.

Wentworth, C. K., 1922, A scale of grade and class terms for clastic sediments: The Journal of Geology, p. 377–392.

Wignall, P., and A. Hallam, 1996, Facies change and the end-Permian mass extinction in SE Sichuan, China: Palaios, p. 587–596.

Wilson, N., 2009, Integrated regional model for the deposition and evolution of the Montney Formation, NE British Columbia.

Wilson, K. M., D. Pollard, W. W. Hay, S. L. Thompson, and C. N. Wold, 1994, General circulation model simulations of Triassic climates: preliminary results: Geological Society of America Special Papers, v. 288, p. 91–116.

Wood, J., 2012, Water Distribution in the Montney Tight Gas Play of the Western Canadian Sedimentary Basin: Significance for Resource Evaluation: Society of Petroleum Engineers, doi:10.2118/161824-MS.

Woods, A. D., 2005, Paleoceanographic and paleoclimatic context of Early Triassic time: Comptes Rendus Palevol, v. 4, no. 6-7, p. 463–472, doi:10.1016/j.crpv.2005.07.003.

Zhenzhong, G., L. Shunshe, H. Youbin, Z. Jisen, and T. Zijun, 1995, The Middle Ordovician contourite on the west margin of Ordos: Acta Sedimentologica Sinica, v. 13, no. 4, p. 16–26.

Zonneveld, J.-P., 2011, Suspending the Rules: Unraveling the ichnological signature of the Lower Triassic post-extinction recovery interval: Palaios, v. 26, no. 11, p. 677–681, doi:10.2110/palo.2011.S06.

Zonneveld, J.-P., G. G. Carrelli, and C. Riediger, 2004, Sedimentology of the Upper Triassic Charlie Lake, Baldonnel and Pardonet formations from outcrop exposures in the southern Trutch region, northeastern British Columbia: Bulletin of canadian petroleum geology, v. 52, no. 4, p. 343–375.

Zonneveld, J.-P., M. K. Gingras, and T. W. Beatty, 2010, Diverse ichnofossil assemblages following the P-T mass extinction, Lower Triassic, Alberta and British Columbia, Canada: Evidence for shallow marine refugia on the northwestern coast of Pangea: Palaios, v. 25, no. 6, p. 368–392, doi:10.2110/palo.2009.p09-135r.

Zonneveld, J.-P., R. B. MacNaughton, J. Utting, T. W. Beatty, S. G. Pemberton, and C. M. Henderson, 2010, Sedimentology and ichnology of the Lower Triassic Montney Formation in the Pedigree-Ring/Border-Kahntah River area, northwestern Alberta and northeastern British Columbia: Bulletin of Canadian Petroleum Geology, v. 58, no. 2, p. 115–140.

Zonneveld, J.-P., and T. F. Moslow, 2014, Perennial River Deltas of the Montney Formation: Alberta and

British Columbia Subcrop Edge.

Zuschin, M., M. Stachowitsch, and R. J. Stanton, 2003, Patterns and processes of shell fragmentation in modern and ancient marine environments: Earth-Science Reviews, v. 63, no. 1, p. 33–82.

Figure Captions

2.1: Map of core datasets in relation to the Montney Formation as a whole during the Greisbachian. The red dots each represent a separate core and they are all located well within the offshore portion of the formation. The Pedigree-Ring Delta is known to be Greisbachian in age, but the Dixonville has only been confirmed to be Smithian, although there are sand bodies of Greisbachian age that are located westward in the Peace River Arch from the delta location. The Meosin High in the southwest is based on subaerial exposure in the outcrop belt. The red block in the inset map shows the location of the above map in relation to modern geographical boundaries of Canada. (The Montney map was compiled and modified from Barclay et al, 1990; Panek, 2000; Zonneveld et al, 2010a; Zonneveld et al, 2010b; Zonneveld and Moslow, 2014; and Zonneveld, pers. comm.).

2.2: The stratigraphic framework of the Lower and Middle Triassic in the Western Canada Sedimentary Basin, and the location and correlation of the Montney Formation with its outcrop equivalents with the horizon of interest to this paper highlighted in grey on the right (modified from Zonneveld, 20 1; compiled from Tozer, 1994; Orchard and Tozer, 1997; Orchard and Zonneveld, 2009).

2.3: The location and study area of all wells logged for this study. These wells were selected as they appeared to have core within the "*Claraia* Zone" based on wireline gamma log signatures.

2.4: SL1: Laminated Siltstone facies. A) Macroscopic example from 14-29-080-20w6. B) Thin section example from 14-29-080-20w6. C) Thin section example from 15-02-080-16w6. Macroscopically and microscopically laminae can be followed across the face of the core or slide in the fine grained, gra , bituminous siltstone. D) Thin section photograph showing the continuous laminated from sample IRG-SA-1412-066.

2.5: LBS: Laminated bioclastic siltstone facies. A) Macroscopic example from 14-29-080-20w6. B) Thin section example from A-10-J/094-B-9. C) Thin section example from C-007-J/094-B-8. Both thin sections B and C are scanned in plain light and are half stained for calcium carbonate. A shows the gradual increase in bioclasts that occurs at the base of the facies. The laminated has of bioclastic material is visible in B and C. D)Thin section photograph showing calcispheres alongside the bioclastic material as well as an ankerite altered valve from 3-30-082-20w6.

2.6: Thin sections of LBS: A) Separate layers of concentrated *Claraia* material (BC13). B) A large concentration of *Claraia* material at the base of the section with a sudden cutoff about a third of the way from the top of the section (BC5). C) Increasing upward concentration of *Claraia* material (14-29-080-20w6). D) High concentration of *Claraia* material increasing upward in the section (14-29-080-20w6).

2.7: Thin section photographs in plane polarized light within LBS. A, B) lenses of bioclastic material from 14-29-080-20w6. C, D, E) Examples of the shell stacking pattern and the fragmented nature of the shells within LBS from A-18-D/094-A-13. F) Calcispheres alongside bioclasts with preferential dolomitization of calcispheres from A-18-D/094-A-13.

2.8: SL2: Heterolithic fine grained sandstone interbedded with fine siltston   A) example from 3-30-082-20w6. This example shows rapid interbedding between the two lithologies as well as multiple scour surfaces. B) Example from 08-30-082-20w6. This sample shows multiple fine grained drapes over sandstone ripples that would not be identifiable save for the fine grained material This horizon is much more discrete compared to A. (Sc) scour surface, (D) Flaser/fine grained offshoots, (L) Lenticular bedding C) Thin section view of the heterolithic structures preserved in the top part of the section, but somewhat obscured in the base of the section (IRG-SA-1412-66). D) Possible HCS feature from B-65-J/094-B-16. E) Thin section photograph of the separated coarse and fine grained sections with ripples (IRG SA-1412-066). F) Thin section photograph of a coarsening upward sequence (IRG-SA-1412-066).

2.9: Preserved original shell material (F) on bedding plane from B-065-J/094-B-16.

2.10: CA: Calcisphere laminated to massive siltstone. A) Macroscopic example of massive to laminated siltstone with calcispheres grading in and out from A-008-D/094-A-13. B) Another laminated siltstone with calcispheres from A-005-C/094-G-10. C) Thin section with calcispheres within laminae from C-074-G/094-B-09. D) Thin section photo of a partially dolomitized calcispheres from A-18-D/094-A-13. E) Thin section photo of calcisphere horizon (BC20). F) Calcispheres alongside bioclasts with preferential dolomitization of calcispheres from A-18-D/094-A-13.

2.11: CO: Calcite concretions common throughout the intervals studied. A, E) Concretions from 14-29-080-20w6 that do not show an internal fabric. B) Concretion from C-074-G/094-B-9 that shows pyrite (red arrow) around the edge of the concretion. C) Concretion from C-007-J/094-B-8 that shows the variation in calcite to dolomite through the concretion. Both thin sections B and C were half stained with a double calcite stain. D) Concretion from 14-29-080-20w6 in which one can follow the beds from outside of the concretion through it. F) Thin section photo of the edge of a concretion (BC19). G) Euhedral pyrite around the rim of a calcite cemented concretion (BC19).

2.12: SL3: Massive siltstone facies. A) a-005-C/094-G-10 B, C) 14-29-080-20w6 Massive fine grained bituminous siltstone that shows no evidence of bioturbation. These thin sections exhibit a brown coloration not seen in other sections. D) Thin section photo of massive fine grained siltstone (IRG SA-1412-036).

2.13: SL4: Bioturbated/Mottled siltstone. A) A08-07-085-18w6 shows bioturbation induced mottling of the sediment. B) Example from A-005-C/094-G-10 which shows unidentifiable burrows visible due to lithological variation in the siltstone. C) Thin section photograph of the coarse grained lenses and discontinuous coarse and fine grained layers (IRG-SA-1412-025)

2.14: SL5: Soft sediment deformed heterolithic coarse grained siltstone and fine grained siltstone. A) An isolated feature in A08-07-085-18w6. B) The strata is more completely convoluted from A-07-19-085-15w6. C) Thin section showing near complete convolution of the heterolithic beds (BC16). D) The middle of this thin section shows convoluted texture while the outer beds still retain the bedforms (IRG-SA-1412-066).

2.15: BF1: *Planolites* bioturbated siltstone. A) A-005-C/094-G-10 B) A-005-C/094-G-10 Layers of *Planolites* bioturbated siltstone with very little lithological variation. C) B-065-J/094-B-16 *Planolites* in discrete sand layers within fine grained siltstone. (P) *Planolites*. D) *Planolites* burrows preserved in the

coarse grained horizon that have been slightly flattened (BC26)

2.16: Bedding plane impressions of Pectinoids. A, B) B-50-H/094-B-16 showing large valves that are somewhat fragmented and disarticulated. C) B-50-H/094-B-16 showing small very fragmented valves.

2.17: Ammonoids from various cores near the "*Claraia* Zone": A) New ammonoid from A-10-J/094-B-9 B) *Wordeioceras wordiei* from A-10-J/094-B-9 C, E) *Ophioceras* sp. from 08-30-082-20w6 D) *Ophioceras*? From A-005-C/094-G-10 surrounded by Pectinoids.

2.18: The bottom current depositional environment with the current shown producing the two different facies associations. A) Represents the fan derived bottom current modified deposits that are closer to the source input of coarse grained sediment (arrows). When the current is active (blue) bivalve shells and ripple structures are created, with suspension sedimentation between current activity. B) Represents the distal bottom current modified deposits where winnowing of fine grained sediment with the deposition o bivalve material in concentrated horizons by the current activity (blue).

2.19: Core lithographic description of Well API: 03-30-082-20w6. There are two distinct sections to this core: the lower showing what is typical of facies SL2 and the first facies association, and the upper showing what is typical of LBS and the second facies association.

2.20: Strike section through the "*Claraia* Zone" across the study area. Horizon B, a supposed flooding surface is used as the datum. Except for one long, 02-07-085-23w6, the "*Claraia* Zone" appears to have a consistent distance from the contact with the Belloy Formation.

2.21: Isopach contour of the measured depth of the top of the "*Claraia* Zone" across the study area. There were 155 wells used to create this contour.

2.22: Map of the Montney Formation during the Greisbachian with possible direction of wind driven bottom currents The currents could be constrained by the ridge at the southwest, but there are no data in that area. Shells and sand could be brought in from the east, or the shells could be from a more local source. (The Montney map was compiled and modified from Barclay et al, 1990; Panek, 2000; Zonneveld et al, 2010a; Zonneveld et al, 2010b; Zonneveld and Moslow, 2014; and Zonneveld, pers. comm.).

2.23: The depositional models for the formation of both facies associations. A-D represents the formation of the fan derived bottom current modified deposits. A, E-G represent the formation of the distal bottom current modified deposits. A) Represents the background conditions of the formation with mostly suspension deposition. B) A bottom water current winnows the sediment already deposited and leaves ripple structures. C) Background conditions return and suspension derived sediment is deposited over the ripples. Processes B and C are repeated until a deposit such as D is formed. E) Represents a distal current process where bivalve shells are transported into the system and concentrated in the winnowing of the fine grained sediment. F) Background conditions return and suspension derived sediment is deposited over the bivalves. Processes E and F are repeated until a deposit such as G is formed.

List of Tables

2.1: Table of cores analyzed and presence or absence of the packstone bed horizon or the "*Claraia* Zone".

2.2: Summary of facies with descriptions of minerology, grain size, sedimentary structures, trace fossils, and body fossils found in each facies.

2.3: Summary of contacts between each facies in and around the *"Claraia* Zone". G = gradational, S = sharp, C = scour, OW = occur within.

Chapter 3: The Altares Packstone Member of the Early Triassic Montney Formation, NE-British Columbia

3.1 Introduction

Bioclastic units of the Montney Formation provide important insight into life in the oceans of northwestern Pangea following the Permian-Triassic Mass Extinction, as well as proxies for assessing ocean chemistry and oceanic circulation in the Peace River Embayment during the Early Triassic. Understanding the origin and preservation of these bioclastic units allows further insight into the factors that controlled the presence and distribution of metazoan life in the Western Canada Sedimentary Basin, which experienced a drastic shift from a carbonate ramp during the Permian (Beauchamp and Desrochers, 1997; Henderson et al., 2002) to a clastic ramp depositional system (Moslow, 2000) as a result of the demise of many Palaeozoic carbonate secreters alongside an environmental shift at the end of the Permian.

The Montney Formation records a complete Lower Triassic succession in the subsurface of the Western Canada Sedimentary Basin (Orchard and Tozer 1997, Orchard and Zonneveld, 2009; Golding et al., 2014). The bioclastic horizons of the Montney Formation, which occur at discrete horizons in the lower and middle Montney Formation (based on the British Columbia paradigm), represent nearly all of the calcareous body fossils preserved in this unit. This lack of preservation has been attributed to changes in the Aragonite Compensation Depth as well as the Calcite Compensation Depth (Rampino and Caldeira, 2005; Woods, 2005; Zonneveld, 2011). Although fossils occur outside of the bioclastic beds, they invariably consist solely of impressions on bedding planes or consist of a material resistant to dissolution (e.g., lingulide brachiopods or vertebrate material composed of calcium phosphate / apatite).

Three main bioclastic intervals have been noted in the Montney Formation, two occurring in British Columbia and the other adjacent to the subcrop limit in Alberta. The oldest Montney bioclastic interval was discussed in Chapter 2 (the '*Claraia* Zone') and has been dated as Late Dienerian (Golding et al., 2014). This unit occurs solely in the western reaches of the subsurface Montney Formation in British Columbia (Chapter 2). The middle Montney bioclastic interval occurs solely in Alberta, in both outcrop and subsurface. This unit, commonly referred to informally as the Coquinal Dolomite Middle Member (Mackenzie Dolomite Lentil in outcrop), has been dated as coincident with the Dienerian-Smithian boundary (Paull et al., 1997; Kendall et al., 1998; Kendall, 1999). The top of the bioclastic interval discussed herein is a regionally correlatable surface throughout the basin that approximates the Smithian-Spathian boundary (Golding et al., 2014). This unit is also limited to northeastern British Columbia although it does have a larger geographical footprint than the Late Dienerian unit in the same area (see chapter 2).

These rare bioclastic intervals provide a stark contrast to the intervening non-fossiliferous siltstone intervals and are a crucial component in paleoecological analyses of the Montney Formation. The interval under consideration in this chapter, the Late Smithian Altares Packstone Member, is recognized as an anomaly within the Montney system. This member is a calcite cemented packstone in which the original body fossils are preserved. The only other calcite cemented deposits (the Coquinal Dolomite Middle Member) only contains molds of the body fossils among the dolomite matrix (Markhasin, 1997; Paull et al., 1997; Kendall, 1999). The present chapter addresses the depositional environment of this unit and provides evidence as to its interpretation as a series of low-relief biostrome deposits.

Both paleontological and sedimentological characteristics must be assessed in order to confidently assign bioclastic units to specific depositional environments (Kidwell and Holland, 1991) This is evidenced by the previous chapter on the Late Dienerian "*Claraia* Zone". In order to understand the bioclastic packstone beds found in the Middle Montney Formation in Northeastern British Columbia, a sedimentary analysis of core data sets was conducted and compared to known bioclastic accumulations from the recent and the geologic record. These packstone beds, which occur in the latest Smithian (middle Olenekian) part of the Montney Formation in northeastern British Columbia (Golding et al., 2014), may represent the earliest known metazoan biostrome deposits in northwestern Pangea after the end Permian mass extinction.

3.2 Background

3.2.1 Triassic

During the Lower Triassic, the Peace River Basin was located at approximately 30°N latitude, and was located in an arid climate on the northeast margin of the Panthalassa Ocean (Habicht, 1979; Tozer, 1982; Wilson et al., 1994; Kidder and Worsley, 2004). Diversity after the extinction event was overall low in the world's oceans, and cosmopolitan taxa (organisms which are found all over the world) represented the majority of biotas (Sepkoski, 1981; Erwin, 2000; Bambach, 2006; Alroy et al, 2008; Payne and Clapham, 2012). Recovery did not occur until the Middle Triassic at the earliest, and was likely delayed by increased alkalinity possibly coupled with the expansion of oxygen minimum zones (Sepkoski, 1981; Woods, 2005; Alroy et al., 2008; Payne et al., 2014). Zonneveld (2011) identified the Middle Montney in northeastern British Columbia as a carbonate recovery interval due both to the resurgence of body fossils and moderately abundant trace fossils in eastern Montney successions. Both body fossils and trace fossils are of overall low abundance and low diversity in the Montney Formation, as a result of ongoing environmental stressors following the extinction event (Zonneveld et al., 2010a; Zonneveld, 2011). High diversity trace fossil assemblages are restricted primarily to rare perennial deltaic succession on the fringe of the basin (Zonneveld et al., 2010a; Zonneveld and Moslow, 2014).

During this time of globally low biodiversity, a number of hotspots with anomalously high diversity have been identified (e.g., Wignall and Hallam, 1996; Lehrmann, 1999; Jin et al., 2000; Boyer et al., 2004; Nutzel and Schubert, 2005; Forel, 2013). Many of these sections occur in sedimentary successions characterized by abundant carbonate (Guizhou Bureau, 1987; Schubert and Bottjer, 1995; Wignall and Hallam, 1996; Wignall and Twitchett, 1999), which certainly is in deficit in the Montney Formation. As carbonate deposits commonly have a better preservation of body fossils (Best and Kidwell, 2000), taphonomic limitations must certainly be considered to explain the low biodiversity in this section. This paper focuses on the low diversity and abundance of body fossils in the Montney Formation in northeastern British Columbia. It is significant to note that the bioclastic horizons described herein show an increase in diversity, albeit moderate, that is lacking elsewhere. It is also worth noting that while the Tethys Sea / eastern Pangaea coastline regions show strong signs of marine environmental stress during the Early Triassic (evidenced by the predominance of 'Lilliput' faunas; e.g., Twitchett et al., 2004; Twitchett, 2006; Forel et al., 2011; Metcalfe et al., 2011; Song et al., 2011; and microbial biostromes;

e.g., Lehrmann, 1999; Jin et al., 2000), there appears to have been even greater stresses on coastal successions at similar paleolatitudes on the western coast of Pangea (Boyer et al., 2004).

3.2.2 Montney stratigraphy and fossil occurrence

The Montney Formation, first identified b Armitage (1962), is a westward thickening package of bituminous siltstone and fine-grained sandstone in western Alberta and northeastern British Columbia, Canada. It has been targeted by petroleum exploration companies in Western Canada for over 50 years, initially as a conventional oil play (Edwards et al., 1994) and subsequently as a liquids-rich unconventional gas reservoir (Fig. 3.1). The subsurface Montney Formation has outcrop equivalents in the deformation belt along the eastern thrust sheets of the Canadian Rocky Mountains and Foothills, which include: the Toad, Grayling, and Sulphur Mountain Formations in the north and the Vega, Phroso and Meosin Mountain members of the Sulphur Mountain Formation to the south (Edwards et al., 1994; Orchard and Zonneveld, 2009) (Fig. 3.2). The Montney Formation has been interpreted as being deposited along a clastic ramp on the western margin of Pangea, with deeper sedimentary facies being deposited westward in the formation (Davies et al., 1997). Although the unit stretches from southern Alberta to northern British Columbia, the Alberta (eastern) succession generally represents the more proximal facies of the formation (Fig. 3.1, 3.2). The shoreline successions are progressively truncated towards the east along the erosional edges of a series of Triassic, Jurassic, and Cretaceous unconformities.

As with all stratigraphic units that host petroleum plays, the Montney Formation is both a stratigraphic entity and an economic entity. The Alberta and British Columbia governments have used widely differing paradigms to identify their economic units. The stratigraphic succession that comprises the Montney Formation in most of Alberta correlates with the Lower part of the Montney Formation in British Columbia. The informally named Upper Montney in British Columbia is a thickening of the unit that is referred to as the Basal Doig Siltstone in Alberta, the boundary of which has been identified as diachronous (Wilson, 2009). Since all of the data presented within this study is located in British Columbia, this study will conform to the BC terminology. It should be noted that the British Columbia model more closely follows the original stratigraphic definitions of the units (sensu Armitage, 1962; Glass, 1990). Since no formal redefinitions of these units have occurred since the original descriptions, the British Columbia model must be taken as the stratigraphically correct nomenclature.

Fossil accumulations have been identified in the southeastern portions of the Montney Formation (and the outcrop-equivalent Sulphur Mountain Formation) in Alberta as part of the coquina-dolomite units (Fig. 3.1; Kendall et al., 1998). The fossils in these horizons are primarily bivalve, and to a lesser extent

Figure 3.1 (Opposing page): Map of core datasets in relation to the Montney Formation as a whole during the Dienerian-Smithian boundary. The two deltas are known to be present on opposite sides of the boundary. The red block in the inset map shows the location of the above map in relation to modern geographical boundaries of Canada. (The Montney map was compiled and modified from Barclay et al., 1990; Panek, 2000; Zonneveld et al., 2010a; Zonneveld et al., 2010b; Zonneveld and Moslow, 2014; and Zonneveld, pers. comm.; the Map of the provinces and coastline of Canada was modified from Government of Canada, 2001).

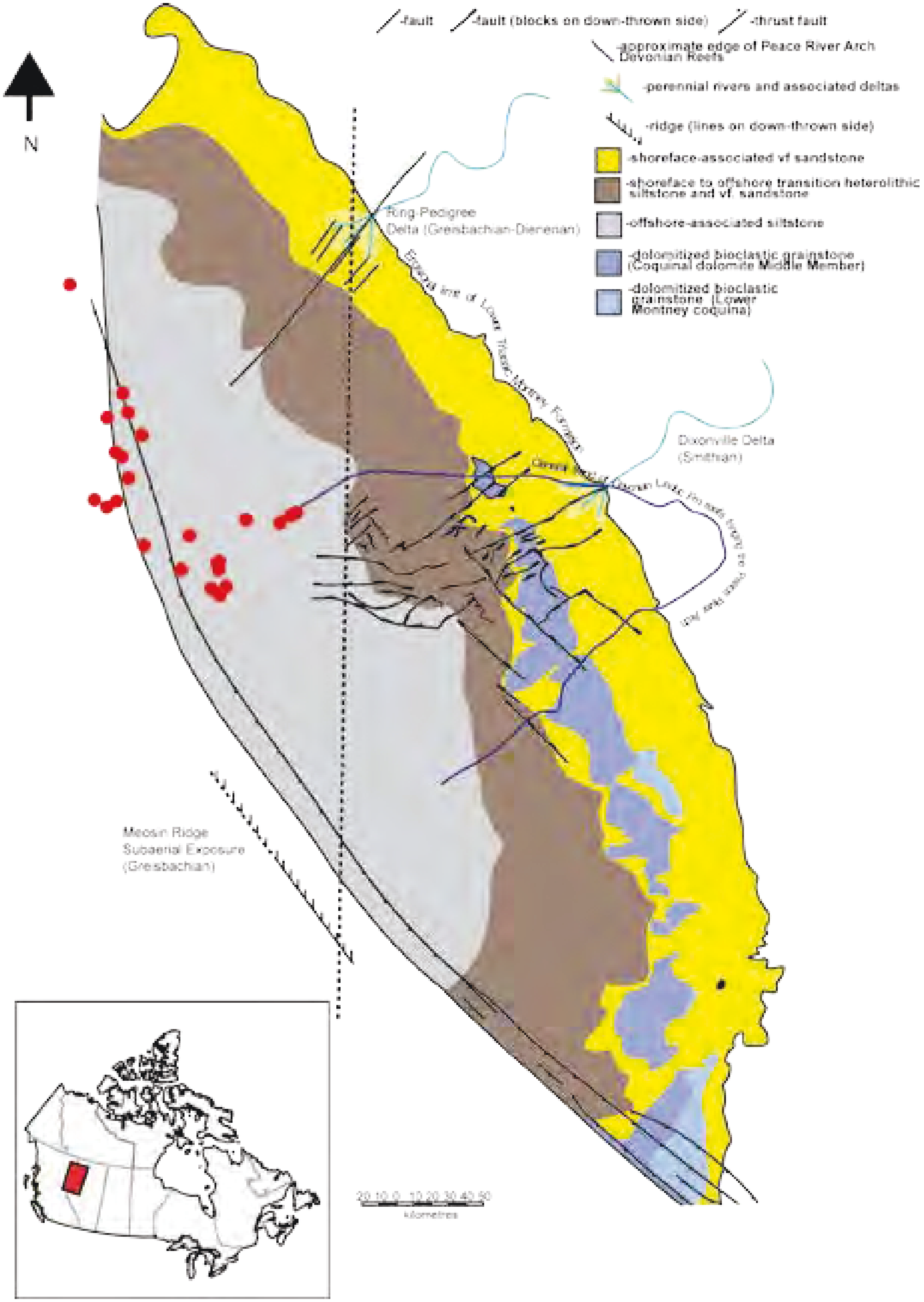N
-fault
-fault (blocks on down-thrown side)
-thrust fault
-approximate edge of Peace River Arch Devonian Reefs
-perennial rivers and associated deltas
-ridge (lines on down-thrown side)
-shoreface-associated vf sandstone
-shoreface to offshore transition heterolithic siltstone and vf. sandstone
-offshore-associated siltstone
-dolomitized bioclastic grainstone (Coquinal dolomite Middle Member)
-dolomitized bioclastic grainstone (Lower Montney coquina)
Ring-Pedigree Delta (Greisbachian-Dienerian)
Erosional line of Lower Triassic Montney Formation
Dixonville Delta (Smithian)
General trend of Devonian Leduc Fm reefs fringing the Peace River Arch
Meosin Ridge Subaerial Exposure (Greisbachian)
20 10 0 10 20 30 40 50
kilometres

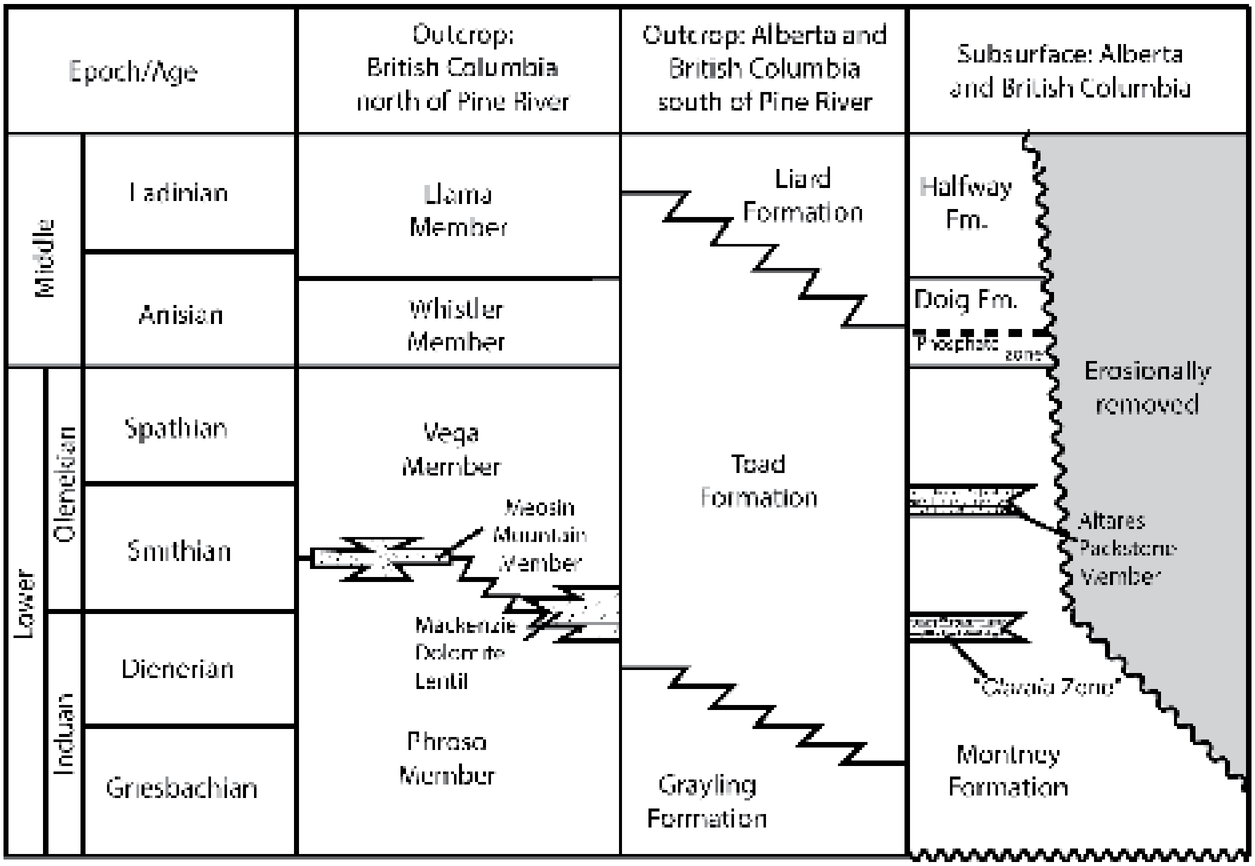
Epoch/Age
Outcrop: British Columbia north of Pine River
Outcrop: Alberta and British Columbia south of Pine River
Subsurface: Alberta and British Columbia
Middle
Ladinian
Anisian
Lower
Olenekian
Spathian
Smithian
Induan
Dienerian
Griesbachian
Llama Member
Whistler Member
Vega Member
Meosin Mountain Member
Mackenzie Dolomite Lentil
Phroso Member
Liard Formation
Toad Formation
Grayling Formation
Halfway Fm.
Doig Fm.
Phosphate zone
Erosionally removed
Altares Packstone Member
"Claraia Zone"
Montney Formation

Figure 3.2: The stratigraphic framework of the Lower and Middle Triassic in the Western Canada Sedimentary Basin, and the location and correlation of the Montney Formation with its outcrop equivalents. With formation names represented for both above and below the Pine River (modified from Zonneveld, 2011; compiled from Tozer, 1994; Orchard and Tozer, 1997; Orchard and Zonneveld, 2009).

gastropod, molds (commonly oil-stained) within a dolomite matrix, with local concentrations of lingulide brachiopods (Markhasin, 1997; Paull et al., 1997; Kendall, 1999). The coquina units, in both the Coquina Dolomite Middle Member (= Mackenzie Dolomite Lentil in outcrop) and the Lower Montney coquina (names that were developed in relation to the Alberta paradigm--each unit would occur in the Lower Montney in relation to the BC terminology), occur adjacent to the several subaerial unconformities that are present in the eastern part of the formation. The unconformity associated with the Coquina Dolomite Middle Member, has been interpreted to represent a possible 2nd or 3rd order Transgressive-Regressive sequence boundary (Markhasin, 1997; Davies et al., 1997; Paull et al., 1997). These coquina units were previously exploited as conventional plays and some companies are still interested, particularly on the fringes of the bioclastic units where coquinal limestone interfingers with siliciclastic siltstone and sandstone. However, identified bioclastic horizons in the western part of the basin are currently being investigated as unconventional plays, including both the "*Claraia* Zone", which occurs in the Griesbachian (lower Induan) section of the lower Montney Formation, and the bioclastic packstone, discussed herein as the Late Smithian Altares Packstone Member, which occur in the late Smithian (middle Olenekian) section of the middle Montney Formation, just below the Smithian-Spathian boundary (Golding et al., 2014).

3.3 Methods

Cores, through the zones of interest from twenty-seven wells (Table 3.1), were logged on a 1 centimeter to 2 meter scale, with attention paid to lithology, bioclastic composition, and physical and biogenic sedimentary structures. Bioclastic zones within the core were logged on a centimeter scale to aid in capturing variability within the zone of interest. The bioclastic packstone beds of the Altares Packstone Member were recognized in 8 of the core logged (Table 3.1). Bedding plane impressions were noted, and select specimens were taken for further photography, petrography, fossil, and trace fossil identification and analysis. Thin sections were then analyzed and described for diagenetic characteristics, fossil identification, and sedimentary characteristics.

Well logs through the horizon of interest were analyzed for unique characters to facilitate correlation between wells and to identify the horizon regionally in cored and non-cored wells (Fig. 3.3). The core gamma log signature was calibrated to match to the core characteristics and further ground truthed to down-hole gamma log signatures. The Late Smithian Altares Packstone Member has the cleanest gamma profile above the Montney-Belloy/Debolt contact and commonly has a blocky character below the cleanest spike. This is interpreted to reflect a drop in total organic carbon (OC). The upper surface is interpreted as a flooding surface, and was therefore used as a datum in regional cross sections (Fig. 3.3). Cross sections were used to determine the extent, distribution, and thickness of the packstone bed interval (Fig. 3.3). Isopach maps were constructed to extrapolate the packstone bed interval between and beyond known core locations (Fig. 3.4).

Core observations and well log correlations were used to construct a sedimentary framework based on 1) facies characteristics that were documented in multiple core and 2) taphonomic observations identified on bedding planes and in thin section. Core and well-log observations were used to assess the distribution of the zone, comparison to modern analogues has allowed the zone to be interpreted in relation to the depositional environment, and finally to make hypotheses about oceanic chemistry and biologic composition and diversity at the time of deposition. These hypotheses may be further tested using geochemical proxies in subsequent research.

3.4 Results

3.4.1 Bioclast Characterization

Bioclasts are the primary component of the packstone beds in this interval. The nature of the bioclasts in each accumulation aids in characterizing the location within the biostrome a particular bed represents as well as the nature of the faunal diversity and biostrome architecture. The taphonomy of the bioclasts themselves and the depositional history that can be drawn from them and the surrounding matrix are what have in turn lead the author to interpret these packstone beds as biostromes (Kidwell, 1991; Kidwell and Holland, 1991).

The packstone beds appear to be organized in two different ways, which are related the thickness of the beds (Fig. 3.5). The thinner beds consist primarily of disarticulated bivalves and/or brachiopod shells that appear to be primarily intact, and often have calcite cement within the internal side of the valves (Fig. 3.6 f). While it is more likely that the disarticulated valves are bivalves, it is nearly impossible

Well I.D.	***Cored Interval***	***"Claraia Zone" MD (m)***	***Packstone Beds MD (m)***	***Presence of "Claraia Zone"***	***Presence of Packstone Beds***
200/a-005-C 094-G-10/00	1854-1872; 2025.5-2043.5	1995	1870.3	x	
200/b-065-J 094-B-16/00	2102-2126	2122.8	1975.6		
200/b-050-H 094-B-16/00	2049.83-2077.3	2142.5	2052.7		x
200/d-008-F 094-B-16/00	2268-2286	2296.5	2177.5		
200/a-010-J 094-B-09/00	2310-2328.27	2318.1	2158.8	x	
200/c-074-G 094-B-09/00	1855-1864; 1954-1945.9	2112.1	1947.2	x	x
200/a-008-D 094-A-13/00	2162-2180	2176.1	2068.4	x	
102/08-07-085-18W6/00	1814-1832		1693		
100/09-21-085-16W6/00	1620.4-1638.85	1750.7	1608.4		x
100/16-17-083-25W6/00	2230-2530	2425.1	2384.1	x	x
100/01-10-082-23W6/00	1995-2013.4	2055.6	2018.6		appears as LBS
100/03-30-082-20W6/00	1899-1926	1900.3		x	
100/09-07-082-20W6/00	2022-2040	2010.2	1956.6		
100/04-11-081-21W6/02	2175.9-2212.17; 2139.75-2175.9		2228.3	x?	
100/14-29-080-20W6/00	2485-2584.05	2570.7	2519.8	x	x
200/c-006-L 094-B-08/00	2610-2845	2781	2660	x	x
200/c-65-F 094-B-08/00	2180-2575	2504	2375	x	x
8-30-82-20w6	1897-1915.45				x
13-11-81-20w6	2306-2323.92				x

Table 3.1: Table of cores analyzed and presence or absence of the packstone bed horizon or the “Claraia Zone”.

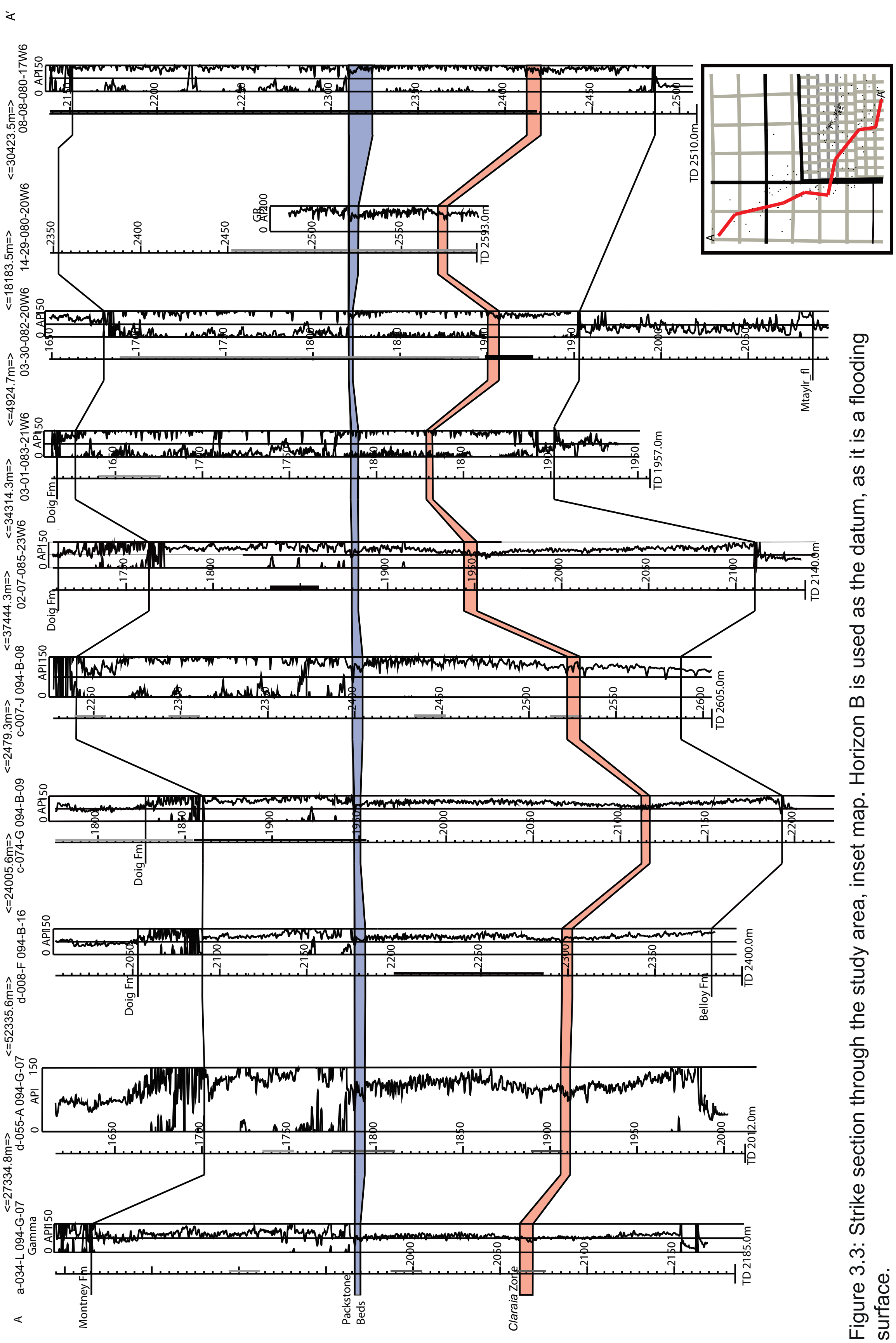

Figure 3.3: Strike section through the study area, inset map. Horizon B is used as the datum, as it is a flooding surface.

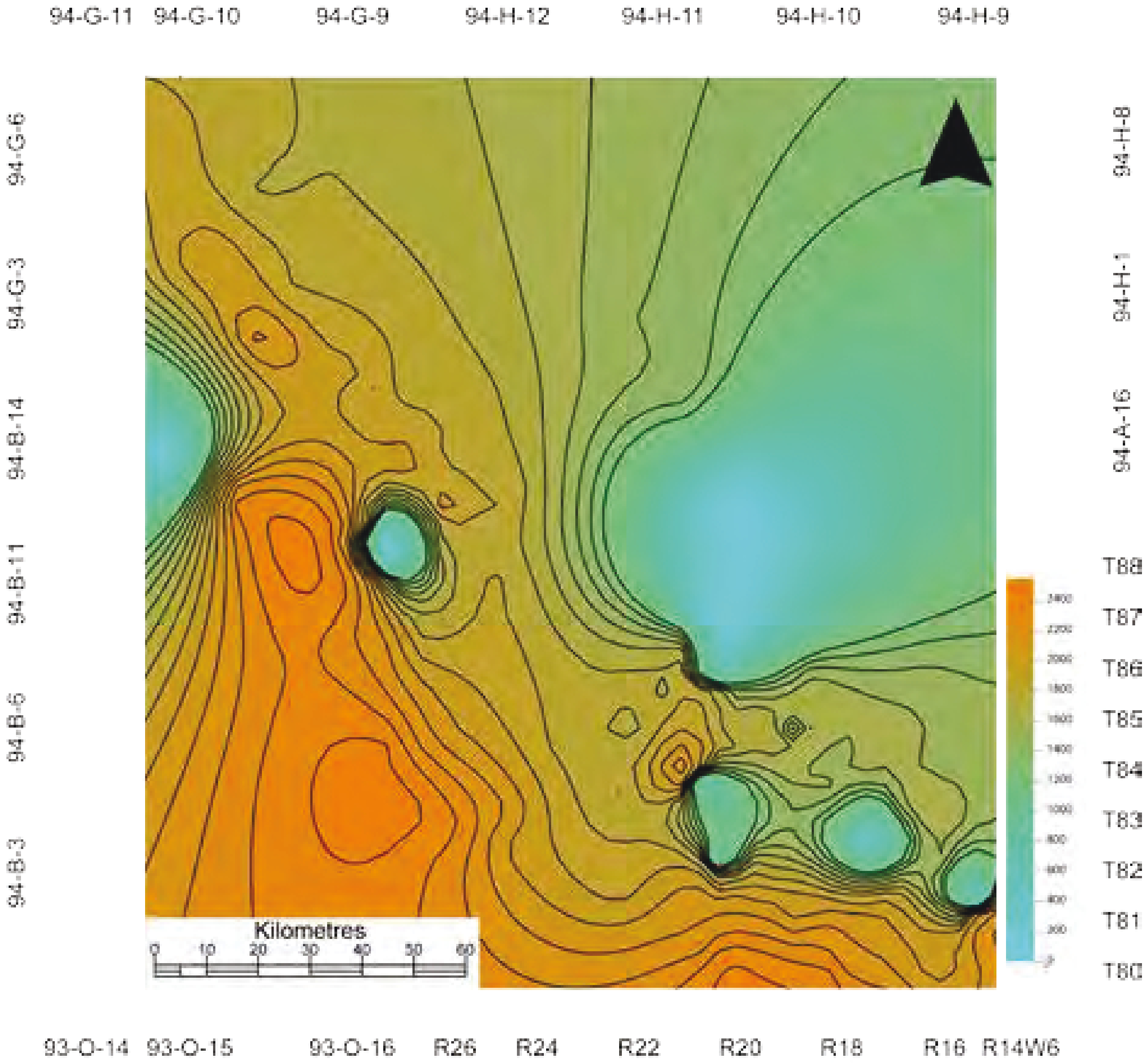
94-G-11
94-G-10
94-G-9
94-H-12
94-H-11
94-H-10
94-H-9
94-G-6
94-G-3
94-B-14
94-B-11
94-B-6
94-B-3
94-H-8
94-H-1
94-A-16
T88
T87
T86
T85
T84
T83
T82
T81
T80
2400
2200
2000
1800
1600
1400
1200
1000
800
600
400
200
0
Kilometres
0
10
20
30
40
50
60
93-O-14
93-O-15
93-O-16
R26
R24
R22
R20
R18
R16
R14W6

Figure 3.4: Isopach map of the top of Horizon B through the study area. Wells were centralized along the NW-SE trend.

---

to differentiate between the two types of valves once they are disarticulated. The cement between the valves is minor in comparison with the thicker beds, and most of the valves appear to be either oriented convex up or convex down, depending on the specific bed.

Within larger beds, a similar pattern is repeated near the base and top of the beds; however within these beds the cement matrix commonly occupies space that is nearly volumetrically equal to that of the bioclasts (Fig. 3.5, 3.6 b, c, e). The bioclasts appear to be nearly suspended in the cement at random orientations and angles and appear to be unfractured from what can be seen in thin section. In one bed in a-5-C/094-G-10, in which the bedding plane at the top of a packstone bed is revealed and likewise the preserved bioclasts are able to be observed, the bioclasts appear to be disarticulated and intact (Fig. 3.5). The thicker beds have a slightly higher taxonomic diversity with the addition of ammonoids, brachiopods, and rare vertebrate bone fragments at the center of the beds. Nonetheless, this

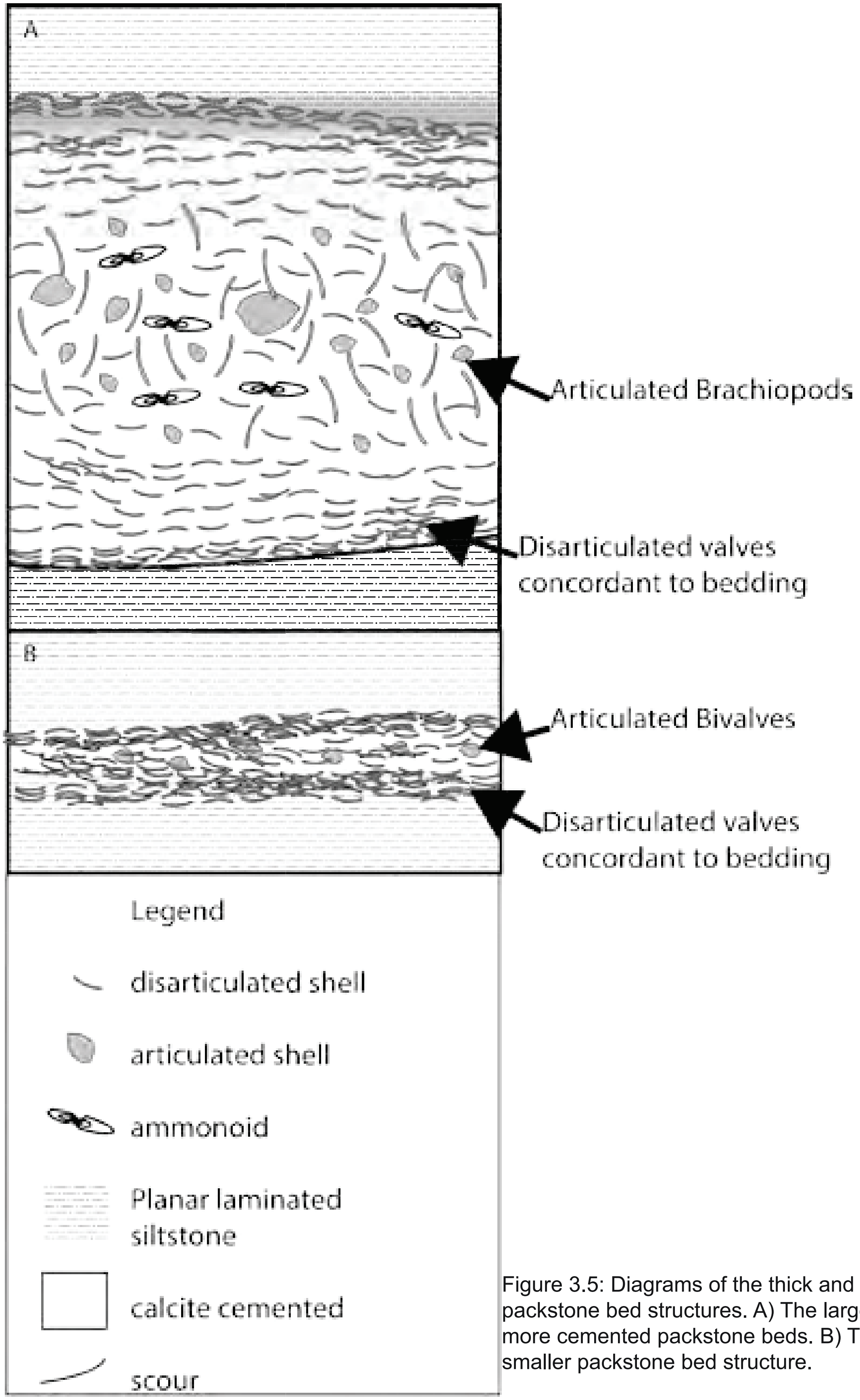
A
Articulated Brachiopods
Disarticulated valves concordant to bedding
B
Articulated Bivalves
Disarticulated valves concordant to bedding
Legend
disarticulated shell
articulated shell
ammonoid
Planar laminated siltstone
calcite cemented
scour

Figure 3.5: Diagrams of the thick and thin packstone bed structures. A) The larger, more cemented packstone beds. B) The smaller packstone bed structure.

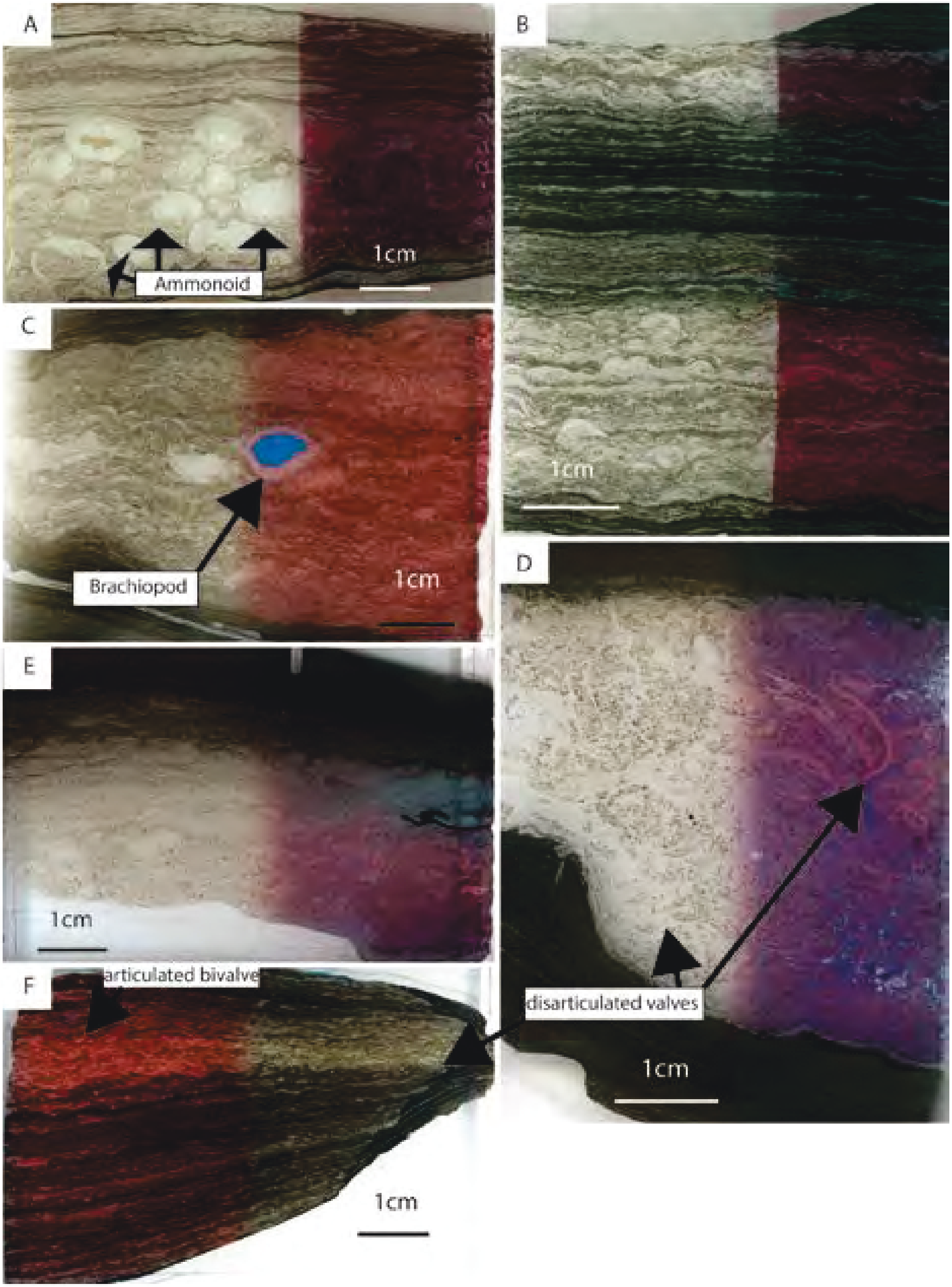
A
Ammonoid
1cm
B
1cm
C
Brachiopod
1cm
D
disarticulated valves
1cm
E
1cm
F
articulated bivalve
1cm

is still a much lower diversity than other biostromes (Hagdorn 1982; Zonneveld, 2001). There are also a few beds which contain bioclasts that are magnitudes of difference in size.

Along the top and bottom contacts of some beds, the bioclasts that occur within the siltstone proximal to the cemented packstone appear to be dolomitized and may have undergone some manner of dissolution (Fig. 3.7). This is in contrast to valves within the packstone that often have a spary calcite rim around the valves (Fig. 3.7). In both cases the number of articulated valves can range from very low ~1-5% of the bioclasts in beds with a higher silt content to ~20% or even more in other beds that are dominated by bioclasts.

Kidwell (1991) pointed out that bottom currents could be a mechanism that allows these shell beds to develop in an otherwise soft sediment environment and a delayed burial would allow for colonizing by organisms that add even more carbonate into the environment (Kidwell and Jablonski, 1983). This mechanism explains the mix of current-mediated fabrics (such as FA1 from the previous chapter) in association with apparently *in situ*, articulated shell material within the Late Smithian Altares Packstone Member.

3.4.1a Ammonoids

Although much of the bioclastic detritus in the packstone beds is fragmentary and recrystallized; several taxa, were found to be identifiable. At the base of the horizon, in well a-005-C/094-G-10, an ammonoid, identified as either cf. *Hypophiceras* sp. or cf. *Tompophiceras* sp., occurs. Additionally, within 16-17-083-25w6 pyritized ammonoids, tentatively identified as cf. *Ophioceras* sp., occur above the packstone beds (Fig. 3.8 a, b).

Ammonoids were primarily identified from impressions that preserved three dimensional molds and casts of the exterior of the shell as well as suture lines that aided in identification. The molds were preserved within the planar laminated siltstone surrounding the packstone intervals. Within thin sections of the packstone beds, ammonoids are typically found near the center of the bed, surrounded by disarticulated shells of other mollusks or brachiopods (Fig. 3.5). In one notable bed, the entire center section is made up of ammonoid shells deposited concordant with bedding with spary calcite filling the inner chambers (Fig. 3.6 a). The *Tompophiceras* sp. specimen occurs in a bed that also contains several bivalve impressions, most of which appear to have been partially crushed as they are missing the umbo region of the shell (Fig. 3.8 b).

Figure 3.6 (Previous page): Facies MBP: Thin section views of the bioclastic packstone. All of the sections are scanned in plane light, have double calcite staining, and the left side of E has staining for aragonite. A) Repetition of the facies within the thin section showing the hiatus of calcite cementation outside of the packstone (Well API = a-64-A/094-B-08). B) Another representation of the packstone in a thinner horizon that pinches out to the right of the thin section. C) This sample shows a brachiopod with particularly inflated valves in the center of the thin section. The internal cavity only is crystalized around the rim (Sample IRG-SA-1412-061). D) Gradation out of packstone back into siltstone facies (Sample BC38). E) The packstone is mostly made of ammonoids that has caused the bedding to be distorted around the packstone (Well API = a-64-A/094-B-8). This is one of the few examples which has an abundance of bioclasts other than bivalves and brachiopods. F) Deformation of the beds below the packstone as well as shells that are not oriented perpendicular to bedding (Sample BC39).

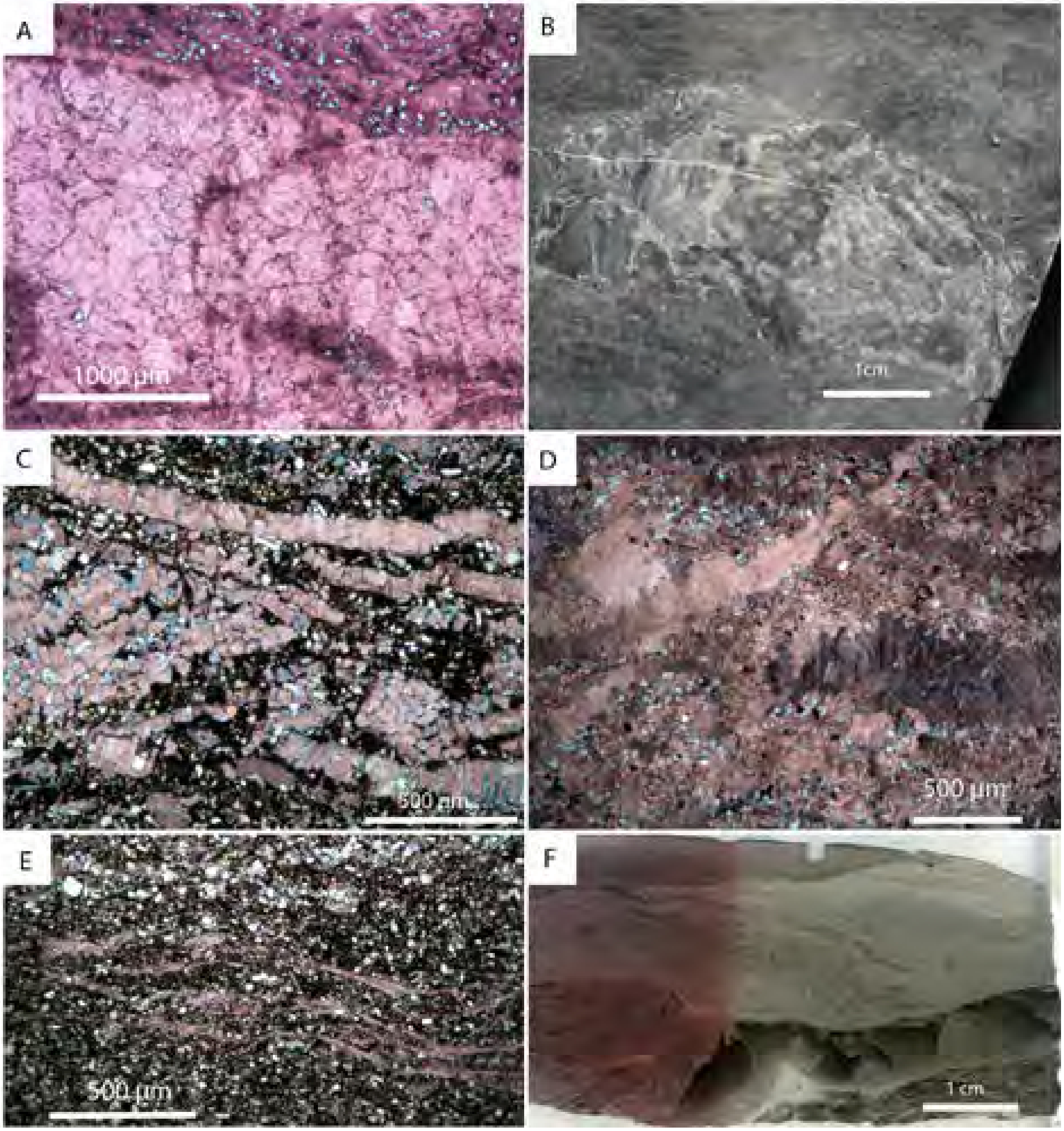

Figure 3.7: Various pictures of the bioclasts within the packstone beds. A) Disarticulated valves alongside whole ammonoids. B) Exposed bedding plane made of disarticulated bivalves on the top of a bioclastic packstone bed (Well API = 8-30-082-20w6). C) Shell structure of Claraia valves from the “Claraia Zone”. D) Valves with spary calcite rims within a packstone bed (photographed in cross-polarized light). E) Dissolved and dolomitized disarticulated valves from around a packstone bed. F) Packstone bed that has multiple erosion surfaces ontop of one another within the bed.

3.4.1b Bivalves

The primary fossil identified within and around the packstone beds is *Claraia clarae*, although *C. stachei* and *C. aurita* also occur within the horizon (Fig. 3.8 d, f). They are primarily preserved as impressions within the planar laminated siltstone separating the packstone beds. Only one bed has had a bedding plane exposed at the top of the bed which indicated that the valves within this horizon were made up of a single taxon (Fig. 3.7), however a whole valve was not exposed to allow for identification. The valves on this bedding plane appear to be intact and composed of the original shell material.

In thin section, bivalve shells in the packstone beds appear much differently than what has previously been observed. The bivalves appear to not have the prismatic shell structure made up of vertical columns of calcite that is typically observed in *Claraia* sp., but appear to have an inner organic layer that is surrounded by small prismatic calcite crystals that are often recrystallized diagenetically (Newell and Boyd, 1994) (Fig 3.7). The valves are much smaller (50-100µm compared to 200-250µm) than those previously documented in the Late Dienerian “*Claraia* Zone” in the same area. Although *Claraia* is the only bivalve that has been identified on bedding planes, it is clear that a second, as yet unidentified, bivalve taxon, is present, which is observed solely in thin section. This discrepancy is likely due to diagenetic alteration and the fact that the calcified layers in the packstone beds do not break apart readily at any planes that would allow the material to be identified. Limitations on core handling protocols preclude manually splitting the core in different horizons, although it is doubted that this would do more than reveal fragments of the second taxon.

3.4.1c Brachiopods

Articulated bivalves and brachiopods were identified in thin-section in the middle of some packstone beds (Fig. 3.6 c). The brachiopods are smooth-shelled and have inflated valves and are identified as terebratulide brachiopods (Figs. 3.6 c; 3.8 c). However minimal detail is preserved. Brachiopods are commonly identified in thin-section but are not identifiable beyond the ordinal level The cavities of articulated shells within thin section are filled with spary calcite, silica or dolomite. Brachiopod shells may make up the majority of the bioclasts observed in some thin-sections because the shell structure observed in articulated shells, as well as the inflation of most of the valves, is similar to that observed in the disarticulated valves. A differentiation based on shell material cannot be made due to the heavy recrystallization of the shell material in thin section.

3.4.1d Vertebrates

Vertebrate fragments are commonly observed on bedding planes and in thin section within the packstone beds, (Fig. 3.8 e). The vertebrate material consists primarily of fish skeletal debris, including both articulated material and isolated, disarticulated elements (Fig. 3.6 e). The articulated material is primarily found on bedding planes within the siltstone horizons around the packstone beds, and is never complete. Ribs and vertebrae are most common, with rare pectoral fins and cranial material also identified. Rare ichthyosaur material, including ribs, mandible fragments and vertebrae, have also been identified in this interval. Processing of this interval for conodont analyses has also revealed the presence of conodonts, a variety of fish teeth, and chondrichthyan dermal denticles.

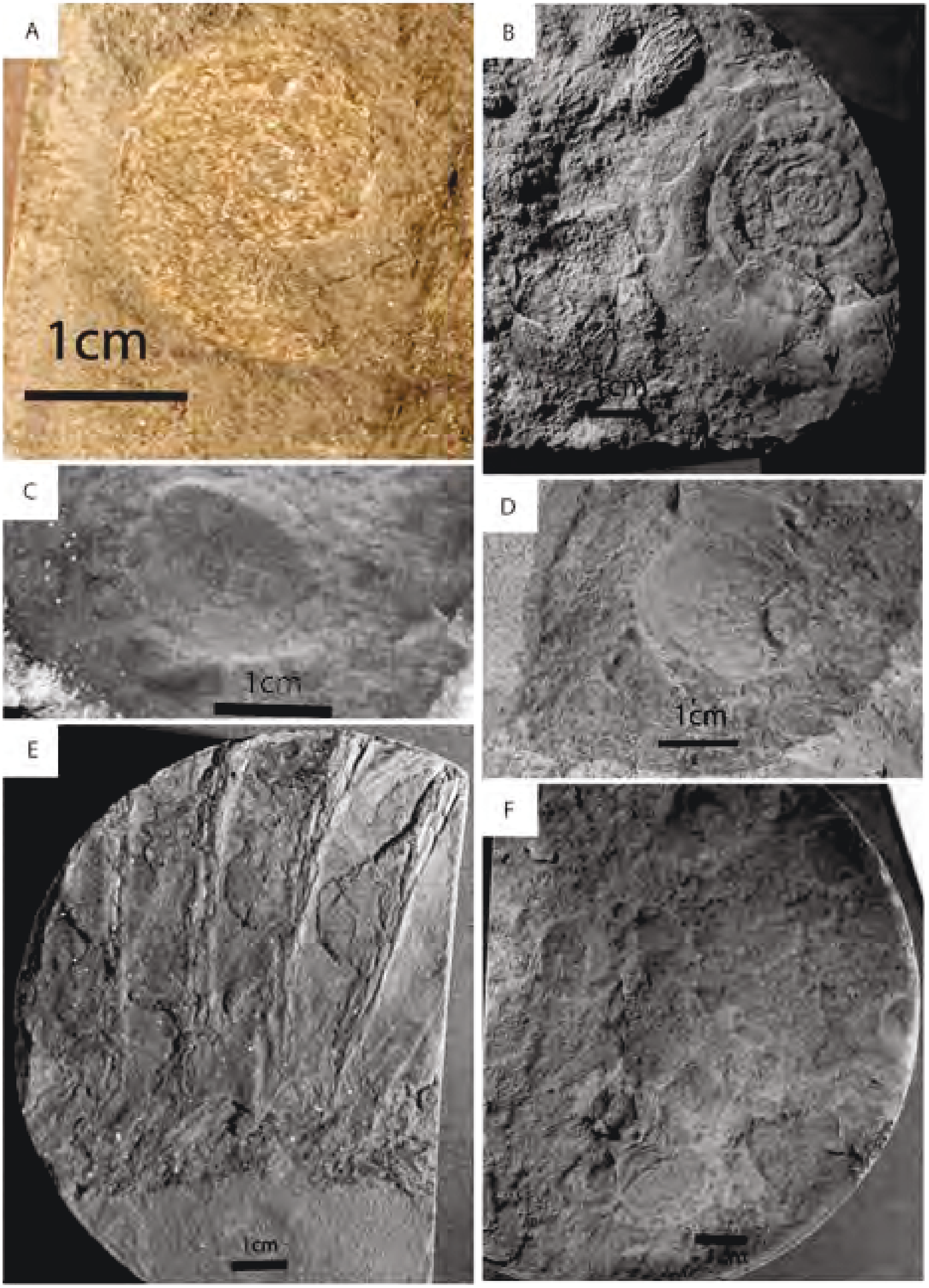
A
1cm
B
1cm
C
1cm
D
1cm
E
1cm
F
1cm

3.4.2 Facies

The facies surrounding the Late Smithian Altares Packstone Member are similar to those discussed in chapter 2, which focused on the "*Claraia* Zone", with the exception of the massive bioclastic packstone (MBP), which is the facies that dominates the Altares Packstone Member. The other facies that surround the MBP facies give more information in regards to the environment in which the Altares Packstone Member was deposited. The grain-sizes used within the facies below follow the Wentworth Classification (entworth, 1922), while the carbonate facies descriptions follow Dunham (1962) and the description of calcispheres follows Versteegh et al. (2009). Facies identified and described include: massive bioclastic packstone (MBP), Laminated siltstone (SL1), Rippled to laminated heterolithic very fine sandstone to fine siltstone (SL2), Calcisphere massive to laminated siltstone subfacies (CA), Calcit cemented concretions subfacies (CO), Massive siltstone (SL3), Bioturbated/mottled siltstone (SL4), Heterolithic convoluted laminated fine to coarse siltstone (SL5), Planolites bioturbated siltstone (BF1). The facies discussed in the previous chapter have been summarized along with MBP in Table 3.2. Table 3.3 shows the contacts of each facies with the surrounding facies.

3.4.2a Massive bioclastic packstone (MBP)

MBP consists of thin beds of bioclastic packstone that have been cemented with calcite (Fig 3.9). The beds of these intervals are massive or convolute. The packstone intervals are less than 8 cm thick, and contain shell material that can be microscopic or several centimeters in shell length. Shell material in this facies, and in the surrounding sediment, has not been compacted to the same degree as bioclastic detritus in LBS. There is commonly a sharp contact between the packstone and the surrounding siltstone. However, there are rare gradational zones, where bioclastic material gradually increases and there are bioclastic-laminated horizons within the siltstone. This sometimes forms crinkled laminae due to their abundance. Usually these intervals overlie, and are overlain, by SL1 or SL2. There is evidence in some cases of compactional deformation of siltstone laminae around packstone beds (Fig. 3.9 a, d). In thin section, MBP commonly exhibits a rim of bivalve shells that are oriented concordant to bedding and are packed together (Fig. 3.5). The shells are more widely spaced the further away from the outside edge of MBP intersections that they are. There can also be a change in the mineralogical composition of the shells along this rim, from dolomitized at the edge to calcite cemented at the center. There are commonly articulated valves of bivalves and brachiopods that may occur in association with ammonoids in the center of packstone beds (Fig. 3.6). The internal chambers of each ammonoid are filled with spary calcite, quartz, and, in some cases, dolomite instead of calcite. Bitumen occurs in the fine-grained siltstone surrounding MBP, but is sparse in the packstone. MBP can vary between a packstone and a wackestone at the center based on Dunham (1962).

3.4.3 Facies Associations

Based on the taphonomy and sedimentology of the bioclastic packstone beds, they are herein interpreted as biostrome deposits. Individual biostrome deposits are not believed to be laterally

---

Figure 3.8 (Previous page): Fossils found in and close to Horizon B in cores. A) Pyritized ammonoid that could possibly be Ophioceras sp. B) Impression of Hypophiceras sp. or Tompophiceras sp. C) Terebratulide impressions. D) Claraia clarae impressions. E) Vertebrate ribs and backbone. F) Claraia stachei.

Facies	***Minerology***	***Thickness***	***Grain Size***	***Sed. Structures***	***Trace Fossils***	***Body Fossils***	***Taphonomy***
MBP	quartz, clay minerals, detrital dolomite or calcite, plagioclase, silica or sometimes calcite cement, and high concentration of bitumen	1-10cm	Fine to coarse silt with pebble or larger size bioclasts	soft sediment deformation, scour, crinkled lamination		ammonoids, brachiopods (terebratulids), bivalves	valves can be disarticulated or articulated, articulated valves often have cement in the cavity. Valves do not appear to be abbraided, and ammonoids are whole.
SL1	quartz, bioclastic hash, some clay minerals, silica cement, and high concentration of bitumen	2cm-10m	fine silt, angular-subangular, mod. well sorted	planar lamination		bivalve and ammonoid impressions	disarticulated bivalve impressions. Sometimes there is fracturing, most ammonoids appear complete
LBS	quartz, silica or calcite cement, clay minerals, pyrite, high bitumen concentration in fine grained fraction	10-20cm	fine silt, angular-subangular, poor-mod. well sorted	planar lamination		Claraia sp.	fractured, disarticulated, sorted and stacked valves concentrated in beds
SL2	Calcispheres (either dolomite or calcite), quartz, small clay fraction occasionally, silica or calcite cement	20cm-5m	fine and coarse silt to very fine sand, angular, well sorted	starved and climbing ripples, flaser and lenticular bedding, mud drapes, scour surfaces	occasional Planolities		
CA	calcite or dolomite cement, pyrite rim, quartz grains, and some clay fraction	20-30cm	fine silt, round calcispheres	massive to planar lamination		occassional Claraia sp.	disarticulated, unfractured valves

Table 3.2: Tabular summary of facies, which details each facies' minerology, grain size, sedimentary structures, trace fossils, and body fossils that have been identified

Facies	***Minerology***	***Thickness***	***Grain Size***	***Sed. Structures***	***Trace Fossils***	***Body Fossils***	***Taphonomy***
CO	clay minerals, quartz, pyrite layers, silica cement	5-20cm	fine or coarse silt	lense shaped features with mostly planar lamination		bivalves	abbraided, fractured, and disarticulated valves
SL3	quartz, clay minerals, detrital dolomite, silica cement	20-50cm	fine silt, angular, well sorted	massive	none observed		
SL4	quartz, clay minerals, pyrite, silica cement	3-10m	fine to coarse silt, angular, mod. well sorted	mottled/bioturbated	observed, but not identified		
SL5	quartz, clay minerals, pyrite, silica cement	5-20cm	fine and coarse silt to very fine sand, angular, well sorted	soft sediment deformation, scour			
BF1	quartz, clay minerals, detrital dolomite or calcite, plagioclase, silica or sometimes calcite cement, and high concentration of bitumen	5-20cm	fine to coarse silt, angular, well sorted	planar lamination, scour	Planolities, Phycosiphon		

		SL1	LBS	SL2	CA	CO	SL3	HB	SL4	SL5	BF1
Laminated Fine siltstone	**SL1**		g/s	s/c	s/g/ow	ow	g	s/g/c	g/c/s	s/g	g
Laminated bioclastic siltstone	**LBS**	g/s		s/g	s/g/ow	ow	g/s			s/g	
Heterolithic rippled to laminated siltstone to very fine sandstone	**SL2**	s/c	s/g		g/ow	ow		s		g	
Laminated to massive calcisphere siltstone	**CA**	s /g/ow	s/g/ow	g/ow							
Calcite cemented concretions	**CO**	ow	ow	ow				ow			
Massive siltstone	**SL3**	g	g/s					s/c	g		
Massive Bioclastic Packstone	**MBP**	s/g/c		s		ow	s/c				
Bioturbated mottled siltstone	**SL4**	g/c/s					g				
Heterolithic convoluted laminated siltstone and vf sandstone	**SL5**	s/g	s/g	g							
Planolites Bioturbated siltstone	**BF1**	g									

Table 3.3: Table of facies contacts. G = gradational, S = sharp, C = Scour, OW = Occurs Within

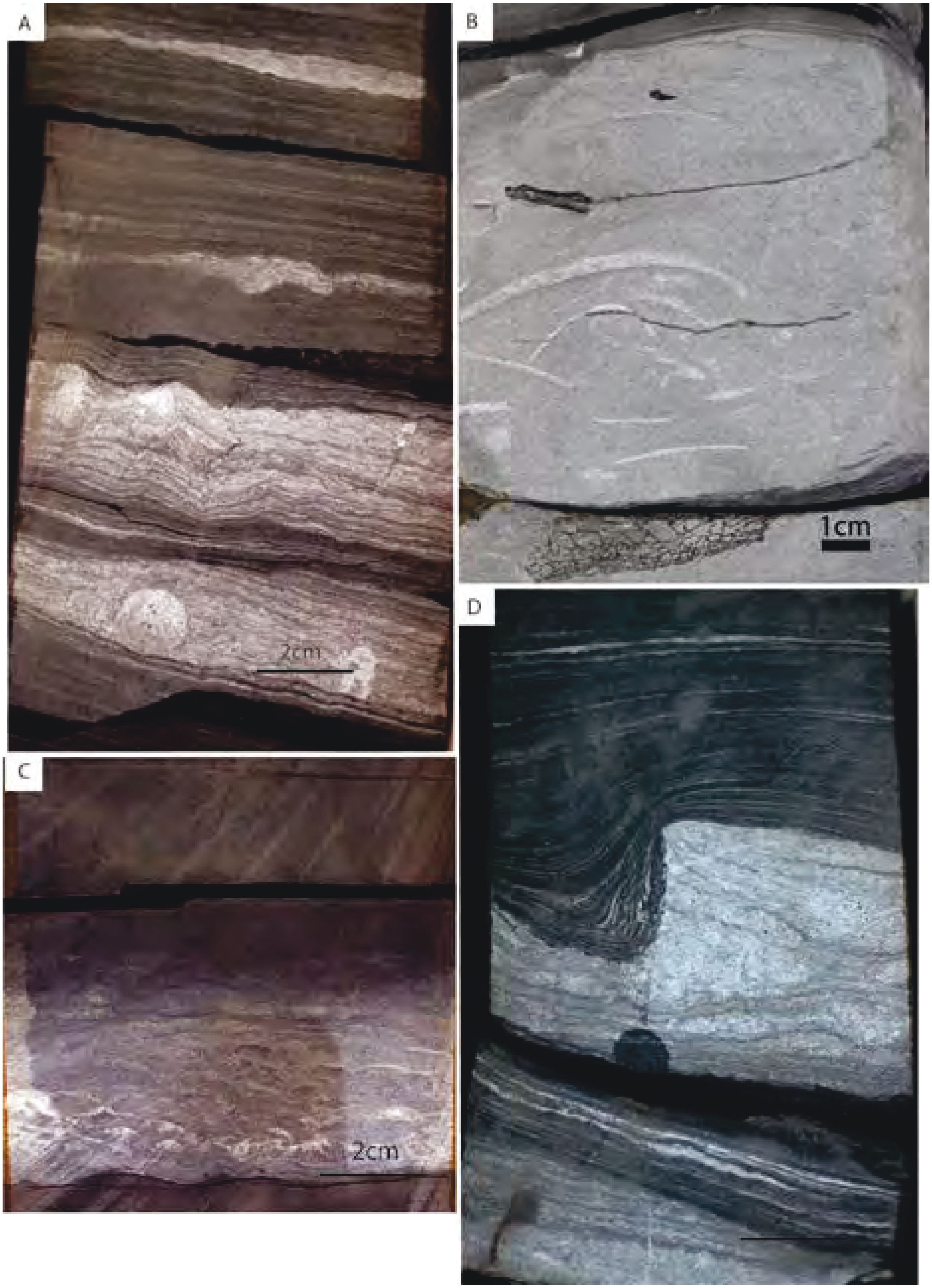
A
2cm
B
1cm
C
2cm
D

continuous on a regional basis (~100s km), and are likely discontinuous on a more local scale (Fig. 3.10). The biostrome facies association comprises a third facies association, distinct from those identified in chapter 2 (Table 3.4). While the previous facies associations represented deposits directly formed by bottom current deposition, this facies would have likely only had minor influence of the currents while the primary depositional mechanisms would have been the result of allogenic taphonomic feedback (Kidwell and Jablonski, 1983).

3.4.3a FA3: Biostromes

While biostromes were first termed by Cummings (1932), there have been multiple attempts at defining and redefining the architecture of biostromes due to their significance both in the econom sector as concentrators of organic material and due to their ecological significance (e.g., Klement, 1967; Kershaw, 1994). The definition by Kershaw (1994) of biostromes as low relief structures of built up biotic material that remain a primarily continuous thickness across their breadth is followed herein. These beds contain layers of bioclasts, particularly valves of bivalves and brachiopods (Fig. 3.6b, f). These layers would most likely represent multiple generations of organisms. The small and large packstone deposits represent the lateral edges and the center of the biostrome deposits respectively. The smaller beds represent the fringes of the biostromes, while the thicker beds represent the well-developed, and typically well-cemented, centers of the biostromes. The shell lags at the base of the biostromes may have been the result of bottom currents similar to those that created Facies Association 1 (FA1) and Facies Association 2 (FA2) or even the result of rare events such as a turbidity currents or storm-generated offshore flow (Fig. 3 1). A strong current would have had to been present to cause the scour surfaces that are common at the bases and/or tops of the beds as well as within the beds (Fig. 3.7). Facies such as SL2 and SL1 are usually adjacent to MBP, which further supports the influence of a bottom current in bed origin and modification

The presence of FA1 adjacent to FA3 in well 8-30-082-20w6 further illustrates the possibility of current mediation in the deposition of FA3. This provides more evidence, in the form of ripples and mud drapes, of wind driven bottom currents influencing Montney deposition in the study area. However, as compared to FA2, FA3 has allowed for carbonate deposits to develop *in situ.* An *in situ* macrofauna biogenic deposit is rare among Triassic deposits in Panthalassa (Pruss et al., 2005 a, b; Mata and Woods, 2007). Oxygen is often called upon in reference to the depauperate fauna in the Early Triassic (Isozaki, 1994; Schubert and Bottjer, 1995; Woods et al., 1999; Greene et al., 2011; Pietsch and Bottjer, 2014). Payne et al. (2014) hypothesized that the anoxia associated with the world's oceans during the Early Triassic was likely the result of expanded Oxygen Minimum Zones (OMZ). The expansion of the OMZ would have had the largest effect on organisms with in the shelf environments (the habitable zone of Beatty et al. (2008)) (Alroy et al., 2008; Doney et al, 2009; Beaufort et al., 2011).

Acidification, in particular, has been an explanation used by researchers for the lack of calcified body fossils within the Montney Formation, however in the Union Wash Formation of the western United

Figure 3.9 (Previous page): Facies MBP: Bioclastic packstone facies A) Packstone beds from 16-17-083-25w6. A shows repetition of the facies with the common wavy appearance of the facies. B) Packstone from 14-29-080-20w6 shows large thick bivalve shells within it along with vertebrate material. C) Packstone from 13-11-081-20w6 shows another variation of the facies with the scoured base and the grading up. D) Packstone beds from 16-17-083-25w6. Similar to A shows the repetition along with soft sediment deformation.

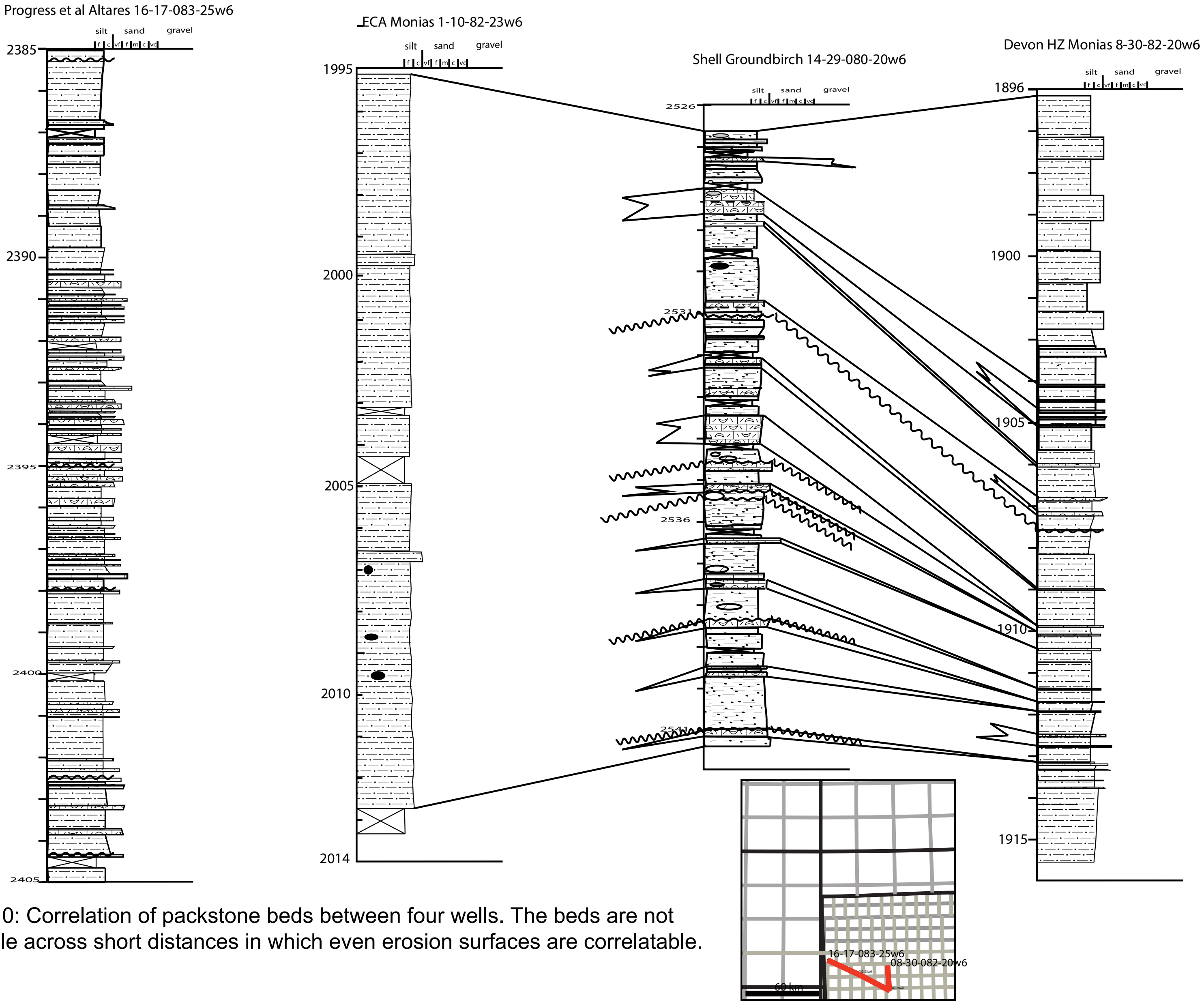
Progress et al Altares 16-17-083-25w6
ECA Monias 1-10-82-23w6
Shell Groundbirch 14-29-080-20w6
Devon HZ Monias 8-30-82-20w6
silt
sand
gravel
f c vf f m c vc
2385
2390
2395
2400
2405
1995
2000
2005
2010
2014
2526
2531
2536
2541
1896
1900
1905
1910
1915
16-17-083-25w6
08-30-082-20w6
60 km

Figure 3.10: Correlation of packstone beds between four wells. The beds are not correlatable across short distances in which even erosion surfaces are correlatable.

Facies Association	***Facies***	***Depositional Environment and Description***
FA1: Fan Derived Bottom Current Modified Deposits	SL1, SL2, CA, CO, SL3, SL4, SL5, BF1	Bottom current winnowing and sedimentation of coarse-grained sediment forming ripples and interbedded with suspension deposition derived fine-grained horizons. This facies association is located near a coarse grained sediment source such as a turbidite fan.
FA2: Distal Bottom Current Modified Deposits	SL1, LBS, CA, CO, SL3	Bottom current winnowing and sedimentation of bioclasts with increasing bioclasts with stronger and longer lasting currents. Bioclast beds are interbedded with fine-grained horizons. This facies association is located further away from any coarse-grain sediment source.
FA3: *In situ* Biostromes	MBP, SL1, SL2, CO	*In situ* accumulations of bioclastic debris that were likely brought in by similar currents to FA1 and FA2 which allowed colonization by hard ground favoring organisms. Allogenic taphonomic feedback allowed these accumulations to self perpetuate until oxygen deficiency likely suffocated the organisms.

Table 3.4: Summary and description of the three facies associations.

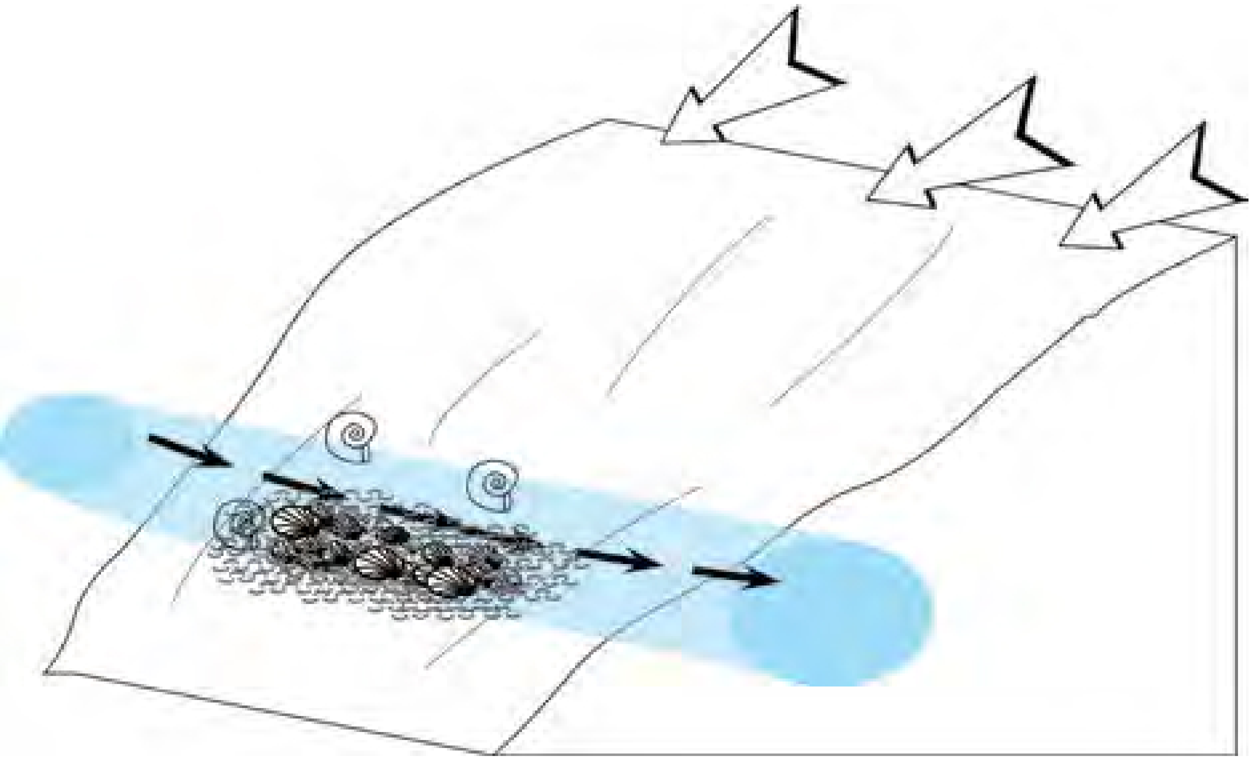

Figure 3.11: Diagram of the location of FA3 within the same environment as FA1 and FA2.

States, Pruss and Bottjer (2004) have interpreted there to have been a super saturation of $CaCO_3$ in the ocean (Hotinski et al., 2001; Zonneveld, 2011; Greene et al., 2012). As noted in the previous chapter, there is a noted difference in preservation potential of calcified body fossils in the Montney Formation. The "*Claraia* Zone" and the Altares Packstone Member are two of the few horizons where calcified body fossil have been preserved. While the *in situ* development of the Altares Packstone Member could be attributed to a change in oxygenation (and perhaps a contraction of the OMZ), the presence of calcified body fossils within this horizon must be associated with another chemical change within the basin.

3.5 Discussion

3.5.1 Biological and Sedimentological Analyses

Early Triassic reef deposits remain unknown from the geologic record, an interval termed the Early Triassic Reef Gap (Flugel, 1994). However, microbial biostromes have been identified in the Tethys Ocean during the Early Triassic alongside the microbial reefs that have been identified within the Virgin Limestone of western United States (Lehrmann, 1999; Jin et al., 2000; Pruss and Bottjer, 2004). Stromatolites and other microbial structures from which these biostromes have been formed have been referred to as "disaster taxa" while a true metazoan biostrome would represent a further stage of recovery (Schubert and Bottjer, 1992; Pruss and Bottjer, 2004). While biostromes are not considered reefs (*sensu stricto*), they still represent important markers of biologic activity within a system and are of particular importance to the recovery story after the Permian-Triassic mass extinction.

As discussed above, articulated shells commonly, both of bivalves and brachiopods, occur in a matrix of recemented calcite and disarticulated shells of a wide variety of sizes and shapes. Both bivalves and brachiopods have been observed to have articulation rates between 5 and 20%, and while that is a low articulation rate for brachiopods it is especially high for Pectinoid bivalves. There may be a bias in the rate observed for brachiopods as identification of brachiopod valves becomes difficult once th have been disarticulated. The abundance of articulated bivalves indicates, when coupled with the lack of abrasion and fragmentation of the valves, that there is a high probability that these fossils were not transported (or were not transported far) (Kidwell and Bosence, 1991). There are three different species of *Claraia* present, along with terebratulide brachiopods, multiple ammonoid taxa of different sizes, and vertebrates, including fish material. This fauna includes nektonic fauna made up of ammonoids (McGowan, 2004), fish, and ichthyosaurs as well as epifaunal taxa made up of brachiopods (Hagdorn, 1982; Zonneveld et al., 1997) and *Claraia* sp. (Newell and Boyd, 1994; Schatz, 2005) in varying abundances within the bioclastic packstone. Although this fauna is not particularly diverse, particularly with respect to modern marine faunas, it is anomalously diverse when compared to other sections within the Montney Formation (Kendall, 1999; Panek, 2000; Zonneveld et al., 2010a,b). However, diversity in the western United States sections is much higher than what can be seen here (Schubert and Bottjer, 1995; McGowan et al., 2004; Mata and Woods, 2008). Schubert and Bottjer (1995) recognize 5 different ecological guilds within the Sinbad Limestone and the Virgin Limestone and 27-28 different species. The Sinbad Limestone represents a gastropod lagerstätten while gastropods are absent from the Altares Packstone Member (Nutzel, 2005; Nutzel and Schulbert, 2005).

Wignall and Hallam (1991; Wignall, 1994) suggested that the presence of both nektonic and benthic organisms is indicative of a moderate level of recovery after a larger scale anoxic event. Wignall and Hallam (1991) argue that dysoxic tolerant organisms, such as *Claraia,* and nektonic ammonoids are present together in environments recovering from an anoxic event. This evidence of recovery in the Altares Packstone Member is contrary to the $\delta^{13}C$ record from the Sverdrup Basin by Grasby et al. (2013) that states that there is an anoxic event at the Smithian-Spathian boundary. Zonneveld (2011) similarly notes the Smithian-Spathian boundary to be devoid of carbonate, and refers to it as the Olenekian carbonate absence zone, which has been found to be false with the presence of the Altares Packstone Member at the Smithian-Spathian boundary. In the western US sections, there is a possible carbonate super saturation that produced carbonate fans, the like of which has not been recorded since the Proterozoic (Pruss and Bottjer, 2004). This is compounding evidence that the Peace River Embayment experienced a different ocean chemistry than other sections on the NW coast of Pangea

Figure 3.9 (d) shows that the packstone was cemented before the subsequent erosion and deposition of the siltstone on top of it. The packstone in this figure has been cut into (note the irregular top boundary) and the sediments above the packstone preferentially fill in the incision with thicker beds concentrated within the incision that can be followed out and across the face of the core. This indicates that at some point, the packstone was an early-cemented hardground. An early-cemented hardground could provide space for colonizing organisms to flourish, however in this instance that does not appear to be the case. There are no borings in the hard ground, nor any subsequent shell beds built on top of it, as has happened in other cases (Fig. 3.7). An absence of borings or other colonizers could indicate that the biostrome in this bed was unable to reestablish before being buried again, possibly due to being within the Oxygen Minimum Zone. Metazoans in particular show a diminishment in diversity and abundance within Oxygen Minimum Zones (Levin et al., 1991; Gooday et al., 2009).

The typical section through one of the packstone beds shows a massive center where most of the articulated bivalves, brachiopods, and ammonoids are located (Fig. 3.5). Compressed, disarticulated valves are aligned parallel to bedding around the outside edges at both the top and the bottom of the packstone. They appear to have been deposited around the same time as the packstone bed itself, however the cementation of the main bed did not extend to those valves. There is commonly a gradient towards the middle of the bed where the disarticulated valves are dispersed within a groundmass of matrix and shell fragments. The shells are arranged concordant to bedding near the bed contacts, whereas in the center of the beds, they have a more chaotic arrangement in the matrix and the rock is more a wackestone than a packstone (Dunham, 1962). The cemented valves progress from a closely packed arrangement around the top and base to a loosely packed arrangement in the center of the bed. Such a change in aggradation of shell material could be related to the presence of fauna attached to the shell lag that buffered water and currents around them (Hagdorn, 1982; Kidwell, 1991)

It is likely from the presented data that these packstone beds represent the earliest Mesozoic metazoan biostromes. Previously, the earliest Mesozoic biostromes in NW Pangea were the Liard Biostromes at Williston Lake (Zonneveld, 2001). Scour surfaces commonly top the packstone beds. The scour surfaces along with the occurrence of fine sandstone ripples, likely reflect either storm reworking o bottom current modification dependent on the location of the beds in relation to storm wave base. Ripples similar to those found in SL2 have been found around the biostromes (Fig. 3.12 a), which formed either by wind driven bottom currents or by storm induced deposition, possibly similar to the deposition of FA2 in the "*Claraia* Zone". Both mechanisms likely attribute to the presence of the anomalously large bioclasts in the environment, and perhaps also for the transportation of new opportunistic fauna into a previously uninhabitable environment (Kidwell and Jablonski, 1983; Kidwell, 1991).

A transported or winnowed pavement of shells would form a hard ground on which organisms such as brachiopods or epifaunal bivalves could colonize (Driscoll and Brandon, 1973; Kidwell and Jablonski, 1983). Once the hard ground is developed, it self-perpetuates until it is suffocated by sediment or anoxia. The addition of each generations' shells to the patch would provide even more surface for colonization and the perpetuation of the deposit (Kidwell and Jablonski, 1983). This idea is similar to the formation of the benthic islands reported by Kauffman (1978) and Zuschin et al. (1999). The epifauna reported in each of these cases attached to a hard structure at the base (Kauffman, 1978; Zuschin et al., 1999), however these benthic islands appear to be short lived and very small in scale such that they may be missed by simple grab sampling (Zuschin et al., 1999; 2000). At present there is no evidence of hardground preferring organisms within the packstone beds. Terebratulide brachiopods have been observed in mud bottoms in New Zealand (Richardson, 1981). Therefore an initial hardground was not a necessary requirement for the formation of the packstone beds within the Montney Formation. Nonetheless, it would have been a result of the accumulation of the shells of multiple generations of fauna.

The biostrome layers are not singular features in the cores. They appear multiple times in core with thin, cemented layers that increase up to a packstone bed, which is normally not more than a few

---

Figure 3.12 (Next page): Bedforms found in and around the Altares Packstone Member. A) Starved mud draped ripples from C-74-G/094-B-8. B) Packstone pinching out on the back of a core piece from 13-11-081-20w6.

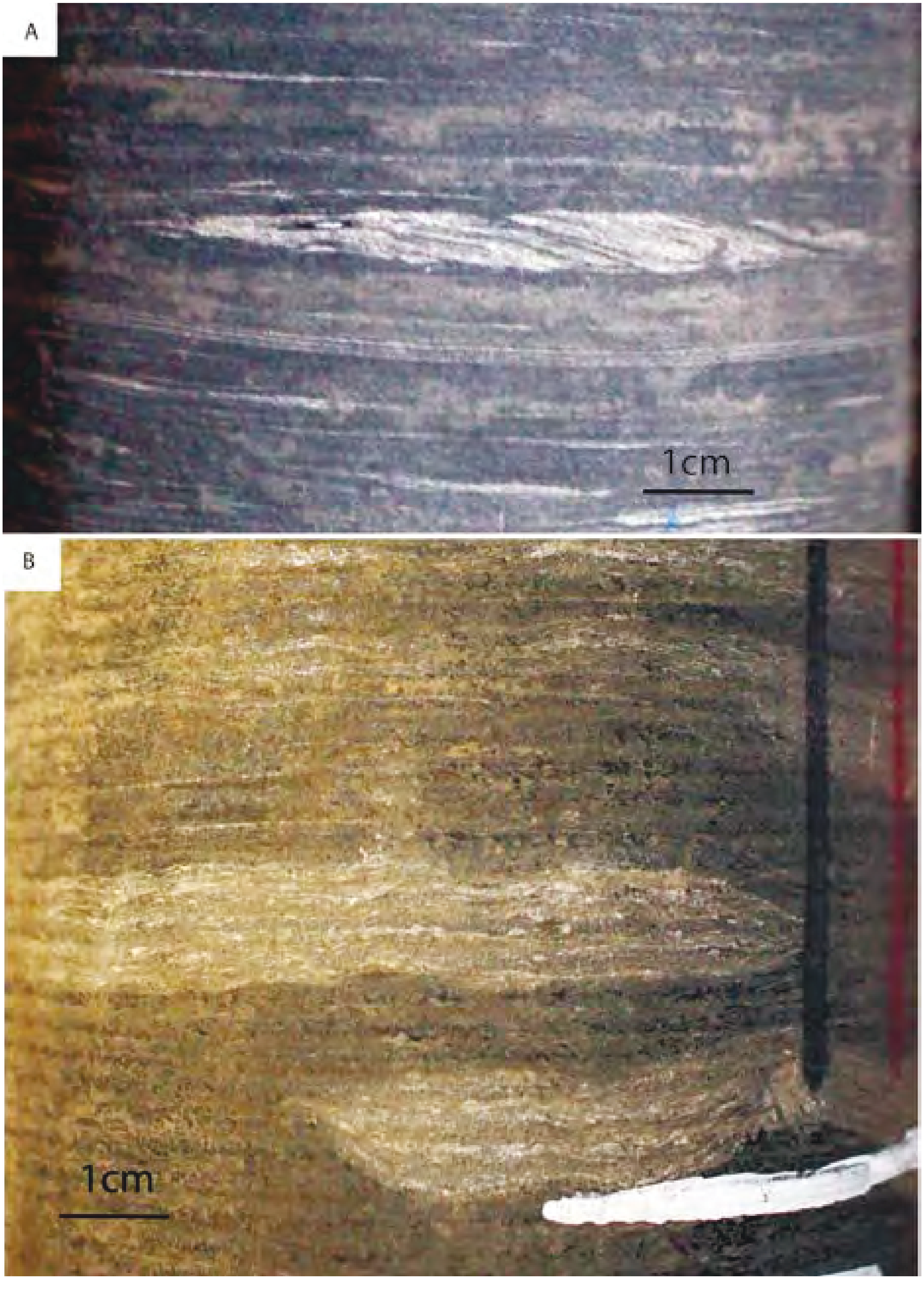
A
1cm
B
1cm

centimeters to a decimeter in thickness. They have been found to be discontinuous over a small area (Fig. 3.13; Fig. 3.9 a,d; Fig 3.12 b; Fig. 3.10). The abundant bioclastic component of individual beds may impart a crinkled appearance to the siltstone layers below the packstone, but in 1-10-082-23w6 there is no cementation of these layers and they appear as LBS even though it is within the same interval on gamma ray density logs. This is another indication that even if the shell pavement existed initially, it had to be colonized to form the biostrome beds present in other core.

It is hypothesized herein that the repeated biostrome layers represent repeated 'attempts' for the carbonate factory to 'restart', which would have resulted in a carbonate ramp, similar to what existed in the study area prior to the P-T boundary. However, the colonization horizons are each short-lived, likely due to an expansion and contraction of the Oxygen Minimum Zone (OMZ) (Levin et al., 1991; Gooday et al., 2009; Payne et al., 2014). If it is related to the OMZ, these packstone beds could record an increase in oxygen allowed for colonization for a brief period before a sudden decrease once again such as Hallam (1987) describes (Fig. 3.14). Macrofauna are significantly affected by the OM and have been identified to be in their lowest abundance and diversity inside of it (Levin et al., 1991; Gooday et al., 2009). The highest macrofaunal diversity is identifiable on the top edges of the OMZ, particularly in bivalves (Levin, 2003). Therefore it follows that these biostromes could have developed on the top margin of the OMZ in the Peace River Embayment. Regardless, it is clear that these features are a widespread, temporally short-lived component of the British Columbia Montney ramp succession. Multiple occurrences, both vertically and laterally, indicate a dynamic balance between silt sedimentation, colonization, and development of the biostrome. Repeated occurrence over several meters of section indicates an environmental instability through the study interval, and yet brief intervals in which living conditions were favorable. The sudden appearance of these features in the late Smithian (mid-Olenekian) in a geographically restricted part of the Montney basin, and their equally rapid disappearance from the broader study area supports the hypothesis of long-term instability of physic-chemical conditions during the Early Triassic of western Canada. Whether this is a function of oxygenation, oceanic chemistry or another environmental factor remains uncertain.

3.5.2 Analogues

3.5.2a Middle Triassic Biostromes

From the evidence outlined above it can be concluded that the bioclastic units around the Middle Montney boundary in BC represent the earliest known Mesozoic biostromes from northwestern Pangea, and possibly the earliest Mesozoic metazoan biostromes. The Montney Formation examples lack the ichnological signature of those described by Zonneveld (2001) from the late Middle Triassic (Ladinian) Liard Formation. They are considerably thinner (decimeter scale versus meter-scale), and likely record a much shorter duration of development. The Middle Triassic examples formed biostromes that were upward of 5 m in thickness, and include a diverse assemblage of invertebrate taxa. The difference between the assemblages reported in the Middle Triassic biostromes versus the beds in the Montney Formation supports the interpretation of unstable environmental conditions in the Peace River Embayment in the Early Triassic. The Montney Formation examples are thinner and likely not as laterally extensive as those found in the Middle Triassic, but the difference in the structure and taxa that make up the center and lateral edges of the biostrome is identifiable (Fig. 3.7 a, b, c, e). The packstone beds on the edge of individual biostromes are thinner and mainly composed of disarticulated shells, as compared

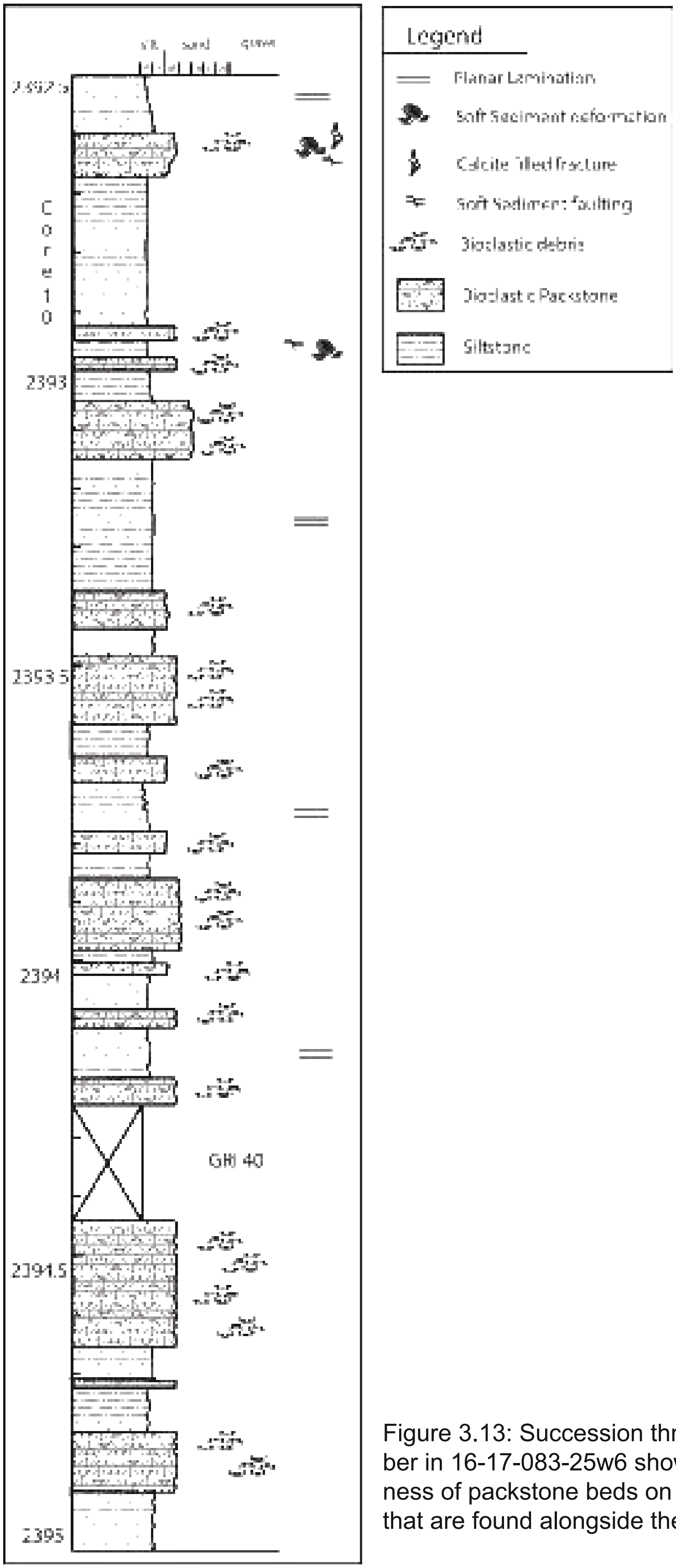
silt
sand
gravel
2392.5
Core 10
2393
2353.5
2394
GR 40
2391.5
2395
Legend
Planar Lamination
Soft Sediment deformation
Calcite filled fracture
Soft Sediment faulting
Bioclastic debris
Bioclastic Packstone
Siltstone

Figure 3.13: Succession through part of the Altares Packstone Member in 16-17-083-25w6 showing the increase and decrease in thickness of packstone beds on a small scale and sedimentary structures that are found alongside the packstone beds.

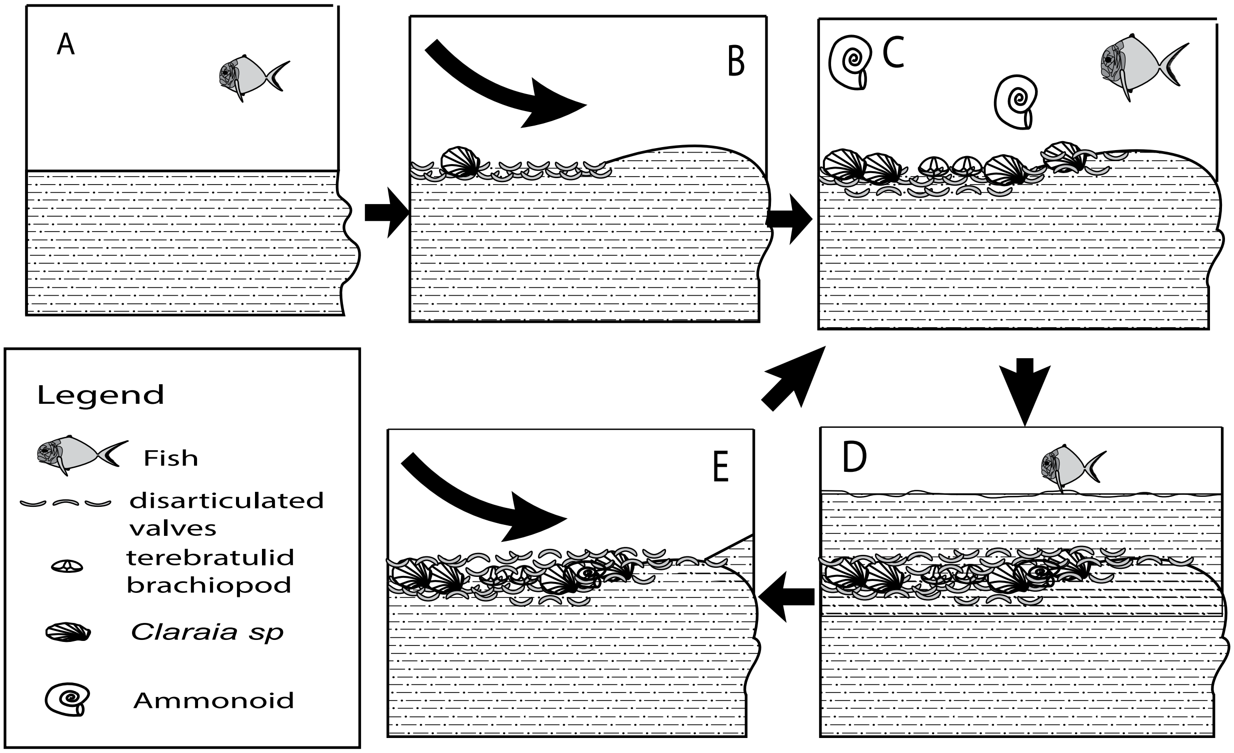

Figure 3.14: Formation of biostromes in the Middle Montney Formation based on Zonneveld (2001). A) Deposition of siltstone in background conditions. B) Storm or current brings in disarticulated valves and live opportunist larvae and adults who recolonize the patch. C) Shells serve as a hard substrate for other colonizers which in turn provide prey for nektobenthic organisms as well as nektonic fauna. D) Either low oxygen kills off fauna or sudden sedimentation buries the organisms. This is a return to background conditions, but beneath the sediment-water interface the packstone is cemented. E) A storm or current uncovers and erodes into the packstone allowing it to become a hardground again.

with those that are located closer towards the center, which contain articulated shells and ammonoids in the packstone. A difference in the duration of buildup and overall faunal diversity of the Embayment in the Lower Triassic compared with the Middle Triassic would account for the differing compositions of the packstone beds as well as the difference in thicknesses of the two biostrome units

3.5.2b Muschelkalk *Placunopsis* Biostromes

The Muschelkalk Biostromes are Middle Triassic in age from Germany (Hagdorn, 1982). The *Placunopsis* beds are pillars that were initially built up by encrusting *Placunopsis* on an exposed surface of ruditic bio-oosparites until the oolite was ripped up so that the biostromes were subsequently formed on top of clasts (Hagdorn, 1982; Hagdorn and Mundlos, 1982). The biostromes accumulated approximately at the same rate as the sediment around them, creating pillar-like/stromatolite-like buildups that were eventually bored by organisms that made *Trypanites, Calciroda,* and *Talpina* traces (Hagdorn, 1982). While the biostromes were only 2-5 m in diameter laterally, the horizon which contains the biostromes are identifiable across tens of kilometers and similar biostromes were identified in Poland (Hagdorn 1982; Bodzoich, 1985). These 40 cm high pillars are in stark contrast to the long thin deposits found in the Montney Formation, but the *Placunopsis* biostromes were identified to be deposited between storm wave base and wave base due to the consolidation of bioclasts and lack of siliclastic sediment, which is somewhat similar to what is found in the bioclastic packstone beds of the Late Smithian biostromes discussed herein (Hagdorn, 1982). This encrustation mechanism that was used in the formation of the *Placunopsis* biostromes does not appear to be the same mechanism used by organisms in the Late Smithian biostromes.

3.5.2c Sinbad Limestone and Virgin Limestone

Two Members of the Moenkopi Formation in western United States have been thoroughly studied in reference to the recovery interval after the Permian-Triassic Mass Extinction, the Sinbad Limestone which is Smithian in age and the Spathian Virgin Limestone (Schubert and Bottjer, 1995; McGowan et al., 2004; Pietsch et al., 2014). The Moenkopi Formation and the coeval Union Wash Formation were deposited in an epicontinental sea on the western coast of Pangea closer to the equator than the Montney formation (Blakey, 1972).

The carbonate factories of the Moenkopi Formation did not appear to have suffered the same severe facies shift that was experienced in the Western Canada Sedimentary Basin (Schubert and Bottjer, 1995). Twenty-seven different species were recognized alongside 5 different ecologic guilds within the Sinbad Limestone (Schubert and Bottjer, 1995). The beds within the Moenkopi Formation are 10cm-2m in thickness and are often monospecific, primarily bivalves and microgastropods; although within the Sinbad Limestone, polytaxic beds are more common (Boyer et al., 2004). The Sinbad Limestone represents the more proximal of the two members, with shoal and lagoon deposits that show increasing storm energy (Goodspeed and Lucas, 2007). The shells within the Sinbad Limestone are highly abraded which indicates that they have undergone extensive transport. This, along with the homogenized internal fabric of the beds and the internal scour surfaces, lead the authors to interpret these deposits to be the result of storm deposition in a shallow water setting (Boyer et al., 2004). The Sinbad Limestone represents the best known gastropod species and generic diversity of the Early Triassic in the world (Nutzel, 2005; Nutzel and Schulbert, 2005).

The Virgin Limestone was deposited on a carbonate ramp and is the more distal of the two units (Mata and Bottjer, 2011). Within the Virgin Limestone, two beds of microbial mound reefs were discovered and interpreted by Pruss and Bottjer (2004). These microbial mounds had undergone early cementation similar to the Altares Packstone Member as they deformed the beds on which they rested, and were interpreted to conform to the definition of a reef (sensu Wood, 1999) as they attained a vertical relief from the seafloor (Pruss and Bottjer, 2004). Bioclastic material is also found within the Virgin Limestone, primarily composed of abraded crinoid, echinoid, and mollusc material (Pietsch et al., 2014). It has been interpreted to be the result of high energy storm events due to the abraded material and the convex up orientation of bivalves (Mata and Bottjer, 2011).

3.6 Conclusion

In conclusion, the numerous packstone beds that are found in the Late Smithian of the Montney Formation in NE British Columbia are likely bivalve and brachiopod dominated biostromes. This is based both on the paleontological and sedimentological evidence which has been gathered from a core dataset in British Columbia. These biostrome deposits are the earliest Mesozoic biostromes in northwestern Pangea, and are one of the first records of the attempt to ‘restart’ the carbonate factory that was shut down in the Peace River Embayment after the Permian-Triassic Boundary.

The Late Smithian biostromes have been identified to be laterally discontinuous packstones. The packstones are carbonate-cemented beds that are primarily composed of bivalve and brachiopod shells, with a large number of articulated specimens (20% or more in places) that indicate that these deposits were accumulated *in situ.* They contain shells of *Claraia* sp., terebratulide brachiopods, ceratitic ammonoids, and fragments of fish skeletons, and appear to be early cemented hard grounds that were repeatedly exposed in some cases. Opportunistic colonizers were able to thrive within these areas allowing a buildup of biologic material to form, at least until oxygen deprivation suffocated the patch reefs. Scouring and erosion of the sediment on either the top and/or the base of the packstone beds is common and provides further evidence that some sort of current reworking was in play in this region. The presence of the heterolithic fine siltstone and very fine sandstone facies adjacent to the packstone beds aids in th identification of bottom currents as the main mechanism that aided in the formation of these biostromes. This is another record of how wind driven bottom currents effected the sedimentary and biologic environments in this part of the Peace River Embayment.

The repeated occurrence of the biostrome beds within this small interval of the Montney Formation in British Columbia, Canada, indicates that there is at least some degree of environmental stability through this interval, even if the overall absence of calcified skeletal material on a broader scale indicates that there was instability with the Peace River Embayment through the Early Triassic. The biostromes were widespread feature within the study area, but they are absent in other parts of the basin which further indicates the restricted nature of the conditions that allowed them to form. Beyond this small interval the physic-chemical conditions in the Peace River Embayment were detrimental to the recovery of life through this time period, whether the cause be anoxia, acidification, or another unidentified fact .

Further research may be conducted to aid in the interpretation of the effect of the Oxygen Minimum Zone on the fauna within these deposits. Their presence indicates that life during this period did attempt to recover and form carbonate deposits, but was repeatedly shut down by some mechanism, either external or internal.

3.7 References

Alroy, J. et al., 2008, Phanerozoic trends in the global diversity of marine invertebrates: Science, v. 321, no. 5885, p. 97–100.

Armitage, J. H., 1962, Triassic Oil and Gas Occurrences in Northeastern British Columbia, Canada: Journal of the Alberta Society of Petroleum Geologists, v. 10, no. 2, p. 35–56.

Bambach, R. K., 2006, Phanerozoic biodiversity mass extinctions: Annual Review of Earth and Planetary Sciences, v. 34, p. 127–155.

Barclay, J., F. Krause, R. Campbell, and J. Utting, 1990, Dynamic casting and growth faulting: Dawson Creek graben complex, Carboniferous-Permian Peace River embayment, western Canada: Bulletin of Canadian Petroleum Geology, v. 38, no. 1, p. 115–145.

Beatty, T. W., J. Zonneveld, and C. M. Henderson, 2008, Anomalously diverse Early Triassic ichnofossil assemblages in northwest Pangea: a case for a shallow-marine habitable zone: Geology, v. 36, no. 10, p. 771–774.

Beauchamp, B., and A. Desrochers, 1997, Permian warm- to very cold- water carbonates and cherts in northwest Pangea, in N. P. James, and J. A. D. Clarke, eds., Cool-Water Carbonates: SEPM (Society for Sedimentary Geology).

Beaufort, L. et al., 2011, Sensitivity of coccolithophores to carbonate chemistry and ocean acidification: Nature, v. 476, no. 7358, p. 80–83.

Best, M. M. R., and S. M. Kidwell, 2000, Bivalve taphonomy in tropical mixed siliciclastic-carbonate settings. I. Environmental variation in shell condition: Paleobiology, v. 26, no. 1, p. 80–102, doi:10.1666/0094-8373(2000)026<0080:BTITMS>2.0.CO;2.

Blakey, R., 1972, Stratigraphy and Depositional Environments of Moenkopi Formation in Southeastern Utah: ABSTRACT: AAPG Bulletin, v. 56, no. 3, p. 604–604.

Bodzoich, A., 1985, Palaeoecology and sedimentary environment of the terebratula beds (lower muschelkalk) from Upper Silesia (south Poland): Annales Societatis Geologorum Poloniae, v. 55, p. 127–138.

Boyer, D. L., D. J. Bottjer, and M. L. Droser, 2004, Ecological Signature of Lower Triassic Shell Beds of the Western United States: Palaios, v. 19, no. 4, p. 372–380, doi:10.1669/0883-1351(2004)019<0372:ESOLTS>2.0.CO;2.

Bureau, G. G., 1987, Regional Geology of Guizhou Province: Geological Memoirs, v. 1, no. 7, p. 1–698.

Cumings, E. R., 1932, Reefs or bioherms?: Geological Society of America Bulletin, v. 43, no. 1, p. 331–352.

Davies, G. R., T. F. Moslow, and M. D. Sherwin, 1997, The Lower Triassic Montney Formation, west-central Alberta: Bulletin of Canadian Petroleum Geology, v. 45, no. 4, p. 474–505.

Doney, S. C., V. J. Fabry, R. A. Feely, and J. A. Kleypas, 2009, Ocean acidification: the other CO2 problem: Marine Science, v. 1.

Driscoll, E., and D. Brandon, 1973, Mollusc-sediment relationships in northwestern Buzzards Bay, Massachusetts, USA: Malacologia, v. 12, no. 1, p. 13–46.

Dunham, R. J., 1962, Classification of carbonate rocks according to depositional textures, in Classification of Carbonate Rocks--A Symposium: AAPG, Memoir, p. 108–121.

Edwards, D. E., J. E. Barclay, D. W. Gibson, G. E. Kvill, and E. Halton, 1994, Triassic Strata of the Western Canada Sedimentary Basin, in G. D. Mossop, and I. Shetsen, eds., Geological Atlas of the Western Canada Sedimentary Basin: Canadian Society of Petroleum Geologists and Alberta Research Council.

Erwin, D. H., 2000, The Permo-Triassic extinction: Shaking the Tree: Readings from Nature in the History of Life, v. 189.

Flügel, E., 1994, Pangean shelf carbonates: controls and paleoclimatic significance of Permian and Triassic reefs: Geological Society of America Special Papers, v. 288, p. 247–266.

Forel, M.-B., 2013, The Permian–Triassic mass extinction: Ostracods (Crustacea) and microbialites: Comptes Rendus Geoscience, v. 345, no. 4, p. 203–211.

Forel, M.-B., S. Crasquin, T. Brühwiler, N. Goudemand, H. Bucher, A. Baud, and C. Randon, 2011, Ostracod recovery after Permian–Triassic boundary mass-extinction: The south Tibet record: Palaeogeography, Palaeoclimatology, Palaeoecology, v. 308, no. 1-2, p. 160–170, doi:10.1016/j.palaeo.2011.02.013.

Glass, D. J., 1990, Lexicon of Canadian Stratigraphy: Volume 4, Western Canada: Canadian Society of Petroleum Geologists.

Golding, M., M. Orchard, J.-P. Zonneveld, C. Henderson, and L. Dunn, 2014, An exceptional record of the sedimentology and biostratigraphy of the Montney and Doig formations in British Columbia: Bulletin of Canadian Petroleum Geology, v. 62, no. 3, p. 157–176.

Gooday, A. et al., 2009, Faunal responses to oxygen gradients on the Pakistan margin: A comparison of foraminiferans, macrofauna and megafauna: Deep Sea Research Part II: Topical Studies in Oceanography, v. 56, no. 6, p. 488–502.

Goodspeed, T. H., and S. G. Lucas, 2007, Stratigraphy, sedimentology, and sequence stratigraphy of the Lower Triassic Sinbad Formation, San Rafael Swell, Utah: New Mexico Museum of Natural History and Science Bulletin, v. 40, p. 91–101.

Grasby, S., B. Beauchamp, A. Embry, and H. Sanei, 2013, Recurrent Early Triassic ocean anoxia: Geology, v. 41, no. 2, p. 175–178.

Greene, S. E., D. J. Bottjer, H. Hagdorn, and J.-P. Zonneveld, 2011, The Mesozoic return of Paleozoic faunal constituents: A decoupling of taxonomic and ecological dominance during the recovery from the end-Permian mass extinction: Palaeogeography, Palaeoclimatology, Palaeoecology, v. 308, no. 1-2, p. 224–232, doi:10.1016/j.palaeo.2010.08.019.

Habicht, J. K. A., 1979, Paleoclimate, paleomagnetism, and continental drift: American Association of Petroleum Geologists Studies in Geology 9.

Hagdorn, H., 1982, The “Bank der kleinen Terebrateln”(Upper Muschelkalk, Triassic) near Schwäbisch Hall (SW-Germany)—A tempestite condensation horizon: Springer.

Hagdorn, H., and R. Mundlos, 1982, Autochthonschille im Oberen Muschelkalk (Mitteltrias) Südwestdeutschlands: Neues Jahrbuch für Geologie und Paläontologie, Abhandlungen, v. 162, p. 332–351.

Hallam, A., 1987, Radiations and extinctions in relation to environmental change in the marine Lower Jurassic of northwest Europe: Paleobiology, p. 152–168.

Henderson, C., S. Mei, and B. Wardlaw, 2002, New conodont definitions at the Guadalupian-Lopingian boundary, in L. Hills, C. Henderson, and E. Bamber, eds., Carboniferous and Permian of the World: Canadian Society of Petroleum Geologists Memoir 19, p. 725–735.

Hotinski, R. M., K. L. Bice, L. R. Kump, R. G. Najjar, and M. A. Arthur, 2001, Ocean stagnation and end-

Permian anoxia: Geology, v. 29, no. 1, p. 7–10.

Isozaki, Y., 1994, Superanoxia across the Permo-Triassic boundary: Record in accreted deep-sea pelagic chert in Japan, in Pangea: Global Environements and Resources: CSPG Memoir 17, p. 805–812.

Jin, Y., Y. Wang, W. Wang, Q. Shang, C. Cao, and D. Erwin, 2000, Pattern of marine mass extinction near the Permian-Triassic boundary in South China: Science, v. 289, no. 5478, p. 432–436.

Kauffman, E., 1978, Short-lived benthic communities in the Solnhofen and Nusplingen Limestones: Neues Jahrbuch für Geologie und Palaeontologie, Monatshefte, p. 717–724.

Kendall, D. R., 1999, Sedimentology and Stratigraphy of the Lower Triassic Montney Formation, Peace River Basin, subsurface of northwestern Alberta, Master of Science: Calgary, Alberta, The University of Calgary, 368 p.

Kendall, D. R., R. Panek, and C. M. Henderson, 1998, Coquina facies of the Lower Triassic Montney Formation, Peace River Embayment, northwestern Alberta.

Kershaw, S., 1994, Classification and geological significance of biostromes: Facies, . 31, no. 1, p. 81–91.

Kidder, D. L., and T. R. Worsley, 2004, Causes and consequences of extreme Permo-Triassic warming to globally equable climate and relation to the Permo-Triassic extinction and recovery: Palaeogeography, Palaeoclimatology, Palaeoecology, v. 203, no. 3-4, p. 207–237, doi:10.1016/S0031-0182(03)00667-9.

Kidwell, S. M., 1991, Taphonomic feedback (live/dead interactions) in the genesis of bioclastic beds: keys to reconstructing sedimentary dynamics., in G. Einsele, W. Ricken, and A. Seilacher, eds., Cycles and Events in Stratigraphy: Berlin, Springer-Verlag, p. 268–282.

Kidwell, S. M., and D. W. Bosence, 1991, Taphonomy and time-averaging of marine shelly faunas: Taphonomy: releasing the data locked in the fossil record. Plenum, New York, p. 115–209.

Kidwell, S. M., and S. M. Holland, 1991, Field description of coarse bioclastic fabrics: Palaios, p. 426–434.

Kidwell, S. M., and D. Jablonski, 1983, Taphonomic feedback ecological consequences of shell accumulation, in Biotic interactions in recent and fossil benthic communities: Springer, p. 195–248.

Klement, K. W., 1967, Practical Classification of Reefs and Banks, Bioherms and Biostromes: ABSTRACT: AAPG Bulletin, v. 51, no. 1, p. 167–168.

Lehrmann, D. J., 1999, Early Triassic calcimicrobial mounds and biostromes of the Nanpanjiang basin, south China: Geology, v. 27, no. 4, p. 359–362.

Levin, L. A., 2003, Oxygen minimum zone benthos: adaptation and community response to hypoxia: Oceanography and Marine Biology: An Annual Review, v. 41, p. 1–45.

Levin, L. A., C. L. Huggett, and K. F. Wishner, 1991, Control of deep-sea benthic community structure by oxygen and organic-matter gradients in the eastern Pacific Ocean: Journal of Marine Research, . 49, no. 4, p. 763–800.

Markhasin, B., 1997, Sedimentology and Stratigraphy of the Lower Triassic Montney Formation, Subsurface of Northwestern Alberta, Master of Science: Calgary, Alberta, University of Calgary, 154 p.

Mata, S. A., and A. D. Woods, 2008, Sedimentology and paleoecology of the Lower Member of the Lower Triassic (Smithian-Spathian) Union Wash Formation, east-central California: Palaios, v. 23, no. 8, p. 514–524.

McGowan, A. J., 2004, Ammonoid taxonomic and morphologic recovery patterns after the Permian–Triassic: Geology, v. 32, no. 8, p. 665–668.

Metcalfe, B., R. J. Twitchett, and N. Price-Lloyd, 2011, Changes in size and growth rate of “Lilliput” animals in the earliest Triassic: Palaeogeography, Palaeoclimatology, Palaeoecology, v. 308, no. 1-2, p. 171–180, doi:10.1016/j.palaeo.2010.09.011.

Moslow, T. F., 2000, Reservoir architecture of a fine-grained turbidite system: Lower Triassic Montney Formation, Western Canada Sedimentary Basin, in Deep-water Reservoirs of the World, Conference Proceedings, Gulf Coast SEPM. P. Weimer, RM Slatt, J. Coleman, NC Rosen, H. Nelson, AH Bouma, MJ Styzen, and DT Lawrence (eds.): SEPM, p. 686–713.

Newell, N., and D. Boyd, 1995, Pectinoid bivalves of the Permian-Triassic crisis.: Bulletin of the American Museum of Natural History, no. 227, p. 5 – 95.

Nützel, A., 2005, Recovery of gastropods in the Early Triassic: Comptes Rendus Palevol, v. 4, no. 6, p. 501–515.

Nützel, A., and C. Schulbert, 2005, Facies of two important Early Triassic gastropod lagerstätten: implications for diversity patterns in the aftermath of the end-Permian mass extinction: Facies, v. 51, no. 1-4, p. 480–500.

Orchard, M. J., and E. T. Tozer, 1997, Triassic conodont biochronology, its calibration with the ammonoid standard, and a biostratigraphic summary for the Western Canada Sedimentary Basin: Bulletin of Canadian Petroleum Geology, v. 45, no. 4, p. 675–692.

Orchard, M. J., and J.-P. Zonneveld, 2009, The Lower Triassic Sulphur Mountain Formation in the Wapiti Lake area: lithostratigraphy, conodont biostratigraphy, and a new biozonation for the lower Olenekian (Smithian) Earth Science Sector (ESS) Contribution 20080714.: Canadian Journal of Earth Sciences, v. 46, no. 10, p. 757–790, doi:10.1139/E09-051.

Paull, R. K., R. A. Paull, and T. S. Laudon, 1997, Conodont biostratigraphy of the Lower Triassic Mackenzie Dolomite Lentil, Sulphur Mountain Formation in the Cadomin area, Alberta: Bulletin of Canadian Petroleum Geology, v. 45, no. 4, p. 708–714.

Payne, J. L., D. Altiner, D. J. DePaolo, J. L. Hinojosa, L. R. Kump, K. V. Lau, D. J. Lehrmann, K. Maher, A. Paytan, and S. Shen, 2014, The End-Permian Mass Extinction and its Aftermath: Insights from Non-Traditional Isotope System: Vancouver,BC.

Payne, J. L., and M. E. Clapham, 2012, End-Permian mass extinction in the oceans: an ancient analog for the twenty-first century?: Annual Review of Earth and Planetary Sciences, v. 40, p. 89–111.

Pietsch, C., and D. J. Bottjer, 2014, The importance of oxygen for the disparate recovery patterns of the benthic macrofauna in the Early Triassic: Earth-Science Reviews, v. 137, p. 65–84.

Pietsch, C., S. A. Mata, and D. J. Bottjer, 2014, High temperature and low oxygen perturbations drive contrasting benthic recovery dynamics following the end-Permian mass extinction: Palaeogeography, Palaeoclimatology, Palaeoecology, v. 399, p. 98–113.

Pruss, S. B., and D. J. Bottjer, 2004, Early Triassic trace fossils of the western United States and their implications for prolonged environmental stress from the end-Permian mass extinction: Palaios, v. 19, no. 6, p. 551–564.

Pruss, S. B., F. A. Corsetti, and D. J. Bottjer, 2005a, Environmental trends of Early Triassic biofabrics: implications for understanding the aftermath of the end-Permian mass extinction: Developments in Palaeontology and Stratigraphy, v. 20, p. 313–332.

Pruss, S. B., F. A. Corsetti, and D. J. Bottjer, 2005b, The unusual sedimentary rock record of the Early Triassic: a case study from the southwestern United States: Palaeogeography, Palaeoclimatology, Palaeoecology, v. 222, no. 1, p. 33–52.

Rampino, M. R., and K. Caldeira, 2005, Major perturbation of ocean chemistry and a “Strangelove Ocean” after the end-Permian mass extinction: Terra Nova, v. 17, no. 6, p. 554–559, doi:10.1111/j.1365-3121.2005.00648.x.

Richardson, J. R., 1981, Brachiopods in mud: resolution of a dilemma: Science, v. 211, no. 4487, p. 1161–1163.

Schatz, W., 2005, Palaeoecology of the Triassic black shale bivalve Daonella—new insights into an old controversy: Palaeogeography, Palaeoclimatology, Palaeoecology, v. 216, no. 3-4, p. 189–201, doi:10.1016/j.palaeo.2004.11.002.

Schubert, J. K., and D. J. Bottjer, 1992, Early Triassic stromatolites as post-mass extinction disaster forms: Geology, v. 20, no. 10, p. 883–886.

Schubert, J. K., and D. J. Bottjer, 1995, Aftermath of the Permian-Triassic mass extinction event: Paleoecology of Lower Triassic carbonates in the western USA: Palaeogeography, Palaeoclimatology, Palaeoecology, v. 116, no. 1, p. 1–39.

Sepkoski Jr, J. J., 1981, A factor analytic description of the Phanerozoic marine fossil record: Paleobiology, p. 36–53.

Song, H., J. Tong, and Z. Q. Chen, 2011, Evolutionary dynamics of the Permian–Triassic foraminifer size: Evidence for Lilliput effect in the end-Permian mass extinction and its aftermath: Palaeogeography, Palaeoclimatology, Palaeoecology, v. 308, no. 1-2, p. 98–110, doi:10.1016/j.palaeo.2010.10.036.

Tozer, E., 1982, Marine Triassic faunas of North America: their significance for assessing plate and terrane movements: Geologische Rundschau, v. 71, no. 3, p. 1077–1104.

Tozer, E. T., 1994, Canadian Triassic ammonoid faunas: Geological Survey of Canada.

Twitchett, R. J., 2006, The palaeoclimatology, palaeoecology and palaeoenvironmental analysis of mass extinction events: Palaeogeography, Palaeoclimatology, Palaeoecology, v. 232, no. 2, p. 190–213.

Twitchett, R., L. Krystyn, A. Baud, J. Wheeley, and S. Richoz, 2004, Rapid marine recovery after the end-Permian mass-extinction event in the absence of marine anoxia: Geology, v. 32, no. 9, p. 805–808.

Versteegh, G. J., T. Servais, M. Streng, A. Munnecke, and D. Vachard, 2009, A discussion and proposal concerning the use of the term calcispheres: Palaeontology, v. 52, no. 2, p. 343–348.

Wentworth, C. K., 1922, A scale of grade and class terms for clastic sediments: The Journal of Geology, p. 377–392.

Wignall, P. B., 1994, Black shales: Clarendon Press Oxford.

Wignall, P. B., and A. Hallam, 1991, Biofacies, stratigraphic distribution and depositional models of British onshore Jurassic black shales: Geological Society, London, Special Publications, v. 58, no. 1, p. 291–309.

Wignall, P., and A. Hallam, 1996, Facies change and the end-Permian mass extinction in SE Sichuan, China: Palaios, p. 587–596.

Wignall, P. B., and R. J. Twitchett, 1999, Unusual intraclastic limestones in Lower Triassic carbonates and their bearing on the aftermath of the end-Permian mass extinction: Sedimentology, v. 46, no. 2, p. 303–316.

Wilson, N., 2009, Integrated regional model for the deposition and evolution of the Montney Formation, NE British Columbia.

Wilson, K. M., D. Pollard, W. W. Hay, S. L. Thompson, and C. N. Wold, 1994, General circulation model simulations of Triassic climates: preliminary results: Geological Society of America Special Papers, v. 288, p. 91–116.

Wood, R., 1999, Reef evolution: Oxford University Press.

Woods, A. D., 2005, Paleoceanographic and paleoclimatic context of Early Triassic time: Comptes Rendus Palevol, v. 4, no. 6-7, p. 463–472, doi:10.1016/j.crpv.2005.07.003.

Woods, A. D., D. J. Bottjer, M. Mutti, and J. Morrison, 1999, Lower Triassic large sea-floor carbonate cements: their origin and a mechanism for the prolonged biotic recovery from the end-Permian mass extinction: Geology, v. 27, no. 7, p. 645–648.

Zonneveld, J.-P., 2001, Middle Triassic biostromes from the Liard Formation, British Columbia, Canada: oldest examples from the Mesozoic of NW Pangea: Sedimentary Geology, v. 145, no. 3, p. 317–341.

Zonneveld, J.-P., 2011, Suspending the Rules: Unraveling the ichnological signature of the Lower Triassic post-extinction recovery interval: Palaios, v. 26, no. 11, p. 677–681, doi:10.2110/palo.2011.S06.

Zonneveld, J.-P., M. K. Gingras, and T. W. Beatty, 2010a, Diverse ichnofossil assemblages following the P-T mass extinction, Lower Triassic, Alberta and British Columbia, Canada: Evidence for shallow marine refugia on the northwestern coast of Pangea: Palaios, v. 25, no. 6, p. 368–392, doi:10.2110/palo.2009.p09-135r.

Zonneveld, J.-P., R. B. MacNaughton, J. Utting, T. W. Beatty, S. G. Pemberton, and C. M. Henderson, 2010b, Sedimentology and ichnology of the Lower Triassic Montney Formation in the Pedigree-Ring/ Border-Kahntah River area, northwestern Alberta and northeastern British Columbia: Bulletin of Canadian Petroleum Geology, v. 58, no. 2, p. 115–140.

Zonneveld, J.-P., and T. F. Moslow, 2014, Perennial River Deltas of the Montney Formation: Alberta and British Columbia Subcrop Edge.

Zonneveld, J.-P., T. F. Moslow, and C. M. Henderson, 1997, Lithofacies associations and depositional environments in a mixed siliciclastic-carbonate coastal depositional system, upper Liard Formation, Triassic, northeastern British Columbia: Bulletin of Canadian Petroleum Geology, v. 45, no. 4, p. 553–575.

Zuschin, M., J. Hohenegger, and F. F. Steininger, 2000, A comparison of living and dead molluscs on coral reef associated hard substrata in the northern Red Sea—implications for the fossil record: Palaeogeography, Palaeoclimatology, Palaeoecology, v. 159, no. 1, p. 167–190.

Zuschin, M., M. Stachowitsch, P. Pervesler, and H. Kollmann, 1999, Structural features and taphonomic pathways of a high-biomass epifauna in the northern Gulf of Trieste, Adriatic Sea: Lethaia, v. 32, no. 4, p. 299–316.

Figure Captions

3.1: Map of core datasets in relation to the Montney Formation as a whole during the Dienerian-Smithian boundary. The two deltas are known to be present on opposite sides of the boundary. The red block in the inset map shows the location of the above map in relation to modern geographical boundaries of Canada. (The Montney map was compiled and modified from Barclay et al., 1990; Panek, 2000; Zonneveld et al., 2010a; Zonneveld et al., 2010b; Zonneveld and Moslow, 2014; and Zonneveld, pers. comm.; the Map of the provinces and coastline of Canada was modified from Government of Canada, 2001).

3.2: The stratigraphic framework of the Lower and Middle Triassic in the Western Canada Sedimentary Basin, and the location and correlation of the Montney Formation with its outcrop equivalents. With formation names represented for both above and below the Pine River (modified from Zonneveld, 2011; compiled from Tozer, 1994; Orchard and Tozer, 1997; Orchard and Zonneveld, 2009).

3.3: Strike section through the study area, inset map. Horizon B is used as the datum, as it is a flooding surface.

3.4: Isopach map of the top of Horizon B through the study area. Wells were centralized along the NW-SE trend.

3.5: Diagrams of the thick and thin packstone bed structures. A) The larger, more cemented packstone beds. B) The smaller packstone bed structure.

3.6: Facies MBP: Thin section views of the bioclastic packstone. All of the sections are scanned in plane light, have double calcite staining, and the left side of E has staining for aragonite. A) Repetition of the facies within the thin section showing the hiatus of calcite cementation outside of the packstone

(Well API = a-64-A/094-B-08). B) Another representation of the packstone in a thinner horizon that pinches out to the right of the thin section. C) This sample shows a brachiopod with particularly inflated valves in the center of the thin section. The internal cavity only is crystalized around the rim (Sample IRG-SA-1412-061). D) Gradation out of packstone back into siltstone facies (Sample BC38). E) The packstone is mostly made of ammonoids that has caused the bedding to be distorted around the packstone (Well API = a-64-A/094-B-8). This is one of the few examples which has an abundance of bioclasts other than bivalves and brachiopods. F) Deformation of the beds below the packstone as well as shells that are not oriented perpendicular to bedding (Sample BC39).

3.7: Various pictures of the bioclasts within the packstone beds. A) Disarticulated valves alongside whole ammonoids. B) Exposed bedding plane made of disarticulated bivalves on the top of a bioclastic packstone bed (Well API = 8-30-082-20w6). C) Shell structure of *Claraia* valves from the "*Claraia* Zone". D) Valves with spary calcite rims within a packstone bed (photographed in cross-polarized light). E) Dissolved and dolomitized disarticulated valves from around a packstone bed. F) Packstone bed that has multiple erosion surfaces ontop of one another within the bed.

3.8: Fossils found in and close to Horizon B in cores. A) Pyritized ammonoid that could possibly be *Ophioceras* sp. B) Impression of *Hypophiceras* sp. or *Tompophiceras* sp. C) Terebratulide impressions. D) *Claraia clarae* impressions. E) Vertebrate ribs and backbone. F) *Claraia stachei*.

3.9: Facies MBP: Bioclastic packstone facies A) Packstone beds from 16-17-083-25w6. A shows repetition of the facies with the common wavy appearance of the facies. B) Packstone from 14-29-080-20w6 shows large thick bivalve shells within it along with vertebrate material. C) Packstone from 13-11-081-20w6 shows another variation of the facies with the scoured base and the grading up. D) Packstone beds from 16-17-083-25w6. Similar to A shows the repetition along with soft sediment deformation.

3.10: Correlation of packstone beds between four wells. The beds are not correlatable across short distances in which even erosion surfaces are correlatable.

3.11: Diagram of the location of FA3 within the same environment as FA1 and FA2.

3.12: Bedforms found in and around the Altares Packstone Member. A) Starved mud draped ripples from C-74-G/094-B-8. B) Packstone pinching out on the back of a core piece from 13-11-081-20w6.

3.13: Succession through part of the Altares Packstone Member in 16-17-083-25w6 showing the increase and decrease in thickness of packstone beds on a small scale and sedimentary structures that are found alongside the packstone beds.

3.14: Formation of biostromes in the Middle Montney Formation based on Zonneveld (2001). A) Deposition of siltstone in background conditions. B) Storm or current brings in disarticulated valves and live opportunist larvae and adults who recolonize the patch. C) Shells serve as a hard substrate for other colonizers which in turn provide prey for nektobenthic organisms as well as nektonic fauna. D) Either low oxygen kills off fauna or sudden sedimentation buries the organisms. This is a return to background conditions, but beneath the sediment-water interface the packstone is cemented. E) A storm or current uncovers and erodes into the packstone allowing it to become a hardground again.

List of Tables

3.1: Table of cores analyzed and presence or absence of the packstone bed horizon or the "*Claraia* Zone".

3.2: Tabular summary of facies, which details each facies' minerology, grain size, sedimentary structures, trace fossils, and body fossils that have been identified

3.3: Table of facies contacts. G = gradational, S = sharp, C = Scour, OW = Occurs Within

3.4: Summary and description of the three facies associations.

Chapter 4: Summary and Conclusions

4.1 *“Claraia* Zone”

This thesis focuses on two, relatively thin, bioclastic units within the Lower Triassic Montney Formation in British Columbia, Canada. These units are both of significant importance as hydrocarbon producing horizons within the formation (Moslow, per. comm.). They also represent two new additions to the list of known bioclastic horizons in the Lower Triassic clastic ramp succession of the Western Canada Sedimentary Basin. The “*Claraia* Zone” and the Late Smithian Altares Packstone Member were the two horizons of interest for this thesis.

Sedimentary analysis of cores was conducted alongside taphonomic and taxonomic analysis of the body fossils found within the same cores. Facies were constructed based on these analyses and then grouped into two facies associations: proximal bottom current modified deposits and distal bottom current modified deposits in the *Claraia* Zone” (Table 4.1, Fig. 4.1). There are many similarities between the laminated bioclastic siltstone facies and the heterolithic fine siltstone to very fine sandstone facies It was determined that the same mechanism formed both units, but with varying distance from the sediment source (Fig. 4.2). The laminated bioclastic siltstone is primarily composed of a hash of *Claraia* valves. There are very few valves that are nearly whole, most being very fragmented. This taphonomic evidence lead the author to interpret these deposits as having been transported based on Kidwell and Bosence (1991). Fragmented and disarticulated valves are more commonly found in transported deposits, particularly if the fragmentation around the edges is of an irregular nature (Kidwell and Bosence, 1991).

While the deposits were most likely not formed by a contour current (e.g., a thermohaline current) it is possible that these deposits were formed by wind currents similar to the Loop Current in the Gulf of Mexico (Cooper et al., 1990). The western coast of Pangea was influenced by strong winds and mega monsoons throughout the Triassic, and either of these could have caused the currents that aided in the deposition of the “*Claraia* Zone” (Barron, 1989; Kidder and Worsley, 2004; Loope et al., 2004).

Finally, the presence of *Claraia* valves both within the zone of calcite preservation and outside of it indicates that these depositional processes were occurring even beyond the “*Claraia* Zone”. A preservation preference was certainly given early in the diagenetic history, as compared with the rest of the formation. This means that there was likely an ocean chemistry imbalance outside of this horizon that prevented the preservation of calcified body fossils within the Peace River Embayment

4.2: Altares Packstone Member

It was determined through facies and taphonomic analysis that these deposits were *in situ* biostromes, and underwent early cementation (Fig. 4.3). There is a higher diversity in these units than seen in most other units within the Montney Formation (particularly the “*Claraia* Zone”), although the diversity changes between individual beds (Kendall, 1999; Panek, 2000). The biostromes contain a large number of articulated bivalves and/or brachiopods (+20% in some cases) which indicates that they formed *in situ* (Fig. 4.4). Colonization of the first shells over time allowed for the perpetuation of a stable substrate on which organisms could live until the beds were likely suffocated by sediment or a change in oxygenation (Kidwell and Jablonski, 1983; Kidwell, 1991).

Facies	*Minerology*	*Thickness*	*Grain Size*	*Sed. Structures*	*Trace Fossils*	*Body Fossils*	*Taphonomy*
MBP	quartz, clay minerals, detrital dolomite or calcite, plagioclase, silica or sometimes calcite cement, and high concentration of bitumen	1-10cm	Fine to coarse silt with pebble or larger size bioclasts	soft sediment deformation, scour, crinkled lamination		ammonoids, brachiopods (terebratulids), bivalves	valves can be disarticulated or articulated, articulated valves often have cement in the cavity. Valves do not appear to be abbraided, and ammonoids are whole.
SL1	quartz, bioclastic hash, some clay minerals, silica cement, and high concentration of bitumen	2cm-10m	fine silt, angular-subangular, mod. well sorted	planar lamination		bivalve and ammonoid impressions	disarticulated bivalve impressions. Sometimes there is fracturing, most ammonoids appear complete
LBS	quartz, silica or calcite cement, clay minerals, pyrite, high bitumen concentration in fine grained fraction	10-20cm	fine silt, angular-subangular, poor-mod. well sorted	planar lamination		Claraia sp.	fractured, disarticulated, sorted and stacked valves concentrated in beds
SL2	Calcispheres (either dolomite or calcite), quartz, small clay fraction occasionally, silica or calcite cement	20cm-5m	fine and coarse silt to very fine sand, angular, well sorted	starved and climbing ripples, flaser and lenticular bedding, mud drapes, scour surfaces	occasional Planolities		
CA	calcite or dolomite cement, pyrite rim, quartz grains, and some clay fraction	20-30cm	fine silt, round calcispheres	massive to planar lamination		occassional Claraia sp.	disarticulated, unfractured valves

Table 4.1: Summary of facies with descriptions of minerology, grain size, sedimentary structures, trace fossils, and body fossils found in each facies.

Facies	***Minerology***	***Thickness***	***Grain Size***	***Sed. Structures***	***Trace Fossils***	***Body Fossils***	***Taphonomy***
CO	clay minerals, quartz, pyrite layers, silica cement	5-20cm	fine or coarse silt	lense shaped features with mostly planar lamination		bivalves	abbraided, fractured, and disarticulated valves
SL3	quartz, clay minerals, detrital dolomite, silica cement	20-50cm	fine silt, angular, well sorted	massive	none observed		
SL4	quartz, clay minerals, pyrite, silica cement	3-10m	fine to coarse silt, angular, mod. well sorted	mottled/bioturbated	observed, but not identified		
SL5	quartz, clay minerals, pyrite, silica cement	5-20cm	fine and coarse silt to very fine sand, angular, well sorted	soft sediment deformation, scour			
BF1	quartz, clay minerals, detrital dolomite or calcite, plagioclase, silica or sometimes calcite cement, and high concentration of bitumen	5-20cm	fine to coarse silt, angular, well sorted	planar lamination, scour	Planolities, Phycosiphon		

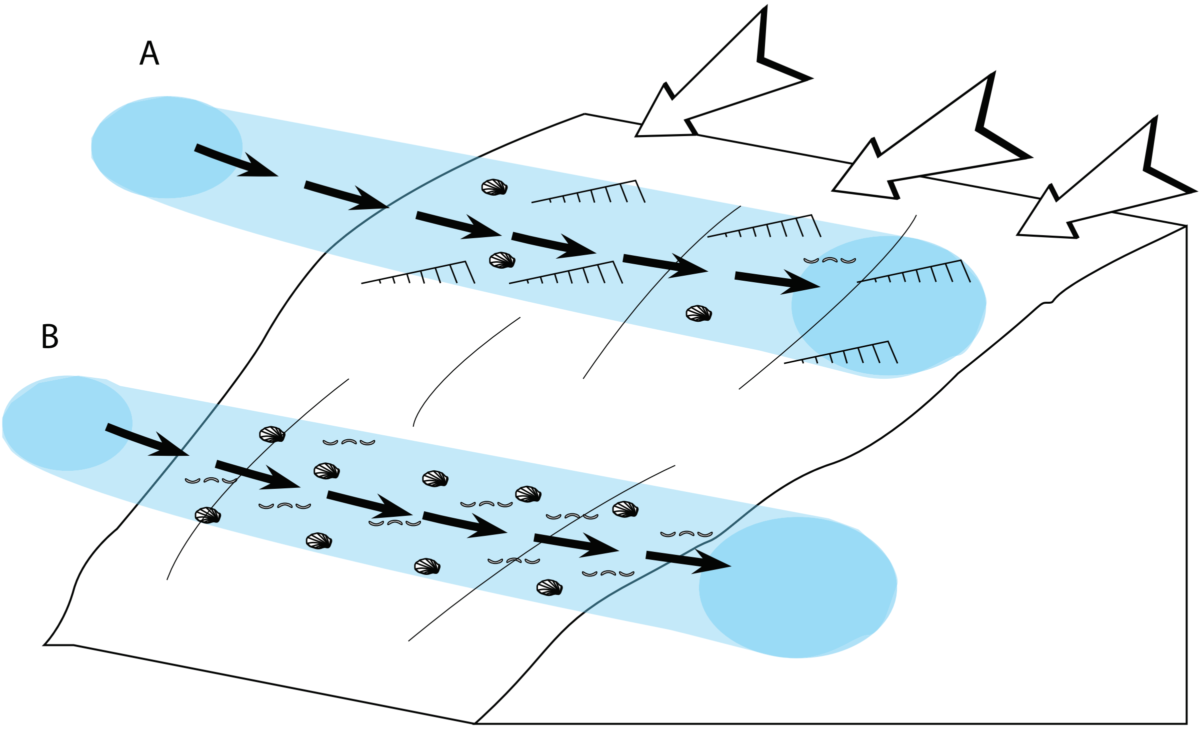

Figure 4.1: The bottom current depositional environment with the current shown producing the two different facies associations. A) Represents the fan derived bottom current modified deposits that are closer to the source input of coarse grained sediment (arrows). When the current is active (blue) bivalve shells and ripple structures are created, with suspension sedimentation between current activity. B) Represents the distal bottom current modified deposits where winnowing of fine grained sediment with the deposition of bivalve material in concentrated horizons by the current activity (blue).

These beds were determined to represent the first biostromes in estern Canada after the Permian-Triassic Mass Extinction. The Montney biostromes were likely effected by a fluctuating oxyge minimum zone. The reduction of the zone would allow for colonization at the top of the zone, while the subsequent expansion would kill off the organisms (Levin et al., 1991; Gooday et al., 2009). These beds represent repeated attempts at restarting the carbonate factory that disappeared at the end of the Permian (Barclay et al., 1990; Edwards et al., 1994; Davies, 1997).

Within the Dienerian *"Claraia* Zone" diversity was much diminished as compared with the Late Smithian Altares Packstone Member, primarily consisting of *Claraia* cf. *stachei, C.* cf. *clarae.* There is some evidence of nektonic organisms such as spines from *Listricanthus* and conodont denticles. *Listricanthus* spines disappear by the deposition of the Altares Packstone Member, but ichthyosaur skeletal elements appear in their place along with a higher number of articulated fish skeletons. Panek (2000) identified lingulide brachiopod and bivalve dominated grainstones in the eastern part of the Montney Formation in the Coquina Dolomite middle member. A trend from primarily *Claraia* deposits to deposits made of *Claraia* and lingulide brachiopods, another opportunistic taxon (Roland and Bottjer, 2001), can be observed then just between the "*Claraia* Zone" and the Coquina Dolomite middle member. By the Late Smithian terebratulide brachiopods, a hard ground preferring organism (Hagdorn, 1982; Zonneveld et al., 1997), are recolonizing specific localities. This provides further evidence to the recovery within the Peace River Basin through the Early Triassic.

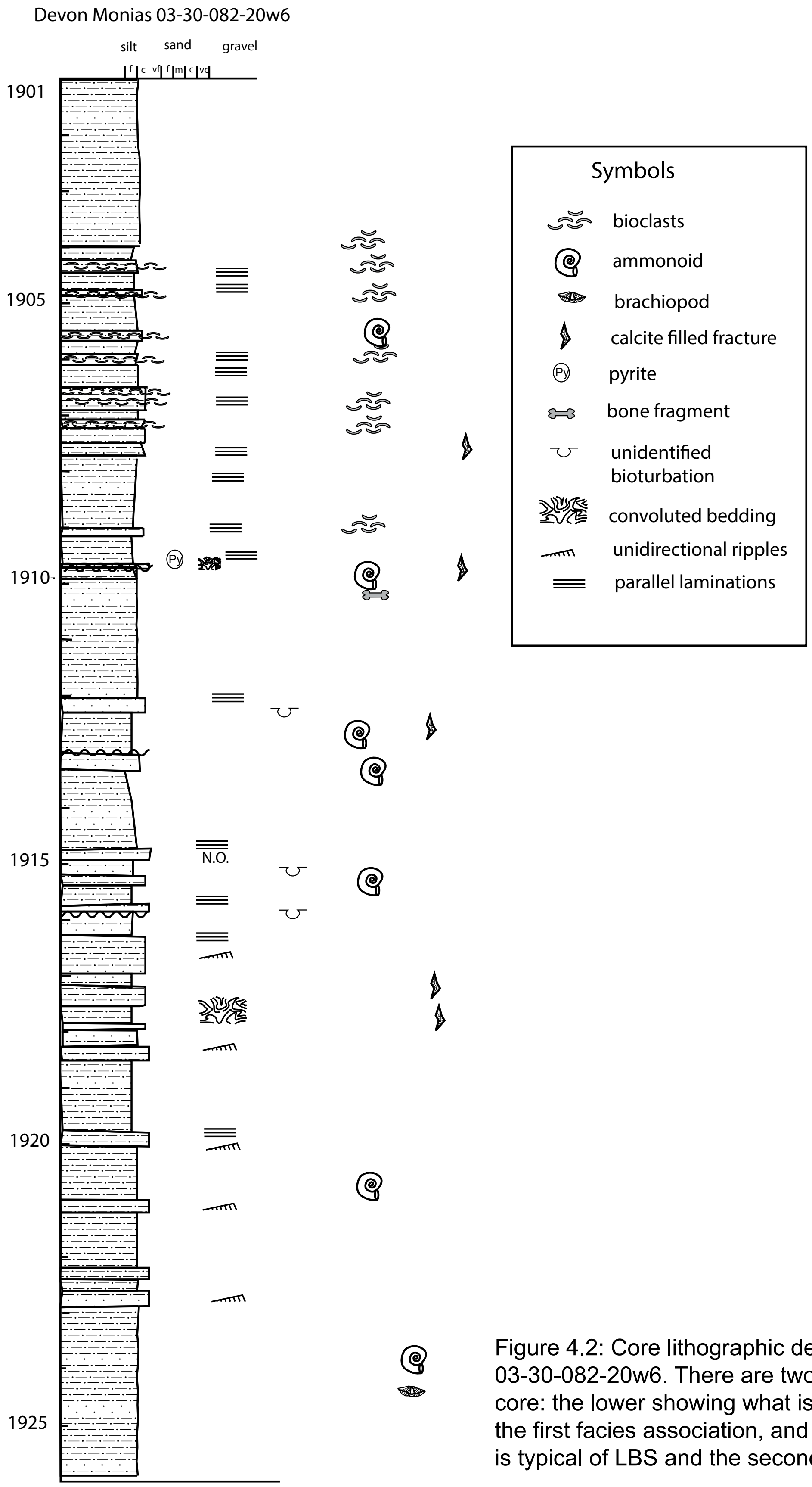
Devon Monias 03-30-082-20w6
silt
sand
gravel
f
c
vf
f
m
c
vc
1901
1905
1910
1915
1920
1925
Py
N.O.
Symbols
bioclasts
ammonoid
brachiopod
calcite filled fracture
pyrite
bone fragment
unidentified bioturbation
convoluted bedding
unidirectional ripples
parallel laminations

Figure 4.2: Core lithographic description of Well API: 03-30-082-20w6. There are two distinct sections to this core: the lower showing what is typical of facies SL2 and the first facies association, and the upper showing what is typical of LBS and the second facies association.

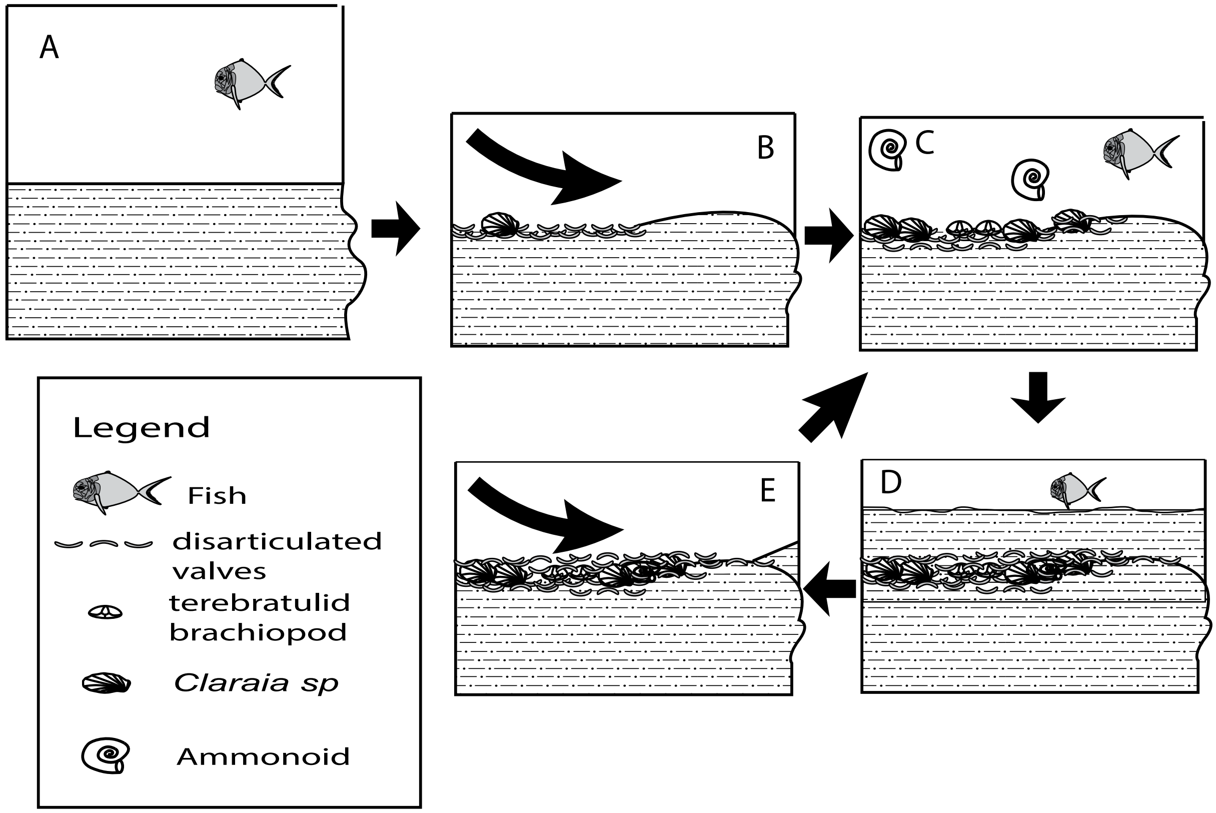

Figure 4.3: Formation of biostromes in the Middle Montney Formation based on Zonneveld (2001). A) Deposition of siltstone in background conditions. B) Storm or current brings in disarticulated valves and live opportunist larvae and adults who recolonize the patch. C) Shells serve as a hard substrate for other colonizers which in turn provide prey for nektobenthic organisms as well as nektonic fauna. D) Either low oxygen kills off fauna or sudden sedimentation buries the organisms. This is a return to background conditions, but beneath the sediment-water interface the packstone is cemented. E) A storm or current uncovers and erodes into the packstone allowing it to become a hardground again.

4.3: Conclusions

Both of these bioclastic horizons are brief glimpses into the biologic history of the Peace River Embayment shortly after the Permian-Triassic Mass Extinction. They provide some of the first preserved calcareous body fossils after the extinction event, and allow for insight into the range of fauna alive at these two time periods. Each deposit also gives insight into how sedimentary processes in the basin affected the organisms that lived within it: one deposit was composed of transported valves and the other preserved *in situ*. The Late Smithian Altares Packstone Member was interpreted to be the oldest biostrome deposit in North Western North America after the Permian-Triassic Mass Extinction. It provides proof that even during the stressful conditions of the Early Triassic Peace River Embayment, calcareous lifeforms tried to restart the carbonate factory similar to what was seen in the Permian.

It appears bottom currents played a major role in the formation of bioclastic units in the lower Montney Formation (Fig. 4.5). Currents likely aided in the deposition of the Late Smithian Altares Packstone Member by transporting in shells and live colonizers to the environment. The "*Claraia* Zone" was likely a deposit that was winnowed and modified directly by bottom currents. These currents may be

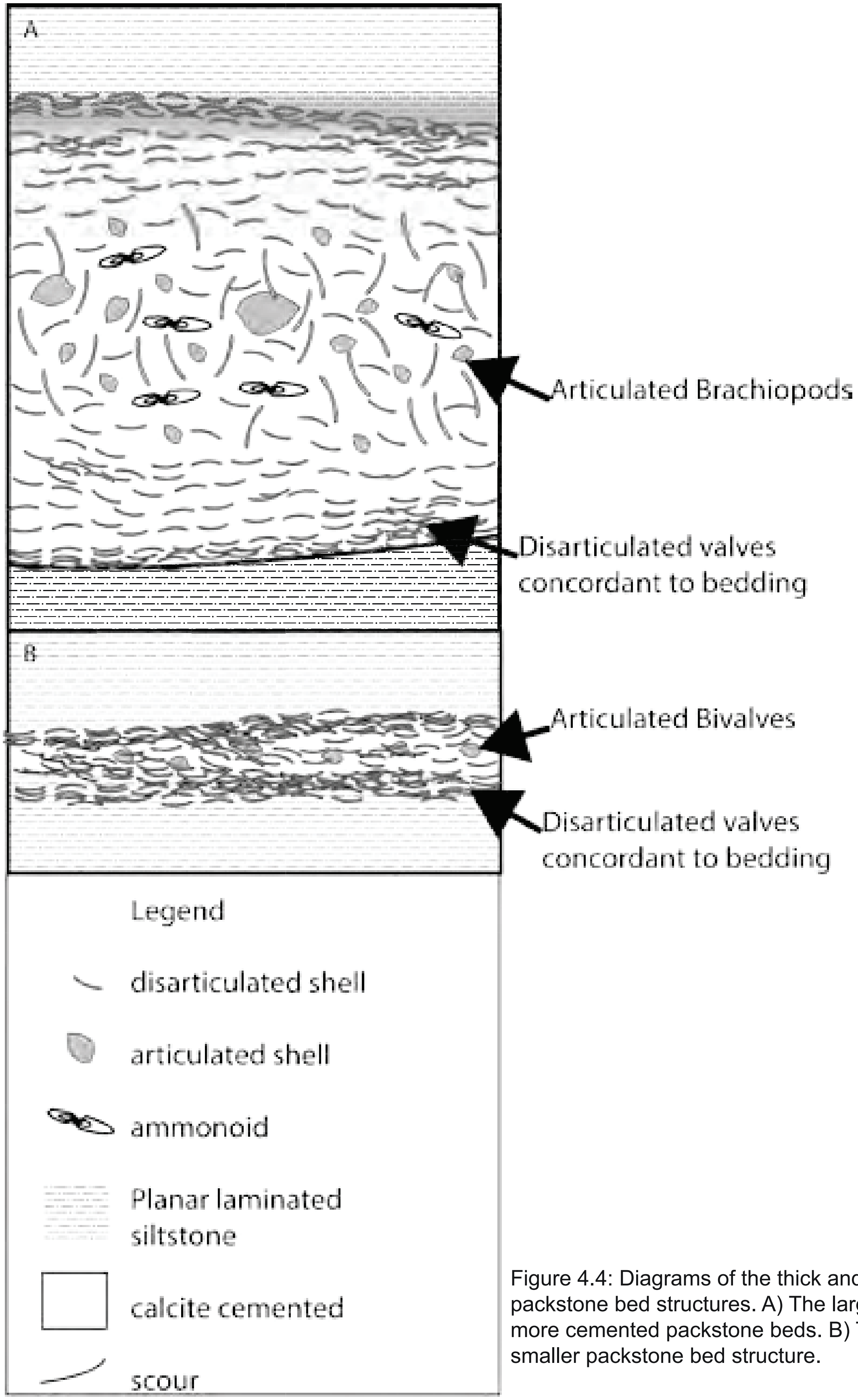
A
Articulated Brachiopods
Disarticulated valves concordant to bedding
B
Articulated Bivalves
Disarticulated valves concordant to bedding
Legend
disarticulated shell
articulated shell
ammonoid
Planar laminated siltstone
calcite cemented
scour

Figure 4.4: Diagrams of the thick and thin packstone bed structures. A) The larger, more cemented packstone beds. B) The smaller packstone bed structure.

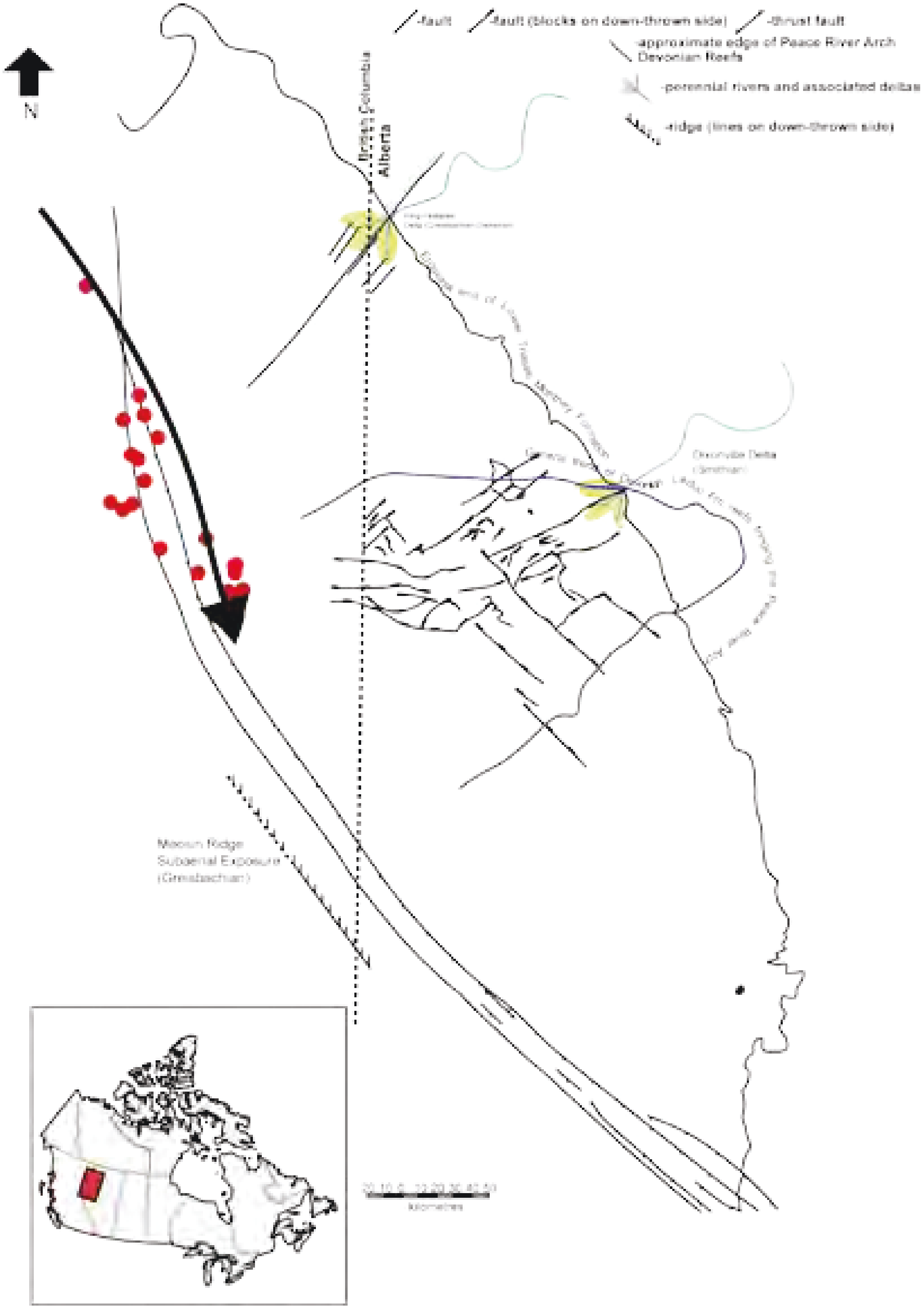
-fault
-fault (blocks on down-thrown side)
-thrust fault
-approximate edge of Peace River Arch Devonian Reefs
-perennial rivers and associated deltas
-ridge (lines on down-thrown side)
N
British Columbia
Alberta
Dixonville Delta (Smithian)
Meosin Ridge Subaerial Exposure (Griesbachian)
20 10 0 10 20 30 40 50
Kilometres

4.5: Map of the Montney Formation during the Greisbachian with possible direction of wind driven bottom currents. The currents could be constrained by the ridge at the southwest, but there is no data in that area. Shells and sand could be brought in from the east, or the shells could be from a more local source. (The Montney map was compiled and modified from Barclay et al, 1990; Panek, 2000; Zonneveld et al, 2010a; Zonneveld et al, 2010b; Zonneveld and Moslow, 2014; and Zonneveld, pers. comm.).

linked to the mega monsoons and high frequency of storms already recorded in the Early Triassic. Both of these deposits in turn provide further evidence of the effect of these storms on the marine life on the eastern margin of Panthalassa.

4.4 References

Barclay, J., F. Krause, R. Campbell, and J. Utting, 1990, Dynamic casting and growth faulting: Dawson Creek graben complex, Carboniferous-Permian Peace River embayment, western Canada: Bulletin of Canadian Petroleum Geology, v. 38, no. 1, p. 115–145.

Barron, E. J., 1989, Climate variations and the Appalachians from the late paleozoic to the present: Results from model simulations: Geomorphology, v. 2, no. 1-3, p. 99–118, doi:10.1016/0169-555X(89)90008-1.

Cooper, C., G. Z. Forristall, and T. M. Joyce, 1990, Velocity and hydrographic structure of two Gulf of Mexico warm-core rings: Journal of Geophysical Research: Oceans (1978–2012), v. 95, no. C2, p. 1663–1679.

Davies, G. R., 1997, The Triassic of the Western Canada Sedimentary Basin: tectonic and stratigraphic framework, paleogeography, paleoclimate and biota: Bulletin of Canadian Petroleum Geology, v. 45, no. 4, p. 434–460.

Edwards, D. E., J. E. Barclay, D. W. Gibson, G. E. Kvill, and E. Halton, 1994, Triassic Strata of the Western Canada Sedimentary Basin, in G. D. Mossop, and I. Shetsen, eds., Geological Atlas of the Western Canada Sedimentary Basin: Canadian Society of Petroleum Geologists and Alberta Research Council.

Gooday, A. et al., 2009, Faunal responses to oxygen gradients on the Pakistan margin: A comparison of foraminiferans, macrofauna and megafauna: Deep Sea Research Part II: Topical Studies in Oceanography, v. 56, no. 6, p. 488–502.

Hagdorn, H., 1982, The “Bank der kleinen Terebrateln”(Upper Muschelkalk, Triassic) near Schwäbisch Hall (SW-Germany)—A tempestite condensation horizon: Springer.

Kendall, D. R., 1999, Sedimentology and Stratigraphy of the Lower Triassic Montney Formation, Peace River Basin, subsurface of northwestern Alberta, Master of Science: Calgary, Alberta, The University of Calgary, 368 p.

Kidder, D. L., and T. R. Worsley, 2004, Causes and consequences of extreme Permo-Triassic warming to globally equable climate and relation to the Permo-Triassic extinction and recovery: Palaeogeography, Palaeoclimatology, Palaeoecology, v. 203, no. 3-4, p. 207–237, doi:10.1016/S0031-0182(03)00667-9.

Kidwell, S. M., 1991, Taphonomic feedback (live/dead interactions) in the genesis of bioclastic beds: keys to reconstructing sedimentary dynamics., in G. Einsele, W. Ricken, and A. Seilacher, eds., Cycles and Events in Stratigraphy: Berlin, Springer-Verlag, p. 268–282.

Kidwell, S. M., and D. W. Bosence, 1991, Taphonomy and time-averaging of marine shelly faunas:

Taphonomy: releasing the data locked in the fossil record. Plenum, New York, p. 115–209.

Kidwell, S. M., and D. Jablonski, 1983, Taphonomic feedback ecological consequences of shell accumulation, in Biotic interactions in recent and fossil benthic communities: Springer, p. 195–248.

Levin, L. A., 2003, Oxygen minimum zone benthos: adaptation and community response to hypoxia: Oceanography and Marine Biology: An Annual Review, v. 41, p. 1–45.

Loope, D. B., M. B. Steiner, C. M. Rowe, and N. Lancaster, 2004, Tropical westerlies over Pangaean sand seas: 100 million years of cross-equatorial flow: Sedimentolog , v. 51, no. 2, p. 315–322, doi:10.1046/j.1365-3091.2003.00623.x.

Panek, R., 2000, The Sedimentology and Stratigraphy of the Lower Triassic Montney Formation in the Subsurface of the Peace River Area, Northwestern Alberta, Master of Science: Calgary, Alberta, University of Calgary.

Rodland, D. L., and D. J. Bottjer, 2001, Biotic recovery from the end-Permian mass extinction: behavior of the inarticulate brachiopod Lingula as a disaster taxon: Palaios, v. 16, no. 1, p. 95–101.

Zonneveld, J.-P., 2001, Middle Triassic biostromes from the Liard Formation, British Columbia, Canada: oldest examples from the Mesozoic of NW Pangea: Sedimentary Geology, v. 145, no. 3, p. 317–341.

Zonneveld, J.-P., T. F. Moslow, and C. M. Henderson, 1997, Lithofacies associations and depositional environments in a mixed siliciclastic-carbonate coastal depositional system, upper Liard Formation, Triassic, northeastern British Columbia: Bulletin of Canadian Petroleum Geology, v. 45, no. 4, p. 553–575.

Zonneveld, J.-P., M. K. Gingras, and T. W. Beatty, 2010, Diverse ichnofossil assemblages following the P-T mass extinction, Lower Triassic, Alberta and British Columbia, Canada: Evidence for shallow marine refugia on the northwestern coast of Pangea: Palaios, v. 25, no. 6, p. 368–392, doi:10.2110/palo.2009.p09-135r.

Zonneveld, J.-P., R. B. MacNaughton, J. Utting, T. W. Beatty, S. G. Pemberton, and C. M. Henderson, 2010, Sedimentology and ichnology of the Lower Triassic Montney Formation in the Pedigree-Ring/Border-Kahntah River area, northwestern Alberta and northeastern British Columbia: Bulletin of Canadian Petroleum Geology, v. 58, no. 2, p. 115–140.

Zonneveld, J.-P., and T. F. Moslow, 2014, Perennial River Deltas of the Montney Formation: Alberta and British Columbia Subcrop Edge. GeoConvention 2014.

Figure Captions

4.1: The bottom current depositional environment with the current shown producing the two different facies associations. A) Represents the fan derived bottom current modified deposits that are closer to the source input of coarse grained sediment (arrows). When the current is active (blue) bivalve shells and ripple structures are created, with suspension sedimentation between current activity. B) Represents the distal bottom current modified deposits where winnowing of fine grained sediment with the deposition o bivalve material in concentrated horizons by the current activity (blue).

4.2: Core lithographic description of Well API: 03-30-082-20w6. There are two distinct sections to this core: the lower showing what is typical of facies SL2 and the first facies association, and the upper showing what is typical of LBS and the second facies association.

4.3: Formation of biostromes in the Middle Montney Formation based on Zonneveld (2001). A) Deposition of siltstone in background conditions. B) Storm or current brings in disarticulated valves and live opportunist larvae and adults who recolonize the patch. C) Shells serve as a hard substrate for other colonizers which in turn provide prey for nektobenthic organisms as well as nektonic fauna. D) Either low oxygen kills off fauna or sudden sedimentation buries the organisms. This is a return to background conditions, but beneath the sediment-water interface the packstone is cemented. E) A storm or current uncovers and erodes into the packstone allowing it to become a hardground again.

4.4: Diagrams of the thick and thin packstone bed structures. A) The larger, more cemented packstone beds. B) The smaller packstone bed structure.

4.5: Map of the Montney Formation during the Greisbachian with possible direction of wind driven bottom currents. The currents could be constrained by the ridge at the southwest, but there is no data in that area. Shells and sand could be brought in from the east, or the shells could be from a more local source. (The Montney map was compiled and modified from Barclay et al, 1990; Panek, 2000; Zonneveld et al, 2010a; Zonneveld et al, 2010b; Zonneveld and Moslow, 2014; and Zonneveld, pers. comm.).

List of Tables

4.1: Summary of facies with descriptions of minerology, grain size, sedimentary structures, trace fossils, and body fossils found in each facies.

References

Alroy, J. et al., 2008, Phanerozoic trends in the global diversity of marine invertebrates: Science, v. 321, no. 5885, p. 97–100.

Armitage, J. H., 1962, Triassic Oil and Gas Occurrences in Northeastern British Columbia, Canada: Journal of the Alberta Society of Petroleum Geologists, v. 10, no. 2, p. 35–56.

Balini, M., S. G. Lucas, J. F. Jenks, and J. A. Spielmann, 2010, Triassic ammonoid biostratigraphy: an overview: Geological Society, London, Special Publications, v. 334, no. 1, p. 221–262, doi:10.1144/SP334.10.

Bambach, R. K., 2006, Phanerozoic biodiversity mass extinctions: Annual Review of Earth and Planetary Sciences, v. 34, p. 127–155.

Barclay, J., F. Krause, R. Campbell, and J. Utting, 1990, Dynamic casting and growth faulting: Dawson Creek graben complex, Carboniferous-Permian Peace River embayment, western Canada: Bulletin of Canadian Petroleum Geology, v. 38, no. 1, p. 115–145.

Barron, E. J., 1989, Climate variations and the Appalachians from the late paleozoic to the present: Results from model simulations: Geomorphology, v. 2, no. 1-3, p. 99–118, doi:10.1016/0169-555X(89)90008-1.

Beatty, T. W., J. Zonneveld, and C. M. Henderson, 2008, Anomalously diverse Early Triassic ichnofossil assemblages in northwest Pangea: a case for a shallow-marine habitable zone: Geology, v. 36, no. 10, p. 771–774.

Beauchamp, B., and A. Desrochers, 1997, Permian warm- to very cold- water carbonates and cherts in northwest Pangea, in N. P. James, and J. A. D. Clarke, eds., Cool-Water Carbonates: SEPM (Society for Sedimentary Geology).

Beaufort, L. et al., 2011, Sensitivity of coccolithophores to carbonate chemistry and ocean acidification: Nature, v. 476, no. 7358, p. 80–83.

Best, M. M. R., and S. M. Kidwell, 2000, Bivalve taphonomy in tropical mixed siliciclastic-carbonate settings. I. Environmental variation in shell condition: Paleobiology, v. 26, no. 1, p. 80–102, doi:10.1666/0094-8373(2000)026<0080:BTITMS>2.0.CO;2.

Best, M. M., T. C. Ku, S. M. Kidwell, and L. M. Walter, 2007, Carbonate preservation in shallow marine environments: Unexpected role of tropical siliciclastics: The Journal of geology, v. 115, no. 4, p. 437–456.

Bird, T., J. Barclay, R. Campbell, and P. Lee, 1994, Triassic Gas Resources of Western Canada Sedimentary Basin, Interior Plains-Geological Play Analysis and Resource Assessment: Western Canadian and International Expertise [Program book with expanded abstracts], p. 352–353.

Blakey, R., 1972, Stratigraphy and Depositional Environments of Moenkopi Formation in Southeastern Utah: ABSTRACT: AAPG Bulletin, v. 56, no. 3, p. 604–604.

Blakey, R.C., Basham, E.L., and Cook, M.J., 1993, Early and Middle Triassic paleogeography, Colorado

Plateau and vicinity, in Morales, M., ed., Aspects of Mesozoic Geology and Paleontology of the Colorado Plateau: Museum of Northern Arizona Bulletin 59, p. 13-26.

Bodzoich, A., 1985, Palaeoecology and sedimentary environment of the terebratula beds (lower muschelkalk) from Upper Silesia (south Poland): Annales Societatis Geologorum Poloniae, v. 55, p. 127–138.

Bottrell, S. H., and R. J. Newton, 2006, Reconstruction of changes in global sulfur cycling from marine sulfate isotopes: Earth-Science Reviews, v. 75, no. 1-4, p. 59–83, doi:10.1016/j.earscirev.2005.10.004.

Boyer, D. L., D. J. Bottjer, and M. L. Droser, 2004, Ecological Signature of Lower Triassic Shell Beds of the Western United States: Palaios, v. 19, no. 4, p. 372–380, doi:10.1669/0883-1351(2004)019<0372:ESOLTS>2.0.CO;2.

Bureau, G. G., 1987, Regional Geology of Guizhou Province: Geological Memoirs, v. 1, no. 7, p. 1–698.

Claypool, G. E., W. T. Holser, I. R. Kaplan, H. Sakai, and I. Zak, 1980, The age curves of sulfur and oxygen isotopes in marine sulfate and their mutual interpretation: Chemical Geology, v. 28, p. 199–260.

Cooper, C., G. Z. Forristall, and T. M. Joyce, 1990, Velocity and hydrographic structure of two Gulf of Mexico warm-core rings: Journal of Geophysical Research: Oceans (1978–2012), v. 95, no. C2, p. 1663–1679.

Cumings, E. R., 1932, Reefs or bioherms?: Geological Society of America Bulletin, v. 43, no. 1, p. 331–352.

Davies, G. R., 1997, The Triassic of the Western Canada Sedimentary Basin: tectonic and stratigraphic framework, paleogeography, paleoclimate and biota: Bulletin of Canadian Petroleum Geology, v. 45, no. 4, p. 434–460.

Davies, G. R., T. F. Moslow, and M. D. Sherwin, 1997, The Lower Triassic Montney Formation, west-central Alberta: Bulletin of Canadian Petroleum Geology, v. 45, no. 4, p. 474–505.

Desrocher, S., I. Hutcheon, D. Kirste, and C. M. Henderson, 2004, Constraints on the generation of H2S and CO2 in the subsurface Triassic, Alberta Basin, Canada: Chemical Geology, v. 204, no. 3-4, p. 237–254, doi:10.1016/j.chemgeo.2003.11.012.

Doney, S. C., V. J. Fabry, R. A. Feely, and J. A. Kleypas, 2009, Ocean acidification: the other CO2 problem: Marine Science, v. 1.

Driscoll, E., and D. Brandon, 1973, Mollusc-sediment relationships in northwestern Buzzards Bay, Massachusetts, USA: Malacologia, v. 12, no. 1, p. 13–46.

Dunham, R. J., 1962, Classification of carbonate rocks according to depositional textures, in Classification of Carbonate Rocks--A Symposium: AAPG, Memoir, p. 108–121.

Edwards, D. E., J. E. Barclay, D. W. Gibson, G. E. Kvill, and E. Halton, 1994, Triassic Strata of the Western Canada Sedimentary Basin, in G. D. Mossop, and I. Shetsen, eds., Geological Atlas of the Western Canada Sedimentary Basin: Canadian Society of Petroleum Geologists and Alberta Research Council.

Erwin, D. H., 2000, The Permo-Triassic extinction: Shaking the Tree: Readings from Nature in the History of Life, v. 189.

Erwin, D., 2007, Disparity: Morphological pattern and developmental context: Palaeontology, v. 50, p. 57–73.

Faugères, J. C., M. L. Mézerais, and D. A. Stow, 1993, Contourite drift types and their distribution in the North and South Atlantic Ocean basins: Sedimentary Geology, v. 82, no. 1, p. 189–203.

Faugères, J.-C., D. A. Stow, P. Imbert, and A. Viana, 1999, Seismic features diagnostic of contourite drifts: Marine Geology, v. 162, no. 1, p. 1–38.

Faugères, J.-C., and D. Stow, 2008, Contourite drifts: nature, evolution and controls: Developments in sedimentology, v. 60, p. 257–288.

Ferri, F., and J. Zonneveld, 2008, Were Triassic rocks of the Western Canada Sedimentary Basin deposited in a foreland: Canadian Society of Petroleum Geologists Reservoir, v. 35, no. 10, p. 12–14.

Flügel, E., 1994, Pangean shelf carbonates: controls and paleoclimatic significance of Permian and Triassic reefs: Geological Society of America Special Papers, v. 288, p. 247–266.

Forel, M.-B., 2013, The Permian–Triassic mass extinction: Ostracods (Crustacea) and microbialites: Comptes Rendus Geoscience, v. 345, no. 4, p. 203–211.

Forel, M.-B., S. Crasquin, T. Brühwiler, N. Goudemand, H. Bucher, A. Baud, and C. Randon, 2011, Ostracod recovery after Permian–Triassic boundary mass-extinction: The south Tibet record: Palaeogeography, Palaeoclimatology, Palaeoecology, v. 308, no. 1-2, p. 160–170, doi:10.1016/j.palaeo.2011.02.013.

Fry, B., S. R. Silva, C. Kendall, and R. K. Anderson, 2002, Oxygen isotope corrections for online ?34S analysis: Rapid Communications in Mass Spectrometry, v. 16, no. 9, p. 854–858, doi:10.1002/rcm.651.

Gibson, D. W., 1974, Triassic rocks of the Southern Canadian Rocky Mountains: Ottawa, [s.n.], Bulletin / Geological survey of Canada;no. 230.

Gibson, D., 1993, Triassic: Sedimentary cover of the craton in Canada. DF Stott and JD Aitken (eds.). Geological Survey of Canada, Geology of Canada, v. 5, p. 294–320.

Gibson, D., and J. Barclay, 1989, Middle Absaroka sequence the Triassic stable craton, in Ricketts, BD, ed., Western Canada Sedimentary Basin - A case history: Calgary, p. 219–231.

Gibson, D., and T. Poulton, 1994, Field Guide to the Triassic and Jurassic stratigraphy and depositional environments in the Rocky Mountain Foothills and Front Ranges in the Banff, Jasper and Cadomin areas, Alberta: Geological Survey of Canada, Open File Report No. 2780, 85 p.

Glass, D. J., 1990, Lexicon of Canadian Stratigraphy: Volume 4, Western Canada: Canadian Society of

Petroleum Geologists.

Golding, M., M. Orchard, J.-P. Zonneveld, C. Henderson, and L. Dunn, 2014, An exceptional record of the sedimentology and biostratigraphy of the Montney and Doig formations in British Columbia: Bulletin of Canadian Petroleum Geology, v. 62, no. 3, p. 157–176.

Golding, M., M. Orchard, J.-P. Zonneveld, and N. Wilson, 2015, Determining the age and depositional model of the Doig Phosphate Zone in northeastern British Columbia using conodont biostratigraphy: Bulletin of Canadian Petroleum Geology, v. 63, no. 2, p. 143–170.

Gooday, A. et al., 2009, Faunal responses to oxygen gradients on the Pakistan margin: A comparison of foraminiferans, macrofauna and megafauna: Deep Sea Research Part II: Topical Studies in Oceanography, v. 56, no. 6, p. 488–502.

Goodspeed, T. H., and S. G. Lucas, 2007, Stratigraphy, sedimentology, and sequence stratigraphy of the Lower Triassic Sinbad Formation, San Rafael Swell, Utah: New Mexico Museum of Natural History and Science Bulletin, v. 40, p. 91–101.

Government of Canada; Natural Resources Canada; Earth Sciences Sector; Canada Centre for Mapping and Earth, 2001, Coastline and Boundaries of Canada.

Grasby, S., B. Beauchamp, A. Embry, and H. Sanei, 2013, Recurrent Early Triassic ocean anoxia: Geology, v. 41, no. 2, p. 175–178.

Greene, S. E., D. J. Bottjer, H. Hagdorn, and J.-P. Zonneveld, 2011, The Mesozoic return of Paleozoic faunal constituents: A decoupling of taxonomic and ecological dominance during the recovery from the end-Permian mass extinction: Palaeogeography, Palaeoclimatology, Palaeoecology, v. 308, no. 1-2, p. 224–232, doi:10.1016/j.palaeo.2010.08.019.

Grice, K., C. Cao, G. D. Love, M. E. Böttcher, R. J. Twitchett, E. Grosjean, R. E. Summons, S. C. Turgeon, W. Dunning, and Y. Jin, 2005, Photic zone euxinia during the Permian-Triassic superanoxic event: Science, v. 307, no. 5710, p. 706–709.

Habicht, J. K. A., 1979, Paleoclimate, paleomagnetism, and continental drift: American Association of Petroleum Geologists Studies in Geology 9.

Hagdorn, H., 1982, The “Bank der kleinen Terebrateln”(Upper Muschelkalk, Triassic) near Schwäbisch Hall (SW-Germany)—A tempestite condensation horizon: Springer.

Hagdorn, H., and R. Mundlos, 1982, Autochthonschille im Oberen Muschelkalk (Mitteltrias) Südwestdeutschlands: Neues Jahrbuch für Geologie und Paläontologie, Abhandlungen, v. 162, p. 332–351.

Hallam, A., 1987, Radiations and extinctions in relation to environmental change in the marine Lower Jurassic of northwest Europe: Paleobiology, p. 152–168.

Hallam, A., 1991, Relative importance of regional tectonics and eustasy for the Mesozoic of the Andes, in D. Macdonald, ed., Sedimentation, tectonics and eustasy, sea-level changes at active margins: International Association of Sedimentologists Special Publication 12, p. 189–200.

Hays, L. E., T. Beatty, C. M. Henderson, G. D. Love, and R. E. Summons, 2007, Evidence for photic zone euxinia through the end-Permian mass extinction in the Panthalassic Ocean (Peace River Basin, Western Canada): Palaeoworld, v. 16, no. 1-3, p. 39–50, doi:10.1016/j.palwor.2007.05.008.

Heezen, B. C., and C. Hollister, 1964, Deep-sea current evidence from abyssal sediments: Marine Geology, v. 1, no. 2, p. 141–174.

Henderson, C., S. Mei, and B. Wardlaw, 2002, New conodont definitions at the Guadalupian-Lopingian boundary, in L. Hills, C. Henderson, and E. Bamber, eds., Carboniferous and Permian of the World: Canadian Society of Petroleum Geologists Memoir 19, p. 725–735.

Hollister, C. D., 1967, Sediment distribution and deep circulation in the western North Atlantic: Columbia University.

Hollister, C. D., and I. N. McCave, 1984, Sedimentation under deep-sea storms: Nature, v. 309, no. 5965, p. 220–225, doi:10.1038/309220a0.

Holser, W. T. et al., 1989, A unique geochemical record at the Permian/Triassic boundary: Nature, v. 337, no. 6202, p. 39–44.

Hotinski, R. M., K. L. Bice, L. R. Kump, R. G. Najjar, and M. A. Arthur, 2001, Ocean stagnation and end-Permian anoxia: Geology, v. 29, no. 1, p. 7–10.

Isozaki, Y., 1994, Superanoxia across the Permo-Triassic boundary: Record in accreted deep-sea pelagic chert in Japan, in Pangea: Global Environements and Resources: CSPG Memoir 17, p. 805–812.

Ito, M., 1996, Sandy contourites of the lower Kazusa Group in the Boso Peninsula, Japan: Kuroshio-Current-influenced deep-sea sedimentation in a Plio-Pleistocene forearc basin: Journal of Sedimentary Research, v. 66, no. 3.

Jin, Y., Y. Wang, W. Wang, Q. Shang, C. Cao, and D. Erwin, 2000, Pattern of marine mass extinction near the Permian-Triassic boundary in South China: Science, v. 289, no. 5478, p. 432–436.

Kajiwara, Y., and K. Kaiho, 1992, Oceanic anoxia at the Cretaceous/Tertiary boundary supported by the sulfur isotopic record: Palaeogeography, palaeoclimatology, palaeoecology, v. 99, no. 1, p. 151–162.

Kato, Y., K. Nakao, and Y. Isozaki, 2002, Geochemistry of Late Permian to Early Triassic pelagic cherts from southwest Japan: implications for an oceanic redox change: Chemical Geology, v. 182, no. 1, p. 15–34.

Kauffman, E., 1978, Short-lived benthic communities in the Solnhofen and Nusplingen Limestones: Neues Jahrbuch für Geologie und Palaeontologie, Monatshefte, p. 717–724.

Kaźmierczak, J., and B. Kremer, 2005, Early post-mortem calcified Devonian acritarchs as a source of calcispheric structures: Facies, v. 51, no. 1-4, p. 554–565.

Kendall, D. R., 1999, Sedimentology and Stratigraphy of the Lower Triassic Montney Formation, Peace River Basin, subsurface of northwestern Alberta, Master of Science: Calgary, Alberta, The University of Calgary, 368 p.

Kendall, D. R., R. Panek, and C. M. Henderson, 1998, Coquina facies of the Lower Triassic Montney Formation, Peace River Embayment, northwestern Alberta.

Kershaw, S., 1994, Classification and geological significance of biostromes: Facies, v. 31, no. 1, p. 81–91.

Kidder, D. L., and T. R. Worsley, 2004, Causes and consequences of extreme Permo-Triassic warming to globally equable climate and relation to the Permo-Triassic extinction and recovery: Palaeogeography, Palaeoclimatology, Palaeoecology, v. 203, no. 3-4, p. 207–237, doi:10.1016/S0031-0182(03)00667-9.

Kidwell, S. M., 1986, Models for fossil concentrations: paleobiologic implications: Paleobiology, p. 6–24.

Kidwell, S. M., 1991, Taphonomic feedback (live/dead interactions) in the genesis of bioclastic beds: keys to reconstructing sedimentary dynamics., in G. Einsele, W. Ricken, and A. Seilacher, eds., Cycles and Events in Stratigraphy: Berlin, Springer-Verlag, p. 268–282.

Kidwell, S. M., and D. Jablonski, 1983, Taphonomic feedback ecological consequences of shell accumulation, in Biotic interactions in recent and fossil benthic communities: Springer, p. 195–248.

Kidwell, S. M., and D. W. Bosence, 1991, Taphonomy and time-averaging of marine shelly faunas: Taphonomy: releasing the data locked in the fossil record. Plenum, New York, p. 115–209.

Kidwell, S. M., and S. M. Holland, 1991, Field Description of Coarse Bioclastic Fabrics: Palaios, v. 6, no. 4, p. 426, doi:10.2307/3514967.

Klement, K. W., 1967, Practical Classification of Reefs and Banks, Bioherms and Biostromes: ABSTRACT: AAPG Bulletin, v. 51, no. 1, p. 167–168.

Kutzbach, J. E., P. J. Guetter, and W. M. Washington, 1990, Simulated circulation of an idealized ocean for Pangaean time: Paleoceanography, v. 5, no. 3, p. 299–317, doi:10.1029/PA005i003p00299.

Lehrmann, D. J., 1999, Early Triassic calcimicrobial mounds and biostromes of the Nanpanjiang basin, south China: Geology, v. 27, no. 4, p. 359–362.

Levin, L. A., 2003, Oxygen minimum zone benthos: adaptation and community response to hypoxia: Oceanography and Marine Biology: An Annual Review, v. 41, p. 1–45.

Levin, L. A., C. L. Huggett, and K. F. Wishner, 1991, Control of deep-sea benthic community structure by oxygen and organic-matter gradients in the eastern Pacific Ocean: Journal of Marine Research, v. 49, no. 4, p. 763–800.

Loope, D. B., M. B. Steiner, C. M. Rowe, and N. Lancaster, 2004, Tropical westerlies over Pangaean sand seas: 100 million years of cross-equatorial flow: Sedimentology, v. 51, no. 2, p. 315–322, doi:10.1046/j.1365-3091.2003.00623.x.

Maiklem, W., 1968, Some hydraulic properties of bioclastic carbonate grains: Sedimentology, v. 10, no.

Markhasin, B., 1997, Sedimentology and Stratigraphy of the Lower Triassic Montney Formation, Subsurface of Northwestern Alberta, Master of Science: Calgary, Alberta, University of Calgary, 154 p.

Marszalek, D., 1975, Calcisphere ultrastructure and skeletal aragonite from the alga Acetabularia antillana: Journal of Sedimentary Research, v. 45, no. 1.

Mata, S. A., and A. D. Woods, 2008, Sedimentology and paleoecology of the Lower Member of the Lower Triassic (Smithian-Spathian) Union Wash Formation, east-central California: Palaios, v. 23, no. 8, p. 514–524.

Mata, S. A., and D. J. Bottjer, 2011, Origin of Lower Triassic microbialites in mixed carbonate-siliciclastic successions: ichnology, applied stratigraphy, and the end-Permian mass extinction: Palaeogeography, Palaeoclimatology, Palaeoecology, v. 300, no. 1, p. 158–178.

McGowan, A. J., 2004, Ammonoid taxonomic and morphologic recovery patterns after the Permian–Triassic: Geology, v. 32, no. 8, p. 665–668.

McRoberts, C. A., 2010, Biochronology of Triassic bivalves: Geological Society, London, Special Publications, v. 334, no. 1, p. 201–219, doi:10.1144/SP334.9.

Mederos, S., 1995, Sedimentology and sequence stratigraphy of the Montney Formation in the Sturgeon Lake A and B pool, MSc: Edmonton, University of Alberta, 229 p.

Metcalfe, B., R. J. Twitchett, and N. Price-Lloyd, 2011, Changes in size and growth rate of “Lilliput” animals in the earliest Triassic: Palaeogeography, Palaeoclimatology, Palaeoecology, v. 308, no. 1-2, p. 171–180, doi:10.1016/j.palaeo.2010.09.011.

Meyer, K., M. Yu, A. Jost, B. Kelley, and J. L. Payne, 2011, d13C evidence that high primary productivity delayed recovery from end-Permian mass extinction: Earth and Planetary Science Letters, v. 302, p. 378–384.

Milliken, K. L., W. L. Esch, R. M. Reed, and T. Zhang, 2012, Grain assemblages and strong diagenetic overprinting in siliceous mudrocks, Barnett Shale (Mississippian), Fort Worth Basin, Texas: Aapg Bulletin, v. 96, no. 8, p. 1553–1578.

Moslow, T. F., 2000, Reservoir architecture of a fine-grained turbidite system: Lower Triassic Montney Formation, Western Canada Sedimentary Basin, in Deep-water Reservoirs of the World, Conference Proceedings, Gulf Coast SEPM. P. Weimer, RM Slatt, J. Coleman, NC Rosen, H. Nelson, AH Bouma, MJ Styzen, and DT Lawrence (eds.): SEPM, p. 686–713.

Newell, N., and D. Boyd, 1995, Pectinoid bivalves of the Permian-Triassic crisis.: Bulletin of the American Museum of Natural History, no. 227, p. 5 – 95.

Nielsen, J. K., and Y. Shen, 2004, Evidence for sulfidic deep water during the Late Permian in the East Greenland Basin: Geology, v. 32, no. 12, p. 1037, doi:10.1130/G20987.1.

Nützel, A., 2005, Recovery of gastropods in the Early Triassic: Comptes Rendus Palevol, v. 4, no. 6, p. 501–515.

Nützel, A., and C. Schulbert, 2005, Facies of two important Early Triassic gastropod lagerstätten: implications for diversity patterns in the aftermath of the end-Permian mass extinction: Facies, v. 51, no. 1-4, p. 480–500.

Orchard, M. J., and E. T. Tozer, 1997, Triassic conodont biochronology, its calibration with the ammonoid standard, and a biostratigraphic summary for the Western Canada Sedimentary Basin: Bulletin of Canadian Petroleum Geology, v. 45, no. 4, p. 675–692.

Orchard, M. J., and J.-P. Zonneveld, 2009, The Lower Triassic Sulphur Mountain Formation in the Wapiti Lake area: lithostratigraphy, conodont biostratigraphy, and a new biozonation for the lower Olenekian (Smithian)Earth Science Sector (ESS) Contribution 20080714.: Canadian Journal of Earth Sciences, v. 46, no. 10, p. 757–790, doi:10.1139/E09-051.

Panek, R., 2000, The Sedimentology and Stratigraphy of the Lower Triassic Montney Formation in the Subsurface of the Peace River Area, Northwestern Alberta, Master of Science: Calgary, Alberta, University of Calgary.

Paull, R. K., R. A. Paull, and T. S. Laudon, 1997, Conodont biostratigraphy of the Lower Triassic Mackenzie Dolomite Lentil, Sulphur Mountain Formation in the Cadomin area, Alberta: Bulletin of Canadian Petroleum Geology, v. 45, no. 4, p. 708–714.

Payne, J. L., D. J. Lehrmann, J. Wei, M. Orchard, D. Schrag, and A. Knoll, 2004, Large Perturbations of the Carbon Cycle During Recovery from the End-Permian Extinction: Science, v. 305, no. 5683, p. 506–509, doi:10.1126/science.1097023.

Payne, J. L., and M. E. Clapham, 2012, End-Permian mass extinction in the oceans: an ancient analog for the twenty-first century?: Annual Review of Earth and Planetary Sciences, v. 40, p. 89–111.

Payne, J. L., D. Altiner, D. J. DePaolo, J. L. Hinojosa, L. R. Kump, K. V. Lau, D. J. Lehrmann, K. Maher, A. Paytan, and S. Shen, 2014, The End-Permian Mass Extinction and its Aftermath: Insights from Non-Traditional Isotope System: Vancouver, BC.

Pietsch, C., and D. J. Bottjer, 2014, The importance of oxygen for the disparate recovery patterns of the benthic macrofauna in the Early Triassic: Earth-Science Reviews, v. 137, p. 65–84.

Pietsch, C., S. A. Mata, and D. J. Bottjer, 2014, High temperature and low oxygen perturbations drive contrasting benthic recovery dynamics following the end-Permian mass extinction: Palaeogeography, Palaeoclimatology, Palaeoecology, v. 399, p. 98–113.

Pruss, S. B., and D. J. Bottjer, 2004, Early Triassic trace fossils of the western United States and their implications for prolonged environmental stress from the end-Permian mass extinction: Palaios, v. 19, no. 6, p. 551–564.

Pruss, S. B., F. A. Corsetti, and D. J. Bottjer, 2005a, Environmental trends of Early Triassic biofabrics: implications for understanding the aftermath of the end-Permian mass extinction: Developments in Palaeontology and Stratigraphy, v. 20, p. 313–332.

Pruss, S. B., F. A. Corsetti, and D. J. Bottjer, 2005b, The unusual sedimentary rock record of the Early Triassic: a case study from the southwestern United States: Palaeogeography, Palaeoclimatology, Palaeoecology, v. 222, no. 1, p. 33–52.

Rampino, M. R., and K. Caldeira, 2005, Major perturbation of ocean chemistry and a “Strangelove Ocean” after the end-Permian mass extinction: Terra Nova, v. 17, no. 6, p. 554–559, doi:10.1111/j.1365-3121.2005.00648.x.

Rebesco, M., A. Camerlenghi, and A. Van Loon, 2008, Contourite research: a field in full development: Contourites, Developments in Sedimentology, v. 60, p. 3–10.

Riccardi, A. L., M. A. Arthur, and L. R. Kump, 2006, Sulfur isotopic evidence for chemocline upward excursions during the end-Permian mass extinction: Geochimica et Cosmochimica Acta, v. 70, no. 23, p. 5740–5752, doi:10.1016/j.gca.2006.08.005.

Richardson, J. R., 1981, Brachiopods in mud: resolution of a dilemma: Science, v. 211, no. 4487, p. 1161–1163.

Robinson B. W., 1993, Sulfur isotope standards. Reference and intercomparison materials for stable isotopes of light elements. Proceedings of a consultants meeting held in Vienna, p. 13–30.

Rodland, D. L., and D. J. Bottjer, 2001, Biotic recovery from the end-Permian mass extinction: behavior of the inarticulate brachiopod Lingula as a disaster taxon: Palaios, v. 16, no. 1, p. 95–101.

Schatz, W., 2005, Palaeoecology of the Triassic black shale bivalve Daonella—new insights into an old controversy: Palaeogeography, Palaeoclimatology, Palaeoecology, v. 216, no. 3-4, p. 189–201, doi:10.1016/j.palaeo.2004.11.002.

Schoepfer, S. D., C. M. Henderson, G. H. Garrison, J. Foriel, P. D. Ward, D. Selby, J. C. Hower, T. J. Algeo, and Y. Shen, 2013, Termination of a continent-margin upwelling system at the Permian–Triassic boundary (Opal Creek, Alberta, Canada): Global and Planetary Change, v. 105, p. 21–35, doi:10.1016/j.gloplacha.2012.07.005.

Schubert, J. K., and D. J. Bottjer, 1992, Early Triassic stromatolites as post-mass extinction disaster forms: Geology, v. 20, no. 10, p. 883–886.

Schubert, J. K., and D. J. Bottjer, 1995, Aftermath of the Permian-Triassic mass extinction event: Paleoecology of Lower Triassic carbonates in the western USA: Palaeogeography, Palaeoclimatology, Palaeoecology, v. 116, no. 1, p. 1–39.

Sepkoski Jr, J. J., 1981, A factor analytic description of the Phanerozoic marine fossil record: Paleobiology, p. 36–53.

Shanmugam, G., 1997, The Bouma sequence and the turbidite mind set: Earth-Science Reviews, v. 42, no. 4, p. 201–229.

Shanmugam, G., T. Spalding, and D. Rofheart, 1993a, Process sedimentology and reservoir quality of deep-marine bottom-current reworked sands (sandy contourites): an example from the Gulf of Mexico: AAPG Bulletin, v. 77, no. 7, p. 1241–1259.

Shanmugam, G., T. D. Spalding, and D. H. Rofheart, 1993b, Traction structures in deep-marine, bottom-current-reworked sands in the Pliocene and Pleistocene, Gulf of Mexico: Geology, v. 21, no. 10, p. 929, doi:10.1130/0091-7613(1993)021<0929:TSIDMB>2.3.CO;2.

Song, H., J. Tong, and Z. Q. Chen, 2011, Evolutionary dynamics of the Permian–Triassic foraminifer size: Evidence for Lilliput effect in the end-Permian mass extinction and its aftermath: Palaeogeograph , Palaeoclimatology, Palaeoecology, v. 308, no. 1-2, p. 98–110, doi:10.1016/j.palaeo.2010.10.036.

Stanley, D. J., D. J. Swift, and H. G. Richards, 1967, Fossiliferous concretions on Georges Bank: Journal of Sedimentary Research, v. 37, no. 4.

Stow, D. A. V., 2001, Deep-Sea Sediment Drifts, in J. H. Steele, K. K. Turekian, and S. A. Thorpe, eds., Encyclopedia of Ocean Sciences: London, Academic Press.

Stow, D. A., J.-C. Faugères, A. Viana, and E. Gonthier, 1998, Fossil contourites: a critical review: Sedimentary Geology, v. 115, no. 1, p. 3–31.

Stow, D. A., J.-C. Faugères, J. A. Howe, C. J. Pudsey, and A. R. Viana, 2002, Bottom currents, contourites and deep-sea sediment drifts: current state-of-the-art: Geological Society, London, Memoirs, v. 22, no. 1, p. 7–20.

Stow, D., and J.-C. Faugères, 2008, Contourite facies and the facies model: Developments in Sedimentology, v. 60, p. 223–256.

Takahashi, S. et al., 2013, Sulfur isotope profiles in the pelagic Panthalassic deep sea during the Permian–Triassic transition: Global and Planetary Change, v. 105, p. 68–78, doi:10.1016/j.gloplacha.2012.12.006.

Thode, H. ., J. Monster, and H. . Dunford, 1961, Sulphur isotope geochemistry: Geochimica et Cosmochimica Acta, v. 25, no. 3, p. 159–174, doi:10.1016/0016-7037(61)90074-6.

Thode, H., 1991, Sulphur isotopes in nature and the environment: an overview: Wiley.

Tozer, E., 1982, Marine Triassic faunas of North America: their significance for assessing plate and terrane movements: Geologische Rundschau, v. 71, no. 3, p. 1077–1104.

Tozer, E. T., 1994, Canadian Triassic ammonoid faunas: Geological Survey of Canada.

Twitchett, R. J., 2006, The palaeoclimatology, palaeoecology and palaeoenvironmental analysis of mass extinction events: Palaeogeography, Palaeoclimatology, Palaeoecology, v. 232, no. 2, p. 190–213.

Twitchett, R. J., and P. B. Wignall, 1996, Trace fossils and the aftermath of the Permo-Triassic mass extinction: evidence from northern Italy: Palaeogeography, Palaeoclimatology, Palaeoecology, v. 124, no. 1, p. 137–151.

Twitchett, R., L. Krystyn, A. Baud, J. Wheeley, and S. Richoz, 2004, Rapid marine recovery after the end-Permian mass-extinction event in the absence of marine anoxia: Geology, v. 32, no. 9, p. 805–808.

Versteegh, G. J., T. Servais, M. Streng, A. Munnecke, and D. Vachard, 2009, A discussion and proposal concerning the use of the term calcispheres: Palaeontology, v. 52, no. 2, p. 343–348.

Viana, A., J.-C. Faugères, and D. Stow, 1998, Bottom-current-controlled sand deposits—a review of modern shallow-to deep-water environments: Sedimentary Geology, v. 115, no. 1, p. 53–80.

Wentworth, C. K., 1922, A scale of grade and class terms for clastic sediments: The Journal of Geology, p. 377–392.

Wignall, P. B., 1994, Black shales: Clarendon Press Oxford.

Wignall, P. B., and A. Hallam, 1991, Biofacies, stratigraphic distribution and depositional models of British onshore Jurassic black shales: Geological Society, London, Special Publications, v. 58, no. 1, p. 291–309.

Wignall, P., and A. Hallam, 1996, Facies change and the end-Permian mass extinction in SE Sichuan, China: Palaios, p. 587–596.

Wignall, P. B., and R. J. Twitchett, 1999, Unusual intraclastic limestones in Lower Triassic carbonates and their bearing on the aftermath of the end-Permian mass extinction: Sedimentology, v. 46, no. 2, p. 303–316.

Wilkin, R. T., and M. A. Arthur, 2001, Variations in pyrite texture, sulfur isotope composition, and iron systematics in the Black Sea: Evidence for late Pleistocene to Holocene excursions of the O 2-H 2 S redox transition: Geochimica et Cosmochimica Acta, v. 65, no. 9, p. 1399–1416.

Wilson, K. M., D. Pollard, W. W. Hay, S. L. Thompson, and C. N. Wold, 1994, General circulation model simulations of Triassic climates: preliminary results: Geological Society of America Special Papers, v. 288, p. 91–116.

Wilson, N., 2009, Integrated regional model for the deposition and evolution of the Montney Formation, NE British Columbia.

Wood, J., 2012, Water Distribution in the Montney Tight Gas Play of the Western Canadian Sedimentary Basin: Significance for Resource Evaluation: Society of Petroleum Engineers, doi:10.2 18/161824-MS.

Wood, R., 1999, Reef evolution: Oxford University Press.

Woods, A. D., 2005, Paleoceanographic and paleoclimatic context of Early Triassic time: Comptes Rendus Palevol, v. 4, no. 6-7, p. 463–472, doi:10.1016/j.crpv.2005.07.003.

Woods, A. D., and D. J. Bottjer, 2000, Distribution of ammonoids in the Lower Triassic Union Wash Formation (Eastern California): Evidence for paleoceanographic conditions during recovery from the end-Permian mass extinction: Palaios, v. 15, p. 535–545.

Woods, A. D., D. J. Bottjer, M. Mutti, and J. Morrison, 1999, Lower Triassic large sea-floor carbonate cements: their origin and a mechanism for the prolonged biotic recovery from the end-Permian mass extinction: Geology, v. 27, no. 7, p. 645–648.

Zhenzhong, G., L. Shunshe, H. Youbin, Z. Jisen, and T. Zijun, 1995, The Middle Ordovician contourite on the west margin of Ordos: Acta Sedimentologica Sinica, v. 13, no. 4, p. 16–26.

Zonneveld, J.-P., 2001, Middle Triassic biostromes from the Liard Formation, British Columbia, Canada: oldest examples from the Mesozoic of NW Pangea: Sedimentary Geology, v. 145, no. 3, p. 317–341.

Zonneveld, J.-P., 2011, Suspending the Rules: Unraveling the ichnological signature of the Lower Triassic post-extinction recovery interval: Palaios, v. 26, no. 11, p. 677–681, doi:10.2110/palo.2011.S06.

Zonneveld, J.-P, and T. F. Moslow, 2013, Regional outcrop to subsurface correlation of the Montney Formation: An evolving understanding of Lower Mesozoic tectono-stratigraphic evolution in Western

Canada: Pennsylvania.

Zonneveld, J.-P., and T. F. Moslow, 2014, Perennial River Deltas of the Montney Formation: Alberta and British Columbia Subcrop Edge.

Zonneveld, J.-P., T. F. Moslow, and C. M. Henderson, 1997, Lithofacies associations and depositional environments in a mixed siliciclastic-carbonate coastal depositional system, upper Liard Formation, Triassic, northeastern British Columbia: Bulletin of Canadian Petroleum Geology, v. 45, no. 4, p. 553–575.

Zonneveld, J.-P., G. G. Carrelli, and C. Riediger, 2004, Sedimentology of the Upper Triassic Charlie Lake, Baldonnel and Pardonet formations from outcrop exposures in the southern Trutch region, northeastern British Columbia: Bulletin of canadian petroleum geology, v. 52, no. 4, p. 343–375.

Zonneveld, J.-P., M. K. Gingras, and T. W. Beatty, 2010a, Diverse ichnofossil assemblages following the P-T mass extinction, Lower Triassic, Alberta and British Columbia, Canada: Evidence for shallow marine refugia on the northwestern coast of Pangea: Palaios, v. 25, no. 6, p. 368–392, doi:10.2110/palo.2009.p09-135r.

Zonneveld, J.-P., R. B. MacNaughton, J. Utting, T. W. Beatty, S. G. Pemberton, and C. M. Henderson, 2010b, Sedimentology and ichnology of the Lower Triassic Montney Formation in the Pedigree-Ring/Border-Kahntah River area, northwestern Alberta and northeastern British Columbia: Bulletin of Canadian Petroleum Geology, v. 58, no. 2, p. 115–140.

Zonneveld, J.-P., C. Furlong, A. Gegolick, M. K. Gingras, M. Golding, T. F. Moslow, M. J. Orchard, T. Playter, D. Prenoslo, and S. C. Sanders, 2015, Stratigraphic architecture of the Montney Formation, Peace district, Alberta and British Columbia: Banff, Canada. Gussow Geoscience Conference: Banff Canada.

Zuschin, M., M. Stachowitsch, P. Pervesler, and H. Kollmann, 1999, Structural features and taphonomic pathways of a high-biomass epifauna in the northern Gulf of Trieste, Adriatic Sea: Lethaia, v. 32, no. 4, p. 299–316.

Zuschin, M., J. Hohenegger, and F. F. Steininger, 2000, A comparison of living and dead molluscs on coral reef associated hard substrata in the northern Red Sea—implications for the fossil record: Palaeogeography, Palaeoclimatology, Palaeoecology, v. 159, no. 1, p. 167–190.

Zuschin, M., M. Stachowitsch, and R. J. Stanton, 2003, Patterns and processes of shell fragmentation in modern and ancient marine environments: Earth-Science Reviews, v. 63, no. 1, p. 33–82.

Appendix A

The data presented within this appendix are the result of sulfur isotope work that was conducted on samples from the "*Claraia* Zone" in an attempt to understand the oxygenation through the interval. The data are inconclusive at this time because separation of sulfide and sulfate minerals was not conducted prior to processing of the samples for isotopes. This study was not included in the main body of the thesis due to the preliminary nature of the data, however its significance as one of the few isotope studies focused on the paleoenvironmental conditions in the Montney Formation warrants its inclusion here.

Oxygenation in the "*Claraia* Zone" of the Lower Triassic Montney Formation of British Columbia, Canada

A.1 Introduction

The Montney Formation and its outcrop equivalents have been the subject of few geochemistry studies, which have focused on other topics beyond hydrocarbon maturation and migration. This formation is a world-class record of the Early Triassic in Panthalassa, and yet has received little attention as to what it could tell us about life through this interval. Oxygenation and acidity have consistently been referred to as being major factors in the low abundance of body and trace fossils through the formation (Rampino and Caldeira, 2005; Woods, 2005; Zonneveld, 2011; Payne et al., 2014). In fact, Schopfer et al. (2013) identified coastal upwelling and euxinia at the base of the formation at a continuous Permian Triassic boundary outcrop section in Opal Creek. Focus on other horizons (particularly those in which body fossils and trace fossils become more abundant) may provide more information about the changes in redox conditions through the formation. This chapter presents preliminary data from sulfur isotopes from the "*Claraia* Zone" of the Lower Montney Formation.

The Late Dienerian "*Claraia* Zone" in northeastern British Columbia, Canada, was identified in chapter 2 as being the result of bottom current transport and deposition on the northwestern margin of Pangea. This horizon is composed of disarticulated *Claraia.* It is the first bioclastic interval above the contact with the Permian Belloy Formation in northeastern British Columbia. Sulfur isotopes may aid in the identification of an oxygenation event during the occurrence of the *"Claraia* Zone". However, at present, only twenty three samples have been collected and processed, and the data remain inconclusive. Additional samples are in the process of being obtained. Although not essential for this thesis, the preliminary data gathered to date are included herein as they provide some support for ideas presented in this study.

A.2 Background

A.2.1 Triassic

The Montney Formation represents the entirety of the Lower Triassic in the Western Canada Sedimentary Basin (Orchard and Tozer 1997, Orchard and Zonneveld, 2009). Thus, fossils within the Montney Formation record the recovery of northwestern Pangean marine biotas after the Permian-Triassic Mass Extinction on the eastern margin of Panthalassa. The Peace River Basin at this time was located at approximately 30°N latitude and was characterized by an arid climate on the east margin of the Panthalassa Ocean (Habicht, 1979; Tozer, 1982; Wilson et al., 1994; Kidder and Worsley, 2004). Diversity after the extinction event was low in the world's oceans and cosmopolitan taxa (organisms with widespread / global distribution), dominated the world's marine biotas (i.e., Sepkoski, 1981; Erwin, 2000; Bambach, 2006; Payne and Clapham, 2012). Recovery did not occur until the Middle Triassic at the earliest and was possibly delayed by increased alkalinity and/or expansion of oxygen minimum zones (e.g., Sepkoski, 1981; Woods, 2005; Payne et al., 2014). In the Montney Formation, trace fossils are also of very low abundance and diversity, pointing towards a stressed environment during deposition (Zonneveld et al, 2010a; 2010b). High diversity occurs only in successions that have been interpreted to record perennial deltaic environments (Zonneveld et al, 2010a; Zonneveld and Moslow, 2014).

A.2.2 The Montney Formation and the "*Claraia* Zone"

The Montney Formation is a westward thickening package of bituminous siltstone and fine grained sandstone in western Alberta and northeastern British Columbia, Canada (Edwards et al, 1994; Davies et al., 1997) (Fig. A.1). It was first identified b Armitage (1962) and has been targeted by petroleum exploration companies in Western Canada as both a conventional target (from the 1950s through the 1990s), and more recently as an unconventional, locally liquids-rich, tight gas reservoir (Bird et al., 1994; Davies et al., 1997; Wood, 2012). The subsurface Montney, and its outcrop equivalents in the western deformation belt along the eastern thrust sheets of the Canadian Rocky Mountains (Toad, Grayling, and Sulphur Mountain Formations), were deposited in the Peace River Basin (Edwards et al, 1994; Davies et al., 1997) (Fig. A.2). The Montney Formation has been interpreted to have been deposited along a clastic ramp on the western margin of Pangea, with deeper sedimentary facies deposited in the west (Edwards et al., 1994; Davies et al, 1997). Although the deposits span both Alberta and British Columbia, the Alberta units generally represent more proximally deposited facies, with the shoreline truncated along the eastern erosional edge by a series of later Mesozoic unconformities including the Late Triassic Coplin Unconformity, the sub-Jurassic unconformity and several sub-Cretaceous unconformities. Units which span the entirety of the Montney Formation on the eastern (Alberta) side of the basin are temporally equivalent to the Lower Montney Formation in the western (British Columbia) part of the basin, whereas the Upper Montney in British Columbia is an expansion of what is referred to as the Basal Doig Siltstone member in Alberta (Wilson, 2009). The Alberta terminology is based on an unpublished consultant report and has not been formally established in the literature. Due to a lack of clear lithological distinctions between the two units, and because all of the data presented herein is located in British Columbia, this study will conform to the British Columbia stratigraphic paradigm.

Figure A.1 (Next page): Map of core datasets in relation to the Montney Formation as a whole during the Greisbachian. The red dots each represent a separate core and they are all located well within the offshore portion of the formation. The Pedigree-Ring Delta is known to be Greisbachian in age, but the Dixonville has only been confirmed to be Smithian, although there are sand bodies of Greisbachian age that are located westward in the Peace River Arch from the delta location. The Meosin High in the southwest is based on subaerial exposure in the outcrop belt. The red block in the inset map shows the location of the above map in relation to modern geographical boundaries of Canada. (The Montney map was compiled and modified from Barclay et al, 1990; Panek, 2000; Zonneveld et al, 2010a; Zonneveld et al, 2010b; Zonneveld and Moslow, 2014; and Zonneveld, pers. comm.).

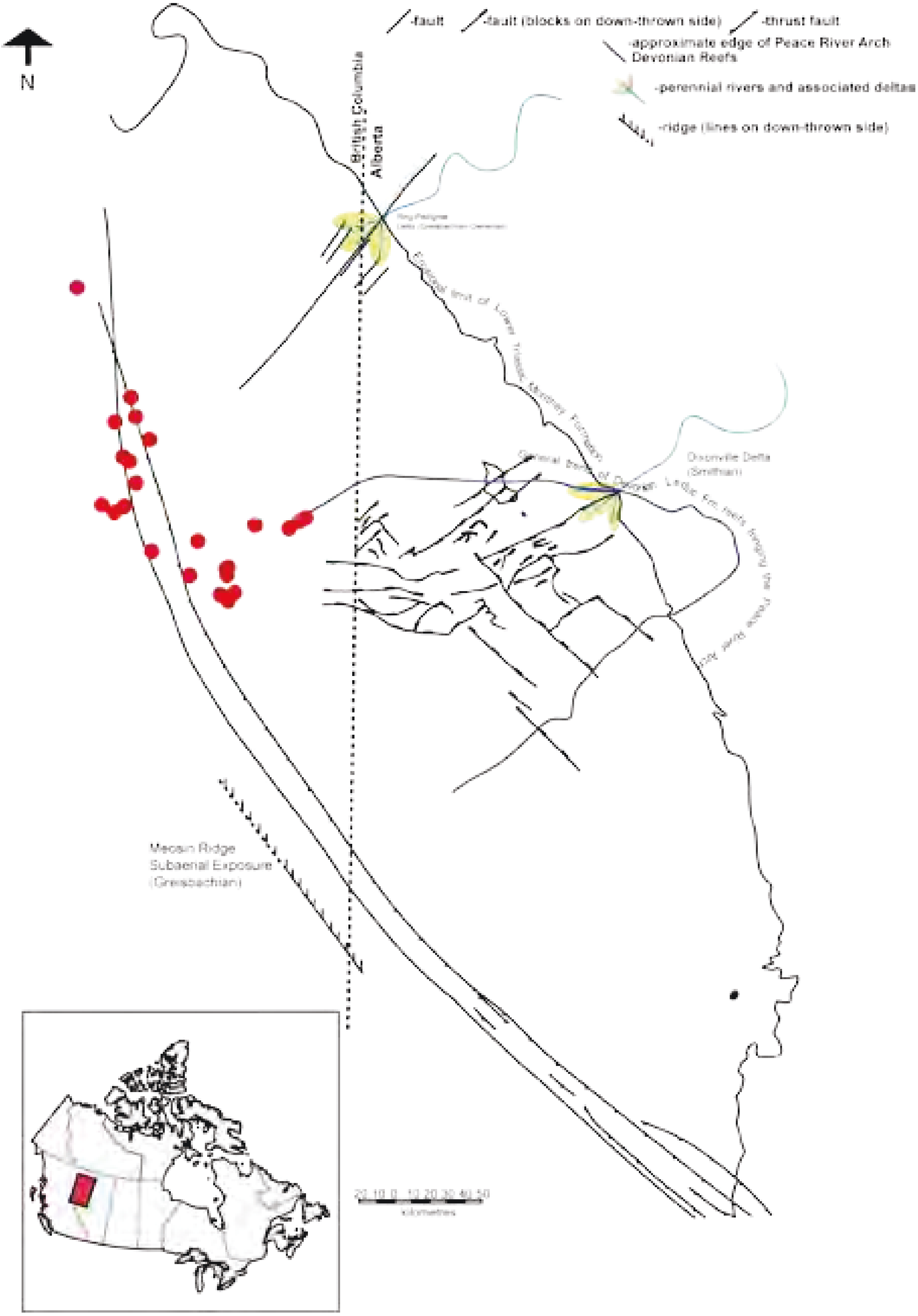
N
-fault
-fault (blocks on down-thrown side)
-thrust fault
-approximate edge of Peace River Arch Devonian Reefs
-perennial rivers and associated deltas
-ridge (lines on down-thrown side)
British Columbia
Alberta
Boy Pedigree
Erosional limit of Lower Triassic Montney Formation
General trend of Devonian Leduc Fm. reefs fringing the Peace River Arch
Dixonville Delta
(Smithian)
Mecsin Ridge
Subaerial Exposure
(Greisbachian)
20 10 0 10 20 30 40 50
kilometres

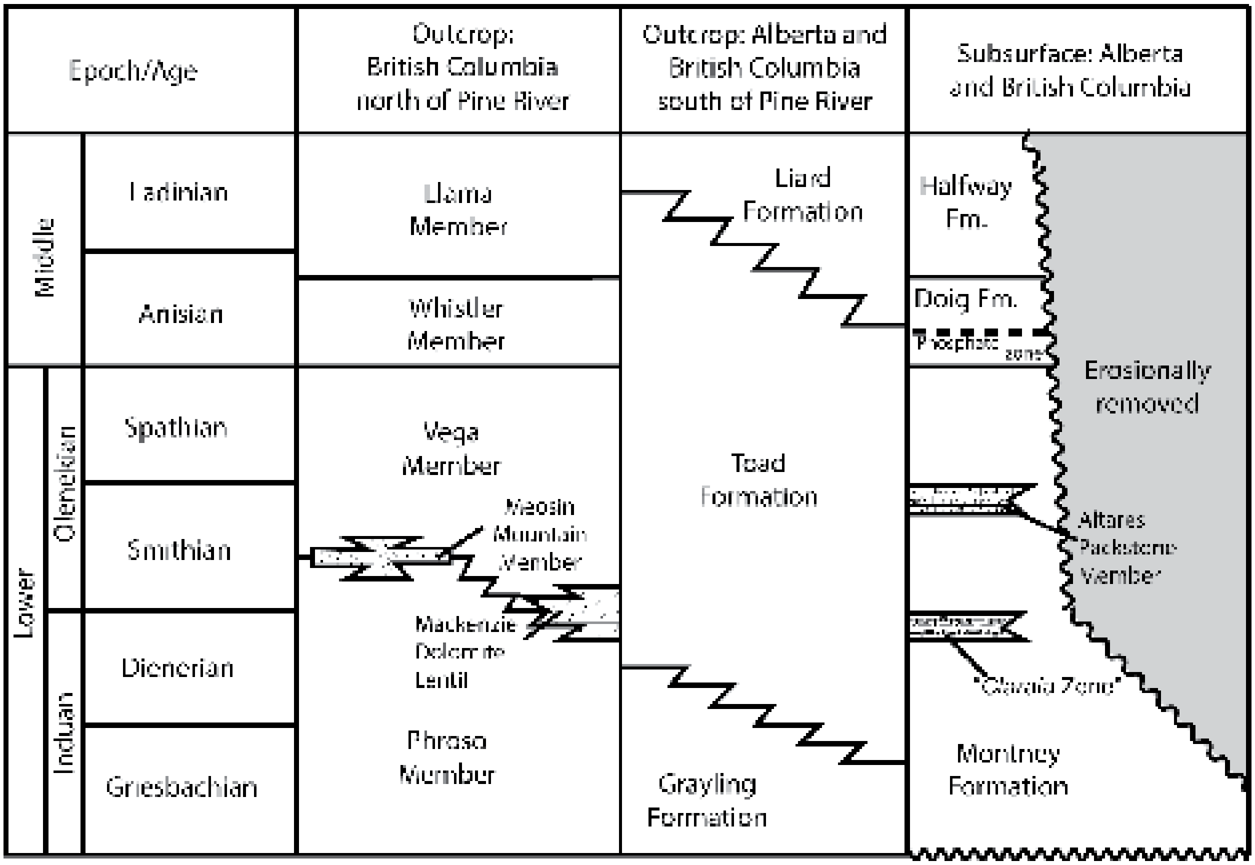
Epoch/Age
Outcrop: British Columbia north of Pine River
Outcrop: Alberta and British Columbia south of Pine River
Subsurface: Alberta and British Columbia
Middle
Ladinian
Anisian
Lower
Olenekian
Spathian
Smithian
Induan
Dienerian
Griesbachian
Llama Member
Whistler Member
Vega Member
Meosin Mountain Member
Mackenzie Dolomite Lentil
Phroso Member
Liard Formation
Toad Formation
Grayling Formation
Halfway Fm.
Doig Fm.
Phosphate zone
Erosionally removed
Altares Packstone Member
"Claraia Zone"
Montney Formation

Figure A.2: The stratigraphic framework of the Lower and Middle Triassic in the Western Canada Sedimentary Basin, and the location and correlation of the Montney Formation with its outcrop equivalents with the horizon of interest to this paper highlighted in grey on the right (modified from Zonneveld, 20 1; compiled from Tozer, 1994; Orchard and Tozer, 1997; and Zonneveld, 2009).

This study focuses on bioclastic horizons recently identified in the northwestern part of the basin, which are being targeted as potential unconventional plays by a number of companies. This unit, referred to informally as the "*Claraia* Zone", consists primarily of bivalve shells encased in laminated bituminous siltstone. The bioclastic horizons of the "*Claraia* Zone" represent nearly all of the preserved calcareous body fossils in the Lower Montney Formation. In intervals above and below this horizon, Montney fossils are represented either by locally abundant impressions of shells, devoid of preserved shell material, or fossils composed of minerals not susceptible to dissolution (e.g., calcium phosphate / apatite). The preferential preservation of calcite body fossils within the "*Claraia* Zone" and the Altares Packstone Member indicates that this pattern of preservation (and non-preservation through the rest of the formation) is unlikely to be related to burial diagenesis and has been attributed to syndepositional changes in the Aragonite Compensation Depth (ACD) and/or Calcite Compensation Depth (CCD) (Rampino and Caldeira, 2005).

The "*Claraia* Zone" in a previous manuscript was identified as a bottom current modified deposi that was transported from outside of the depo center. This was concluded from the evidence of traction sedimentation structures (e.g., ripples) present in the heterolithic, rippled, very fine sandstone and fin siltstone facies that have been correlated with the "*Claraia* Zone" in certain wells. The goal of this current chapter is to ascertain if oxygenation had any effect on the appearance of the bivalves in question.

A.2.3 Previous Sulfur Isotope Studies

Isotope studies have been conducted on the Montney Formation and its outcrop equivalents at Opal Creek (Schopfer et al., 2013) and the Le Glace area of the subsurface (Desrocher et al., 2004). Analyses at Opal Creek were performed on whole rock samples and focused on the Permian-Triassic boundary section (Schopfer et al., 2013). Schopfer et al. (2013) corroborated evidence set out by Hays et al. (2007) from biomarkers supporting the hypothesis of euxinic conditions within the Peace River Embayment through the Permian-Triassic boundary interval into the middle Induan.

Sulfur isotopes have been used in numerous studies in the Tethys Ocean and western Panthalassa regions to establish physio-chemical oceanic conditions during the Triassic, primarily to assess the presence, intensity and duration of anoxic events at the Permian-Triassic boundary (eg. Kato et al., 2002; Hosler et al., 1989; Grice et al., 2005; Nielsen and Shen, 2004; Riccardi et al., 2006). Sulphur isotope ratios from most Tethyan carbonate analyses exhibit strong negative values for $\delta^{34}S$ (Nielsen and Shen, 2004; Riccardi et al., 2006). Positive shifts in the isotope ratios (dominance of lighter isotopes) have been attributed to anoxia, whereas more negative values (heavier isotopes) have been attributed to Bacterial Sulfide Reduction (BSR) and possibly more normal conditions (Thode, 1991; Kajiwara and Kaiho, 1992; Kato et al., 2002). However, extremely negative isotopes (e.g., -60‰ in the Black Sea) are attributed to anoxia and euxinia as well (Wilikin and Arthur, 2001; Takahashi et al., 2013). Therefore moderately negative isotope values between 0‰ and ~-50‰ could represent normal oxic conditions (Kajiwara and Kaiho, 1992; Kato et al., 2002). This is based on the normal BSR of the oceanic water at the time of deposition. Oceanic $\delta^{34}S$ ratios were thought to be between 10‰ to 30‰ at the Permian-Triassic boundary and shifting towards the more positive values (30‰) in the Triassic (Claypool et al., 1980; Bottrell and Newton, 2006).

A.3 Methods

Twenty-three samples, which each weighed ≥ 10 grams, were obtained from the informal type cores of the "*Claraia* Zone" (c-65-F/094-B-8 and c-006-L/094-B-8) for an initial $\delta^{34}S$ survey through the horizon of interest. The "*Claraia* Zone" in c-65-F/094-B-8 was approximately 4m thick, while it was approximately 3m thick in c-006-L/094-B-8. Samples were obtained below, through and above the "*Claraia* Zone". The sparsity of data points was due to a limited amount of data allowed to be collected for the initial investigation (BC government sampling rules) in hopes that more data could be collected later if this investigation proved useful. The samples were sent to the IsoLab at the University of Washington for Sulphur isotope processing. Samples were chipped and crushed, then reacted with silver to form Ag_2S. This compound was then reacted with O_2 to form SO_2, which was then analyzed on the ThermoFinnigan MAT253 isotope ratio mass spectrometer and compared to the Vienna Canyon Diablo Troilite (VCDT) to obtain the parts per mil difference. The ThermoFinnigan Conflow III was used to nullify the effect o oxygen isotope ratios in measuring $\delta^{34}S$ through the methods described in Fry et al. (2002). Finally, the values were corrected to the VCDT scale using a linear regression on the raw $\delta^{34}S$ values with a precision and error provided for each value. $\delta^{34}S$ is measured compared to the VCDT as per the following equation (Thode et al., 1961; Robinson, 1993):

$$\delta^{34}S \text{ ‰} = (((S^{34} / S^{32})_{sample} - (S^{34} / S^{32})_{VCDT}) / ((S^{34} / S^{32})_{VCDT})) \cdot 1000$$

A.4 Results

The raw sulfur isotope data are presented in Table 4.1. Core c-65-F/094-B-8 had a mean δ^{34}S value relative to VCDT 5.452‰ and a standard deviation (σ) of 3.355 (Table A.1). The values range from 12.138‰ to -0.573‰. The ten data points from this core are concentrated around 8m of core, specifically the ”*Claraia* Zone” (Fig A.3). The variation in results from samples that were reprocessed is minimal, at most 0.436‰ difference. There is a sharp increase from the base of the section sampled to positive values around the *“Claraia* Zone” (Fig. A.3). The positive values are recorded through the “*Claraia* Zone”. There is an abrupt positive spike recorded just after the ”*Claraia* Zone”, but the values return to lower values immediately after. The presence of 4 beds with macroscopically visible pyrite through the sampled interval did not appear to change the δ^{34}S levels significantly. Both spikes are significant as they fall outside of the range of one standard deviation.

The isotope samples were spread across a larger depth interval in c-006-L/094-B-8 (13m as compared with 8m) (Fig. A.4). The mean δ^{34}S value relative to VCDT is 4.741‰ with a standard deviation (σ) of 1.742 (Table A.1). The values range from 11.598‰ to -4.549‰. The same signal recorded in c-65-F/094-B-8 appears to be recorded at the base of the “*Claraia* Zone” in this core with another significant drop off to negative values at 2783m (Fig. A.4). Except for one additional spike a meter above, the δ^{34}S values continue to decrease upward through the core. There is another large spike at the very base of the section (2790m) that is significantly larger than any other spike through the core. It coincides with a calcisphere horizon and occurs above two pyrite intervals. Pyrite is again prevalent through the “*Claraia* Zone” and coincides with the level part of the signal within the horizon. The largest variance in resampled values is 1.411‰ and is located at 2782m, but it is still less than significant

The spikes present within c-065-F/094-B-08 and c-006-L/094-B-08 do not correlate between the two cores, and the signals observed are not consistent through the “*Claraia* Zone” in the two cores. Although there appears to be a similar signal in both cores, it is not correlatable between the “*Claraia* Zone” of the cores (Fig A.3; A.4).

A.5 Discussion

Since the signals from the two cores are not consistent within the “*Claraia* Zone”, interpretation of the δ^{34}S values is speculative at best. The signal through c-065-F/094-B-08 is consistently level, which is contrary to the signal from c-006-L/094-B-08 where the δ^{34}S becomes more negative with decreasing depth (Fig. A.3; A.4). A negative trend could be interpreted as a continually more oxic environment from the base of the “*Claraia* Zone” towards the top of the section with increasing BSR influence (Thode, 1991; Kajiwara and Kaiho, 1992; Kato et al., 2002). The positive spikes could represent short pulses of anoxia; however, the data points are currently sparse, and while the data points in c-065-F/094-B-08 are about 1m apart, the data points in c-006-L/094-B-08 are much further apart. This could allow for signals to be lost in contrasting scales. This problem is apparent in c-006-L/094-B-08 where there is no conclusive background signal before the erosive surface at the base of the “*Claraia* Zone”.

Sulfur isotopes, as mentioned before, are dependent on multiple factors that could complicate the interpretation (eg. Schopfer et al., 2013). In this study sulfate minerals were not separated from the sulfide minerals before processing, which causes a mixed signal due to the separate formation mechanisms

Sample	Well ID	Depth (m)	Amount (mg)	PeakArea (Vs)	Percent S	Percent S Accuracy	Percent S Precision	d34S vs VCDT (permil)	d34S Accuracy	d34S Precision
IRG-SA-0415-001	C-65-F/094-B-8	2509.76	6.092	44.27	1.4743	-0.18448	1.9704	-0.57273	-0.082515	0.15763
IRG-SA-0415-002	C-65-F/094-B-8	2508.9	5.927	12.005	0.46268	-0.18448	1.9704	4.9877	-0.082515	0.15763
IRG-SA-0415-002	C-65-F/094-B-8	2508.9	14.952	38.8	0.52929	-0.17953	0.23776	4.6574	0.025011	0.11674
IRG-SA-0415-003	C-65-F/094-B-8	2507.73	6.016	36.09	1.23	-0.18448	1.9704	5.725	-0.082515	0.15763
IRG-SA-0415-004	C-65-F/094-B-8	2507.12	8.082	66.273	1.5203	0.29373	0.39701	4.6985	0.23626	0.28949
IRG-SA-0415-005	C-65-F/094-B-8	2506.08	10.06	58.036	1.0747	0.29373	0.39701	5.1211	0.23626	0.28949
IRG-SA-0415-006	C-65-F/094-B-8	2505.73	8.235	52.868	1.2005	0.29373	0.39701	6.7253	0.23626	0.28949
IRG-SA-0415-007	C-65-F/094-B-8	2504.84	7.987	65.01	1.5101	0.29373	0.39701	5.3837	0.23626	0.28949
IRG-SA-0415-008	C-65-F/094-B-8	2503.79	9.026	14.101	0.32592	0.29373	0.39701	11.6747	0.23626	0.28949
IRG-SA-0415-008	C-65-F/094-B-8	2503.79	21.714	16.348	0.17058	-0.17953	0.23776	12.1379	0.025011	0.11674
IRG-SA-0415-009	C-65-F/094-B-8	2502.99	9.456	60.541	1.1908	0.29373	0.39701	2.7981	0.23626	0.28949
IRG-SA-0415-010	C-65-F/094-B-8	2501.56	7.745	53.615	1.2937	0.29373	0.39701	3.1663	0.23626	0.28949
IRG-SA-0415-011	C-006-L/094-B-8	2792.75	7.51	39.752	1.0036	0.29373	0.39701	-0.38336	0.23626	0.28949
IRG-SA-0415-012	C-006-L/094-B-8	2790.84	9.89	26.809	0.52762	0.29373	0.39701	10.7182	0.23626	0.28949
IRG-SA-0415-012	C-006-L/094-B-8	2790.84	15.221	38.702	0.51873	-0.17953	0.23776	11.5981	0.025011	0.11674

Table A.1: The table of the raw sulfur isotope data including sulfur content of each sample and the accuracy and precision of each data point.

Sample	Well ID	Depth (m)	Amount (mg)	PeakArea (Vs)	Percent S	Percent S Accuracy	Percent S Precision	d34S vs VCDT (permil)	d34S Accuracy	d34S Precision
IRG-SA-0415-013	C-006-L/094-B-8	2789.59	8.897	69.001	1.436	0.29373	0.39701	1.6297	0.23626	0.28949
IRG-SA-0415-014	C-006-L/094-B-8	2787.59	7.252	57.679	1.4821	0.29373	0.39701	0.54656	0.23626	0.28949
IRG-SA-0415-015	C-006-L/094-B-8	2786.02	7.803	65.365	1.5539	0.29373	0.39701	4.1946	0.23626	0.28949
IRG-SA-0415-016	C-006-L/094-B-8	2784.86	7.02	55.625	1.4786	0.29373	0.39701	2.6056	0.23626	0.28949
IRG-SA-0415-017	C-006-L/094-B-8	2783.64	7.432	22.297	0.59337	0.29373	0.39701	5.4226	0.23626	0.28949
IRG-SA-0415-017	C-006-L/094-B-8	2783.64	10.419	11.023	0.25967	-0.17953	0.23776	6.7864	0.025011	0.11674
IRG-SA-0415-018	C-006-L/094-B-8	2783.19	6.987	59.87	1.5945	0.29373	0.39701	-0.55257	0.23626	0.28949
IRG-SA-0415-019	C-006-L/094-B-8	2782.03	8.947	16.176	0.37035	0.29373	0.39701	-0.82791	0.23626	0.28949
IRG-SA-0415-019	C-006-L/094-B-8	2782.03	17.537	23.839	0.29131	-0.17953	0.23776	0.58339	0.025011	0.11674
IRG-SA-0415-020	C-006-L/094-B-8	2781.07	7.736	73.406	1.7535	0.29373	0.39701	-2.484	0.23626	0.28949
IRG-SA-0415-021	C-006-L/094-B-8	2779.83	8.67	79.717	1.695	0.29373	0.39701	-3.4695	0.23626	0.28949
IRG-SA-0415-022	C-006-L/094-B-8	2777.75	7.565	67.814	1.6607	0.29373	0.39701	-3.9523	0.23626	0.28949
IRG-SA-0415-023	C-006-L/094-B-8	2776.37	6.241	50.486	1.5157	0.29373	0.39701	-4.5494	0.23626	0.28949

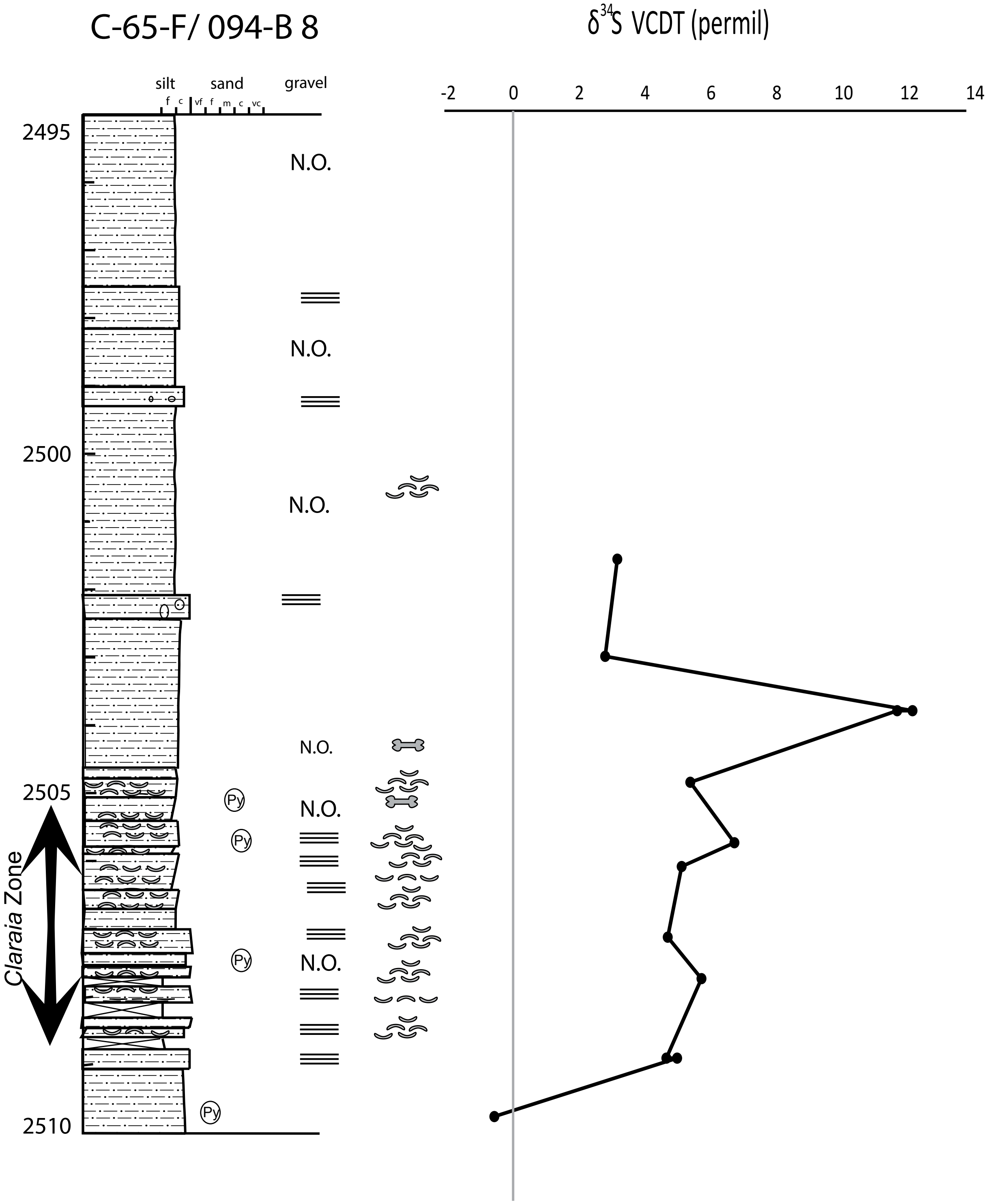

Figure A.3: Core lithology log of C-065-F/094-B-08 alongside the δ34S data points for the core.

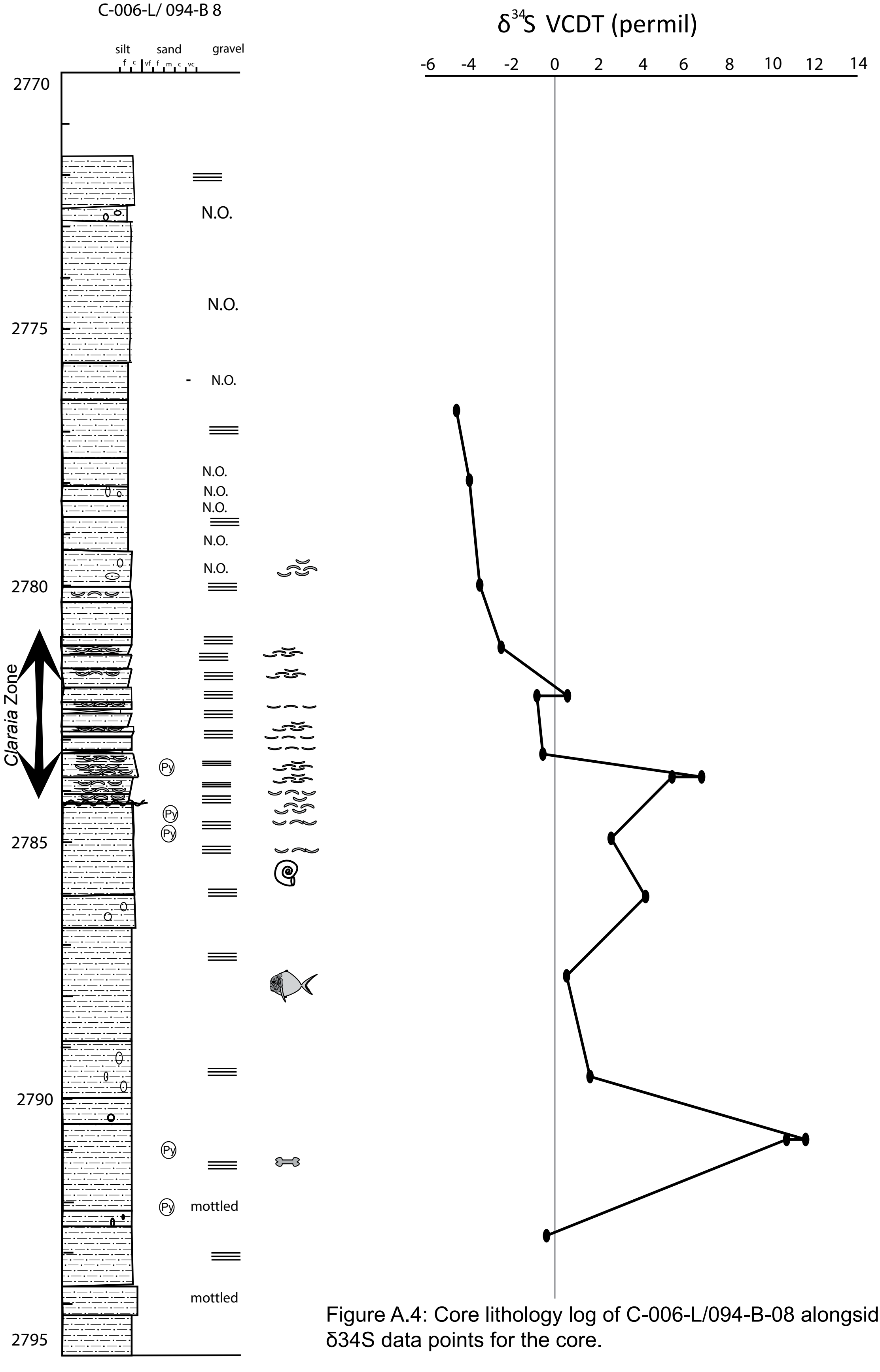

Figure A.4: Core lithology log of C-006-L/094-B-08 alongside the δ34S data points for the core.

involved. This is also true for euhedral vs. frambiodal pyrite (Wiliken and Arthur, 2001). Further analyses could help determine if the $\delta^{34}S$ signal is from a mixed source or if it is showing the true redox conditions at this time. Nonetheless the values obtained from the "*Claraia* Zone" samples are between 14‰ and -6‰. While there are possible changes in how much BSR effected the isotopes, most of the values would fall in what would be a normal range for BSR. The values above 10‰ could represent times of anoxia if the $\delta^{34}S$ of the ocean was 10‰ (Claypool et al., 1980; Bottrell and Newton, 2006). It can be inferred that euxinic conditions are unlikely during this interval due to the moderate $\delta^{34}S$ values.

It is also possible that because the "*Claraia* Zone" represents transported fauna that these analyses will not provide any information to further understand environment during deposition. The effects of the environment on the *Claraia* through this horizon are likely related to a different area within the formation. In fact, examining the Altares Packstone Member discussed in the chapter 3 may provide more conclusive evidence about the redox conditions that existed at the time as it is an *in situ* fauna.

A.6 Conclusion

Although sulfur isotopes seemed to be a sensible choice in an interval composed of abundant pyrite, the current twenty-three samples that were collected likely show a mixed signal. The current data indicates that it is possible that the ocean at the time of deposition of the "*Claraia* Zone" was an oxic environment. Only a few of the points within the samples collected could be related to an anoxic environment, and that is only in the case of an ocean with a low sulfur content (i.e., 10‰). A combination of mixed signals and a coarse resolution may be responsible for the lack of a correlatable signal between the two type wells of the "*Claraia* Zone". Further analyses could refute or affirm this in order to develo a more concrete interpretation, however nearly all of the current data points fall within an oxic value and unless this is the result of a mixed signal it is unlikely that the signal will significantly move out of this zone. It is also possible that there is a gradual increase in oxygenation from the base of the "*Claraia* Zone" to the top of the interval sampled. However, even if this interpretation is correct it is likely that the redox conditions did not affect the *Claraia* that were incorporated in the horizon as they were transported into the region.

A.7 References

Armitage, J. H., 1962, Triassic Oil and Gas Occurrences in Northeastern British Columbia, Canada: Journal of the Alberta Society of Petroleum Geologists, v. 10, no. 2, p. 35–56.

Bambach, R. K., 2006, Phanerozoic biodiversity mass extinctions: Annual Review of Earth and Planetary Sciences, v. 34, p. 127–155.

Barclay, J., F. Krause, R. Campbell, and J. Utting, 1990, Dynamic casting and growth faulting: Dawson Creek graben complex, Carboniferous-Permian Peace River embayment, western Canada: Bulletin of Canadian Petroleum Geology, v. 38, no. 1, p. 115–145.

Bird, T., J. Barclay, R. Campbell, and P. Lee, 1994, Triassic Gas Resources of Western Canada Sedimentary Basin, Interior Plains-Geological Play Analysis and Resource Assessment: Western Canadian and International Expertise [Program book with expanded abstracts], p. 352–353.

Bottrell, S. H., and R. J. Newton, 2006, Reconstruction of changes in global sulfur cycling from marine sulfate isotopes: Earth-Science Reviews, v. 75, no. 1-4, p. 59–83, doi:10.1016/j.earscirev.2005.10.004.

Claypool, G. E., W. T. Holser, I. R. Kaplan, H. Sakai, and I. Zak, 1980, The age curves of sulfur and oxygen isotopes in marine sulfate and their mutual interpretation: Chemical Geology, v. 28, p. 199–260.

Davies, G. R., T. F. Moslow, and M. D. Sherwin, 1997, The Lower Triassic Montney Formation, west-central Alberta: Bulletin of Canadian Petroleum Geology, v. 45, no. 4, p. 474–505.

Desrocher, S., I. Hutcheon, D. Kirste, and C. M. Henderson, 2004, Constraints on the generation of H2S and CO2 in the subsurface Triassic, Alberta Basin, Canada: Chemical Geology, v. 204, no. 3-4, p. 237–254, doi:10.1016/j.chemgeo.2003.11.012.

Edwards, D. E., J. E. Barclay, D. W. Gibson, G. E. Kvill, and E. Halton, 1994, Triassic Strata of the Western Canada Sedimentary Basin, in G. D. Mossop, and I. Shetsen, eds., Geological Atlas of the Western Canada Sedimentary Basin: Canadian Society of Petroleum Geologists and Alberta Research Council.

Erwin, D. H., 2000, The Permo-Triassic extinction: Shaking the Tree: Readings from Nature in the History of Life, v. 189.

Fry, B., S. R. Silva, C. Kendall, and R. K. Anderson, 2002, Oxygen isotope corrections for online ?34S analysis: Rapid Communications in Mass Spectrometry, v. 16, no. 9, p. 854–858, doi:10.1002/rcm.651.

Grice, K., C. Cao, G. D. Love, M. E. Böttcher, R. J. Twitchett, E. Grosjean, R. E. Summons, S. C. Turgeon, W. Dunning, and Y. Jin, 2005, Photic zone euxinia during the Permian-Triassic superanoxic event: Science, v. 307, no. 5710, p. 706–709.

Habicht, J. K. A., 1979, Paleoclimate, paleomagnetism, and continental drift: American Association of Petroleum Geologists Studies in Geology 9.

Hays, L. E., T. Beatty, C. M. Henderson, G. D. Love, and R. E. Summons, 2007, Evidence for photic zone euxinia through the end-Permian mass extinction in the Panthalassic Ocean (Peace River Basin, Western Canada): Palaeoworld, v. 16, no. 1-3, p. 39–50, doi:10.1016/j.palwor.2007.05.008.

Holser, W. T. et al., 1989, A unique geochemical record at the Permian/Triassic boundary: Nature, v. 337, no. 6202, p. 39–44.

Kajiwara, Y., and K. Kaiho, 1992, Oceanic anoxia at the Cretaceous/Tertiary boundary supported by the sulfur isotopic record: Palaeogeography, palaeoclimatology, palaeoecology, v. 99, no. 1, p. 151–162.

Kato, Y., K. Nakao, and Y. Isozaki, 2002, Geochemistry of Late Permian to Early Triassic pelagic cherts from southwest Japan: implications for an oceanic redox change: Chemical Geology, v. 182, no. 1, p. 15–34.

Kidder, D. L., and T. R. Worsley, 2004, Causes and consequences of extreme Permo-Triassic warming to globally equable climate and relation to the Permo-Triassic extinction and recovery: Palaeogeography, Palaeoclimatology, Palaeoecology, v. 203, no. 3-4, p. 207–237, doi:10.1016/S0031-0182(03)00667-9.

Nielsen, J. K., and Y. Shen, 2004, Evidence for sulfidic deep water during the Late Permian in the East Greenland Basin: Geology, v. 32, no. 12, p. 1037, doi:10.1130/G20987.1.

Orchard, M. J., and E. T. Tozer, 1997, Triassic conodont biochronology, its calibration with the ammonoid standard, and a biostratigraphic summary for the Western Canada Sedimentary Basin: Bulletin of Canadian Petroleum Geology, v. 45, no. 4, p. 675–692.

Orchard, M. J., and J.-P. Zonneveld, 2009, The Lower Triassic Sulphur Mountain Formation in the Wapiti Lake area: lithostratigraphy, conodont biostratigraphy, and a new biozonation for the lower Olenekian (Smithian)Earth Science Sector (ESS) Contribution 20080714.: Canadian Journal of Earth Sciences, v. 46, no. 10, p. 757–790, doi:10.1139/E09-051.

Panek, R., 2000, The Sedimentology and Stratigraphy of the Lower Triassic Montney Formation in the Subsurface of the Peace River Area, Northwestern Alberta, Master of Science: Calgary, Alberta, University of Calgary.

Payne, J. L., D. Altiner, D. J. DePaolo, J. L. Hinojosa, L. R. Kump, K. V. Lau, D. J. Lehrmann, K. Maher, A. Paytan, and S. Shen, 2014, The End-Permian Mass Extinction and its Aftermath: Insights from Non-Traditional Isotope System: Vancouver,BC.

Payne, J. L., and M. E. Clapham, 2012, End-Permian mass extinction in the oceans: an ancient analog for the twenty-first century?: Annual Review of Earth and Planetary Sciences, v. 40, p. 89–111.

Rampino, M. R., and K. Caldeira, 2005, Major perturbation of ocean chemistry and a “Strangelove Ocean” after the end-Permian mass extinction: Terra Nova, v. 17, no. 6, p. 554–559, doi:10.1111/j.1365-3121.2005.00648.x.

Riccardi, A. L., M. A. Arthur, and L. R. Kump, 2006, Sulfur isotopic evidence for chemocline upward excursions during the end-Permian mass extinction: Geochimica et Cosmochimica Acta, v. 70, no. 23, p. 5740–5752, doi:10.1016/j.gca.2006.08.005.

Robinson B. W., 1993, Sulfur isotope standards. Reference and intercomparison materials for stable isotopes of light elements. Proceedings of a consultants meeting held in Vienna, p. 13–30.

Schoepfer, S. D., C. M. Henderson, G. H. Garrison, J. Foriel, P. D. Ward, D. Selby, J. C. Hower, T. J. Algeo, and Y. Shen, 2013, Termination of a continent-margin upwelling system at the Permian–Triassic boundary (Opal Creek, Alberta, Canada): Global and Planetary Change, v. 105, p. 21–35, doi:10.1016/j.gloplacha.2012.07.005.

Sepkoski Jr, J. J., 1981, A factor analytic description of the Phanerozoic marine fossil record: Paleobiology, p. 36–53.

Takahashi, S. et al., 2013, Sulfur isotope profiles in the pelagic Panthalassic deep sea during the Permian–Triassic transition: Global and Planetary Change, v. 105, p. 68–78, doi:10.1016/j.gloplacha.2012.12.006.

Thode, H., 1991, Sulphur isotopes in nature and the environment: an overview: Wiley.

Thode, H. ., J. Monster, and H. . Dunford, 1961, Sulphur isotope geochemistry: Geochimica et Cosmochimica Acta, v. 25, no. 3, p. 159–174, doi:10.1016/0016-7037(61)90074-6.

Tozer, E. T., 1994, Canadian Triassic ammonoid faunas: Geological Survey of Canada.

Tozer, E., 1982, Marine Triassic faunas of North America: their significance for assessing plate and terrane movements: Geologische Rundschau, v. 71, no. 3, p. 1077–1104.

Wilkin, R. T., and M. A. Arthur, 2001, Variations in pyrite texture, sulfur isotope composition, and iron systematics in the Black Sea: Evidence for late Pleistocene to Holocene excursions of the O 2-H 2 S redox transition: Geochimica et Cosmochimica Acta, v. 65, no. 9, p. 1399–1416.

Wilson, N., 2009, Integrated regional model for the deposition and evolution of the Montney Formation, NE British Columbia.

Wilson, K. M., D. Pollard, W. W. Hay, S. L. Thompson, and C. N. Wold, 1994, General circulation model simulations of Triassic climates: preliminary results: Geological Society of America Special Papers, v. 288, p. 91–116.

Wood, J., 2012, Water Distribution in the Montney Tight Gas Play of the Western Canadian Sedimentary Basin: Significance for Resource Evaluation: Society of Petroleum Engineers, doi:10.2 18/161824-MS.

Woods, A. D., 2005, Paleoceanographic and paleoclimatic context of Early Triassic time: Comptes Rendus Palevol, v. 4, no. 6-7, p. 463–472, doi:10.1016/j.crpv.2005.07.003.

Zonneveld, J.-P., 2011, Suspending the Rules: Unraveling the ichnological signature of the Lower Triassic post-extinction recovery interval: Palaios, v. 26, no. 11, p. 677–681, doi:10.2110/palo.2011.S06.

Zonneveld, J.-P., M. K. Gingras, and T. W. Beatty, 2010, Diverse ichnofossil assemblages following the P-T mass extinction, Lower Triassic, Alberta and British Columbia, Canada: Evidence for shallow marine refugia on the northwestern coast of Pangea: Palaios, v. 25, no. 6, p. 368–392, doi:10.2110/palo.2009.p09-135r.

Zonneveld, J.-P., R. B. MacNaughton, J. Utting, T. W. Beatty, S. G. Pemberton, and C. M. Henderson, 2010, Sedimentology and ichnology of the Lower Triassic Montney Formation in the Pedigree-Ring/Border-Kahntah River area, northwestern Alberta and northeastern British Columbia: Bulletin of Canadian Petroleum Geology, v. 58, no. 2, p. 115–140.

Zonneveld, J.-P., and T. F. Moslow, 2014, Perennial River Deltas of the Montney Formation: Alberta and British Columbia Subcrop Edge.

Figure captions

A.1: Map of core datasets in relation to the Montney Formation as a whole during the Greisbachian. The red dots each represent a separate core and they are all located well within the offshore portion of the formation. The Pedigree-Ring Delta is known to be Greisbachian in age, but the Dixonville has only been confirmed to be Smithian, although there are sand bodies of Greisbachian age that are located westward in the Peace River Arch from the delta location. The Meosin High in the southwest is based on subaerial exposure in the outcrop belt. The red block in the inset map shows the location of the above map in relation to modern geographical boundaries of Canada. (The Montney map was compiled and modified from Barclay et al, 1990; Panek, 2000; Zonneveld et al, 2010a; Zonneveld et al, 2010b; Zonneveld and Moslow, 2014; and Zonneveld, pers. comm.).

A.2: The stratigraphic framework of the Lower and Middle Triassic in the Western Canada Sedimentary Basin, and the location and correlation of the Montney Formation with its outcrop equivalents with the horizon of interest to this paper highlighted in grey on the right (modified from Zonneveld, 20 1; compiled from Tozer, 1994; Orchard and Tozer, 1997; and Zonneveld, 2009).

A.3: Core lithology log of C-065-F/094-B-08 alongside the $\delta^{34}S$ data points for the core.

A.4: Core lithology log of C-006-L/094-B-08 alongside the $\delta^{34}S$ data points for the core.

List of Tables

A.1: The table of the raw sulfur isotope data including sulfur content of each sample and the accuracy and precision of each data point.

Appendix B

Fossil identification by depth within cores

08-30-082-20w6

1908.45

fish

same as 1908.6, part and counterpart

1908.6

fish

vertebrate bone fragments, likely from a fish

1909.84

vertebrate

bone fragment

11-04-085-16w6

1793.15

Ophioceras sp.

calcite crystallized ammonoid, also likely *Ophioceras*

13-11-081-20w6

2312.25

bivalve

shells of bivalve? Partially sticking up out of matrix

2321.99

bivalve

similar to 2312.25 with some other hashed material

2323

Claraia clarae

concentric folds of Pectinoids visible, *Claraia clarae*

13-18-065-5w6

3176.84

Claraia stachei

Claraia stachei impression

3182.8

Claraia stachei

Claraia stachei fragment impression

13-18-65-5w6

3176.84

Claraia stachei

most of a preserved valve of a Pectinoid shell (unwinged) *Claraia stachei* LV, very equant

3182.8

Claraia stachei

impressions of multiple Pectinoid shells most likely *Claraia stachei* from age and ornamentation, but no observed hinges. Possibly left valves. The center of the valves has commonly been broken and compressed.

14-19-77-10w6

2163.1
Fish
fish fossil with scales
14-29-080-20w6

2577.71
Fish
ribs, spine, and fins of fish
same as 037, part and counterpart
15-02-080-16w6

2294.5
vertebrate
vertebrate fragments and scales
16-17-083-25w6

2249.26
Eumorphotis multiformis or *Leptochondria curtocardinalis*
impression of LV of *Eumorphotis multiformis* or *Leptochondria curtocardinalis*
2267.03
ammonoid
ammonoid impressions
2269
ammonoid
pyritized ammonoid impression
2276.95
Eumorphotis multiformis
Eumorphotis multiformis impressions and shell hash
Eumorphotis multiformis, brachiopod
shell has as with c,d, but another round shell with only concentric ornamentation is visible (terebratulide?)
shell hash, could be same as a,b,e, also present is an internal mold that is very inflated (may be terebratulide)
similar to f, but more of shell is visible
2277.05
Claraia clarae and *Eumorphotis* sp.
Claraia clarae fragments and possible *Eumorphotis* sp. fragments
2299.45
Ophioceras sp.
ammonoid impression possibly *Ophioceras* sp. , b has multiples that are unidentifiable
2390.1
Claraia clarae
Claraia clarae impressions most approximately 2 cm in size
2391.17
vertebrate
bone fragments

vertebrate bone fragments

2430.4

Listricanthus

Listricanthus

2432.6

vertebrate

vertebrate fragments

2448.66

fish

fish tail, fin, and jaw bone

2455

fish

fish backbone and ribs

2473.5

fish

fish fin

2477.5

brachiopod

barely visible spiriferid brachiopods

2479.1

Claraia stachei

Claraia stachei impressions in matrix

2480.85

Ellesmerella aranea

Ellesmerella aranea

6-14-66-6w6

3039.2

bivalve

bivalve, Pectinoid fragments, both relatively large, but mostly obscured by matrix

Claraia sp.

Claraia sp. broken edges and missing hinge line, buried in matrix

3042.3

Claraia sp.

Claraia sp. One visible hinge line that shows the wing. Beak does not go far past the hinge. All external molds, all large valves greater than 3cm.

Claraia clarae

incomplete hinge and shell margins, but most likely *Claraia clarae*.

Pectinoid (*Claraia* sp.) fragments that are all relatively large. Impressions, but visible ribs and growth lines. *Claraia clarae*

6-36-67-27w6

3089.2

bivalves

internal casts and molds of bivalves in coquina, bitumen stained

A-005-C/094-G-10

1867.78
Ophioceras sp.
Ophioceras sp. Impression with indentation running around mid whorl, may have had ribbing
1867.8
Ophioceras sp.

1867.89
Ophioceras sp.
Ammonoid impression, *Ophioceras* sp.
1869.14
ammonoid
pyritized ammonoid impressions
1869.22
Ophioceras sp.
pyritized ammonoid impression, possibly *Ophioceras* sp.
vertebrate
vertebrate ribs and backbone
1870.25
vertebrate
vertebrate ribs and backbone
1870.89
Claraia stachei
very round impression *Claraia stachei* LV
1871
Claraia aurita
Claraia aurita impression, no visible hinge
1871.17
Claraia clarae
Claraia clarae impression, no visible hinge
1871.6
Hypophiceras sp. Or *Tompophiceras* sp.
Hypophiceras sp. Or *Tompophiceras* sp. But ribs are not visible

A07-29-085-25w6

1776.5
ammonoid
top of core full of has of stuff, showing ammonoid perpendicular to bedding

A-10-J/094-B-09

2315.17
New ammonoid
similar to *Ophioceras*, but possibly new species with constriction along inside of whorl with ridges
2319.4
Claraia clarae

Claraia clarae impressions

2328.06

Claraia clarae

some preserved original material and fragments of *Claraia clarae*

A-18-D/094-A-13

2171

Wordeioceras wordiei

Wordeioceras wordiei impression

a-64-A/094-B-8

2389

Claraia clarae

bioclastic hash similar to the top with one location with impressions of concentric folds indicative of *Claraia clarae*

2389.05

Claraia clarae

bioclastic material hash with some visible concentric folds indicative of *Claraia clarae*

Claraia clarae impressions of left valves 1-2 cm in size

Claraia clarae valves approximately 1cm across, visible on bedding plane

2389.1

Claraia clarae

Claraia clarae impressions of left valve all between 1-2cm across

Claraia clarae left valve mostly visible in center

2547.6

ammonoid

ammonoid impression of last whorl

2555.95

*Ophiocera*s sp.

Possibly *Ophioceras* sp. Impression

2559.55

sponge

sponge spicules

2561.38

sponge

sponge spicules

2806.25

fish

side of core showing smeared bone fragments.

a-78-C/094-G-1

1148.5

Leiophyllites sp.

Leiophyllites sp. Ammonoid

b-064-I/094-A-11

1713.4

Daonella elagans
Daonella elegans impressions

B-65-J/094-B-16

2114.71
Claraia aurita
recrystallized material of large *Claraia aurita*? Incomplete hinge line, but possible RV
2116.56
Claraia stachei
Claraia stachei impression external of RV

C-007-J/094-B-08

2253.79
brachiopod
a few brachiopod impressions
2446.98
vertebrate
vertebrate fragment

carbon film that is in the shape of a bivalve

C-074-G/094-B-09

1947.1
brachiopod
pieces of brachiopods sticking out of matrix
1949.64
brachiopod
brachiopod impressions (terebratulids)

C-74-G/094-B-9

1945.75

hash of stuff, not really identifiable, possibly vertebrate
thing, maybe shell
1947
Peribositria sp.

C-85-I/094-B-1

2370.3
Anaxenaspis sp.

Melagathiceras depressum

DD b-050-H/094-B-16

2063.25
Claraia clarae

2064

Claraia clarae
fragmented valves of *Claraia clarae*
2066.07
Claraia clarae

2066.2
Claraia clarae
large nearly complete LVs of *Claraia clarae*
2069.41
Claraia sp.
small molds of bivalves and fragments, some of the larger fragments could be *Claraia* sp.
2069.49
Claraia sp.

2074.23
Claraia clarae
large fragments of *Claraia clarae*
2074.24
Claraia clarae
Claraia clarae small fragments
2075
Claraia clarae
Claraia clarae 2+ cm in size

Appendix C: Thin section descriptions by well and depth (m)
03-30-082-20w6
1905.48
BC4
Fine grained siltstone that is only visible laminated due to layers of bioclasts. Bitumen is abundant interstitially. The bioclasts (bivalves) are highly fragmented and concentrated in layers. Some of the bioclasts are extremely thin, but most are much thicker. Outside of the bioclasts calcite is mostly absent from the section. Bioclasts become suddenly much more abundant at the bottom of the section. Pyrite is present.
1907
BC5a
The top of the section is a laminated siltstone with only minor presence of calcite and dolomite. There is not that much bitumen present. Going down in the section bioclasts appear with pyrite then they suddenly become the most dominant particle along with calcispheres through the rest of the section. The bivalves are all thick shelled *Claraia* and are oriented plane parallel and are mostly fragmentary. Some of the bivalves have another mineral replacing at their core other than calcite. Bitumen is very abundant in this layer.
BC5b
Interlayered bituminous fine grained laminated siltstone and bituminous bioclastic has in siltstone with abundant calcispheres. Mineral from BC5a is seen again at base where bioclasts take over again. Bioclasts are very fragmented, but are present through the section. Laminations are only visible due to bioclasts. Mostly thick shelled *Claraia*.
1924.8
BC 6
Mostly planar laminated coarse grained siltstone. There is an abrupt shift in the cement, but not grainsize, which appears to be an erosive surface near the top of the section. A vertebrate bone fragment is caught at this boundary. Any calcite, which is prevalent beneath this horizon disappears and gives way to mostly coarse grained siltstone. There are rare heavily weathered bioclasts evident in the bottom horizon, mainly Claraia. Calcispheres also are present. Both calcispheres and bioclasts become dolomitized closer to the boundary between the two layers. Most of the calcite in the bottom layer appears to be grown as cement between the silt grains. Calcite overwhelmingly dominates the bottom horizon.
08-30-082-20w6
1897.88
BC 26
Very fine to medium grain size siltstone with planar bedding that alternates on a cm scale between coarser and finer grained horizons. There is no calcite detectable within the section and a larger clay size fraction towards the base of the section. There are a few coarse grained lenses within a fine grained horizon that are visible macroscopically and could be burrows that have been flattened.
1897.89
BC27

Alternating beds of very fine to fine/medium grained siltstone. Bedding is distinct both macroscopically and microscopically.
1904.72
BC28
Both units contain slightly concave up bedding, there is evidence of some soft sediment deformation in the upper part of the section. There is a sharp contact between the two units. The top unit is mainly made up with fine to coarse silt sized grains with occasional bioclastic material that has been highly weathered. There are coarse silt sized clastic grains throughout this section as well, but to a smaller extent than in the bottom section which is a fine to coarse grained siltstone with no apparent calcite grains. Bedding is visible in the bottom horizon at both scales, but only at the macroscopic scale in the top horizon. The distortion appears to have been caused by a mostly articulated bivalve that is oriented at about a 45 degree angle in the sediment.
1907.5
BC29
Fine to medium grain sized siltstone that is planar bedded macroscopically. The beds appear more discontinuous microscopically, although this may be due to the sparse nature of the coarser grain sizes.
1908.45
BC30
Fine to coarse grained siltstone, with a slight increase of coarse grained material towards the top of the section. At the base of the section there is a large Claraia shell that has been partially dolomitized. There are no other bioclastic or carbonate material until the top of the section where there is a bed of bioclastic material and occasional dolomite grains in the coarser section of sediments. They disappear again as the grain size decreases at the very top of the section.
1909.84
BC32
There is a distortion of the bedding to the right side of the slide that may have been caused by the cementation of the upper beds with calcite. Clastic grains are still very prevalent in the calcite cemented horizon, although only the coarser grain size seems to remain as compared to the lower horizon which contains a high amount of fine to very fine silt sized grains. There are occasional calcispheres present in the calcite cemented horizon. The clastic component is very fine to coarse grained siltstone that grades up into the calcite cemented horizon and on the left side of the slide appears to grade back to mostly siltstone above the calcite horizon.
1914
BC33
Fine to medium grain siltstone that is planar laminated with rare bioclastic and calcite grains. The calcite component decreases towards the top of the section until there is no visible component. There are a couple very small articulated bivalves towards the bottom of the section that have been filled with partially dolomitized calcite even though their shells are still calcite. All of the bioclastic material appears to be Claraia.
1915.05
BC34

Fine to medium grained planar laminated siltstone with rare calcite component, mostly from bioclastic input. There is a concentration of bioclastic material in two beds to the top of the section, but there are small amounts of shell material through the section. The shells appear to be from another thin shelled bivalve, but do not appear to be Claraia. There are also small horizons that are made up of mostly coarser grained clasts that appears to have some calcite cementation between the grains. None of the valves are articulated and most appear to be very weathered.
1915.12
BC35
Fine to coarse grain siltstone that fines upward slightly. The beds are planar laminated and are not very apparent in the microscopic scale as there is not much differentiation in grain size; although a few beds that are composed of coarser grains can be followed over much of the slide.
1-10-082-23w6
1997.35
BC25
Predominantly planar laminated fine to coarse grained planar laminated siltstone with the very rare calcite clast. There are a few beds that are discontinuous across the slide with clay sized grains that are unable to be distinguished. Most of the bedding across the slide is discontinuous, but there is no other evidence of bioturbation within this section.
13-11-081-20w6
2312.25
BC36
The base of the section is a fine grained siltstone composed of predominantly calcite grains with occasional calcispheres and bioclasts. The shells are mainly of thin walled bivalves and brachiopods. Most of the shells are still articulated and the interior chambers are filled with calcite or silica in some cases. Most of the disarticulated shells do not appear to be heavily weathered either. This unit has a sharp transition into a coarse siltstone with calcite cementation. The bioclasts do not disappear here but appear to accumulate towards the base of the unit. One has an interior chamber that has been partially dolomitized. There is a high abundance of anisotropic granules, possibly phosphate as the grain size increases to coarse silt. Halfway through the coarse siltstone horizon all calcite material disappears and only the occasional dolomite clast appears. There is another sharp transition at the top into a very fine grained siltstone that is planar laminated.
2312.35
BC37
Mostly planar laminated fine grain siltstone with abundant calcite clasts and bioclasts. There are a few calcispheres, but there are very abundant articulated thin walled bivlaves throught the section. The interiors of these specimens are mainly calcite, but several also have silica crystalized along the margins of their shells. There are several horizons towards the base of the section where calcite veins seem to have crystalized along the bedding.
2313.25
BC38

The base of the section is mainly bioclastic and calcite cemented material with clasts of both thin walled bivalves and possibly also ammonoids. Some of the spary calcite has been partially dolomitized. There is gradually more clastic input upward in the section with an increase of coarse silt sized clasts and a decrease in bioclastic material at the same time; although there is still prevalent calcite cementation. There is also a streak of pyrite granules when the coarse sediment is first introduced. The clastic sediment fines upwards to the top of the section until it has become very fine siltstone. Dolomite grains are also more common in these upper sections. There is a single bed of bioclastic material at the top of the section. After that bed calcite and dolomite become increasingly rare. There is a vertebrate bone fragment to the left side of the slide that is situated in the middle of a highly dolomitized zone.
2313.45
BC39
A skeletal packstone is surrounded on each side by fine to medium grained siltstone beds that are distorted around the packstone. The siltstone beds are planar laminated except for where they have been distorted due to compaction. The packstone is made up of both thin shelled bivalves, and ammonoids. The ammonoids and the area around many of the bivalves has had crystallization of spary calcite that has been partially dolomitized in many cases. There are a few cases of very thick walled bivalve shells among the bioclastic material. At the top of the packstone there is a sudden increase in coarse grained siltstone clasts that have been cemented with calcite and dolomite. There is a sharp change after that back to a fine grained siltstone unit that is identical to the one below the packstone.
2321.25
BC40
The base of the section begins with alternating beds of fine to medium grained siltstone with only occasional dolomite grains. A bioclastic bed is introduced about 1cm up in the section in a fine grained bed. Some of the material in this bed has been dolomitized. The bioclastic material grades out until there is a sharp increase in calcite. Most of the grains in this bed are calcite; although they remain between medium and coarse silt size. The amount of bioclasts increase, but the shells do not change thickness. Calcispheres are also present alongside the thin walled bivalves. In a coarse grained bed in the middle of this bioclastic zone there is a streak of pyrite grains among the coarse grained silt. The calcite horizon continues with most of the bioclastic material concentrating in the coarser grained beds as the grain size continues to alternate in beds. This continues to the top of the section. The beds in this section are mainly planar laminated, but they also distort around the bioclastic beds.
2321.99
BC41
The majority of the section is made up of fine grained siltstone interlaminated with layers of medium to coarse grained siltstone. There are bioclastic beds of thin shelled bivalves throughout most of the section. The beds are more abundant towards the base of the section, but the bioclastic material does not appear to be preferentially located in any grain size. Throughout this section there are common larger grains of dolomite, some of which could have been calcispheres, but they are not always circular. These are the largest grains in the horizon. At the very top of the section there is a small portion of a calcite cemented skeletal packstone horizon with occasional coarse silt grains. It is composed mostly of thin walled bivalves, some of which are articulated. The interiors of the articulated bivalves are partially dolomitized along with any space that has been caught between two disarticulated shells that are arranged to form a cavity.

2323
BC42
Primarily fine grained siltstone with occasional interlaminations of medium grained siltstone. The coarser grained horizons are more common towards the base of the section. Calcispheres are moderately abundant within this section and have all been at least partially dolomitized. They become very abundant towards the top of the section. The laminations are not uniform in thickness across the slide.
13-18-65-5w6
3176.84
IRG-SA-0614-16
Fine to medium siltstone. Macroscopically it appears to be planar laminated, and microscopically certain beds can be followed across the thin section. This becomes difficult due to the mostly uniform grainsize across the slide. No biogenic structures can be confidently observed.
3182.8
IRG-SA-0614-17
Macroscopically appears to be planar laminated, but microscopically there are only a few laminations that can be followed across the section. The section is mainly fine to medium grained siltstone with no apparent calcite present. There could be crypto bioturbation present as some of the coarse grains appear to be arranged in circles around finer grained material.
14-29-080-20w6
2526.97
IRG-SA-1412-066a
Macroscopically there are starved and climbing ripples throughout and evidence of bioturbation in the upper 2/3rds of the section. Planolites and other trace fossils disrupt many of the bedforms. Mud drapes make the ripples visible. Microscopically there are distinct layers of coarse and fine siltstone at the base and top with detrital grains of calcite throughout. Bitumen is concentrate in fine grained layers. In the center the coarse and fine grained material is homogenized save for obvious burrows that concentrate coarse grained material. The layers are convoluted, but recognizable at the top of the section.
IRG-SA-1412-066b
Macroscopically the bottom half of the section has been disturbed and convoluted to where in some areas bedforms are not visible while in the top half ripples and laminations are clearly visible and only the occasional burrow is visible. Microscopically the base of the section is a homogenous medium grained siltstone with moderate bitumen content. A coarser grained bed cuts through this with higher detrital calcite content. Further up distinct beds of fine and coarse grained siltstone are distinguishable with bitumen concentration in the fine grained beds. There are still a few homogenized layers, but they are less abundant further up and disappear to the top of the section. The burrow concentrate coarse grained material and calcite is predominantly in coarse grained beds.
2527.18
IRG-SA-1412-065a

Mainly mixed fine and coarse grained siltstone with very few identifiable beds on the microscopic scale. There is a small clay fraction and detrital calcite and dolomite. Bitumen is dominant throughout the section. There are two large calcite blebs close to the base of the section. It appears laminated on the macroscopic scale.

IRG-SA-1412-065b

At the base and the top of the section it is a macroscopically laminate coarse and fine grained bituminous siltstone with occasional calcite blebs and a small amount of detrital calcite (less at the top than at the base). There is a sudden change in the middle with less than a cm grade into overwhelming bioclastic material. It becomes a bioclastic silty packstone/wackestone with abundant pyrite. Many of the bioclasts in the packstone are articulate. All are thin shelled and most are oriented parallel to bedding. Calcite and silica crystallized in the centers of the articulated bivalves. AT the top of the packstone calcite is gradually lost and bioclasts are less abundant until they disappear. Pyrite is abundant in the packstone.

2527.5

IRG-SA-1412-067

The very base of the slide is a bioclastic silty packstone/wackestone that is predominantly fine grained silt with bitumen. This grades up into a coarse grained silty limestone which may have at one time contained bioclasts, but they are nearly indistinguishable from the rest of the calcite cement. There are a few beds with fine grained silt (still containing bitumen) in this horizon, bit it is much less abundant. This grades up into alternating layers of coarse and fine grained siltstone with discrete layers of abundant bioclasts and bitumen still concentrated in fine grained laminae. Pyrite is very abundant in the center horizon.

2527.77

IRG-SA-1412-064a

For most of the section it is a bioclastic silty packstone to wackestone. With abundant pyrite and bitumen in fine grained layers. Bioclasts are predominantly disarticulate and oriented parallel to bedding, but closer to the base there are a few that are articulated and have calcite and silica crystallized in their inner chambers. Shells of bivalves are thin and in some cases closer to the top spary calcite has crystallized along the margins. About 2 cm from the top of the calcite cement and bioclasts disappear and it becomes an interlaminate coarse and fine grained siltstone with some dolomite and calcite cement in the coarser layers while bitumen is concentrate in the fine layers. In some cases the beds appear to coarsen upwards. The coarse grained beds are always much thinner than the fines.

IRG-SA-1412-064b

Interlaminated fine and coarse siltstone with bitumen concentrated in the fine layers. There is minor clay and detrital dolomite. There is a calcite filled fracture close to the top of the section and some of the beds appear to coarsen upward. Coarse grained beds are always thinner and will often pinch and swell. The beds in this section are curved upward on the right.

2528.99

IRG-SA-1412-063a

Alternating layers of fine and coarse grained siltstone (interlaminated) with calcite cement (may be classified as a silty wackestone). Moderately abundant bioclasts oriented parallel to bedding and calcispheres. Bitumen is present in fine silt. Bioclasts are predominantly thin, but not very fragmented (or obviously), disarticulated. Coarse beds are thin, wavy, and discontinuous.

IRG-SA-1412-063b

Silty bioclastic packstone with more abundant bioclasts at the top that are often articulate with calcite crystallized into the inner spaces of the shell. Shells are thin and predominantly oriented parallel to bedding. Abundant calcispheres. Bitumen present in areas overwhelmed with fine silt that are pressing to wackstone. Pyrite is abundant.
2530.87
IRG-SA-1412-062a
The base of the section is a bioclastic packstone cemented with calcite. This grades up into a bioclastic limestone/wackestone with moderately abundant bioclasts oriented parallel to bedding and abundant calcispheres. Within the packstone there are articulated bivalves. Within the wackestone there is alternation of predominantly fine and coarse grained silt. Pyrite is moderately abundant and bitumen is present in fine grained portion.
IRG-SA-1412-062b
Ammonoid and bivalve packstone at top cemented with calcite and calcite, quartz, and dolomite crystallized in interior spaces of shell which are oriented at random. This grades into a silty wackestone similar to 062a with calcispheres and bioclasts oriented parallel to bedding and alternating laminated layers of coarse and fine silt.
2531.1
IRG-SA-1412-061
Laminae of coarse and fine grained siltstone is differentially compacted around a bioclastic packstone cemented with calcite. The laminae to the right of the slide contain some bioclasts oriented parallel to bedding as calcite becomes more abundant suddenly at the margins of the packstone. Calcite outside of the packstone is much rarer and often partially dolomitized. Within the packstone bioclasts are oriented randomly and pyrite is abundant at the edges. There are both articulate and disarticulate bivalves in the packstone which often have calcite crystallized in the center. Bitumen is much rarer in the packstone, but still is present in the finer portion as in the siltstone. Bioclasts appear to be solely bivalves.
2531.29
IRG-SA-1412-060
Coarse grained siltstone cemented with micrite with abundant bioclasts throughout and abundant calcispheres. Bitumen is present and the amount of micrite and quartz grains varies minimally across the section. The bioclasts (bivalves) are thin and fragmented and mostly oriented parallel to bedding.
2532.98
IRG-SA-1412-058a
At the base of the section there is a small portion of the bioclastic calcispheres laminated siltstone that is calcite cemented It quickly transitions into alternating layers of coarse and fine grained silt where the fine grained material is full of bitumen and the coarse grained material has a small amount more of calcite. Most of the calcite above the initial horizon is detrital, however some of the calcite between the grains appears to be the remains of bioclasts, but they are almost indistinguishable. Most of the coarse grained beds are discontinuous and pinch and swell. Macroscopically there appears to be a few erosive surfaces higher in the section. The bottom of the section may have suffered differential compaction.
IRG-SA-1412-058b

At the base there is a sharp contact between a bioclastic packstone above and a medium grained bituminous siltstone below with minor amounts of bioclasts. At the edge of the packstone there is abundant pyrite. The shells in the packstone are oriented mainly parallel to bedding and are disarticulated and cemented together with micrite. Towards the top of the section the shells are more compacted and a small quartz fragment returns along with abundant pyrite.
2533.52
IRG-SA-1412-057
At the base of the section it is alternating beds of fine and coarse grained silt with an overwhelming micrite and bioclastic component with abundant calcispheres. The shells are thin and may have undergone dissolution and recrystallization of spary calcite along the margins. They are oriented parallel to bedding. Some of the calcispheres show concentric layers. Bioclasts become rarer upward in the section until they disappear. Calcite cement lessens although there is still prevalent detrital grains. Near the top of the section the bitumen content decreases drastically and the grain size decreases in several alternating dark/light beds with the darker beds containing some bitumen. Macroscopically these beds display starved ripples. Above these beds the grain size decreases again into a very fine brown siltstone with rare detrital dolomite that is massive in appearance. The grain are about the same size as the clay minerals.
2533.76
IRG-SA-1412-056a
Most of the section starting at the base is alternating layers of fine and coarse siltstone with approximately 20% detrital dolomite and calcite. There are a few thin bioclasts that look to have suffered dissolution. There are fewer bioclasts upward in the section until a horizon at the top where bioclasts and calcite cement take over with calcispheres. There is very little bitumen in this horizon. The bioclasts are still oriented parallel to bedding.
IRG-SA-1412-056b
Most of the section is made up of alternating layers of fine and coarse siltstone with a few large grains of detrital dolomite/calcite. Bitumen is concentrated in the fine grained portion. Towards the top of the section bioclasts appear parallel to bedding. They are concentrated in a few beds in the fine grain portion and are thin and somewhat fragmented. There is a small portion of pyrite in these beds and some dolomite between shells.
2534.75
IRG-SA-1412-55a
Alternating laminations of fine and coarse grained siltstone. The coarse grained laminations are often discontinuous and pinch and swell. There is one bed with an accumulation of bioclasts that are thin and parallel with the bedding. Bitumen is concentrated in the finer fraction. Other than the bioclasts the only calcite appears to be detrital fragments of calcite and dolomite.
IRG-SA-1412-55b
The section is made up of alternating layers of fine and coarse siltstone with bitumen concentration in the finer fraction. At the base of the section it is primarily cemented with calcite and calcispheres. Bioclasts are present and oriented parallel to the bedding. There is a short hiatus in calcite before another layer with mainly micrite in the center with bioclasts rimming the edges with pyrite. After this small horizon the only calcite is a small detrital fraction. The coarse grained layers are relatively large and appear to be continuous. Clay does make up a reasonable fraction of the finer beds.

IRG-SA-1412-55c
Calcite demented fine grained bioclastic siltstone. The shells are oriented parallel to bedding, and calcispheres are very abundant. The shells appear to have undergone minor dissolution, but are mostly intact, and are often concentrated around beds of coarse grained silt. There are a few beds where no bioclasts can be discerned, but there is still an overwhelming micrite fraction.
2535.36
IRG-SA-1412-054a
Fine and coarse grained siltstone laminated with small detrital grains of dolomite and calcite. The coarser grained fraction is very minor and discontinuous.
IRG-SA-1412-054b
Alternating layers of fine and coarse grained siltstone with a larger fraction of bitumen in the fine grained layers. Highly dissolved bioclasts are prevalent throughout and are likely the source of the calcite cement through most of the section, which is prevalent until the very top of the section. At the base the bivalves are more abundant and in better condition than higher up, and in some cases have spary calcite formed between valves. Most of the bivalves are oriented plane parallel.
2536.7
IRG-SA-1412-053
The top of the section is a bioclastic packstone mainly made of bivalves that are oriented in random directions. It is rimmed by pyrite, and towards the edges the shells become more compacted a a quartz fraction starts to appear between the shells instead of just micrite. There is one vertebrate bone fragment. Below the packstone there is interlaminations of coarse and fine grained siltstone. Bioclasts (bivalves) are still present, but they are much more degraded/dissolved. For approximately 2 cm of the section there is still a calcite cement along with interstitial bitumen (mainly in the finer fraction) the coarse laminations are not often continuous and are extremely thin, often on a few grains in thickness. Below this horizon the calcite cement disappears, although there are still some large grains of detrital dolomite in the alternating layers of fine and coarse silt. There is an erosive surface between these two horizons, but it is not erosive between the siltstone and packstone.
2538.11
IRG-SA-1412-052
Alternating laminations of fine and medium grained siltstone. The fine grained fraction contains a larger fraction of bitumen than the coarser grained layers. There is no visible calcite fraction. Some of the coarse grained layers are continuous, but many of the smaller ones are discontinuous. There does not appear to be a large clay fraction at all.
2538.61
IRG-SA-1412-051
Fine grained siltstone interlaminated with medium to coarse grained siltstone. Occasional dolomite detrital grains, can be more concentrated in coarser fraction. The coarser grained laminae are lighter in color and contain less bitumen. There are rare isotropic blebs (pyrite or phosphate). Clay minerals are moderately abundant and are oriented with bedding. Coarser grained layers could be calcite cemented. There are a couple thin calcite laminations that could be very thin bioclasts, but it is unclear. The detrital dolomite grains are the largest grains visible, most twice the size or more of any other grains.
14-29-080-20w6

2539.53
IRG-SA-1412-050
Laminated bioclastic siltstone/packstone, evidence of differential compaction creating a macro scale wedge. Shells are primarily oriented parallel to bedding with some spary calcite grown between shell that are close together or articulated. Most of the shells are not articulated and are often very fragmented. The siltstone portion is calcite cemented. The shells are concentrated in discrete layers with increasing articulation and spary calcite towards the top of the section. The shells are from bivalves, but it does not appear to be Claraia. In the small band outside of the concretion quartz grains that are very fine sand size appear in the fine siltstone matrix and evidence of shells starts to disappear or are much more degraded.
2539.75
IRG-SA-1412-049
Laminated siltstone with calcisphere and bioclasts. Partial dolomitization of calcispheres, discrete laminae of very fine sandstone, increase bioclasts towards top of section. Vein of dolomite, bioclasts in discrete horizons overall appears to have a calcite cement, large amounts of bitumen between grains. More dolomite at bottom of section.
2540.35
IRG-SA-1412-048
Laminated coarse siltstone and very fine sandstone. Very small amount of calcite dement. Continuous laminae of very fine siltstone, some discontinuous lenses of very fine sand in the fine-coarse siltstone matrix.
2540.91
IRG-SA-1412-046
Mostly a massive bioclastic packstone with interstitial micrite and occasional quartz grains at the top. Pyrite is very abundant through the middle of the section. The bioclasts are mainly large thin walled bivalve shells that re disarticulated and deposited at random orientations. The bioclasts disappear at the very top of the section.
2542.94
IRG-SA-1412-047
At the top of the section there is vertebrate material. Bioclastic packstone with abundant quartz grains mixed in with the calcite grains and thin shelled bivalves that are mostly oriented parallel to bedding. A small amount of bitumen is preserved between grains.
2573.51
IRG-SA-1412-045
Medium to fine siltstone, appears massive with a few large Claraia. Shells are disarticulated and somewhat fragmented, oriented parallel to what would be bedding. There are some larger blebs of fragmented disarticulated material. The shells are isolated at the base of the section and are the only evidence of calcite in the section.
2574.7
IRG-SA-1412-044
Isolated very fragmented shell throughout section. Some evidence of a shell hash. Most are oriented parallel to bedding in the fine grained siltstone matrix. High bitumen content. Partial dolomitization of cement between shells. Often shells are stacked on top of one another.

2575.33
IRG-SA-1412-043
Layers of bioclastic Claraia hash in fine grained-medium grained siltstone with lots of bitumen. Very little dolomite fraction, only in a few spaces between shells. Shells are oriented parallel to bedding, and are often only evidence of bedding. Hash layers become thicker towards top of section. Siltstone layers between hash layers are devoid of calcite or have much thinner shells. Possible agglutinated foraminifera.
2575.6
IRG-SA-1412-042
Fine to medium siltstone with bitumen, very occasional bioclastic fragments. Massive, possibly because there is no change in the lithology or color to show the bedding. Larger bioclasts are parallel to supposed bedding direction.
2575.63
IRG-SA-1412-041
Massive, no apparent macro bedding or change in lithology. Rare bioclastic material and pyrite that orient parallel to what would be bedding. Bioclasts are small and fragmented. Large amount of bitumen in fine siltstone.
2576.4
IRG-SA-1412-040
Bioclastic hash layers alternating with siltstone – shells are oriented parallel to bedding. Shells are calcite, but dolomite often crystalized between or on rim of fragments. Possible agglutinated foraminifera. Caclispheres are present and mostly dolomitized. Honey comb texture in calcite at some places, could be part of shell (columnar structure). Calcispheres only appear with bivalves (Claraia).
2576.7
IRG-SA-1412-039
Massive to laminated medium grain siltstone. Less bitumen, but still present. Occasional fragmented bivalve shells with a small amount of partial dolomitization between shells (Claraia). Very little macroscopic bedforms, laminations only visible due to bivalves. No calcite besides bivalves.
15-02-080-16w6
2294.5
BC21
Planar laminated fine grained siltstone with occasional micrometer scale laminations of medium grained siltstone.
16-17-083-25w6
2249.26
BC1
Coarse to fine grained siltstone with abundant black grains. There are some macroscopic starved ripples, but very little visible laminations. There is little to no calcite within the section. Towards the top of the section there are beds that are finer grained with no coarse grained component.
A-005-C/094-G-10
1869.14
IRG-SA-1412-009

Layers of very fine sandstone interbedded with fine siltstone with occasional very fine sand grains. Calcite cementation prevalent through section with occasional bioclasts and several very large bivalve shell (concentrated to top) fragments. Most bioclasts are fragmentary and/or small and oriented parallel to bedding. Pyrite and bitumen are prevalent.
A-10-J/094-B-09
2328.06
BC10
Fine to medium grained siltstone with no visible bedding except where the bioclastic material, solely Claraia, lie parallel with the bedding. The shell material is highly abraided, but still shows the typical calcite structure associated with Claraia. There are very rare dolomite grains within the matrix.
A-18-D/094-A-13
2166.27
IRG-SA-1412-021
Very Fine laminated to massive siltstone with spotty bitumen presence. Coarser grained layers are not continuous across the section and they pinch and swell across the section.
2170.8
IRG-SA-1412-020
Massive fine grained siltstone with very little bitumen. A few large bivalve fragments that have been stacked on top of one another in some places. Small amounts of dolomitization around edges.
2173.39
IRG-SA-1412-019
Laminations only visible due to bioclastic component. Bivalves are largely fragmentary. Possible agglutinated foraminifera. Shells are oriented parallel to bedding in fine grained siltstone with large bitumen content. Shells appear to be Claraia. There are a few small beds of larger bioclast accumulations.
2173.93
IRG-SA-1412-018
Laminated bitumen heavy fine grained siltstone with abundant calcispheres. Bivalve fragments are somewhat abundant and oriented parallel to bedding. There is a preferential dolomitization of calcisphere through the section and a few coarser grained beds that have abundant bivalve hash. The bivalves tend to be present mostly in discrete beds. More calcite preservation at the top of the section.
2174
IRG-SA-1412-017
Bitumen abundant fine grained siltstone that is laminated to massive, often laminations only visible due to bioclasts. Bivalve fragments are moderately abundant through section and parallel to bedding. There are a couple horizons with color change due to amount of bitumen, but not grain size. The one coarser grained layer has abundant bioclast fragments that are very ground up. Bivalve fragments are often stacked on top of one another and in those horizons pyrite is visible. Claraia is the most common bivalve, and there are possible agglutinated foraminifera.
2175.67
IRG-SA-1412-016

Macroscopic laminated fine grained siltstone only visible due to color change. Very rare bivalve fragments, often partially dolomitized. One bed of stacked bivalve (Claraia) shells.
2175.99
IRG-SA-1412-015
Laminated fine grained siltstone with interlayered beds of siltstone and a bioclastic hash. One coarser grained layer contains very ground up bivalve material (Claraia). Pyrite present, siltstone is bitumen filled. Shells are occasionally partially dolomitized more towards base of section. Shells are oriented parallel to bedding. There is abundant clay grains mixed in with the siltstone.
2177.08
IRG-SA-1412-014
Laminated bioclast rich fine grained siltstone with bitumen present most often in discrete layers. Possible agglutinated foraminifera. These layers contain both abundant fragments as well as a few largely complete specimens. Siltstone between these layers is largely devoid of bioclasts, or only very small fragments. Clay is present alongside quartz.
2179.04
IRG-SA-1412-012a
Fine grained bitumen filled siltstone laminated with abundant dolomitized calcispheres and bioclasts (Claraia). The bivalves tend to mostly occur in concentrated layers, but are present through the whole section. Bivalve shells are mostly fragmentary, but are thick. Pyrite is present.
IRG-SA-1412-012b
Laminated fine grained siltstone with abundant bitumen. There are a few coarser grained layers. Bioclast fragments are present in the coarser grained layers. The bioclasts (bivalves) are thin and small and mainly only concentrated in these discrete layers. There are a couple occurrences of vertebrate bone material. Clay is present in siltstone component. The coarse grain layers are continuous across the section.
a-64-A/094-B-8
2386
IRG-SA-0614-07
Fine to coarse grained siltstone alternating and grading into a skeletal packstone. The siltstone horizons contain sparse calcite or dolomite, but as they grade up into the packstone horizons they contain progressively more bioclasts, mainly Claraia, until in the packstone horizons there is calcite cement as well as abundant bioclasts (some of which are still articulated) and occasional calcispheres. The packstone horizons grade up, losing the amount of bioclasts into the siltstone horizons again. This is repeated twice in the section with the second bioclastic horizon having thicker shells, but a smaller accumulation of them. These bioclasts also appear to be more abraded and distorted. The section ends with a third siltstone horizon similar to the two previous. The bedding has been distorted and is wavy in a macroscopic scale, possibly due to the loading of the bioclastic layers.
2389
IRG-SA-0614-02

Mostly fine grained siltstone with abundant bioclasts of Claraia in specific beds throughout. A few coarse grained beds appear towards the top of the section, but it ends with a fine grained bed with very low calcite. Calcite is abundant through the section in both coarse and fine grained beds, mostly in the form of bioclasts aligned parallel to the bedding. There is a scour surface before the final fine grained bed separating it from the bioclast rich horizons. The shells are thin and often heavily abraded and broken, none appear to be articulated.

2389.05

IRG-SA-0614-11

Fine to coarse grained siltstone with alternating beds of fine and coarse grained material. Coarse grained beds increase in abundance towards the top of the section. There is minor dolomite at the base of the section with increasing amounts of calcite towards the top. The dolomite does not disappear through the section, but becomes overwhelmed by the calcite. The calcite and dolomite in this case is mainly found in the fine grained horizons including a few beds of Claraia that start about 2cm from the top of the section. The Claraia increase in size from their first appearance to double their thickness in the subsequent beds. Most are oriented parallel to the bedding and appear to be disarticulated; although some of the shells could still be attached with calcite filling in the inner chamber. After the bed of large Claraia they decrease in thickness and abundance again towards the top of the section along with a decrease in abundance of calcite. About 1cm from the bottom of the section there is a cross section through vertebrate bone material.

2389.4

(blank)

Alternating beds of fine to coarse grained siltstone with occasional dolomite cement. At the base of the thin section there are abundant thick Claraia both in fine and coarse grained beds, although more abundant in fine grained beds. Above this the Claraia decrease in thickness and abundance. They are more dolomitized and decrease in abundance upwards through the fine grained bed. The specimens towards the top of the bed are highly abraded. Just after a scour surface the Claraia return to the same thickness from the base of the section and are found in a mostly coarse grained horizon. The shells in this horizon are highly abraded and as the beds become finer grained again the shells decrease in thickness and dolomite becomes more abundant. The bioclasts disappear quickly after the grain size decreases.

2410.05

IRG-SA-0614-08

Bedding at the base of the section has been distorted by loading from the bed of abundant ammonoid and bivalve bioclasts just above them. The clastic component alternates between fine and coarse grained siltstone, with coarse grained siltstone more prevalent in the bioclastic horizon. The base of the section begins with very little calcite or dolomite input, only the occasional dolomitized grain. Just above those beds, where the bedding starts to become very contorted, calcite immediately becomes abundant in the form of bioclasts. Both Claraia and brachiopods seem to contribute along with much larger ammonoids. The bivalve and brachiopod bioclasts are the only indication of bedding through the skeletal packstone interval. This quickly grades up into an interval with more clastic input that against starts to alternate between fine and coarse grained siltstone, although still with a heavy calcite input. The bioclastic material appears more abraided the further up in the section and is more common in the coarser grained horizons. The laminations at the top of the section are distorted by preserved starved ripples. There is no evidence of any preserved aragonite in the ammonoid specimens.

Mostly fine grained siltstone with abundant bioclasts of Claraia in specific beds throughout. A few coarse grained beds appear towards the top of the section, but it ends with a fine grained bed with very low calcite. Calcite is abundant through the section in both coarse and fine grained beds, mostly in the form of bioclasts aligned parallel to the bedding. There is a scour surface before the final fine grained bed separating it from the bioclast rich horizons. The shells are thin and often heavily abraded and broken, none appear to be articulated.
2389.05
IRG-SA-0614-11
Fine to coarse grained siltstone with alternating beds of fine and coarse grained material. Coarse grained beds increase in abundance towards the top of the section. There is minor dolomite at the base of the section with increasing amounts of calcite towards the top. The dolomite does not disappear through the section, but becomes overwhelmed by the calcite. The calcite and dolomite in this case is mainly found in the fine grained horizons including a few beds of Claraia that start about 2cm from the top of the section. The Claraia increase in size from their first appearance to double their thickness in the subsequent beds. Most are oriented parallel to the bedding and appear to be disarticulated; although some of the shells could still be attached with calcite filling in the inner chamber. After the bed of large Claraia they decrease in thickness and abundance again towards the top of the section along with a decrease in abundance of calcite. About 1cm from the bottom of the section there is a cross section through vertebrate bone material.
2389.4
(blank)
Alternating beds of fine to coarse grained siltstone with occasional dolomite cement. At the base of the thin section there are abundant thick Claraia both in fine and coarse grained beds, although more abundant in fine grained beds. Above this the Claraia decrease in thickness and abundance. They are more dolomitized and decrease in abundance upwards through the fine grained bed. The specimens towards the top of the bed are highly abraded. Just after a scour surface the Claraia return to the same thickness from the base of the section and are found in a mostly coarse grained horizon. The shells in this horizon are highly abraded and as the beds become finer grained again the shells decrease in thickness and dolomite becomes more abundant. The bioclasts disappear quickly after the grain size decreases.
2410.05
IRG-SA-0614-08
Bedding at the base of the section has been distorted by loading from the bed of abundant ammonoid and bivalve bioclasts just above them. The clastic component alternates between fine and coarse grained siltstone, with coarse grained siltstone more prevalent in the bioclastic horizon. The base of the section begins with very little calcite or dolomite input, only the occasional dolomitized grain. Just above those beds, where the bedding starts to become very contorted, calcite immediately becomes abundant in the form of bioclasts. Both Claraia and brachiopods seem to contribute along with much larger ammonoids. The bivalve and brachiopod bioclasts are the only indication of bedding through the skeletal packstone interval. This quickly grades up into an interval with more clastic input that against starts to alternate between fine and coarse grained siltstone, although still with a heavy calcite input. The bioclastic material appears more abraided the further up in the section and is more common in the coarser grained horizons. The laminations at the top of the section are distorted by preserved starved ripples. There is no evidence of any preserved aragonite in the ammonoid specimens.

2423.65
(blank)
Fine to very fine siltstone with very rare calcite or dolomite grains. Distinct planar laminations of alternating grainsize. There appears to be no difference in cement for the beds. There is possibly an erosional surface 1cm from the base of the section.
a-64-A/94-B-8
(blank)
fish
Bedding at the base of the section has been macroscopically depressed and contorted. A fish ribcage is present and is oriented almost vertically in the thin section. The bedding is contorted around it and several ammonoids (approx. 2cm in cross section); although a short distance away from the fish planar beds and starved ripples are observable. After the fish the beds return quickly to planar lamination with minor depression. There is a scour surface approx. 1.5 cm from the top of the section where there is a drastic grain size change from coarser grained silt (with abundant calcite cementation) to fine grained silt with no calcite observable. The first bed fines upward then the bedding starts to alternate between fine grained and coarse grained silt. The coarse grained silt horizons have starved ripples and rare calcite. Towards the middle of the section, around the fish fossil there is a bed with abundant abraded Claraia and other thin shelled bivalves. Most are deposited parallel to the bedding. This bed also is only about 30-40% coarse silt.
B-65-J/094-B-16
2024.5
BC9
Interlaminated fine and medium grained siltstone where the medium grained has less bitumen than the fine grained making it visibly lighter. Very little calcite in the section, mostly small grains in coarser layers. Small bone fragment.
C-006-L/094-B-8
2796.46
IRG-SA-1504-024
Fish fossil with pyrite rim around calcite concretion that has been differentially compacted. Laminated fine grained bituminous siltstone with a small component of dolomite outside of concretion. Pyrite is abundant in the concretion along with possible calcispheres. The laminations are preserved, but are discontinuous in the concretion. The lighter layers are cemented with calcite and there is little quartz in the concretion. There is a quartz filled vein at the base of the concretion.
C-007-J/094-B-08
2253.79
BC16
Medium to coarse grained siltstone that fines upwards. There are very rare bioclasts towards the base of the section with an increase in calcite, and rare dolomite, grains towards the top of the section. Macroscopically there is evidence of bedding that is not easily visible microscopically.
2438.85
BC 15

Planar laminated alternating coarse and fine grained siltstone with moderately abundant partially dolomitized grains. Both bioclasts and calcispheres have been dolomitized. Bioclasts, Claraia, are very thin and are more common in the bottom of the section compared to calcispheres which are more common after the first 0.5cm of the section. Bioclasts are more common in the coarser grained beds while calcispheres are more common in fine grained sections. The bioclasts appear to be highly abraded and are oriented parallel with the bedding.
2441.72
BC18
Section through a calcite pinch out. Coarse to fine grained siltstone is distorted around a bed of skeletal packstone. Dolomite grains are rare within the siltstone beds, although there appear to be a few bioclastic fragments within those beds that have been dolomitized. At the base of the packstone there is a coarse grained siltstone that contains more bioclastic material as it grades upward into the packstone. The packstone appears to entirely consist of Claraia shell material that is not oriented in any specific pattern. There appears to be some dissolution and cementation around the edges of the shell material that may have aided in the shells resisting compaction. The upper part of the packstone appears to have undergone partial dolomitization with the process becoming more prevalent towards the boundary between the packstone and the upper siltstone beds. The shells are thickest in the center of the packstone layer and decrease in thickness towards the edges.
2446.98
BC14
Alternating beds of fine to medium grained siltstone. Most of the section is plane parallel laminated, but some of the coarser grained horizons show evidence of ripples macroscopically. The bedding is fairly distinct microscopically.
2529.46
BC13
Fine to medium grained siltstone with no visible bedding except where the bioclastic material lies parallel to the bedding and where there are distinct horizons that have an absence of the bioclastic material. Most of the bioclastic material, Claraia shell material, has been partially dolomitized around the edges of the shell and highly abraded. There are occasional anisotropic grains that could be phosphate.
C-074-G/094-B-09
1947.1
BC20
Fine to medium grained siltstone that is mainly planar laminated. There are alternating layers of the siltstone with fine grains of calcite interspersed within them and layers in which most of the fabric is composed of large sand sized calcite grains. Some of the calcite grains exhibit partial dolomitization within these sections. The amount of calcite in the section increases towards the top of the section until it makes up most of the silt size particles within the horizon. Some of the calcite grains could be calcispheres due to their round shape.
1949.64
BC19

At the base of the section there is a calcite cemented horizon that may contain bioclasts, but there are none that are distinct. If they are present they have had major recrystallization. There is abundant pyrite at the top of this section. Above this unit there is a layer of alternating fine grained and medium to coarse grained planar laminated siltstone that is partially distorted around the calcite horizon. There is visible porosity within the coarser grained horizons between the grains. At the top of the section there is a thin horizon of spary calcite that has undergone moderate dolomitization.
DD b-050-H/094-B-16
2055.37
IRG-SA-1412-036
Fine grained bituminous siltstone with minor clay content and a few discontinuous layer of fine siltstone with less bitumen content that is the only evidence of laminations and bedforms in the section. Otherwise the siltstone appears massive.
2057.54
IRG-SA-1412-035a
Medium to fine grained siltstone laminated with large quantities of calcite cement and low amounts of bitumen. Very few if any bioclasts are observed and several large layers of crystalline calcite are bedded with the calcite. What bioclasts are present are parallel to bedding.
IRG-SA-1412-035b
Bitumen filled stylolite. Alternating layer of fine to coarse grained silt with a few bioclasts and calcite cement and minor bitumen content in finer layers grades into a silty limestone with occasional bioclasts and abundant calcispheres. Bitumen levels stay constant and there is abundant pyrite. This grades out back into the siltstone with minor calcite that is seen at the base.
IRG-SA-1412-035c
Alternating predominantly fine and coarse silt layers with bitumen concentrated in the fine grained layers. The coarse grained layers are thin, few in number and often discontinuous.
2063.01
IRG-SA-1412-034
Mostly fine grained siltstone with interspersed coarse grained material that except for a few instances does not appear to make discrete layers. Bitumen is concentrated in the fine grained layers. At the very base of the section there is some bioclastic material that quickly grades out, but is partially dolomitized. The bioclasts are all oriented parallel to bedding. Above that there are a few detrital calcite and dolomite grains.
2063.25
IRG-SA-1412-033a
Hydrocarbon filled stylolite on the right side. Alternating layers of fine and coarse grained siltstone which start off with a high concentration of bioclasts and calcite cement at the base. Bitumen is concentrated in fine grained intervals through the section. Bioclasts are thin and are very recrystallized through the section. Above the point where bioclasts disappear, any calcite fraction is much smaller and is partially dolomitized. Dolomite is detrital and there is a small amount of detrital calcite. There is a very small clay fraction.
IRG-SA-1412-033b

Vertical stylolite on right side of the section, hydrocarbon filled. Alternating layers of coarse and fine grained siltstone in a bioclastic silty wackestone. Bitumen is concentrated in fine grained portion and pyrite is abundant. Bioclasts are larger towards the top of the section and oriented parallel to bedding. Calcite cement is prevalent through the section, although it appears to have dissolved and recrystallized around bioclasts at the base. Spary calcite around shell margins at the base. Coarse grained layers are few in number and are very thin, but coarse grained material is interspersed throughout.
2063.34
IRG-SA-1412-032
Macroscopically the bedding in this section is very convoluted. Vertical hydrocarbon filled stylolite in the center of section. At the base there are convoluted layers of coarse and fine siltstone. At the very base there is no carbonate fraction, but just above that detrital dolomite grains become a major constituent in both the fine and coarse grained layers. Bioclasts are rare and partially dolomitized at the base. At the middle of the section it is primarily coarse grained silt, but fine grained material is interspersed randomly in clumps. At the top of this horizon calcite becomes more abundant in the fine grained fraction, which is separated out in layer again, in the form of bioclasts. The coarse and fine grained fractions are homogenized again until the very top fine grained layer. Bioclasts are all oriented parallel to bedding and are thicker at the top of the section.
2064
IRG-SA-1412-031a
Alternating layers of laminated fine and coarse grained siltstone where the bitumen is concentrated in the fine grained layers and calcite and bioclasts are often found in the coarse grained horizons which are thin and very often pinch and swell across the section. Dolomite replaces a good portion of the calcite towards the top of the section.
IRG-SA-1412-031b
Horizon of pyrite 1 cm from the top. Alternating layers of fine and coarse grained siltstone that is calcite cemented all except the top 1cm above the pyrite which is cemented with dolomite. Bioclasts are oriented parallel to bedding and are most abundant around coarse grained horizons. They are moderately thick and individual pyrite crystals are found around the bioclasts. Above the pyrite layer the bioclasts are very thin. Bitumen is a minor component due to calcite, but is still present in fine grained horizons.
2066.07
IRG-SA-1412-030a
Same as 029b.
IRG-SA-1412-030b
Same as 030a, but with more abundant and larger bioclasts that are concentrated around the coarser layers towards the base of the section. (One near the top of the section may be an agglutinated foraminifera).
2066.2
IRG-SA-1412-029a
Alternating layers of coarse and fine grained siltstone with abundant detrital dolomite through section. Bitumen is concentrate in fines and there are rare partially dolomitized very thin bioclasts. The coarse grained layers are thin, wavy, and discontinuous lamination.
IRG-SA-1412-029b

Same as 029a, but with less dolomite towards the base, fewer coarse grained horizons that are thinner, but more laterally continuous.
2069.19
IRG-SA-1412-026
Alternating beds of very fine sandstone and fine siltstone. They layers are often discontinuous and there is no visible carbonate fraction. The cement in the coarser layers appears to be silica. The finer layers are filled with bitumen.
2069.41
IRG-SA-1412-027
Heterolithic, slightly deformed laminations with vertical bitumen filled fracture that appears to be syndepositional. At the top of the section there are only a few dolomite grains, but about 2 cm down there is a transition where calcite immediately becomes prevalent (at first alongside dolomite). It does not appear to be an erosional contact. The fracture ends at this horizon. Layers alternate between very fine sandstone and fine siltstone through the section. Bivalve shells are increasingly prevalent with increasing calcite starting off very thin and only mildly abundant to become slightly thicker and form beds of mainly bioclasts oriented parallel to bedding. Their bedding orientation is deformed with bedding. They are common in both fine siltstone and very fine sandstone layers. Pyrite is abundant.
2069.49
IRG-SA-1412-028a
A coarse grained dolomite siltstone with rare bioclasts, grades up into a bioclastic micritic limestone with occasional layers of coarse siltstone and abundant pyrite. The bioclast concentrate around the coarse silt layers and are oriented parallel to bedding the bioclasts and silt give it a wavy laminated bedding.
IRG-SA-1412-028b
The section is composed of alternating layers of fine silt and coarse silt. The majority of the slide contains detrital dolomite and very thin bivalves that are parallel to bedding. Throughout the section bitumen is concentrated in the fine grained layers. The coarse grained layers are discontinuous and wavy laminated. Shells in the dolomite horizons have been partially dolomitized. Stylolites are present. A few calcispheres are present. A centimeter thick horizon is calcite cemented with abundant bioclasts. The shells are much better preserved in this layer and pyrite is present.
IRG-SA-1412-028c
Major vertical stylolites, one filled with dolomite. Alternating layers of coarse and fine grained siltstone with abundant detrital dolomite through section. Bitumen is concentrated in fines and there are rare partially dolomitized very thin bioclasts. The coarse grained layers are thin, wavy, and discontinuous.
2074.23
IRG-SA-1412-025a
Alternating layers of fine and coarse grained silt with bitumen concentrated in the fine grained material. Detrital dolomite is concentrated in the coarser grained layers which pinch and swell across the section. It appears to be laminated macroscopically with possible evidence of erosion in pinch and swell layers.
IRG-SA-1412-025b

The section is composed of alternating laminations of fine and coarse grained siltstone with bitumen concentrated in the fine grained fraction. Detrital dolomite is present for most of the section up until about a centimeter from the top. Coarse grained beds are commonly discontinuous and there are rare thin bioclasts in the bottom half.
2074.24
IRG-SA-1412-024
Alternating layers of fine and coarse grained siltstone with bitumen concentrated in the fine grained layers. Bioclasts become increasingly prevalent in the fine grained layers towards the top of the section, increasing with calcite cement at the very top. At the base calcite and dolomite are very minor, but still contained in fine grained layers. Coarse grained layers are very discontinuous and thin throughout the section.
Ursula Creek
(blank)
UC 1D
Fine grained siltstone with abundant calcite both as cement and in the form of calcispheres (possibly radiolaria?). Most laminations appear disturbed and discontinuous with rare beds that appear to be mostly calcite. Streaks of what appears to be bitumen are common in thin section and often contribute to the discontinuity of beds. There is partial dolomitization that increases in intensity towards the top of the section.
UC1A
Planar laminated very fine to medium grain size siltstone with abundant partially dolomitized calcite, some appear to be calcispheres. The medium silt mainly appears in thin laminations through the section. Some of the calcite has formed around the coarser silt grains, and could be some form of early cementation, but those cases are rare in this section.
UC1B
Very fine to medium siltstone that is planar laminated with moderate degrees of dolomitization towards the top and base of the section. Save for a few calcite cemented beds, most of the calcite appears to be of the same grain size as the clastic element. There appear to be black bitumen filled streaks through the section and no bioclastic element to it. There are a few blebs and one vein towards the top of the section that appear to be large quartz grains. There is also a small section of pyritization towards the top of the section.
UC1C
Fine to medium grained siltstone with abundant calcite and calcispheres. Black streaks, possibly bitumen, cross the rock fabric. There is no change in the rock texture save for a few beds of calcite that cross the section. There is no distinct bedding macroscopically other than these features.
UC1E
Very fine grained siltstone with occasional grains or stringers of coarser grained material. Abundant calcispheres that have all been partially dolomitized. Black material runs through the fabric that macroscopically appears to be planar laminated, but no continuous beds are identifiable across the thin section.
UC2

The section is mostly, 80-90%, composed of calcite with very low clastic input. What clasts that are there are coarse silt sized grains, and most of the calcite grains are of the same size, bioclasts and the occasional calcisphere being the only exception. Black streaks are present across the fabric. Claraia make up the bioclastic input and are mainly oriented with the bedding. The bioclastic material is found in two to three main zones and is rare to the top and bottom of the section. The bedding is distorted macroscopically most likely due to the bioclasts.
UC3
The section is bounded on both surfaces by distinct darkened horizons (fine grained siltstone) otherwise it appears to be a uniform texture. Has black streaks that run haphazardly through the fabric, perhaps bitumen? There is no apparent bedding within this horizon. Coarse grained siltstone with abundant calcite in the forms of prismatic, circular possibly calcispheres, and linear features that could be bioclasts. There is very rare partial dolomitization. The two surfaces bounding the calcite filled bed appear to be erosive.
A07-19-085-15w6
1763
BC23
Fine grained siltstone with layers of plane parallel bioclasts (bivalves) and interstitial bitumen. The bioclasts are concentrated in a few layers which are the only indication of bedding. On the left (unstained) side of the section there is a small area that has been differentially compacted and contains abundant calcispheres. The shells are thick and appear to be Claraia, but are very fragmented. Possible agglutinated foraminifera. Some bivalves at the top of the section are very thin shelled.
1776.5
BC24
Mostly fine to coarse grained siltstone matrix with large pebble to very coarse sand size angular clasts both made up of bioclastic debris-very abraded material-or mud clasts. There are many different types of bioclasts within the section including vertebrate bone material, bivalve shell material, and possible microfossils; although they are mostly shell material from bivalves. There is no macroscopic or microscopic bedding in the section.

Appendix D: Well Data

Well I.D.	"*Claraia* Zone" MD (m)	"*Claraia* Zone" thickness (m)	Altares Packstone Member MD (m)	Altares Packstone Member Thickness (m)
100/06-18-080-15W6/00	2285.8	4.4	2146.6	6.5
100/10-21-080-16W6/00			2029.9	6.5
100/08-08-080-17W6/00	2412.3	8	2310.1	13.5
100/15-13-080-17W6/00	2249.6	4	2135.8	3.4
100/13-14-080-18W6/00	2369.6	4.4	2271.6	2.3
100/13-16-080-18W6/00			2428.5	2.3
100/15-34-080-18W6/00	2316.5	5.9	2222.2	4
100/14-29-080-20W6/00	2570.7	5.5	2519.8	5.1
100/06-29-081-15W6/00	2070	3	2016.9	9.8
100/11-32-081-15W6/00	2020.1	5.4		
100/03-33-081-15W6/00	1989.3	7.2	1792	7.5
100/14-15-081-16W6/00	2088.4	6.9	1914	9.3
100/03-17-081-18W6/00	2320.9	6	2254.9	1.7
100/08-08-081-19W6/00	2431.1	5	2349	2.7
100/05-23-081-19W6/00	2150.1	5.2	2051.3	2.4
100/13-11-081-20W6/00	2373.4	5.2	2311.5	3
100/04-11-081-21W6/00	2276.6	8.8	2231.2	8.9
100/04-11-081-21W6/02	2345	4.2	2228.3	3.5
100/10-28-082-16W6/00	1854.1	10.3	1662	4
100/07-05-082-17W6/00	2107.7	5.4	1985.7	5.4
100/08-10-082-17W6/00	2001.9	4.6	1872.8	5.3
100/05-03-082-18W6/00	2071.8	5.7	1969.3	8.7
102/07-05-082-19W6/00			2083.2	3.3
100/14-12-082-19W6/00	2062.2	4.1	1940.2	3
100/05-18-082-19W6/00	2133.8	6.2	2014.7	4
100/09-07-082-20W6/00	2010.2	6.8	1956.6	2.6
100/09-17-082-20W6/00			1917.5	5.6

100/08-22-082-20W6/00	1994.1	4.6	1900.6	2.9
100/10-27-082-20W6/00	1961	2	1859.5	3.1
100/03-30-082-20W6/00	1900.3	6.7	1820.6	2.3
100/08-30-082-20W6/00	1892	3.7		
100/13-08-082-22W6/00	1978.1	3.5	1944	6.1
100/01-10-082-23W6/00	2055.6	5.1	2018.6	6.9
100/06-13-083-16W6/00	1839.5	5.8	1666.2	10.8
100/06-30-083-16W6/00	1830.1	6.6	1654	14.3
100/04-09-083-17W6/00	1777.7	4.3		
100/03-01-083-21W6/00	1828.6	3.7	1785.1	4.3
100/06-34-083-21W6/00	---		1700.6	3.8
100/05-05-083-24W6/00	---		2086.6	8.8
100/12-07-083-24W6/00	2174.2	6.9	2125.5	3.1
100/01-31-083-24W6/00	2265.8	4.1	2215.9	5.1
100/16-17-083-25W6/00	2425.1	4.7	2384.1	11.8
100/06-14-084-15W6/00	1695.4	8.6	1540.7	6.3
100/08-23-084-15W6/00	1695.2	5.2	1545.5	13.2
100/07-22-084-16W6/00	1706.1	4.9	1562.8	11.1
100/10-23-084-16W6/00	1713.4	5	1572	7.5
100/16-11-084-17W6/00	1757.5	7.7	1597.5	12.5
100/14-14-084-17W6/00	1709.1	4.9	1566.6	12.2
100/14-19-084-17W6/00	1770.8	5.5	1625.4	15.7
100/12-30-084-17W6/00	1790.1	4	1642.4	7.1
100/08-10-084-18W6/00	1804	5.9	1641	14.8
100/14-10-084-18W6/00	1750.6	5.2	1596.2	14.1
100/16-10-084-18W6/00	1737.5	5.1	1587.4	14.9
100/06-15-084-18W6/00	1875.6	3.7	1671	15.4
100/03-16-084-18W6/00	1674.9	4.8	1517.5	14.9
100/08-16-084-18W6/00	1660.3	4	1514.1	13.7
100/16-18-084-18W6/00	1782.1	5.3	1639.9	5.1

100/06-19-084-18W6/00	1770.9	10.8	1623.2	17.4
100/11-19-084-18W6/00	1756	4.9	1615.4	16.8
100/14-20-084-18W6/00	1685.3	4.2	1547.2	15.8
100/09-21-084-18W6/00	1822.6	6	1668.8	13.2
100/06-22-084-18W6/00	1747.9	5		
100/10-22-084-18W6/00	1744.3	5.4	1592.9	16.6
100/12-23-084-18W6/00	1560.3	4.1	1396.5	14.8
100/04-25-084-18W6/00	1807.9	3.8	1653.1	14
100/08-25-084-18W6/00	1790.8	3.8	1643.7	22.4
100/09-25-084-18W6/00	---		1640.8	12.9
100/11-25-084-18W6/02	1776.4		1629	
100/04-26-084-18W6/03	1835.2	5	1688	13.9
100/07-26-084-18W6/00	1525.1	6.7	1387.7	14.2
100/09-26-084-18W6/00	1581.2	3.3	1431.9	2.8
100/15-26-084-18W6/02	1819	3.5	1663.1	15.5
100/02-27-084-18W6/00	1725.9	3.3	1581.4	14.2
100/04-27-084-18W6/00			1582.5	16.3
100/10-27-084-18W6/00	1718.2	6.2	1580.6	2.5
100/04-29-084-18W6/00	1780.5	4.6	1636.6	16
100/05-29-084-18W6/00	1764	4.9	1624.9	16.7
100/06-29-084-18W6/00	1769.9	5.4	1630.2	16.3
100/08-29-084-18W6/00	---		1615	14.5
100/12-29-084-18W6/00	1787.1	4.3	1647	16.2
100/14-29-084-18W6/00	1863.7	6.5	1719.7	14.4
100/01-30-084-18W6/00	1948.6	5	1792.8	14.4
100/03-30-084-18W6/00	1809.6	4.9	1665.1	14.6
100/12-30-084-18W6/00	1867.9	4.5	1707.5	3.8
100/02-31-084-18W6/00	1747.5	5.4	1608.5	14.3
100/04-32-084-18W6/00	1829.5	6	1685.8	13.9
100/16-32-084-18W6/00			1667.5	15.9

100/04-33-084-18W6/00	1746.7	5.2	1604.8	15.7
100/08-34-084-18W6/00	1712.3	4.4	1576.8	12.7
100/01-35-084-18W6/00	1592.5	5.4	1432.1	16.2
100/03-35-084-18W6/00	1725.1	4.6	1588.1	13.2
100/14-35-084-18W6/00	1717.8	5.4	1581.5	13.5
100/06-36-084-18W6/00	1531.4	5	1380.9	15.4
100/16-23-084-19W6/00			1664.5	3.8
100/14-24-084-19W6/00			1636.3	5.7
100/08-26-084-19W6/00			1643.6	15.6
100/16-26-084-19W6/00	1789	6.5	1646.7	9.7
100/14-35-084-19W6/00	1856.7	4.9	1714.2	15.5
100/06-34-084-20W6/00	1965	7.6	1836.7	16.8
100/06-13-084-21W6/00	2043.8	4.9	1919.5	14.1
100/08-13-084-21W6/00	2056.9		1924.8	
100/15-13-084-21W6/00	2014	4.9	1886.4	16.1
100/04-09-084-22W6/00	---		1790	10.7
100/04-14-084-23W6/00	---		1867.4	5.7
100/04-20-084-24W6/00	---		2098.4	5.1
100/09-21-085-16W6/00	1750.7	4.1	1608.4	22.7
100/10-04-085-18W6/00	1740.5	5.7	1602.5	9.3
100/06-05-085-18W6/00	1835.1	5.9	1698.5	5.3
100/16-05-085-18W6/00	1769.1	8.7	1633.3	10.8
100/04-06-085-18W6/00	1743.6	9.4	1596.4	8.9
100/08-06-085-18W6/00	1811.9	9.7	1672.5	8.6
100/12-06-085-18W6/00	1769.1	6.1	1635.1	13.3
100/04-07-085-18W6/00	1746.7	6.4	1622.2	8.4
102/08-07-085-18W6/00			1693	5.9
100/10-07-085-18W6/00	1804.9	7.1	1676.4	5.2
100/04-09-085-18W6/00	1743.3	8.1	1617.4	5.4
102/07-11-085-18W6/00	1699.5	7.6	1584	5.4

100/04-01-085-19W6/00	1796.6	3.7	1655.6	6.2
100/07-01-085-19W6/00			1612.3	5.4
100/08-01-085-19W6/00	1830.7	6.9	1682	11.3
100/09-01-085-19W6/00	1796	6.2	1651.1	5.8
100/16-01-085-19W6/00	1887.1	4.9	1734.2	8.4
100/06-03-085-19W6/00	1898.7	5.2	1768	5.9
100/08-07-085-19W6/00			1738.5	5.7
100/06-09-085-19W6/00			1708.3	8.4
100/08-11-085-19W6/00			1645.1	8
100/14-11-085-19W6/00			1665.1	9.5
100/16-11-085-19W6/00	---			
100/02-12-085-19W6/00			1697.2	5.6
100/12-12-085-19W6/00	1765.2	5.8	1617.2	4.8
100/04-13-085-19W6/00	---		1606.3	9.4
100/14-18-085-19W6/00	1835.5	7.1	1729.5	7.6
100/14-19-085-19W6/00			1770.9	5.1
100/16-19-085-19W6/00	---		1764.9	5.2
102/06-20-085-19W6/00	---		1753	5.7
100/06-21-085-19W6/00	---		1751.2	10.5
100/06-30-085-19W6/00	---		1753.2	16.9
100/14-16-085-20W6/00	---		1776.7	5.6
100/08-21-085-20W6/00			1747.9	6.2
102/16-21-085-20W6/00	---		1733	9.9
100/12-22-085-20W6/00	---		1722	10.3
100/14-22-085-20W6/00	---		1737.7	10.2
100/08-23-085-20W6/00	---		1704.3	10.8
100/06-25-085-20W6/00			1740.8	10.9
100/08-25-085-20W6/00	---		1727.7	11
100/16-25-085-20W6/00			1747.7	10.7
100/06-26-085-20W6/00	---		1712.1	7.8

100/08-26-085-20W6/00	---		1740.1	10.5
100/13-26-085-20W6/00	---		1696.3	9.9
100/09-27-085-20W6/00	---		1680.2	4.3
100/10-27-085-20W6/00			1707.8	10.8
100/11-27-085-20W6/00			1755	8.1
100/16-27-085-20W6/00	---		1673.9	8.1
100/08-28-085-20W6/00	---		1742.5	6.8
100/08-33-085-20W6/00			1781.6	7.6
100/02-34-085-20W6/00	---		1692.4	10.2
100/10-34-085-20W6/00	---		1685.9	10.8
100/12-36-085-20W6/00	---		1769.1	11.4
100/15-12-085-22W6/00	---		1872.7	6.3
100/03-22-085-22W6/00			1768.1	
100/02-07-085-23W6/00	1943.9	7.4	1879.5	3.8
100/09-07-085-25W6/00	2234.3	5.7	2128.2	13.4
100/14-22-086-16W6/00	1622.1	4.8	1500.6	5.1
103/06-17-086-18W6/00			1654.1	10.5
100/02-04-086-20W6/00			1733.4	7.2
100/16-04-086-20W6/00	---		1686.6	8.4
100/11-17-086-20W6/00	---		1689.7	7.8
100/11-20-086-20W6/00	---			
100/13-05-086-21W6/00			1737.3	8.4
100/14-14-086-21W6/00	1945.1	6.5	1834	7
100/01-18-086-21W6/00			1749.9	6.7
100/10-35-086-21W6/00			1755.6	8.7
100/10-12-086-22W6/00			1860.6	6
100/06-06-087-20W6/00			1728.8	8.9
100/07-21-087-20W6/00	---			
102/12-06-087-24W6/00	2063	4.5	1948	21.9
100/04-08-088-24W6/00			1941	8.7

100/14-20-088-25W6/00	1902.6	4.1	1764.2	13.4
202/b-058-L 094-A-04/00	2518.7	4.7	2458.7	3.7
200/c-050-K 094-A-12/00	1874.7	13.4	---	
200/c-060-K 094-A-12/00			1779.4	11.5
200/d-096-K 094-A-12/00	2017.8	3.4	1917.5	4.2
200/a-039-L 094-A-12/00	1873.9	7.9	1769.8	12
202/c-058-B 094-A-13/00			1836.4	11.4
200/b-070-C 094-A-13/00			1899.8	4.2
200/a-018-D 094-A-13/00	2176.1	4.3	2068.4	3.5
202/b-007-E 094-A-13/00	---		1939.9	5.2
200/c-021-L 094-A-13/00	1966.2	5.8	1865.4	5.7
200/a-026-A 094-A-14/00	1525.5	6.7		
200/d-080-I 094-A-14/00	1497.5	4.6	1392.6	8.1
200/c-005-J 094-A-14/00			1496.7	2.7
200/b-015-I 094-B-01/00	2496.8	5.7	2439.3	4
200/b-017-I 094-B-01/00	2539.7	5.7	2484.3	2.9
202/c-048-I 094-B-01/00	2601.5	6.8	2536.3	8.9
200/c-085-I 094-B-01/00			2534.5	5.2
200/d-022-G 094-B-08/00	2634	4.1	2511.5	6.8
200/d-046-G 094-B-08/00	2577.1	14.4	2479.3	6.6
202/c-003-H 094-B-08/00			2276.9	4.4
200/c-057-I 094-B-08/00	2304.5	4.3	2160.8	2.7

200/b-030-A 094-B-09/00	2359	3.8	2193.7	3.4
200/b-035-A 094-B-09/00	2085.1	18.2	1926.6	6
200/b-046-A 094-B-09/00	2128.9	5.1	1956.5	6
200/d-048-A 094-B-09/00	2228.2	4.1	2061.8	5.4
200/c-037-B 094-B-09/00	2415.9	7.9	2257.9	22.4
200/c-033-C 094-B-09/00			2339.1	13.9
200/d-002-G 094-B-09/00	2165.7	7.2	2015.1	21.4
200/c-074-G 094-B-09/00	2112.1	4.8	1947.2	3.6
200/a-020-H 094-B-09/00	2076.4	4.2	1906.2	8.1
202/a-001-J 094-B-09/00	2168.4	5.3		
200/a-010-J 094-B-09/00	2318.1	4.6	2158.8	5.3
200/c-054-J 094-B-09/00	2161.2	7.2		
200/d-067-J 094-B-09/00	2112.2	10.1	1960.3	4.7
200/a-031-B 094-B-15/00	2598	3	2446.9	9
200/a-028-F 094-B-15/00			2502.7	
200/b-033-A 094-B-16/00	1982	4.8	1875.4	17.3
200/b-078-A 094-B-16/00	2177.7	3.1	2068.4	4.9
200/a-065-E 094-B-16/00			2047.9	16.6
200/d-075-E 094-B-16/00			2036.2	5.4

200/d-008-F 094-B-16/00	2296.5	6	2177.5	6.1
203/d-063-G 094-B-16/00	2026.2	5	1930.7	6.3
200/d-050-H 094-B-16/00	2142.5	3.2	2052.7	5.8
200/c-068-I 094-B-16/00	2008.7	4.4	1860.5	5.6
200/a-069-I 094-B-16/00			1879.6	5.7
200/d-038-J 094-B-16/00			1912.5	5.6
200/b-065-J 094-B-16/00	2122.8	6.5	1975.6	5.7
200/d-100-J 094-B-16/00			2098.5	6.2
200/b-013-B 094-G-01/00			1930.4	5.2
200/a-078-C 094-G-01/00			1971.8	5.7
200/a-050-D 094-G-01/00	2280.1	6.1	2196.5	4.7
202/c-056-E 094-G-01/00			1899.1	5.5
200/c-066-A 094-G-02/00	2318.7	3.3	2231.3	6.6
200/d-088-F 094-G-02/00	2043.2	3.7	1923.3	12.6
200/d-028-J 094-G-02/00	2191.8	5.2	2099.1	7.8
200/d-055-A 094-G-07/00	1906.1	5.6	1787.8	5.8
202/c-054-B 094-G-07/00			1896.3	6.1
200/a-034-L 094-G-07/00	2061.2	7.5	1966.5	3.3
200/c-004-F 094-G-08/00	1899.2	4.8	1800.8	6.5
200/a-005-C 094-G-10/00	1995	7	1870.3	6.5

200/c-100-C 094-H-03/00			1502.5	8.6

“*Claraia* Zone” Avg depth (m)	1968.14	**Altares Packstone Member Avg depth (m)**	1834.55
“*Claraia* Zone” Avg thickness (m)	5.65	**Altares Packstone Member Avg Thickness (m)**	8.9
“*Claraia* Zone” Max thickness (m)	18.2	**Altares Packstone Member Max Thickness (m)**	22.7
“*Claraia* Zone” Min Thickness (m)	2	**Altares Packstone Member Min Thickness (m)**	1.7

Appendix E: Core Lithology Logs

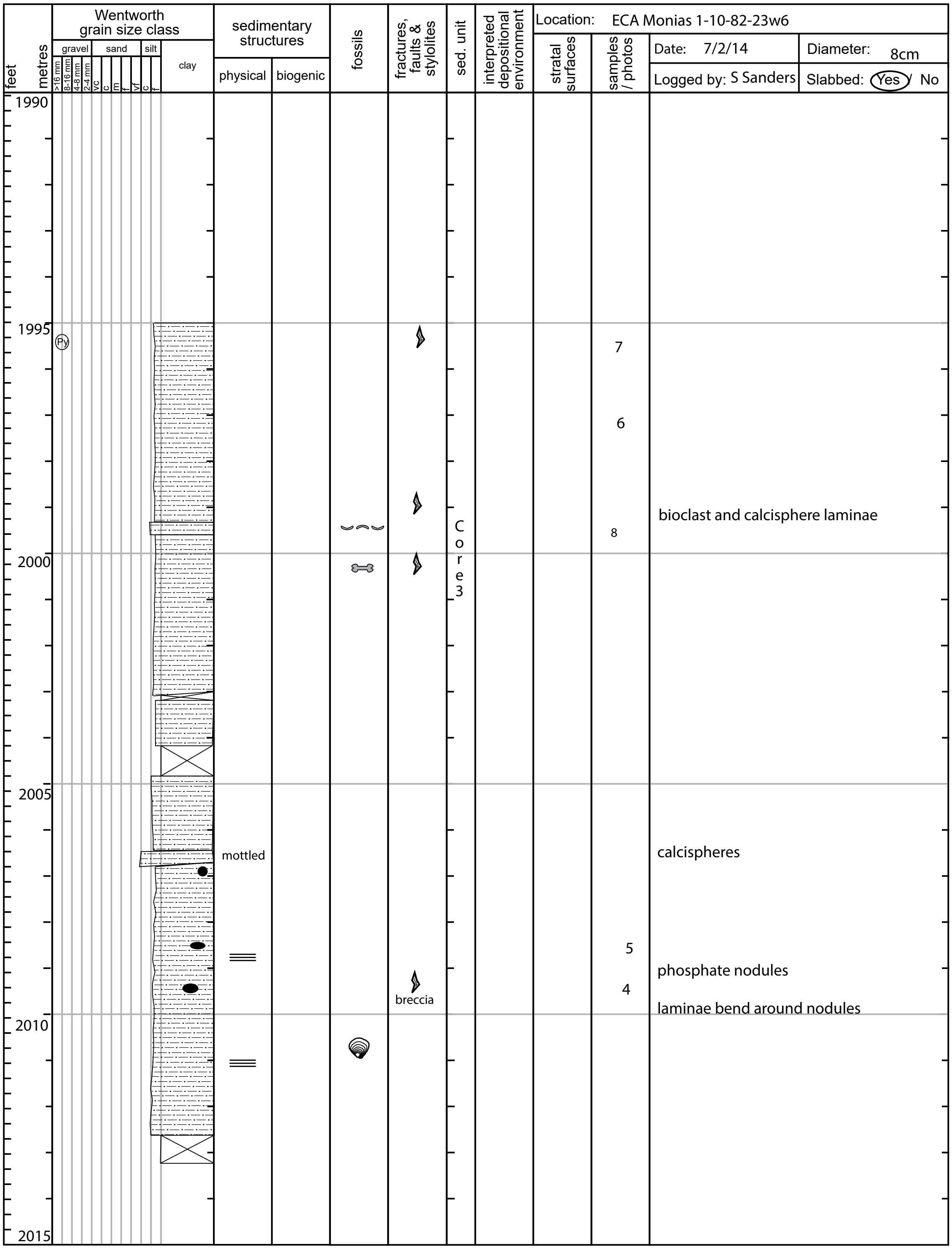

Location: ECA Monias 1-10-82-23w6

Date: 7/2/14

Diameter: 8cm

Logged by: S Sanders

Slabbed: [✓ Yes] / No

feet
metres
Wentworth grain size class
gravel
sand
silt
clay
>16 mm
8-16 mm
4-8 mm
2-4 mm
vc
c
m
f
vf
c
f
sedimentary structures
physical
biogenic
fossils
fractures, faults & stylolites
sed. unit
interpreted depositional environment
stratal surfaces
samples / photos
1990
1995
Py
7
6
bioclast and calcisphere laminae
8
Core 3
2000
2005
mottled
calcispheres
5
phosphate nodules
4
breccia
laminae bend around nodules
2010
2015

Location: Devon Monias 03-30-082-20w6 p1

Date: 7/2/14

Diameter: 8.5cm

Logged by: S Sanders

Slabbed: [✓ Yes]/ No

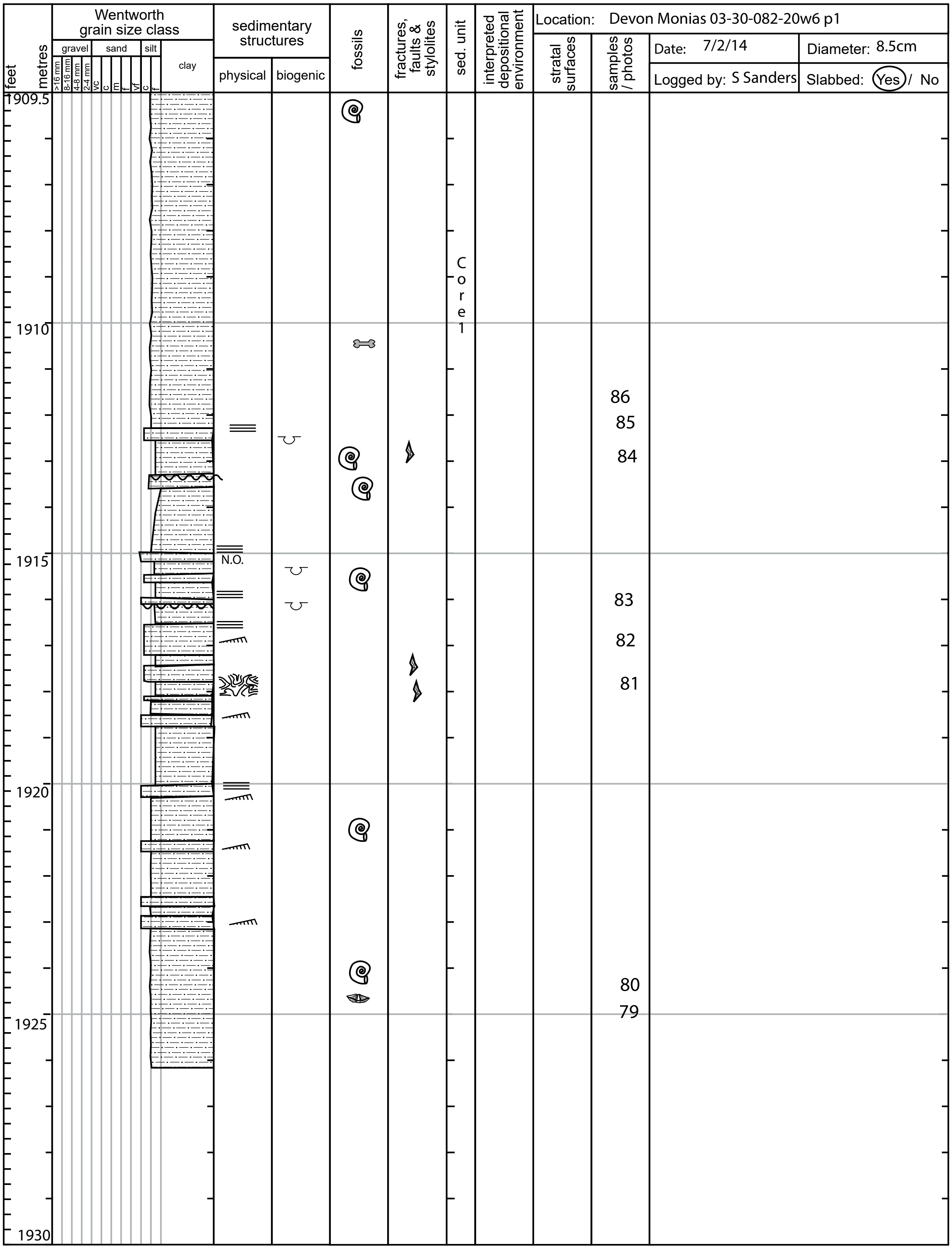
feet
metres
Wentworth grain size class
gravel
sand
silt
clay
>16 mm
8-16 mm
4-8 mm
2-4 mm
vc
c
m
f
vf
c
f
sedimentary structures
physical
biogenic
fossils
fractures, faults & stylolites
sed. unit
interpreted depositional environment
stratal surfaces
samples / photos
1909.5
1910
1915
1920
1925
1930
Core 1
N.O.
86
85
84
83
82
81
80
79

Location: Devon Monias 03-30-082-20w6 p2

Date: 7/2/14

Diameter: 8.5cm

Logged by: S Sanders

Slabbed: [✓ Yes] / No

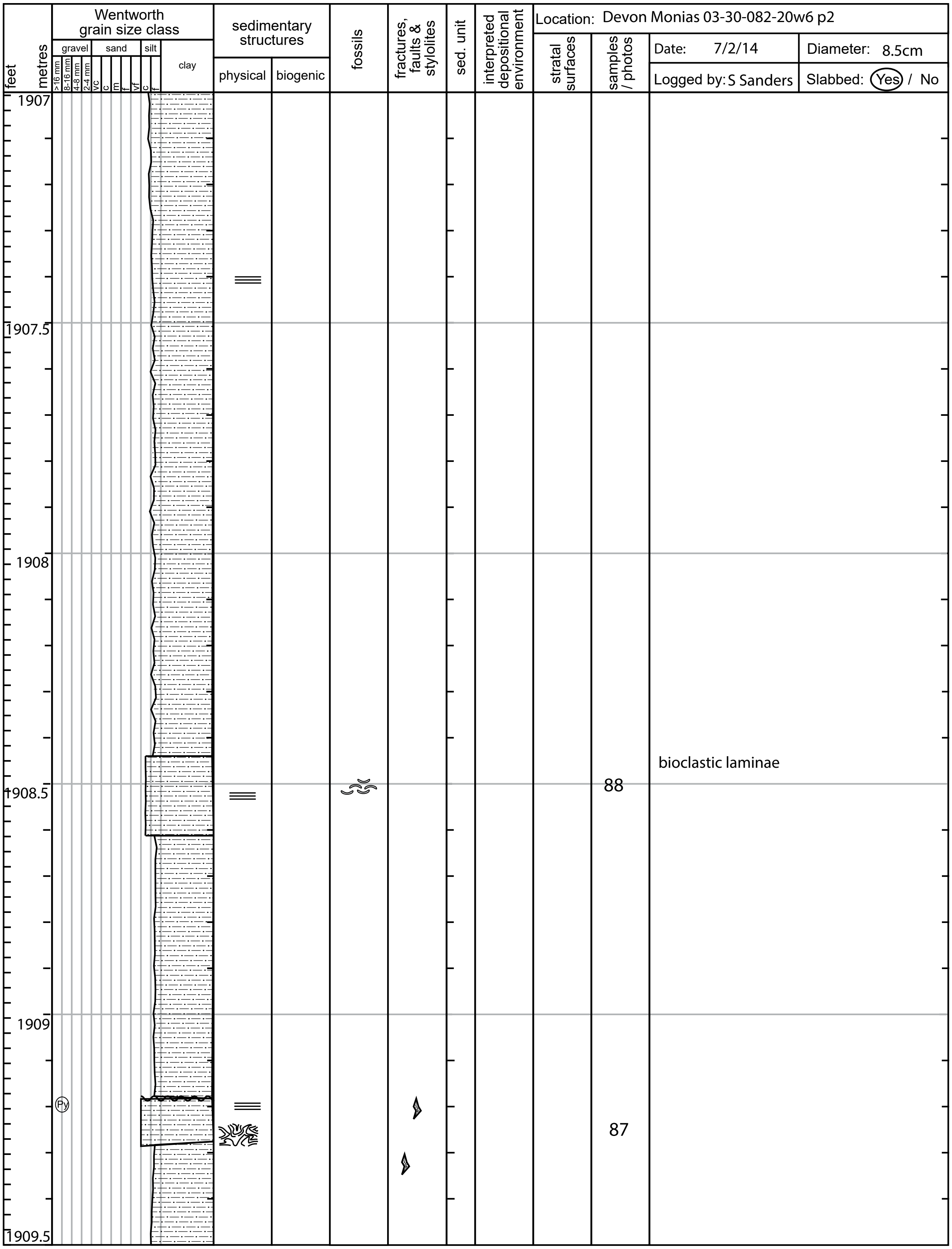

feet
metres
Wentworth grain size class
gravel
sand
silt
clay
>16 mm
8-16 mm
4-8 mm
2-4 mm
vc
c
m
f
vf
c
f
sedimentary structures
physical
biogenic
fossils
fractures, faults & stylolites
sed. unit
interpreted depositional environment
stratal surfaces
samples / photos
1907
1907.5
1908
1908.5
1909
1909.5
Py
88
87

bioclastic laminae

Location: Devon Monias 03-30-082-20w6 p3

Date: 7/2/14

Diameter: 8.5cm

Logged by: S Sanders

Slabbed: [✓ Yes] / No

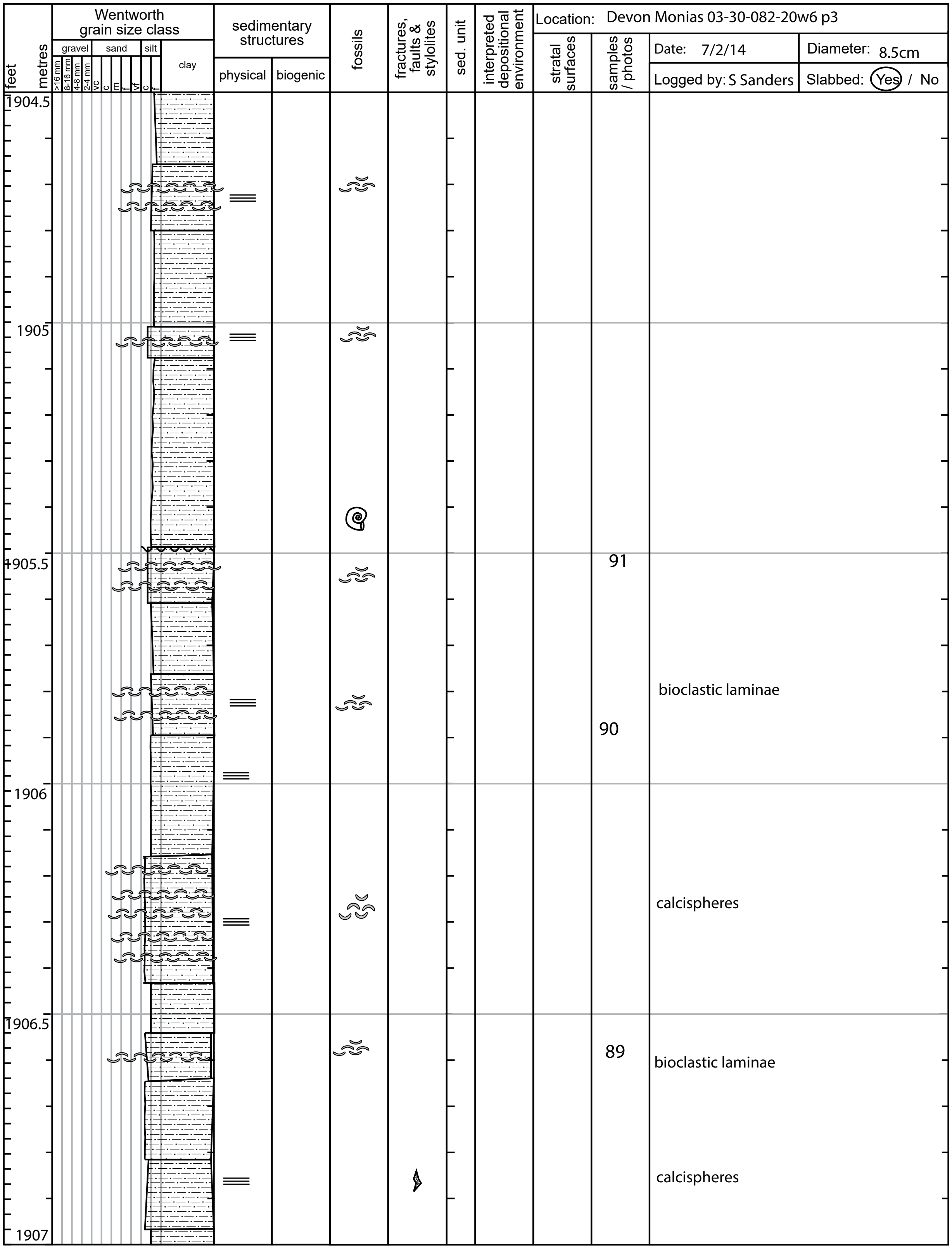

feet
metres
Wentworth grain size class
gravel
sand
silt
clay
>16 mm
8-16 mm
4-8 mm
2-4 mm
vc
c
m
f
vf
c
f
sedimentary structures
physical
biogenic
fossils
fractures, faults & stylolites
sed. unit
interpreted depositional environment
stratal surfaces
samples / photos
1904.5
1905
1905.5
1906
1906.5
1907
91
90
89
bioclastic laminae
calcispheres
bioclastic laminae
calcispheres

Location: Devon Monias 03-30-082-20w6 p4

Date: 7/2/14

Diameter: 8.5cm

Logged by: S Sanders

Slabbed: [✓ Yes] / No

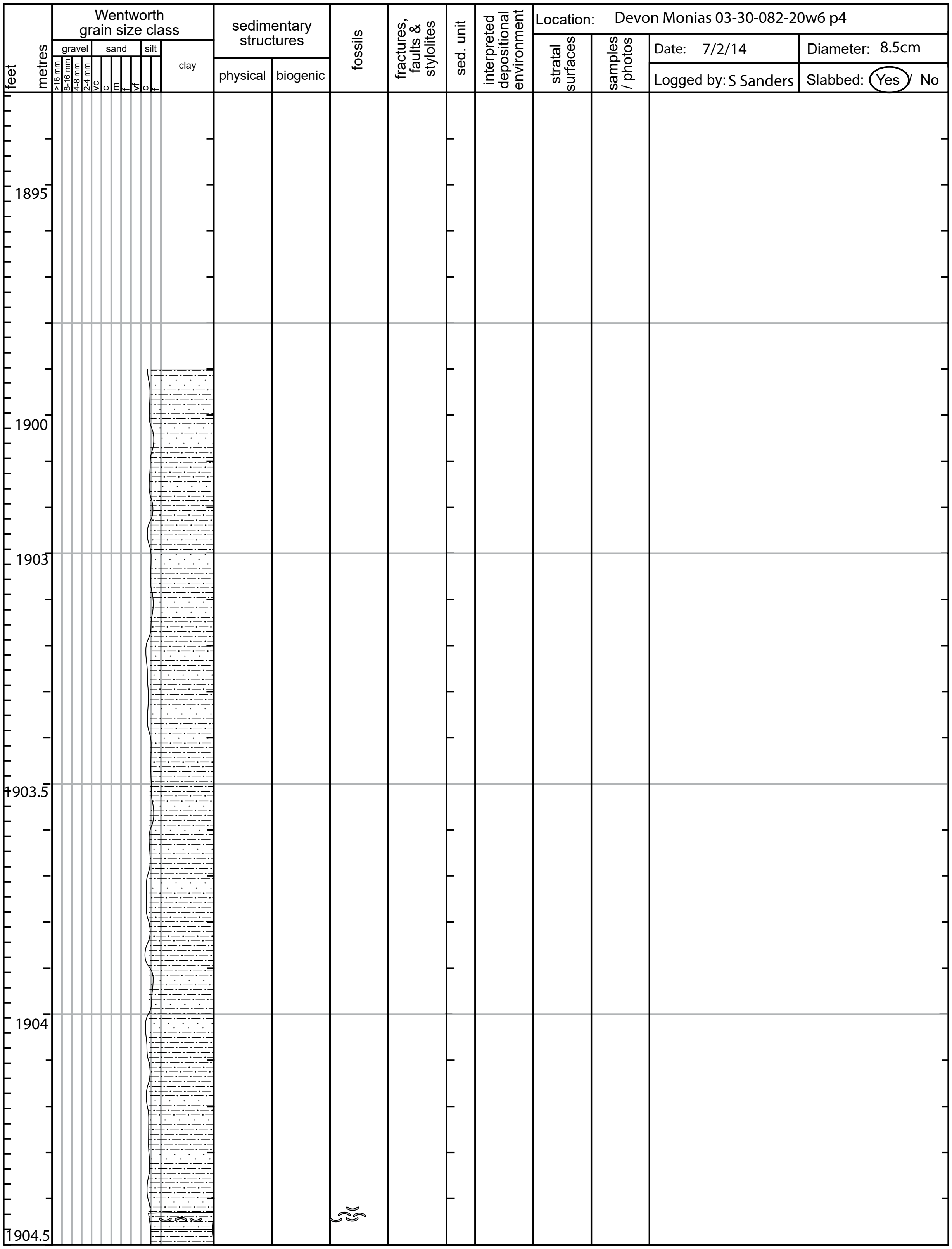
feet
metres
Wentworth grain size class
gravel
sand
silt
clay
>16 mm
8-16 mm
4-8 mm
2-4 mm
vc
c
m
f
vf
c
f
sedimentary structures
physical
biogenic
fossils
fractures, faults & stylolites
sed. unit
interpreted depositional environment
stratal surfaces
samples / photos
1895
1900
1903
1903.5
1904
1904.5

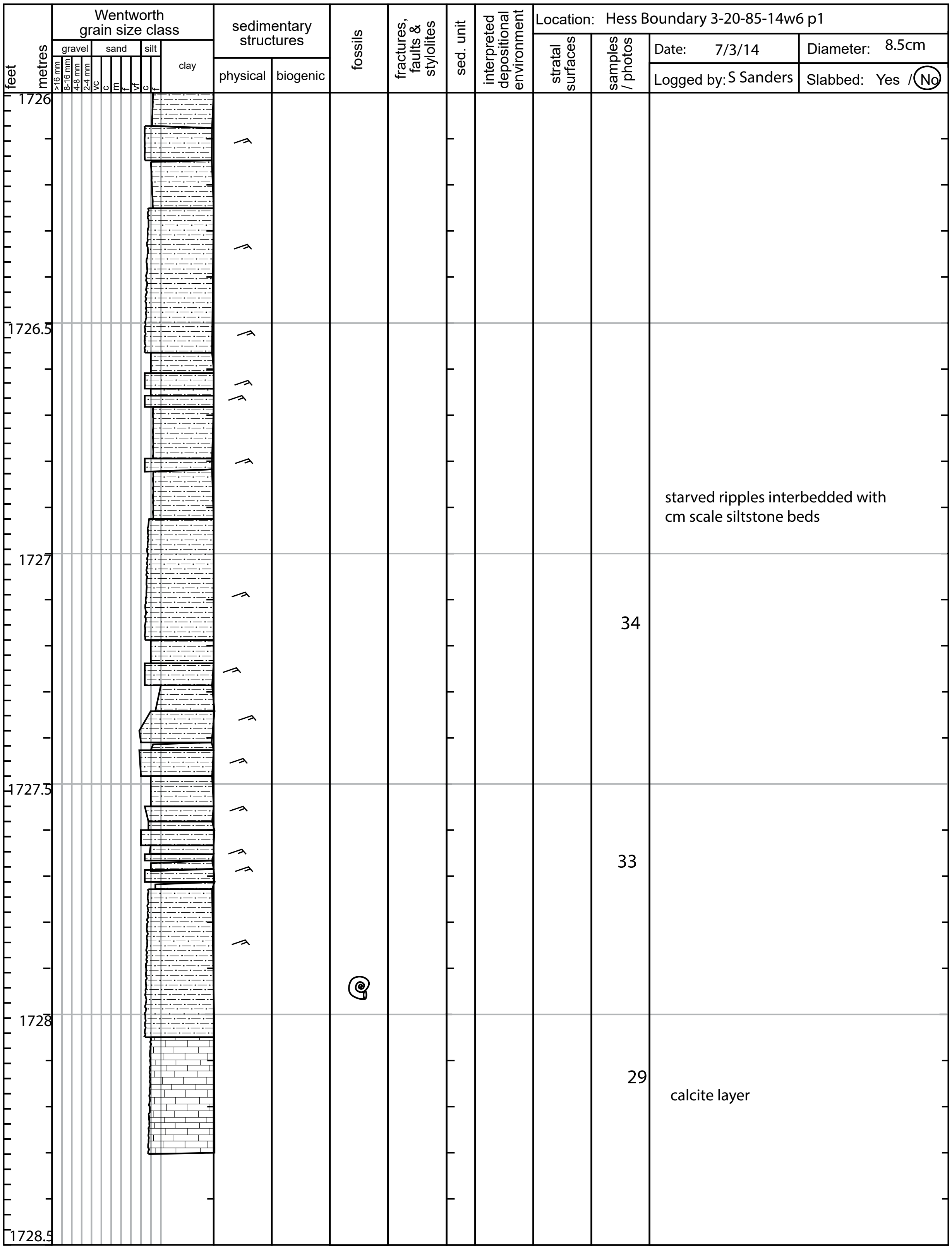
feet
metres
Wentworth grain size class
gravel
sand
silt
clay
>16 mm
8-16 mm
4-8 mm
2-4 mm
vc
c
m
f
vf
c
f
sedimentary structures
physical
biogenic
fossils
fractures, faults & stylolites
sed. unit
interpreted depositional environment
stratal surfaces
samples / photos
1726
1726.5
1727
1727.5
1728
1728.5

Location: Hess Boundary 3-20-85-14w6 p1

Date: 7/3/14

Diameter: 8.5cm

Logged by: S Sanders

Slabbed: Yes / [✓ No]

34

33

29

starved ripples interbedded with cm scale siltstone beds

calcite layer

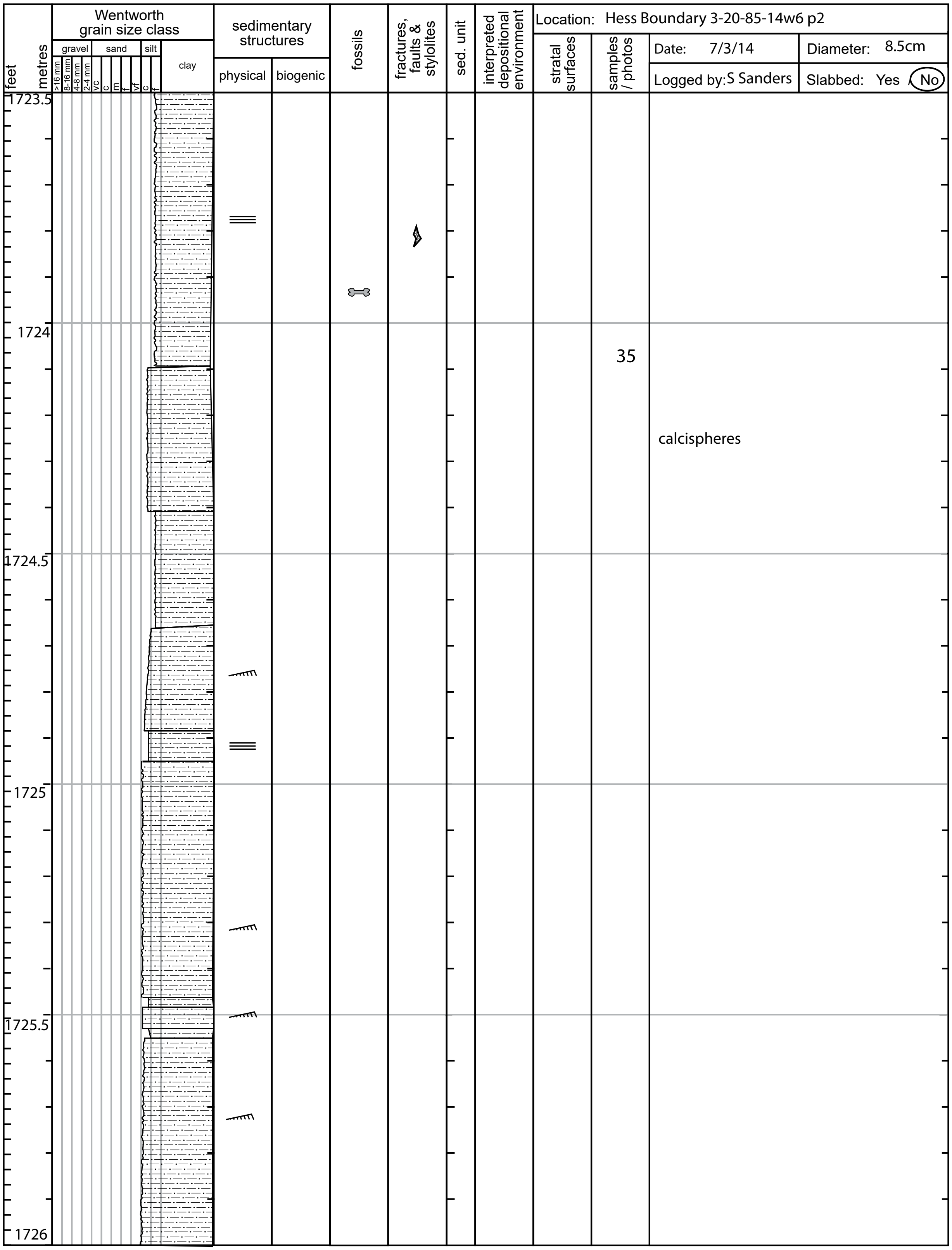
feet
metres
Wentworth grain size class
gravel
sand
silt
clay
>16 mm
8-16 mm
4-8 mm
2-4 mm
vc
c
m
f
vf
c
f
sedimentary structures
physical
biogenic
fossils
fractures, faults & stylolites
sed. unit
interpreted depositional environment
stratal surfaces
samples / photos
1723.5
1724
1724.5
1725
1725.5
1726

Location: Hess Boundary 3-20-85-14w6 p2

Date: 7/3/14

Diameter: 8.5cm

Logged by: S Sanders

Slabbed: Yes [✓ No]

35

calcispheres

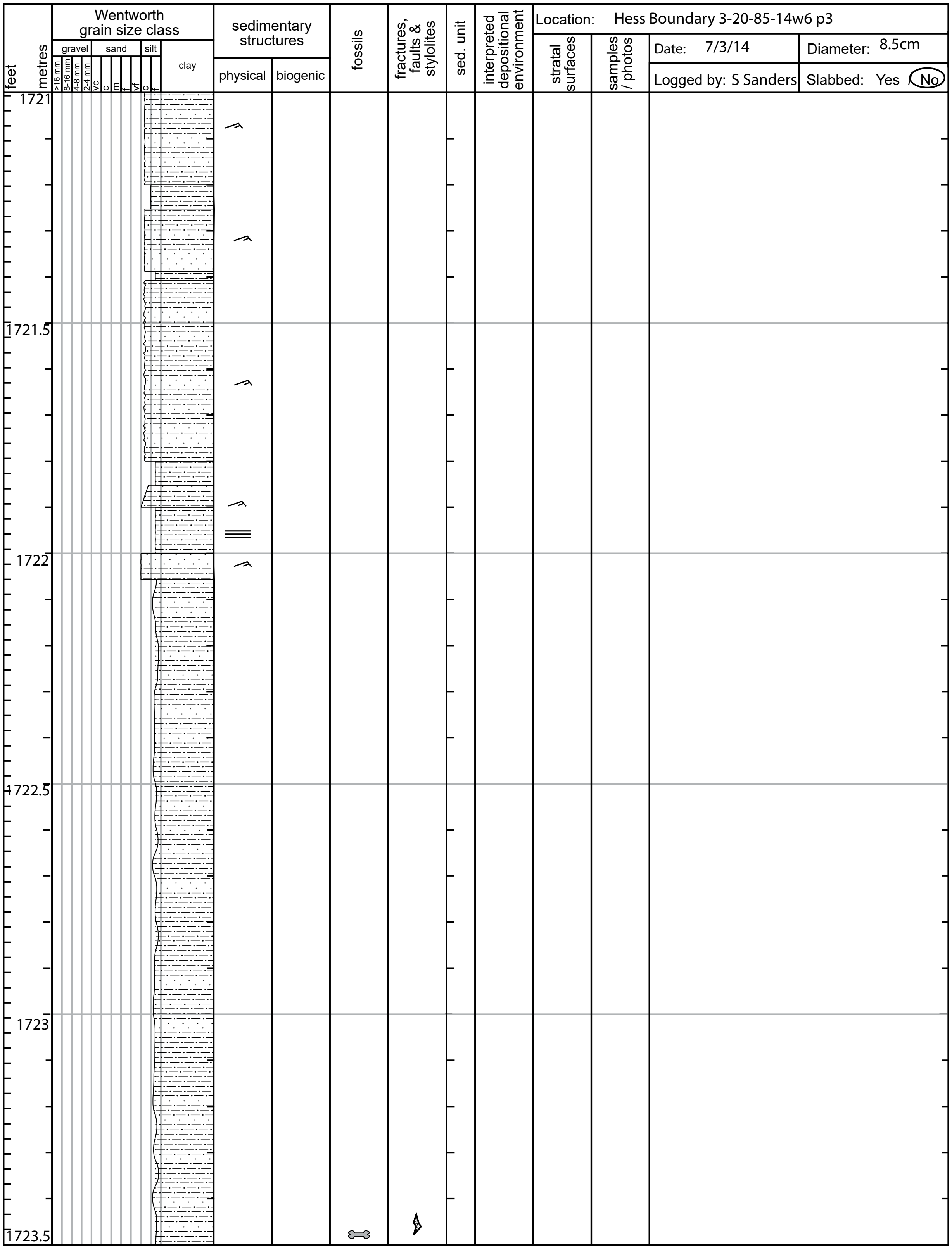
feet
metres
Wentworth grain size class
gravel
sand
silt
clay
>16 mm
8-16 mm
4-8 mm
2-4 mm
vc
c
m
f
vf
c
f
sedimentary structures
physical
biogenic
fossils
fractures, faults & stylolites
sed. unit
interpreted depositional environment
stratal surfaces
samples / photos
1721
1721.5
1722
1722.5
1723
1723.5

Location: Hess Boundary 3-20-85-14w6 p3

Date: 7/3/14

Diameter: 8.5cm

Logged by: S Sanders

Slabbed: Yes [✓ No]

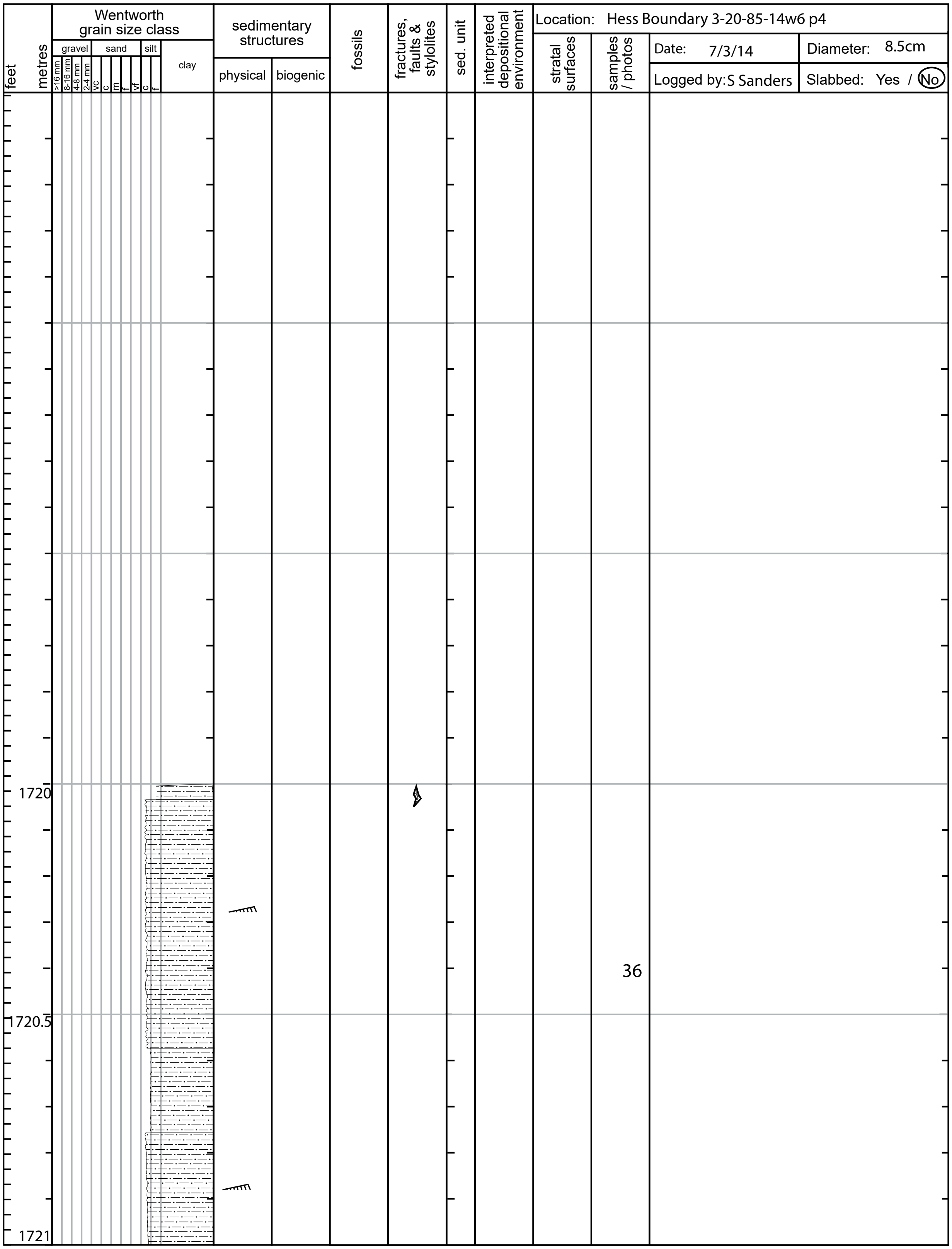
feet
metres
Wentworth grain size class
gravel
sand
silt
clay
>16 mm
8-16 mm
4-8 mm
2-4 mm
vc
c
m
f
vf
c
f
sedimentary structures
physical
biogenic
fossils
fractures, faults & stylolites
sed. unit
interpreted depositional environment
stratal surfaces
samples / photos
1720
1720.5
1721
36

Location: Hess Boundary 3-20-85-14w6 p4

Date: 7/3/14

Diameter: 8.5cm

Logged by: S Sanders

Slabbed: Yes / [✓ No]

Location: Arcres Attachie 04-09-084-22w6

Date: 7/3/14

Diameter: 8cm

Logged by: S Sanders

Slabbed: [✓ Yes] / No

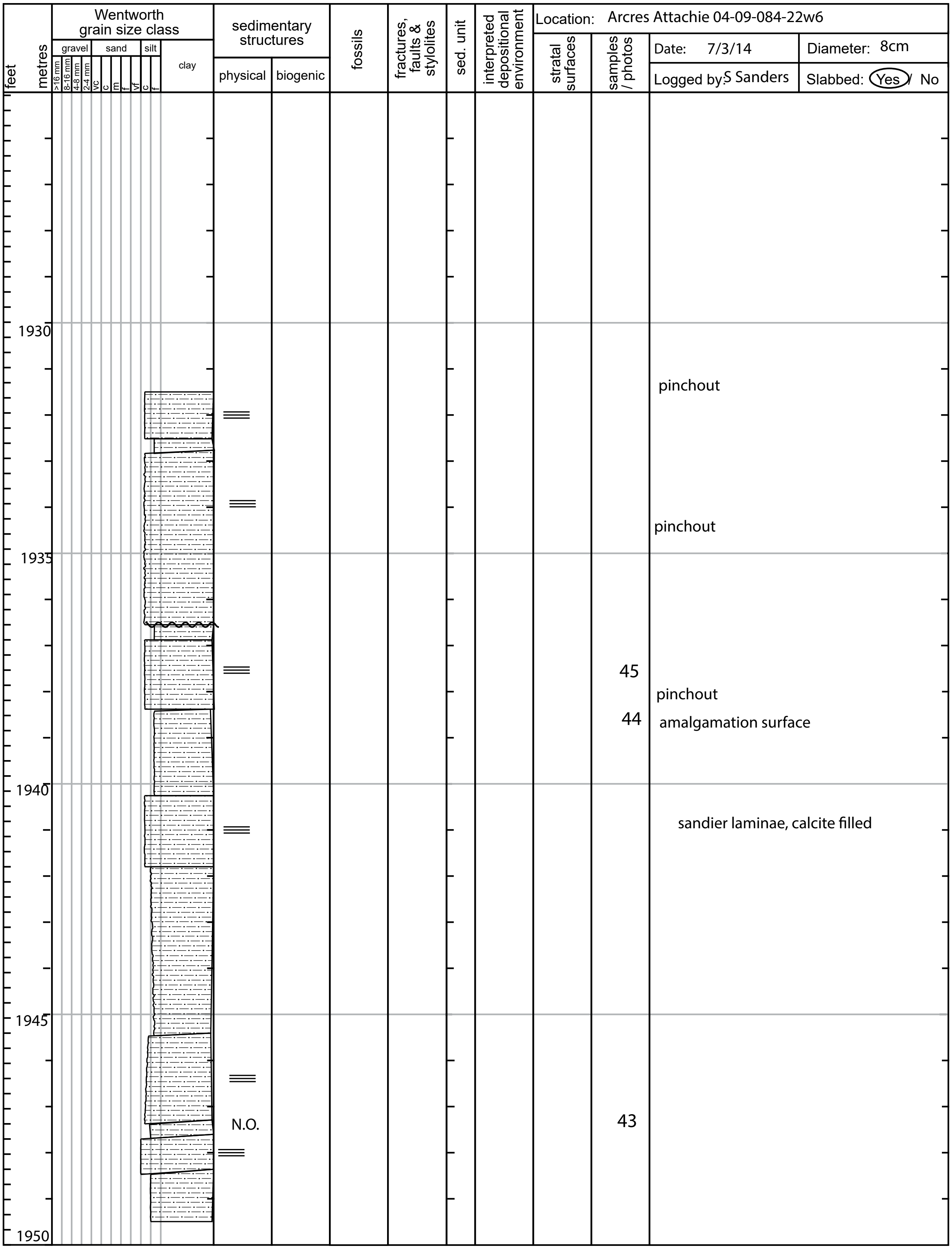
feet
metres
Wentworth grain size class
gravel
sand
silt
clay
>16 mm
8-16 mm
4-8 mm
2-4 mm
vc
c
m
f
vf
c
f
sedimentary structures
physical
biogenic
fossils
fractures, faults & stylolites
sed. unit
interpreted depositional environment
stratal surfaces
samples / photos
1930
1935
1940
1945
1950
pinchout
pinchout
45
pinchout
44
amalgamation surface
sandier laminae, calcite filled
N.O.
43

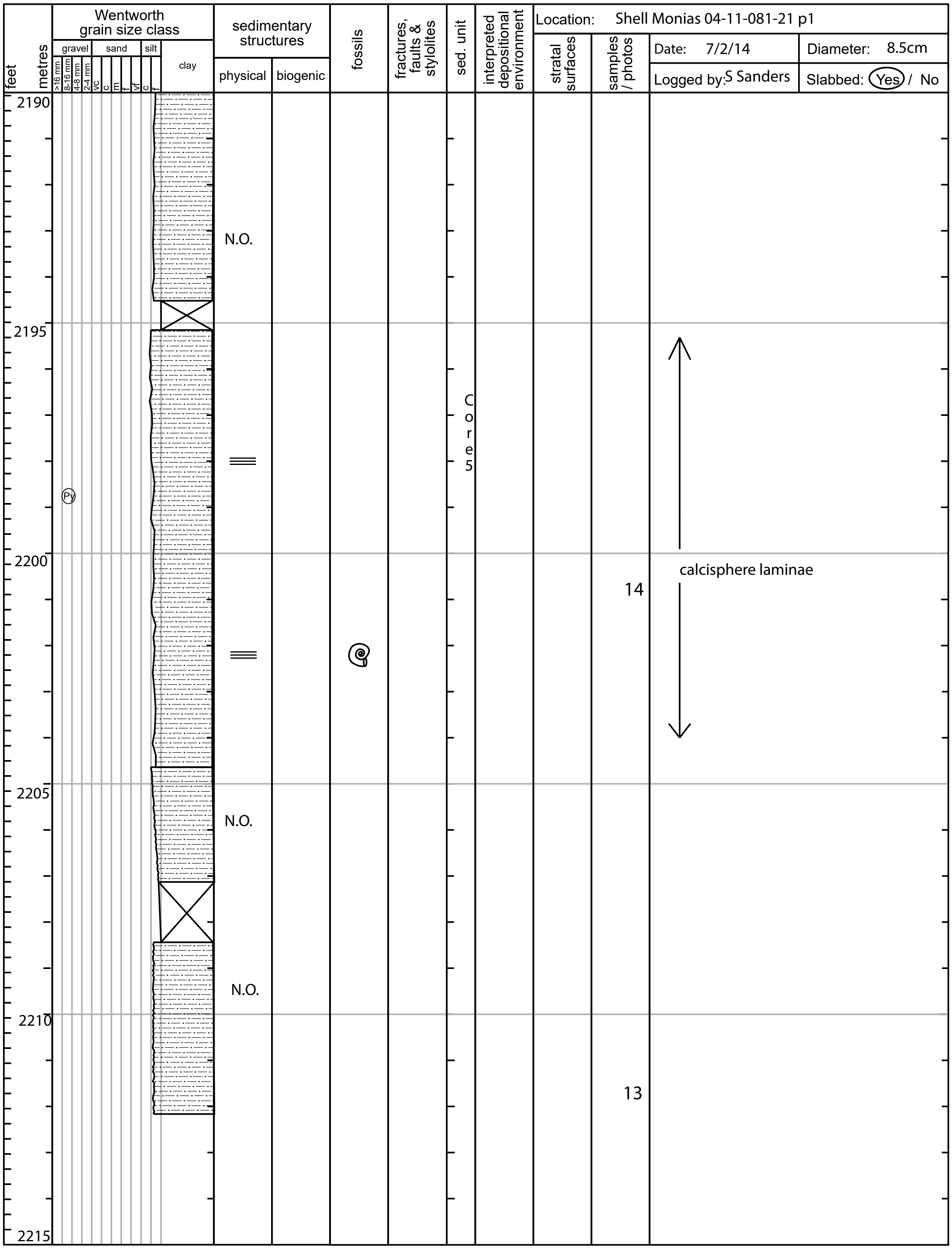
Location: Shell Monias 04-11-081-21 p1

Date: 7/2/14

Diameter: 8.5cm

Logged by: S Sanders

Slabbed: [✓ Yes] / No

feet
metres
Wentworth grain size class
gravel
sand
silt
clay
>16 mm
8-16 mm
4-8 mm
2-4 mm
vc
c
m
f
vf
c
f
sedimentary structures
physical
biogenic
fossils
fractures, faults & stylolites
sed. unit
interpreted depositional environment
stratal surfaces
samples / photos
2190
2195
2200
2205
2210
2215
N.O.
Py
Core 5
14
calcisphere laminae
N.O.
N.O.
13

Location: Shell Monias 04-11-081-21 p2

Date: 7/2/14

Diameter: 8.5cm

Logged by: S Sanders

Slabbed: [✓ Yes] / No

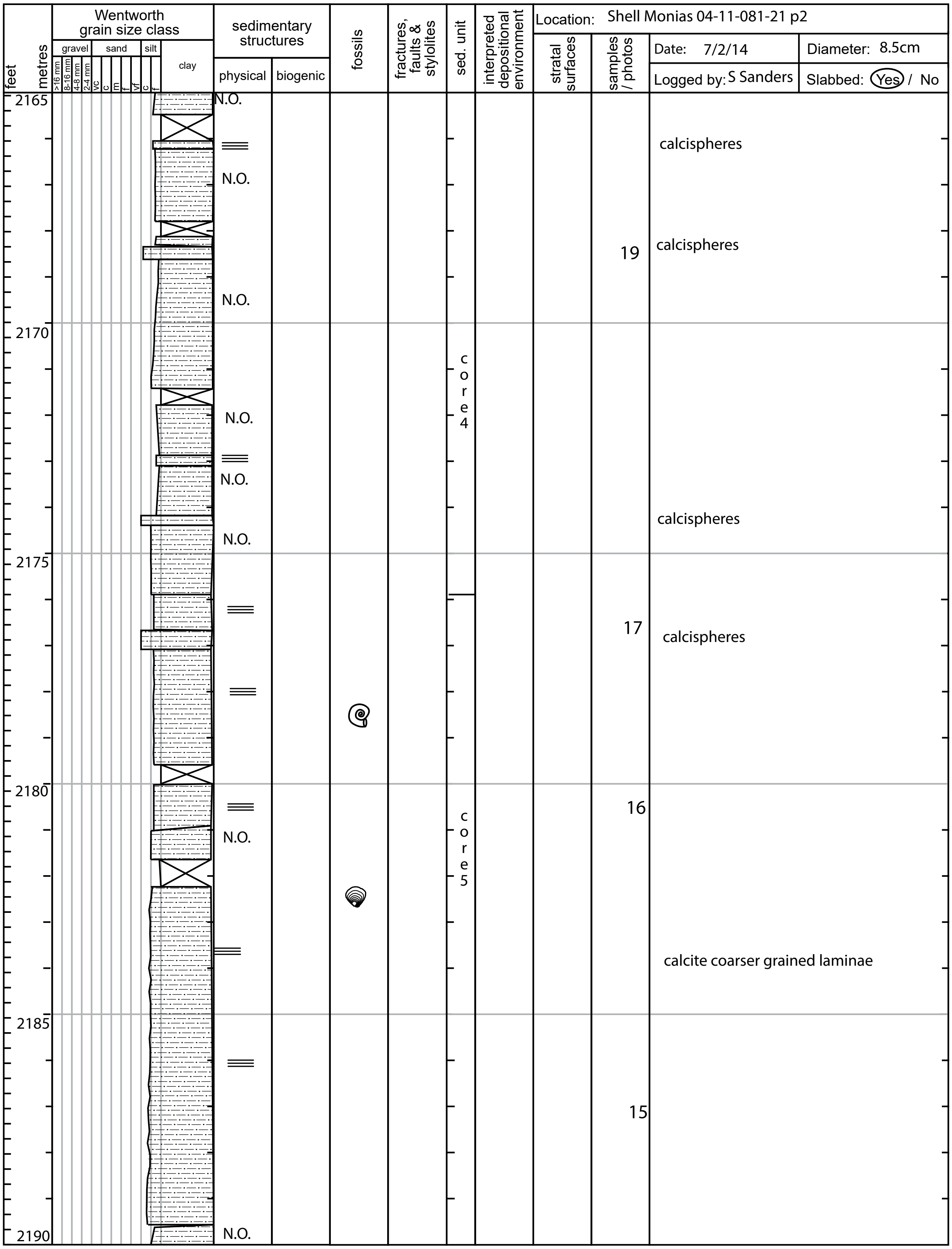

feet
metres
Wentworth grain size class
gravel
sand
silt
clay
>16 mm
8-16 mm
4-8 mm
2-4 mm
vc
c
m
f
vf
c
f
sedimentary structures
physical
biogenic
fossils
fractures, faults & stylolites
sed. unit
interpreted depositional environment
stratal surfaces
samples / photos
2165
2170
2175
2180
2185
2190
N.O.
N.O.
N.O.
N.O.
N.O.
N.O.
N.O.
N.O.
core 4
core 5
19
17
16
15
calcispheres
calcispheres
calcispheres
calcispheres
calcite coarser grained laminae

Location: Shell Monias 04-11-081-21 p3

Date: 7/2/14

Diameter: 8.5cm

Logged by:S Sanders

Slabbed: [✓ Yes] / No

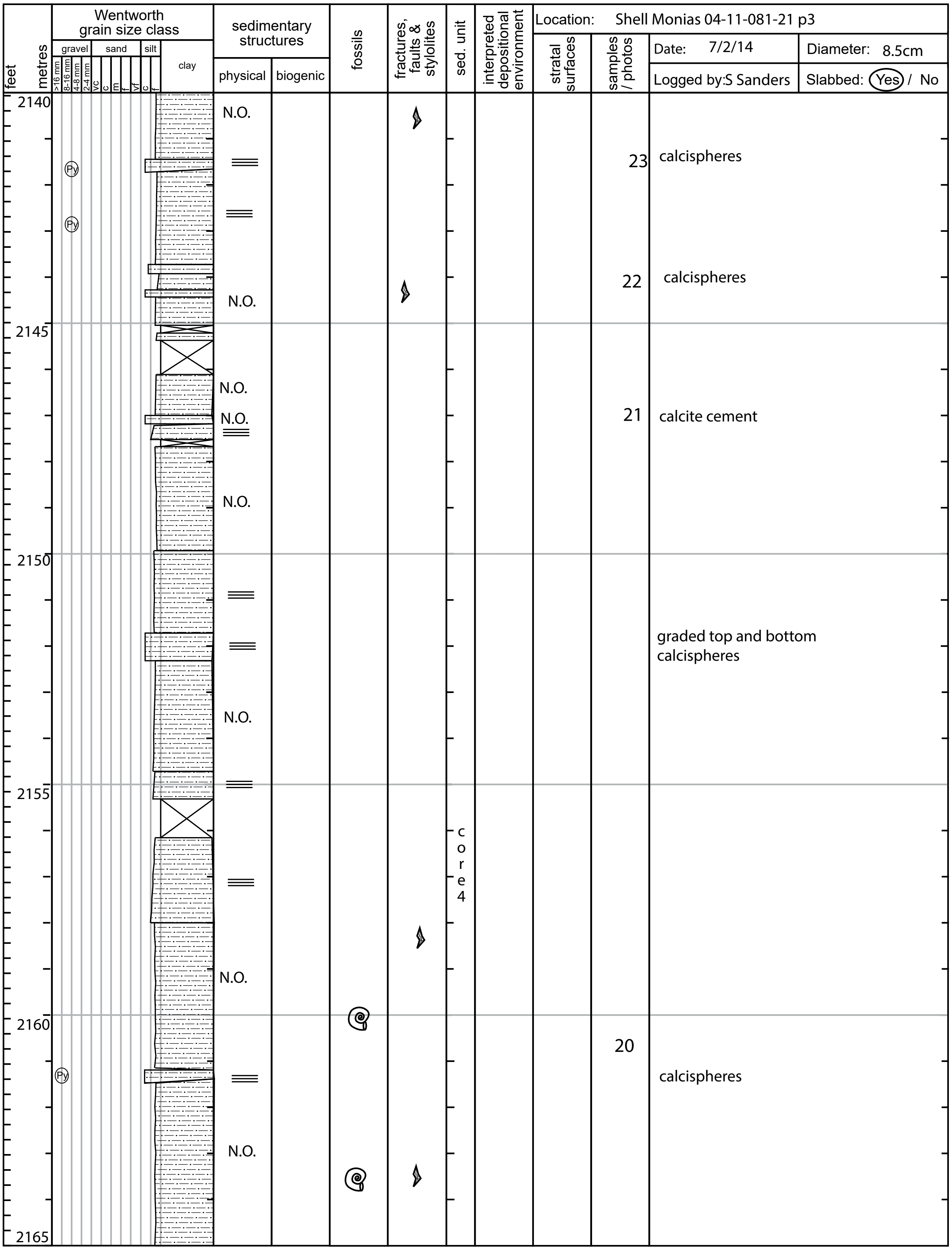
feet
metres
Wentworth grain size class
gravel
sand
silt
clay
>16 mm
8-16 mm
4-8 mm
2-4 mm
vc
c
m
f
vf
c
f
sedimentary structures
physical
biogenic
fossils
fractures, faults & stylolites
sed. unit
interpreted depositional environment
stratal surfaces
samples / photos
2140
2145
2150
2155
2160
2165
Py
Py
Py
N.O.
N.O.
N.O.
N.O.
N.O.
N.O.
N.O.
N.O.
N.O.
core 4
23
calcispheres
22
calcispheres
21
calcite cement
graded top and bottom
calcispheres
20
calcispheres

Location: Shell Monias 04-11-081-21 p4
Date: 7/2/14
Diameter: 8.5cm
Logged by: S Sanders
Slabbed: [✓ Yes] / No

feet	metres	Wentworth grain size class gravel: >16 mm, 8-16 mm, 4-8 mm, 2-4 mm sand: vc, c, m, f, vf silt: c, f clay	sedimentary structures: physical	sedimentary structures: biogenic	fossils	fractures, faults & stylolites	sed. unit	interpreted depositional environment	stratal surfaces	samples / photos	
2135											
							Core 4				
2140			N.O.								

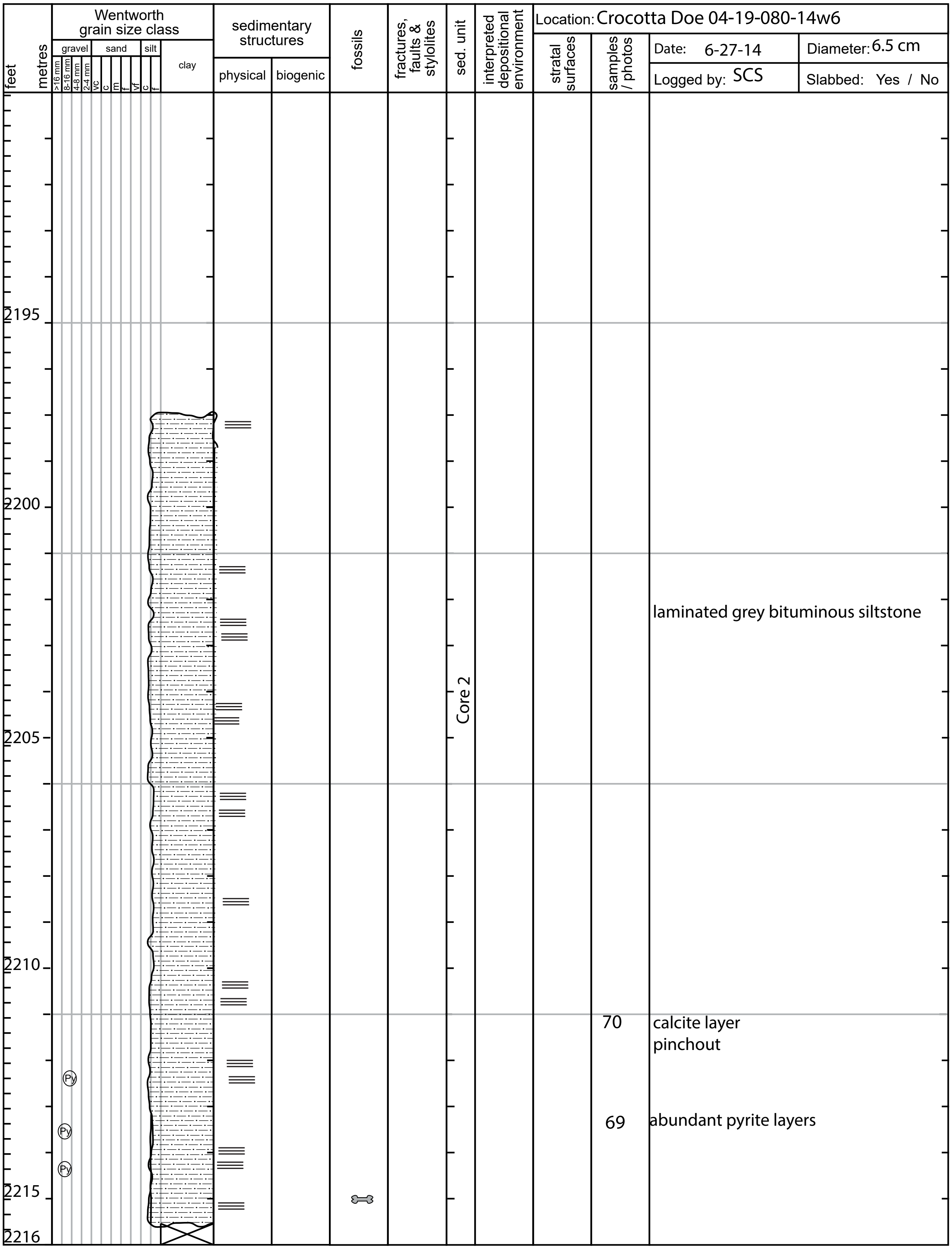
Wentworth grain size class
gravel
sand
silt
clay
>16 mm
8-16 mm
4-8 mm
2-4 mm
vc
c
m
f
vf
c
f
feet
metres
sedimentary structures
physical
biogenic
fossils
fractures, faults & stylolites
sed. unit
interpreted depositional environment
strata surfaces
samples / photos
2195
2200
2205
2210
2215
2216
Core 2
Py
Py
Py

Location: Crocotta Doe 04-19-080-14w6

Date: 6-27-14

Diameter: 6.5 cm

Logged by: SCS

Slabbed: Yes / No

laminated grey bituminous siltstone

70 calcite layer pinchout

69 abundant pyrite layers

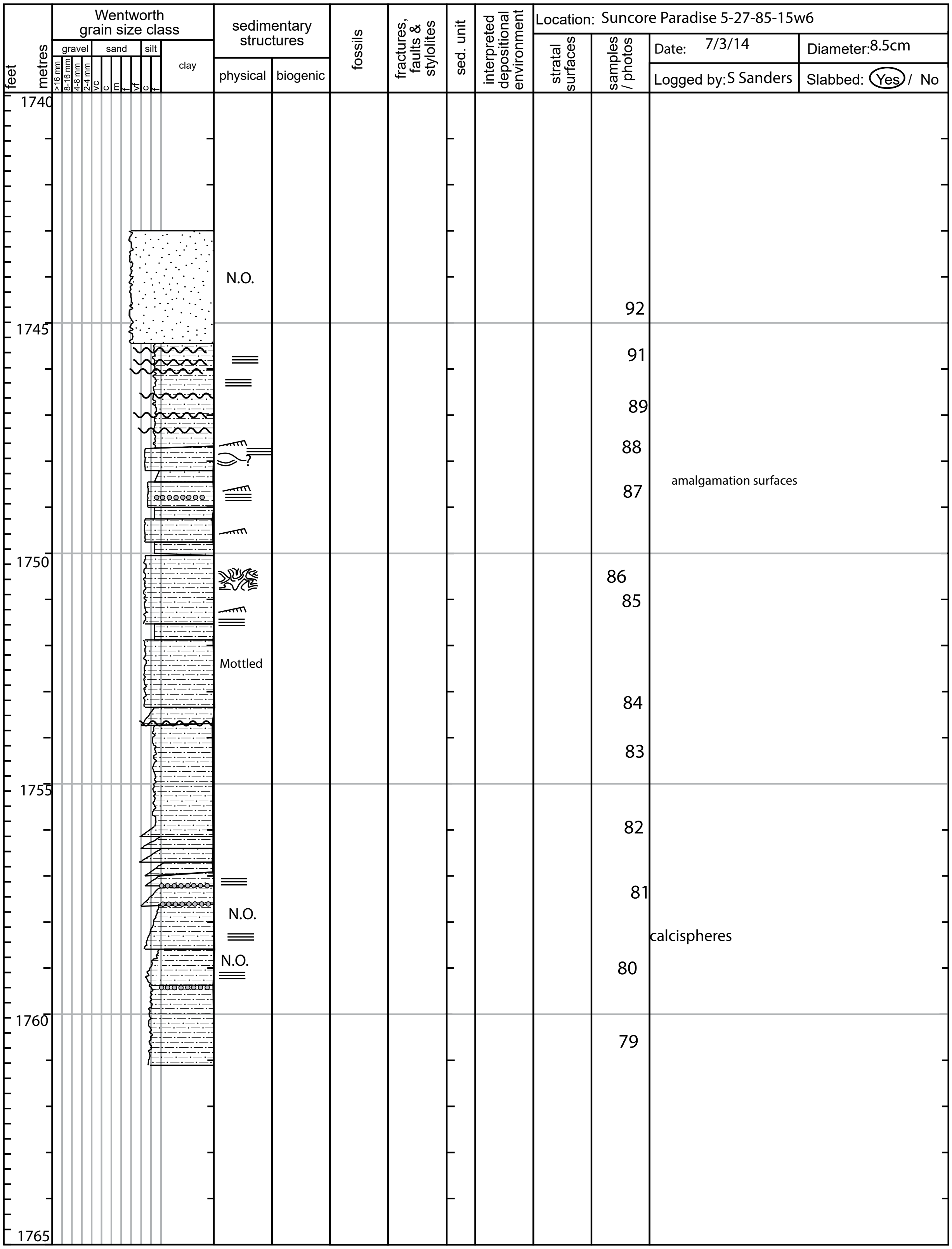
feet
metres
Wentworth grain size class
gravel
sand
silt
clay
>16 mm
8-16 mm
4-8 mm
2-4 mm
vc
c
m
f
vf
c
f
sedimentary structures
physical
biogenic
fossils
fractures, faults & stylolites
sed. unit
interpreted depositional environment
stratal surfaces
samples / photos
1740
1745
1750
1755
1760
1765
N.O.
Mottled
N.O.
N.O.
?
92
91
89
88
87
86
85
84
83
82
81
80
79
amalgamation surfaces
calcispheres

Location: Suncore Paradise 5-27-85-15w6

Date: 7/3/14

Diameter: 8.5cm

Logged by: S Sanders

Slabbed: [✓ Yes] / No

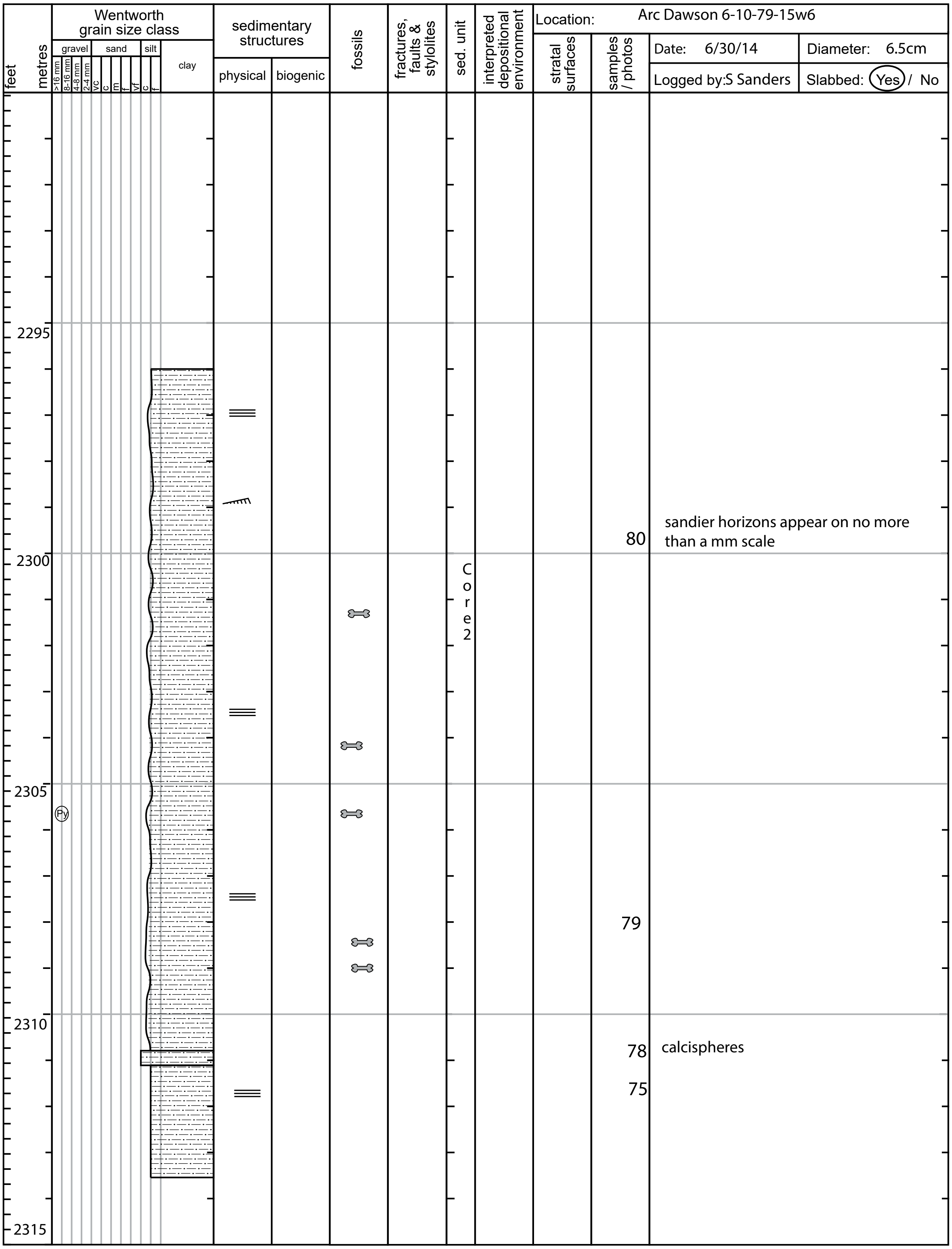

Location: Arc Dawson 6-10-79-15w6

Date: 6/30/14

Diameter: 6.5cm

Logged by: S Sanders

Slabbed: [✓ Yes] / No

80 sandier horizons appear on no more than a mm scale

78 calcispheres

feet
metres
Wentworth grain size class
gravel
sand
silt
clay
>16 mm
8-16 mm
4-8 mm
2-4 mm
vc
c
m
f
vf
c
f
sedimentary structures
physical
biogenic
fossils
fractures, faults & stylolites
sed. unit
interpreted depositional environment
stratal surfaces
samples / photos
2295
2300
2305
2310
2315
Py
Core 2
80
79
78
75

Location: AEC Flatrock 8-21-85-16w6 p1

Date: 7/4/14

Diameter: 8cm

Logged by: S Sanders

Slabbed: [✓ Yes] / No

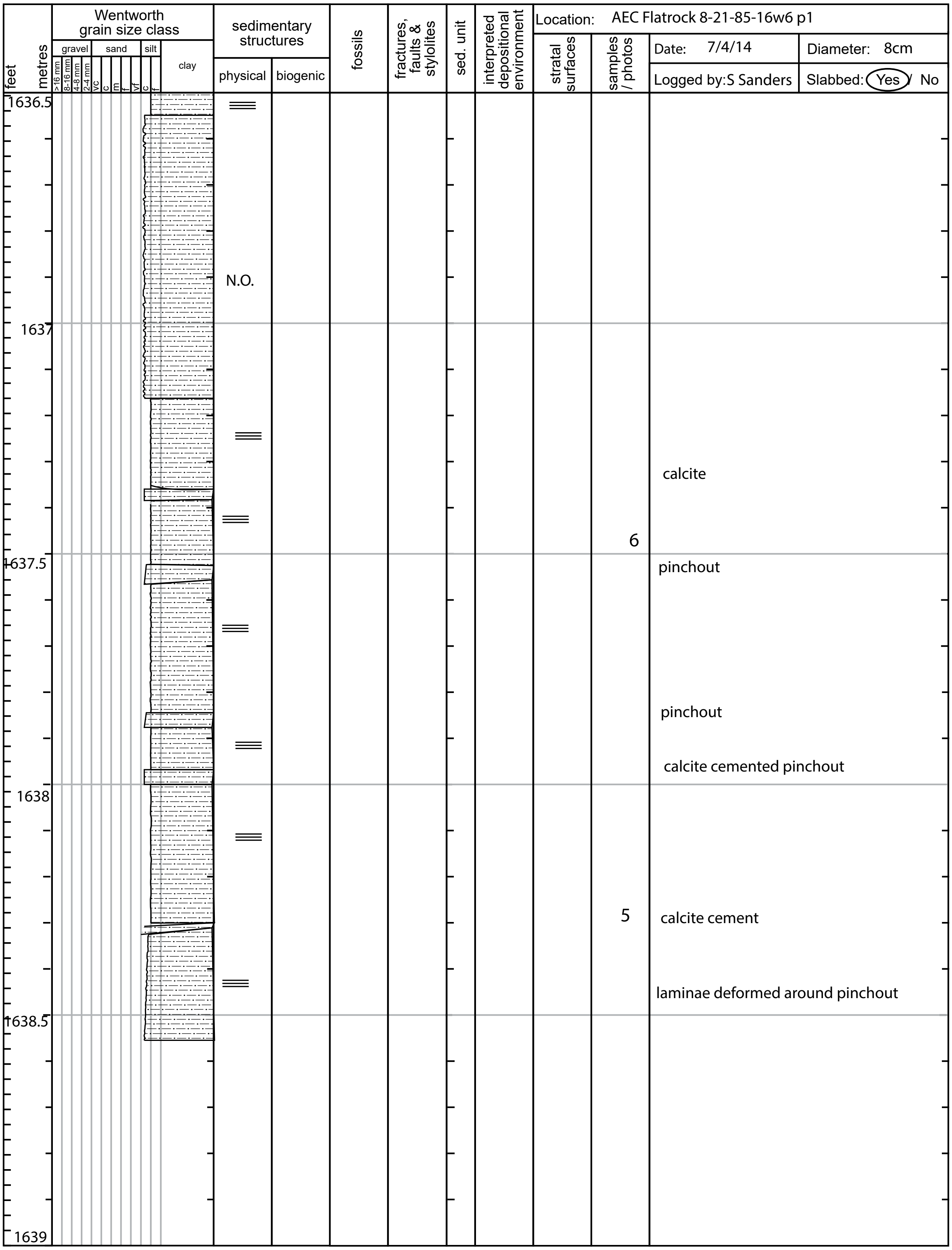
feet
metres
Wentworth grain size class
gravel
sand
silt
clay
>16 mm
8-16 mm
4-8 mm
2-4 mm
vc
c
m
f
vf
c
f
sedimentary structures
physical
biogenic
fossils
fractures, faults & stylolites
sed. unit
interpreted depositional environment
stratal surfaces
samples / photos
1636.5
N.O.
1637
6
1637.5
1638
5
1638.5
1639

calcite

pinchout

pinchout

calcite cemented pinchout

calcite cement

laminae deformed around pinchout

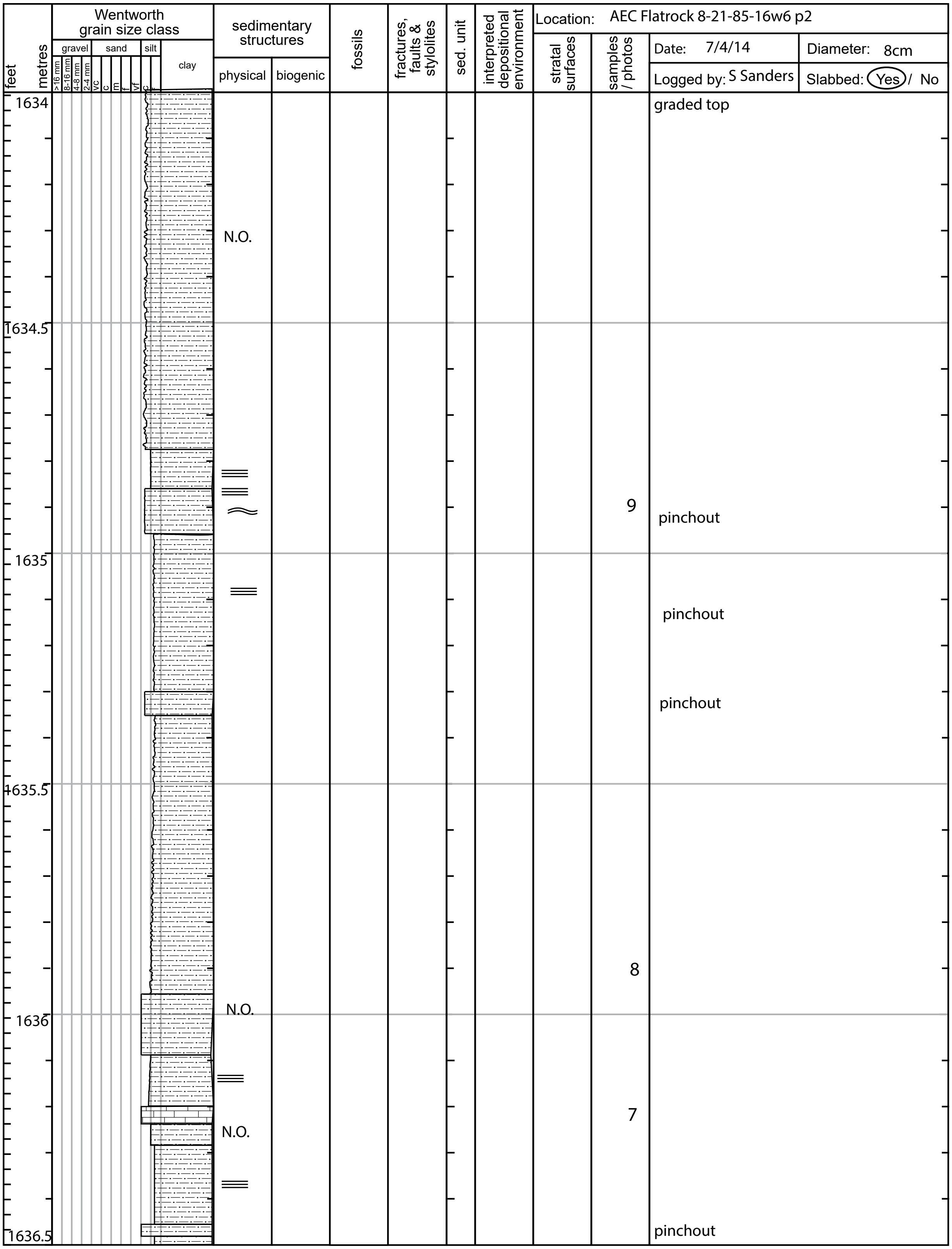
feet
metres
Wentworth grain size class
gravel
sand
silt
clay
>16 mm
8-16 mm
4-8 mm
2-4 mm
vc
c
m
f
vf
c
sedimentary structures
physical
biogenic
fossils
fractures, faults & stylolites
sed. unit
interpreted depositional environment
stratal surfaces
samples / photos
1634
1634.5
1635
1635.5
1636
1636.5
N.O.
N.O.
N.O.
9
8
7
graded top
pinchout
pinchout
pinchout
pinchout

Location: AEC Flatrock 8-21-85-16w6 p2

Date: 7/4/14

Diameter: 8cm

Logged by: S Sanders

Slabbed: [✓ Yes] / No

Location: AEC Flatrock 8-21-85-16w6 p3

Date: 7/4/14

Diameter: 8cm

Logged by: S Sanders

Slabbed: [✓ Yes] / No

feet	metres	Wentworth grain size class (gravel: >16 mm, 8-16 mm, 4-8 mm, 2-4 mm; sand: vc, c, m, f, vf; silt: c, f; clay)	sedimentary structures: physical	sedimentary structures: biogenic	fossils	fractures, faults & stylolites	sed. unit	interpreted depositional environment	stratal surfaces	samples / photos

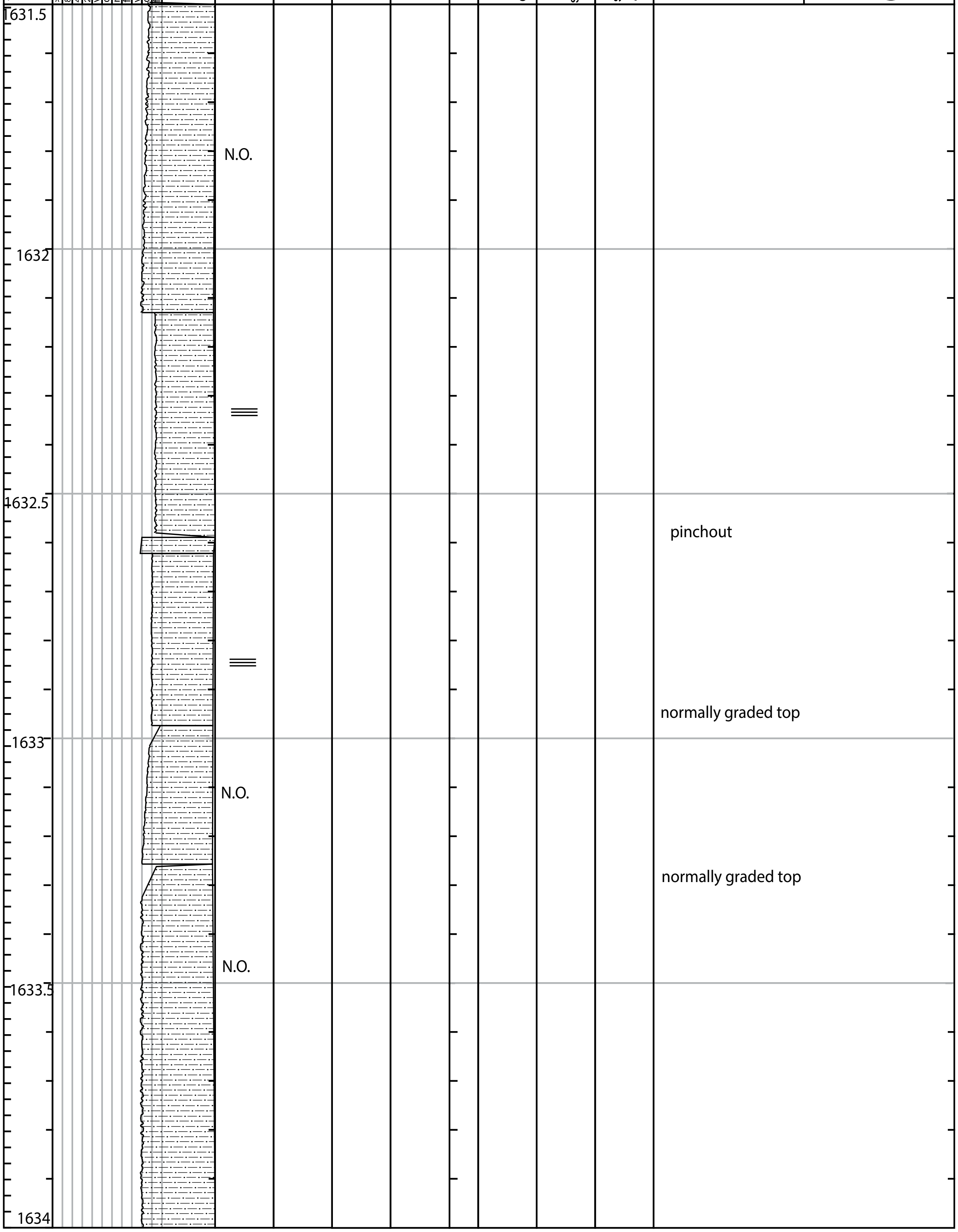
1631.5
N.O.
1632
1632.5
pinchout
1633
normally graded top
N.O.
normally graded top
N.O.
1633.5
1634

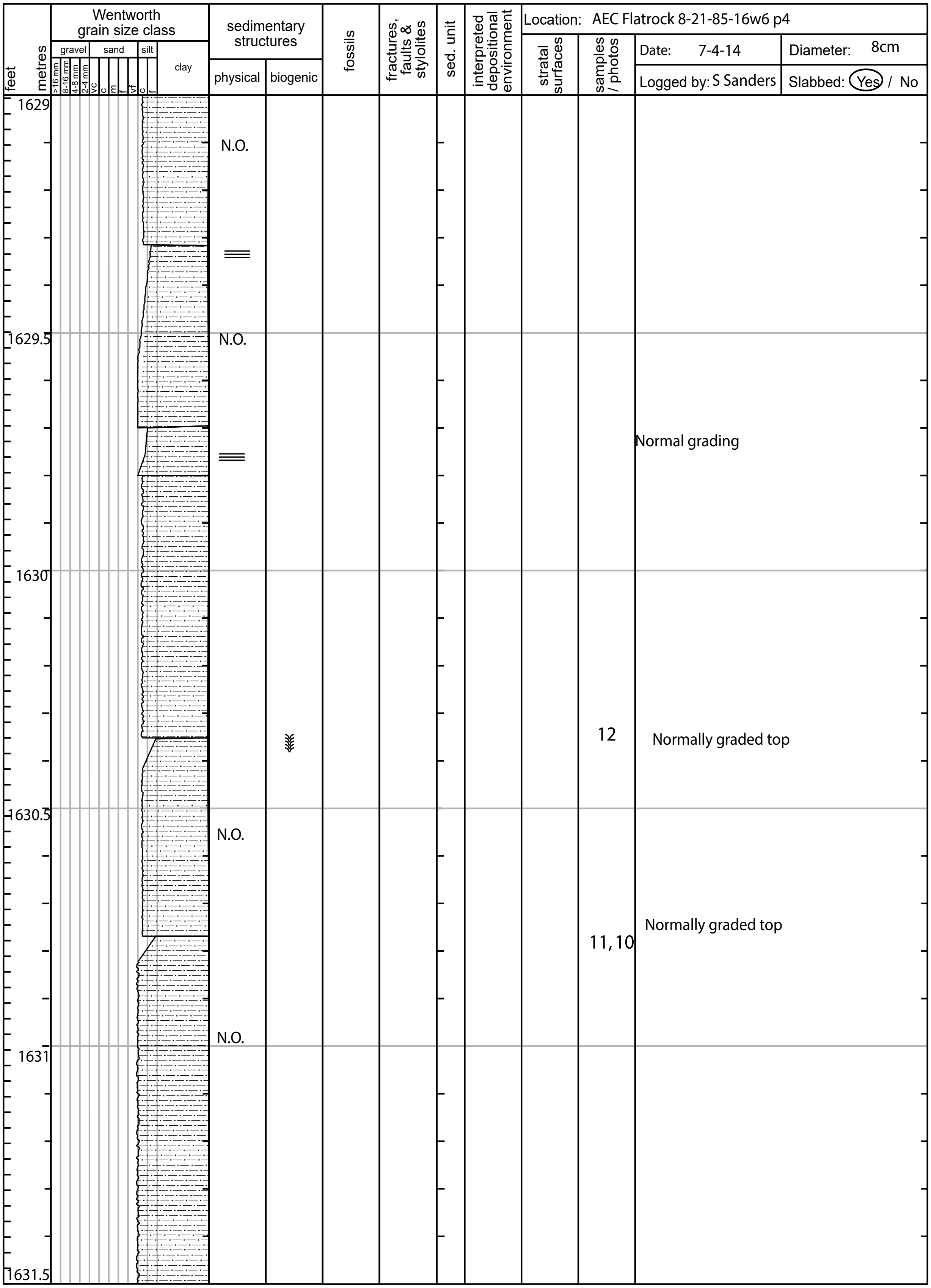
feet
metres
Wentworth grain size class
gravel
sand
silt
clay
>16 mm
8-16 mm
4-8 mm
2-4 mm
vc
c
m
f
vf
c
f
sedimentary structures
physical
biogenic
fossils
fractures, faults & stylolites
sed. unit
interpreted depositional environment
stratal surfaces
samples / photos
1629
1629.5
1630
1630.5
1631
1631.5
N.O.
N.O.
N.O.
N.O.
12
11, 10

Location: AEC Flatrock 8-21-85-16w6 p4

Date: 7-4-14

Diameter: 8cm

Logged by: S Sanders

Slabbed: [✓ Yes] / No

Normal grading

Normally graded top

Normally graded top

Location: AEC Flatrock 8-21-16w6 p5

Date: 7/4/14

Diameter: 8cm

Logged by: S Sanders

Slabbed: [✓ Yes] / No

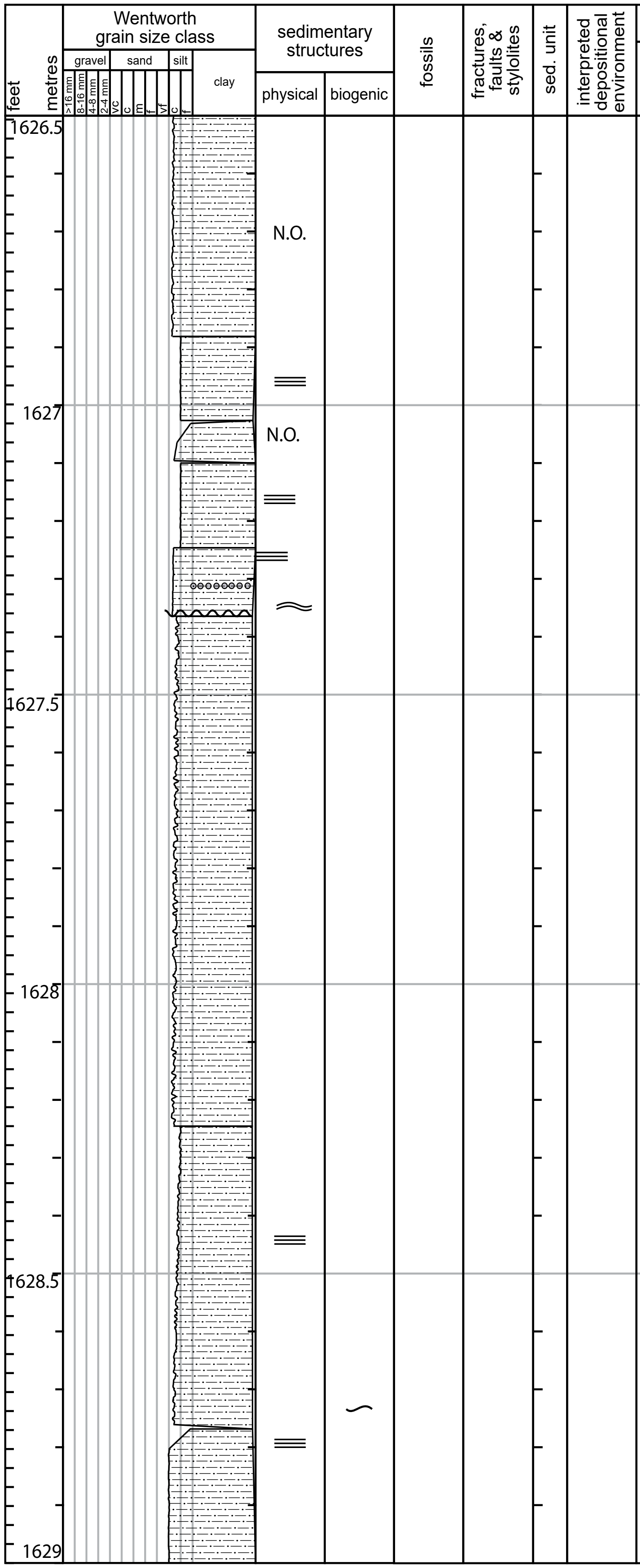
feet
metres
Wentworth grain size class
gravel
sand
silt
clay
>16 mm
8-16 mm
4-8 mm
2-4 mm
vc
c
m
f
vf
c
f
sedimentary structures
physical
biogenic
fossils
fractures, faults & stylolites
sed. unit
interpreted depositional environment
1626.5
N.O.
1627
N.O.
1627.5
1628
1628.5
1629

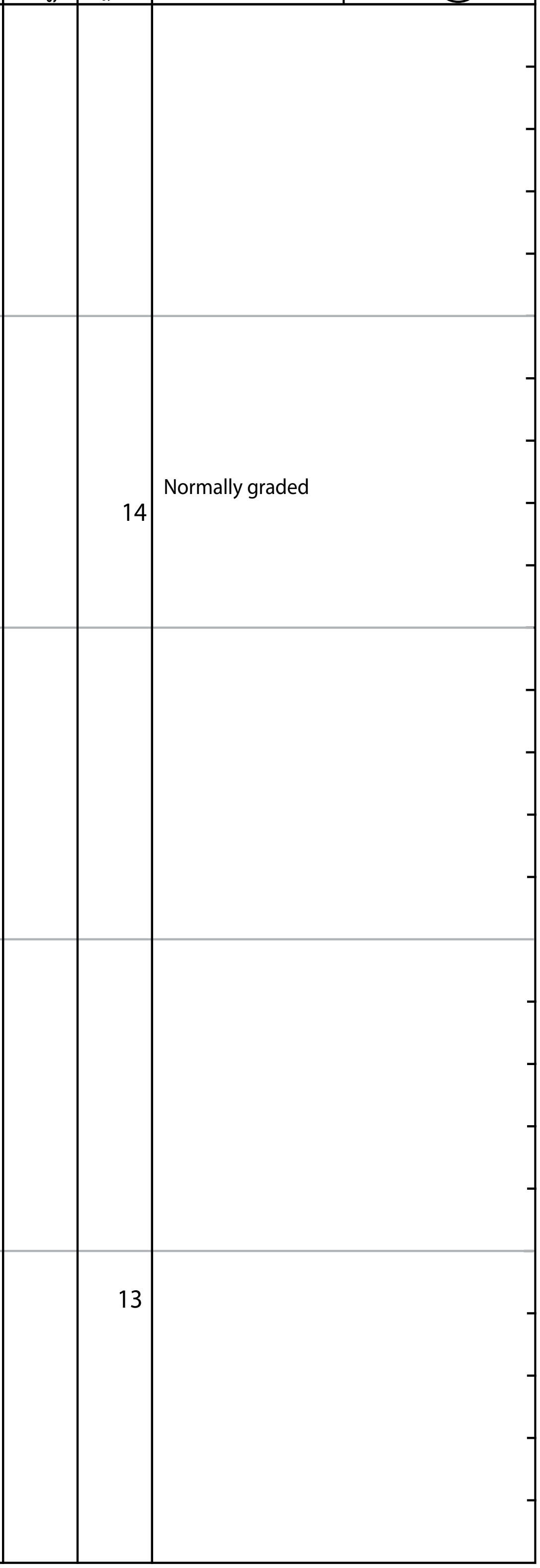
stratal surfaces
samples / photos
14
Normally graded
13

Location: AEC Flatrock 8-21-85-16w6 p6

Date: 7/4/14

Diameter: 8cm

Logged by: S Sanders

Slabbed: [✓ Yes] / No

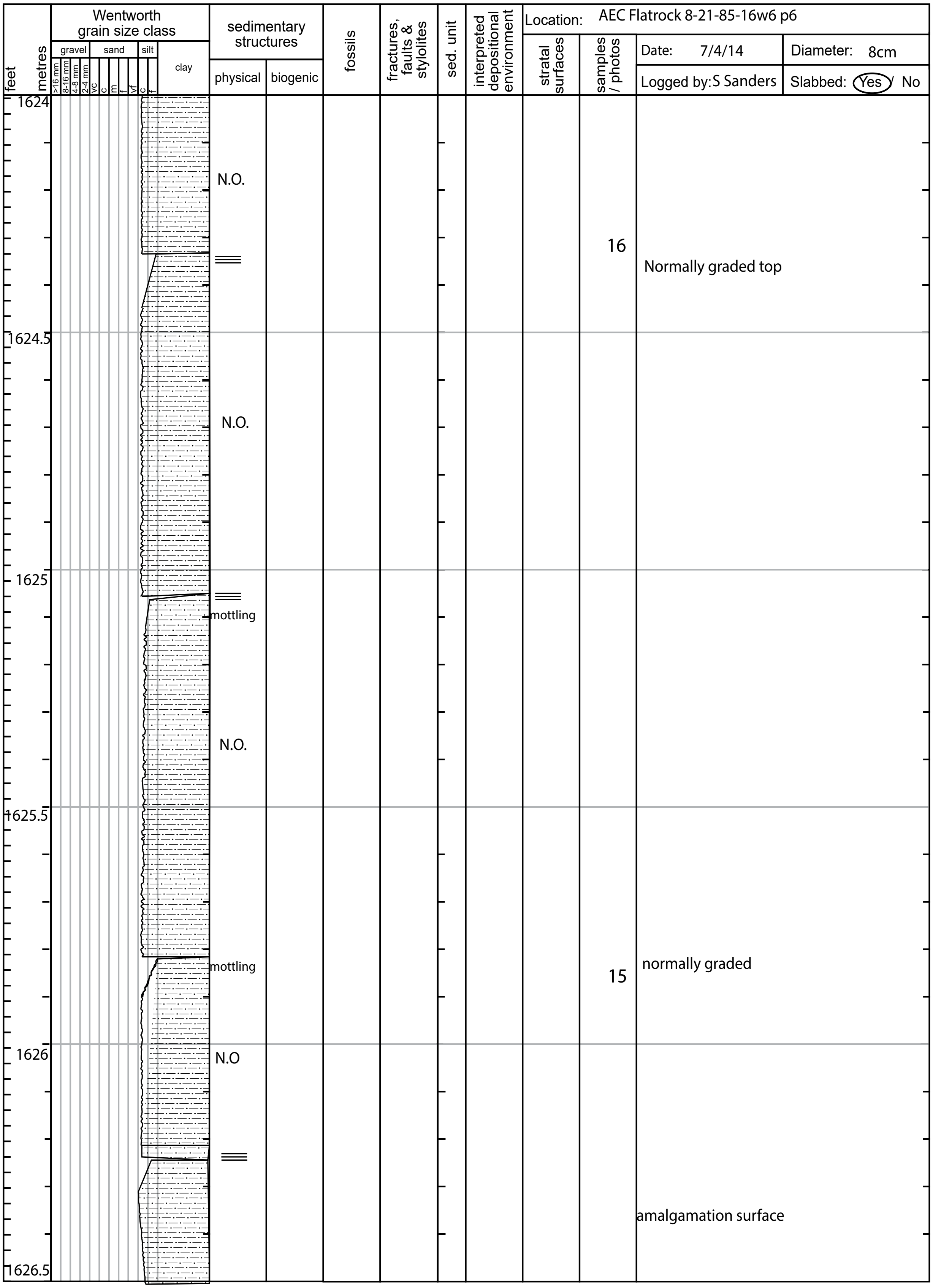

feet
metres
Wentworth grain size class
gravel
sand
silt
clay
>16 mm
8-16 mm
4-8 mm
2-4 mm
vc
c
m
f
vf
c
f
sedimentary structures
physical
biogenic
fossils
fractures, faults & stylolites
sed. unit
interpreted depositional environment
stratal surfaces
samples / photos
1624
1624.5
1625
1625.5
1626
1626.5
N.O.
16
Normally graded top
N.O.
mottling
N.O.
mottling
15
normally graded
N.O
amalgamation surface

Location: AEC Flatrock 8-21-85-16w6 p7

Date: 7/4/14

Diameter: 8cm

Logged by: S Sanders

Slabbed: [✓ Yes] / No

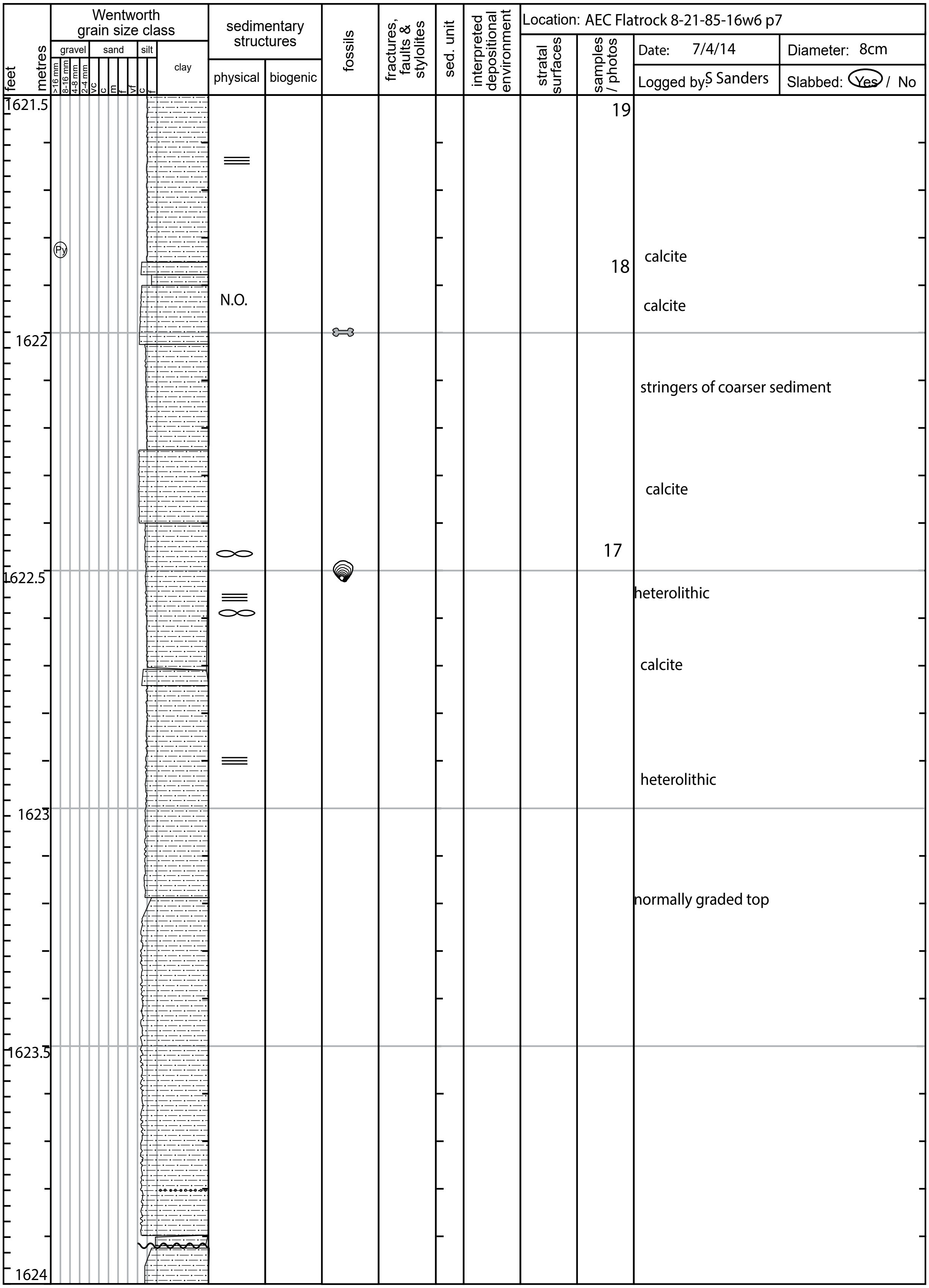
feet
metres
Wentworth grain size class
gravel
sand
silt
clay
>16 mm
8-16 mm
4-8 mm
2-4 mm
vc
c
m
f
vf
c
f
sedimentary structures
physical
biogenic
fossils
fractures, faults & stylolites
sed. unit
interpreted depositional environment
stratal surfaces
samples / photos
1621.5
1622
1622.5
1623
1623.5
1624
Py
N.O.
19
18
17
calcite
calcite
stringers of coarser sediment
calcite
heterolithic
calcite
heterolithic
normally graded top

Location: AEC Flatrock 8-21-85-16w6 p8

Date: 7/4/14

Diameter: 8cm

Logged by: S Sanders

Slabbed: [✓ Yes] / No

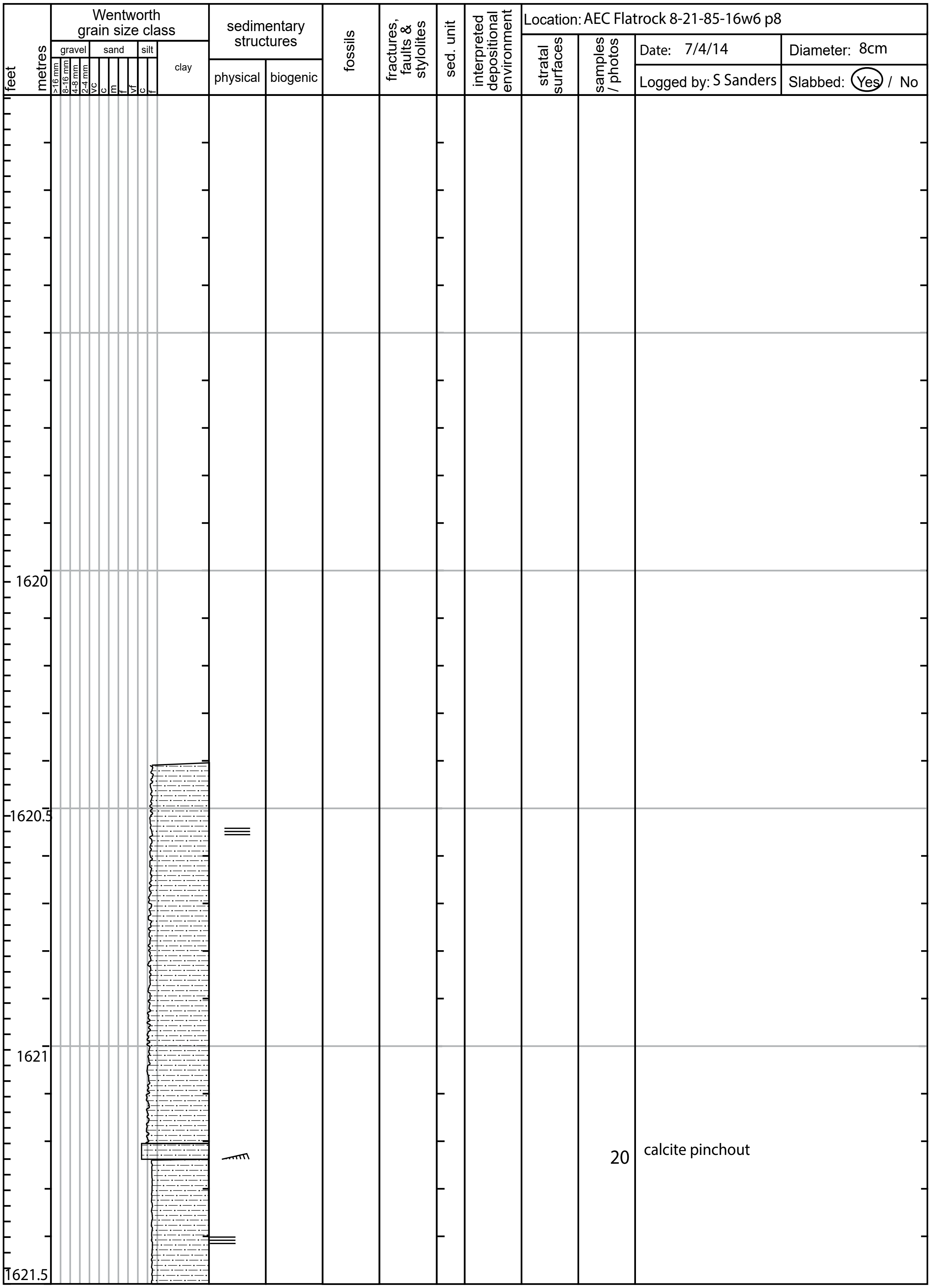
feet
metres
Wentworth grain size class
gravel
sand
silt
clay
>16 mm
8-16 mm
4-8 mm
2-4 mm
vc
c
m
f
vf
c
f
sedimentary structures
physical
biogenic
fossils
fractures, faults & stylolites
sed. unit
interpreted depositional environment
stratal surfaces
samples / photos
1620
1620.5
1621
1621.5
20
calcite pinchout

Location: Devon HZ Monias 8-30-82-20w6 p1

Date: 6-30-14

Diameter: 8.5cm

Logged by:S Sanders

Slabbed: [✓ Yes] / No

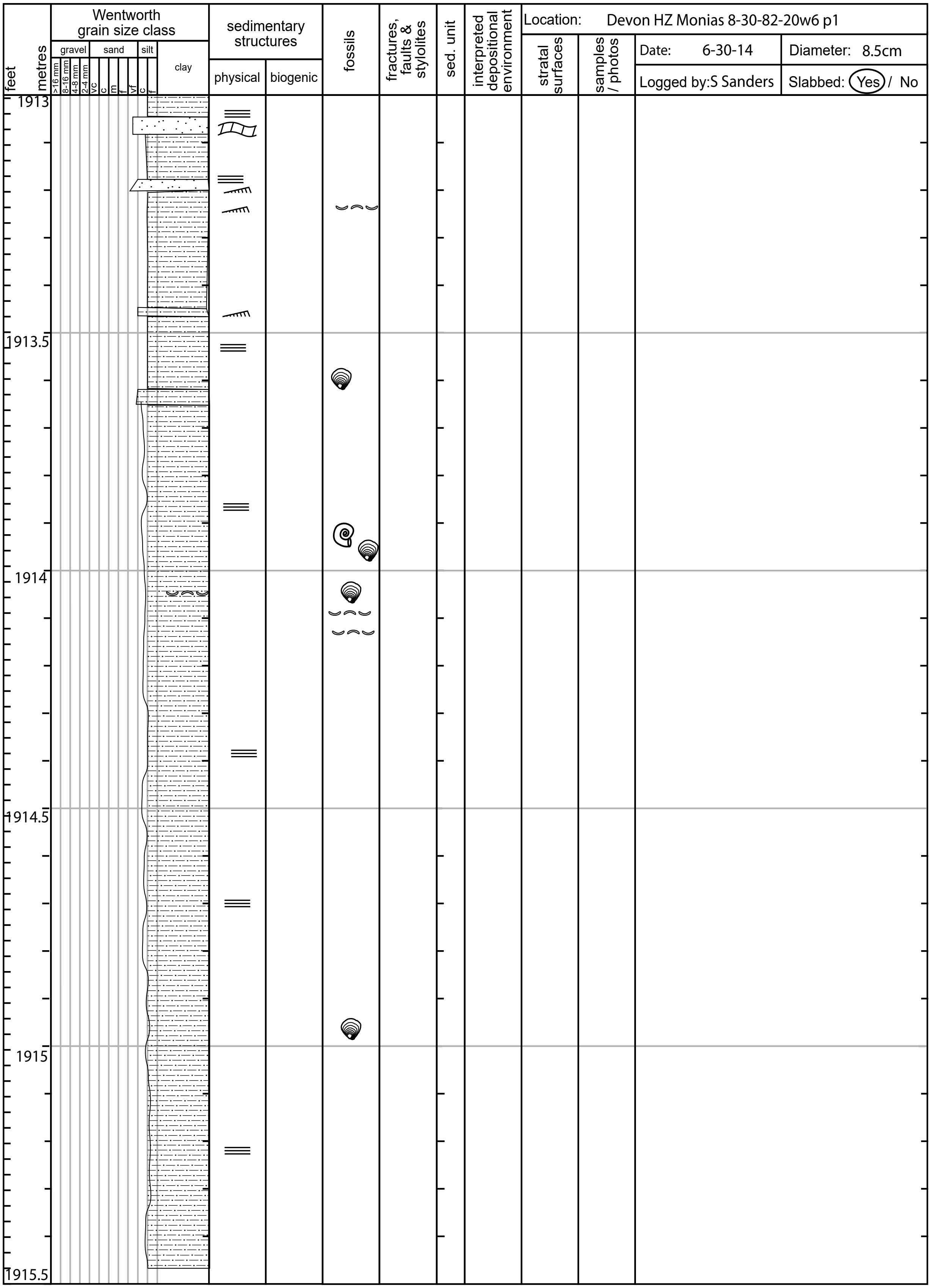
feet
metres
Wentworth grain size class
gravel
sand
silt
clay
>16 mm
8-16 mm
4-8 mm
2-4 mm
vc
c
m
f
vf
c
f
sedimentary structures
physical
biogenic
fossils
fractures, faults & stylolites
sed. unit
interpreted depositional environment
stratal surfaces
samples / photos
1913
1913.5
1914
1914.5
1915
1915.5

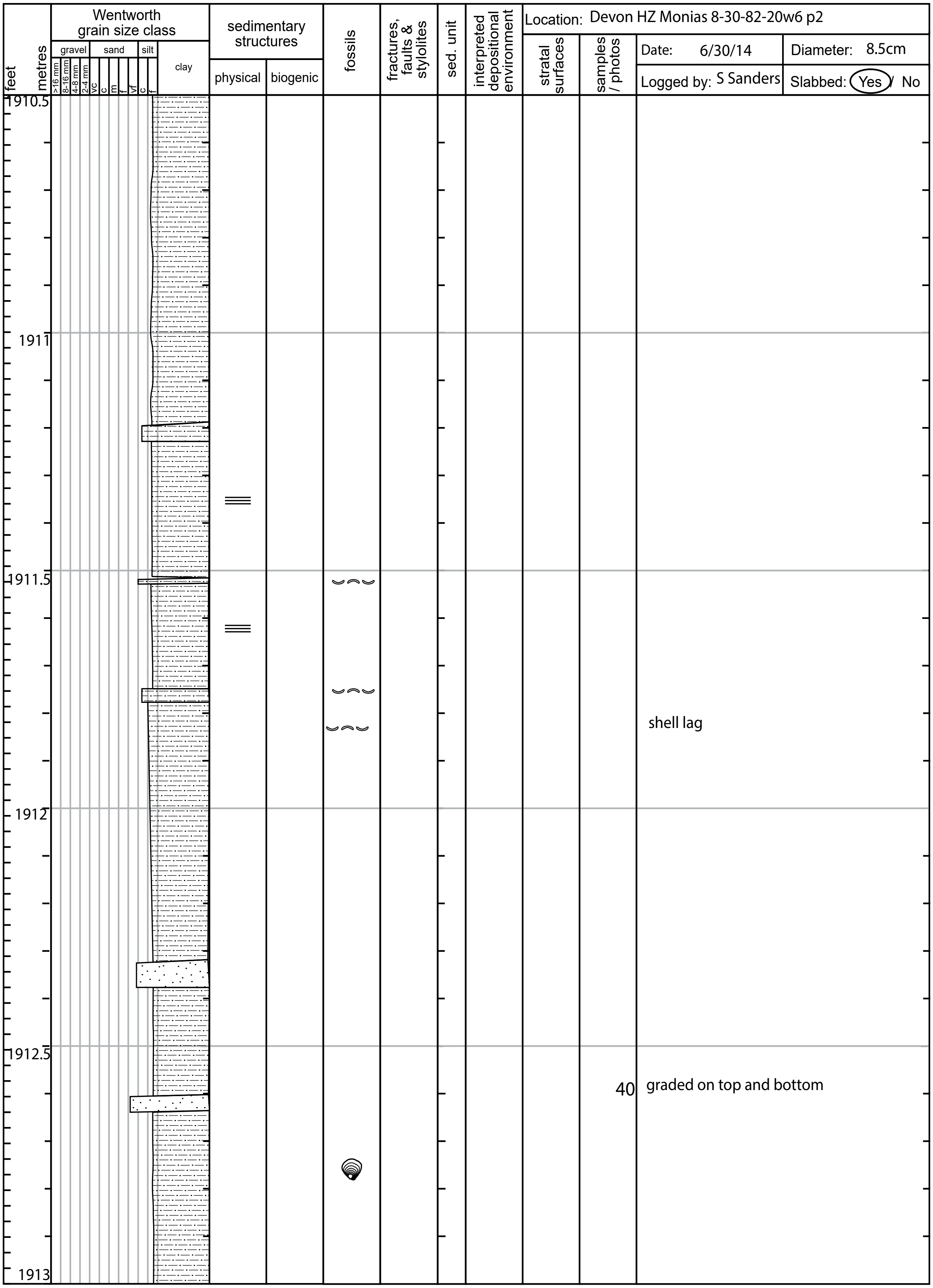
feet
metres
Wentworth grain size class
gravel
sand
silt
clay
>16 mm
8-16 mm
4-8 mm
2-4 mm
vc
c
m
f
vf
c
f
sedimentary structures
physical
biogenic
fossils
fractures, faults & stylolites
sed. unit
interpreted depositional environment
stratal surfaces
samples / photos
1910.5
1911
1911.5
1912
1912.5
1913

Location: Devon HZ Monias 8-30-82-20w6 p2

Date: 6/30/14

Diameter: 8.5cm

Logged by: S Sanders

Slabbed: [✓ Yes] / No

shell lag

40 graded on top and bottom

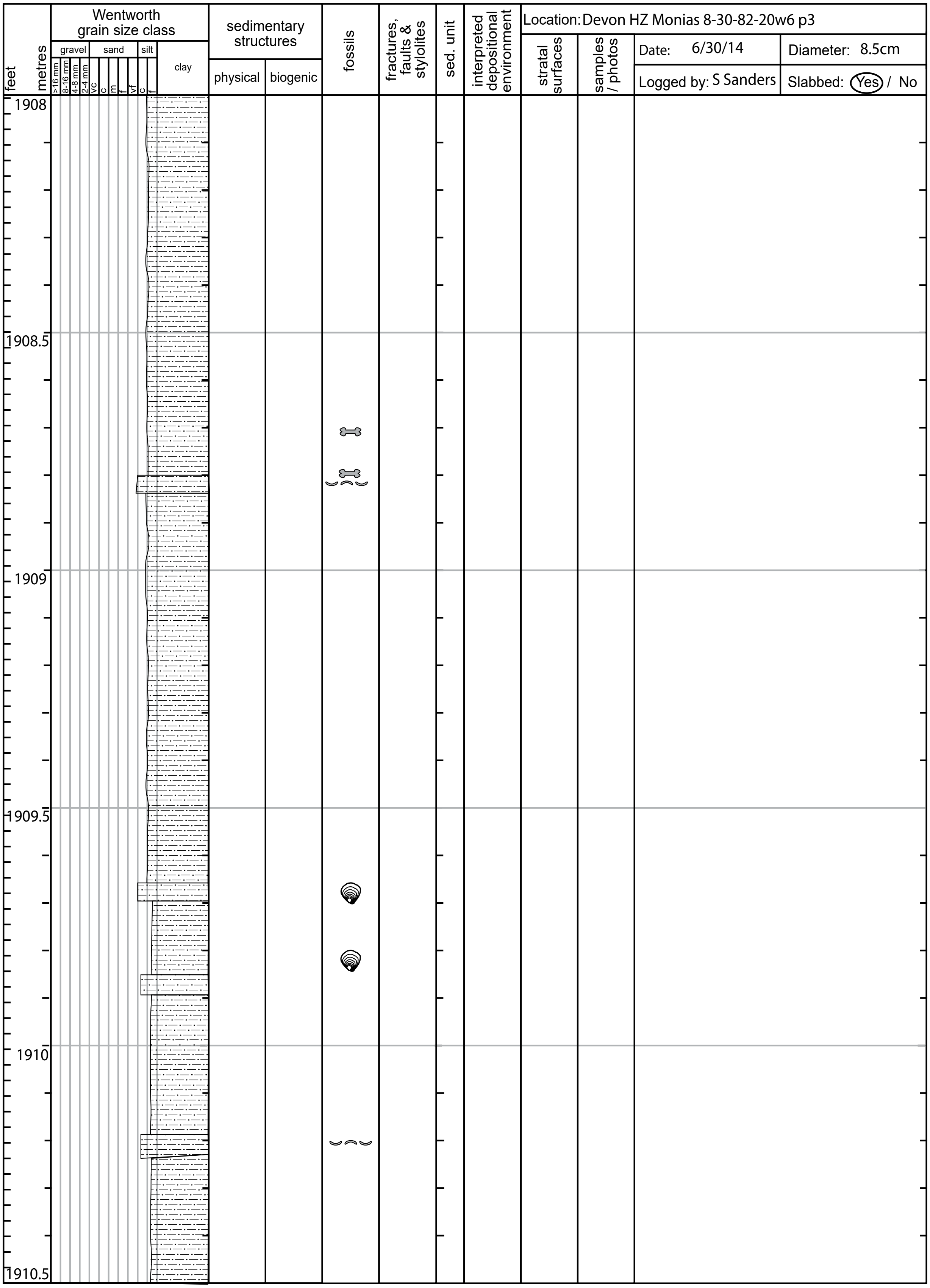
feet
metres
Wentworth grain size class
gravel
sand
silt
clay
>16 mm
8-16 mm
4-8 mm
2-4 mm
vc
c
m
f
vf
c
f
sedimentary structures
physical
biogenic
fossils
fractures, faults & stylolites
sed. unit
interpreted depositional environment
stratal surfaces
samples / photos
1908
1908.5
1909
1909.5
1910
1910.5

Location: Devon HZ Monias 8-30-82-20w6 p3

Date: 6/30/14

Diameter: 8.5cm

Logged by: S Sanders

Slabbed: [✓ Yes] / No

Location: Devon HZ Monias 8-30-82-20w6 p4

Date: 6/30/14

Diameter: 8.5cm

Logged by: S Sanders

Slabbed: [✓ Yes] / No

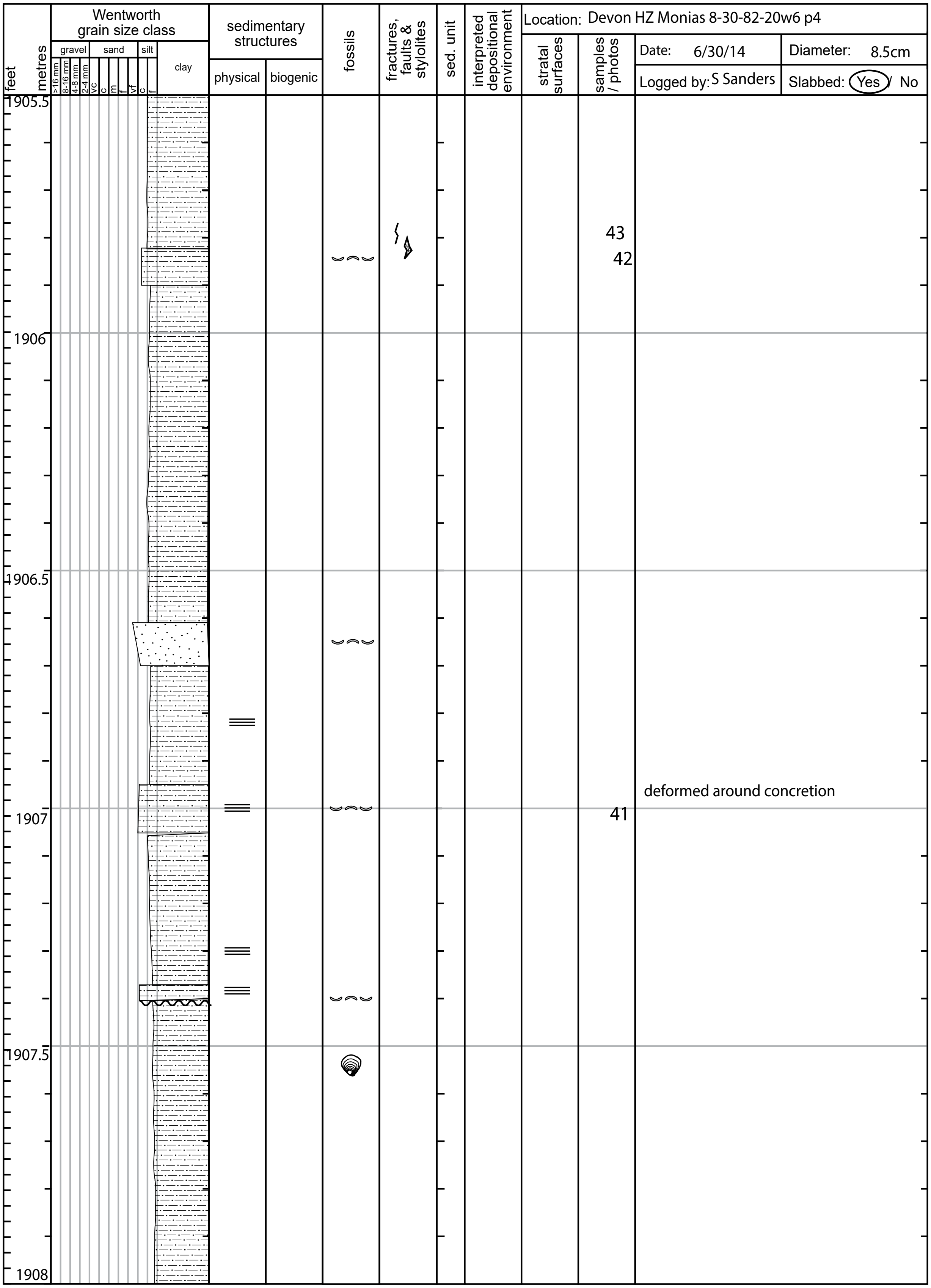
Wentworth grain size class
gravel
sand
silt
clay
>16 mm
8-16 mm
4-8 mm
2-4 mm
vc
c
m
f
vf
c
f
feet
metres
sedimentary structures
physical
biogenic
fossils
fractures, faults & stylolites
sed. unit
interpreted depositional environment
stratal surfaces
samples / photos
1905.5
1906
1906.5
1907
1907.5
1908
43
42
41
deformed around concretion

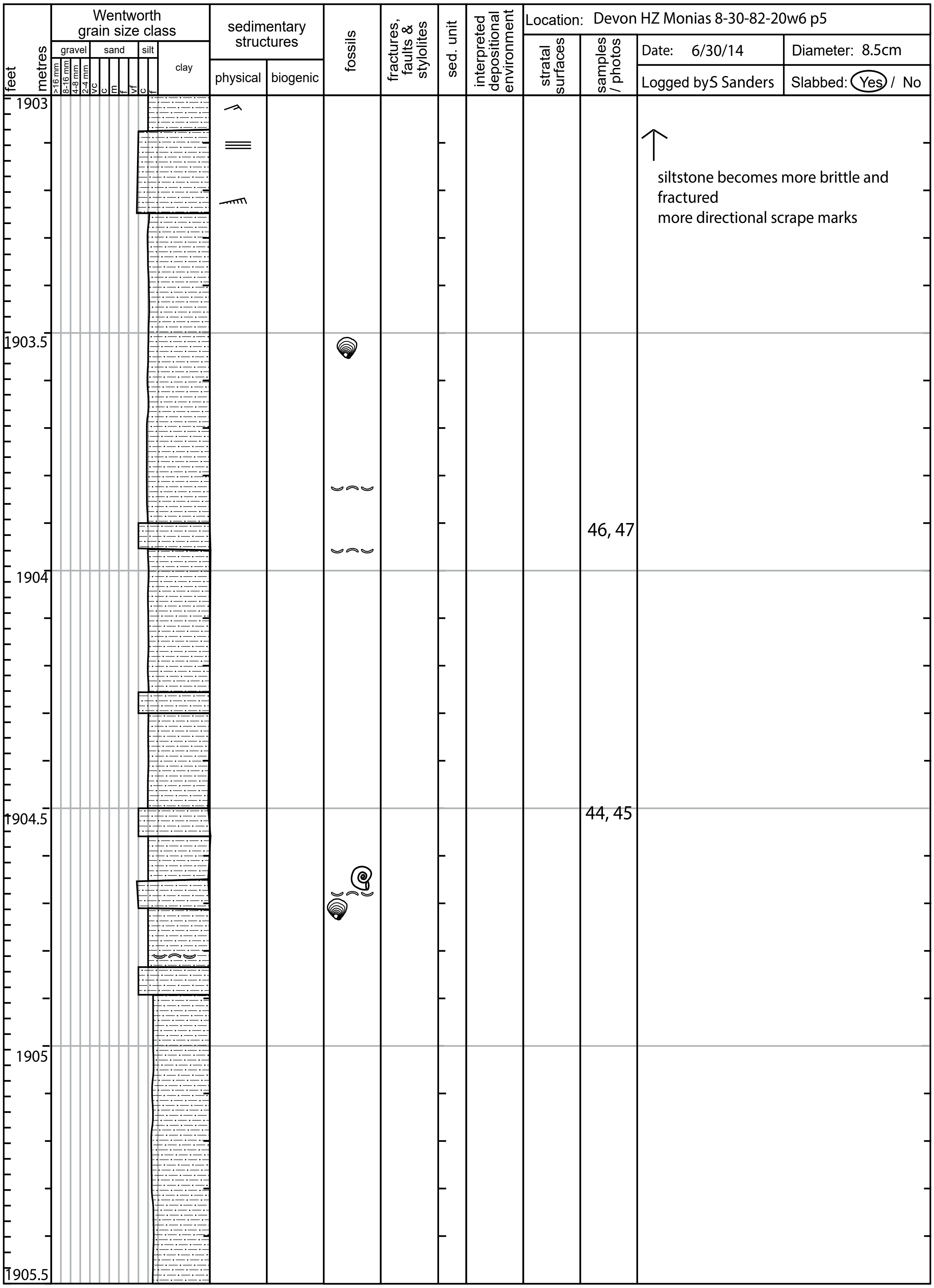
feet
metres
Wentworth grain size class
gravel
sand
silt
clay
>16 mm
8-16 mm
4-8 mm
2-4 mm
vc
c
m
f
vf
c
f
sedimentary structures
physical
biogenic
fossils
fractures, faults & stylolites
sed. unit
interpreted depositional environment
stratal surfaces
samples / photos
1903
1903.5
1904
1904.5
1905
1905.5
46, 47
44, 45

Location: Devon HZ Monias 8-30-82-20w6 p5

Date: 6/30/14

Diameter: 8.5cm

Logged byS Sanders

Slabbed: [✓ Yes] / No

↑

siltstone becomes more brittle and fractured
more directional scrape marks

Location: Devon HZ Monias 8-30-82-20w6 p6	
Date: 6/30/14	Diameter: 8.5cm
Logged by: S Sanders	Slabbed: [✓ Yes] / No

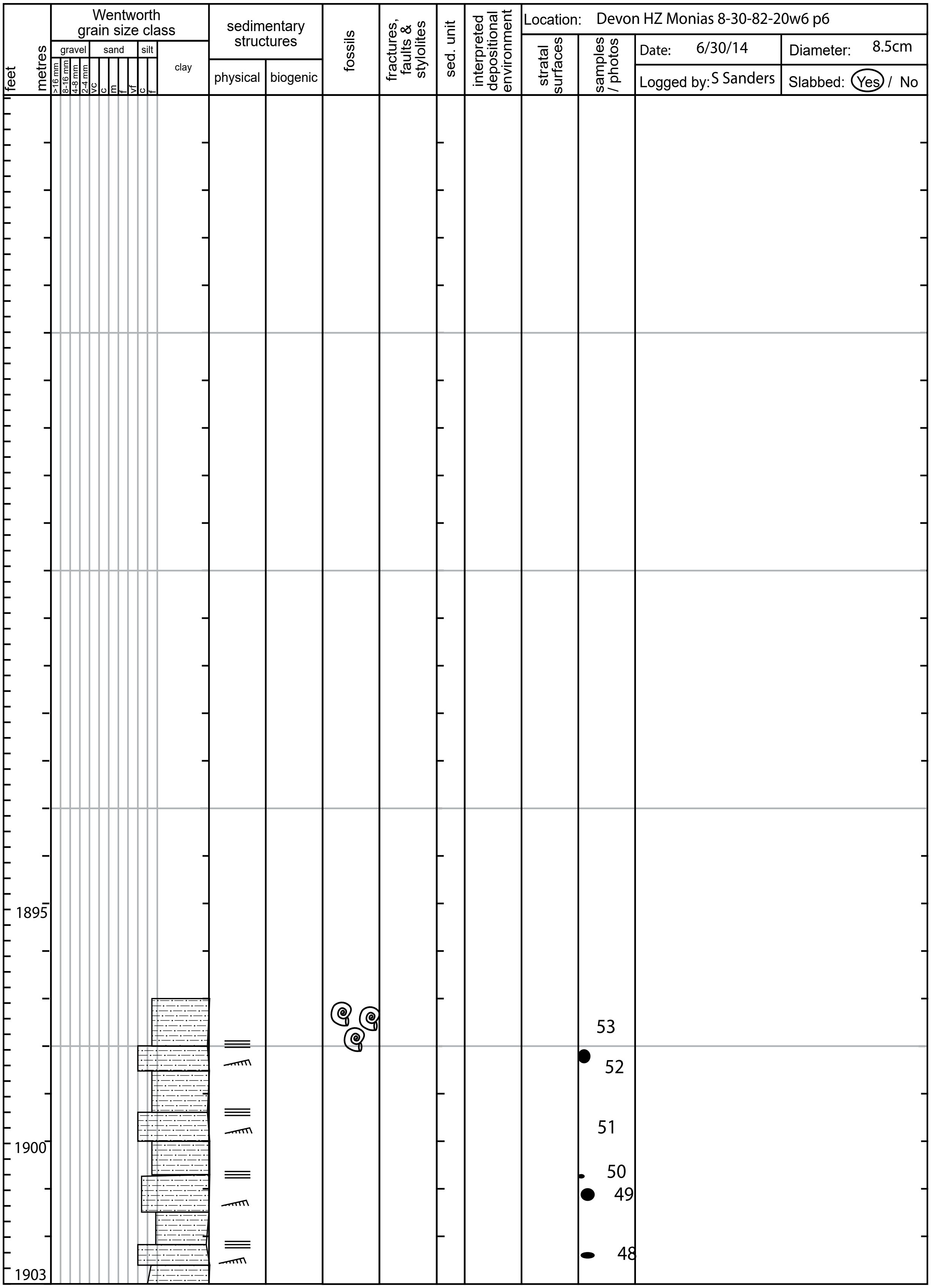

feet
metres
Wentworth grain size class
gravel
sand
silt
clay
>16 mm
8-16 mm
4-8 mm
2-4 mm
vc
c
m
f
vf
c
f
sedimentary structures
physical
biogenic
fossils
fractures, faults & stylolites
sed. unit
interpreted depositional environment
stratal surfaces
samples / photos
1895
1900
1903
53
52
51
50
49
48

feet	metres	Wentworth grain size class gravel: >16 mm, 8-16 mm, 4-8 mm, 2-4 mm sand: vc, c, m, f, vf silt: c, f clay	sedimentary structures physical biogenic	fossils	fractures, faults & stylolites	sed. unit	interpreted depositional environment	stratal surfaces	samples / photos	Location: Arc Monias 09-07-082-20w6 Date: 6/30/14 — Diameter: 6.5cm Logged by: S Sanders — Slabbed: [✓ Yes] / No

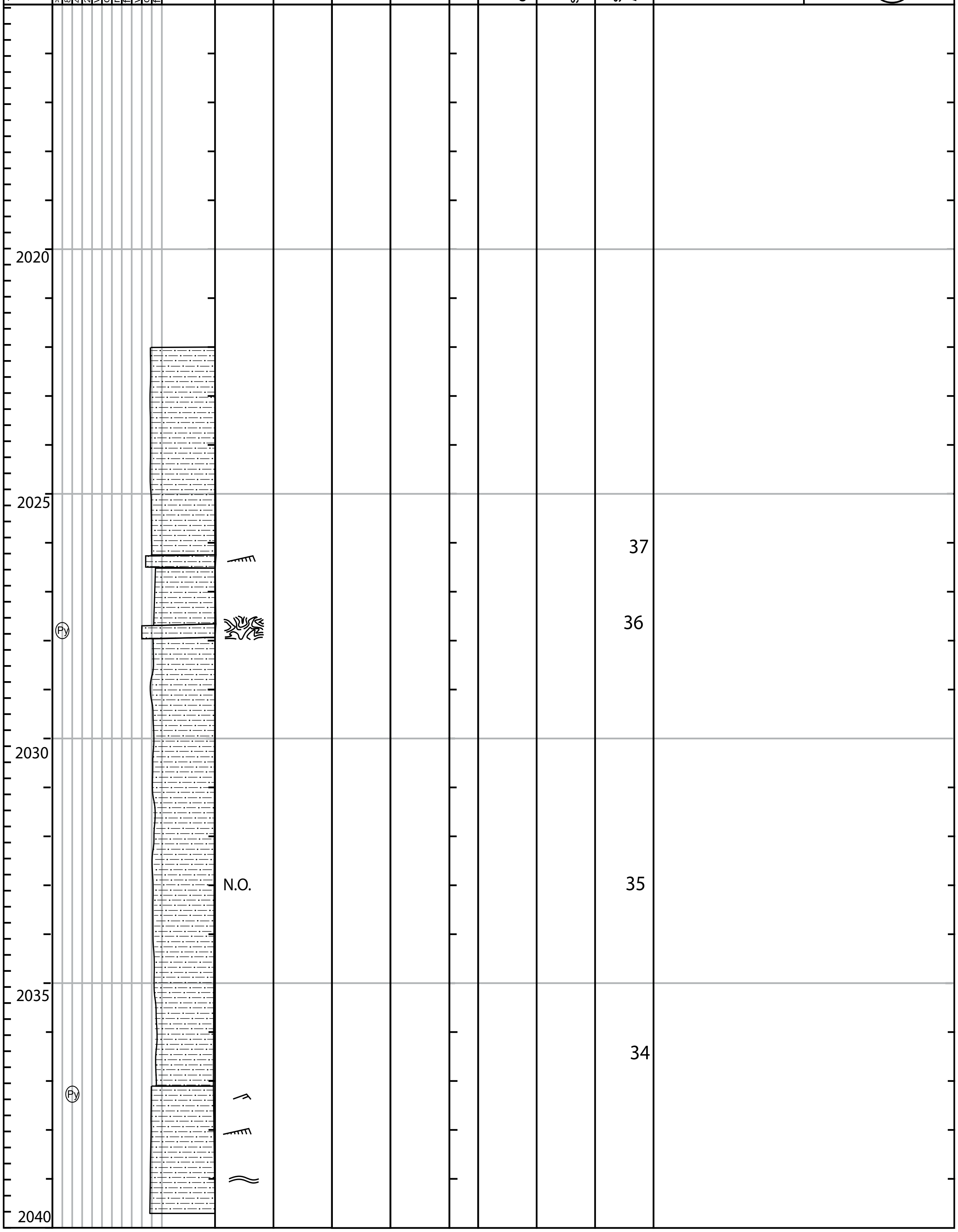

2020
2025
2030
2035
2040
37
36
Py
N.O.
35
34
Py

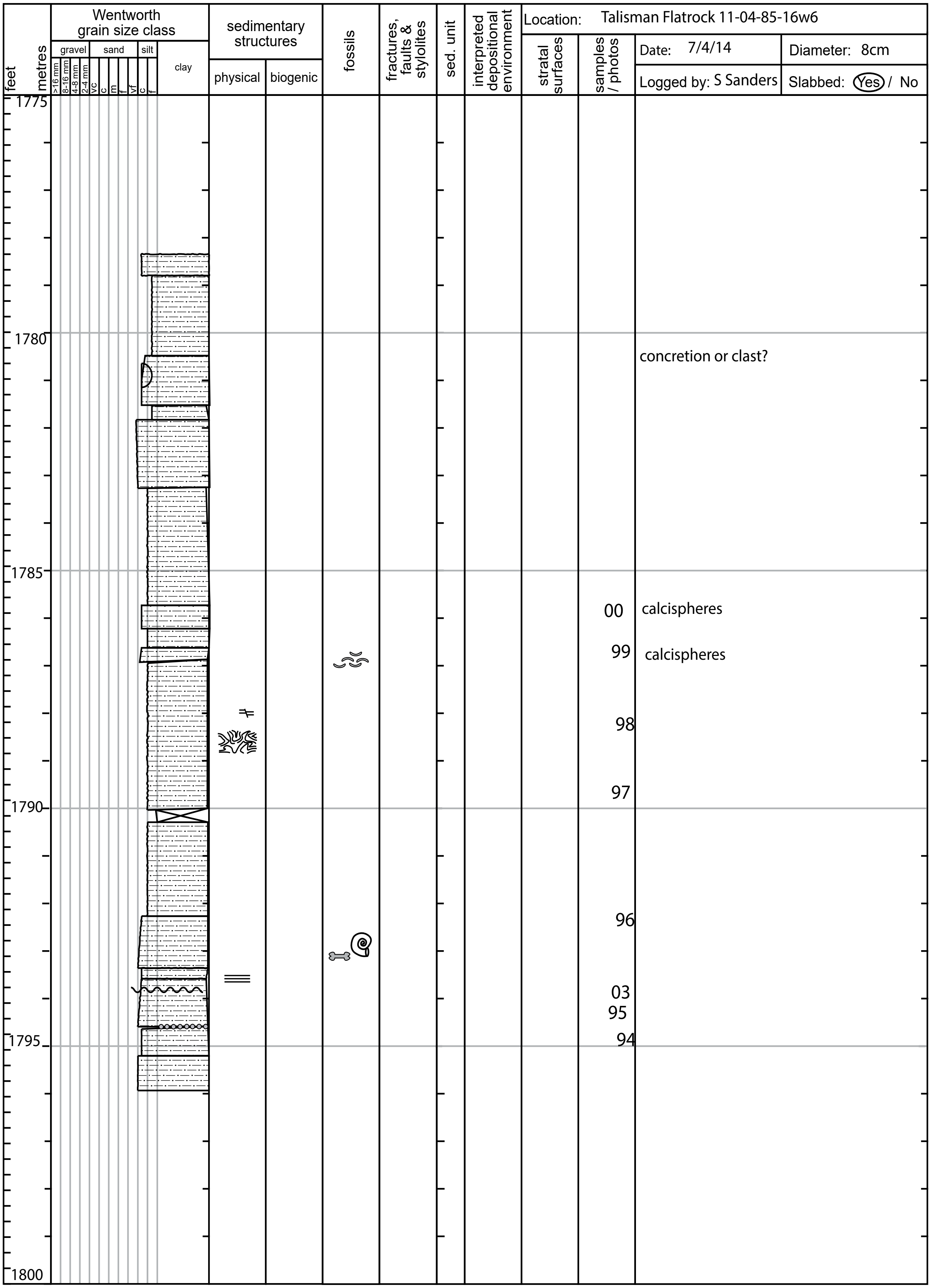
feet
metres
Wentworth grain size class
gravel
sand
silt
clay
>16 mm
8-16 mm
4-8 mm
2-4 mm
vc
c
m
f
vf
c
f
sedimentary structures
physical
biogenic
fossils
fractures, faults & stylolites
sed. unit
interpreted depositional environment
stratal surfaces
samples / photos
1775
1780
1785
1790
1795
1800

Location: Talisman Flatrock 11-04-85-16w6

Date: 7/4/14

Diameter: 8cm

Logged by: S Sanders

Slabbed: [✓ Yes] / No

concretion or clast?

00 calcispheres

99 calcispheres

98

97

96

03

95

94

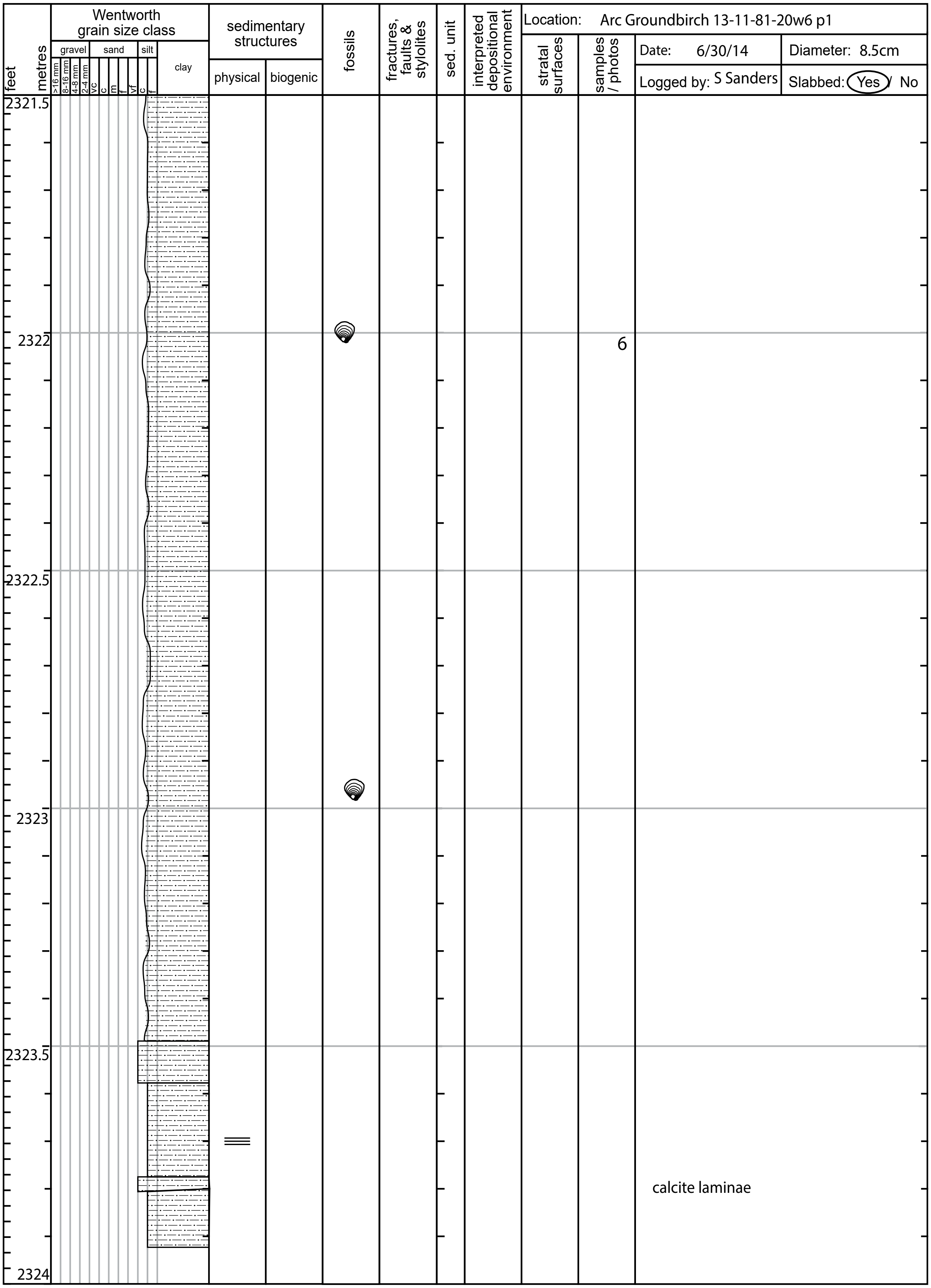
feet
metres
Wentworth grain size class
gravel
sand
silt
clay
>16 mm
8-16 mm
4-8 mm
2-4 mm
vc
c
m
f
vf
c
f
sedimentary structures
physical
biogenic
fossils
fractures, faults & stylolites
sed. unit
interpreted depositional environment
stratal surfaces
samples / photos
2321.5
2322
2322.5
2323
2323.5
2324

Location: Arc Groundbirch 13-11-81-20w6 p1

Date: 6/30/14

Diameter: 8.5cm

Logged by: S Sanders

Slabbed: [✓ Yes] / No

6

calcite laminae

Location: Arc Groundbirch 13-11-81-20w6 p2

Date: 6/30/14

Diameter: 8.5cm

Logged by: S Sanders

Slabbed: [✓ Yes] / No

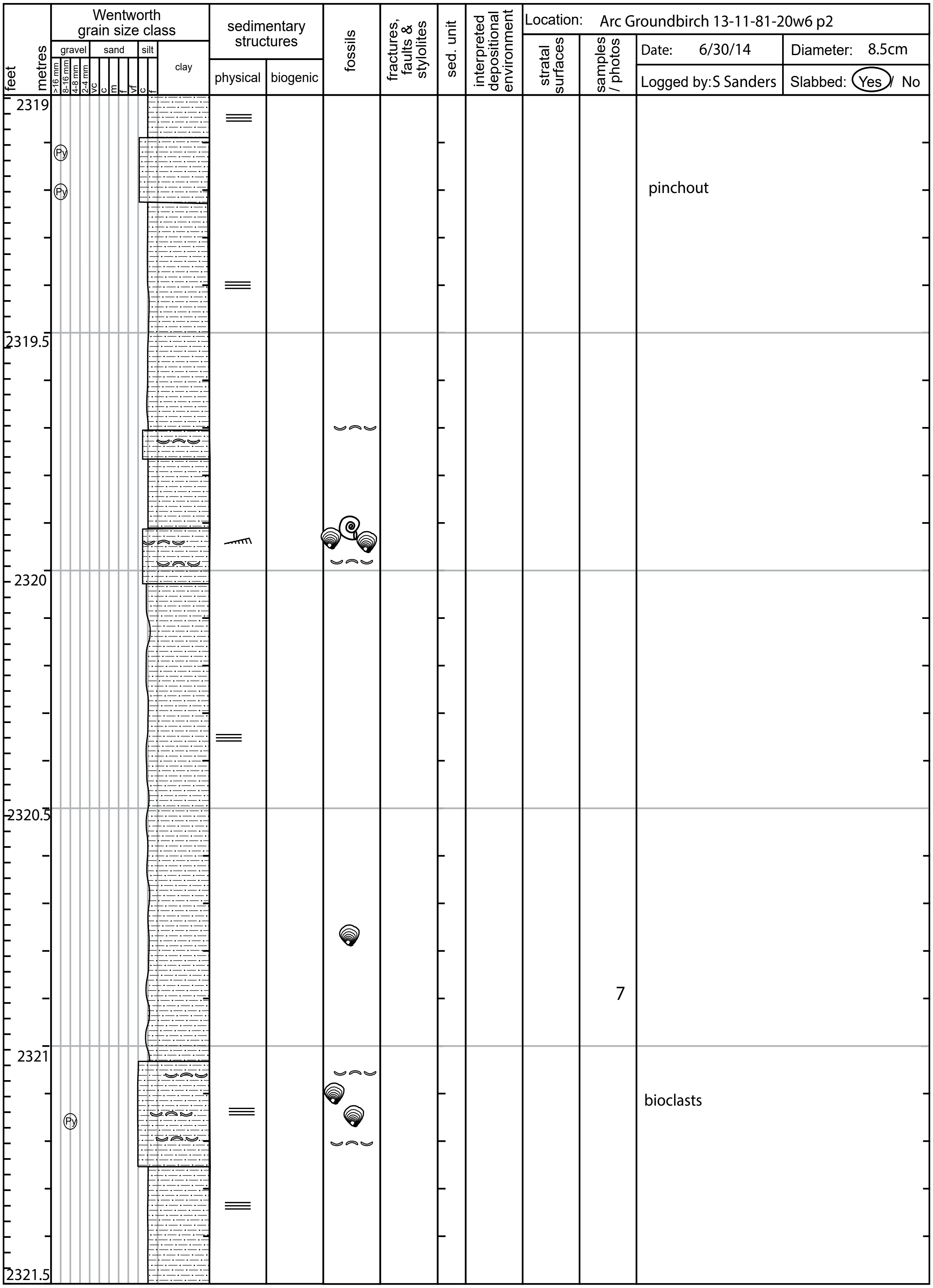

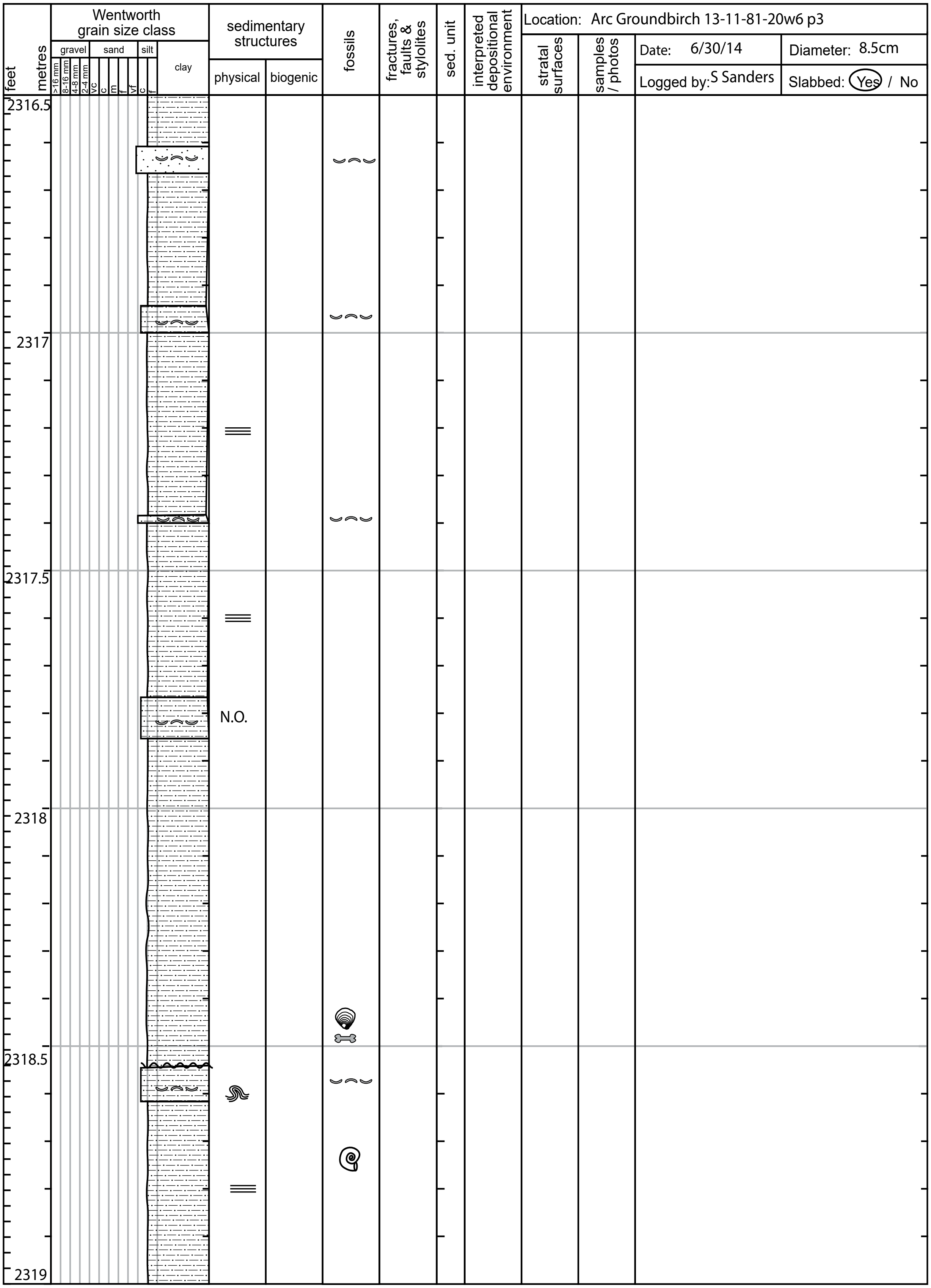

feet
metres
Wentworth grain size class
gravel
sand
silt
clay
>16 mm
8-16 mm
4-8 mm
2-4 mm
vc
c
m
f
vf
c
f
sedimentary structures
physical
biogenic
fossils
fractures, faults & stylolites
sed. unit
interpreted depositional environment
stratal surfaces
samples / photos
2316.5
2317
2317.5
2318
2318.5
2319
N.O.

Location: Arc Groundbirch 13-11-81-20w6 p3

Date: 6/30/14

Diameter: 8.5cm

Logged by: S Sanders

Slabbed: [✓ Yes] / No

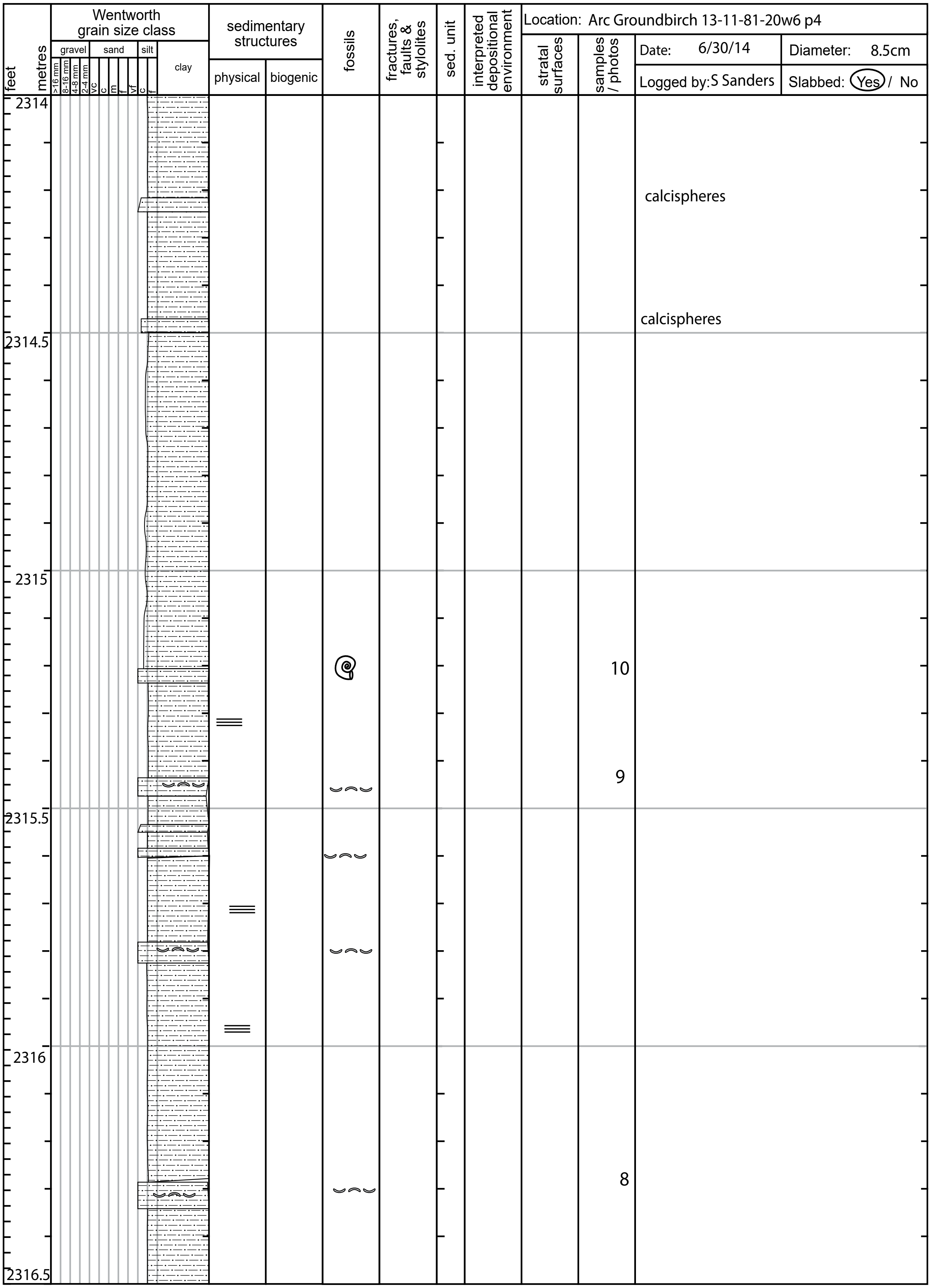
feet
metres
Wentworth grain size class
gravel
sand
silt
clay
>16 mm
8-16 mm
4-8 mm
2-4 mm
vc
c
m
f
vf
c
f
sedimentary structures
physical
biogenic
fossils
fractures, faults & stylolites
sed. unit
interpreted depositional environment
stratal surfaces
samples / photos
2314
2314.5
2315
2315.5
2316
2316.5
10
9
8

Location: Arc Groundbirch 13-11-81-20w6 p4

Date: 6/30/14

Diameter: 8.5cm

Logged by: S Sanders

Slabbed: [✓ Yes] / No

calcispheres

calcispheres

Location: Arc Groundbirch 13-11-81-20w6 p5

Date: 6/30/14

Diameter: 8.5cm

Logged by: S Sanders

Slabbed: [✓ Yes] / No

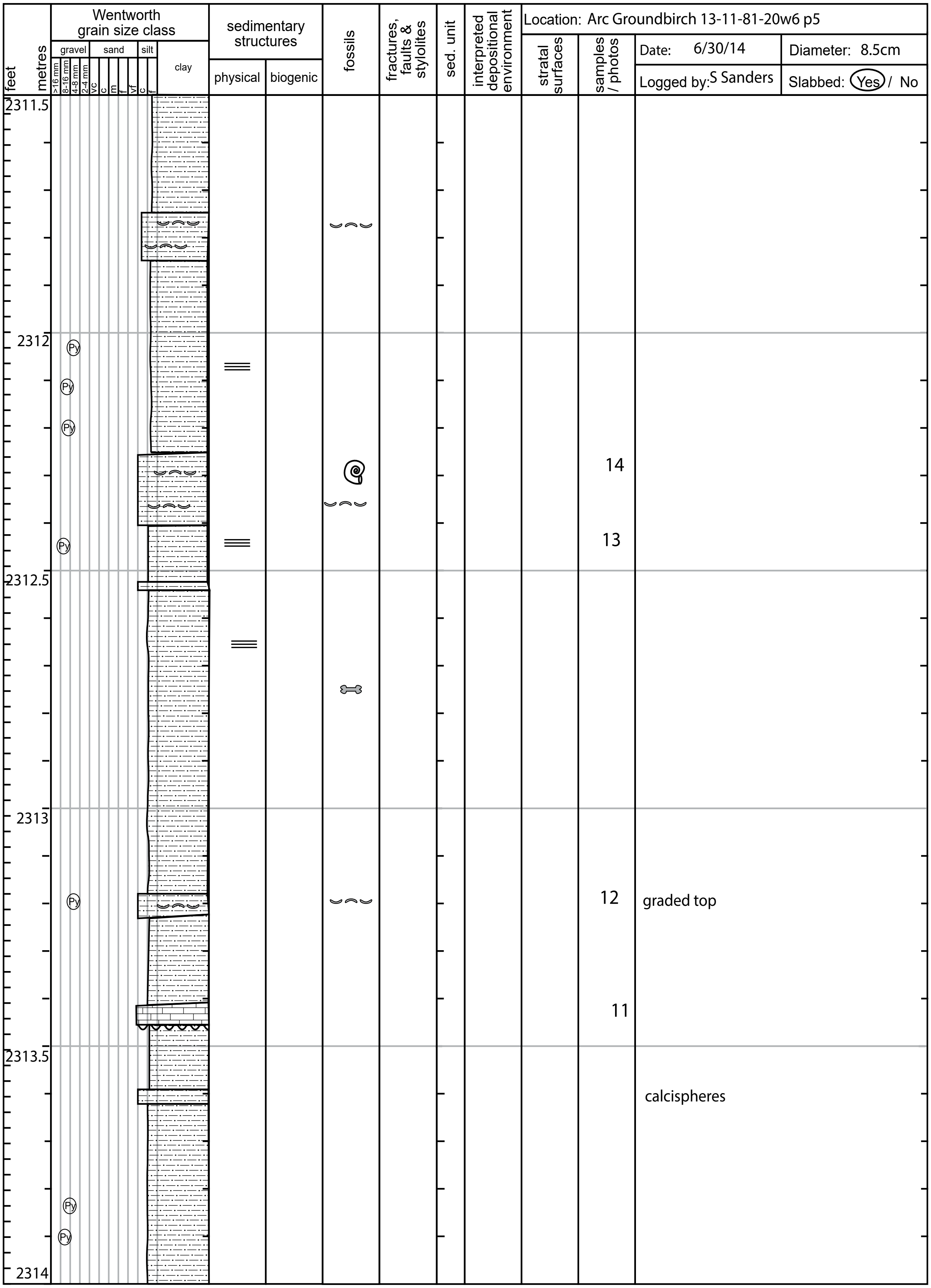
feet
metres
Wentworth grain size class
gravel
sand
silt
clay
>16 mm
8-16 mm
4-8 mm
2-4 mm
vc
c
m
f
vf
c
f
sedimentary structures
physical
biogenic
fossils
fractures, faults & stylolites
sed. unit
interpreted depositional environment
stratal surfaces
samples / photos
2311.5
2312
2312.5
2313
2313.5
2314
Py
Py
Py
Py
Py
Py
Py

samples / photos	
14	
13	
12	graded top
11	
	calcispheres

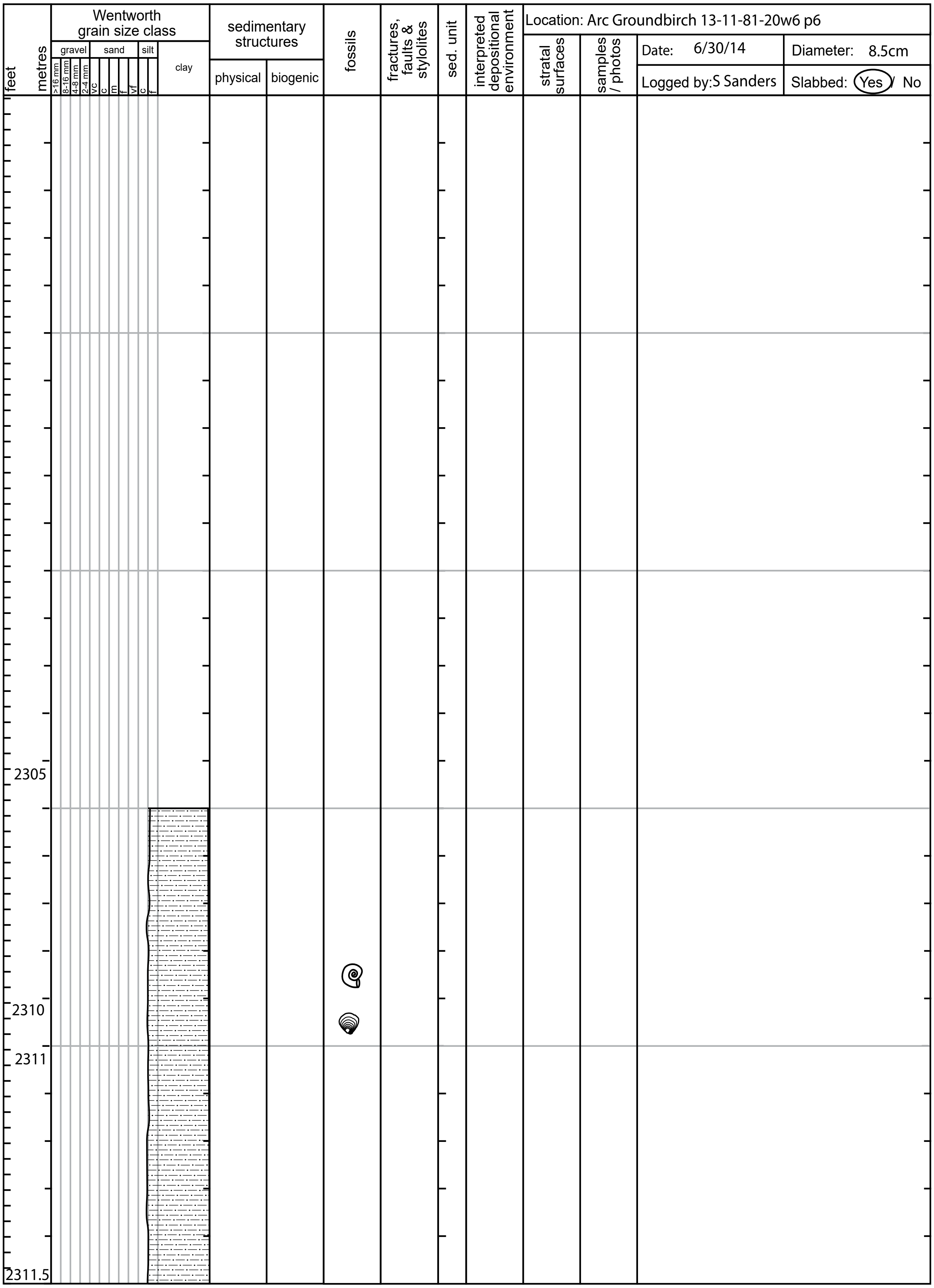
feet
metres
Wentworth grain size class
gravel
sand
silt
>16 mm
8-16 mm
4-8 mm
2-4 mm
vc
c
m
f
vf
c
f
clay
sedimentary structures
physical
biogenic
fossils
fractures, faults & stylolites
sed. unit
interpreted depositional environment
stratal surfaces
samples / photos
2305
2310
2311
2311.5

Location: Arc Groundbirch 13-11-81-20w6 p6

Date: 6/30/14

Diameter: 8.5cm

Logged by:S Sanders

Slabbed: [✓ Yes] / No

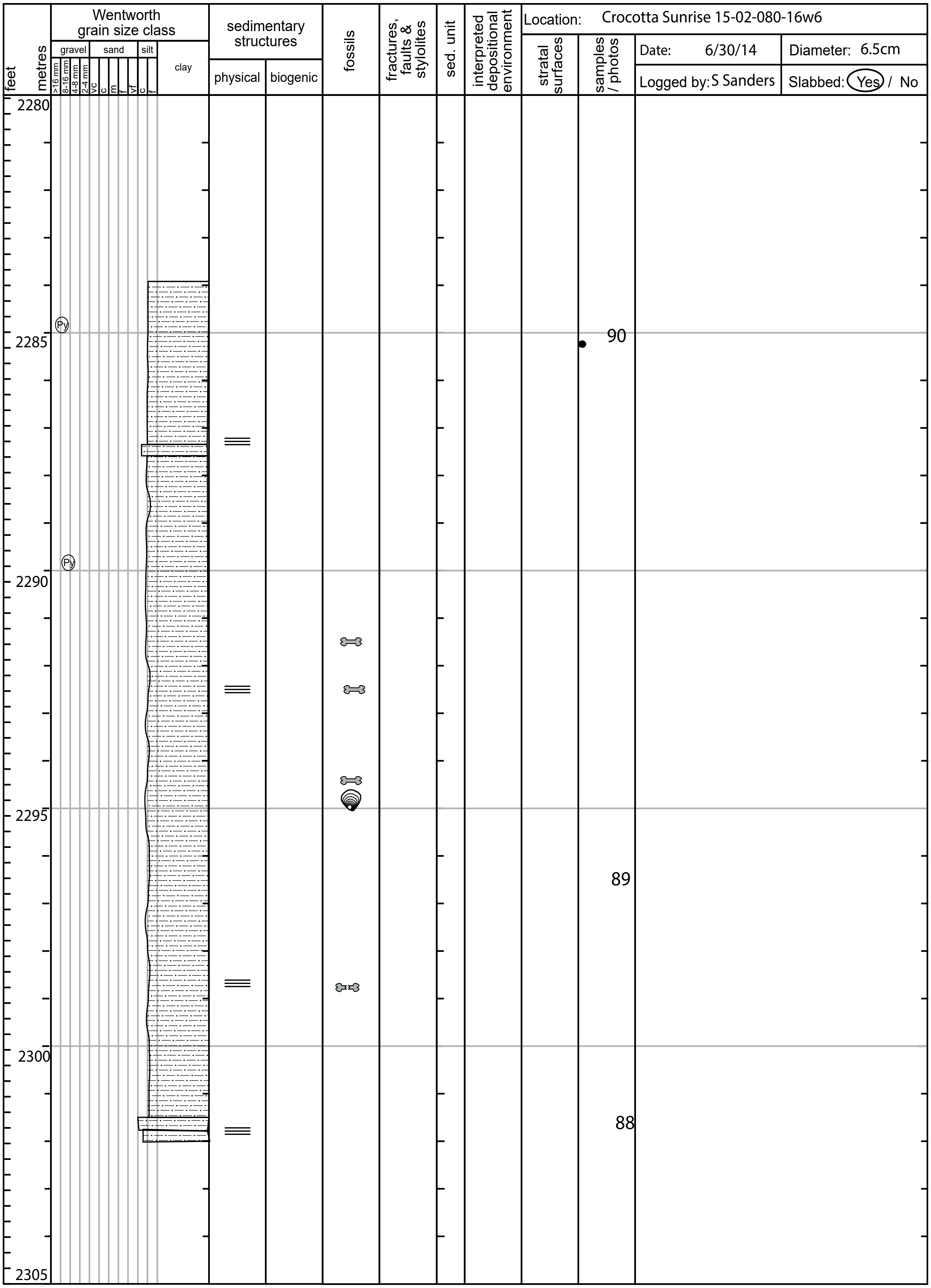

Location: Crocotta Sunrise 15-02-080-16w6

Date: 6/30/14

Diameter: 6.5cm

Logged by: S Sanders

Slabbed: [✓ Yes] / No

feet
metres
Wentworth grain size class
gravel
sand
silt
clay
>16 mm
8-16 mm
4-8 mm
2-4 mm
vc
c
m
f
vf
c
f
sedimentary structures
physical
biogenic
fossils
fractures, faults & stylolites
sed. unit
interpreted depositional environment
stratal surfaces
samples / photos
2280
Py
2285
90
Py
2290
2295
89
2300
88
2305

Location: Progress et al Altares 16-17-083-25w6

Date: 6/25/14

Diameter:

Logged by: S Sanders

Slabbed: [✓ Yes] / No

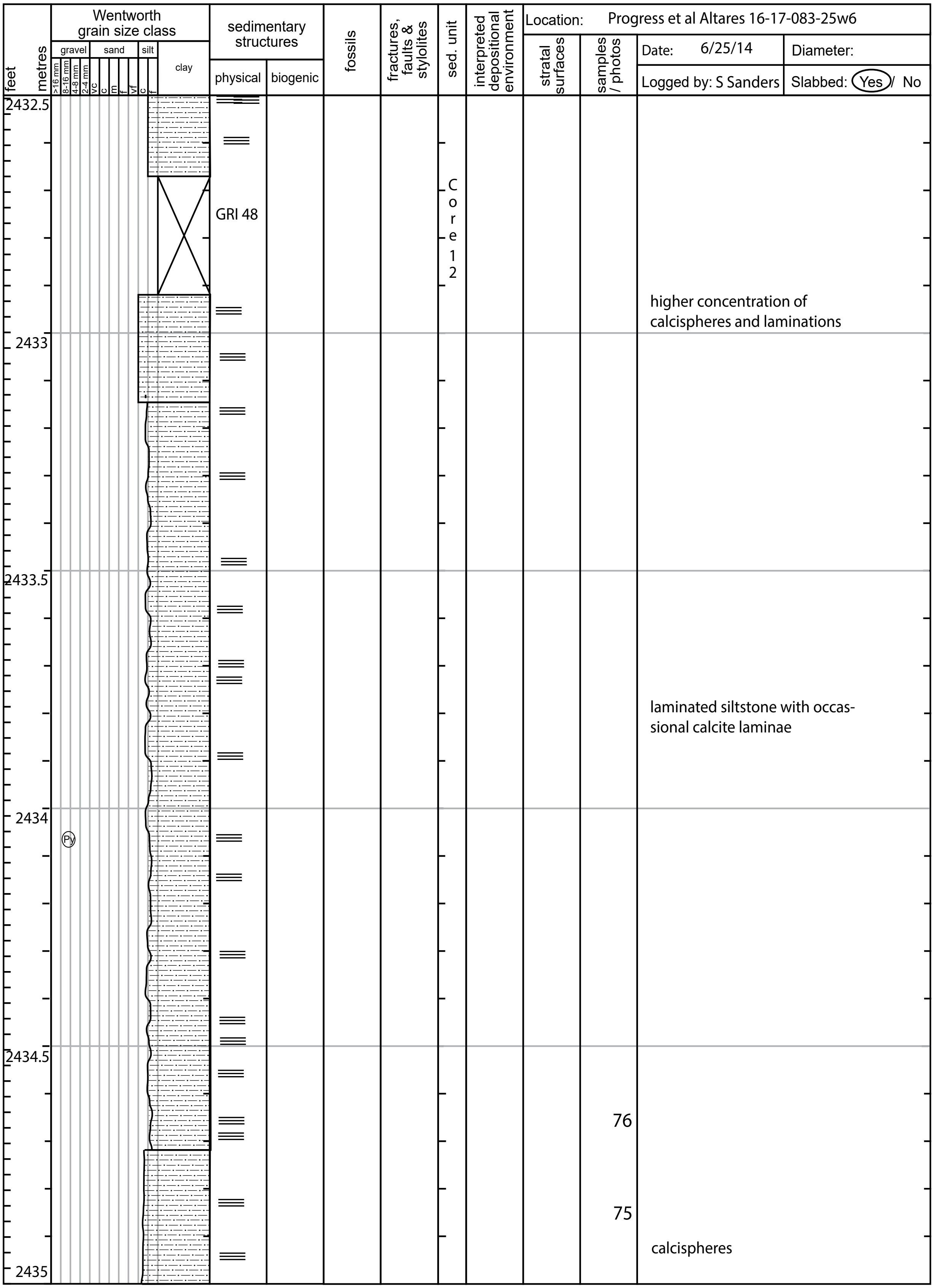
feet
metres
Wentworth grain size class
gravel
sand
silt
clay
>16 mm
8-16 mm
4-8 mm
2-4 mm
vc
c
m
f
vf
c
f
sedimentary structures
physical
biogenic
fossils
fractures, faults & stylolites
sed. unit
interpreted depositional environment
stratal surfaces
samples / photos
2432.5
2433
2433.5
2434
2434.5
2435
GRI 48
Core 12
Py
76
75

higher concentration of calcispheres and laminations

laminated siltstone with occasional calcite laminae

calcispheres

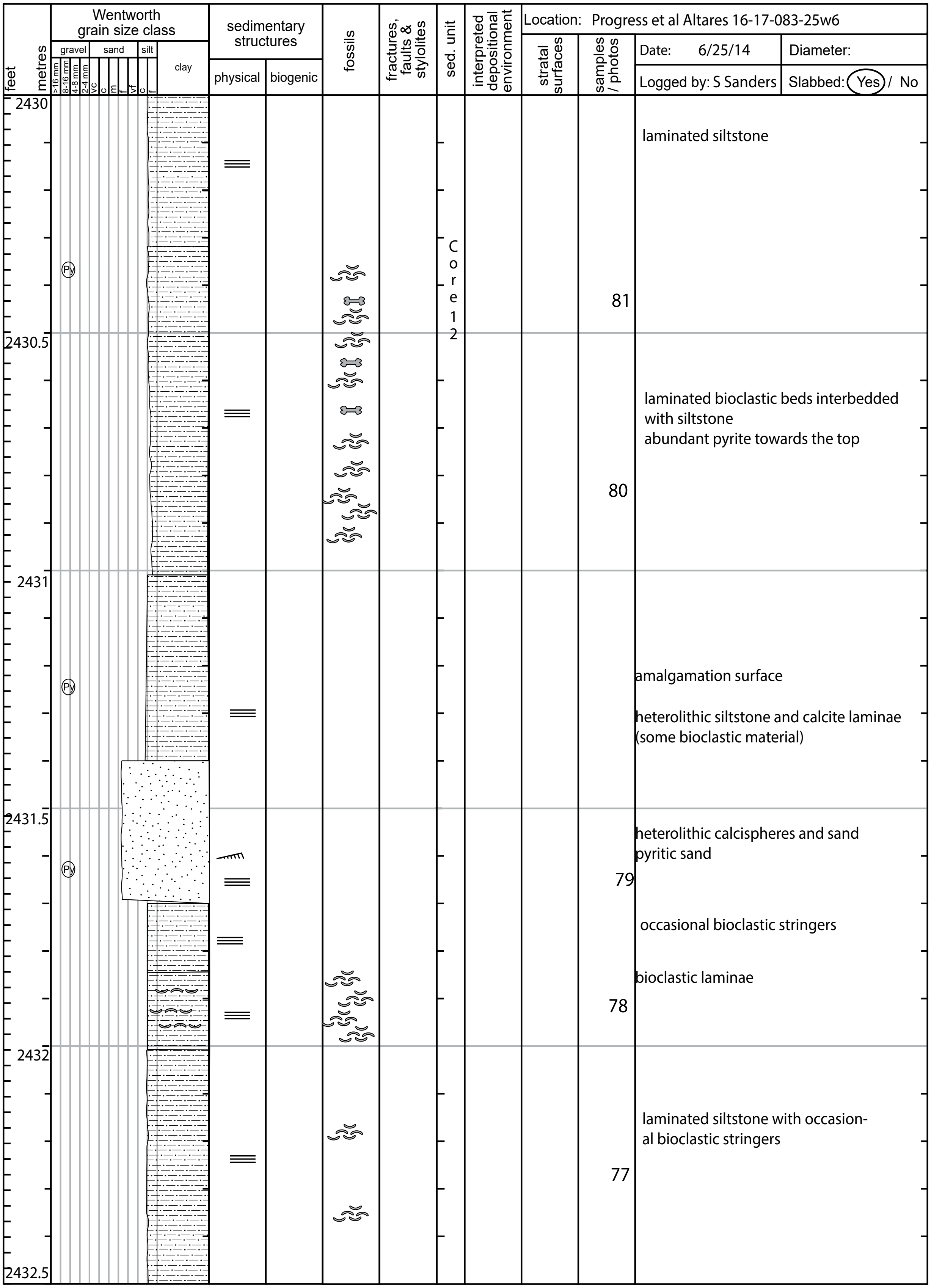
feet
metres
Wentworth grain size class
gravel
sand
silt
clay
>16 mm
8-16 mm
4-8 mm
2-4 mm
vc
c
m
f
vf
c
f
sedimentary structures
physical
biogenic
fossils
fractures, faults & stylolites
sed. unit
interpreted depositional environment
stratal surfaces
samples / photos
2430
2430.5
2431
2431.5
2432
2432.5
Py
Py
Py
Core 12
81
80
79
78
77

Location: Progress et al Altares 16-17-083-25w6

Date: 6/25/14

Diameter:

Logged by: S Sanders

Slabbed: [✓ Yes] / No

laminated siltstone

laminated bioclastic beds interbedded with siltstone
abundant pyrite towards the top

amalgamation surface

heterolithic siltstone and calcite laminae (some bioclastic material)

heterolithic calcispheres and sand
pyritic sand

occasional bioclastic stringers

bioclastic laminae

laminated siltstone with occasional bioclastic stringers

Location: Progress et al Altares 16-17-083-25w6

Date: 6/25/14

Diameter:

Logged by: S Sanders

Slabbed: [✓ Yes] / No

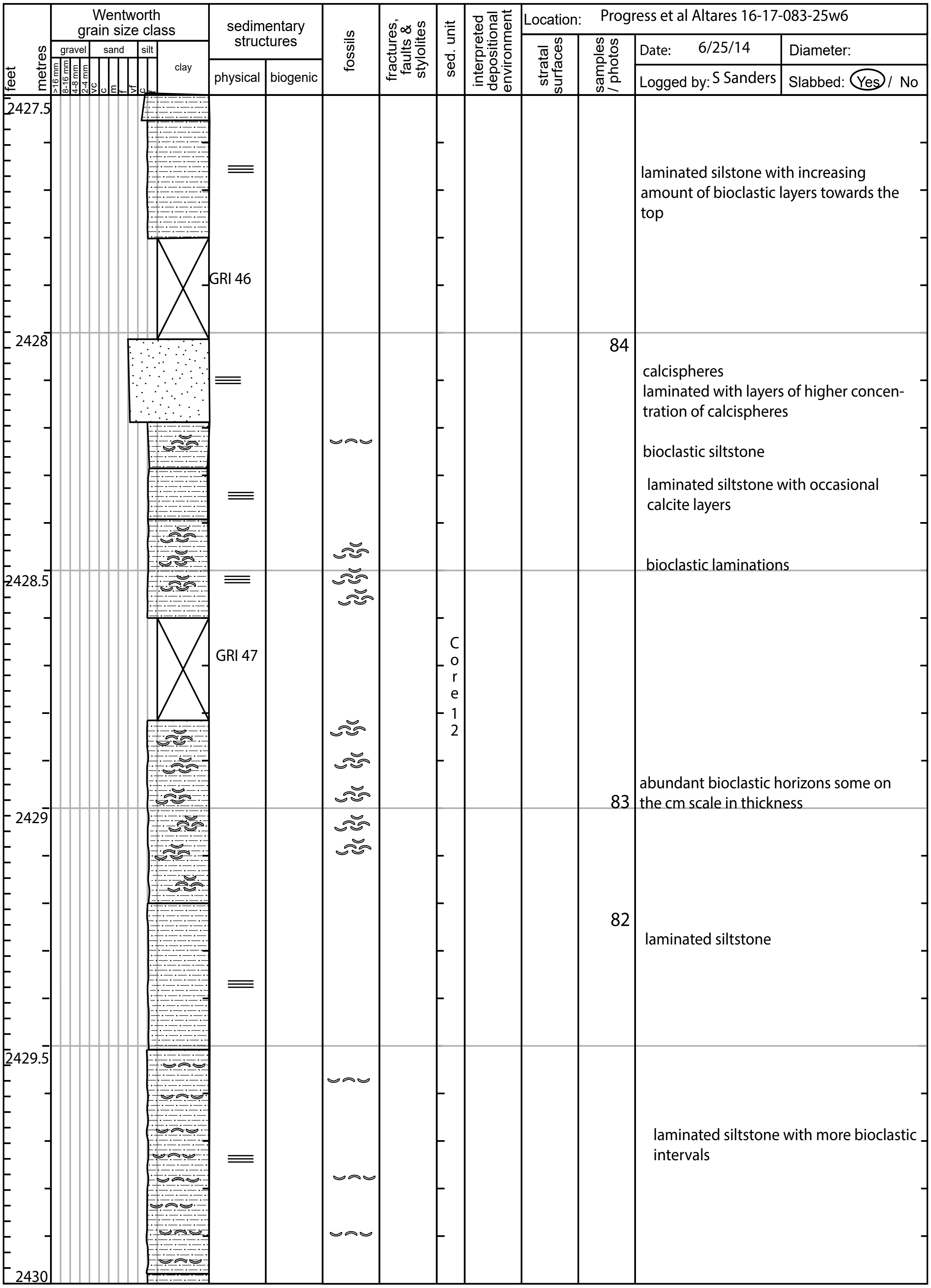
feet
metres
Wentworth grain size class
gravel
sand
silt
clay
>16 mm
8-16 mm
4-8 mm
2-4 mm
vc
c
m
f
vf
c
sedimentary structures
physical
biogenic
fossils
fractures, faults & stylolites
sed. unit
interpreted depositional environment
stratal surfaces
samples / photos
2427.5
2428
2428.5
2429
2429.5
2430
GRI 46
GRI 47
Core 12
84
83
82

laminated siltstone with increasing amount of bioclastic layers towards the top

calcispheres

laminated with layers of higher concentration of calcispheres

bioclastic siltstone

laminated siltstone with occasional calcite layers

bioclastic laminations

abundant bioclastic horizons some on the cm scale in thickness

laminated siltstone

laminated siltstone with more bioclastic intervals

Location: Progress et al Altares 16-17-083-25w6

Date: 6/25/14

Diameter:

Logged by: S Sanders

Slabbed: [✓ Yes] / No

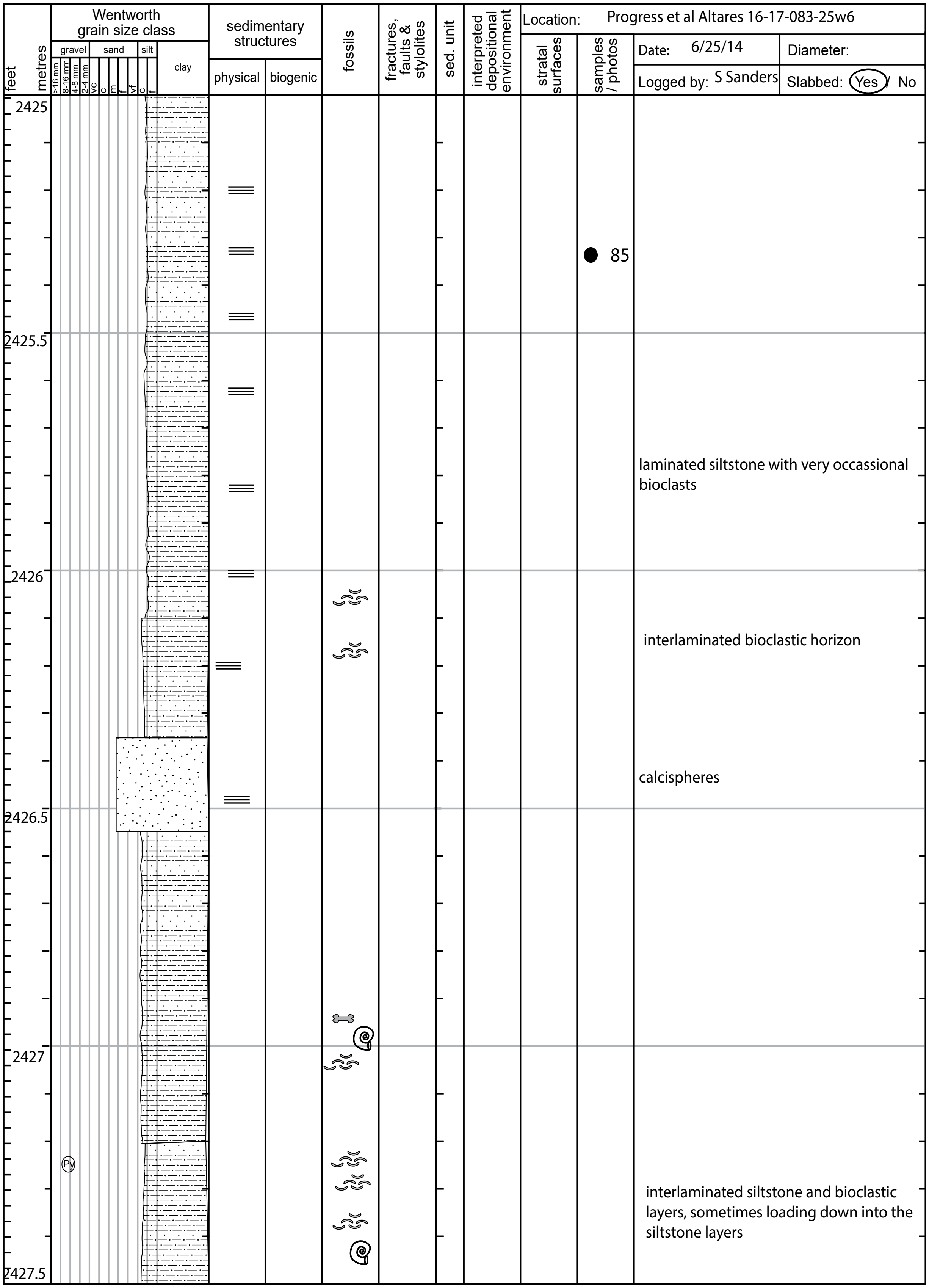
feet
metres
Wentworth grain size class
gravel
sand
silt
clay
>16 mm
8-16 mm
4-8 mm
2-4 mm
vc
c
m
f
vf
c
f
sedimentary structures
physical
biogenic
fossils
fractures, faults & stylolites
sed. unit
interpreted depositional environment
strata surfaces
samples / photos
2425
2425.5
2426
2426.5
2427
2427.5
85
Py

laminated siltstone with very occassional bioclasts

interlaminated bioclastic horizon

calcispheres

interlaminated siltstone and bioclastic layers, sometimes loading down into the siltstone layers

Location: Progress et al Altares 16-17-083-25w6

Date: 6/25/14

Diameter:

Logged by: S Sanders

Slabbed: [✓ Yes] / No

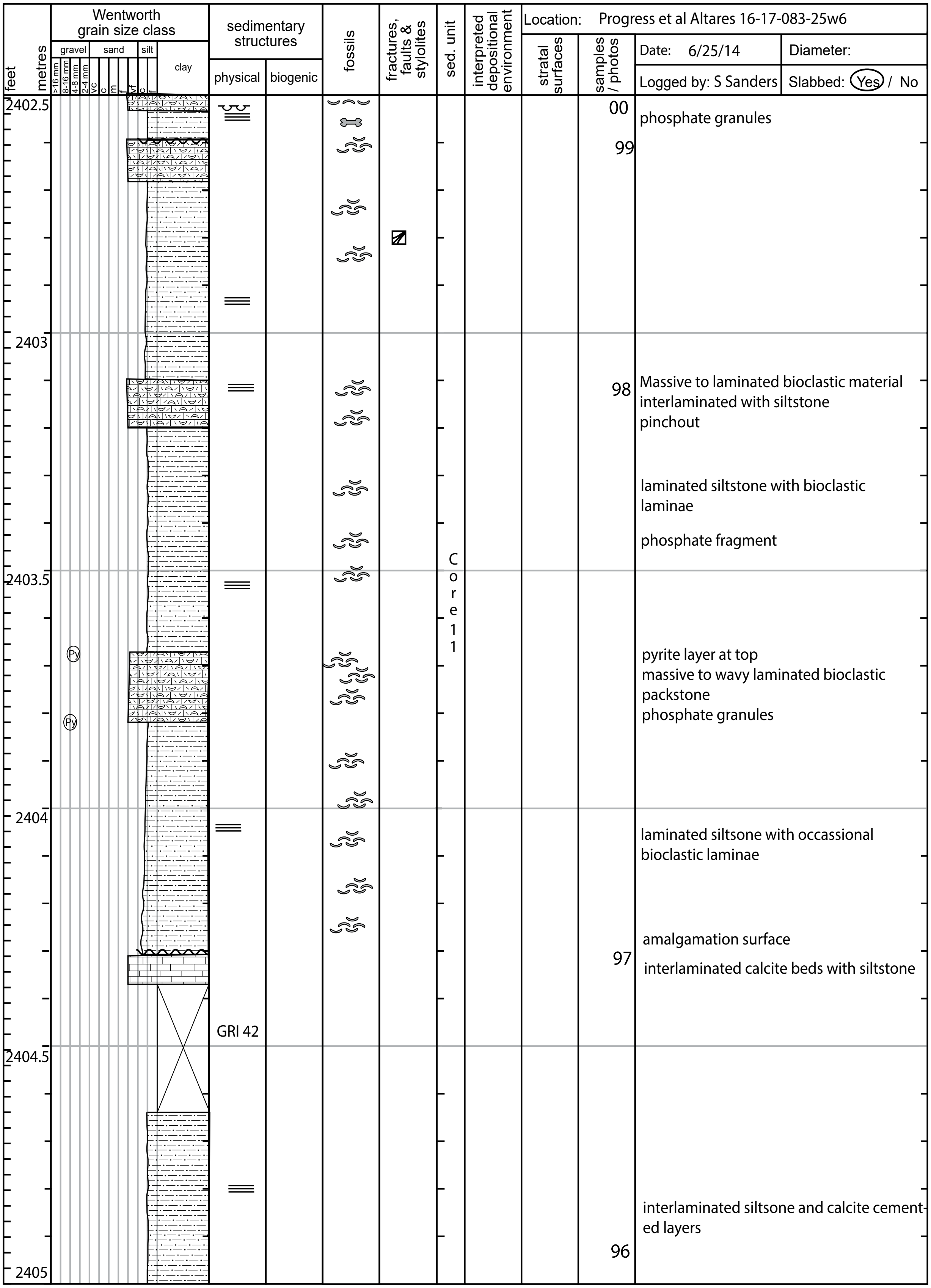
feet
metres
Wentworth grain size class
gravel
sand
silt
clay
>16 mm
8-16 mm
4-8 mm
2-4 mm
vc
c
m
f
vf
c
f
sedimentary structures
physical
biogenic
fossils
fractures, faults & stylolites
sed. unit
interpreted depositional environment
stratal surfaces
samples / photos
2402.5
2403
2403.5
2404
2404.5
2405
Py
Py
GRI 42
Core 11
00
99
98
97
96

phosphate granules

Massive to laminated bioclastic material interlaminated with siltstone

pinchout

laminated siltstone with bioclastic laminae

phosphate fragment

pyrite layer at top

massive to wavy laminated bioclastic packstone

phosphate granules

laminated siltsone with occassional bioclastic laminae

amalgamation surface

interlaminated calcite beds with siltstone

interlaminated siltsone and calcite cemented layers

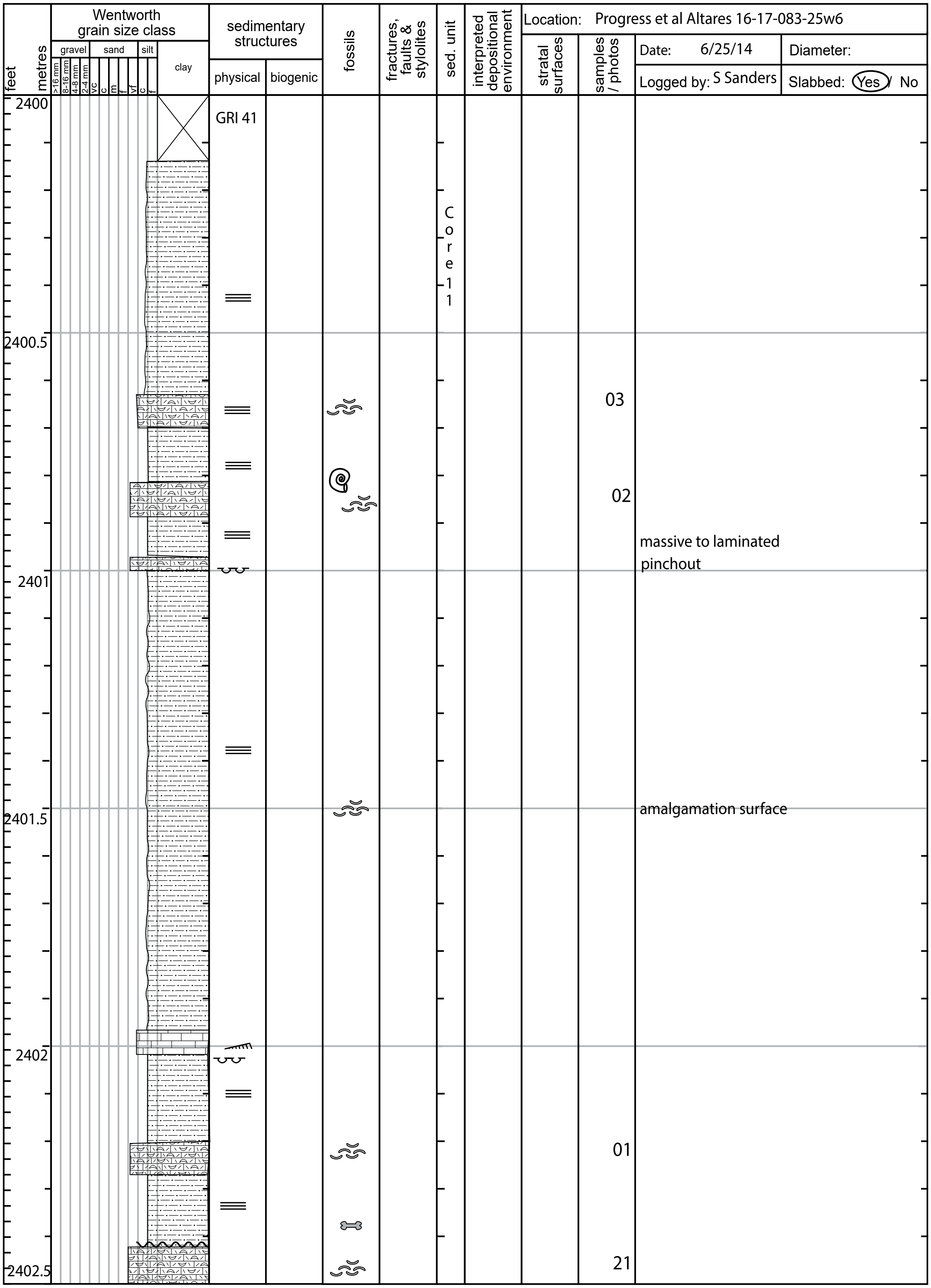

Location: Progress et al Altares 16-17-083-25w6

Date: 6/25/14

Diameter:

Logged by: S Sanders

Slabbed: [✓ Yes] / No

feet
metres
Wentworth grain size class
gravel
sand
silt
clay
>16 mm
8-16 mm
4-8 mm
2-4 mm
vc
c
m
f
vf
c
f
sedimentary structures
physical
biogenic
fossils
fractures, faults & stylolites
sed. unit
interpreted depositional environment
stratal surfaces
samples / photos
2400
2400.5
2401
2401.5
2402
2402.5
GRI 41
Core 11
03
02
01
21
massive to laminated
pinchout
amalgamation surface

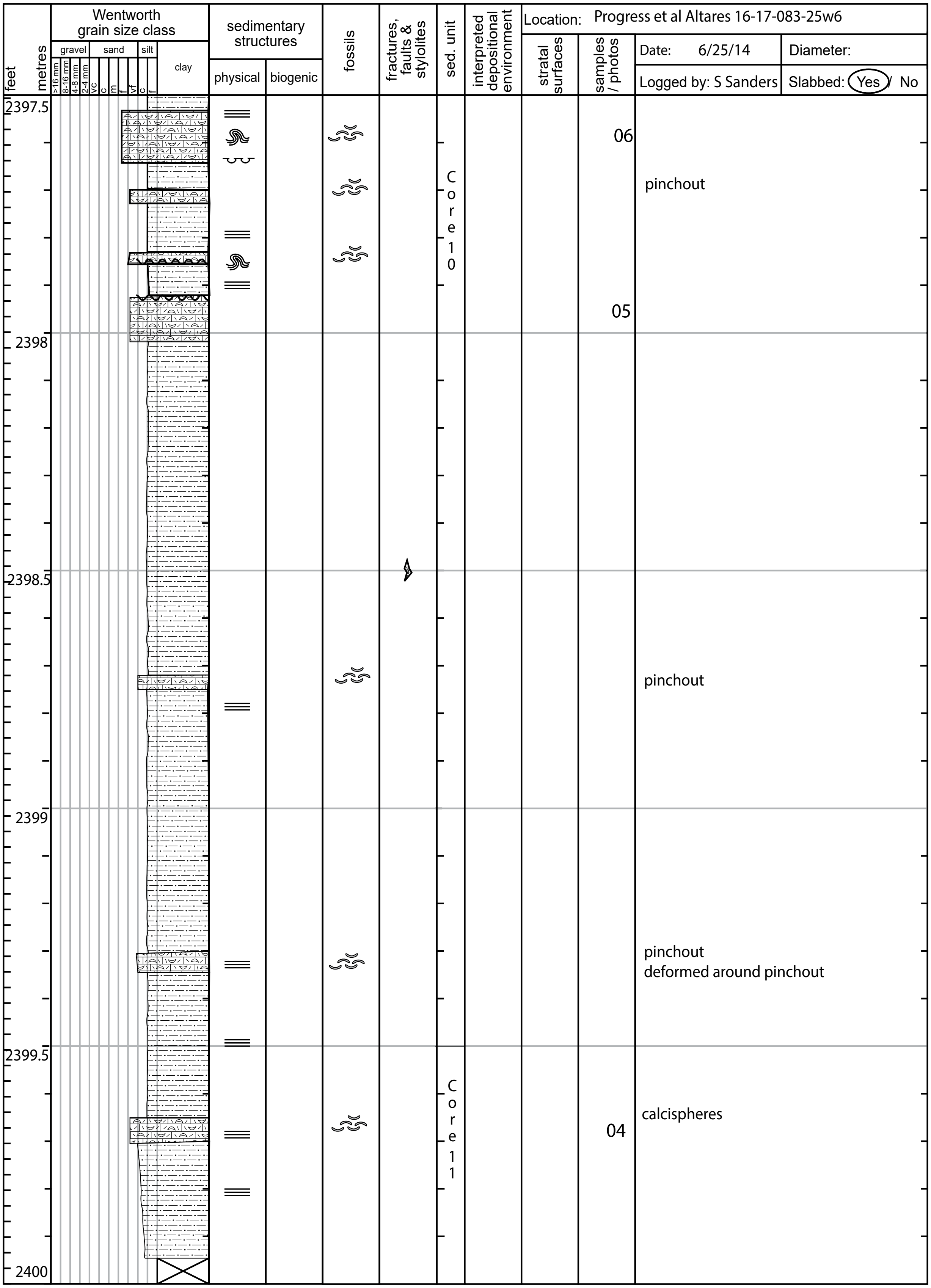
Location: Progress et al Altares 16-17-083-25w6

Date: 6/25/14

Diameter:

Logged by: S Sanders

Slabbed: [✓ Yes] / No

feet
metres
Wentworth grain size class
gravel
sand
silt
clay
>16 mm
8-16 mm
4-8 mm
2-4 mm
vc
c
m
f
vf
c
f
sedimentary structures
physical
biogenic
fossils
fractures, faults & stylolites
sed. unit
interpreted depositional environment
stratal surfaces
samples / photos
2397.5
2398
2398.5
2399
2399.5
2400
Core 10
Core 11
06
05
04
pinchout
pinchout
pinchout
deformed around pinchout
calcispheres

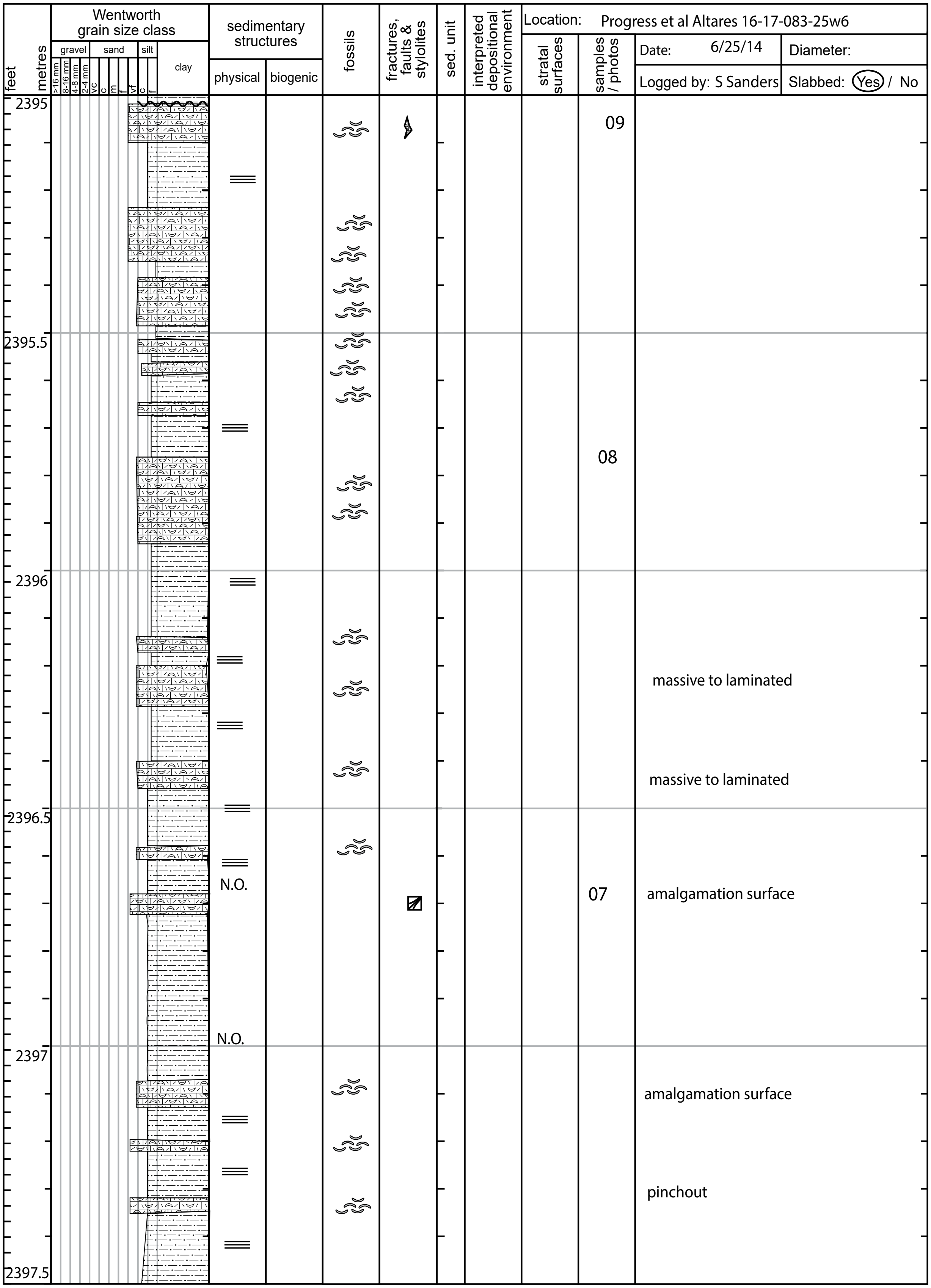
Wentworth grain size class
gravel
sand
silt
clay
>16 mm
8-16 mm
4-8 mm
2-4 mm
vc
c
m
f
vf
c
f
feet
metres
sedimentary structures
physical
biogenic
fossils
fractures, faults & stylolites
sed. unit
interpreted depositional environment
stratal surfaces
samples / photos
2395
2395.5
2396
2396.5
2397
2397.5
N.O.
N.O.
09
08
07
massive to laminated
massive to laminated
amalgamation surface
amalgamation surface
pinchout

Location: Progress et al Altares 16-17-083-25w6

Date: 6/25/14

Diameter:

Logged by: S Sanders

Slabbed: [✓ Yes] / No

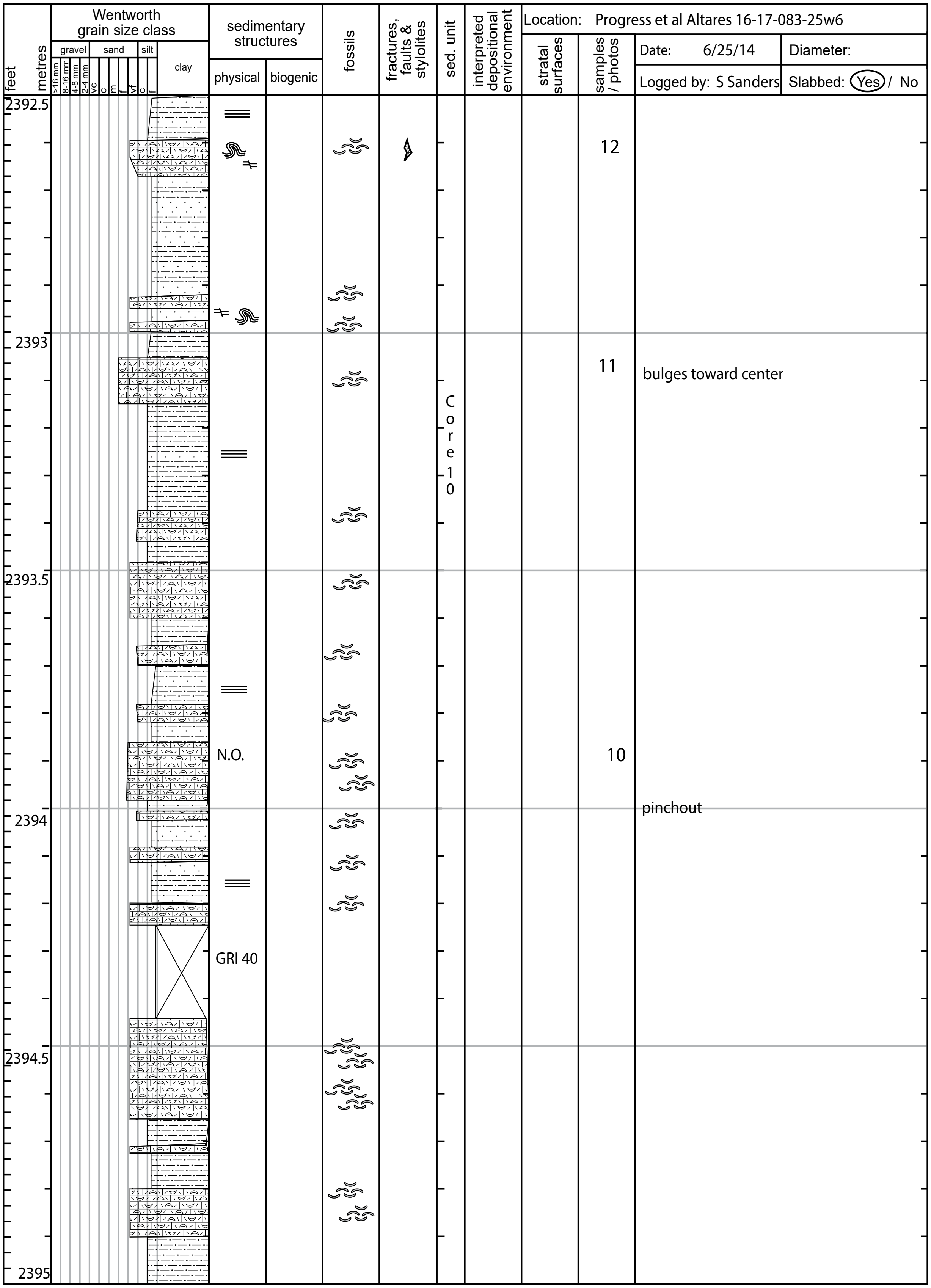

Location: Progress et al Altares 16-17-083-25w6

Date: 6/25/14

Diameter:

Logged by: S Sanders

Slabbed: [✓ Yes] / No

feet
metres
Wentworth grain size class
gravel
sand
silt
clay
>16 mm
8-16 mm
4-8 mm
2-4 mm
vc
c
m
f
vf
c
f
sedimentary structures
physical
biogenic
fossils
fractures, faults & stylolites
sed. unit
interpreted depositional environment
stratal surfaces
samples / photos
2392.5
2393
2393.5
2394
2394.5
2395
12
11
10
Core 10
N.O.
GRI 40
bulges toward center
pinchout

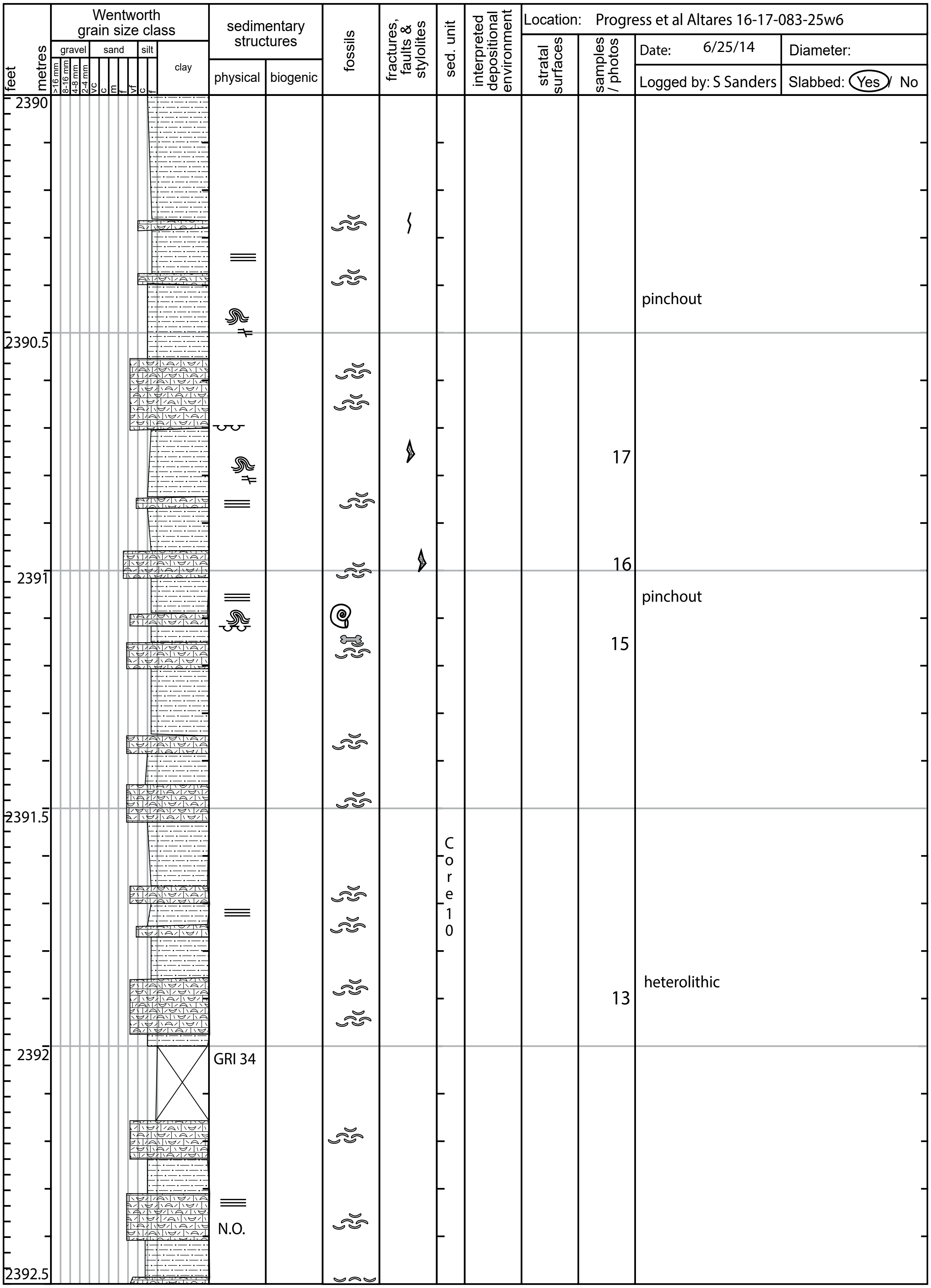
feet
metres
Wentworth grain size class
gravel
sand
silt
clay
>16 mm
8-16 mm
4-8 mm
2-4 mm
vc
c
m
f
vf
c
f
sedimentary structures
physical
biogenic
fossils
fractures, faults & stylolites
sed. unit
interpreted depositional environment
stratal surfaces
samples / photos
2390
2390.5
2391
2391.5
2392
2392.5
17
16
15
13
GRI 34
N.O.
C o r e 1 0
pinchout
pinchout
heterolithic

Location: Progress et al Altares 16-17-083-25w6

Date: 6/25/14

Diameter:

Logged by: S Sanders

Slabbed: [✓ Yes] / No

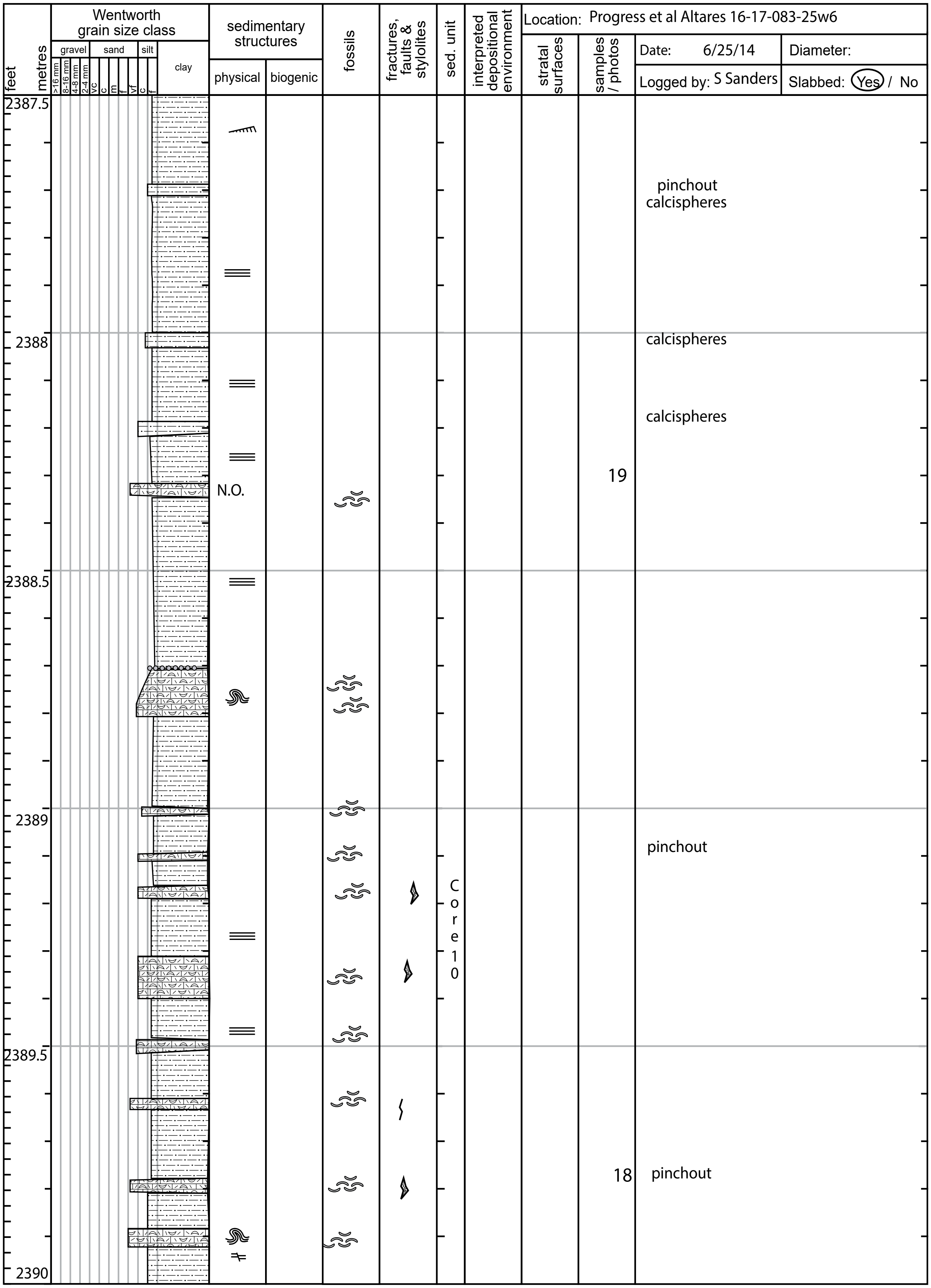
feet
metres
Wentworth grain size class
gravel
sand
silt
clay
>16 mm
8-16 mm
4-8 mm
2-4 mm
vc
c
m
f
vf
c
f
sedimentary structures
physical
biogenic
fossils
fractures, faults & stylolites
sed. unit
interpreted depositional environment
stratal surfaces
samples / photos
2387.5
2388
2388.5
2389
2389.5
2390
N.O.
Core 10
19
18

Location: Progress et al Altares 16-17-083-25w6

Date: 6/25/14

Diameter:

Logged by: S Sanders

Slabbed: [✓ Yes] / No

pinchout
calcispheres

calcispheres

calcispheres

pinchout

pinchout

Location: Progress et al Altares 16-17-083-25w6

Date: 6/25/14

Diameter:

Logged by: S Sanders

Slabbed: [✓ Yes] / No

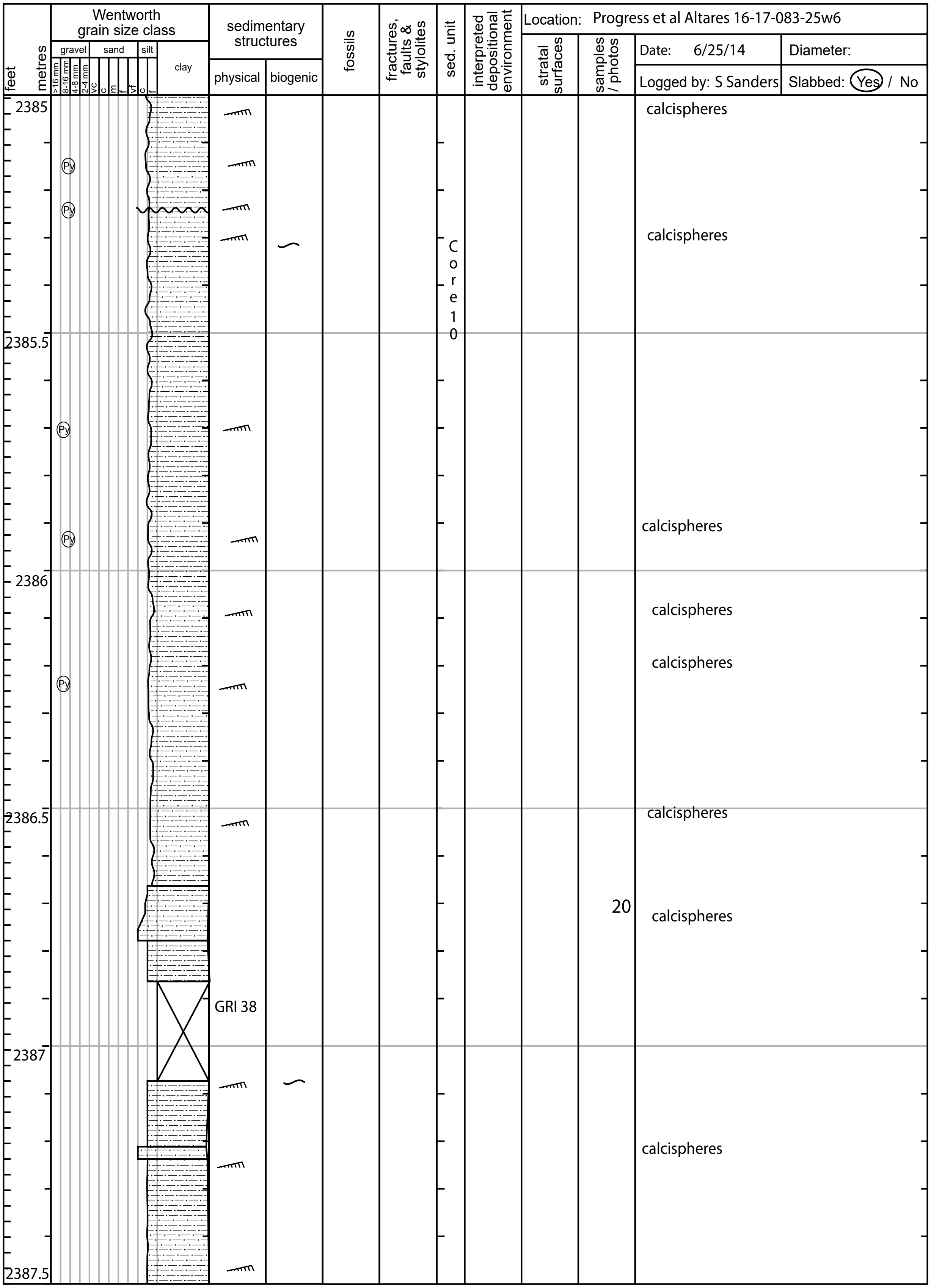

feet
metres
Wentworth grain size class
gravel
sand
silt
clay
>16 mm
8-16 mm
4-8 mm
2-4 mm
vc
c
m
f
vf
c
f
sedimentary structures
physical
biogenic
fossils
fractures, faults & stylolites
sed. unit
interpreted depositional environment
stratal surfaces
samples / photos
2385
2385.5
2386
2386.5
2387
2387.5
Py
Py
Py
Py
Py
Core 10
GRI 38
20
calcispheres
calcispheres
calcispheres
calcispheres
calcispheres
calcispheres
calcispheres
calcispheres

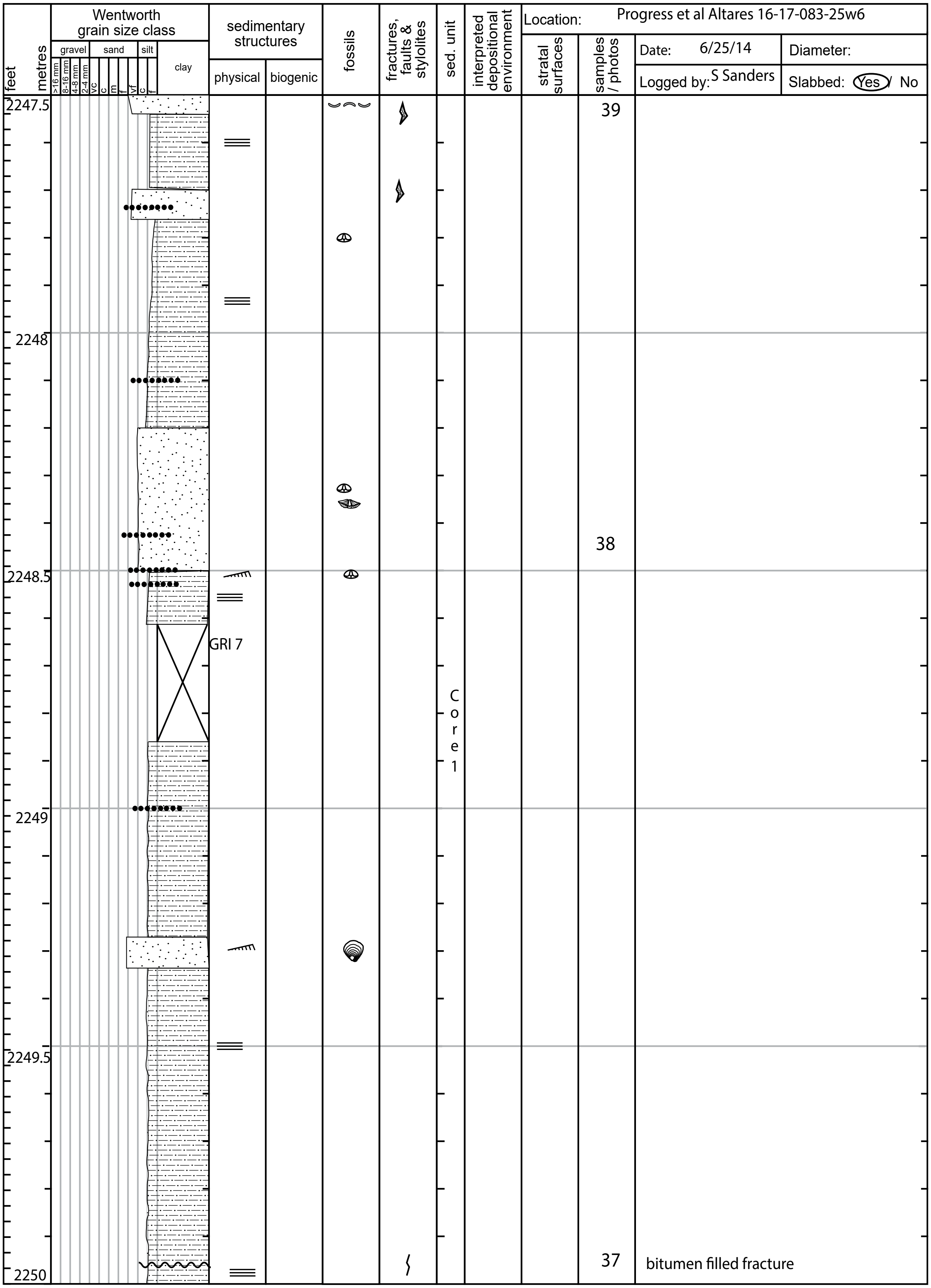

feet
metres
Wentworth grain size class
gravel
sand
silt
clay
>16 mm
8-16 mm
4-8 mm
2-4 mm
vc
c
m
f
vf
c
f
sedimentary structures
physical
biogenic
fossils
fractures, faults & stylolites
sed. unit
interpreted depositional environment
stratal surfaces
samples / photos
2247.5
2248
2248.5
2249
2249.5
2250
39
38
37
GRI 7
Core 1
bitumen filled fracture

Location: Progress et al Altares 16-17-083-25w6

Date: 6/25/14

Diameter:

Logged by: S Sanders

Slabbed: [✓ Yes] / No

Location: Progress et al Altares 16-17-083-25w6

Date: 6/25/14

Diameter:

Logged by: S Sanders

Slabbed: [✓ Yes] / No

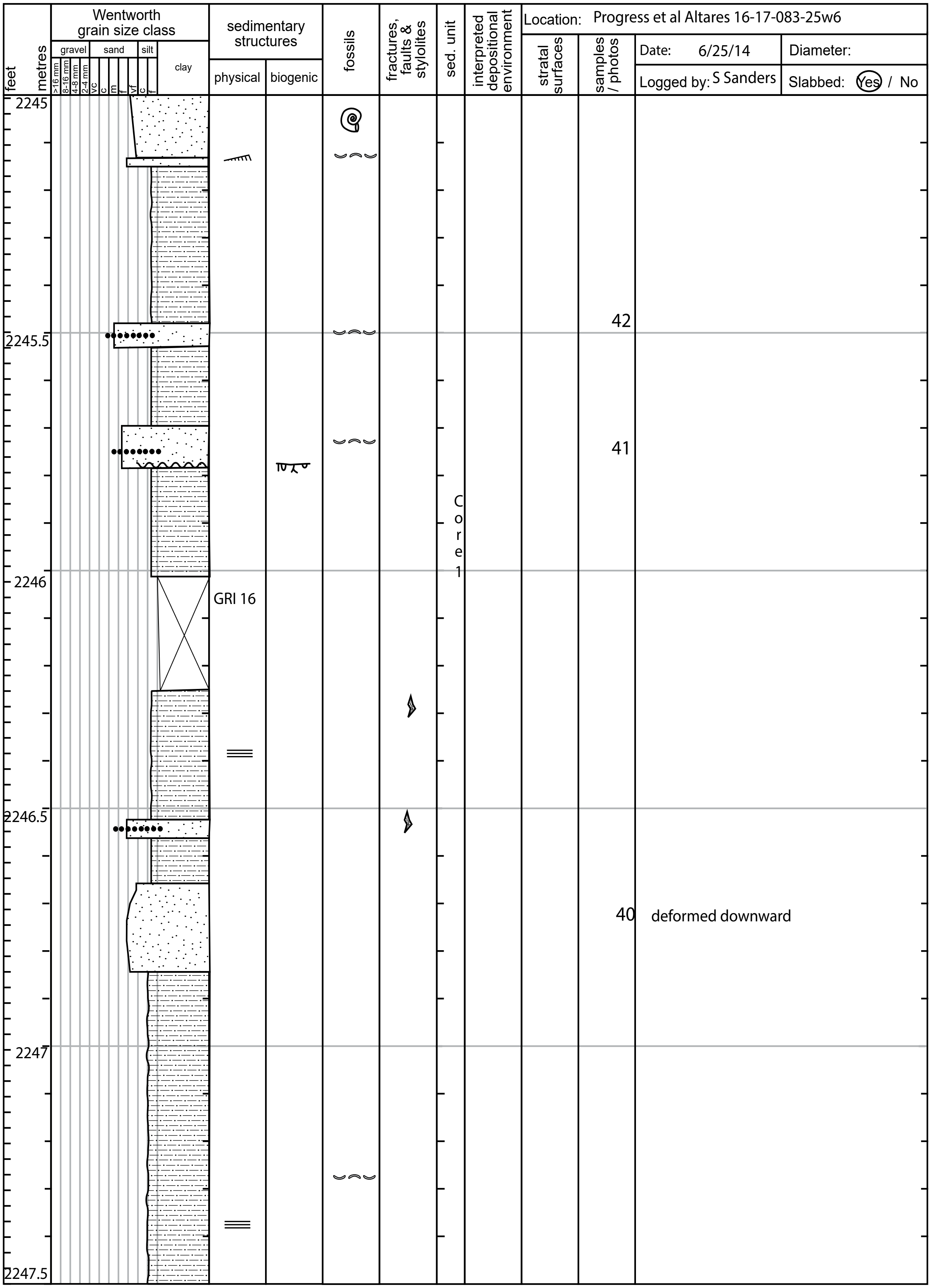

feet
metres
Wentworth grain size class
gravel
sand
silt
clay
>16 mm
8-16 mm
4-8 mm
2-4 mm
vc
c
m
f
vf
c
f
sedimentary structures
physical
biogenic
fossils
fractures, faults & stylolites
sed. unit
interpreted depositional environment
stratal surfaces
samples / photos
2245
2245.5
2246
2246.5
2247
2247.5
GRI 16
Core 1
42
41
40
deformed downward

Location: Progress et al Altares 16-17-083-25w6

Date: 6/25/14

Diameter:

Logged by: S Sanders

Slabbed: Yes [✓ Yes] / No

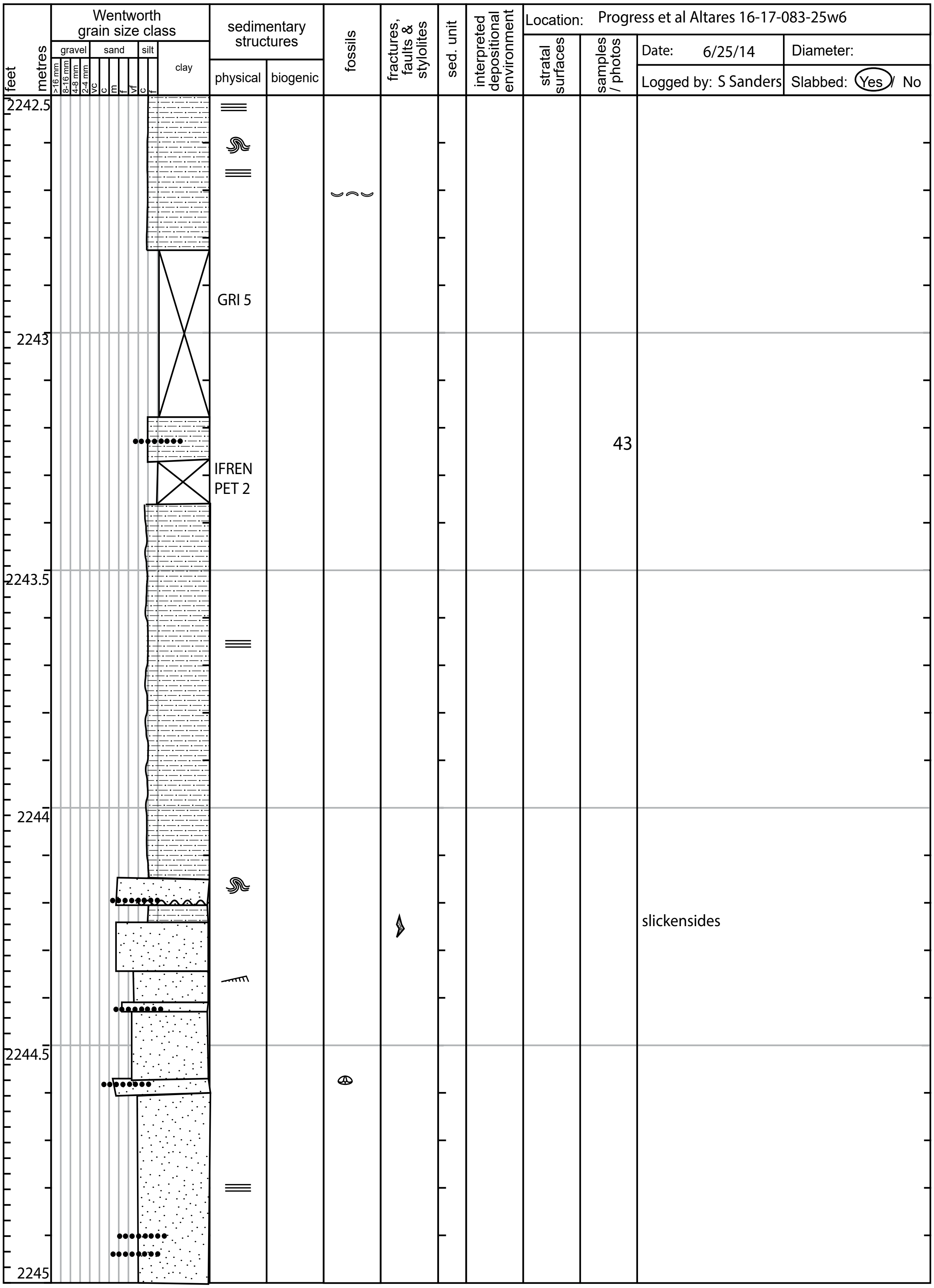
feet
metres
Wentworth grain size class
gravel
sand
silt
clay
>16 mm
8-16 mm
4-8 mm
2-4 mm
vc
c
m
f
vf
c
f
sedimentary structures
physical
biogenic
fossils
fractures, faults & stylolites
sed. unit
interpreted depositional environment
stratal surfaces
samples / photos
2242.5
2243
2243.5
2244
2244.5
2245
GRI 5
IFREN PET 2
43
slickensides

Location: Progress et al Altares 16-17-083-25w6

Date: 6/25/14

Diameter:

Logged by: S Sanders

Slabbed: [✓ Yes] / No

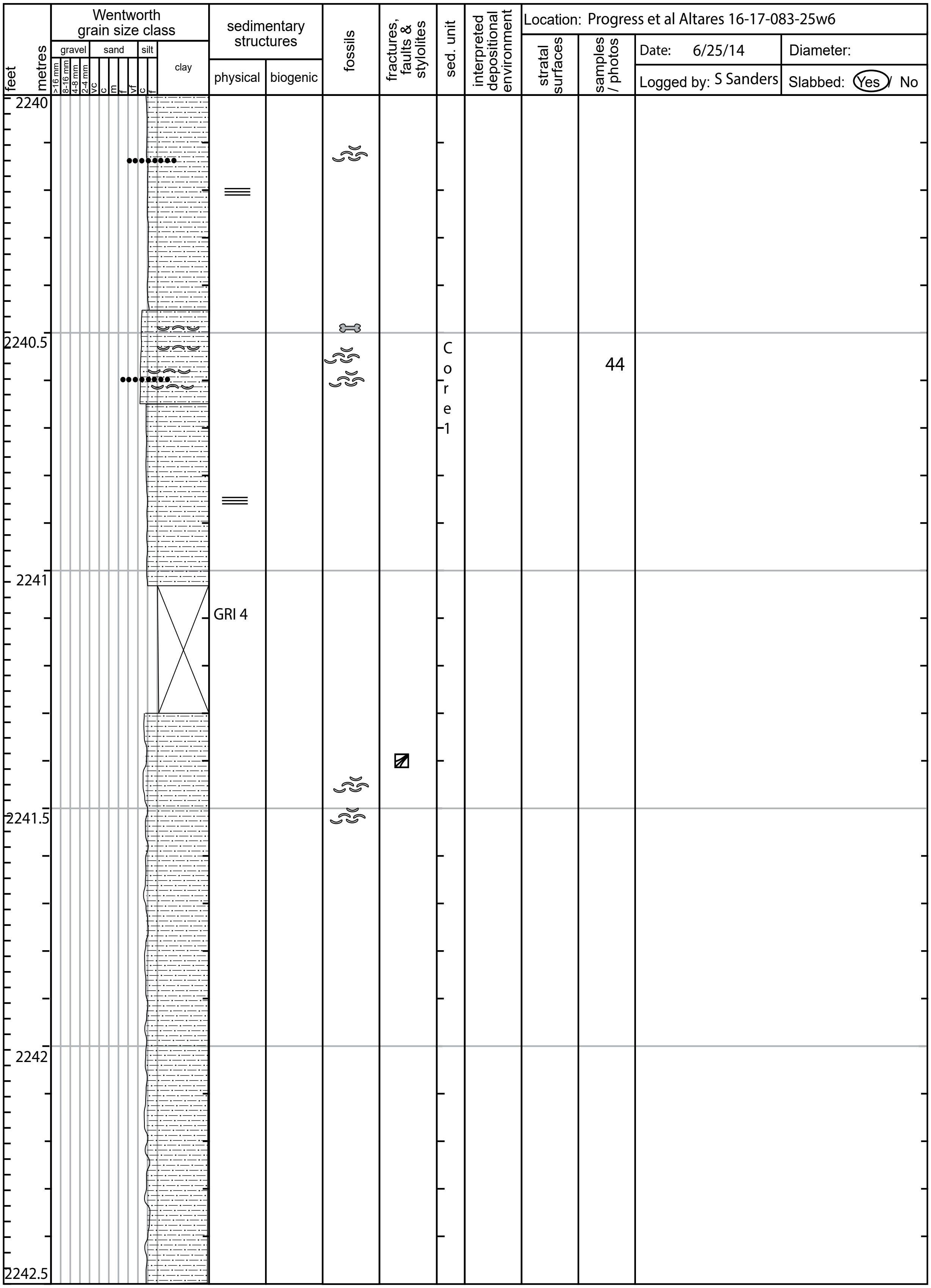

feet
metres
Wentworth grain size class
gravel
sand
silt
clay
>16 mm
8-16 mm
4-8 mm
2-4 mm
vc
c
m
f
vf
c
f
sedimentary structures
physical
biogenic
fossils
fractures, faults & stylolites
sed. unit
interpreted depositional environment
stratal surfaces
samples / photos
2240
2240.5
2241
2241.5
2242
2242.5
GRI 4
Core 1
44

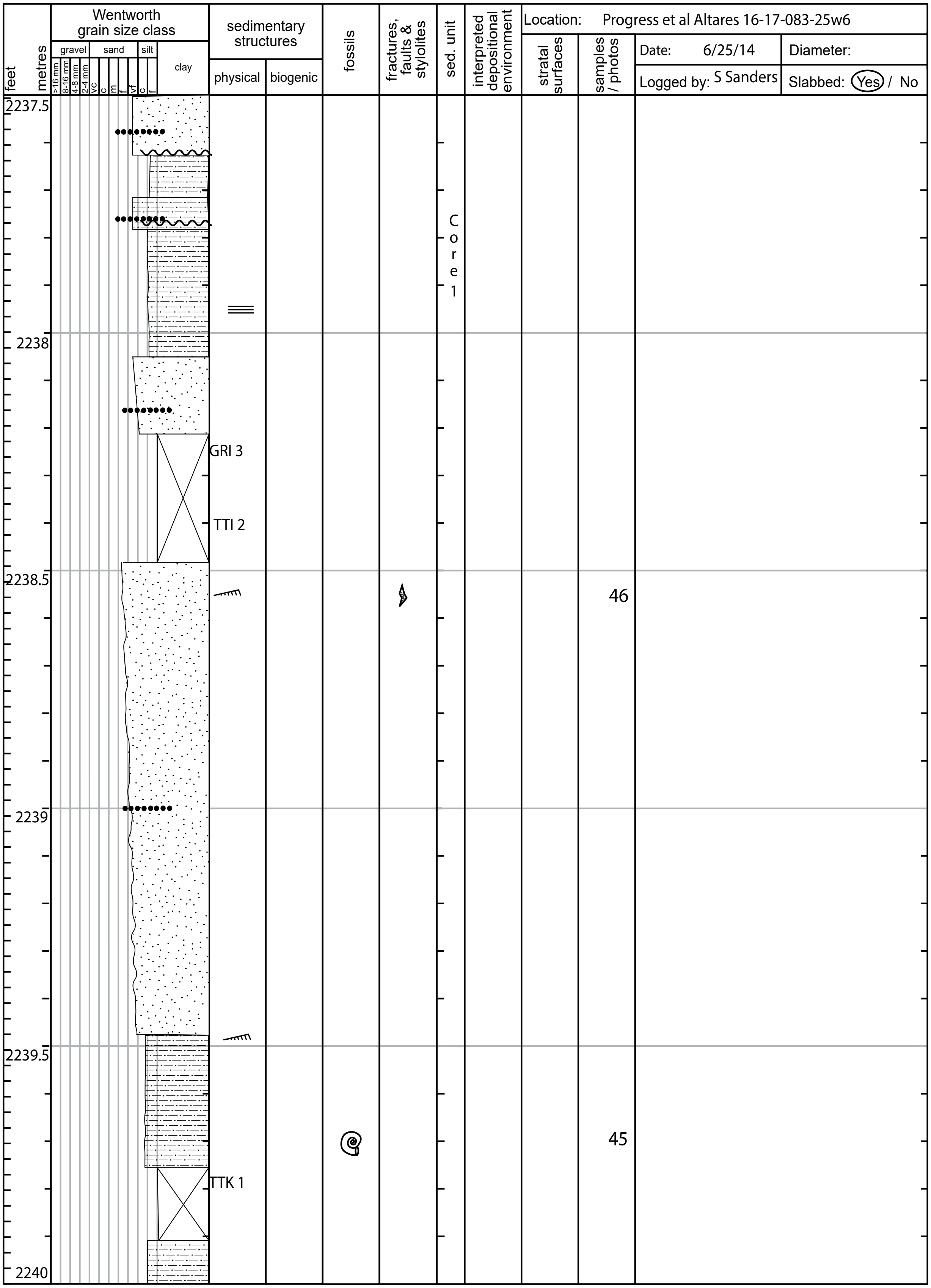
feet
metres
Wentworth grain size class
gravel
sand
silt
clay
>16 mm
8-16 mm
4-8 mm
2-4 mm
vc
c
m
f
vf
c
f
sedimentary structures
physical
biogenic
fossils
fractures, faults & stylolites
sed. unit
interpreted depositional environment
stratal surfaces
samples / photos
2237.5
2238
2238.5
2239
2239.5
2240
GRI 3
TTI 2
TTK 1
Core 1
46
45

Location: Progress et al Altares 16-17-083-25w6

Date: 6/25/14

Diameter:

Logged by: S Sanders

Slabbed: [✓ Yes] / No

Location: Progres et al Altares 16-17-083-25w6

Date: 6/25/14

Diameter:

Logged by: S Sanders

Slabbed: [✓ Yes] / No

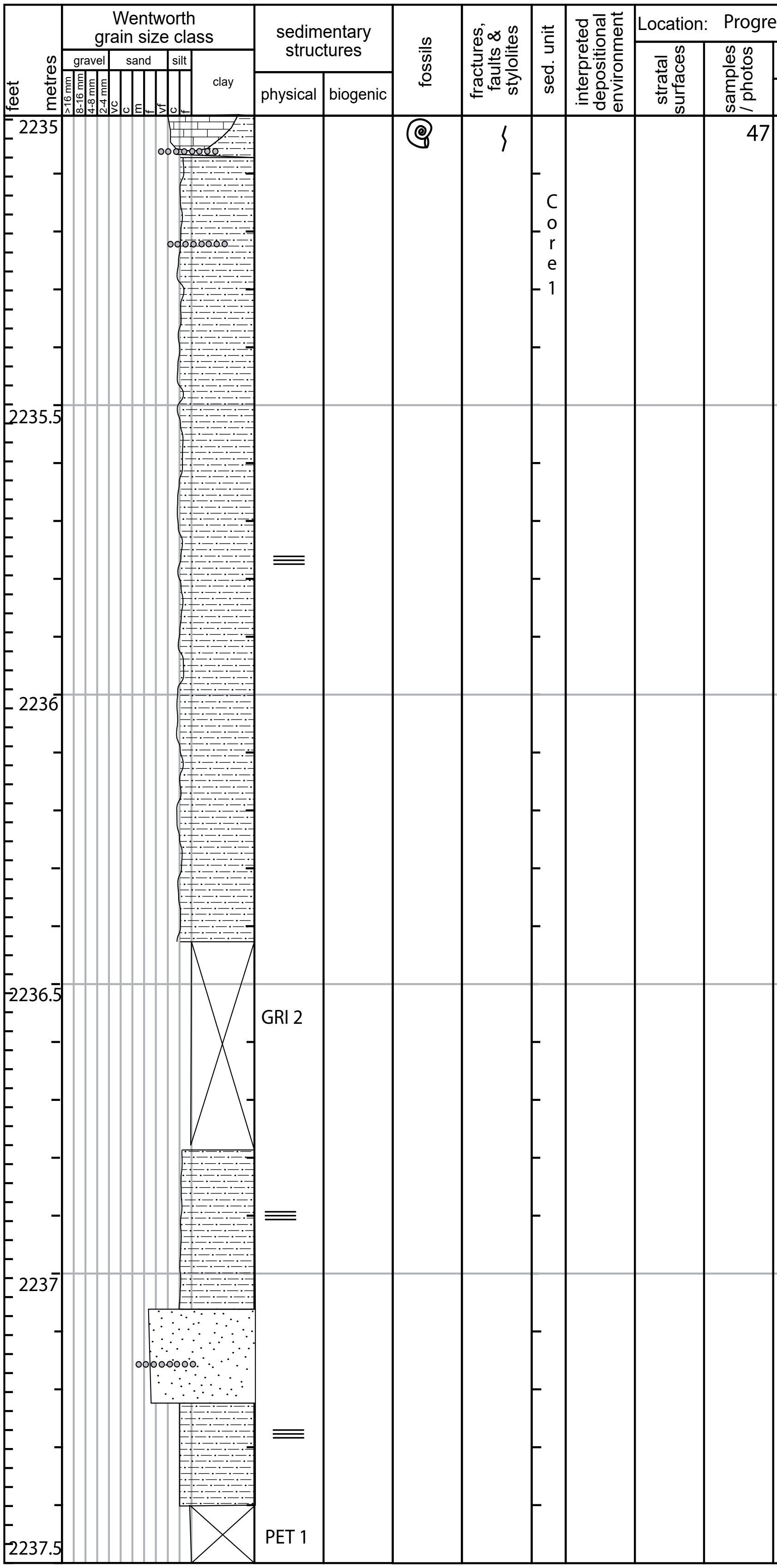
feet
metres
Wentworth grain size class
gravel
sand
silt
clay
>16 mm
8-16 mm
4-8 mm
2-4 mm
vc
c
m
f
vf
c
f
sedimentary structures
physical
biogenic
fossils
fractures, faults & stylolites
sed. unit
interpreted depositional environment
stratal surfaces
samples / photos
2235
2235.5
2236
2236.5
2237
2237.5
Core 1
47
GRI 2
PET 1

ammonoid concretion
beds deformed around concretion
fractures around concretion

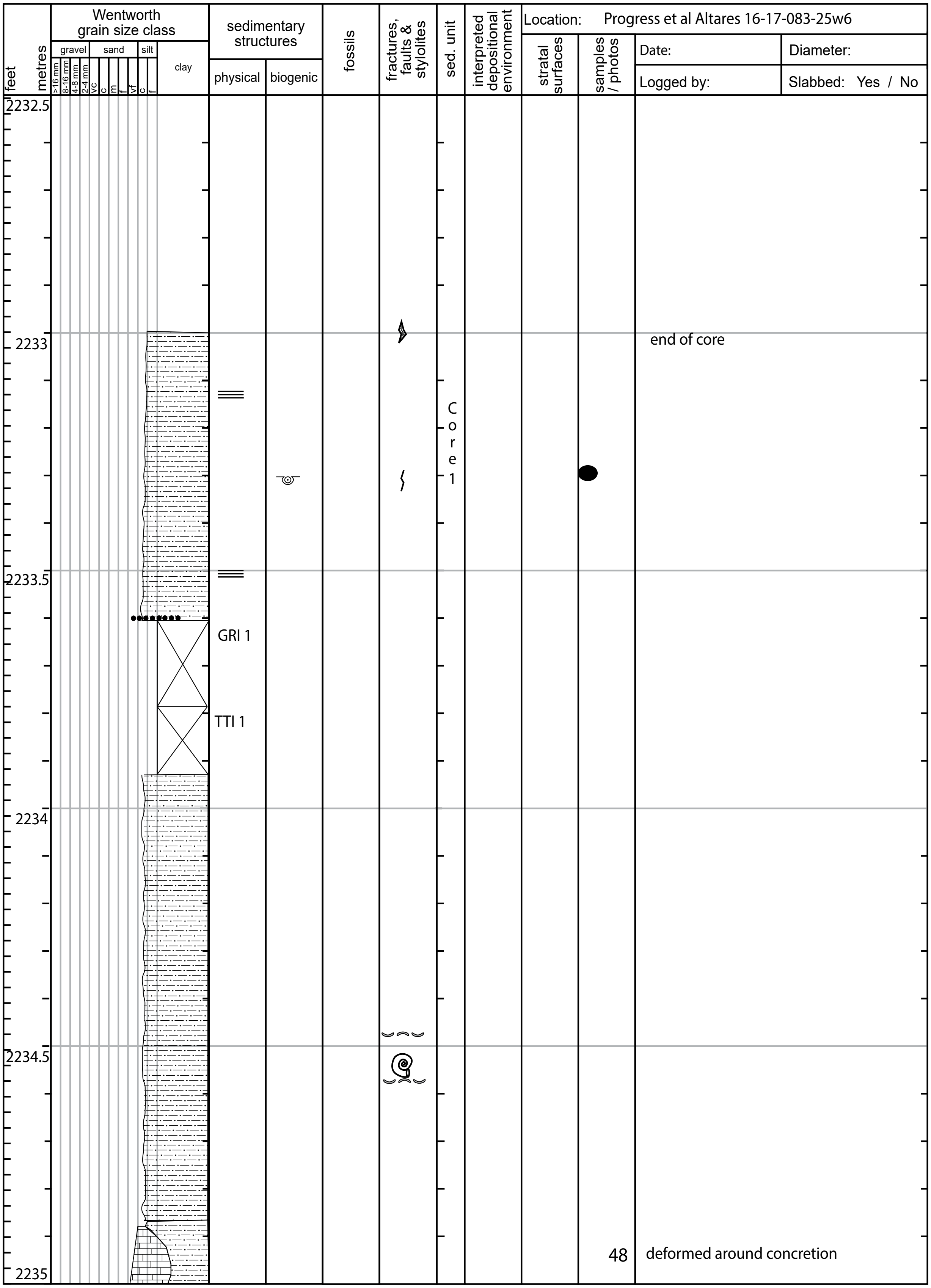

feet
metres
Wentworth grain size class
gravel
sand
silt
clay
>16 mm
8-16 mm
4-8 mm
2-4 mm
vc
c
m
f
vf
c
f
sedimentary structures
physical
biogenic
fossils
fractures, faults & stylolites
sed. unit
interpreted depositional environment
stratal surfaces
samples / photos
2232.5
2233
2233.5
2234
2234.5
2235
GRI 1
TTI 1
Core 1

Location: Progress et al Altares 16-17-083-25w6

Date:

Diameter:

Logged by:

Slabbed: Yes / No

end of core

48 deformed around concretion

Location: Suncor EV Paradise a07-19-085-15w6 p1

Date: 7/3/14

Diameter: 10cm

Logged by: S Sanders

Slabbed: [✓ Yes] / No

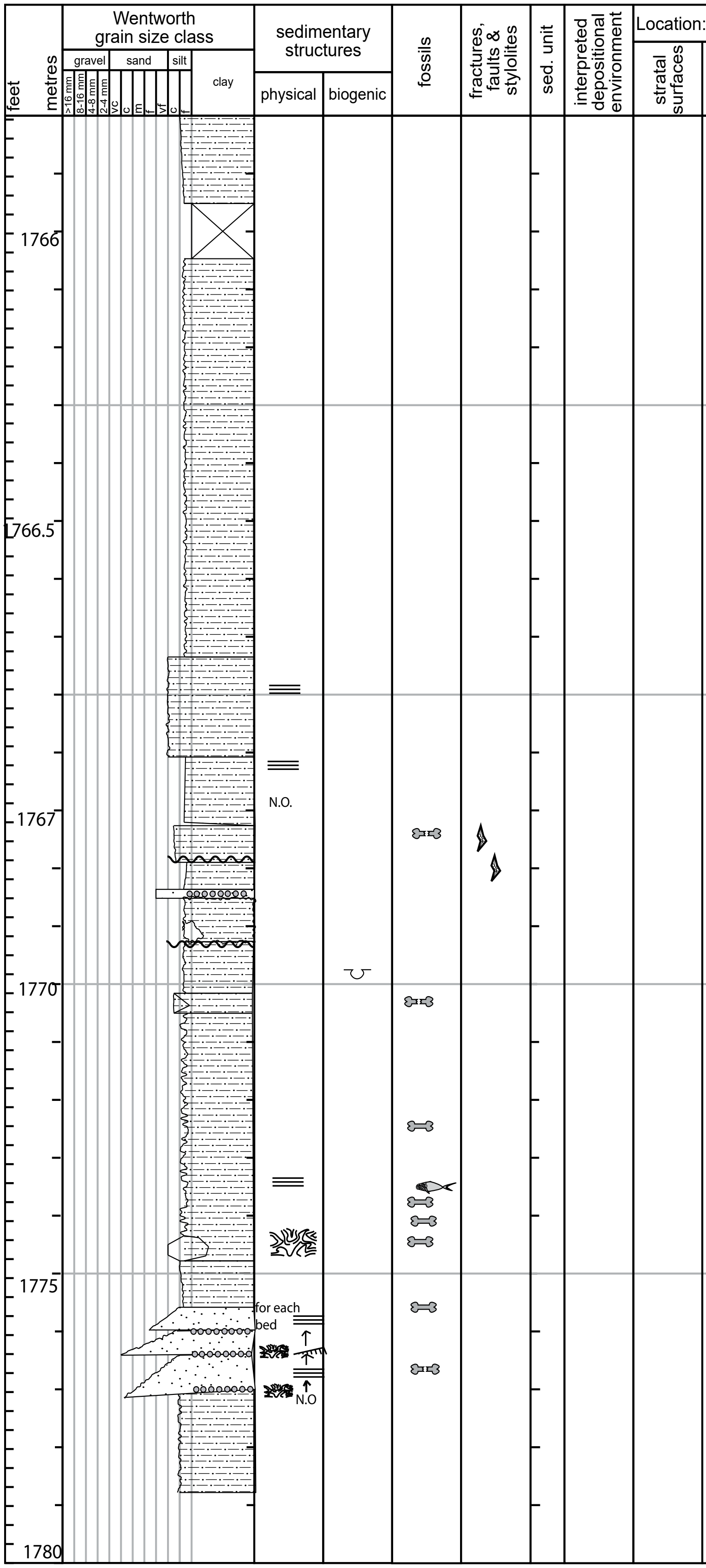
feet
metres
Wentworth grain size class
gravel
sand
silt
clay
>16 mm
8-16 mm
4-8 mm
2-4 mm
vc
c
m
f
vf
c
f
sedimentary structures
physical
biogenic
fossils
fractures, faults & stylolites
sed. unit
interpreted depositional environment
stratal surfaces
1766
1766.5
1767
1770
1775
1780
N.O.
for each bed
N.O

samples / photos

same as below

occasional calcite laminae (usually calcispheres)
60

59 calcispheres

58 calcispheres

57 concretion

56

55

54 concretion

53

52

51 concretion

50

49

48

pinchout

47 prevalent fossilized organic debris through core

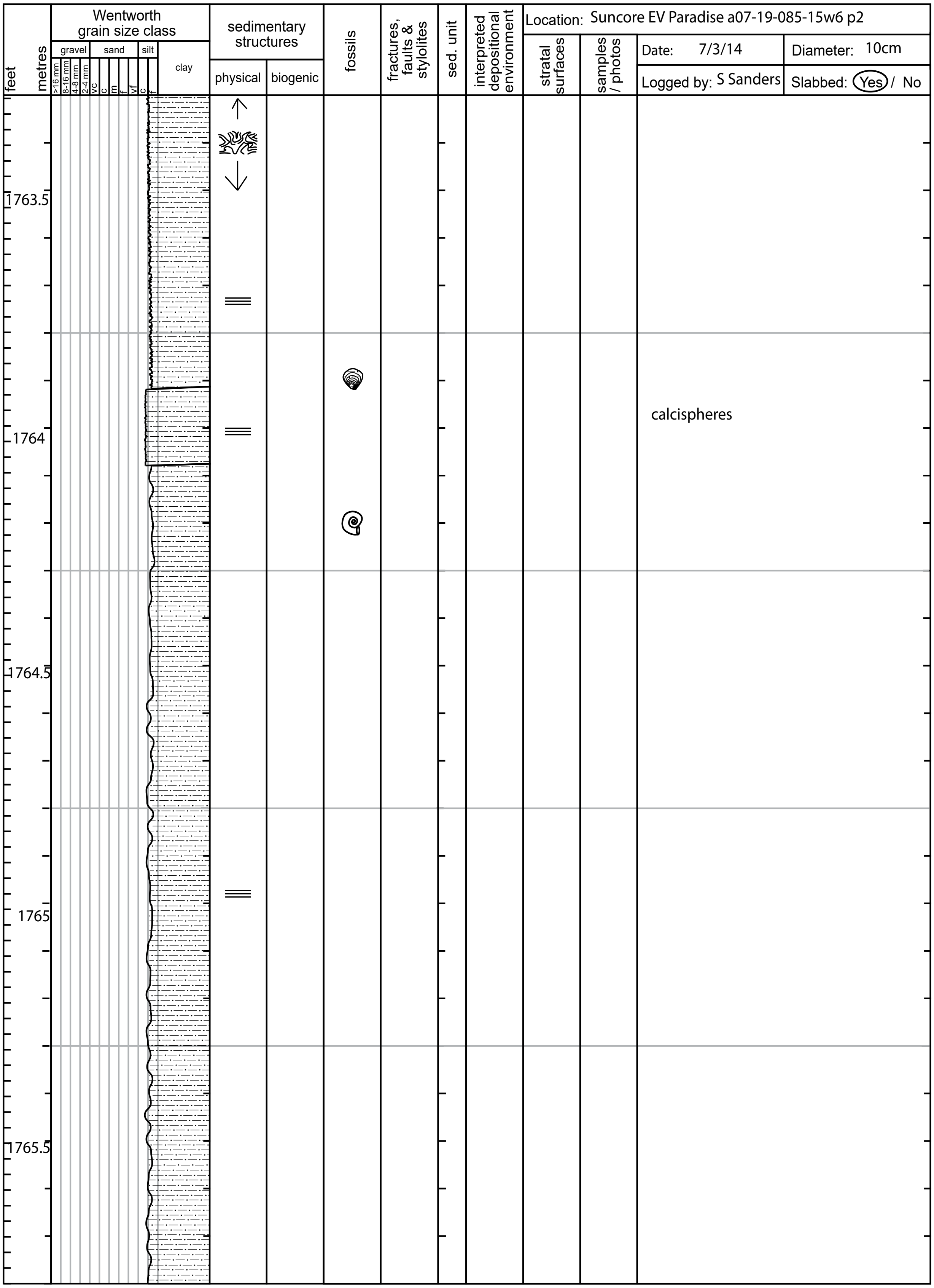
feet
metres
Wentworth grain size class
gravel
sand
silt
>16 mm
8-16 mm
4-8 mm
2-4 mm
vc
c
m
f
vf
c
f
clay
sedimentary structures
physical
biogenic
fossils
fractures, faults & stylolites
sed. unit
interpreted depositional environment
stratal surfaces
samples / photos
1763.5
1764
1764.5
1765
1765.5

Location: Suncore EV Paradise a07-19-085-15w6 p2

Date: 7/3/14

Diameter: 10cm

Logged by: S Sanders

Slabbed: [✓ Yes] / No

calcispheres

Location: Suncor EV Paradise a07-19-85-15w6 p3

Date: 7/3/14

Diameter: 10cm

Logged by: S Sanders

Slabbed: [✓ Yes] / No

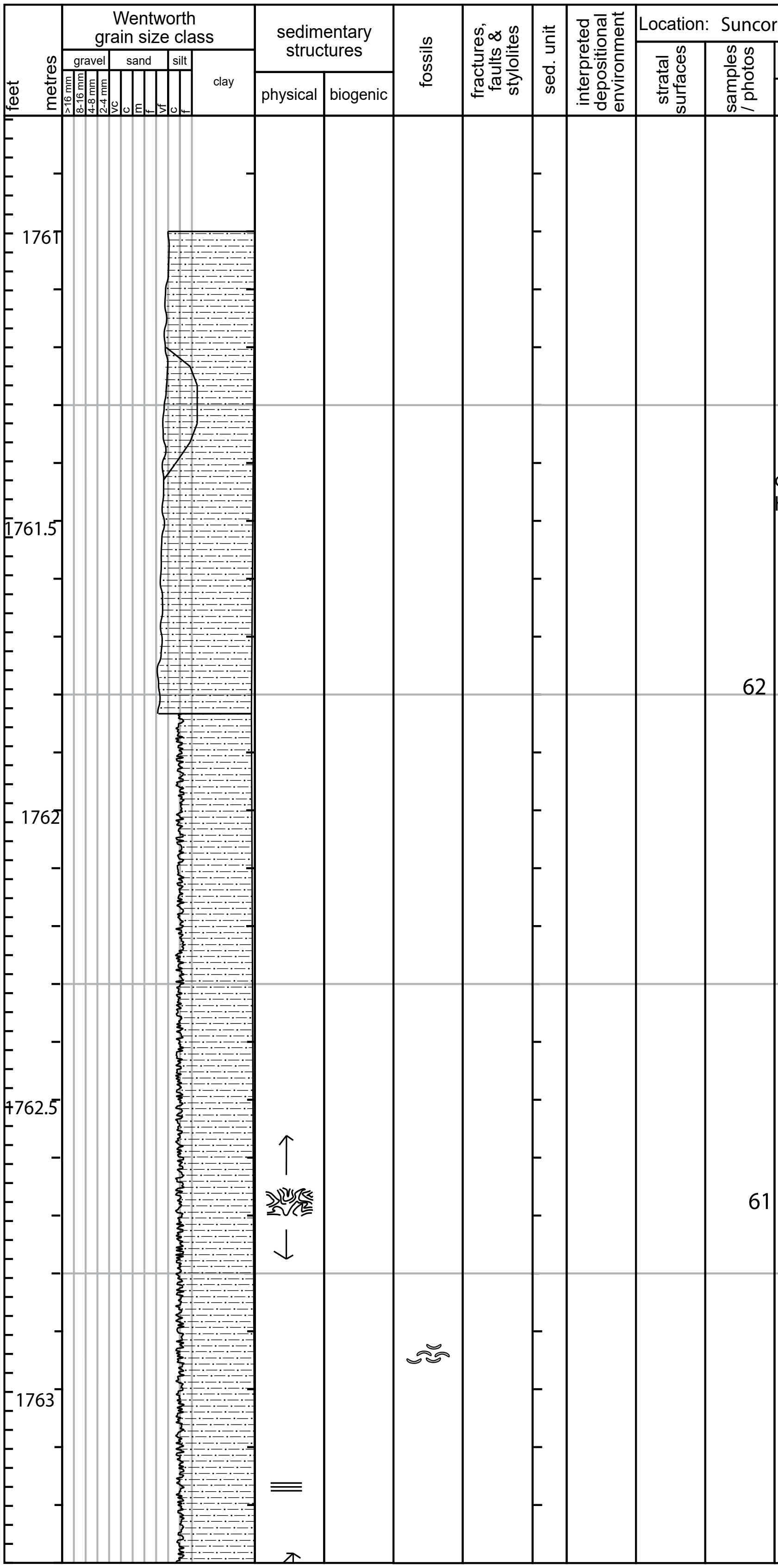
feet
metres
Wentworth grain size class
gravel
sand
silt
clay
>16 mm
8-16 mm
4-8 mm
2-4 mm
vc
c
m
f
vf
c
f
sedimentary structures
physical
biogenic
fossils
fractures, faults & stylolites
sed. unit
interpreted depositional environment
strata surfaces
samples / photos
1761
1761.5
1762
1762.5
1763
62
61

concretion?

calcite cemented coarser grained horizon

Location: Scurry Placer West Eage A8-7-85-18w6 p1

Date: 7/4/14

Diameter: 8.5cm

Logged by: SCS

Slabbed: [✓ Yes] / No

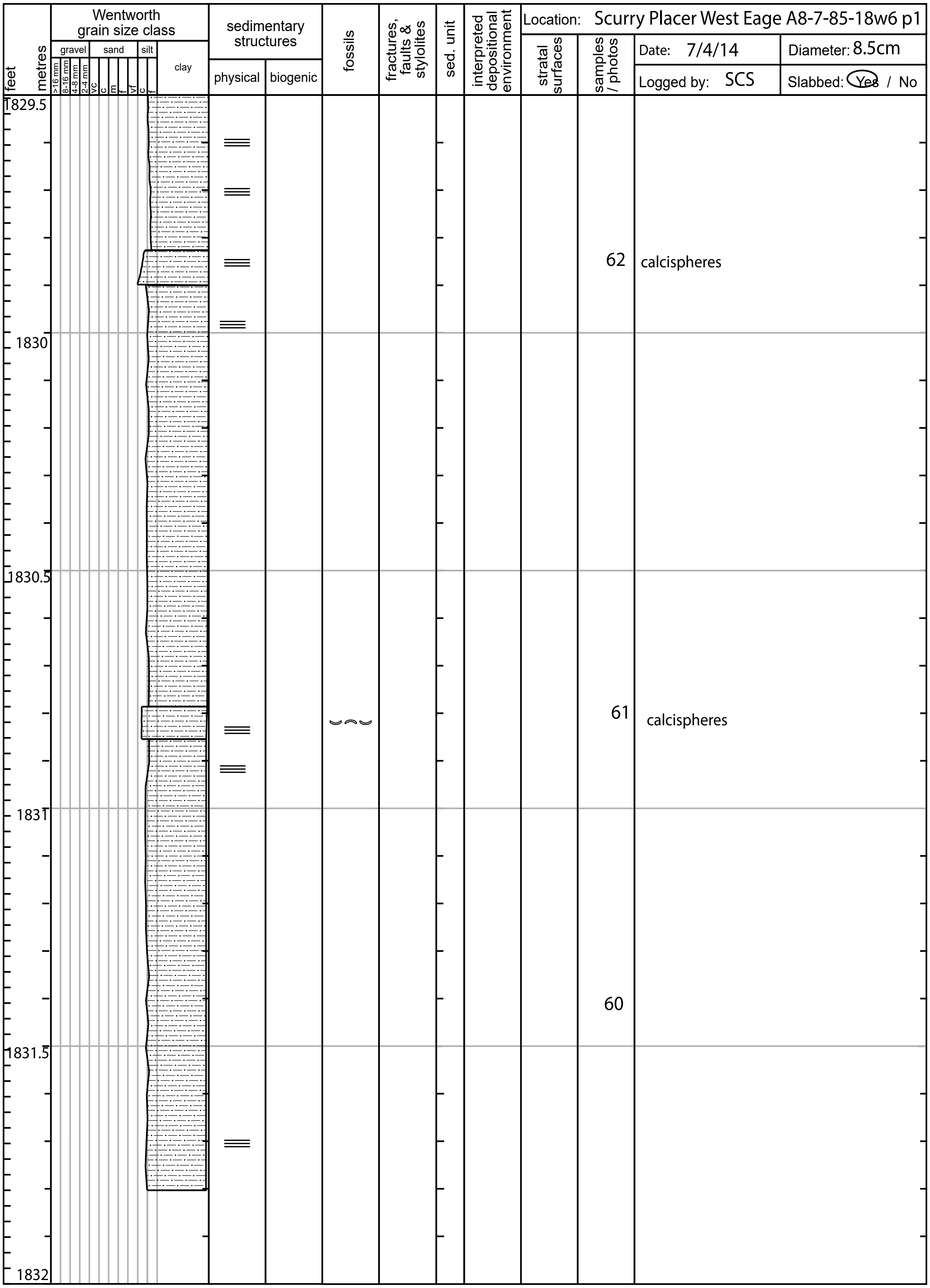
feet
metres
Wentworth grain size class
gravel
sand
silt
clay
>16 mm
8-16 mm
4-8 mm
2-4 mm
vc
c
m
f
vf
c
f
sedimentary structures
physical
biogenic
fossils
fractures, faults & stylolites
sed. unit
interpreted depositional environment
stratal surfaces
samples / photos
1829.5
1830
1830.5
1831
1831.5
1832

62 calcispheres

61 calcispheres

60

Location: Scurry Placer West Eagle A8-7-85-18w6 p2

Date: 7/4/14

Diameter: 8.5cm

Logged by: S Sanders

Slabbed: [✓ Yes] / No

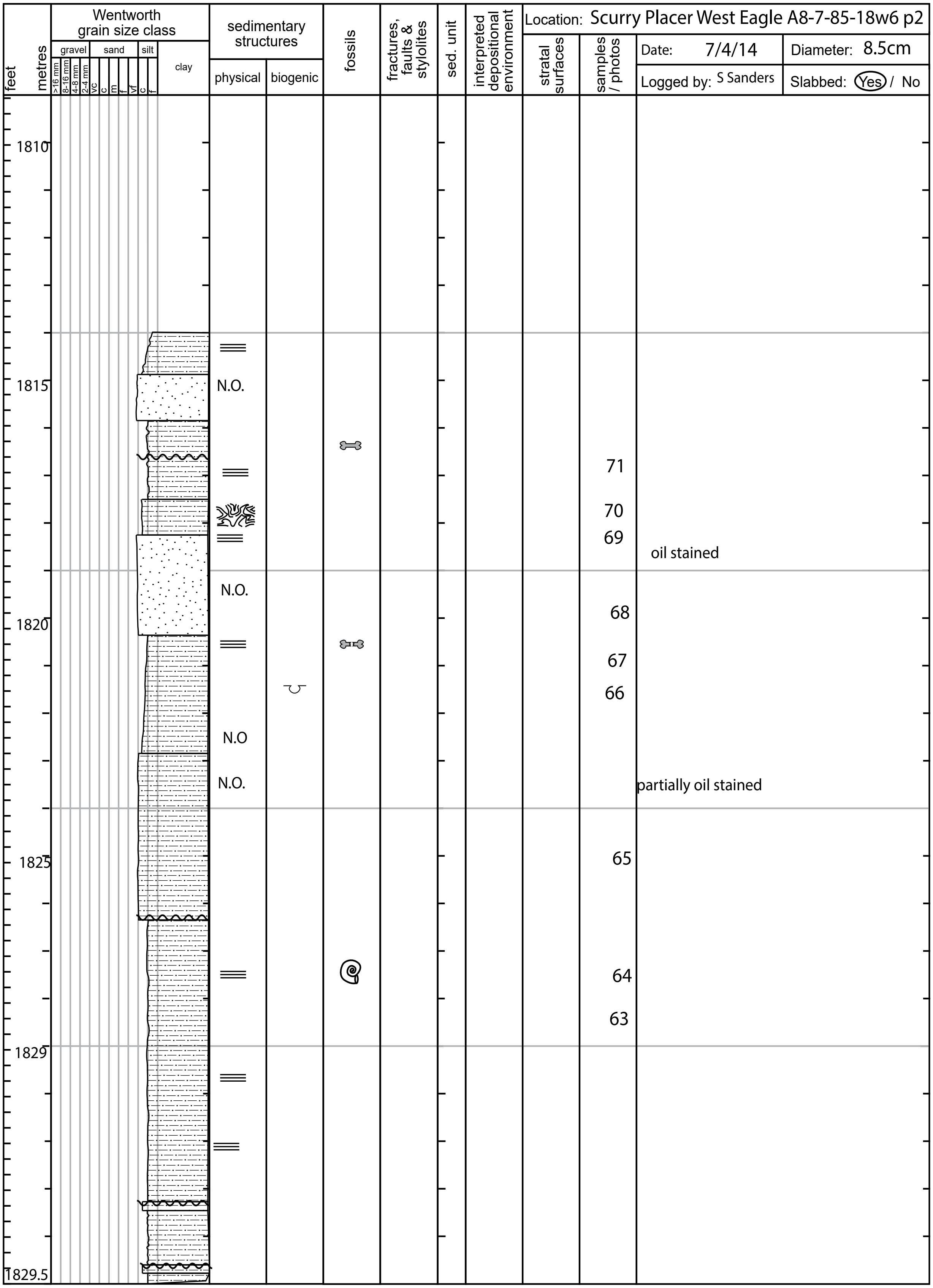
feet
metres
Wentworth grain size class
gravel
sand
silt
clay
>16 mm
8-16 mm
4-8 mm
2-4 mm
vc
c
m
f
vf
c
f
sedimentary structures
physical
biogenic
fossils
fractures, faults & stylolites
sed. unit
interpreted depositional environment
stratal surfaces
samples / photos
1810
1815
N.O.
71
70
69
N.O.
68
1820
67
66
N.O
N.O.
1825
64
63
1829
1829.5

oil stained

partially oil stained

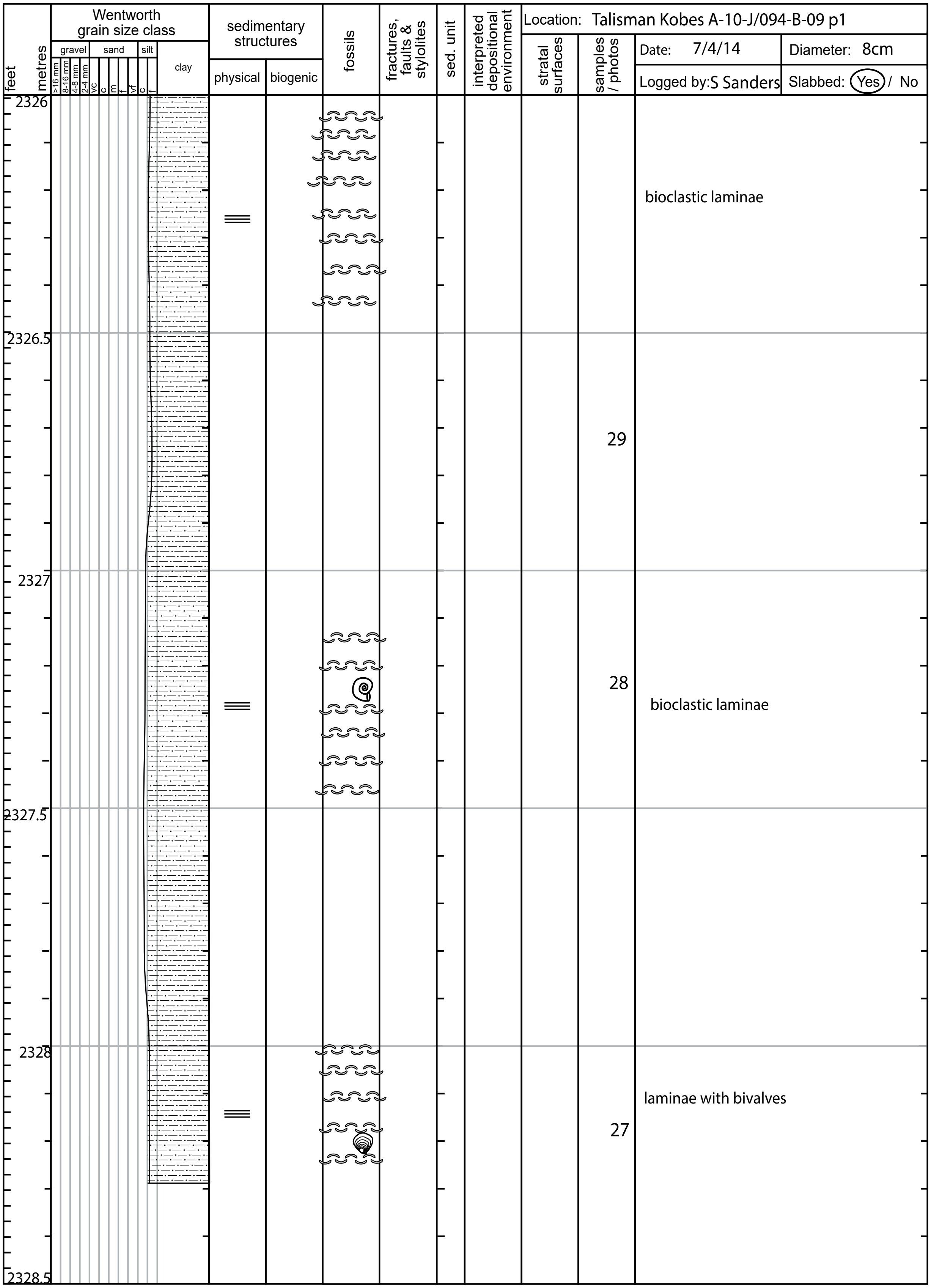
feet
metres
Wentworth grain size class
gravel
sand
silt
clay
>16 mm
8-16 mm
4-8 mm
2-4 mm
vc
c
m
f
vf
c
f
sedimentary structures
physical
biogenic
fossils
fractures, faults & stylolites
sed. unit
interpreted depositional environment
stratal surfaces
samples / photos
2326
2326.5
2327
2327.5
2328
2328.5
29
28
27
bioclastic laminae
bioclastic laminae
laminae with bivalves

Location: Talisman Kobes A-10-J/094-B-09 p1

Date: 7/4/14

Diameter: 8cm

Logged by: S Sanders

Slabbed: [✓ Yes] / No

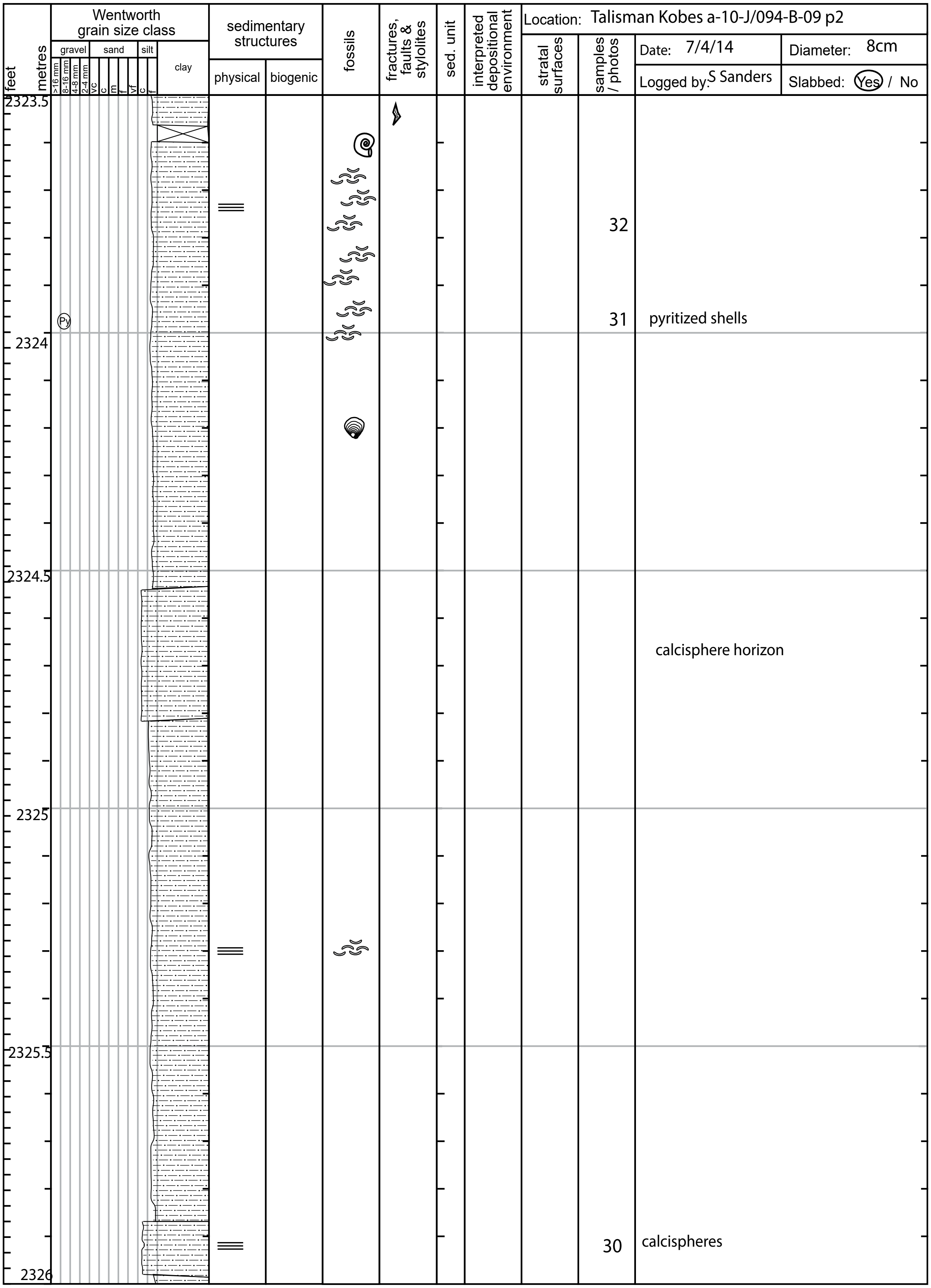
feet
metres
Wentworth grain size class
gravel
sand
silt
clay
>16 mm
8-16 mm
4-8 mm
2-4 mm
vc
c
m
f
vf
c
f
sedimentary structures
physical
biogenic
fossils
fractures, faults & stylolites
sed. unit
interpreted depositional environment
stratal surfaces
samples / photos
2323.5
2324
2324.5
2325
2325.5
2326
Py
32
31
30

Location: Talisman Kobes a-10-J/094-B-09 p2

Date: 7/4/14

Diameter: 8cm

Logged by: S Sanders

Slabbed: [✓ Yes] / No

pyritized shells

calcisphere horizon

calcispheres

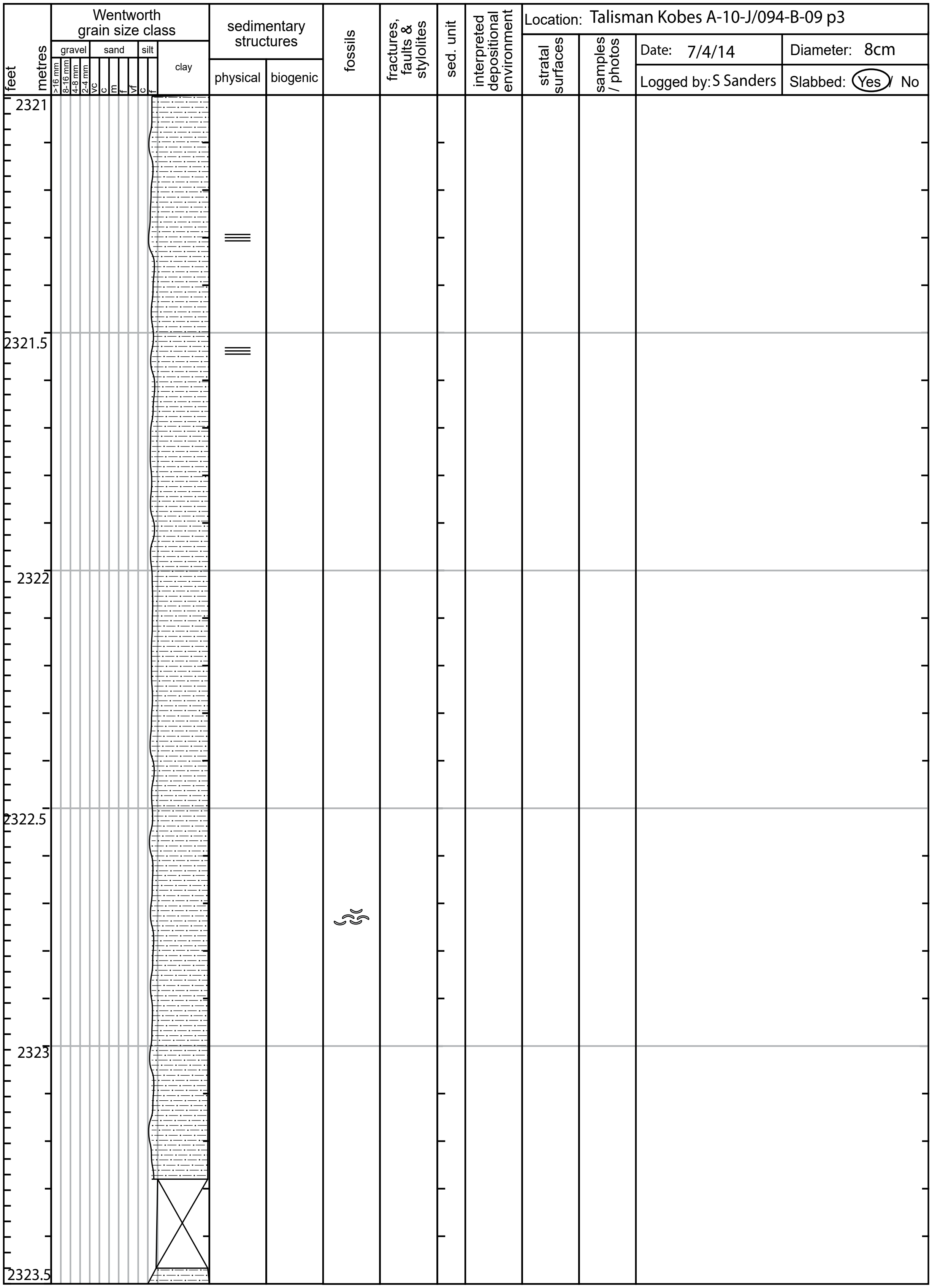
feet
metres
Wentworth grain size class
gravel
sand
silt
clay
>16 mm
8-16 mm
4-8 mm
2-4 mm
vc
c
m
f
vf
c
f
sedimentary structures
physical
biogenic
fossils
fractures, faults & stylolites
sed. unit
interpreted depositional environment
stratal surfaces
samples / photos
2321
2321.5
2322
2322.5
2323
2323.5

Location: Talisman Kobes A-10-J/094-B-09 p3

Date: 7/4/14

Diameter: 8cm

Logged by: S Sanders

Slabbed: [✓ Yes] / No

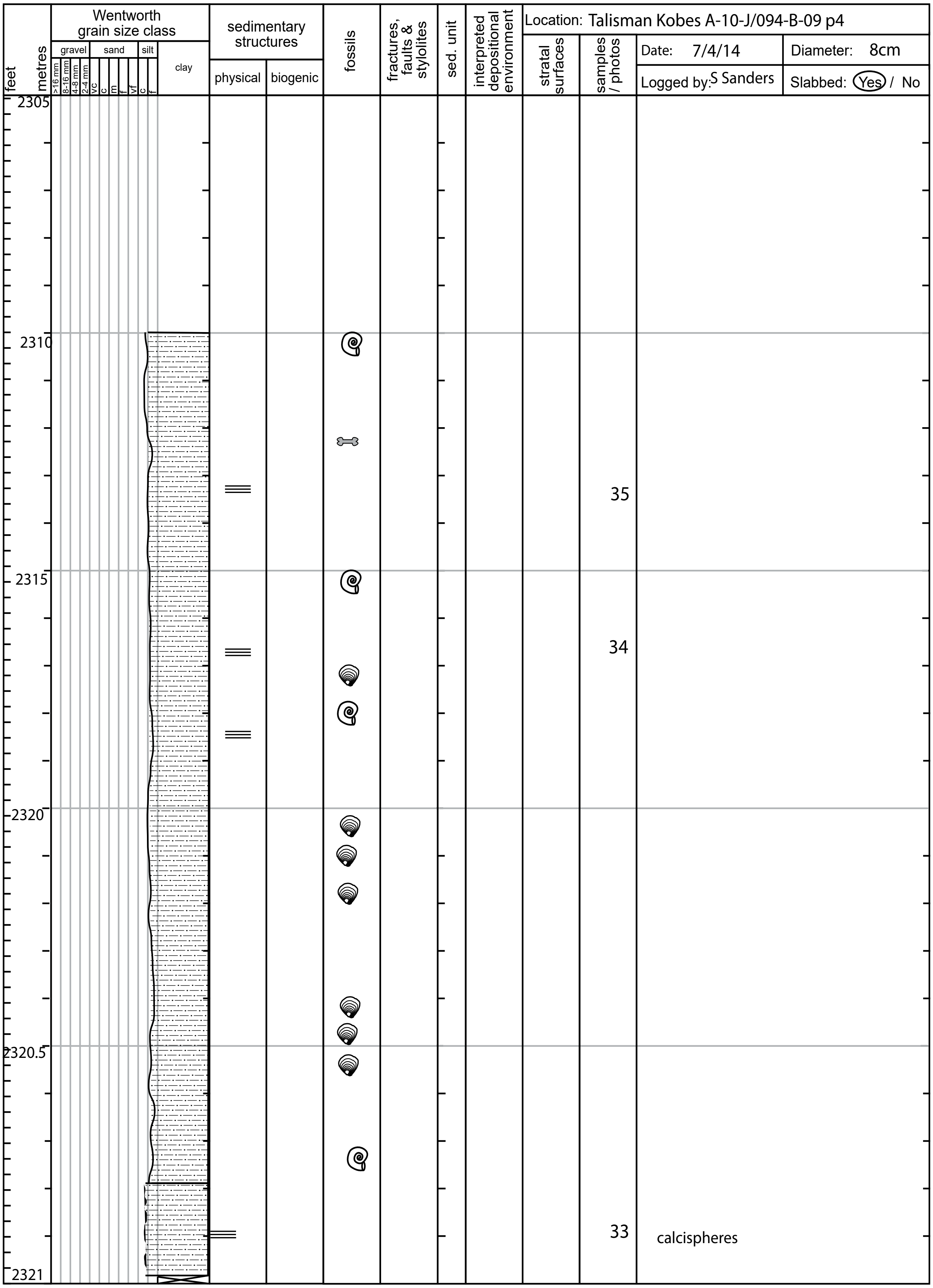

Location: Talisman Kobes A-10-J/094-B-09 p4

Date: 7/4/14

Diameter: 8cm

Logged by: S Sanders

Slabbed: [✓ Yes] / No

feet
metres
Wentworth grain size class
gravel
sand
silt
clay
>16 mm
8-16 mm
4-8 mm
2-4 mm
vc
c
m
f
vf
c
f
sedimentary structures
physical
biogenic
fossils
fractures, faults & stylolites
sed. unit
interpreted depositional environment
stratal surfaces
samples / photos
2305
2310
2315
2320
2320.5
2321
35
34
33
calcispheres

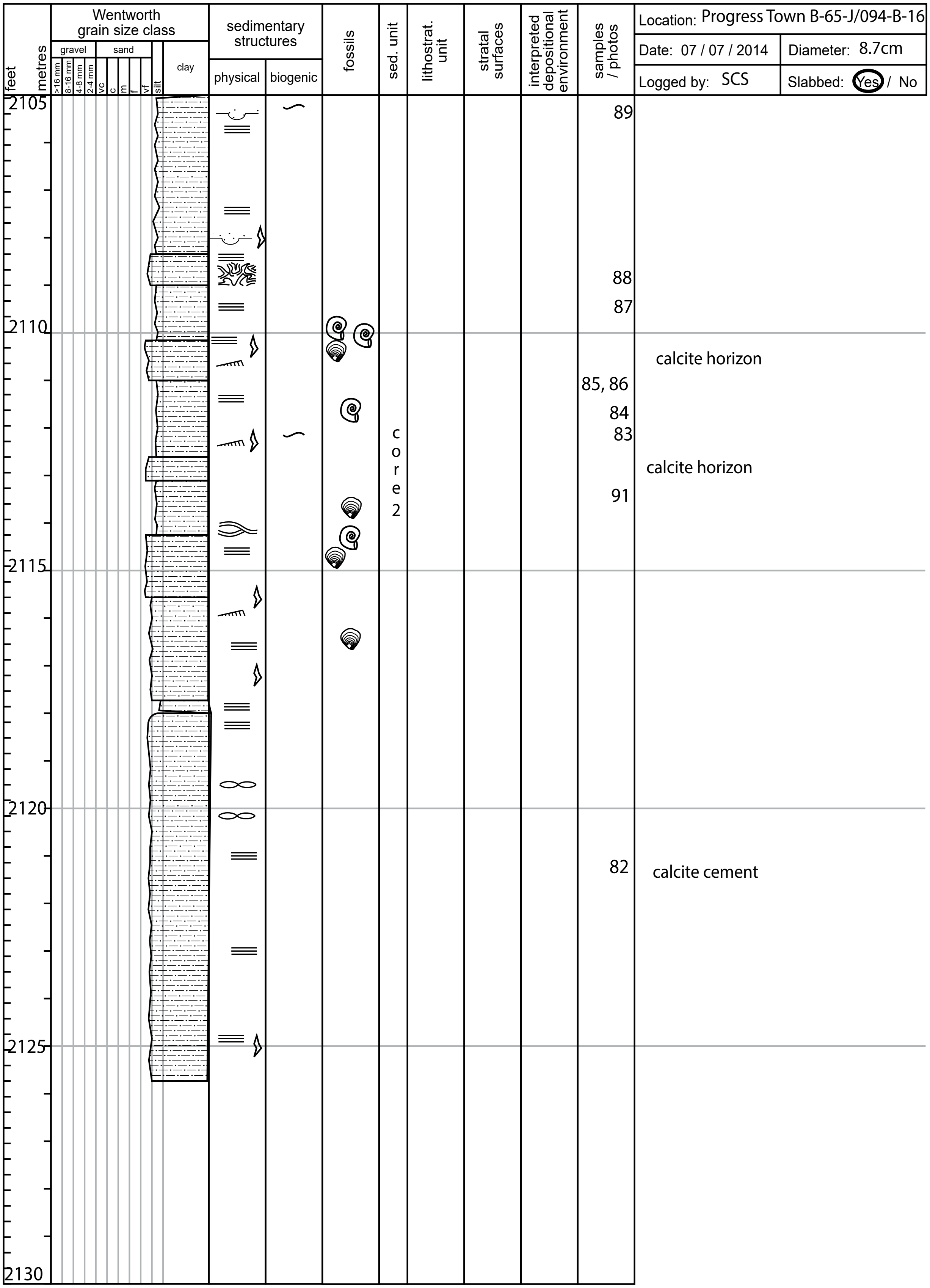

Location: Progress Town B-65-J/094-B-16

Date: 07 / 07 / 2014

Diameter: 8.7cm

Logged by: SCS

Slabbed: [✓ Yes] / No

feet
metres
Wentworth grain size class
gravel
sand
>16 mm
8-16 mm
4-8 mm
2-4 mm
vc
c
m
f
vf
silt
clay
sedimentary structures
physical
biogenic
fossils
sed. unit
lithostrat. unit
stratal surfaces
interpreted depositional environment
samples / photos
2105
2110
2115
2120
2125
2130
core 2
89
88
87
85, 86
84
83
91
82
calcite horizon
calcite horizon
calcite cement

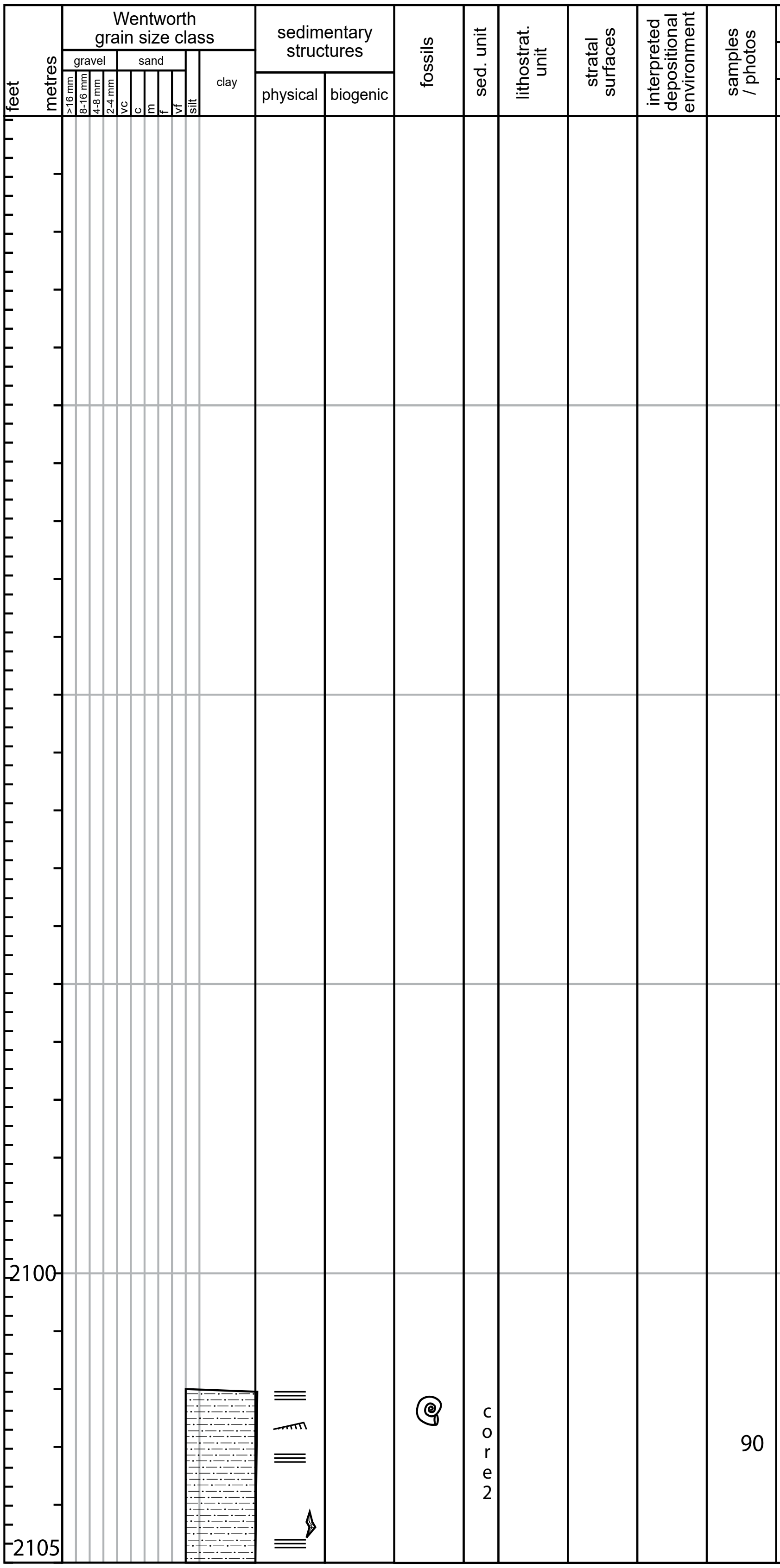
feet
metres
Wentworth grain size class
gravel
sand
>16 mm
8-16 mm
4-8 mm
2-4 mm
vc
c
m
f
vf
silt
clay
sedimentary structures
physical
biogenic
fossils
sed. unit
lithostrat. unit
stratal surfaces
interpreted depositional environment
samples / photos
2100
2105
core 2
90

Location: Progress Town B-065-J/094-B-16

Date: 07 / 07 / 2014

Diameter: 8.7cm

Logged by: SCS

Slabbed: [✓ Yes] / No

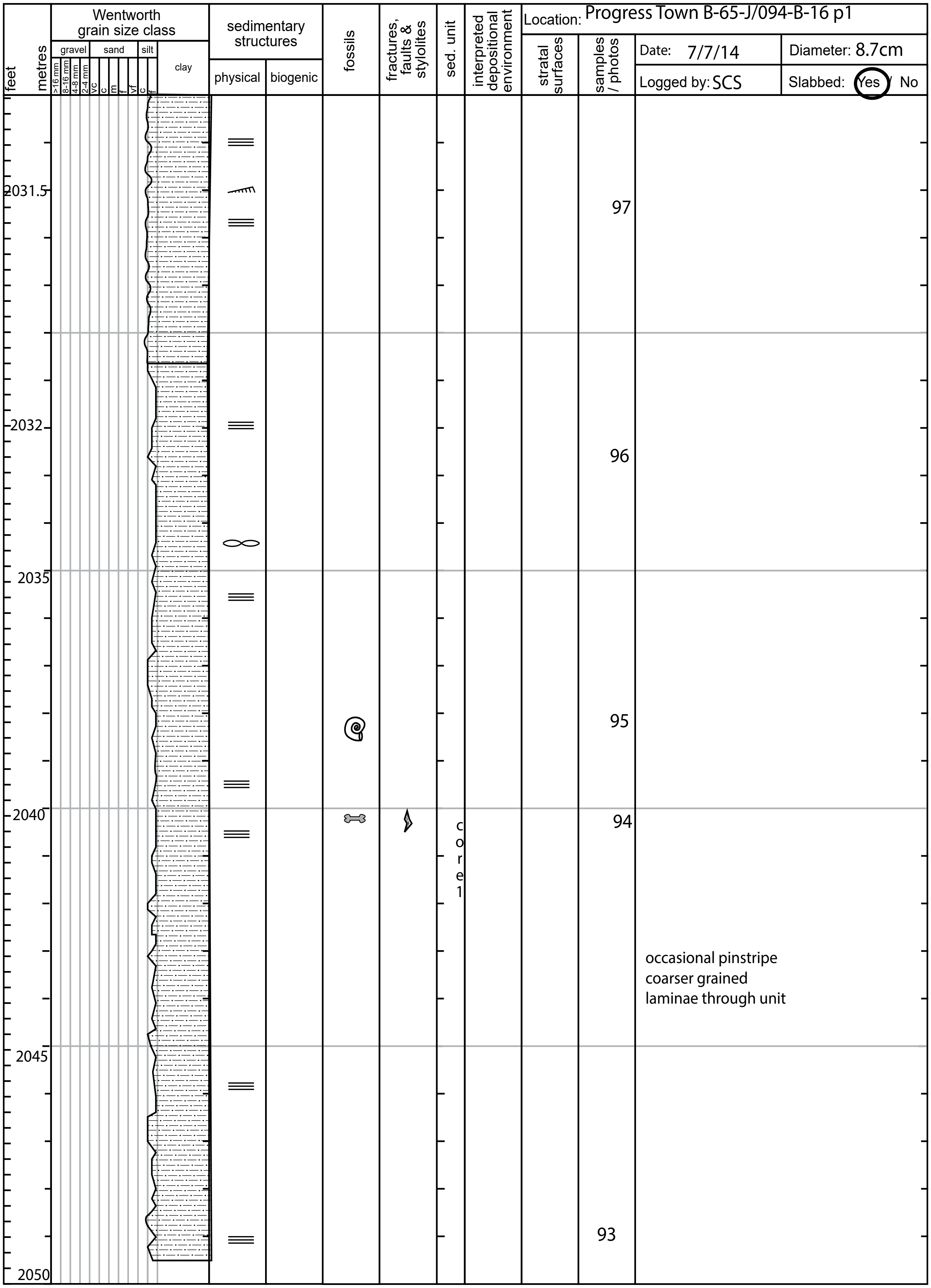
Location: Progress Town B-65-J/094-B-16 p1

Date: 7/7/14

Diameter: 8.7cm

Logged by: SCS

Slabbed: [✓ Yes] / No

occasional pinstripe coarser grained laminae through unit

feet
metres
Wentworth grain size class
gravel
sand
silt
clay
>16 mm
8-16 mm
4-8 mm
2-4 mm
vc
c
m
f
vf
c
f
sedimentary structures
physical
biogenic
fossils
fractures, faults & stylolites
sed. unit
interpreted depositional environment
stratal surfaces
samples / photos
2031.5
2032
2035
2040
2045
2050
97
96
95
94
93
core 1

Location: Progress Town B-65-J/094-B-16 p2

Date: 7/7/14

Diameter: 8.7cm

Logged by: SCS

Slabbed: [✓ Yes] / No

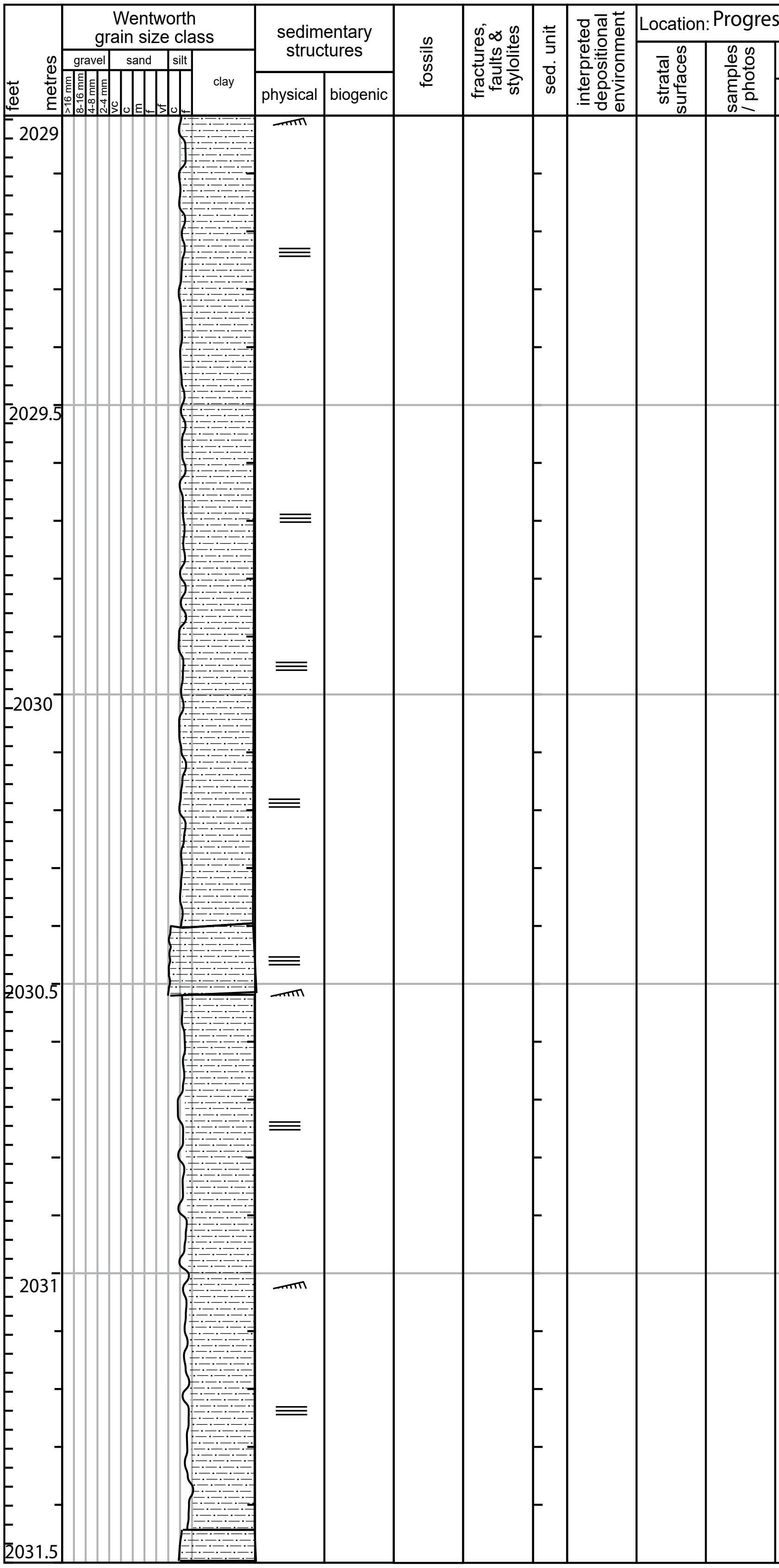
feet
metres
Wentworth grain size class
gravel
sand
silt
clay
>16 mm
8-16 mm
4-8 mm
2-4 mm
vc
c
m
f
vf
c
f
sedimentary structures
physical
biogenic
fossils
fractures, faults & stylolites
sed. unit
interpreted depositional environment
stratal surfaces
samples / photos
2029
2029.5
2030
2030.5
2031
2031.5

occassional laminae

Location: Progress Town B-65-J/094-B-16 p3

Date: 7/7/14

Diameter: 8.7cm

Logged by: SCS

Slabbed: [✓ Yes] / No

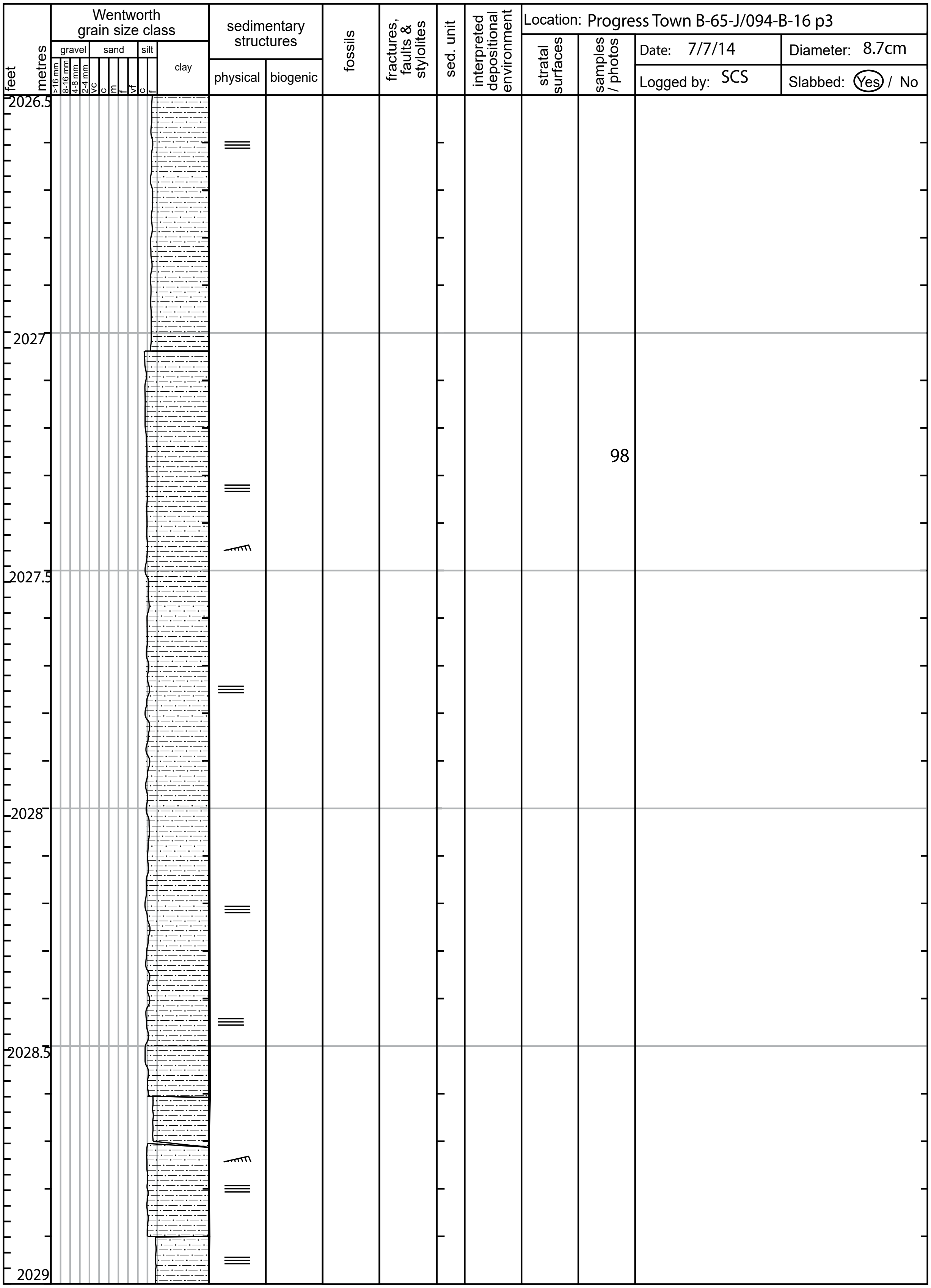
feet
metres
Wentworth grain size class
gravel
sand
silt
clay
>16 mm
8-16 mm
4-8 mm
2-4 mm
vc
c
m
f
vf
c
f
sedimentary structures
physical
biogenic
fossils
fractures, faults & stylolites
sed. unit
interpreted depositional environment
stratal surfaces
samples / photos
2026.5
2027
2027.5
2028
2028.5
2029
98

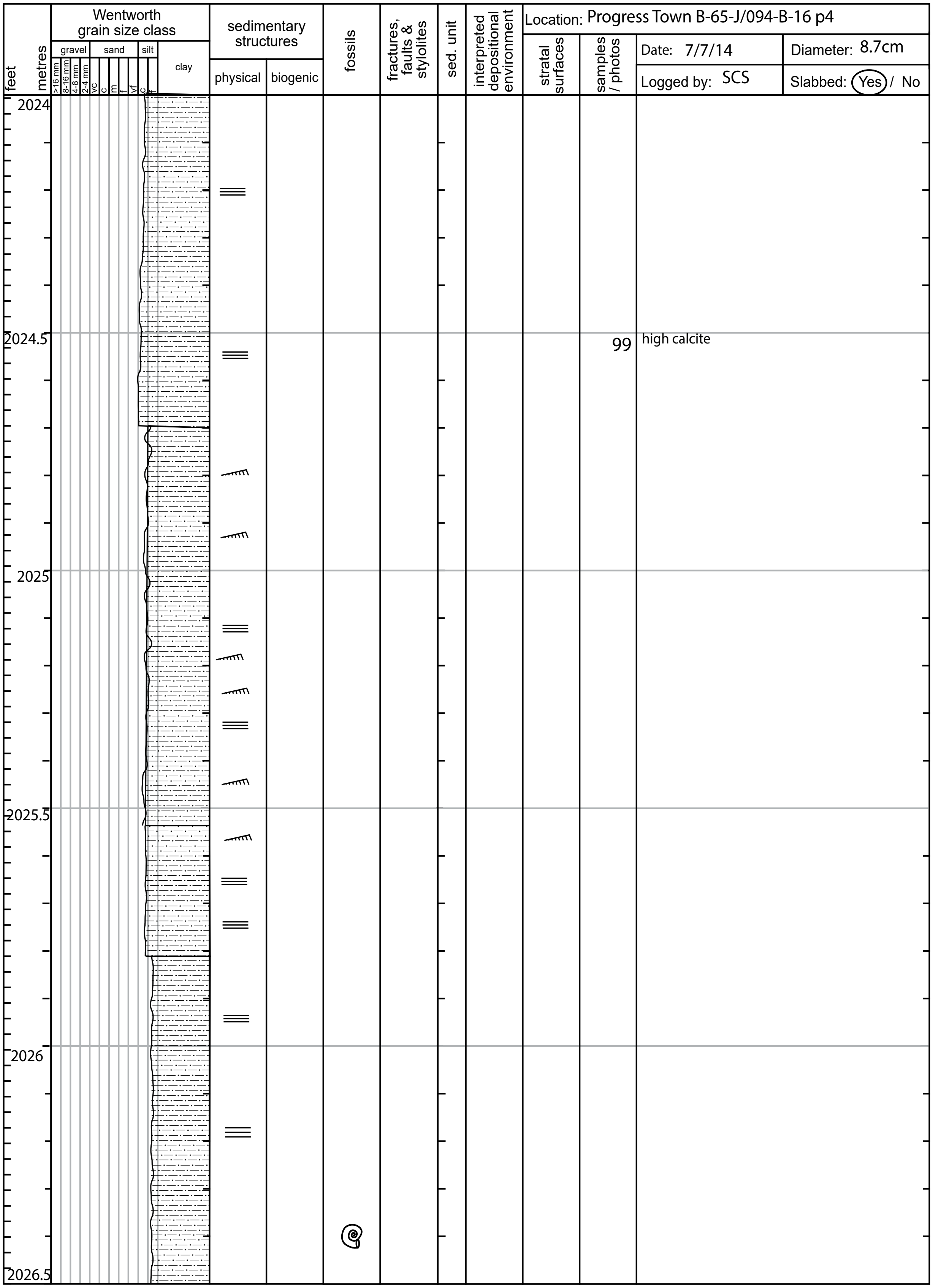
Wentworth grain size class
gravel
sand
silt
>16 mm
8-16 mm
4-8 mm
2-4 mm
vc
c
m
f
vf
c
f
clay
sedimentary structures
physical
biogenic
fossils
fractures, faults & stylolites
sed. unit
interpreted depositional environment
stratal surfaces
samples / photos
feet
metres
2024
2024.5
2025
2025.5
2026
2026.5

Location: Progress Town B-65-J/094-B-16 p4

Date: 7/7/14

Diameter: 8.7cm

Logged by: SCS

Slabbed: [✓ Yes] / No

99 high calcite

Location: Progress Town B-65-J/094-B-16

Date: 7/7/14

Diameter: 8.7cm

Logged by: SCS

Slabbed: [✓ Yes] / No

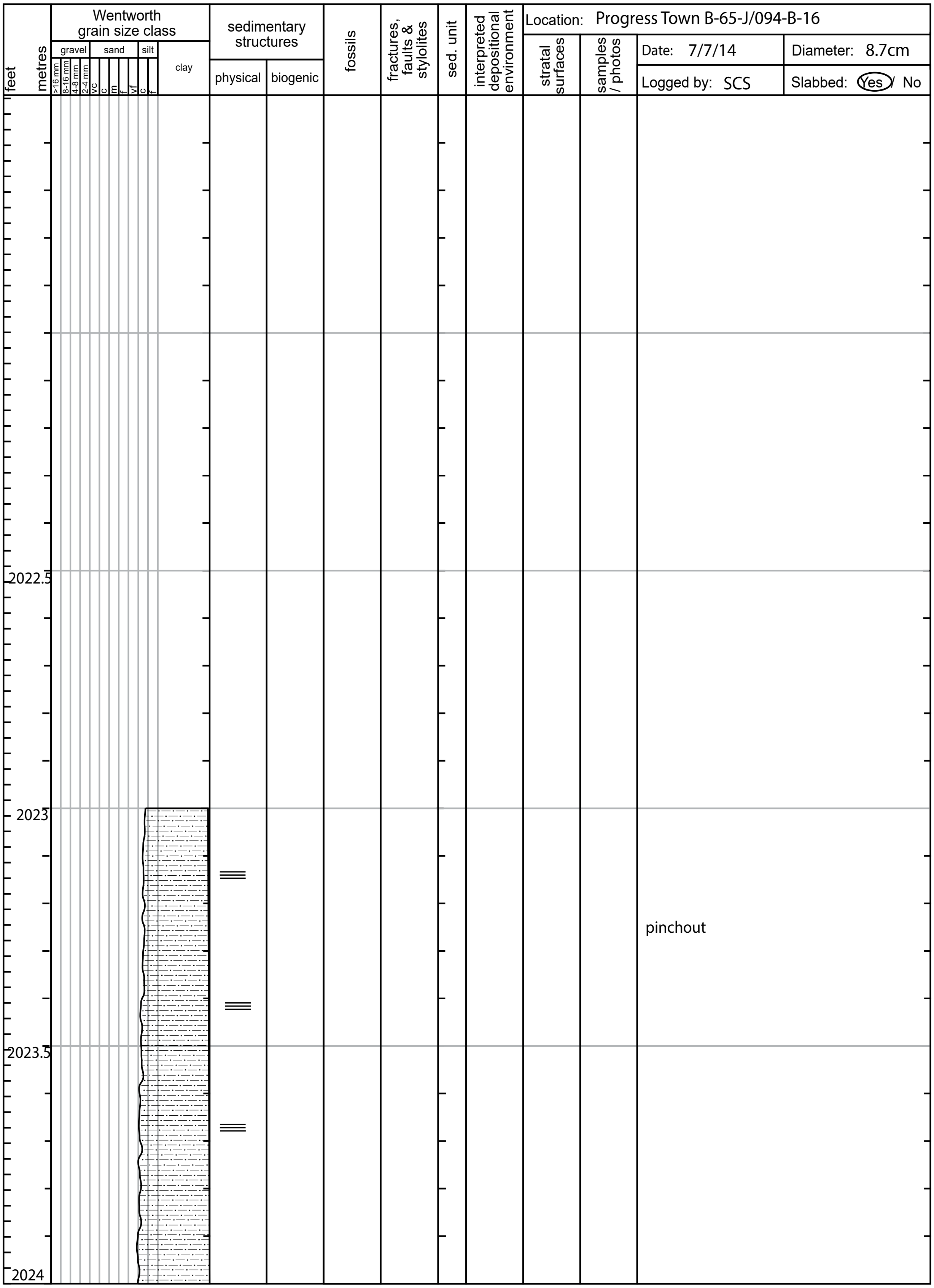
feet
metres
Wentworth grain size class
gravel
sand
silt
clay
>16 mm
8-16 mm
4-8 mm
2-4 mm
vc
c
m
f
vf
c
f
sedimentary structures
physical
biogenic
fossils
fractures, faults & stylolites
sed. unit
interpreted depositional environment
stratal surfaces
samples / photos
2022.5
2023
2023.5
2024

pinchout

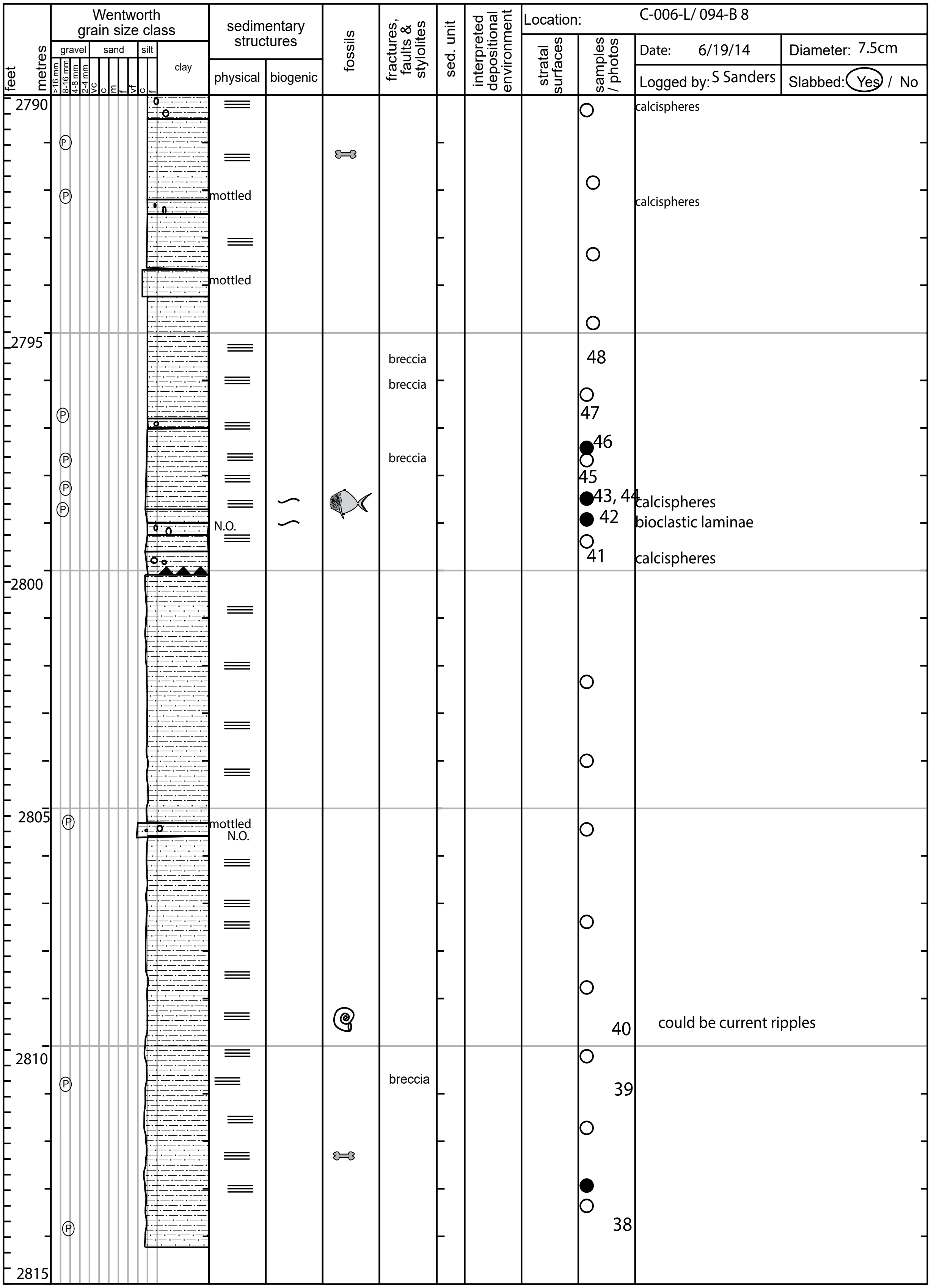

Location: C-006-L/ 094-B 8

Date: 6/19/14

Diameter: 7.5cm

Logged by: S Sanders

Slabbed: [✓ Yes] / No

feet
metres
Wentworth grain size class
gravel
sand
silt
clay
>16 mm
8-16 mm
4-8 mm
2-4 mm
vc
c
m
f
vf
c
f
sedimentary structures
physical
biogenic
fossils
fractures, faults & stylolites
sed. unit
interpreted depositional environment
strata surfaces
samples / photos
2790
2795
2800
2805
2810
2815
P
mottled
mottled
N.O.
mottled
N.O.
breccia
breccia
breccia
breccia
48
47
46
45
43, 44
42
41
40
39
38
calcispheres
calcispheres
calcispheres
bioclastic laminae
calcispheres
could be current ripples

Location: C-006-L/ 094-B-08

Date: 6/19/14

Diameter: 7.5cm

Logged by:S Sanders

Slabbed: [✓ Yes] / No

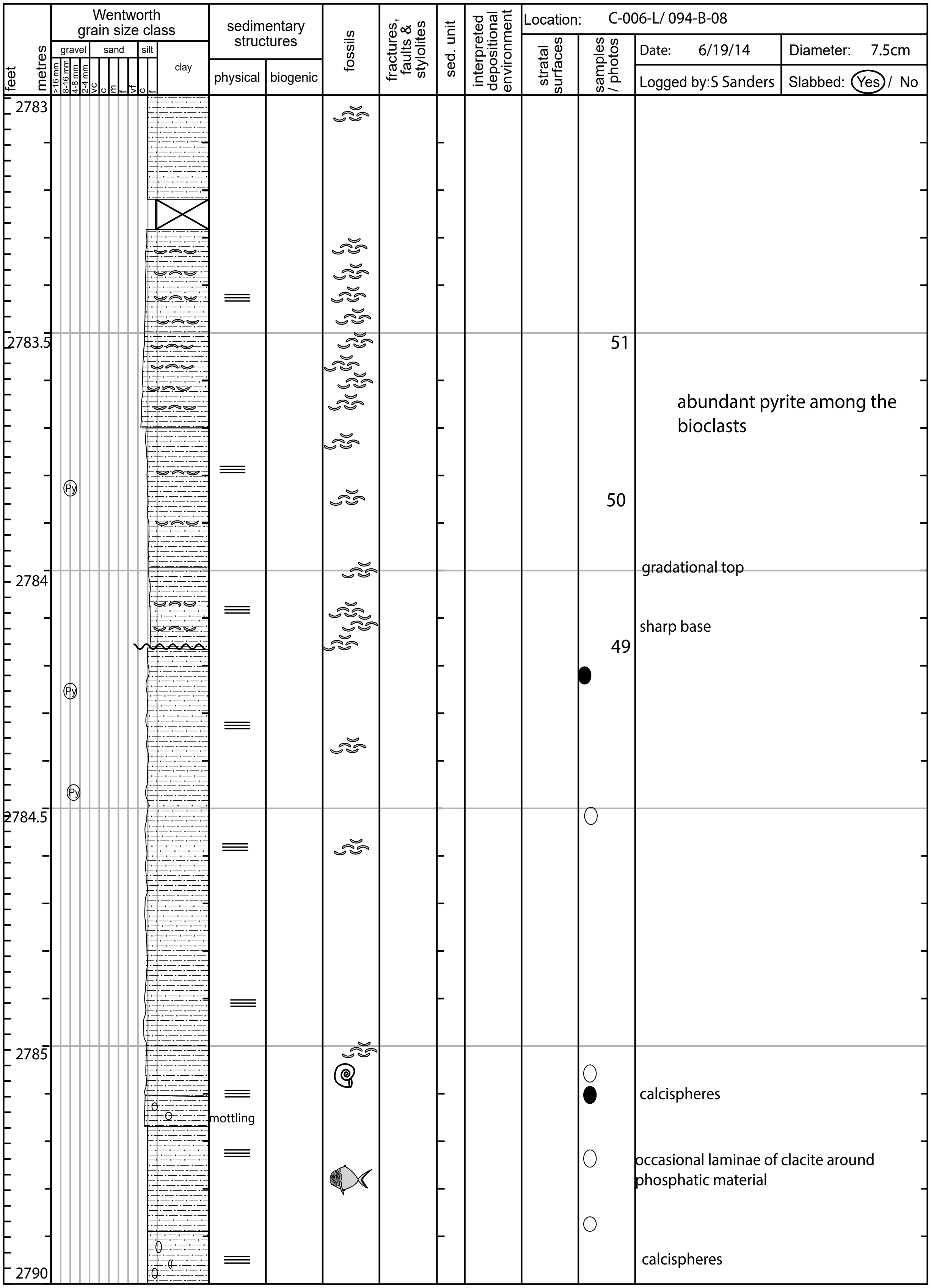
feet
metres
Wentworth grain size class
gravel
sand
silt
clay
>16 mm
8-16 mm
4-8 mm
2-4 mm
vc
c
m
f
vf
c
f
sedimentary structures
physical
biogenic
fossils
fractures, faults & stylolites
sed. unit
interpreted depositional environment
stratal surfaces
samples / photos
2783
2783.5
2784
2784.5
2785
2790
Py
Py
Py
mottling
51
50
49

abundant pyrite among the bioclasts

gradational top

sharp base

calcispheres

occasional laminae of clacite around phosphatic material

calcispheres

Location: C-006-L/ 094-B 08

Date: 6/19/14

Diameter: 7.5cm

Logged by: S Sanders

Slabbed: [✓ Yes] / No

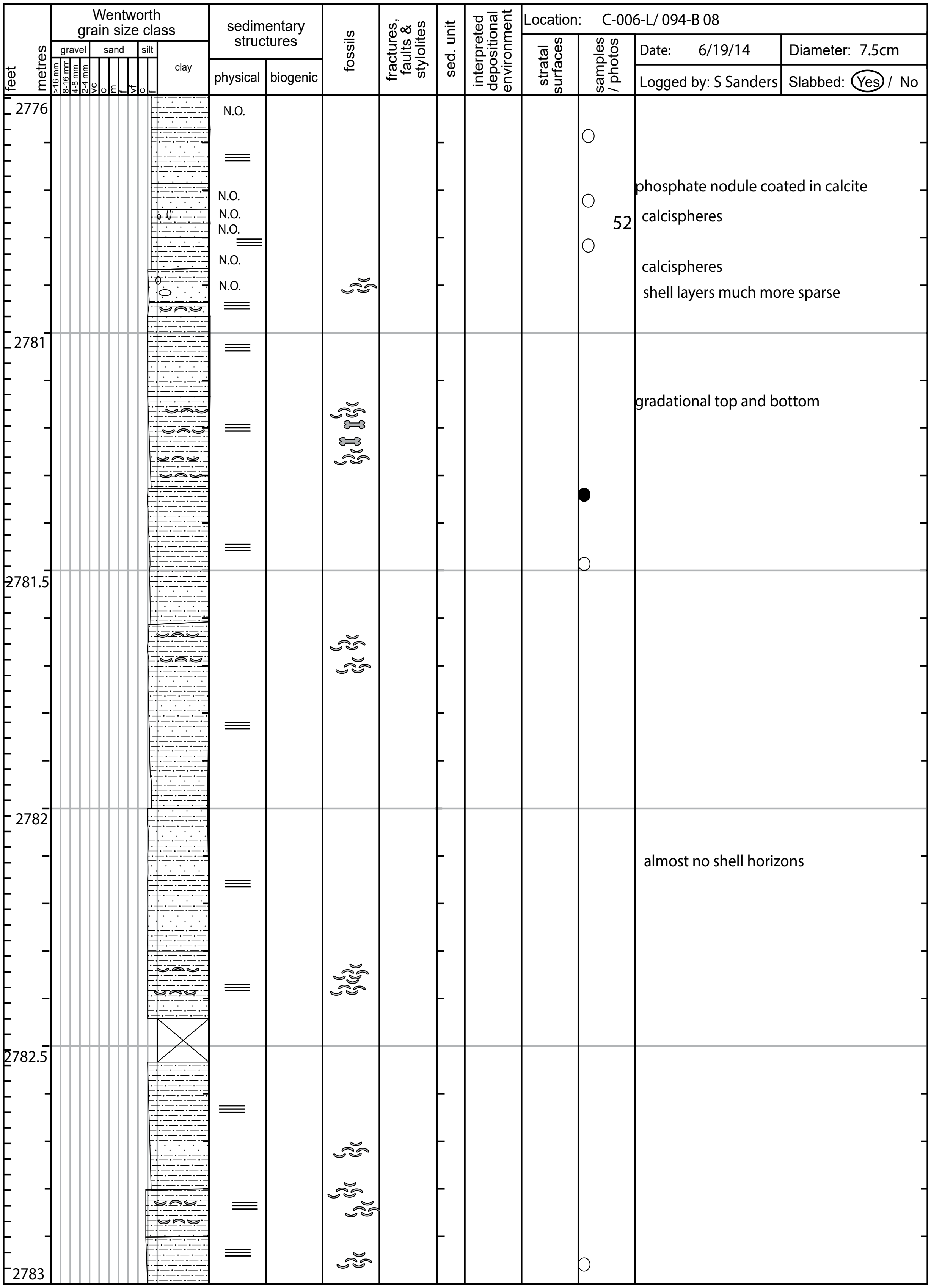
feet
metres
Wentworth grain size class
gravel
sand
silt
clay
>16 mm
8-16 mm
4-8 mm
2-4 mm
vc
c
m
f
vf
c
f
sedimentary structures
physical
biogenic
fossils
fractures, faults & stylolites
sed. unit
interpreted depositional environment
stratal surfaces
samples / photos
2776
2781
2781.5
2782
2782.5
2783
N.O.
N.O.
N.O.
N.O.
N.O.
N.O.

phosphate nodule coated in calcite

52 calcispheres

calcispheres

shell layers much more sparse

gradational top and bottom

almost no shell horizons

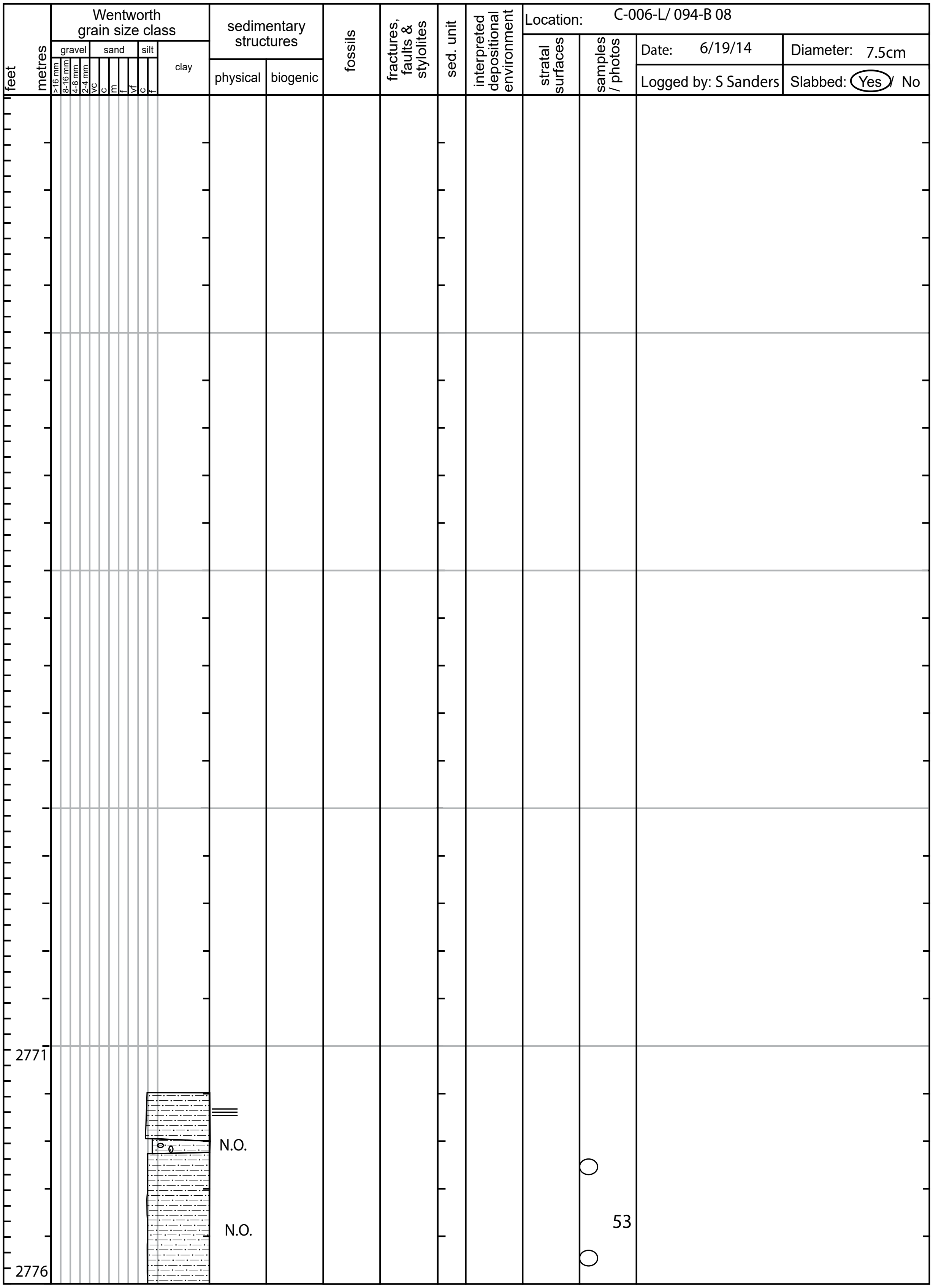
Wentworth grain size class
gravel
sand
silt
clay
>16 mm
8-16 mm
4-8 mm
2-4 mm
vc
c
m
f
vf
c
f
feet
metres
sedimentary structures
physical
biogenic
fossils
fractures, faults & stylolites
sed. unit
interpreted depositional environment
stratal surfaces
samples / photos
2771
N.O.
N.O.
53
2776

Location: C-006-L/ 094-B 08

Date: 6/19/14

Diameter: 7.5cm

Logged by: S Sanders

Slabbed: [✓ Yes] / No

Location: Progress HZ Altares C-007-J/094 B-08

Date: 6/27/14

Diameter: 6.5cm

Logged by: S Sanders

Slabbed: [✓ Yes] / No

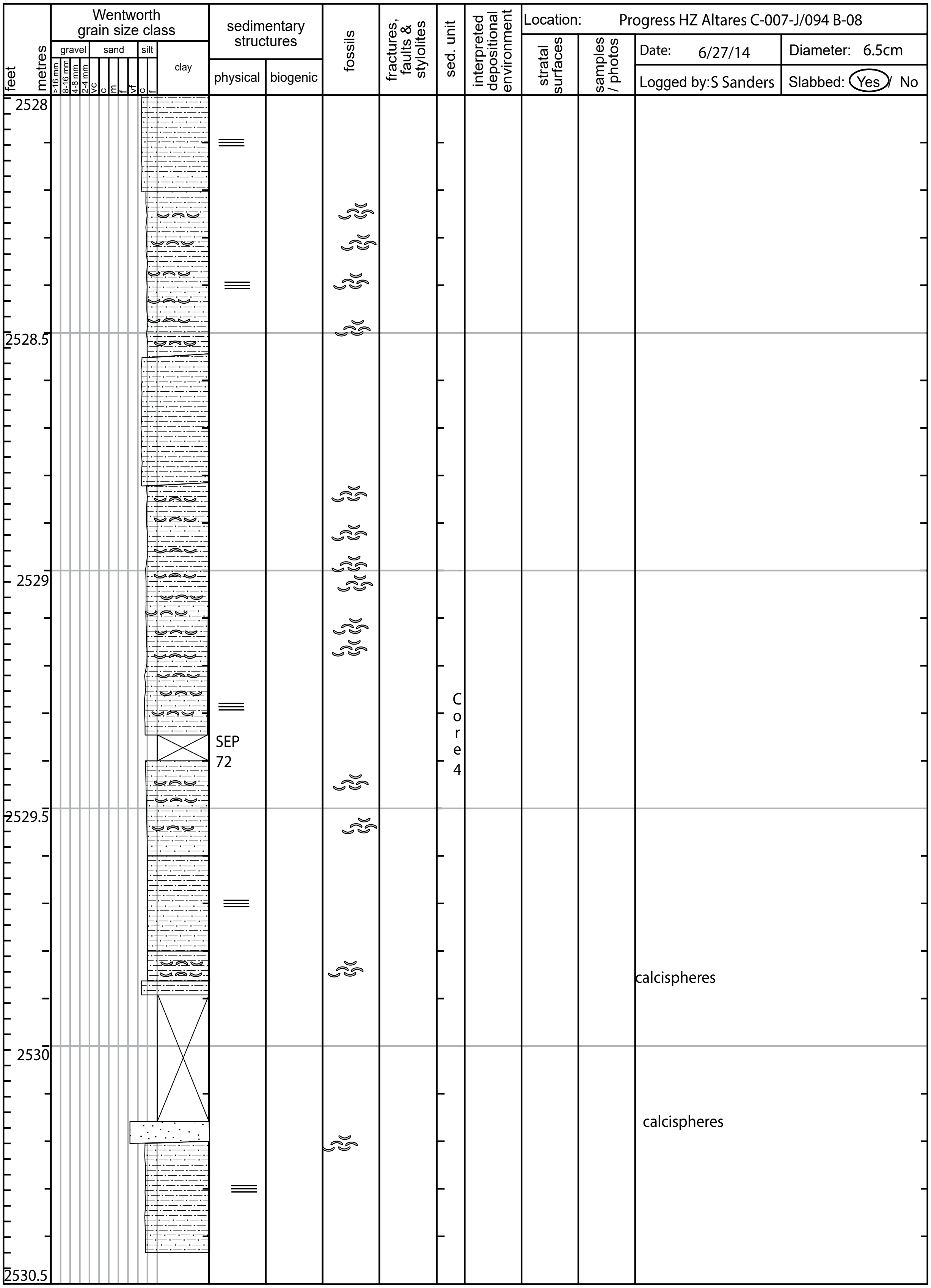

feet
metres
Wentworth grain size class
gravel
sand
silt
clay
>16 mm
8-16 mm
4-8 mm
2-4 mm
vc
c
m
f
vf
c
f
sedimentary structures
physical
biogenic
fossils
fractures, faults & stylolites
sed. unit
interpreted depositional environment
stratal surfaces
samples / photos
2528
2528.5
2529
2529.5
2530
2530.5
SEP 72
Core 4

calcispheres

calcispheres

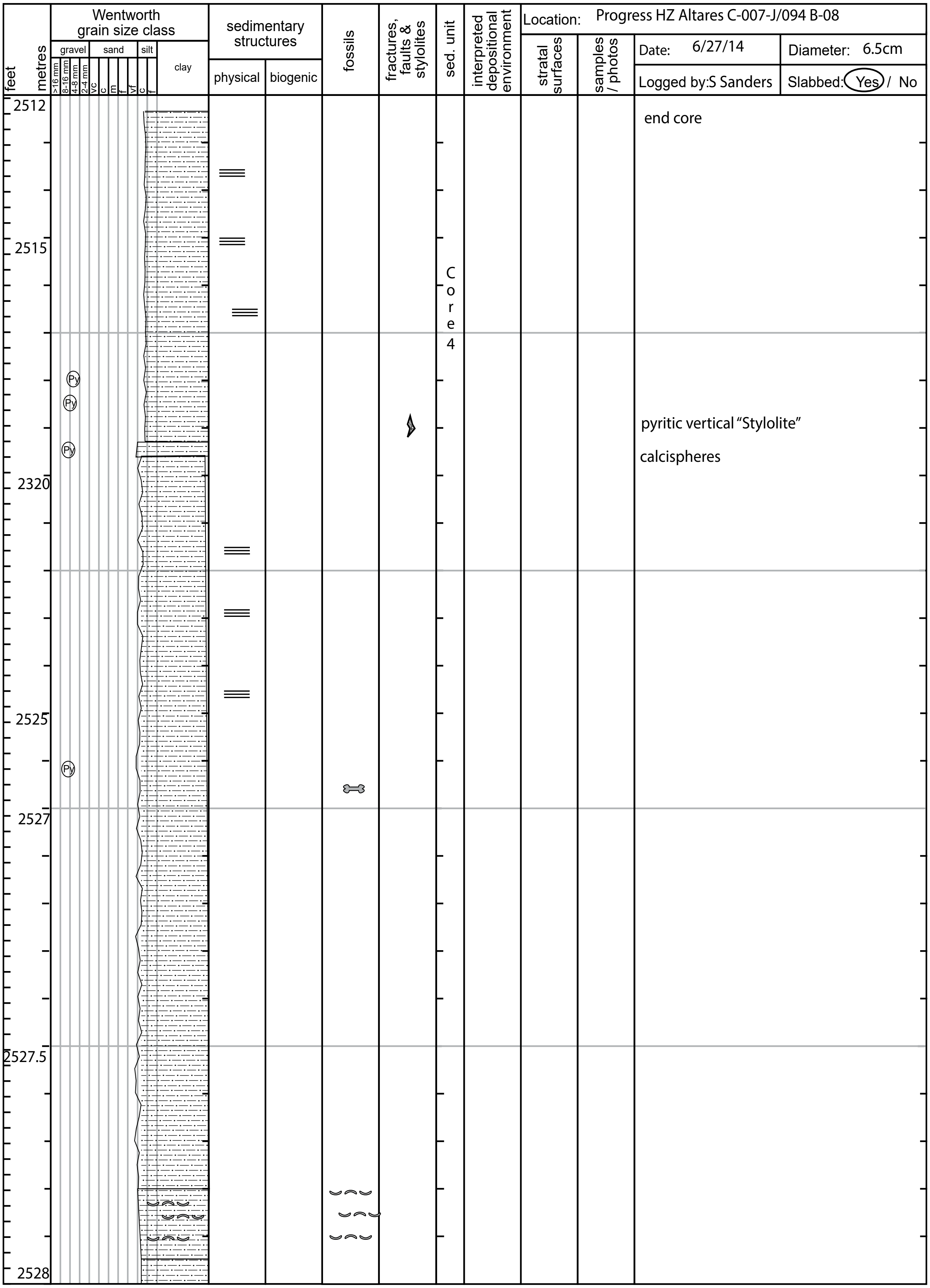
feet
metres
Wentworth grain size class
gravel
sand
silt
clay
>16 mm
8-16 mm
4-8 mm
2-4 mm
vc
c
m
f
vf
c
f
sedimentary structures
physical
biogenic
fossils
fractures, faults & stylolites
sed. unit
interpreted depositional environment
stratal surfaces
samples / photos
2512
2515
2320
2525
2527
2527.5
2528
Py
Py
Py
Py
Core 4

Location: Progress HZ Altares C-007-J/094 B-08

Date: 6/27/14

Diameter: 6.5cm

Logged by:S Sanders

Slabbed: [✓ Yes] / No

end core

pyritic vertical “Stylolite”

calcispheres

Location: Progress HZ Altares C-007-J/ 094 B-08

Date: 6/27/14

Diameter: 6.5cm

Logged by: S Sanders

Slabbed: [✓ Yes] / No

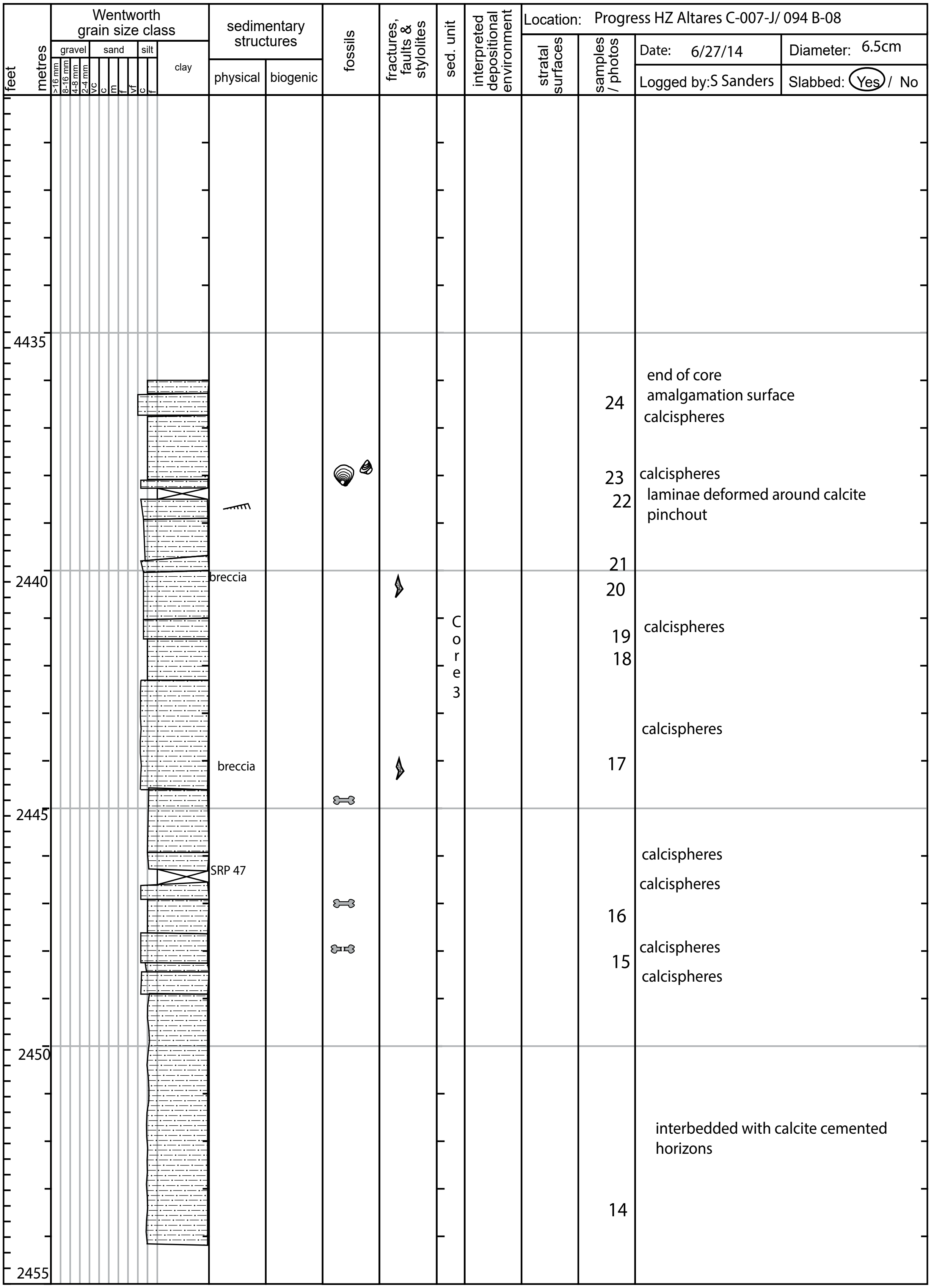
feet
metres
Wentworth grain size class
gravel
sand
silt
clay
>16 mm
8-16 mm
4-8 mm
2-4 mm
vc
c
m
f
vf
c
f
sedimentary structures
physical
biogenic
fossils
fractures, faults & stylolites
sed. unit
interpreted depositional environment
stratal surfaces
samples / photos
4435
2440
2445
2450
2455
breccia
breccia
SRP 47
Core 3
24
23
22
21
20
19
18
17
16
15
14

end of core

amalgamation surface

calcispheres

calcispheres

laminae deformed around calcite pinchout

calcispheres

calcispheres

calcispheres

calcispheres

calcispheres

calcispheres

interbedded with calcite cemented horizons

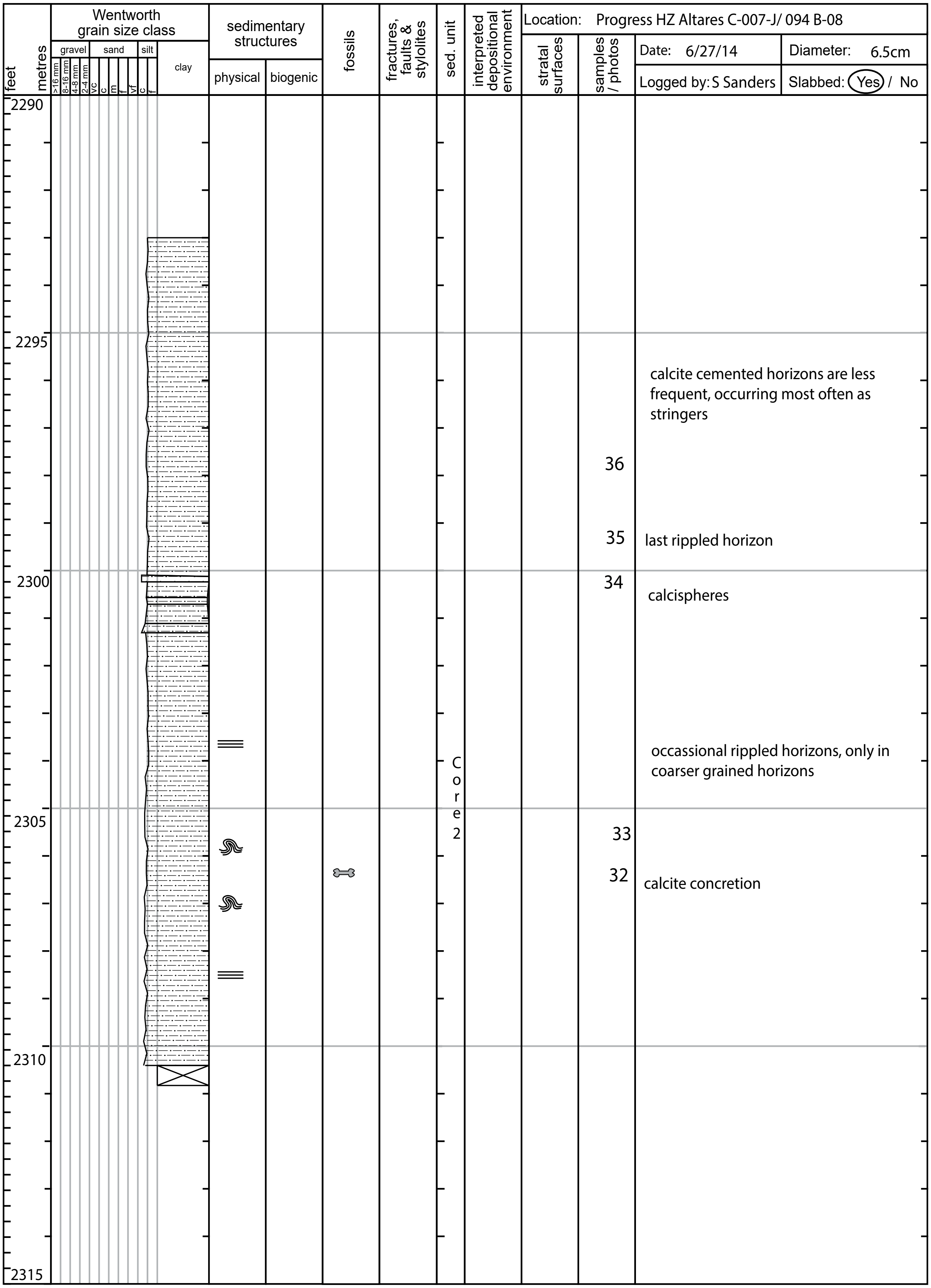
feet
metres
Wentworth grain size class
gravel
sand
silt
clay
>16 mm
8-16 mm
4-8 mm
2-4 mm
vc
c
m
f
vf
c
f
sedimentary structures
physical
biogenic
fossils
fractures, faults & stylolites
sed. unit
interpreted depositional environment
stratal surfaces
samples / photos
2290
2295
2300
2305
2310
2315
C
o
r
e
2
36
35
34
33
32

Location: Progress HZ Altares C-007-J/ 094 B-08

Date: 6/27/14

Diameter: 6.5cm

Logged by: S Sanders

Slabbed: [✓ Yes] / No

calcite cemented horizons are less frequent, occurring most often as stringers

last rippled horizon

calcispheres

occassional rippled horizons, only in coarser grained horizons

calcite concretion

Location: Progress HZ Altares C-007-J/094 B-08

Date: 06/27/14

Diameter: 6.5cm

Logged by: S Sanders

Slabbed: [✓ Yes] / No

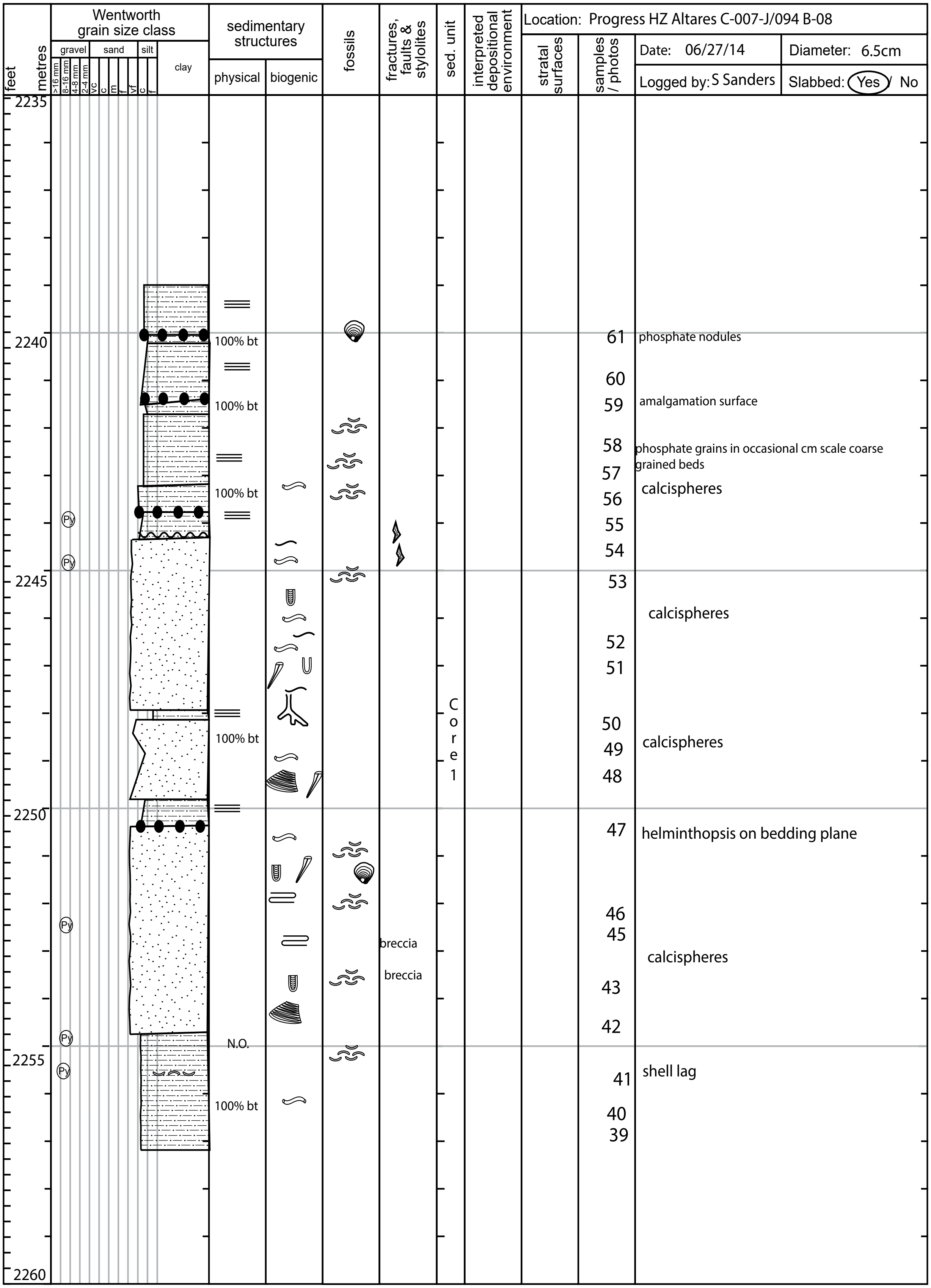

feet
metres
Wentworth grain size class
gravel
sand
silt
clay
>16 mm
8-16 mm
4-8 mm
2-4 mm
vc
c
m
f
vf
c
f
sedimentary structures
physical
biogenic
fossils
fractures, faults & stylolites
sed. unit
interpreted depositional environment
stratal surfaces
samples / photos
2235
2240
2245
2250
2255
2260
100% bt
100% bt
100% bt
100% bt
100% bt
N.O.
Py
Py
Py
Py
Py
breccia
breccia
Core 1
61 phosphate nodules
60
59 amalgamation surface
58 phosphate grains in occasional cm scale coarse grained beds
57
56 calcispheres
55
54
53
calcispheres
52
51
50
49 calcispheres
48
47 helminthopsis on bedding plane
46
45
calcispheres
43
42
41 shell lag
40
39

Location: C-65-F/ 094-B 8

Date: 6/18/14

Diameter: 7.5cm

Logged by: S Sanders

Slabbed: [✓ Yes] / No

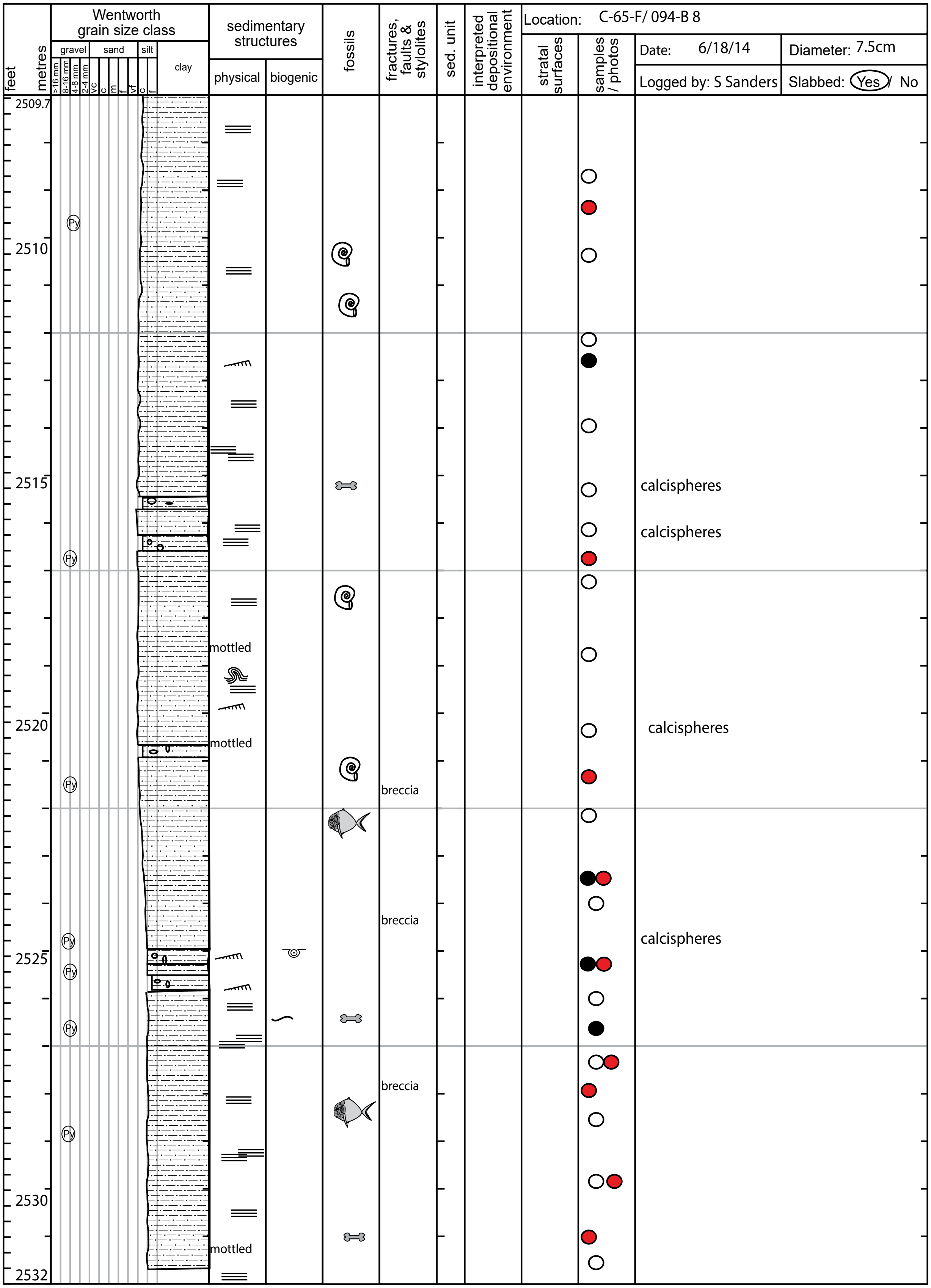
feet
metres
Wentworth grain size class
gravel
sand
silt
clay
>16 mm
8-16 mm
4-8 mm
2-4 mm
vc
c
m
f
vf
c
f
sedimentary structures
physical
biogenic
fossils
fractures, faults & stylolites
sed. unit
interpreted depositional environment
stratal surfaces
samples / photos
2509.7
2510
2515
2520
2525
2530
2532
Py
Py
Py
Py
Py
Py
Py
mottled
mottled
mottled
breccia
breccia
breccia
calcispheres
calcispheres
calcispheres
calcispheres

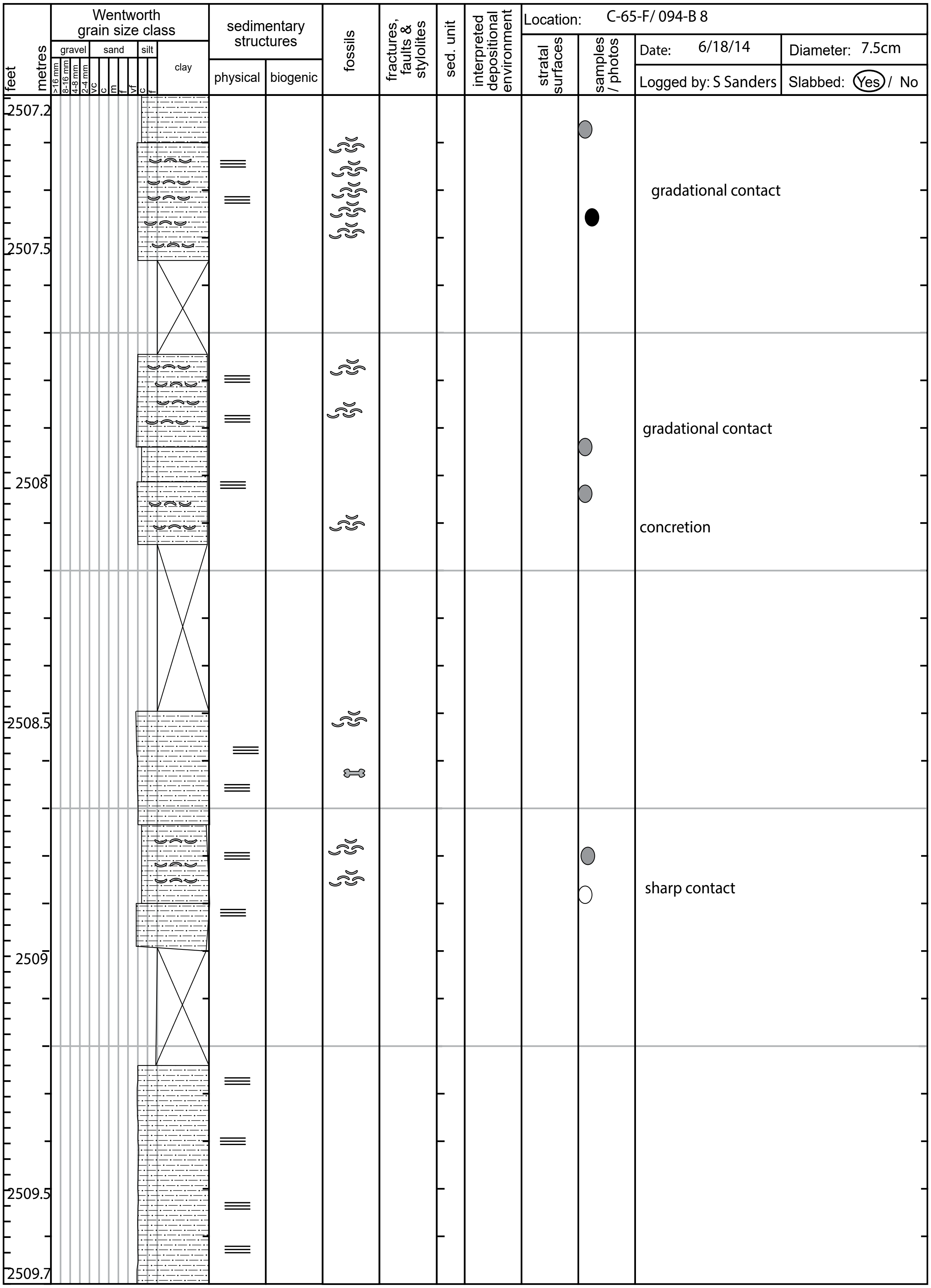

Location: C-65-F/ 094-B 8

Date: 6/18/14

Diameter: 7.5cm

Logged by: S Sanders

Slabbed: [✓ Yes] / No

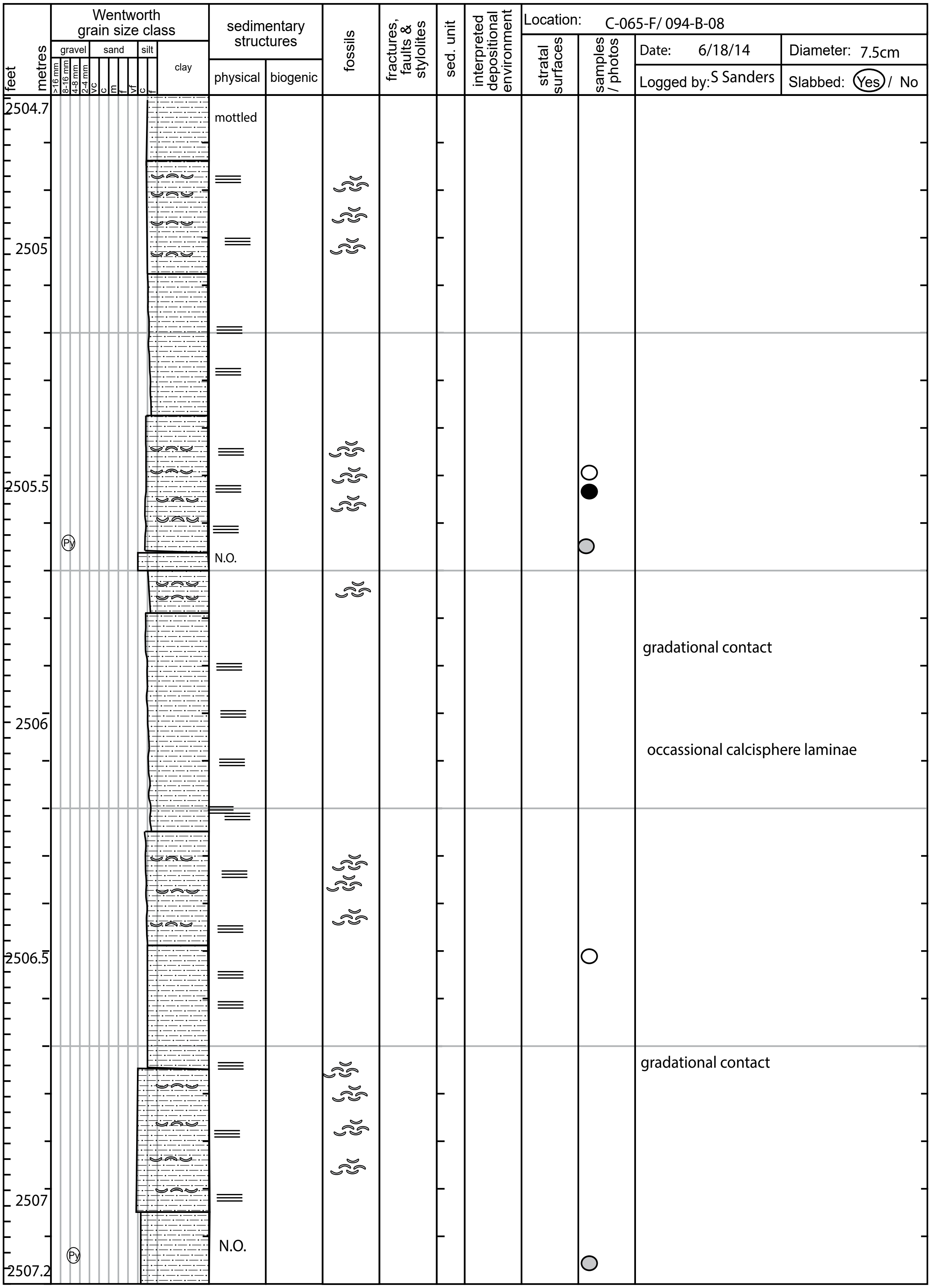
Location: C-065-F/ 094-B-08

Date: 6/18/14

Diameter: 7.5cm

Logged by: S Sanders

Slabbed: [✓ Yes] / No

feet
metres
Wentworth grain size class
gravel
sand
silt
clay
>16 mm
8-16 mm
4-8 mm
2-4 mm
vc
c
m
f
vf
c
f
sedimentary structures
physical
biogenic
fossils
fractures, faults & stylolites
sed. unit
interpreted depositional environment
stratal surfaces
samples / photos
2504.7
2505
2505.5
2506
2506.5
2507
2507.2
mottled
N.O.
Py
N.O.
Py
gradational contact
occassional calcisphere laminae
gradational contact

Location: C-065-F/ 094-B 08

Date: 6/18/14

Diameter: 7.5cm

Logged by: S Sanders

Slabbed: [✓ Yes] / No

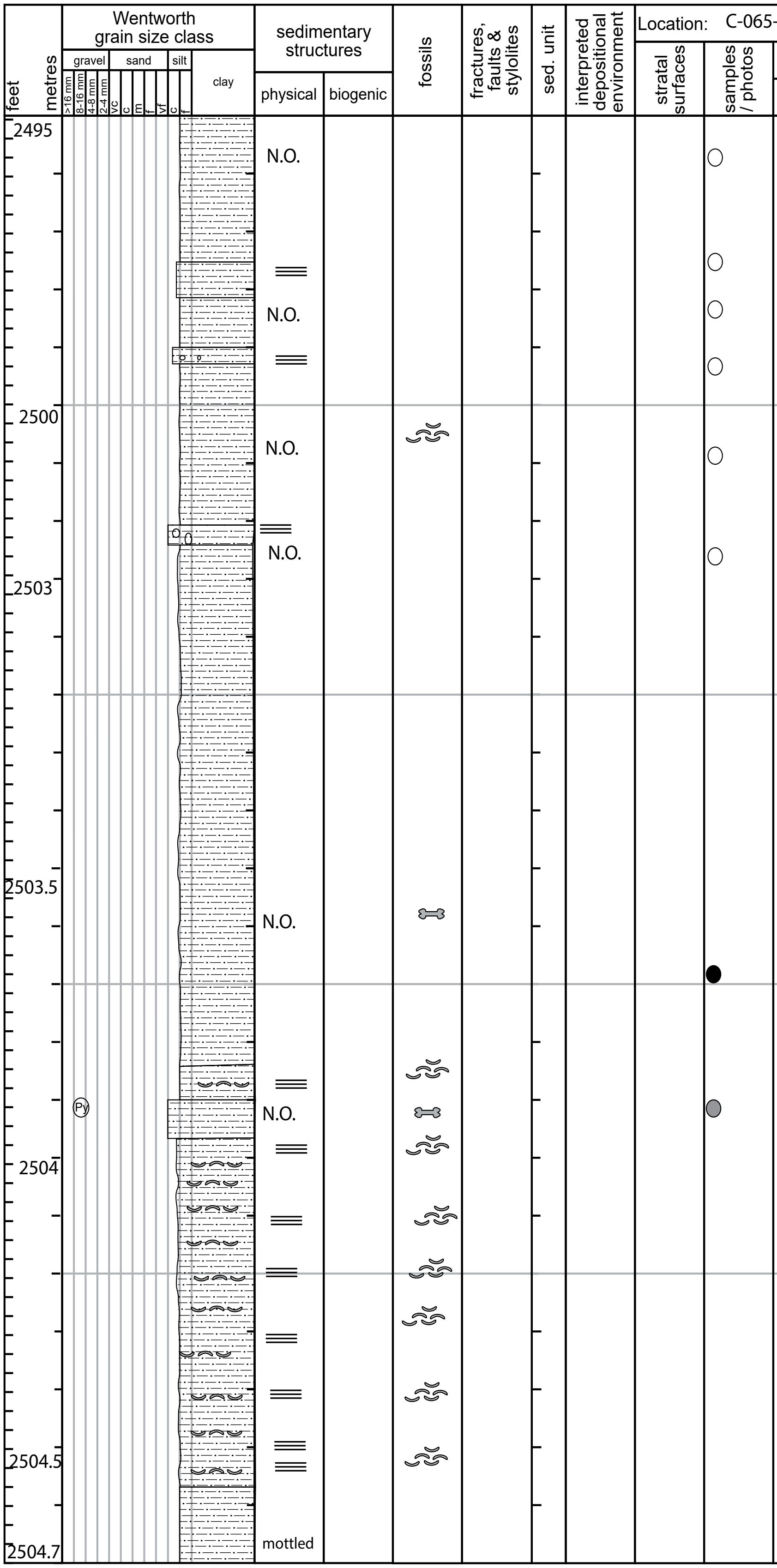
Wentworth grain size class
gravel
sand
silt
clay
>16 mm
8-16 mm
4-8 mm
2-4 mm
vc
c
m
f
vf
c
f
feet
metres
sedimentary structures
physical
biogenic
fossils
fractures, faults & stylolites
sed. unit
interpreted depositional environment
stratal surfaces
samples / photos
2495
N.O.
N.O.
2500
N.O.
N.O.
2503
2503.5
N.O.
Py
N.O.
2504
2504.5
2504.7
mottled

sharp contact

concretion

sharp contact

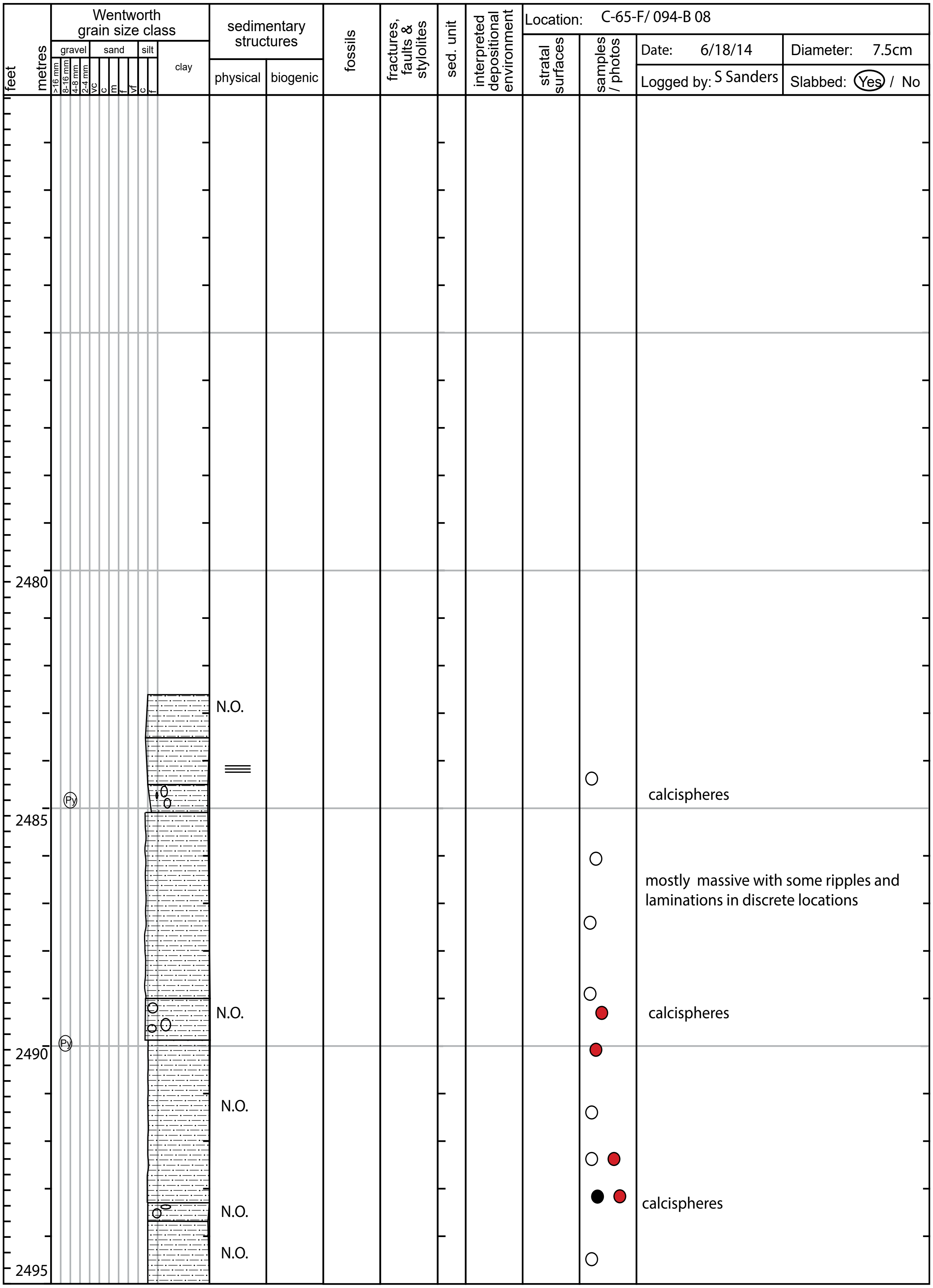
feet
metres
Wentworth grain size class
gravel
sand
silt
clay
>16 mm
8-16 mm
4-8 mm
2-4 mm
vc
c
m
f
vf
c
f
sedimentary structures
physical
biogenic
fossils
fractures, faults & stylolites
sed. unit
interpreted depositional environment
stratal surfaces
samples / photos
2480
2485
2490
2495
N.O.
Py
calcispheres
mostly massive with some ripples and laminations in discrete locations
N.O.
calcispheres
Py
N.O.
N.O.
calcispheres
N.O.

Location: C-65-F/ 094-B 08

Date: 6/18/14

Diameter: 7.5cm

Logged by: S Sanders

Slabbed: [✓ Yes] / No

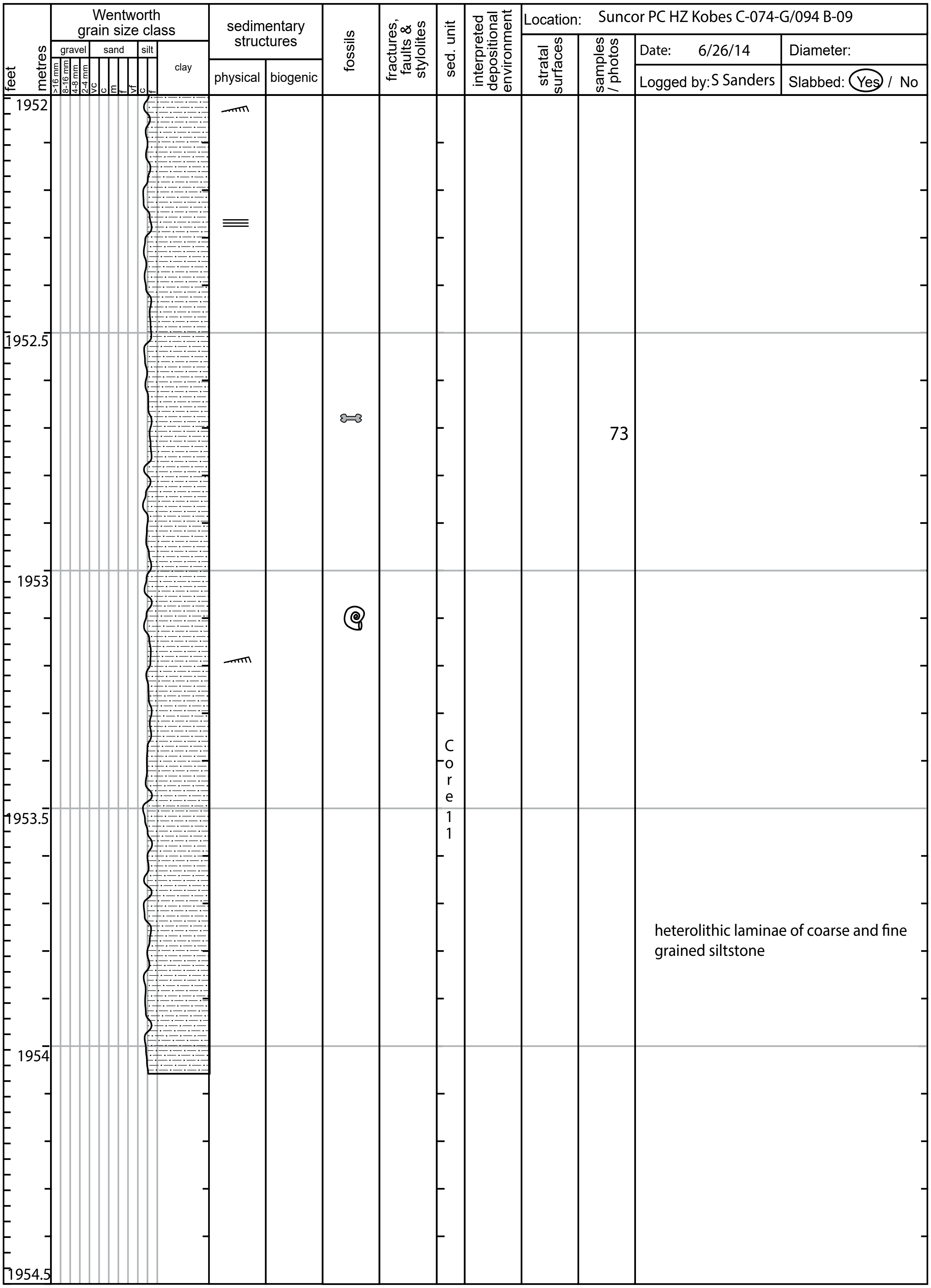
feet
metres
Wentworth grain size class
gravel
sand
silt
clay
>16 mm
8-16 mm
4-8 mm
2-4 mm
vc
c
m
f
vf
c
f
sedimentary structures
physical
biogenic
fossils
fractures, faults & stylolites
sed. unit
interpreted depositional environment
stratal surfaces
samples / photos
1952
1952.5
1953
1953.5
1954
1954.5
73
Core 11

Location: Suncor PC HZ Kobes C-074-G/094 B-09

Date: 6/26/14

Diameter:

Logged by: S Sanders

Slabbed: [✓ Yes] / No

heterolithic laminae of coarse and fine grained siltstone

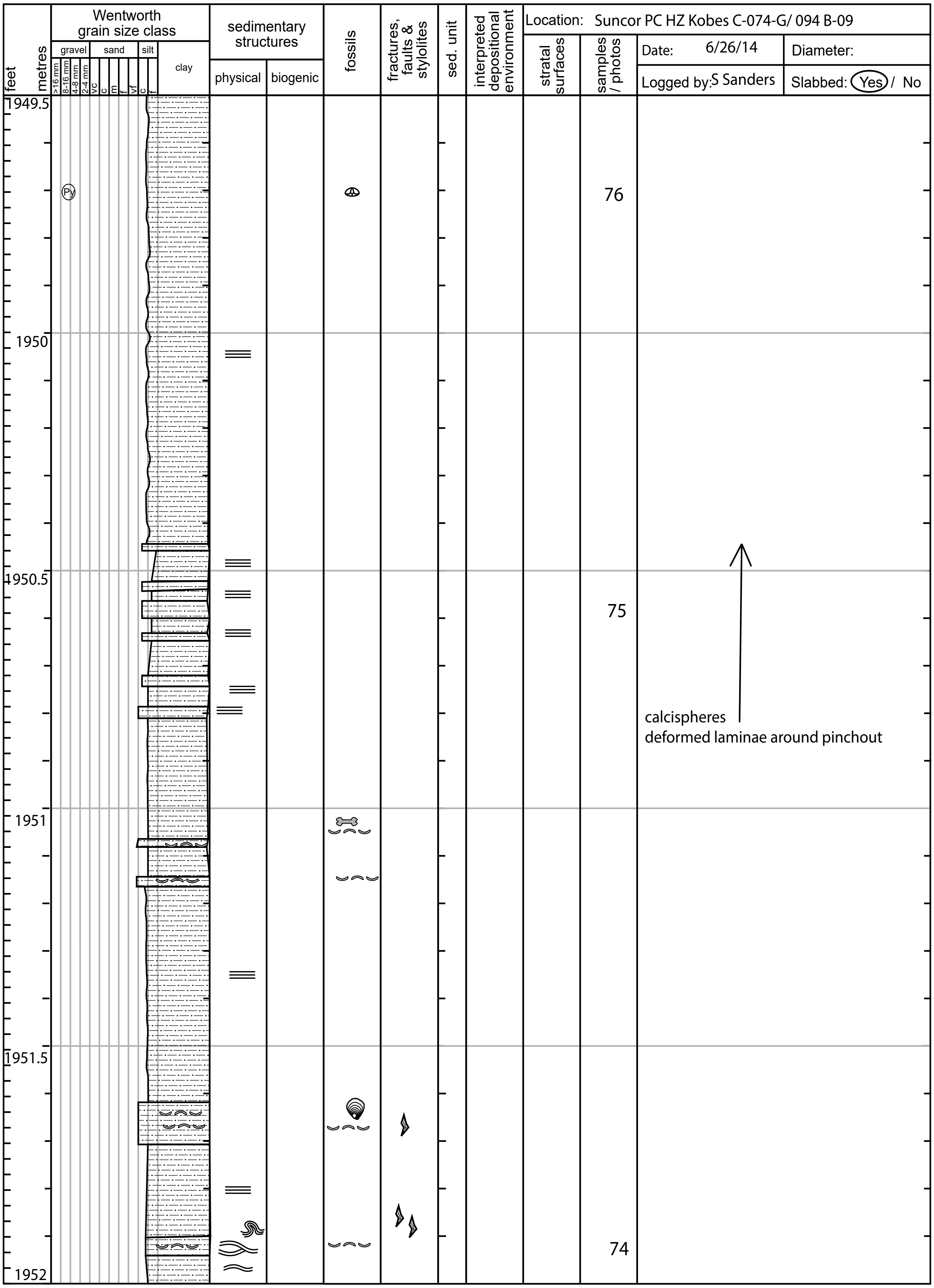

feet
metres
Wentworth grain size class
gravel
sand
silt
clay
>16 mm
8-16 mm
4-8 mm
2-4 mm
vc
c
m
f
vf
c
f
sedimentary structures
physical
biogenic
fossils
fractures, faults & stylolites
sed. unit
interpreted depositional environment
stratal surfaces
samples / photos
1949.5
Py
1950
1950.5
1951
1951.5
1952
76
75
74

Location: Suncor PC HZ Kobes C-074-G/ 094 B-09

Date: 6/26/14

Diameter:

Logged by: S Sanders

Slabbed: [✓ Yes] / No

calcispheres
deformed laminae around pinchout

Location: Suncor PC HZ Kobes C-074-G/ 094 B-09

Date: 6/26/14

Diameter:

Logged by: S Sanders

Slabbed: [✓ Yes] / No

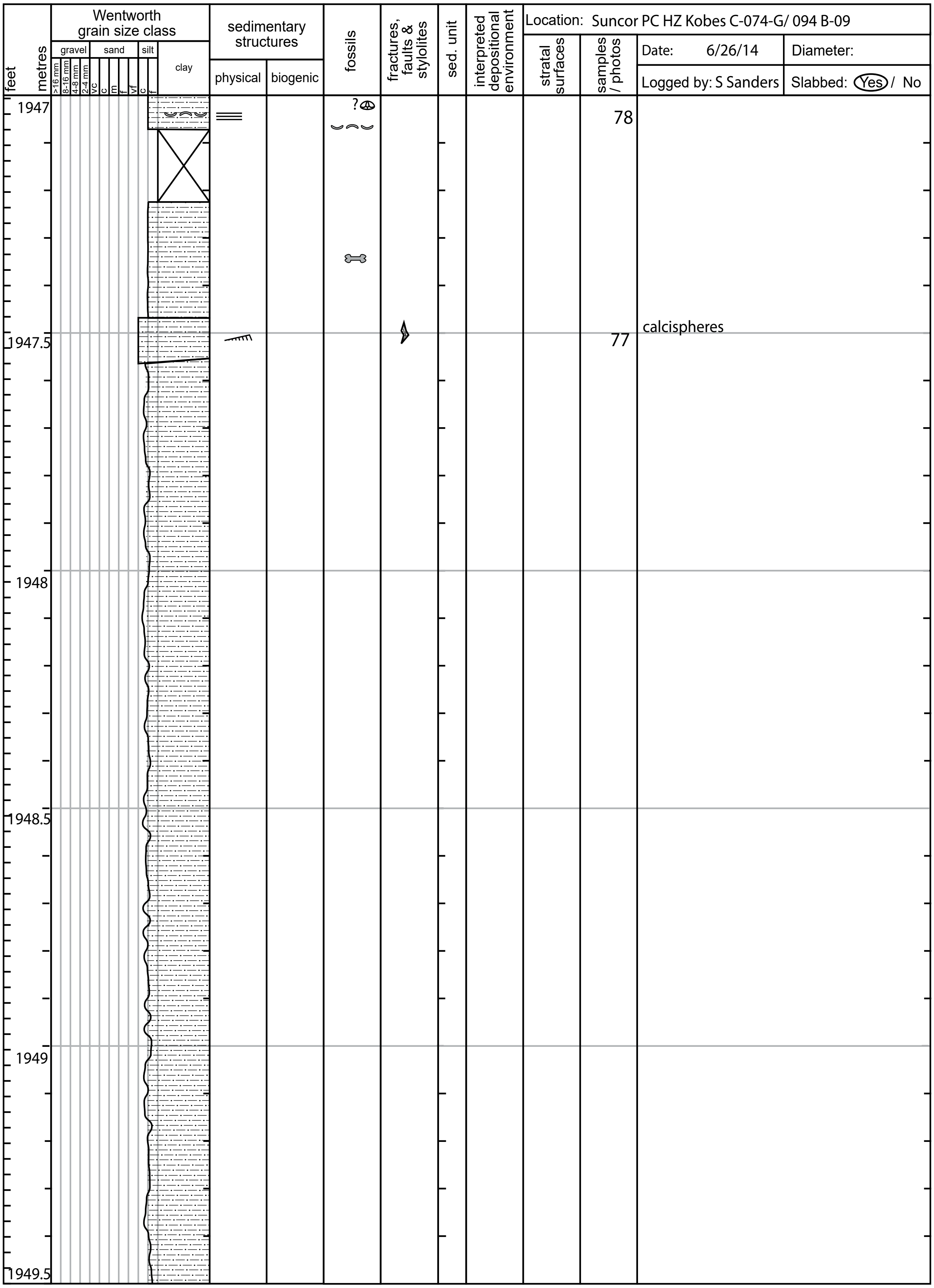

feet
metres
Wentworth grain size class
gravel
sand
silt
clay
>16 mm
8-16 mm
4-8 mm
2-4 mm
vc
c
m
f
vf
c
f
sedimentary structures
physical
biogenic
fossils
fractures, faults & stylolites
sed. unit
interpreted depositional environment
stratal surfaces
samples / photos
1947
?
1947.5
1948
1948.5
1949
1949.5

samples / photos: 78 (1947); 77 (1947.5)

calcispheres

Location: Suncor PC HZ Kobes C-074-G/ 094 B-09

Date: 6/26/14

Diameter:

Logged by: S Sanders

Slabbed: [✓ Yes] / No

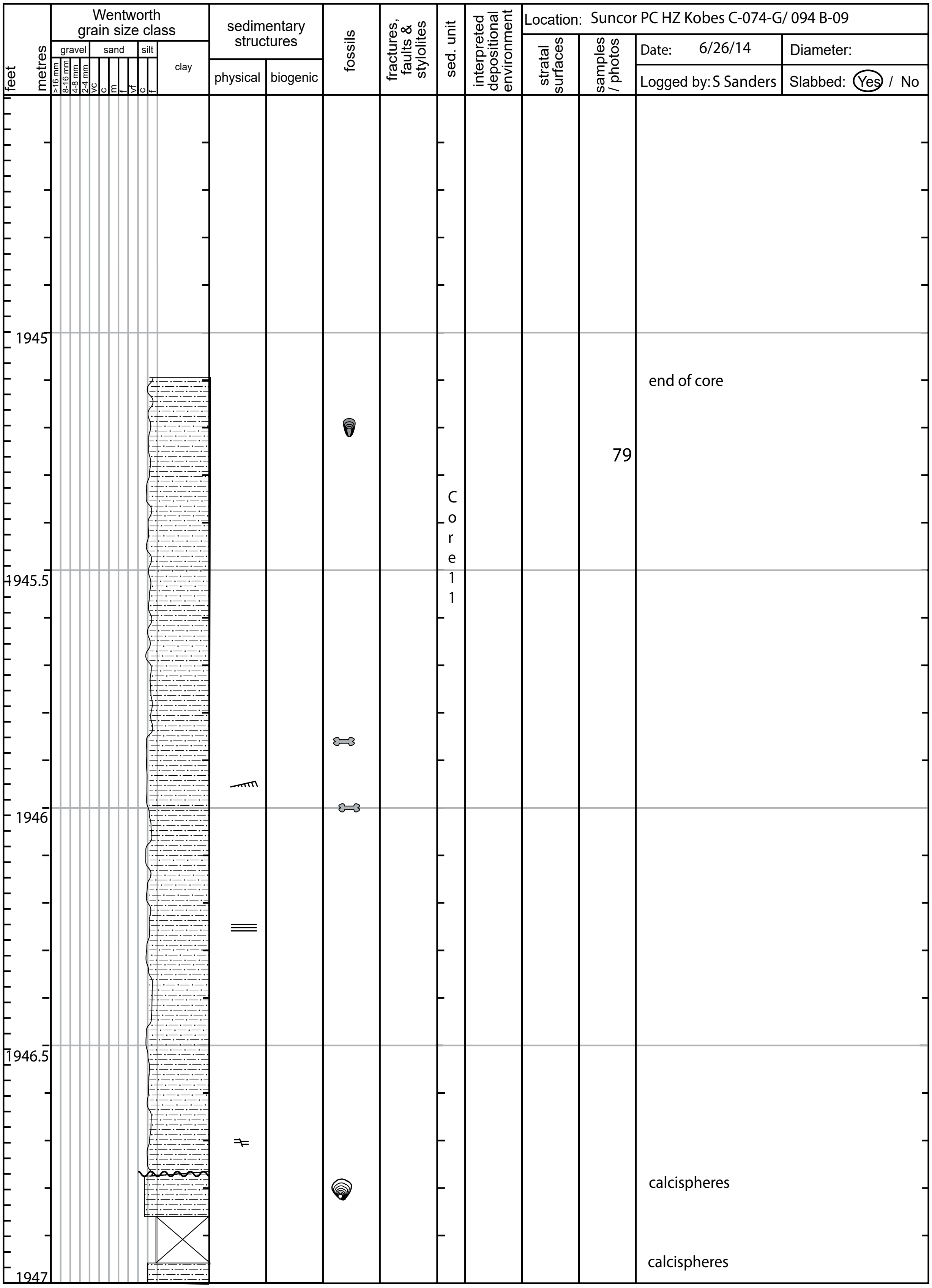
feet
metres
Wentworth grain size class
gravel
sand
silt
clay
>16 mm
8-16 mm
4-8 mm
2-4 mm
vc
c
m
f
vf
c
f
sedimentary structures
physical
biogenic
fossils
fractures, faults & stylolites
sed. unit
interpreted depositional environment
stratal surfaces
samples / photos
1945
1945.5
1946
1946.5
1947
79
Core 11
end of core
calcispheres
calcispheres

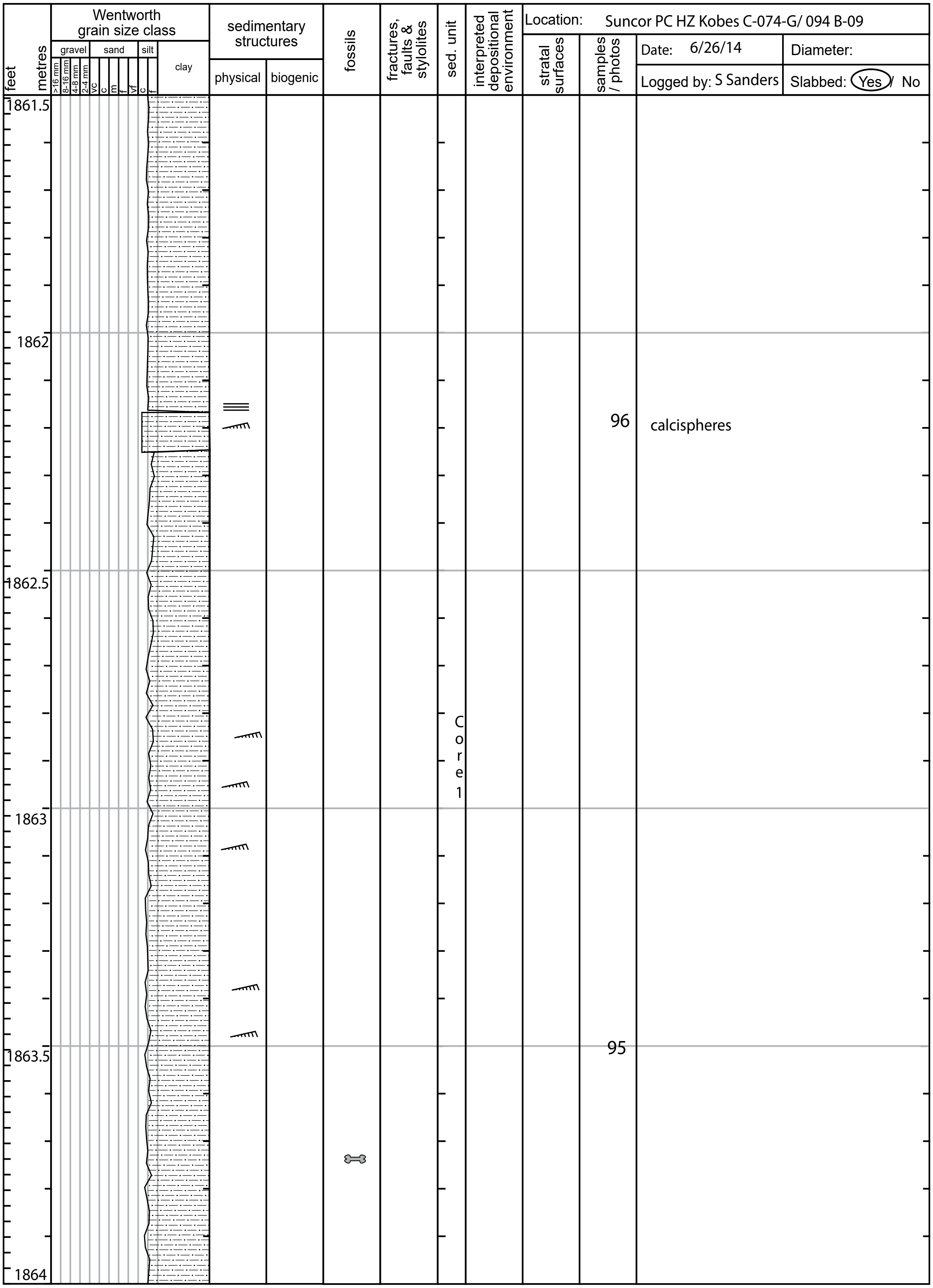

Location: Suncor PC HZ Kobes C-074-G/ 094 B-09

Date: 6/26/14

Diameter:

Logged by: S Sanders

Slabbed: [✓ Yes] / No

Location: Suncor PC HZ Kobes C-074-G/ 094 B-09

Date: 6/26/14

Diameter:

Logged by: S Sanders

Slabbed: [✓ Yes]/ No

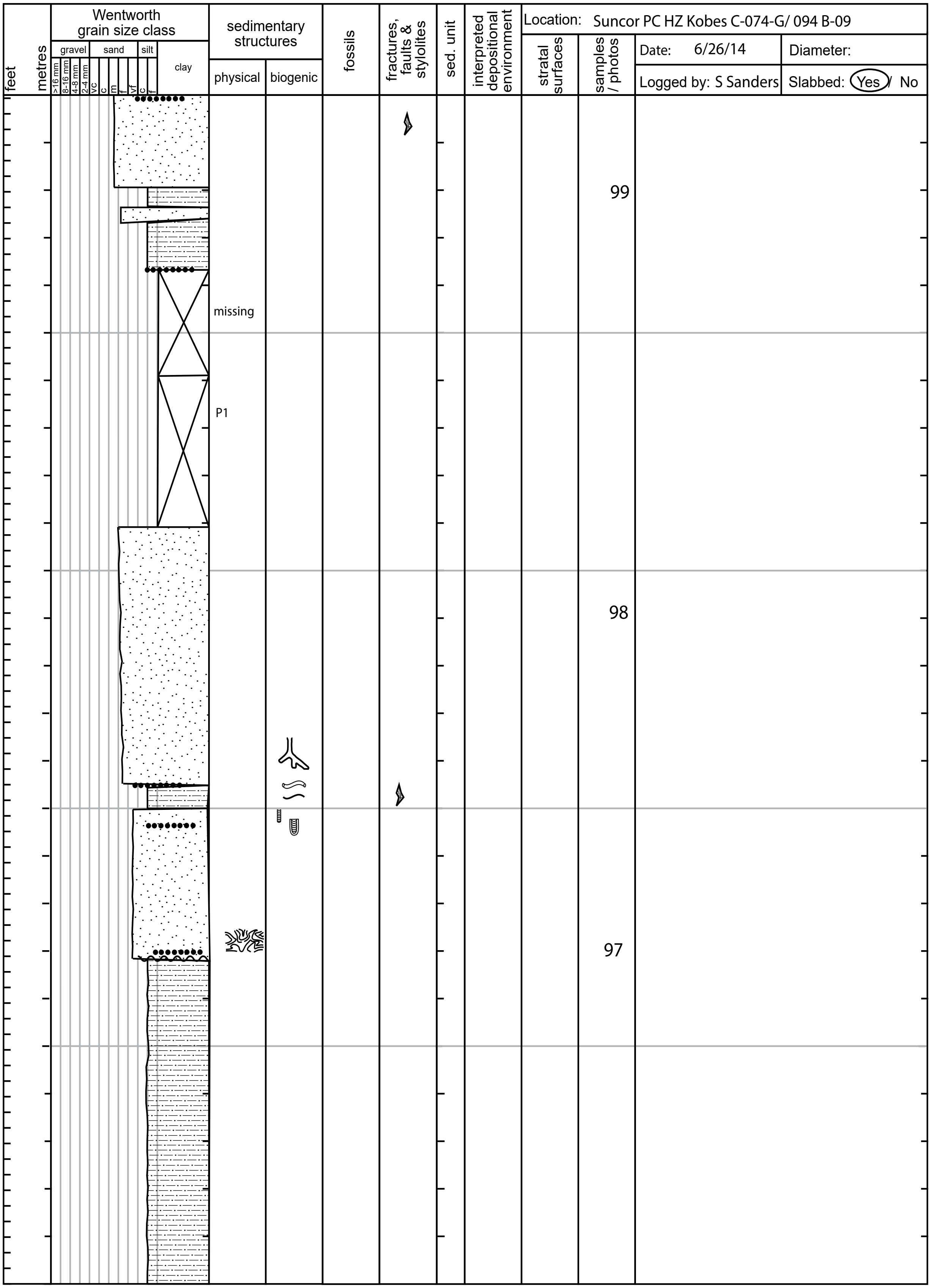
feet
metres
Wentworth grain size class
gravel
sand
silt
clay
>16 mm
8-16 mm
4-8 mm
2-4 mm
vc
c
m
f
vf
c
f
sedimentary structures
physical
biogenic
fossils
fractures, faults & stylolites
sed. unit
interpreted depositional environment
stratal surfaces
samples / photos
99
missing
P1
98
97

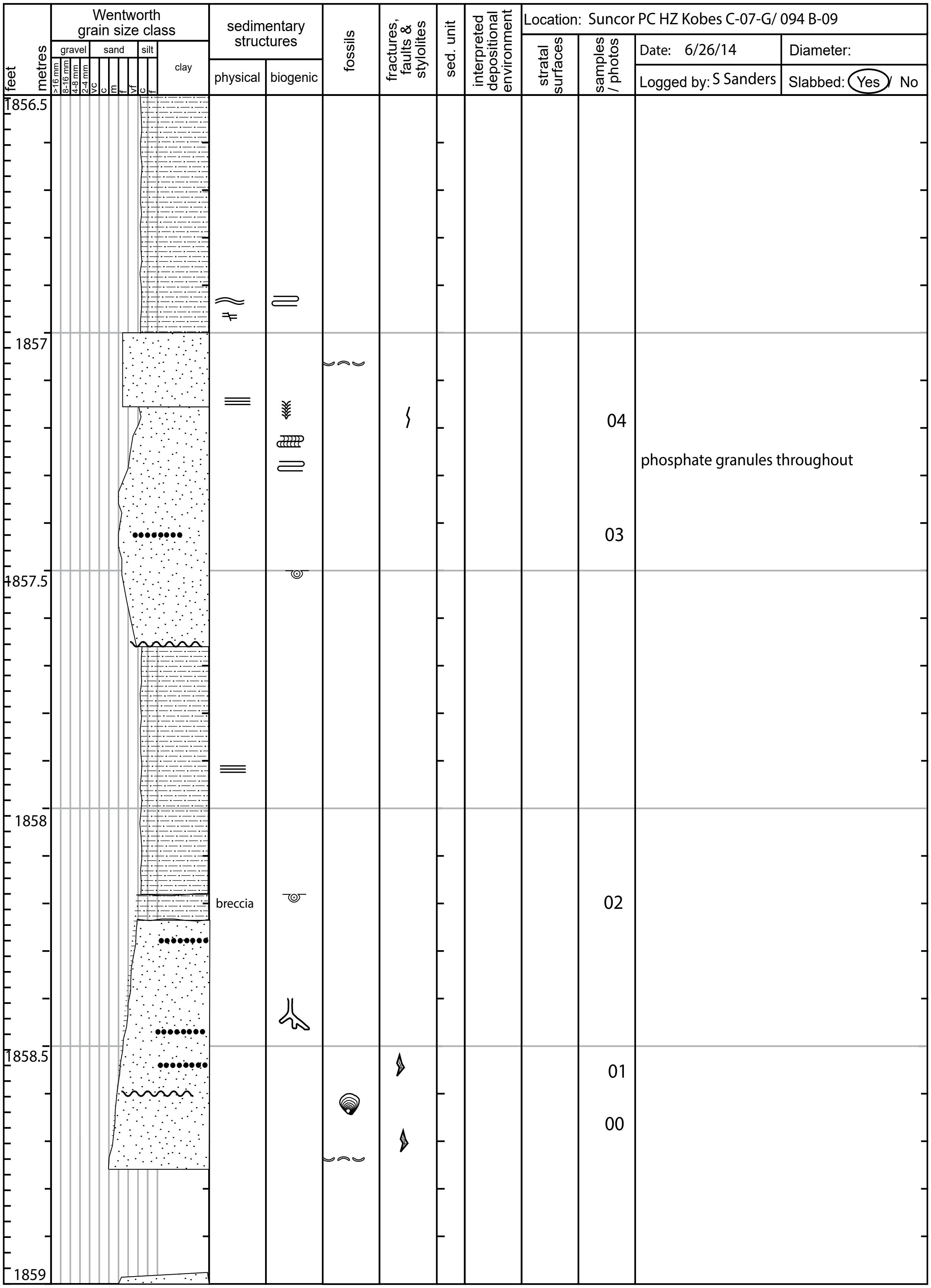

Wentworth grain size class
gravel
sand
silt
clay
>16 mm
8-16 mm
4-8 mm
2-4 mm
vc
c
m
f
vf
c
f
feet
metres
sedimentary structures
physical
biogenic
fossils
fractures, faults & stylolites
sed. unit
interpreted depositional environment
stratal surfaces
samples / photos
1856.5
1857
1857.5
1858
1858.5
1859
breccia
04
03
02
01
00

Location: Suncor PC HZ Kobes C-07-G/ 094 B-09

Date: 6/26/14

Diameter:

Logged by: S Sanders

Slabbed: [✓ Yes] / No

phosphate granules throughout

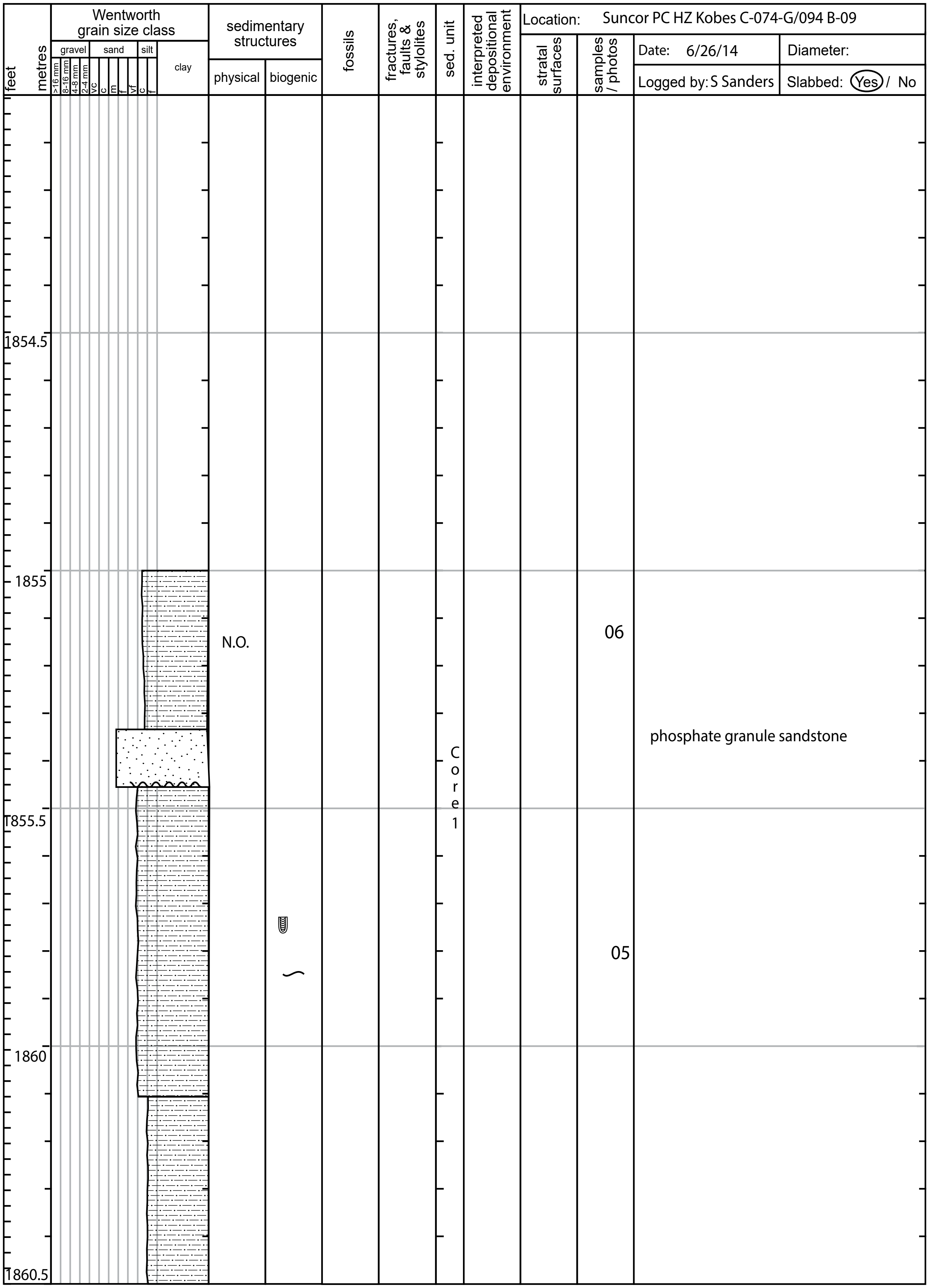
feet
metres
Wentworth grain size class
gravel
sand
silt
clay
>16 mm
8-16 mm
4-8 mm
2-4 mm
vc
c
m
f
vf
c
f
sedimentary structures
physical
biogenic
fossils
fractures, faults & stylolites
sed. unit
interpreted depositional environment
stratal surfaces
samples / photos
1854.5
1855
1855.5
1860
1860.5
N.O.
06
Core 1
05

Location: Suncor PC HZ Kobes C-074-G/094 B-09

Date: 6/26/14

Diameter:

Logged by: S Sanders

Slabbed: [✓ Yes] / No

phosphate granule sandstone

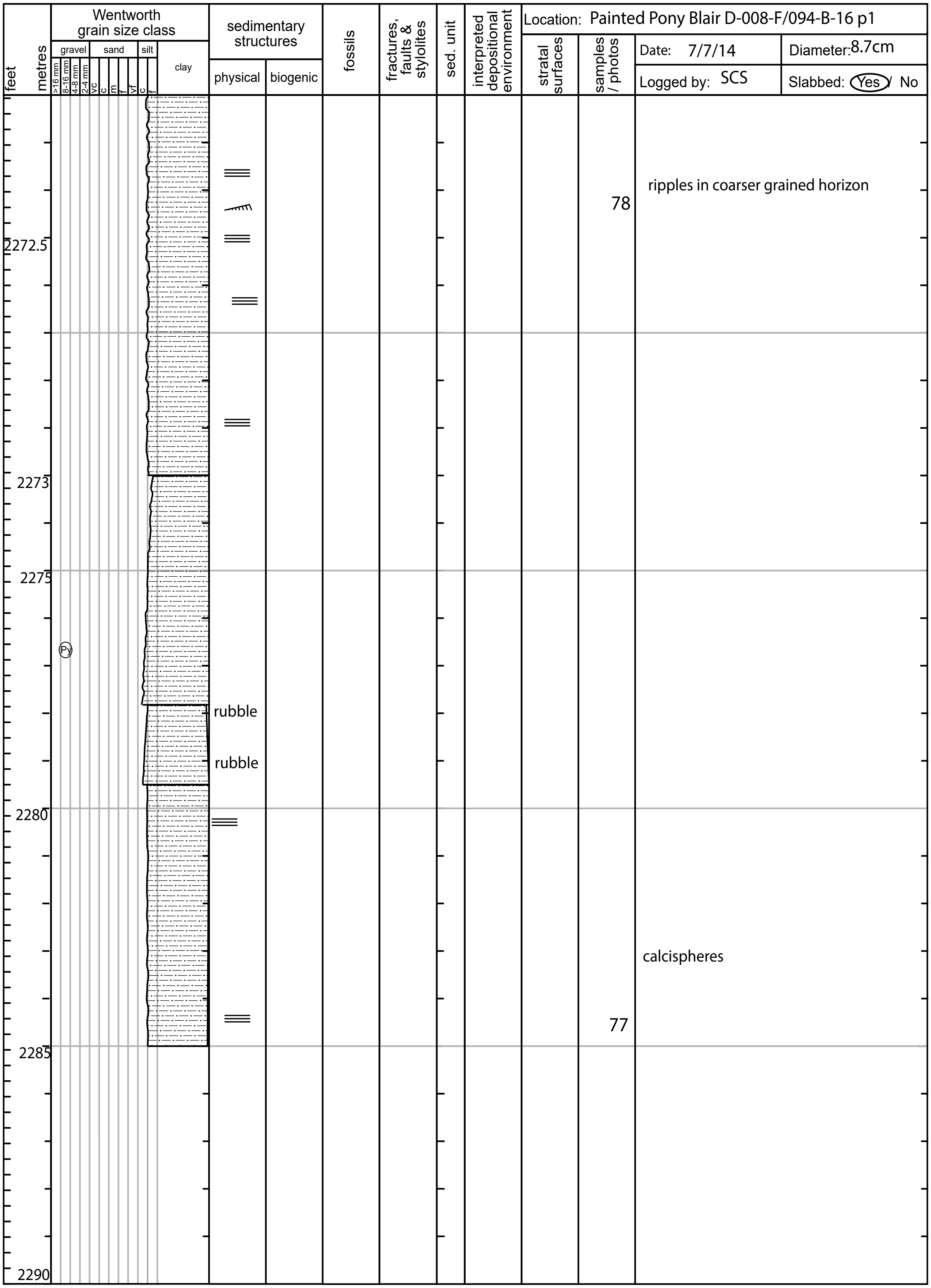

Location: Painted Pony Blair D-008-F/094-B-16 p2

Date: 7/7/14

Diameter: 8.7cm

Logged by: SCS

Slabbed: [✓ Yes] / No

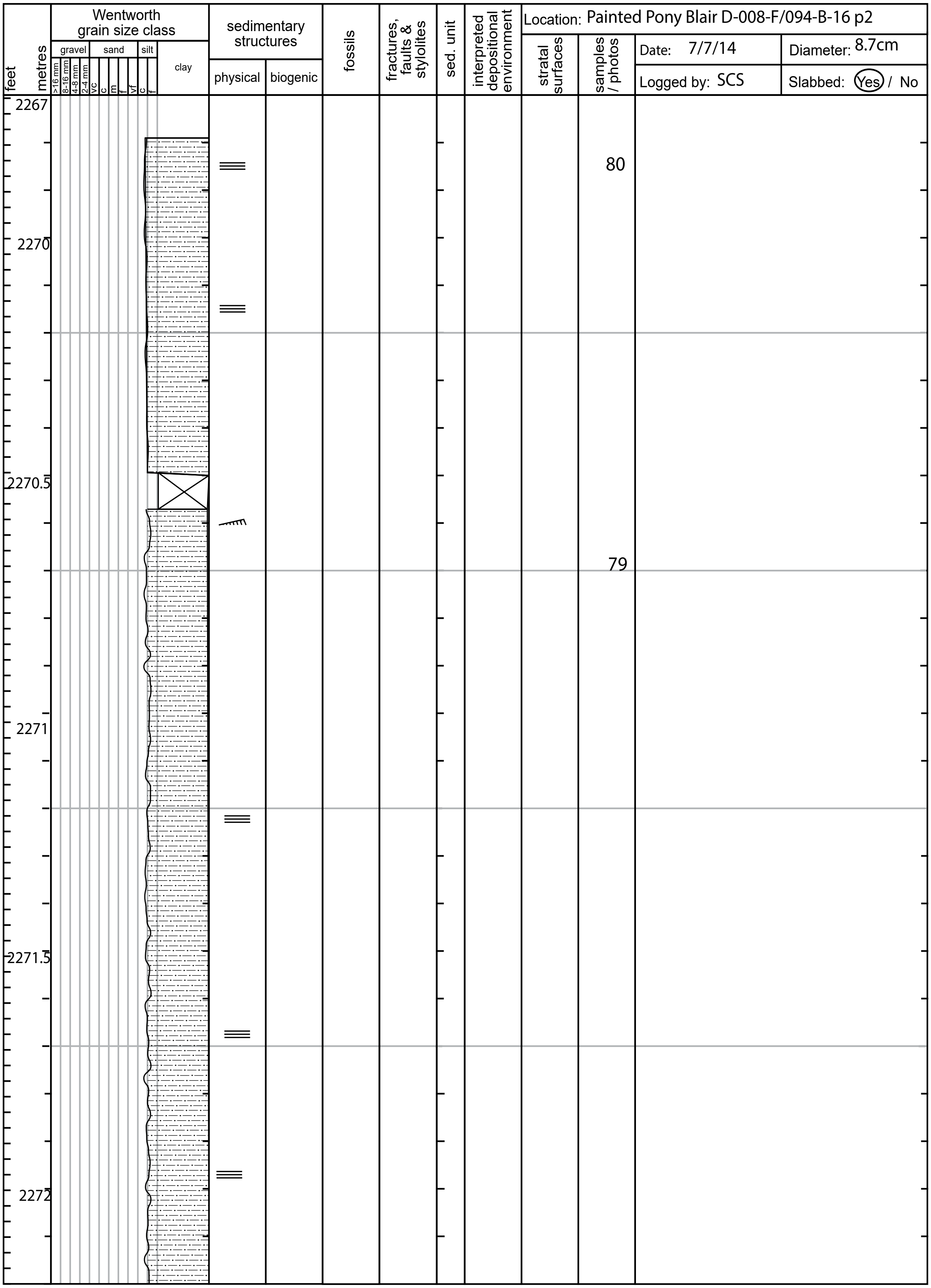
feet
metres
Wentworth grain size class
gravel
sand
silt
clay
>16 mm
8-16 mm
4-8 mm
2-4 mm
vc
c
m
f
vf
c
f
sedimentary structures
physical
biogenic
fossils
fractures, faults & stylolites
sed. unit
interpreted depositional environment
stratal surfaces
samples / photos
2267
2270
2270.5
2271
2271.5
2272
80
79

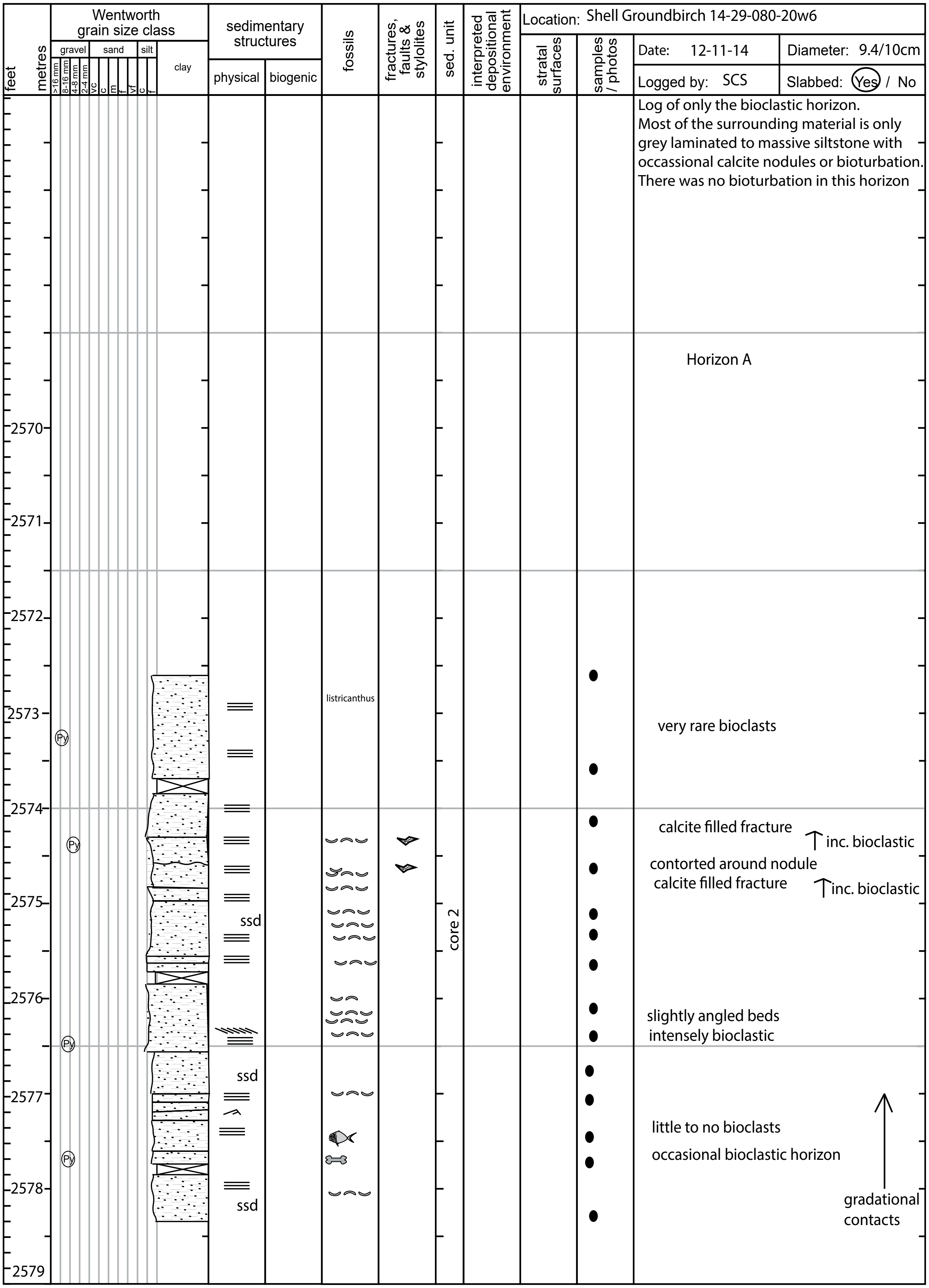
feet
metres
Wentworth grain size class
gravel
sand
silt
>16 mm
8-16 mm
4-8 mm
2-4 mm
vc
c
m
f
vf
c
f
clay
sedimentary structures
physical
biogenic
fossils
fractures, faults & stylolites
sed. unit
interpreted depositional environment
stratal surfaces
samples / photos
2570
2571
2572
2573
2574
2575
2576
2577
2578
2579
Py
Py
Py
Py
ssd
ssd
ssd
listricanthus
core 2

Location: Shell Groundbirch 14-29-080-20w6

Date: 12-11-14

Diameter: 9.4/10cm

Logged by: SCS

Slabbed: [✓ Yes] / No

Log of only the bioclastic horizon.
Most of the surrounding material is only grey laminated to massive siltstone with occassional calcite nodules or bioturbation.
There was no bioturbation in this horizon

Horizon A

very rare bioclasts

calcite filled fracture

↑ inc. bioclastic

contorted around nodule

calcite filled fracture

↑ inc. bioclastic

slightly angled beds

intensely bioclastic

little to no bioclasts

occasional bioclastic horizon

↑ gradational contacts

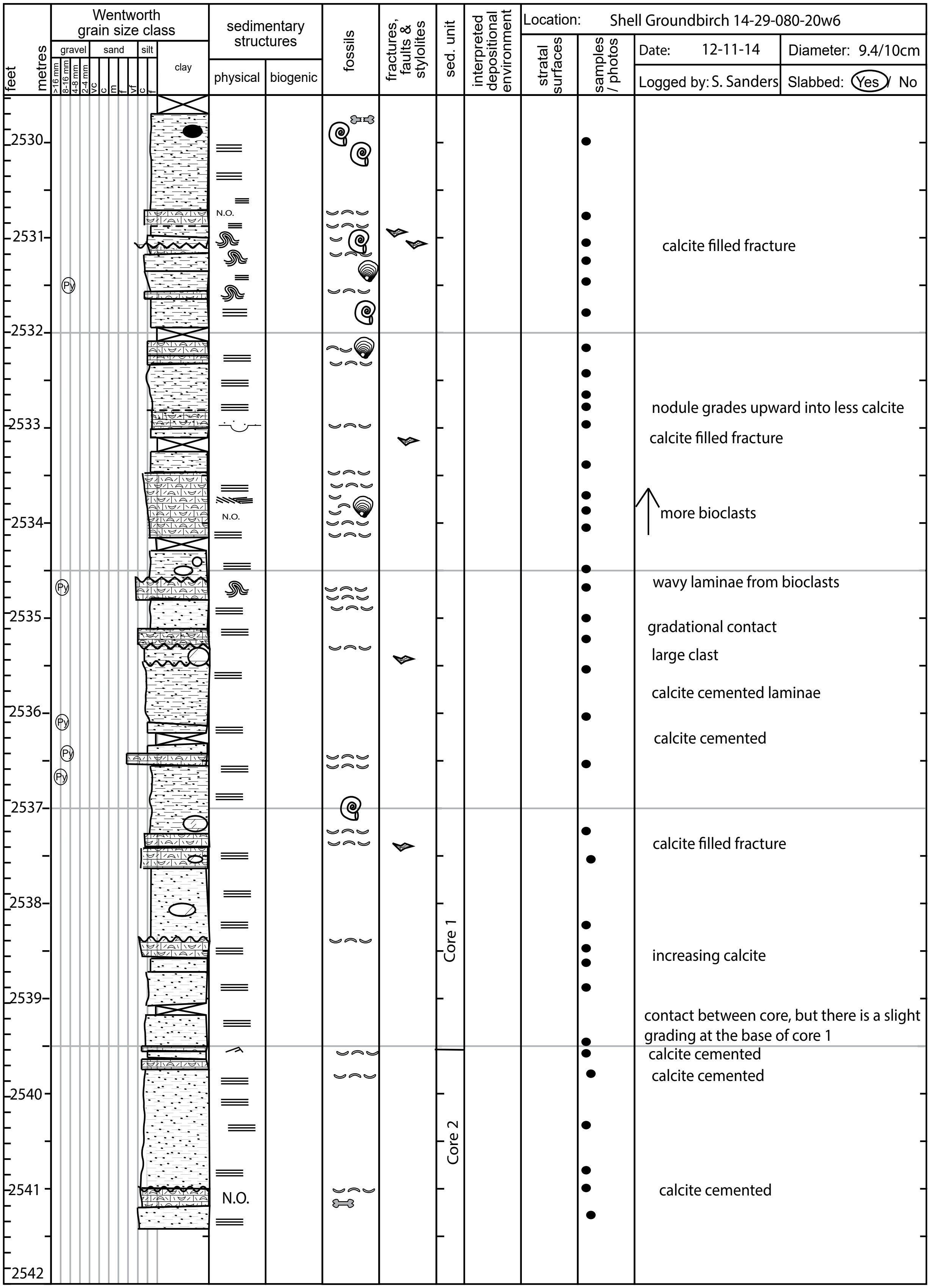
feet
metres
Wentworth grain size class
gravel
sand
silt
clay
>16 mm
8-16 mm
4-8 mm
2-4 mm
vc
c
m
f
vf
c
f
sedimentary structures
physical
biogenic
fossils
fractures, faults & stylolites
sed. unit
interpreted depositional environment
stratal surfaces
samples / photos
2530
2531
2532
2533
2534
2535
2536
2537
2538
2539
2540
2541
2542
N.O.
N.O.
N.O.
Py
Py
Py
Py
Py
Core 1
Core 2

Location: Shell Groundbirch 14-29-080-20w6

Date: 12-11-14

Diameter: 9.4/10cm

Logged by: S. Sanders

Slabbed: [✓ Yes] / No

calcite filled fracture

nodule grades upward into less calcite

calcite filled fracture

more bioclasts

wavy laminae from bioclasts

gradational contact

large clast

calcite cemented laminae

calcite cemented

calcite filled fracture

increasing calcite

contact between core, but there is a slight grading at the base of core 1

calcite cemented

calcite cemented

calcite cemented

Location: Shell Groundbirch 14-29-080-20w6

Date: 12-11-14

Diameter: 9.4/10cm

Logged by: S. Sanders

Slabbed: [✓ Yes] / No

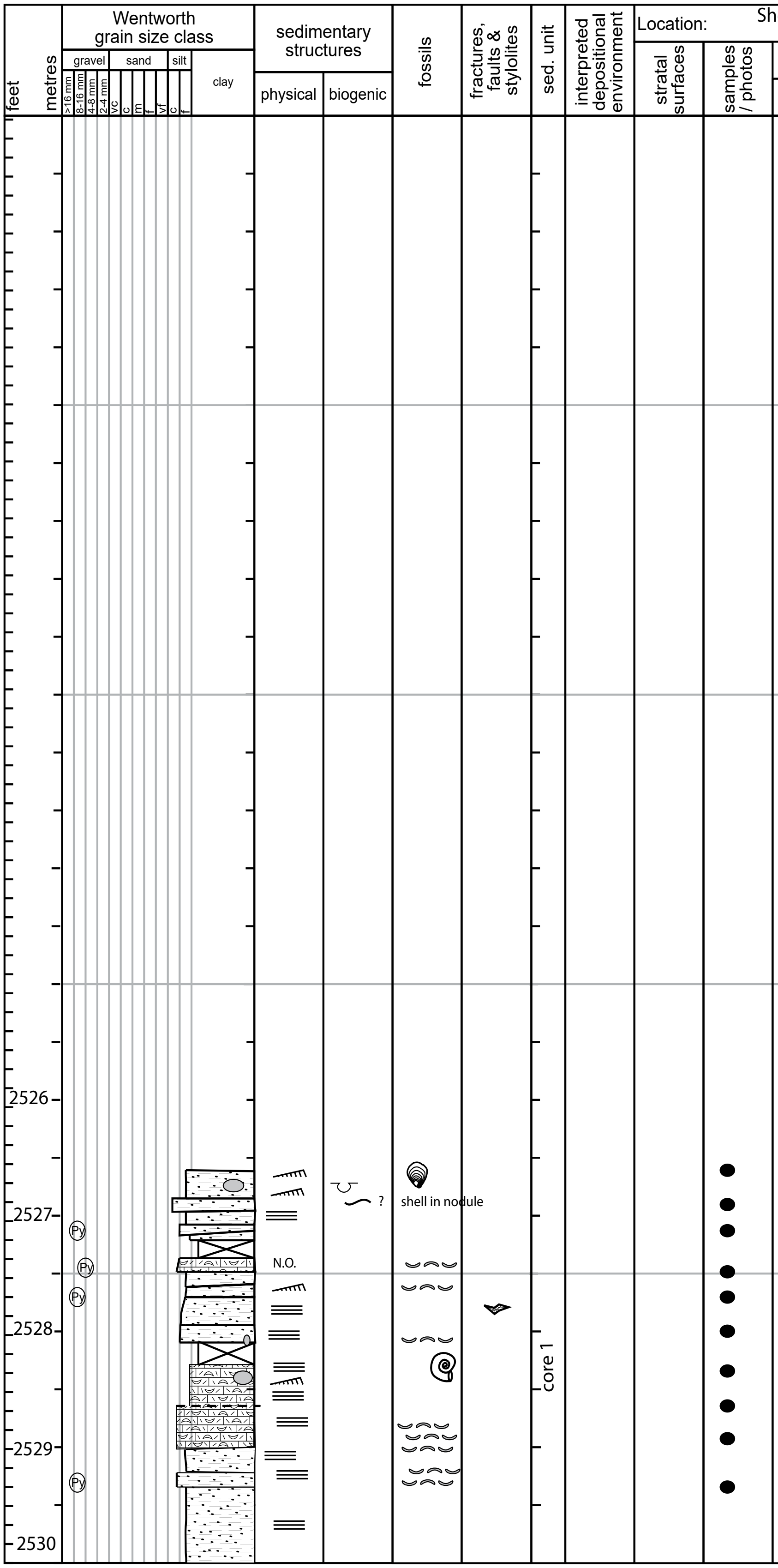

feet
metres
Wentworth grain size class
gravel
sand
silt
clay
>16 mm
8-16 mm
4-8 mm
2-4 mm
vc
c
m
f
vf
c
f
sedimentary structures
physical
biogenic
fossils
fractures, faults & stylolites
sed. unit
interpreted depositional environment
stratal surfaces
samples / photos
2526
2527
2528
2529
2530
Py
Py
Py
Py
N.O.
?
shell in nodule
core 1

Horizon B

End of Section

nodule and rippled/bioturbated horizons
are coarser grained

wavy laminae at center and more
laminated edges
calcite filled fracture
nodule at base

nodule

less distinct laminae at base
grading up into less bioclastic material
nodule in middle

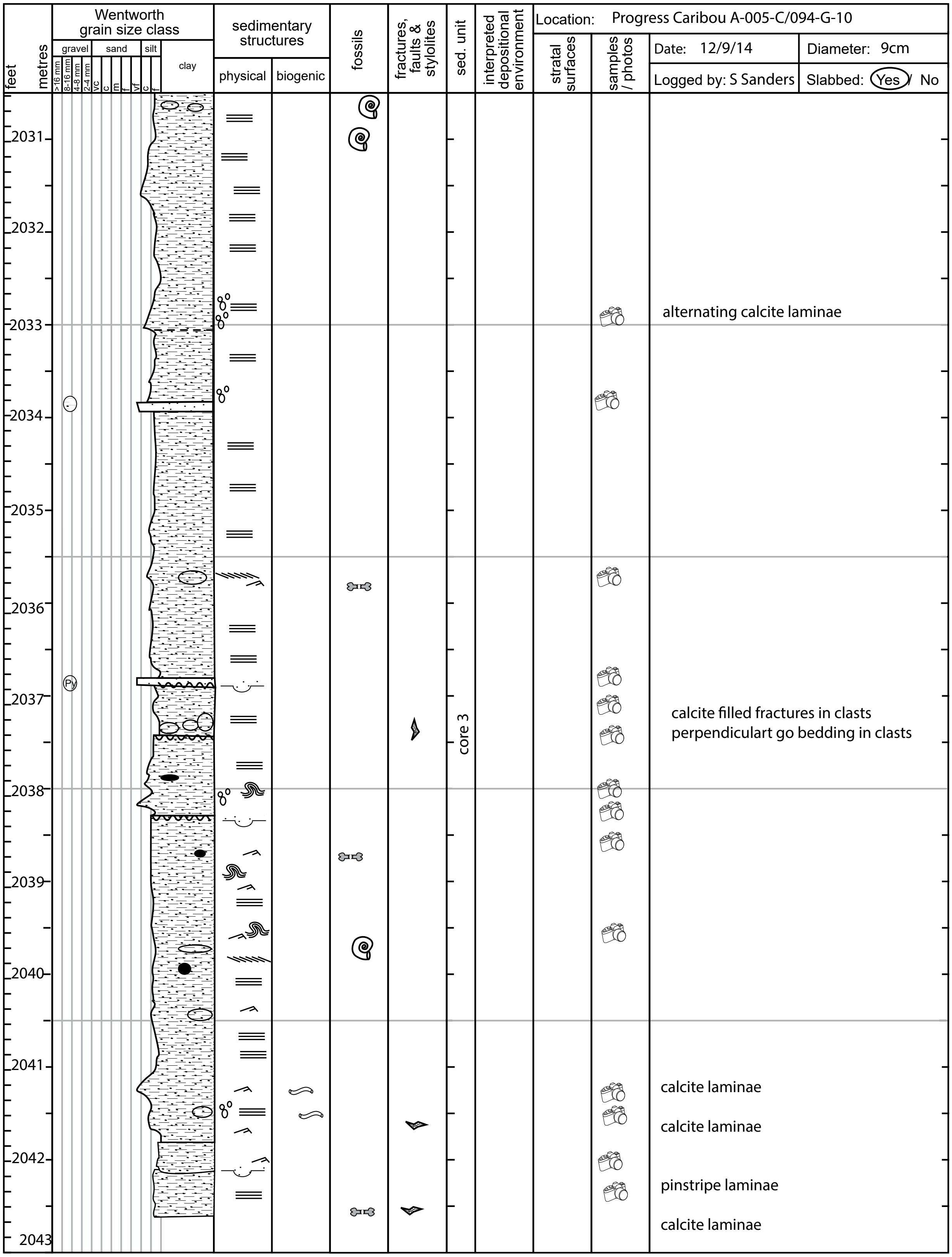
feet
metres
Wentworth grain size class
gravel
sand
silt
clay
>16 mm
8-16 mm
4-8 mm
2-4 mm
vc
c
m
f
vf
c
f
sedimentary structures
physical
biogenic
fossils
fractures, faults & stylolites
sed. unit
interpreted depositional environment
strata surfaces
samples / photos
2031
2032
2033
2034
2035
2036
2037
2038
2039
2040
2041
2042
2043
Py
core 3

Location: Progress Caribou A-005-C/094-G-10

Date: 12/9/14

Diameter: 9cm

Logged by: S Sanders

Slabbed: [✓ Yes] / No

alternating calcite laminae

calcite filled fractures in clasts
perpendicualart go bedding in clasts

calcite laminae

calcite laminae

pinstripe laminae

calcite laminae

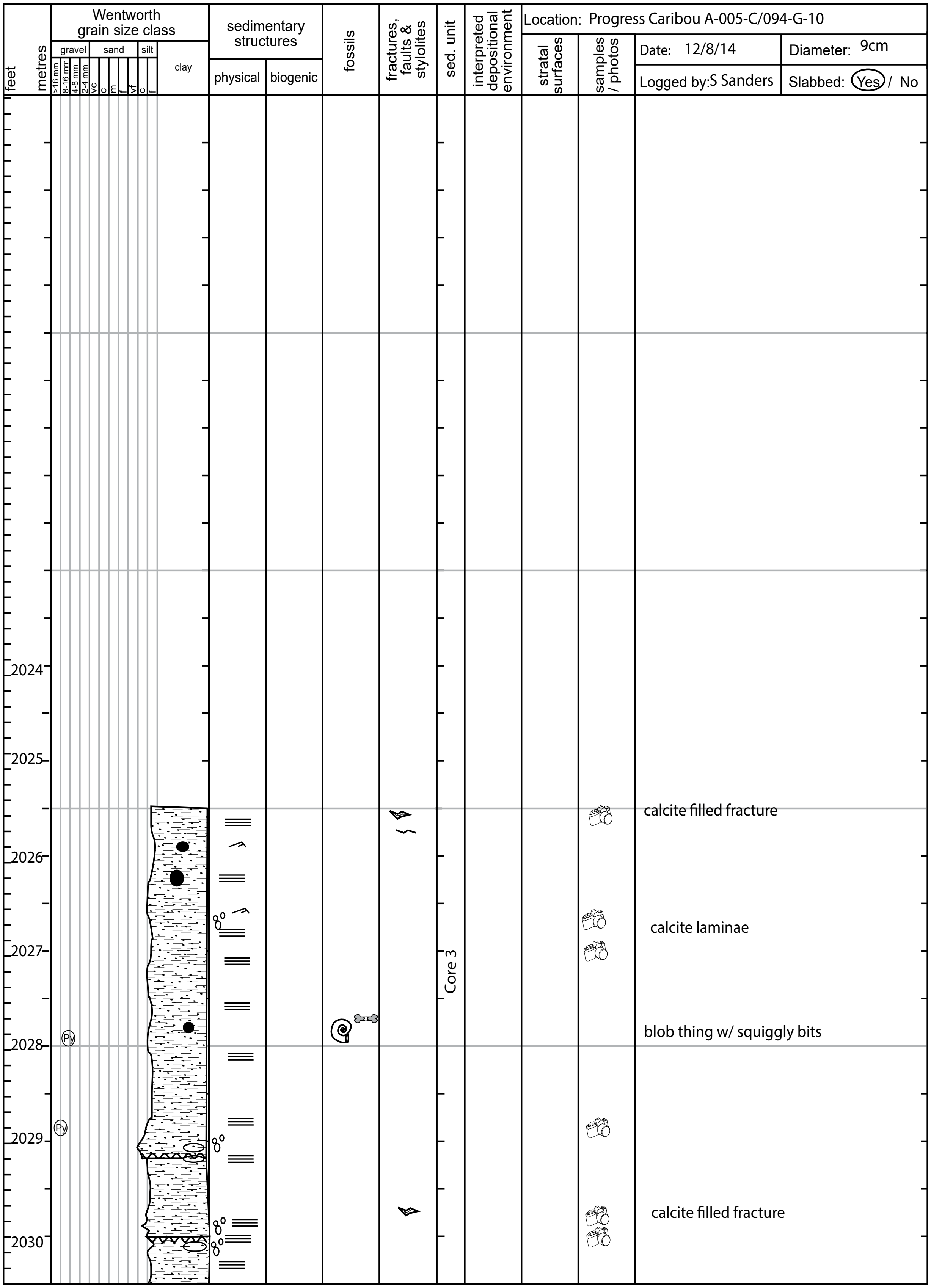

Location: Progress Caribou A-005-C/094-G-10

Date: 12/8/14

Diameter: 9cm

Logged by:S Sanders

Slabbed: [✓ Yes] / No

calcite filled fracture

calcite laminae

blob thing w/ squiggly bits

calcite filled fracture

feet
metres
Wentworth grain size class
gravel
sand
silt
clay
>16 mm
8-16 mm
4-8 mm
2-4 mm
vc
c
m
f
vf
c
f
sedimentary structures
physical
biogenic
fossils
fractures, faults & stylolites
sed. unit
interpreted depositional environment
stratal surfaces
samples / photos
2024
2025
2026
2027
2028
2029
2030
Py
Py
Core 3

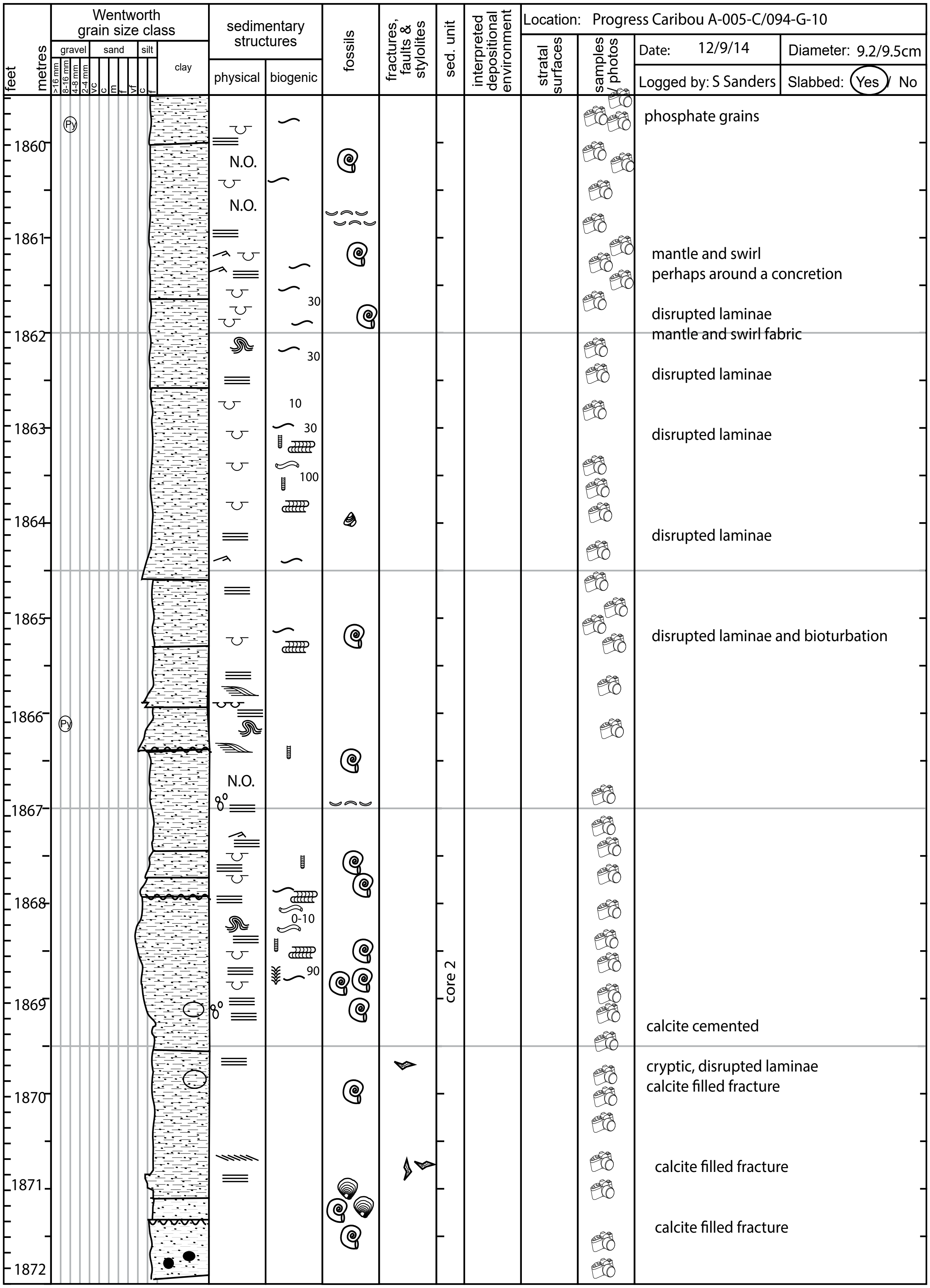
feet
metres
Wentworth grain size class
gravel
sand
silt
clay
>16 mm
8-16 mm
4-8 mm
2-4 mm
vc
c
m
f
vf
c
f
sedimentary structures
physical
biogenic
fossils
fractures, faults & stylolites
sed. unit
interpreted depositional environment
stratal surfaces
samples / photos
1860
1861
1862
1863
1864
1865
1866
1867
1868
1869
1870
1871
1872
Py
Py
N.O.
N.O.
N.O.
30
30
10
30
100
0-10
90
core 2

Location: Progress Caribou A-005-C/094-G-10

Date: 12/9/14

Diameter: 9.2/9.5cm

Logged by: S Sanders

Slabbed: [✓ Yes] / No

phosphate grains

mantle and swirl
perhaps around a concretion

disrupted laminae
mantle and swirl fabric

disrupted laminae

disrupted laminae

disrupted laminae

disrupted laminae and bioturbation

calcite cemented

cryptic, disrupted laminae
calcite filled fracture

calcite filled fracture

calcite filled fracture

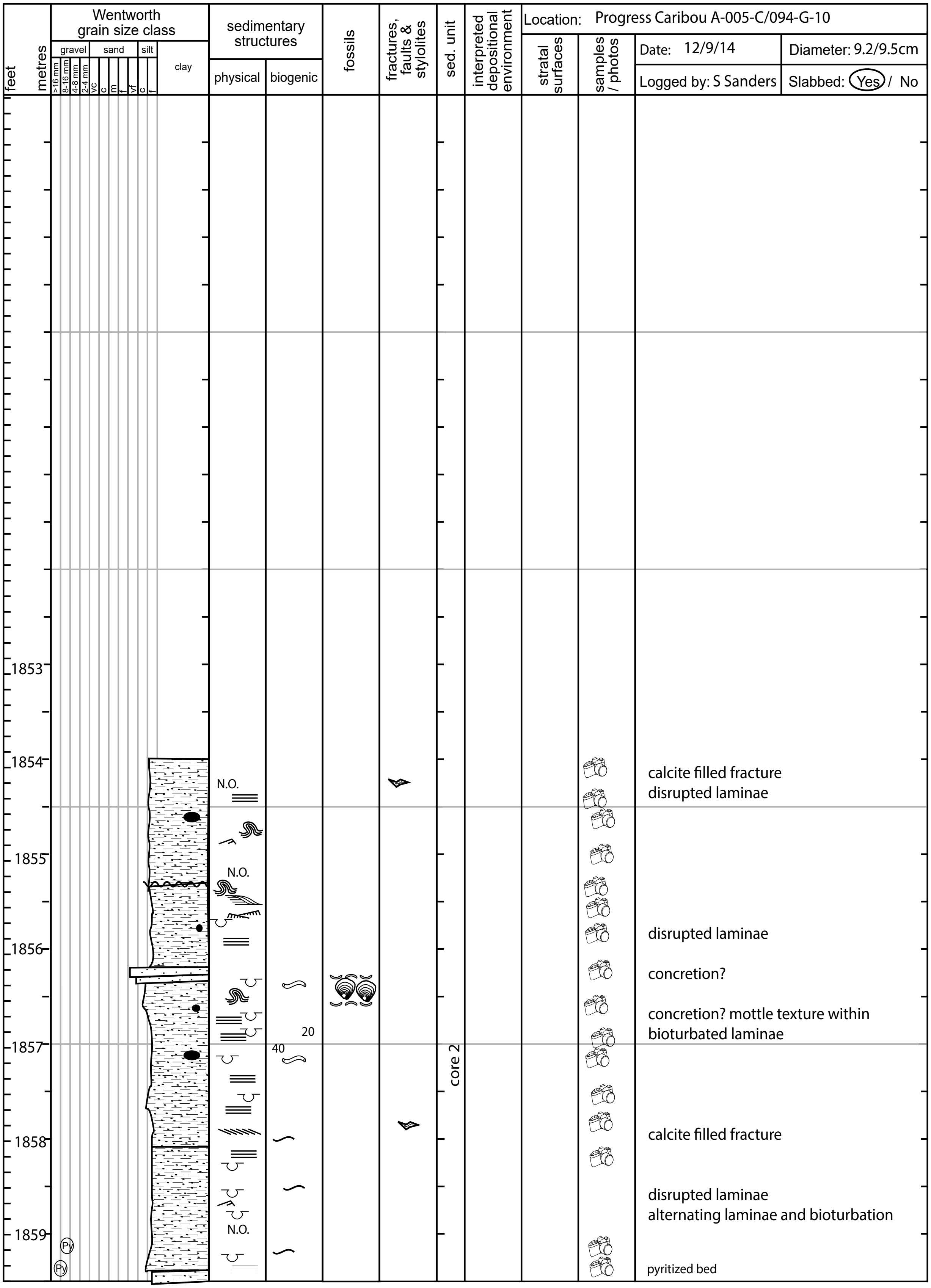
feet
metres
Wentworth grain size class
gravel
sand
silt
clay
>16 mm
8-16 mm
4-8 mm
2-4 mm
vc
c
m
f
vf
c
f
sedimentary structures
physical
biogenic
fossils
fractures, faults & stylolites
sed. unit
interpreted depositional environment
stratal surfaces
samples / photos
1853
1854
1855
1856
1857
1858
1859
N.O.
N.O.
20
40
N.O.
core 2
Py
Py

Location: Progress Caribou A-005-C/094-G-10

Date: 12/9/14

Diameter: 9.2/9.5cm

Logged by: S Sanders

Slabbed: [✓ Yes] / No

calcite filled fracture
disrupted laminae

disrupted laminae

concretion?

concretion? mottle texture within
bioturbated laminae

calcite filled fracture

disrupted laminae
alternating laminae and bioturbation

pyritized bed

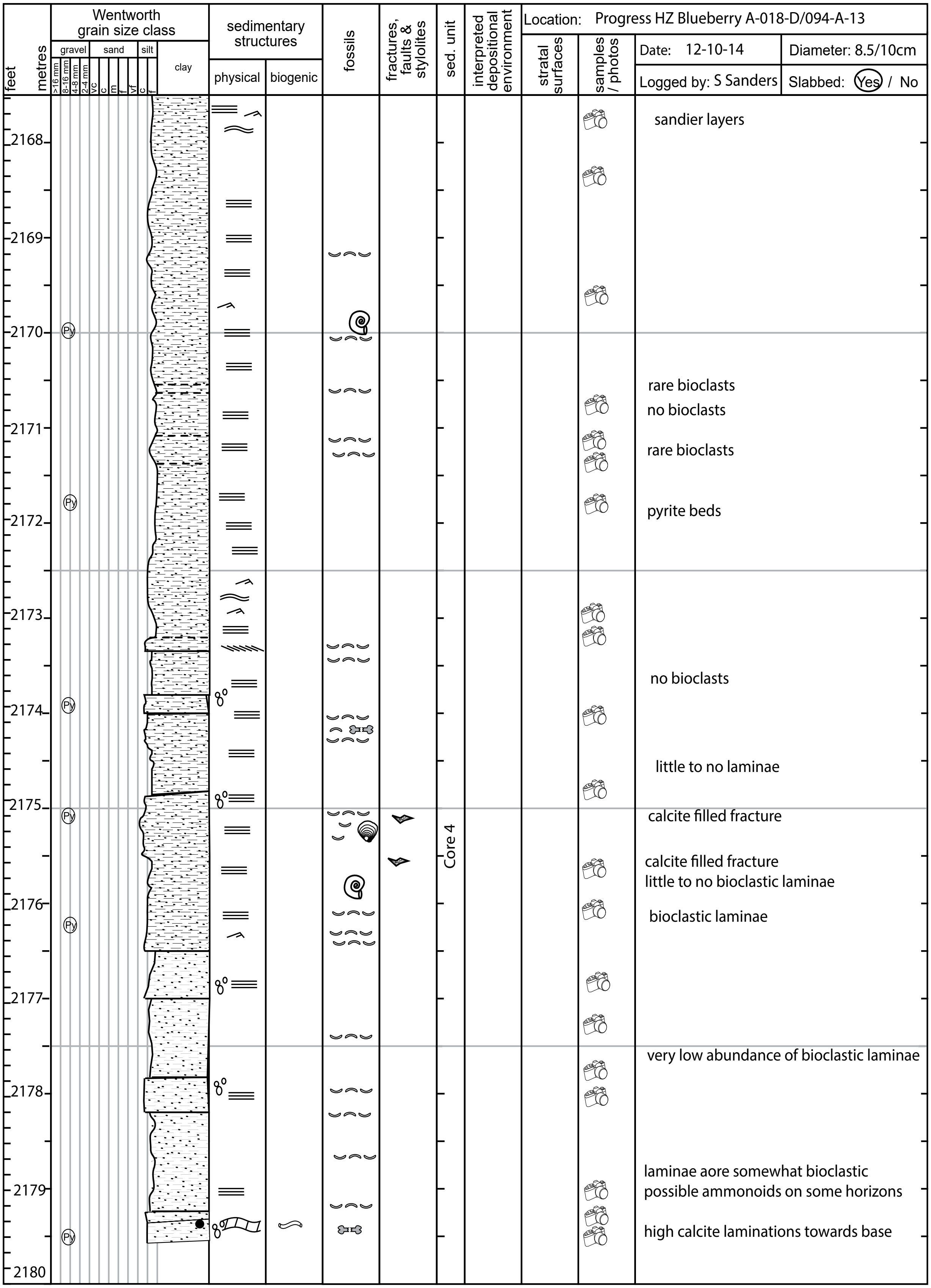
feet
metres
Wentworth grain size class
gravel
sand
silt
clay
>16 mm
8-16 mm
4-8 mm
2-4 mm
vc
c
m
f
vf
c
f
sedimentary structures
physical
biogenic
fossils
fractures, faults & stylolites
sed. unit
interpreted depositional environment
stratal surfaces
samples / photos
2168
2169
2170
2171
2172
2173
2174
2175
2176
2177
2178
2179
2180
Py
Py
Py
Py
Py
Py
Core 4

Location: Progress HZ Blueberry A-018-D/094-A-13

Date: 12-10-14

Diameter: 8.5/10cm

Logged by: S Sanders

Slabbed: [✓ Yes] / No

sandier layers

rare bioclasts

no bioclasts

rare bioclasts

pyrite beds

no bioclasts

little to no laminae

calcite filled fracture

calcite filled fracture

little to no bioclastic laminae

bioclastic laminae

very low abundance of bioclastic laminae

laminae aore somewhat bioclastic

possible ammonoids on some horizons

high calcite laminations towards base

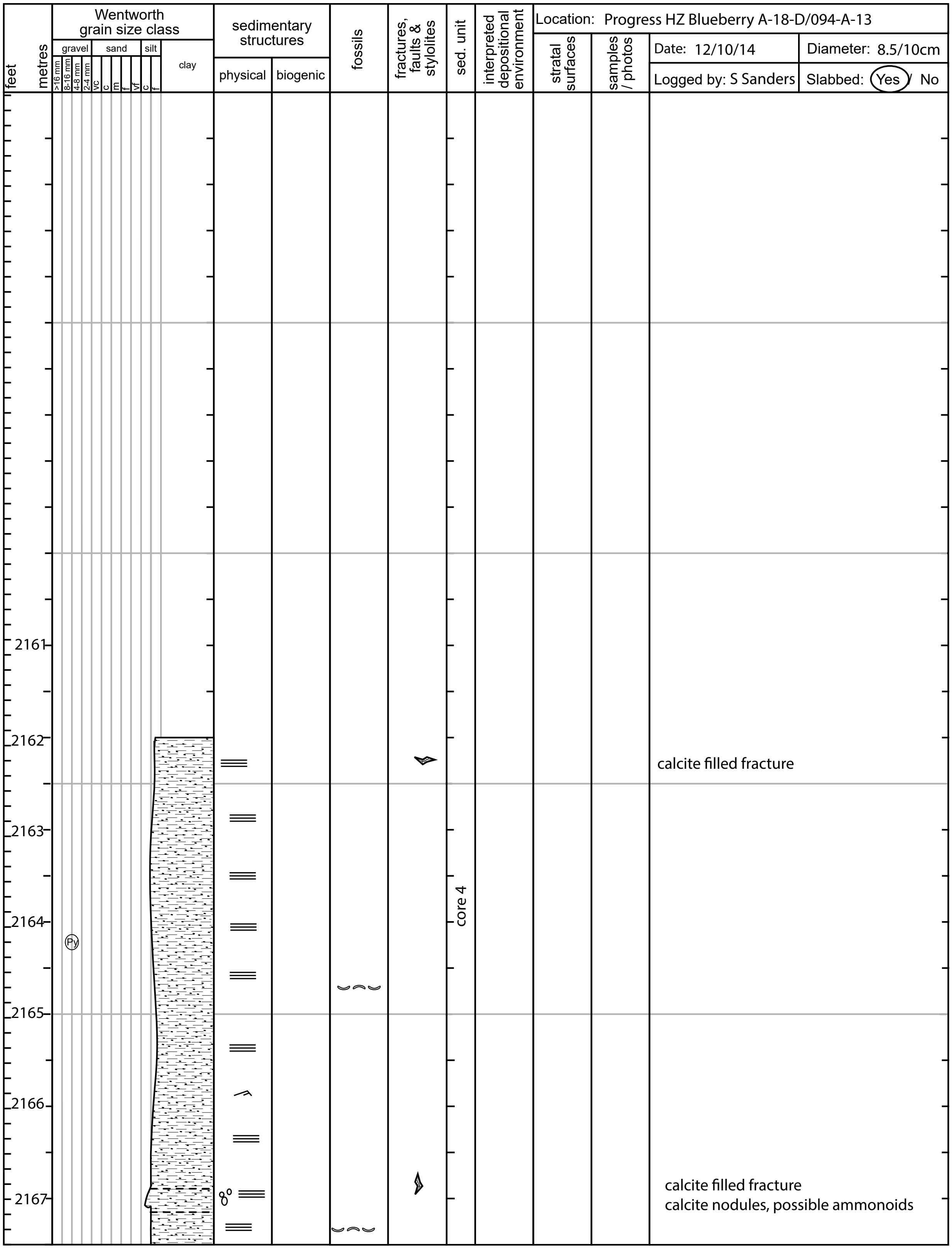
feet
metres
Wentworth grain size class
gravel
sand
silt
clay
>16 mm
8-16 mm
4-8 mm
2-4 mm
vc
c
m
f
vf
c
f
sedimentary structures
physical
biogenic
fossils
fractures, faults & stylolites
sed. unit
interpreted depositional environment
stratal surfaces
samples / photos
2161
2162
2163
2164
2165
2166
2167
Py
core 4
calcite filled fracture
calcite filled fracture
calcite nodules, possible ammonoids

Location: Progress HZ Blueberry A-18-D/094-A-13

Date: 12/10/14

Diameter: 8.5/10cm

Logged by: S Sanders

Slabbed: [✓ Yes] / No

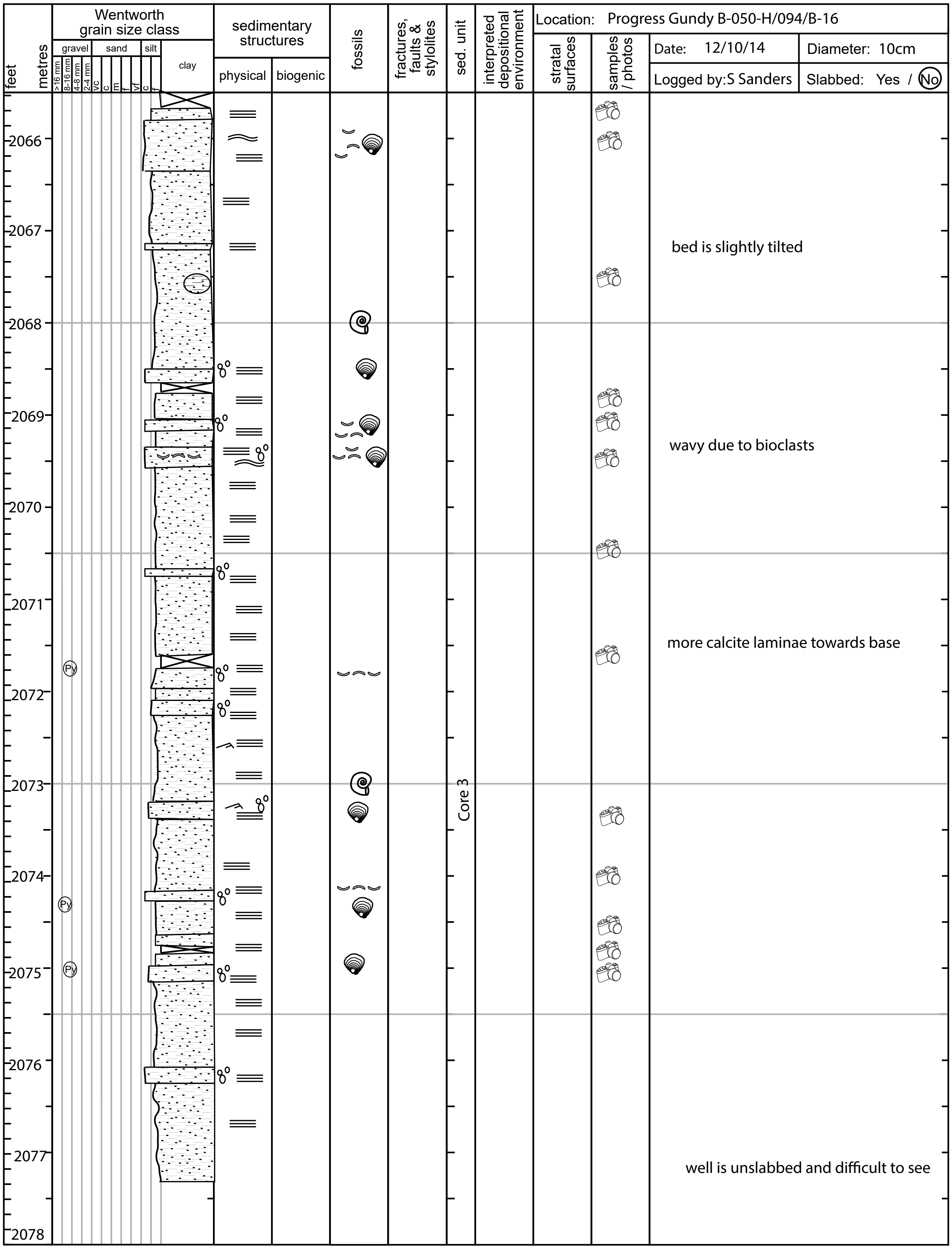

Location: Progress Gundy B-050-H/094/B-16

Date: 12/10/14

Diameter: 10cm

Logged by:S Sanders

Slabbed: Yes [✓ No]

bed is slightly tilted

wavy due to bioclasts

more calcite laminae towards base

well is unslabbed and difficult to see

feet
metres
Wentworth grain size class
gravel
sand
silt
clay
>16 mm
8-16 mm
4-8 mm
2-4 mm
vc
c
m
f
vf
c
f
sedimentary structures
physical
biogenic
fossils
fractures, faults & stylolites
sed. unit
interpreted depositional environment
stratal surfaces
samples / photos
2066
2067
2068
2069
2070
2071
2072
2073
2074
2075
2076
2077
2078
Py
Py
Py
Core 3

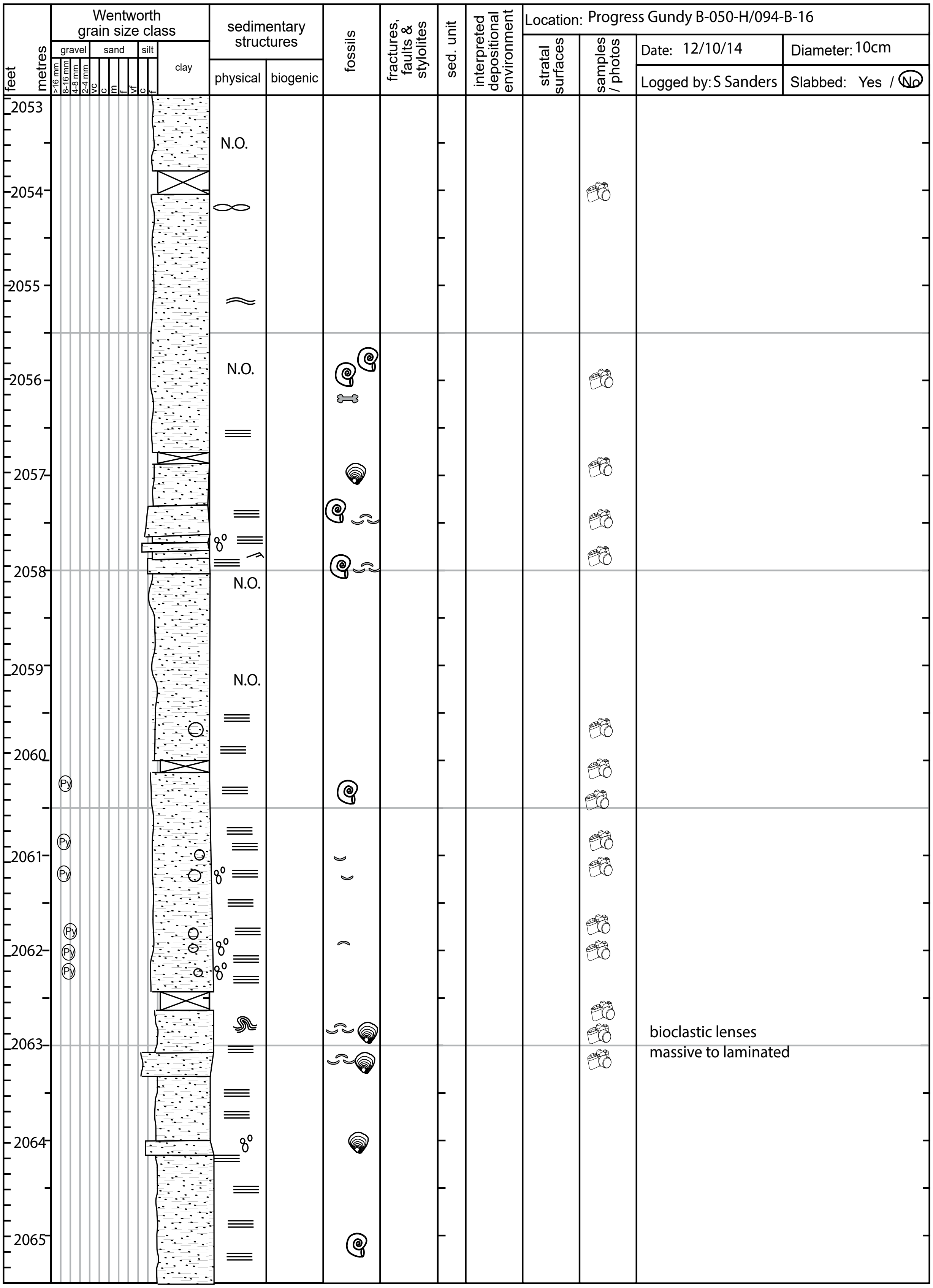

Location: Progress Gundy B-050-H/094-B-16

Date: 12/10/14

Diameter: 10cm

Logged by: S Sanders

Slabbed: Yes / [✓ No]

bioclastic lenses
massive to laminated

feet
metres
Wentworth grain size class
gravel
sand
silt
clay
>16 mm
8-16 mm
4-8 mm
2-4 mm
vc
c
m
f
vf
c
f
sedimentary structures
physical
biogenic
fossils
fractures, faults & stylolites
sed. unit
interpreted depositional environment
stratal surfaces
samples / photos
2053
2054
2055
2056
2057
2058
2059
2060
2061
2062
2063
2064
2065
N.O.
N.O.
N.O.
N.O.
Py
Py
Py
Py
Py
Py

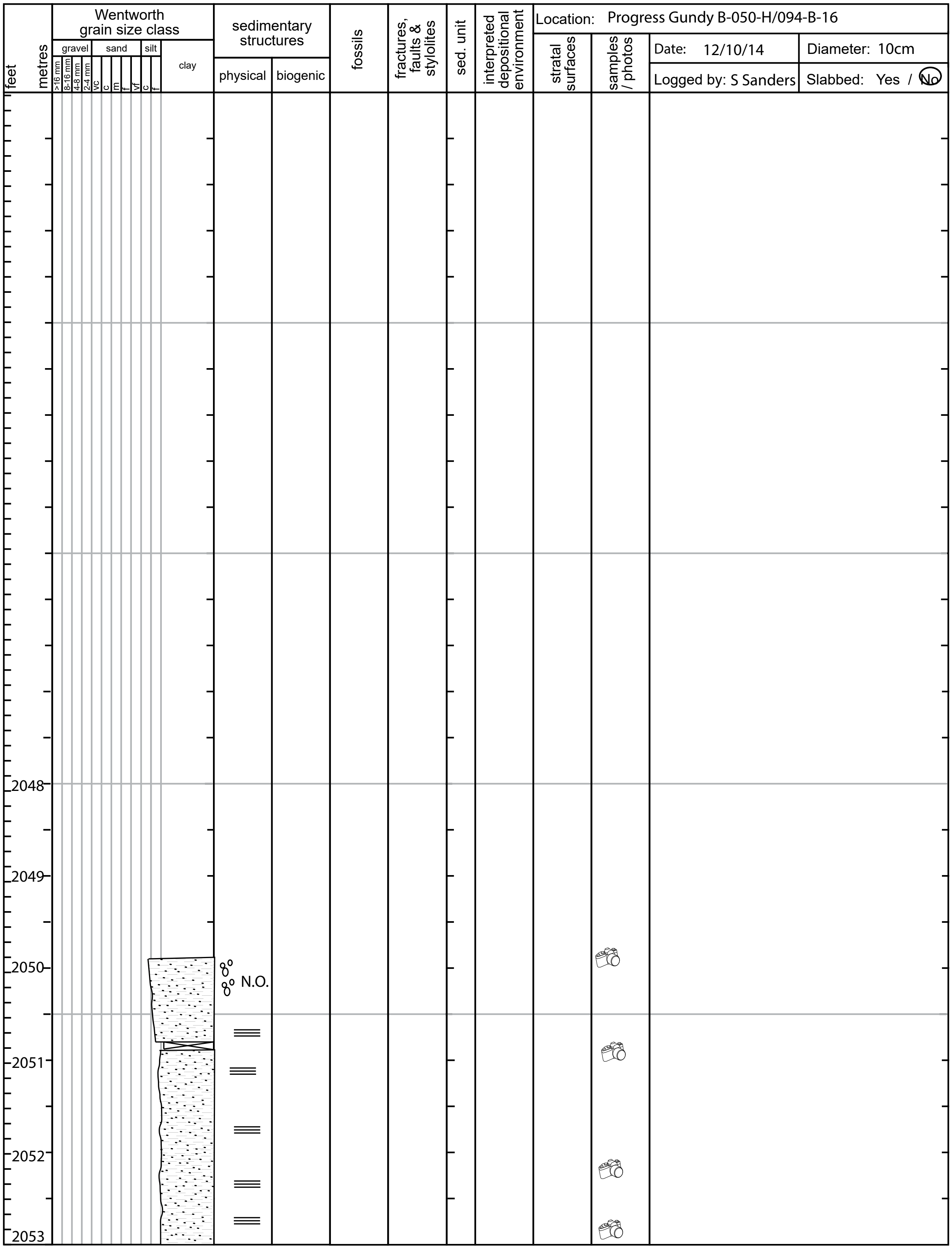
feet
metres
Wentworth grain size class
gravel
sand
silt
>16 mm
8-16 mm
4-8 mm
2-4 mm
vc
c
m
f
vf
c
f
clay
sedimentary structures
physical
biogenic
fossils
fractures, faults & stylolites
sed. unit
interpreted depositional environment
stratal surfaces
samples / photos
2048
2049
2050
2051
2052
2053
N.O.

Location: Progress Gundy B-050-H/094-B-16

Date: 12/10/14

Diameter: 10cm

Logged by: S Sanders

Slabbed: Yes / [✓ No]

Location: Bonavista Blueberry C-060-C/094-A-13	
Date: 12/11/14	Diameter: 9/10cm
Logged by: S Sanders	Slabbed: Yes / No

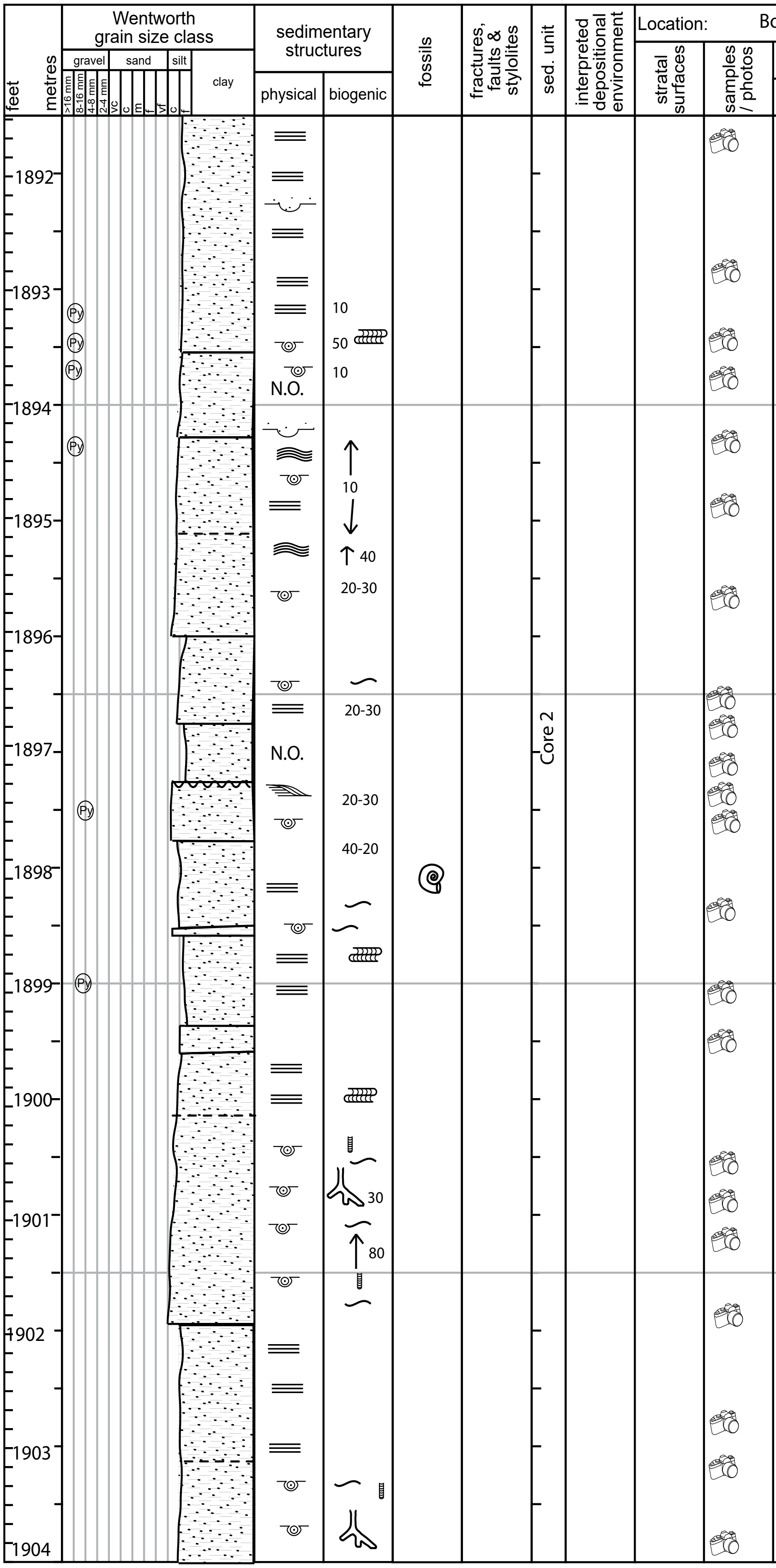
feet
metres
Wentworth grain size class
gravel
sand
silt
clay
>16 mm
8-16 mm
4-8 mm
2-4 mm
vc
c
m
f
vf
c
f
sedimentary structures
physical
biogenic
fossils
fractures, faults & stylolites
sed. unit
interpreted depositional environment
stratal surfaces
samples / photos
1892
1893
1894
1895
1896
1897
1898
1899
1900
1901
1902
1903
1904
Py
Py
Py
Py
Py
Py
10
50
10
N.O.
10
40
20-30
20-30
N.O.
20-30
40-20
30
80
Core 2

1/3 slab in the box. Mostly slabbed except where samples were taken.

possible bioturbation
disrupted laminae

ripples in pyritized laminae

salt and peppery look
disrupted laminae

disrupted laminae

occassional laminae

disrupted laminae

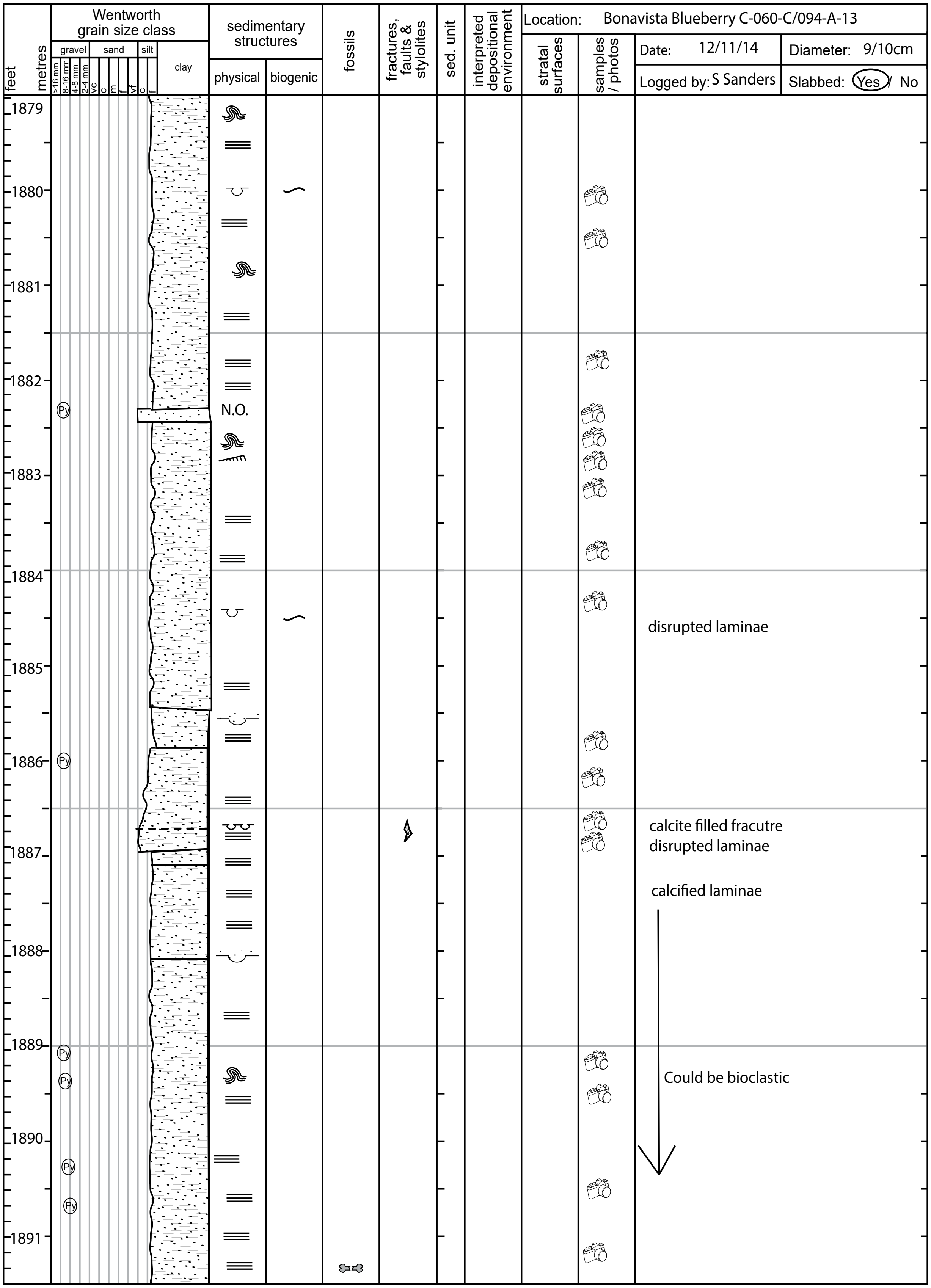

feet
metres
Wentworth grain size class
gravel
sand
silt
clay
>16 mm
8-16 mm
4-8 mm
2-4 mm
vc
c
m
f
vf
c
f
sedimentary structures
physical
biogenic
fossils
fractures, faults & stylolites
sed. unit
interpreted depositional environment
stratal surfaces
samples / photos
1879
1880
1881
1882
1883
1884
1885
1886
1887
1888
1889
1890
1891
Py
N.O.

Location: Bonavista Blueberry C-060-C/094-A-13

Date: 12/11/14

Diameter: 9/10cm

Logged by: S Sanders

Slabbed: [✓ Yes] / No

disrupted laminae

calcite filled fracutre
disrupted laminae

calcified laminae

Could be bioclastic

Location: Bonavista Blueberry C-060-C/094-A-13

Date: 12/11/14	Diameter: 9/10cm
Logged by: S Sanders	Slabbed: [✓ Yes] / No

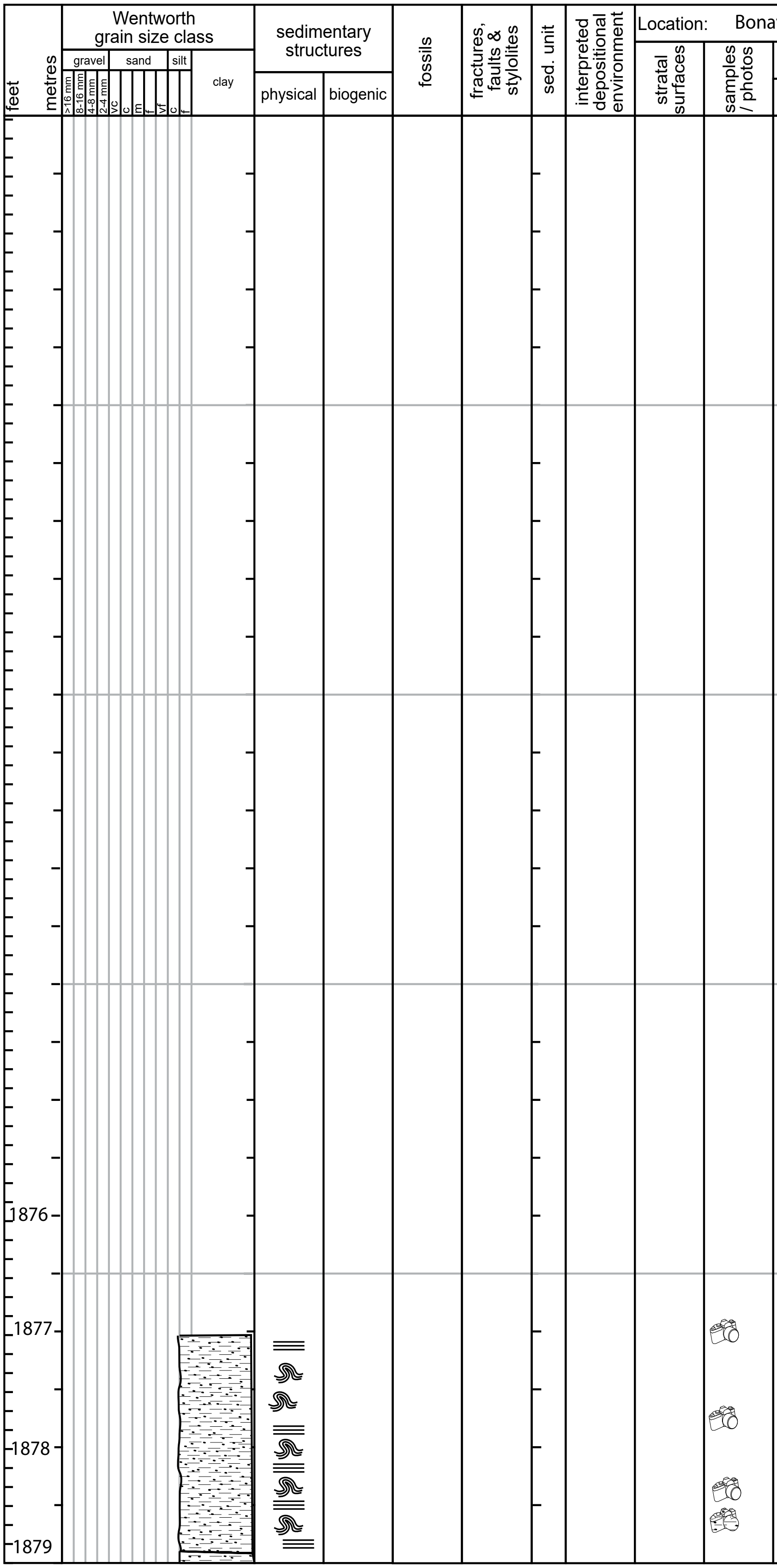
feet
metres
Wentworth grain size class
gravel
sand
silt
clay
>16 mm
8-16 mm
4-8 mm
2-4 mm
vc
c
m
f
vf
c
f
sedimentary structures
physical
biogenic
fossils
fractures, faults & stylolites
sed. unit
interpreted depositional environment
stratal surfaces
samples / photos
1876
1877
1878
1879

SYMBOLS: CORE/OUTCROP LOGGING FORMS

Ichnofossil Symbols

- Root Traces
- *Scalarituba*
- *Gyrochorte*
- tubular tidalite
- *Planolites*
- *Treptichnus*
- *Gyrolithes*
- *Trichichnus*
- *Fugichnia*
- *Asteriacites*
- *Chondrites*
- feeding pit
- *Lingulichnus*
- *Cylindrichnus*
- *Asterosoma*
- *Roselia*
- *Zoophycos*
- *Siphonichnus*
- *Lockeia*
- vertical discoidal & plug-shaped burrows
- *Glossifungites* surface

- Undifferentiated Bioturbation
- *Phycosiphon/Anconichnus*
- *Helminthopsis/Helminthoida*
- *Skolithos/Monocraterion*
- *Conichnus/Bergaueria*
- *Rhizocorallium*
- *Teichichnus*
- *Diplocraterion*
- *Arenicolites*
- *Spongelliomorpha*
- *Thalassinoides/Camborygma*
- *Ophiomorpha*
- *Cruziana*
- *Lunulichnos*
- *Palaeophycus*
- *"Terebellina"*
- *Schaubcylindrichnus*
- *Macaronichnus*
- bivalve resting trace
- *Trypanites* surface

- *Trichophycus*
- *Undichna*
- *Aulichnites*
- *Diplichnites*
- *Monomorphichnus*
- *Phycodes*
- *Scolicia*
- *Halapoa*
- *Fustiglyphus*
- *Macanopsis*
- *Merdelineaus*
- *Psilonichnus*
- *Beaconichnus*

Fossil Symbols

- Conodont
- Foraminifera
- Gastropod
- Ammonoid
- Bivalved pelecypods
- Nautaloid
- Echinoid/ echinoid debris
- Ophiuroid
- Asteroid
- Crinoid/ crinoid debris
- Spirifirid Brachiopod
- Lingulide Brachiopod
- Terebratulid Brachiopod
- Acrotretid brachiopod
- Atrypid Brachiopod
- Decapod crustacean
- Phyllocarid arthropod
- Tabulate Coral
- Rugose Coral
- Spongiomorph
- Sponge
- / Scleractinian Coral (branching / encrusting)
- Cryptalgal laminae
- Wrinkle structures / Runzelmarken
- Bioclastic debris
- Vertebrate skeletal elements
- Wood
- Leaves
- Carbonaceous matter
- Carbonaceous laminae
- Carbonaceous debris on ripple foresets

- - - - - - - conformable contact
- marine flooding surface
- erosional surface

Physical Sedimentary Structures

- Flaser Bedding
- Lenticular Bedding
- Tidal Couplets
- Wavy bedding (heterolithic)
- Wavy bedding (homogeneous)
- Ripple Laminae (wave/current)
- Ripple Laminae (bidirectional/starved)
- Climbing Ripples
- Low angle cross-stratification
- Hummocky cross-stratification
- Planar cross-stratification
- Swaley cross-stratification
- Trough cross-stratification
- Over steepened beds

- Sediment-filled fracture
- Shrinkage/Dessication cracks
- Planar bedding
- Scour and Fill
- Bird's eye structure
- Tool marks
- Pedogenic slickensides

- Calcispheres
- Stylolite
- Load casts
- Synaeresis cracks
- Soft sediment faulting
- Soft sediment deformation
- Dewatering structure
- Convolute lamination

Extras

- ▲ ▲▲▲ Mud clasts
- Pebble lag
- ------ Shale laminae
- Imbricated clasts
- Photo Available
- Sample collected

- outcrop locality
- subsurface locality
- Ⓢ Siderite
- (Gl) Glauconite
- (Py) Pyrite
- Ⓟ Phosphate

- fracture (vertical)
- fracture (horizontal)
- fracture (open)
- fracture (open, crystal lined)